DISSERTATION

MEASUREMENT OF THE DIFFERENTIAL CHARGED CURRENT SINGLE PION CROSS SECTION USING MUON MOMENTUM AND MUON ANGLE IN THE PI ZERO DETECTOR OF THE T2K EXPERIMENT

Submitted by

Jaclyn Schwehr

Department of Physics

In partial fulfillment of the requirements

For the Degree of Doctor of Philosophy

Colorado State University

Fort Collins, Colorado

Spring 2018

Doctoral Committee:

Advisor: Robert J. Wilson

Bruce Berger
Walter Toki
Michael Mooney
Alexander Brandl

ABSTRACT

MEASUREMENT OF THE DIFFERENTIAL CHARGED CURRENT SINGLE PION CROSS SECTION USING MUON MOMENTUM AND MUON ANGLE IN THE PI ZERO DETECTOR OF THE T2K EXPERIMENT

A measurement of the charged current single pion differential cross section in the pi-zero detector of the T2K experiment is presented as a function of reconstructed muon momentum and muon angle. This measurement is done with particular care taken to minimize model dependence throughout the analysis, specifically with careful signal definition and efficiency corrections. New methods for improving the reconstruction of low energy pions are included, as is a method for fitting background events induced by signal physics without introducing model dependence to the fit. Run 4 water-in data is used to make this measurement, which corresponds to an exposure of 1.63×10^{20} protons on target. The differential cross section measurement is made per nucleon for all targets in the fiducial volume of the pi-zero detector over muon angles of 0° to 90° with respect to the incident neutrino beam direction, and muon momenta from 150 MeV to 5 GeV. The measured cross sections are lower than those predicted by the default Rein Sehgal resonance and coherent models, favoring the Minoo resonance and Berger Sehgal coherent models.

ACKNOWLEDGEMENTS

There are a great many people who helped me get here, and while these words are hardly enough to thank them, they are a good start.

The T2K Collaboration - For building and running a great experiment, for all the people who taught me so much about that experiment, and for after-collaboration-meeting karaoke parties.

T2K Subgroups: Cross Section and NIWG - For advice, encouragement, and assistance from a great number of experts, and for bribery chocolate.

CSU CC1pi Group: Dan Cherdack and Matt Hogan - For invaluable assistance throughout the analysis, for being willing to debate almost everything, and for pushing me to do my best work.

My Thesis Advisor: Bob Wilson - For helping me find the motivation necessary to complete my analysis, for support and assistance when I needed it, and for patience as I found my path.

My Masters Advisor: Bruce Berger - For giving me the job that brought me to CSU and led to me joining the graduate school, and for encouraging me to take on interesting and challenging research.

My Parents - For always believing in me, and for constant and unending support whenever I needed it.

My Friends: Cheri, Raj, Dave, and Gus - For reminding me to have fun, for having faith in me even when I lost it, for chats over beer and delves through dungeons and everything in between.

TABLE OF CONTENTS

LIST OF TABLES

LIST OF FIGURES

Chapter 1

Introduction

1.1 Foreword

This thesis describes the analysis done to measure the charged-current single-charged-pion production cross section for events occurring within the pi-zero detector of the T2K near detector. This measurement is done as a function of the outgoing muon momentum and angle. One overriding theme in this measurement is to take special care in ensuring that this measurement is as model independent as possible. The nature of neutrino experiments is such that simulations of events are vital to any measurement, and thus it is only through special effort that these simulations do not influence what is being measured. The chapters to follow provide all the introductory information necessary to understand the measurement being made, as well as full description of the tools and techniques used and developed to make the measurement. A short description of each chapter is provided here:

Chapter 1 contains an introduction to the physics of neutrinos, the meaning and measuring of cross sections, the T2K experiment, and the Pi-Zero detector.

Chapter 2 presents the methods and models used to simulate data. These simulations are a crucial part of all neutrino cross section measurements, and careful consideration is necessary to use these tools without letting a measurement be wholly dependent on them.

Chapter 3 details the reconstruction of passing track momenta and angles by studying the energy these passing particles leave in the detector. A new reconstruction algorithm developed for this analysis, the Cluster Track Fitter, is presented. The characteristics of the track reconstruction are carefully considered and play a role in the development of the analysis.

Chapter 4 introduces the multivariate analysis techniques used by this analysis to determine the identity of the tracks passing through the detector.

Chapter 5 defines the signal this analysis is attempting to measure as well as the method for selecting events defined as signal. The final analysis samples are detailed here, both those containing the purest sample of signal events, as well as defined sideband regions developed to most accurately characterize the backgrounds present in the analysis.

Chapter 6 explains the procedure used to extract the final number of signal events, using a likelihood fitter developed for this analysis. The details and functionality are provided for the fitter together with the characterization of the systematic errors as applied to the measurement.

Chapter 7 presents the final measured signal and efficiency corrected cross section measurement, complete with errors. Comparison of this result to other measurements and models is also done.

1.2 Neutrino Interactions

Neutrinos interact very rarely, making them difficult to study. Unlike charged particles that can ionize particles as they pass through media, neutrinos are neutral thus and only through weak interactions can their presence be detected. The only way in which neutrinos can be measured is by looking for the products of neutrinos interacting with other matter, hopefully resulting in charged particles that can show up in a detector. This means that the outgoing particles from a neutrino interaction are what are really being seen by detectors, not the neutrinos themselves. Neutrinos can interact with individual nucleons, both protons and neutrons, and also with an entire nucleus as a whole.

1.2.1 Charged-Current vs. Neutral-Current

When they do interact, neutrinos interact via the weak force, which means they exchange a W or Z boson with the target of the interaction. In particle physics it is useful to use diagrams to depict different particle interactions, with the standard depiction being the Feynman diagram. All the Feynman diagrams depicted here will have time moving from left to right, meaning particles on the left side are the initial particles in the interaction, while all the particles on the right side are particles leaving the interaction. The diagram in Figure 1.1 depicts two types of neutrino interactions, defined by the exchange boson mediating the interaction.

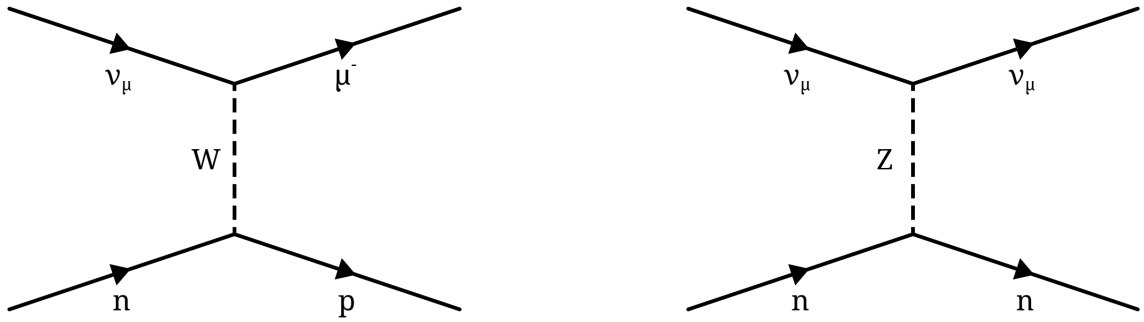

(a) Charged-Current **(b)** Neutral-Current

Figure 1.1: Feynman diagrams for (a) charged-current and (b) neutral-current neutrino interactions.

Figure 1.1a is a charged-current interaction because it is mediated by the charge carrying W boson. In charged-current interactions a neutrino is incident on a particle (in this case a neutron), and since the W^+ in this example carries positive charge away from the neutral neutrino, the resulting lepton is negatively charged. What type of lepton comes from a charged-current interaction depends on the flavor of the incoming neutrino: $\nu_e \rightarrow e$, $\nu_\mu \rightarrow \mu$, $\nu_\tau \rightarrow \tau$. It is through these charged-current interactions that the flavor of interacting neutrino can be determined.

Figure 1.1b is a neutral-current interaction mediated by the neutral Z boson. For the neutral-current interaction the incoming and outgoing leptons are both neutrinos, so only the struck target and any other particles created by the interaction will be seen in a detector. For neutral-current

interactions, there is no way to be sure what type of neutrino interacted, as there is no lepton to measure.

1.2.2 Types of Neutrino Interactions

In addition to charge-current and neutral-current, neutrino interactions can be further broken down into three broad categories that are defined by the energy of the neutrino, the amount of energy transferred from the neutrino to the target particle, and the resulting type and number of particles. From low to high neutrino energy, these three categories are: quasi elastic (QE), resonant (RES), and deep inelastic scattering (DIS). The cross sections for these interactions are given in Figure 1.2a. For all neutrino interactions, there are corresponding anti-neutrino interactions that can also be measured. For this analysis the anti-neutrino interactions are mostly negligible, but for completeness Figure 1.2b contains the interaction cross sections for anti-neutrinos.

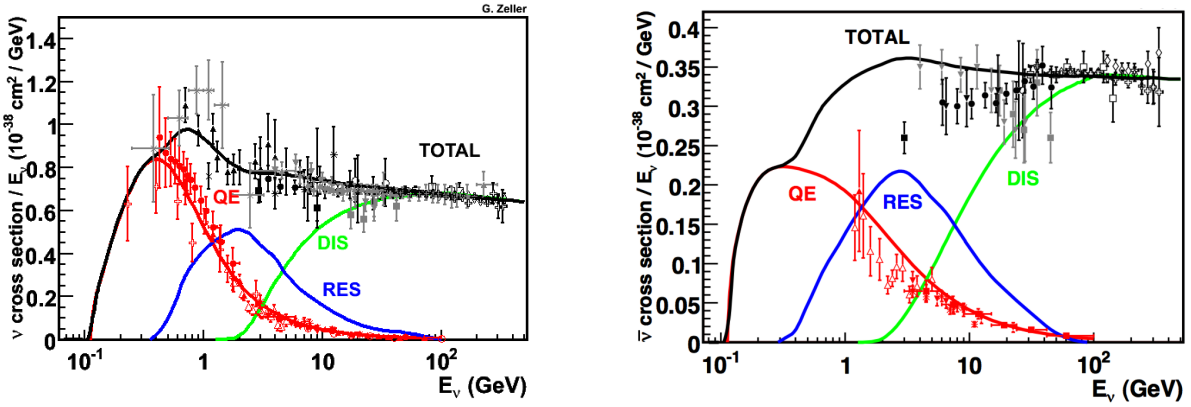

(a) Neutrino **(b)** Anti-Neutrino

Figure 1.2: Interaction cross section as a function of neutrino energy for quasi elastic (QE), resonant (RES), and deep inelastic scattering (DIS) interactions for neutrinos and anti-neutrinos [1].

Resonant Pion Production

When a sufficiently energetic neutrino interacts with a nucleon it can excite that nucleon into a resonant state that immediately decays into a pion. This process is called resonant pion production, and results in a charged or neutral pion along with a nucleon and lepton in the final state. There are

a total of 14 resonances that can be probed with neutrinos and anti-neutrinos, six charged-current resonances:

$$\begin{aligned} \nu_\mu p &\rightarrow \mu^- p\pi^+ & \overline{\nu}_\mu + n &\rightarrow \mu^+ n\pi^- \\ \nu_\mu n &\rightarrow \mu^- p\pi^0 & \overline{\nu}_\mu + p &\rightarrow \mu^+ n\pi^0 \\ \nu_\mu n &\rightarrow \mu^- n\pi^+ & \overline{\nu}_\mu + p &\rightarrow \mu^+ p\pi^- \end{aligned} \tag{1.1}$$

and 8 neutral-current resonances:

$$\begin{aligned} \nu p &\rightarrow \nu p\pi^0 & \overline{\nu} p &\rightarrow \overline{\nu} p\pi^0 \\ \nu p &\rightarrow \nu n\pi^+ & \overline{\nu} p &\rightarrow \overline{\nu} n\pi^+ \\ \nu n &\rightarrow \nu n\pi^0 & \overline{\nu} n &\rightarrow \overline{\nu} n\pi^0 \\ \nu n &\rightarrow \nu p\pi^- & \overline{\nu} n &\rightarrow \overline{\nu} p\pi^- \end{aligned} \tag{1.2}$$

Note that when a neutrino undergoes a charged-current interaction, the outgoing lepton is negatively charged, while when an anti-neutrino interacts the outgoing lepton is positively charged. This example of charge conservation is how an event can be identified as resulting from a neutrino or anti-neutrino.

For this analysis the goal is to measure neutrino induced charged-current single-charged-pion production, so there are only two interaction channels of interest, both of which are shown in Figure 1.3. For these interactions there is either a neutron or a proton in the final state along with a positively charged muon and pion. Neutrons do not give off ionization light when they pass through the detectors, so the interactions this analysis will be looking for will have either a muon and pion or will have a muon, pion, and a proton.

Coherent Pion Production

Coherent pion production occurs when the neutrino interacts with a whole nucleus coherently, leaving the nucleus in its ground state, and produces an outgoing lepton and a single-charged-pion.

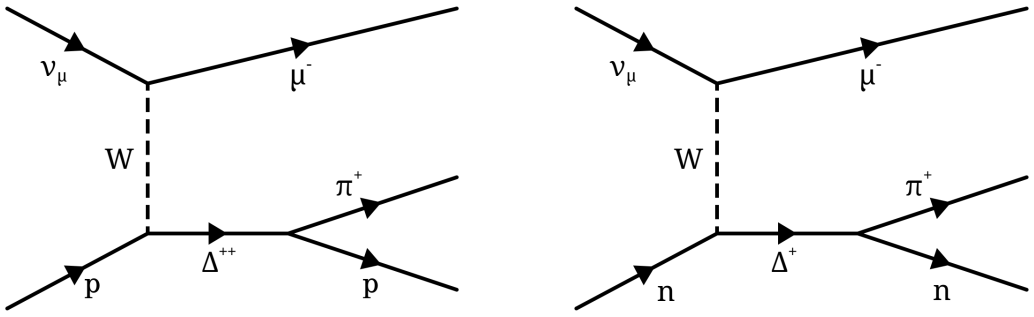

(a) On Proton **(b)** On Neutron

Figure 1.3: Feynman diagrams for neutrino-induced charged-current resonant π^+ production on (a) proton or (b) neutron.

Because the nucleus must remain in its ground state, and none of the nucleons can be excited individually, the amount of energy and momentum transferred to the nucleus must stay small. Because of the small amount of energy and momentum transferred to the nucleus, the outgoing muon and pion are restricted in their phase space and travel predominantly in the direction of the incident neutrino.

As with other interactions, coherent pion production has charged-current interactions:

$$\nu N \to \mu^- N \pi^+ \qquad\qquad \overline{\nu} N \to \mu^+ N \pi^- \tag{1.3}$$

as well as neutral-current interactions:

$$\nu N \to \mu^- N \pi^0 \qquad\qquad \overline{\nu} N \to \mu^+ N \pi^0 \tag{1.4}$$

Because coherent pion production involves scattering off an entire nucleus, instead of individual nuclei, this interaction does not result in any individual nucleons in the final state. The Feynman diagram for charged-current coherent pion production is given in Figure 1.4. In coherent pion production, the small amount of energy and momentum transferred to the nucleus is carried by a pomeron, represented as $\mathcal{P}$.

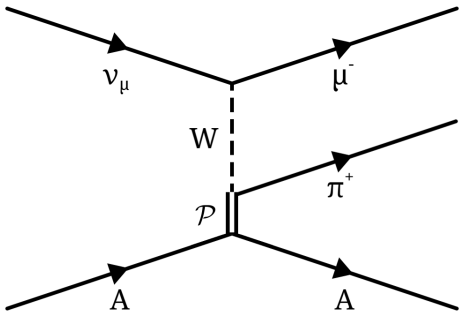

Figure 1.4: Feynman Diagram for neutrino-induced charged-current coherent π^+ production.

Deep Inelastic Scattering

When a neutrino is of sufficient energy it can probe not just a single nucleon in a nucleus, but the individual quarks within that nucleon. In this case, the interaction is referred to as Deep Inelastic Scattering (DIS), and the result is a shower of hadronic particles. DIS interactions occur as the neutrino energy increases, with the lower energy DIS events producing fewer particles than DIS events with neutrinos of higher energy. For these lower energy DIS events, it is possible for the only outgoing particles to be the lepton, a single charged pion, and the resulting nucleon. These low-energy DIS events can then resemble resonant pion production, and therefore must be considered when looking for single-charged-pion events. At higher energies DIS events result in showers of hadronic particles in the final state. The Feynman Diagram for DIS events is shown in Figure 1.5.

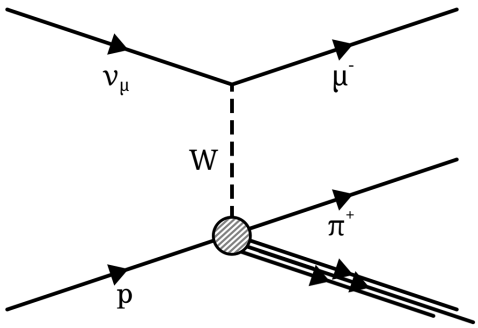

Figure 1.5: Feynman diagram for neutrino-induced charged-current deep inelastic scattering resulting in single π^+ production.

Quasi-Elastic

At lower neutrino energies, a neutrino interacting with a nucleon will not excite a resonance and no pion will be created. In these cases all that occurs is four momentum transfer to the nucleon, resulting in just a lepton and a nucleon in the final state. These interactions are called quasi-elastic; "quasi" because unlike elastic interactions QE events have different particles in the final states than in the initial states. Charge-current quasi-elastic interactions have been very well measured in past experiments because in addition to being the dominant channel for low-energy neutrino sources, this channel can give a very good measurement of the neutrino energy just by observing the outgoing lepton angle and momentum. The charged current quasi-elastic (CCQE) interactions are:

$$\nu_\mu n \rightarrow \mu^- p \qquad\qquad \overline{\nu_\mu} p \rightarrow \mu^+ + n \tag{1.5}$$

And the neutral-current interactions are:

$$\begin{aligned} \nu_\mu n &\rightarrow \nu_\mu n & \overline{\nu_\mu} n &\rightarrow \overline{\nu_\mu} n \\ \nu_\mu p &\rightarrow \nu_\mu p & \overline{\nu_\mu} p &\rightarrow \overline{\nu_\mu} p \end{aligned} \tag{1.6}$$

In recent years there has been much attention to the CCQE interaction as experiments have measured it on more complex targets than the early experiments.

This increased precision has lead to the measurement of additional nuclear effects that change the expected final state particles for the CCQE interaction. The current expansion to CCQE is the MEC (meson exchange current) or 2p2h (two particle, two hole) interaction that occurs when a neutrino interacts with a bound pair of nucleons, resulting in two nucleons in a final state [2]. These additional nuclear effects seen in CCQE interactions are probably present in other neutrino interaction modes as well, and are still being studied with numerous models being introduced and tested in an attempt to better understand the latest experimental results.

For this analysis, the importance of CCQE is that it is the predominant background - an interaction mode that will be confused for CC $1\pi^+$ interactions within the detector. The wealth of models and measurements for CCQE means that the interaction is very well understood, making it much easier to deal with throughout the analysis.

1.2.3 Charge-Current Single-Pion

All the interaction modes discussed above are the primary physics interactions that are separately modeled by theorists. When it comes to comparing these models to data, the separation of interaction modes becomes much more difficult. For this analysis, the goal is to measure charged-current single-charged-pion production. From the discussion above, charged-current means that the final state should contain a muon, and single-charged-pion production means there should be one charged pion. That said, there are three different interactions described above that can result in a pion being created from the initial neutrino interaction. In order to keep this analysis independent of signal models, this analysis does not differentiate between the different modes of generating a CC $1\pi^+$ event. The experiment and analysis to be described in this thesis does not have the ability to distinguish the primary physics mechanism, and thus all interactions are valid.

1.3 Detector

1.3.1 T2K

The Tokai to Kamioka (T2K) [3] experiment is a long-baseline neutrino experiment in Japan built to study neutrino flavor oscillations. Tokai, a town located approximately 80 miles northeast of Tokyo, is the location of the particle accelerator that is the source of the neutrinos and also the location of the near detector ND280 that characterizes the neutrinos at the start of their flight. Kamioka is the location of the far detector Super Kamiokande, a 50 kiloton water Cerenkov detector 185 miles west of Tokai, and is where the neutrinos are finally detected. The main goal of T2K is to study neutrino oscillation, which is done primarily by looking at CCQE events. As the most common interaction mode after CCQE, CC $1\pi^+$ is the dominant background to many of the

oscillation measurements, and thus a better understanding of the CC $1\pi^+$ cross section will lead to more precise oscillation measurements. In addition to the oscillation analyses there are a number of additional measurements that can and have been made using the different detectors, including many neutrino cross section measurements.

1.3.2 Neutrino Beam

The source of neutrinos for the T2K experiment is the proton accelerator located at JPARC. The 30 GeV protons are directed to a graphite target where they interact and produce pions that quickly decay into neutrinos. The neutrino beam that the detectors see is a distribution peaked at 600 MeV with a full width at half max around 400 MeV, making it a more tightly peaked neutrino beam than many other experiments. The tight energy distribution is due to the detectors being positioned 2.5 degrees off axis from the center of the neutrino beam, a design feature of T2K, that results in the neutrino event spectrum shown in Figure 1.6.

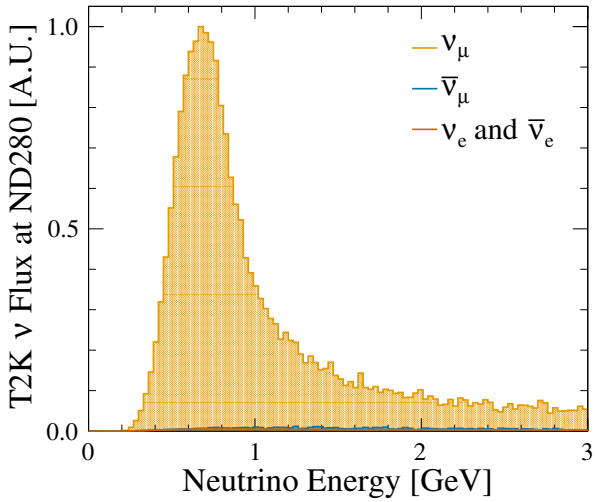

Figure 1.6: T2K neutrino flux at ND280.

1.3.3 ND280

The near detector in T2K is located 280 meters from the neutrino source, which gives it the name ND280. This detector is actually a detector complex made of a number of different subdetectors collected together and contained within a 0.2 T electromagnet, as shown in Figure 1.7.

The goals of ND280 are to characterize the neutrino beam and to help constrain cross section parameters in the oscillation measurement. Additionally the nature of the different subdetectors lends itself well to cross section measurements, with different subdetectors optimized for different measurements. The alignment of the subdetectors is such that (for the most part) the detectors are in a line parallel to the incoming neutrino beam. This alignment leads to the labeling of positions and directions relative to the neutrino beam, with detectors closer to the source of neutrinos labeled as "upstream" of their counterparts, which are considered to be "downstream" of the first detectors.

During data collection, ND280 is monitored continuously to ensure the detector is operating correctly. In addition to continuous monitoring of standard systems (temperatures, air and water flow, etc), the data that is collected undergoes quality checks every week to ensure that all collected data is of good quality (properly calibrated), that all subdetectors are functioning within acceptable ranges (temperatures, voltages, etc.), and that any data that does not meet these standards is flagged such that it can be identified and excluded from physics analyses.

Only two subdetectors in ND280 are used in this analysis, the pi-zero detector (PØD) and the most upstream time projection chamber (TPC), both of which are described in more detail below.

1.3.4 PØD

The most upstream subdetector in the ND280 detector complex is the pi-zero detector (PØD), which was designed to measure one of the dominant background interactions that occur in SK, specifically resonant interactions that result in a neutral pion (a pi-zero). To that end, the PØD was designed to operate both with and without an internal water target so as to match the water target of SK, and the PØD was filled with both active detecting layers and radiator layers that were designed to optimize the detection of and contain the pi-zeros it was designed to measure. A schematic of

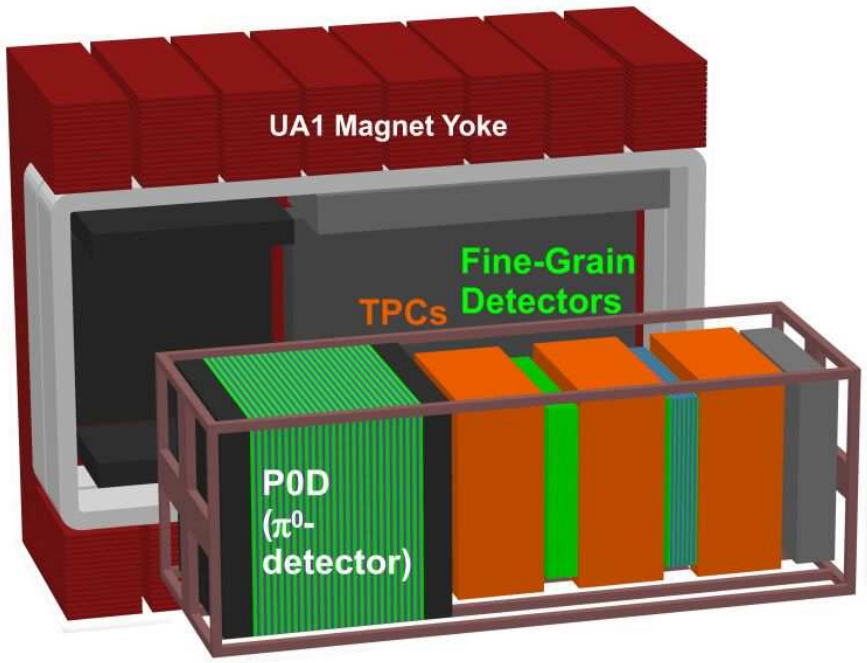

Figure 1.7: Diagram of ND280 with the different subdetectors labeled.

the PØD can be seen in Figure 1.8. The full specifications of the PØD can be found in the technical publication [4], with the pertinent details given below.

Composition

The PØD is composed of four large substructures called super PØDules each of which is made up of smaller structures called PØDules. The PØDules consist of active light detection material in the form of two detection planes - X and Y - and material in which measurements cannot be made, "dead material," in the form of sheets of lead or sheets of brass and bags of water, depending on the PØDule.

Detection planes The detection planes are composed of stacks of triangular bars of scintillating plastic designed to give off scintillation light when charged particles pass through them. The outside of the bars have a coating of titanium dioxide to keep any scintillation light from escaping, while a wavelength shifting fiber runs down the center of each bar to collect the light and direct it to a photon collector. The distance between the read out fibers is 16.5 mm, which provides the coarse

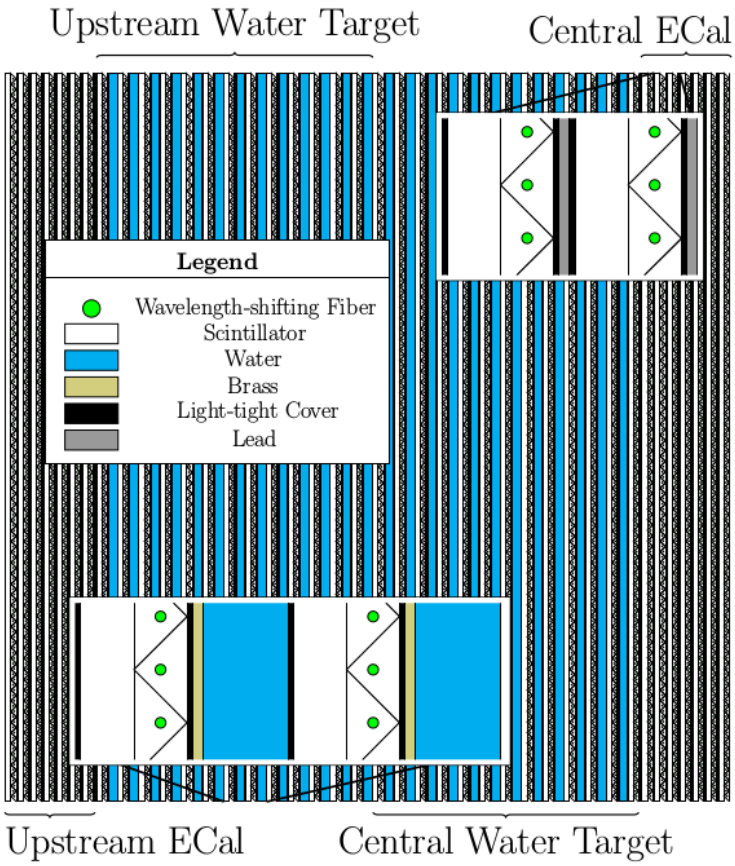

Figure 1.8: Diagram of the PØD.

resolution in the position readout. The triangular bars were chosen to ensure that any passing particle would cross multiple bars so that the proportion of light collected in the two bars could be used to give an indication of where between the two fiber readouts the particle had traveled. The two detection planes in each PØDule are oriented at 90° to one another providing two dimensional position information, these dimensions defined as X and Y, both perpendicular to the neutrino beam direction which is defined as the Z direction.

PØDules The first seven PØDules combine to form the first super PØDule: the up-stream electromagnetic calorimeter (USECal). The "dead" material used in the PØDules of the USECal is lead, which for this analysis means that it will slow down and stop any backwards going tracks that could otherwise escape the detection region of the PØD. The next 25 PØDules contain brass sheets in place of lead, again providing a target and slowing down passing particles. Sandwiched between each PØDule is a layer of water, contained in bags that can be either full or empty, depending on the desired configuration. These PØDules make up the up-stream and central water target super PØDules. Last is the central ECal, matching the US-ECal in design and purpose.

Water Target and Radiators The spacing between different PØDules provides the third dimension for track reconstruction, and is the most coarse distance resolution. In the ECal regions, the size of the PØDules (and thus the distance between pairs of XY detection planes) is 43.5 mm, while the presence of the water bags pushes the distance between detection planes in the water target region to 68.3 mm. The spacing between detection planes makes it difficult for the PØD to detect high angle particles, as they will pass though fewer PØDules than forward going tracks. If tracks are of sufficiently high angle, it is possible for them to escape the PØD without ever traversing a detection plane.

Fiducial Volume

The fiducial volume defines the number of targets the interaction is being measured on, and is defined as a volume sitting slightly within the boundaries of the detector. The inset is designed

to help reject any particles that may originate outside the detector and be mis-reconstructed as originating inside, as well as to define the region of the detector for which the mass is known well. For the PØD, the depth of the water in the water bags influences the fiducial volume, because the fiducial volume needs to be defined such that when the bags are full the top of the water in the bags is above the fiducial volume, ensuring the fiducial volume region does not have a mix of air and water. Additionally the fiducial volume is inset to avoid the side and bottom support structures for the water bags, reducing the amount of dead material within the fiducial volume.

For this analysis, the fiducial volume definition in X and Y is the standard one used throughout the PØD analyses, though the upstream and downstream Z cuts are different. The standard PØD fiducial volume includes all the water layers in the Z fiducial volume, as well as the Y detection plane on the first water target PØDule, and the X detection plane on the last. For this analysis, the fiducial boundary was placed in the middle of the most upstream water layer and in the middle of the most downstream water layer, containing entire PØDules in between. The goal was to not split any pairs of detection layers (X and Y readout layers) with the fiducial volume, as there can be slight mis-alignments between pairs of detection planes, and these definitions use only the Z axis, which may end up including part of a detection plane if there is any shift or tilt in the detector.

The dimensions of the fiducial volume used in this analysis are given in Table 1.1.

Table 1.1: Fiducial Volume Definition using the ND280 coordinate system.

Dimension	Width (mm)	Minimum (mm)	Maximum (mm)
X	1600	-836	764
Y	1740	-871	869
Z	1705	-2969	-1264

The fiducial volume is the definition of the target for the analysis, and thus it is important to know the number of targets within that volume. The number of targets used for the cross section calculation is specific to an analysis, as it can be the number of a particular nuclei, the number of all nuclei, or the number of individual nucleons or just the number of protons. For this analysis, the

interaction producing the signal events is either resonant or coherent pion production. For coherent pion production, the number of nuclei is the relevant target, because coherent pion production is an interaction with the whole nucleus. For resonant pion production interactions can occur off of both the proton and the neutron, so the number of total nucleons is more relevant. For this analysis the final result is reported per nucleon, but with the number of nuclei also provided for completeness. The total mass of the PØD within the fiducial volume is given in Table 1.2 and the error on that mass is given in Table 1.3 and Table 1.4, all calculated from measurements reported in [5].

Table 1.2: PØD Fiducial Mass in Kilograms

Component	Mass/PØDule [kg]	# PØDules	Total Mass [kg]	Total Nuclei	Total Nucleons
PØDule	106.98	24	2567.54	1.17×10^{29}	1.54×10^{30}
Brass	30.28	24	726.72	6.83×10^{27}	4.38×10^{29}
Cover	16.62	1	16.62	7.14×10^{26}	9.99×10^{27}
Water Bags	5.2	24	124.80	4.06×10^{27}	7.51×10^{28}
Water	76.08	24	1825.92	6.10×10^{28}	1.10×10^{30}

Table 1.3: Non-Water Fiducial Mass Error Calculation

Component	Mass/PØDule [kg]	Mass err/PØDule [kg (%)]	# PØDules	Total Mass [kg]	Total Error [kg (%)]
PØDule	106.98	0.96 (0.90%)	24	2567.52	23.04 (0.90%)
Brass	30.29	0.89 (2.94%)	24	726.96	21.36 (2.94%)
Cover	16.62	1.34 (8.06%)	1	16.62	1.34 (8.06%)
Water Bag	5.2	0.29 (5.58%)	24	124.8	6.96 (5.58%)
Total Mass and Error				3435.9	52.70 (1.53%)

A full breakdown of materials within the PØD for an elemental analysis of the fiducial volume is provided in Table 1.6, with a summary of the different elements given in Table 1.5.

Table 1.4: Water Fiducial Mass Error Calculation

Water	Mass/PØDule [kg]	mass err/layer [kg (%)]	# PØDules	Total Mass [kg]	Total Error [kg (%)]
Central bags	76.08	7.608 (10%)	23	1749.84	36.49 (2.9%)
Edge bags	76.08	38.04 (50%)	1	76.08	38.04 (50%)
Total Volume				1825.92	36.52 (2%)
Total Mass and Error				1825.92	64.12 (3.51%)

Table 1.5: Fiducial Volume Breakdown by Element

Material	PØDules	Water	Brass	Water Bags	Water Cover	Total
Nucleons	1.54×10^{30}	1.10×10^{30}	4.38×10^{29}	7.51×10^{28}	9.99×10^{27}	3.17×10^{30}
Nuclei	1.17×10^{29}	6.10×10^{28}	6.83×10^{27}	4.06×10^{27}	7.14×10^{26}	1.90×10^{29}
H	1.18×10^{29}	1.22×10^{29}		6.11×10^{27}	1.43×10^{27}	2.48×10^{29}
C	1.15×10^{29}			3.33×10^{27}	7.14×10^{26}	1.19×10^{29}
N	9.69×10^{26}					9.69×10^{26}
O	7.77×10^{26}	6.1×10^{28}				6.18×10^{28}
Si	5.21×10^{25}					5.21×10^{25}
Cl				5.57×10^{26}		5.57×10^{26}
Ti	3.02×10^{26}					3.02×10^{26}
Fe				1.65×10^{26}		1.65×10^{26}
Cu			4.82×10^{27}			4.82×10^{27}
Zn			2.01×10^{27}			2.01×10^{27}

Table 1.6: Fiducial Volume Target By PØDule and Material

Component	Material	Mass Fraction [%]	Composition	Atomic Weight [amu]
		PØDule		
bars	Polystyrene	90.97	C_8H_8	104.1
	Titanium dioxide	1.56	TiO_2	79.866
	PPO	0.93	$C_{15}H_{11}NO$	221.26
	POPOP	0.03	$C_{24}H_{16}N_2O_2$	364.4
PØDule covers	Polystyrene	3.75	C_8H_8	104.1
fibers	Polystyrene	0.09	C_8H_8	104.1
epoxy	Tetraethylene pentamine	1.22	$C_8H_{23}N_5$	189.307
	N,N'-bis(3-aminopropyl) piperazine	0.95	$C_{10}H_{24}N_4$	200.32
	Silica	0.20	SiO_2	60.08
	3,6,9,12-tetraazatetradeca-methylenediamine	0.20	$C_{10}H_{34}N_6$	238.414
	Triethylenetetramine	0.08	$C_6H_{18}N_4$	146.23
	Carbon black	0.01	C	12.011
		Brass		
	Copper	70	Cu	63.546
	Zinc	30	Zn	65.38
		Water Target Cover		
	Polyethylene	100	C_2H_4	28.05
		Water Bag Accessories		
central support	HDPE	15.77	C_2H_4	28.05
water bags	HDPE	17.23	C_2H_4	28.05
fill/drain pipes	PVC	16.08	C_2H_3Cl	62.5
sensor cables	HDPE	8.42	C_2H_4	28.05
sensor pipes	PVC	30.25	C_2H_3Cl	62.5
sensor casing	Steel	12.25	Fe	55.845
		Water		
	Water	100	H_2O	18.02

1.3.5 TPC

ND280 has three time projection chambers (TPCs), each one consisting of approximately four cubic meters of argon gas inside an electric and magnetic field. The TPCs are designed to provide momentum and charge information about the particles passing through the tracker region, which is made up of the three TPCs with two fine-grain tracking detectors (FGDs) sandwiched in between. Full details of the TPCs can be found in the documentation [6].

The TPCs work on the principle of transiting charged particles ionizing the gas of the TPC, and then an electric field guides the ionized gas across the chamber to be detected on one side. The low density of the gas allows the charged particles to pass without losing much energy or reinteracting and changing their trajectory. For these reasons, the spatial resolution of the TPC is very good. The presence of the magnetic field curves passing particles proportional to their momentum in a direction determined by their charge. Using the TPC in an analysis thus allows for detailed momentum reconstruction.

TPC 1 is the most upstream of the three TPCs, and is the first subdetector immediately downstream of the PØD. Tracks that exit the downstream face of the PØD can then enter the TPC and allow an analysis to make use of the charge and momentum measurements available from the TPC.

1.4 Cross Sections

A cross section is a measurement of the interaction probability of a particle for a given target. The probability of a neutrino interacting at all is called the total (or inclusive) cross section while the probability of a neutrino interacting through a specific interaction mode is a called an exclusive cross section. The cross section can also be broken down further into what particles are produced by the interaction and with what angles and momenta, which can be expressed as differential cross sections. The specifics of the interactions are dependent on both the properties of the neutrinos, but also on the nuclear physics modeling the target the neutrino is interacting with. Both the exact properties of nuclear targets and the specific neutrino interactions are poorly understood, and thus

measurements of a variety of cross sections and cross section parameters are useful in advancing the field.

1.4.1 Uses

One of the most important uses of neutrino cross sections is modeling the neutrino interactions in oscillation experiments. Knowing the exact interaction modes available for a beam of neutrinos of a given energy spectrum allows experiments to design detectors to optimally detect the neutrino interactions, and to properly measure the number of particles that interact in the detector.

1.4.2 Calculation

Measuring a neutrino cross section requires counting the number of particles that interact with a given amount of target material for a given number of total neutrinos impinging on the same target material. (1.7) gives the simple equation for a cross section (σ):

$$\sigma = \frac{N}{\Phi T} \tag{1.7}$$

with N representing the number of interactions, T the number of target nuclei, and Φ the integrated neutrino flux (the number of neutrinos per area per unit time, integrated over the run time being studied). Measuring the neutrino interactions is not a simple matter, and the imperfection of our detectors make it difficult if not impossible to detect all the interactions that happen and to differentiate the desired interactions from other background interactions that also occur in the detector. Because of these complications, the cross section equation can be written:

$$\sigma = \frac{N^{obs} - B}{\epsilon \Phi T} \tag{1.8}$$

where now N^{obs} is the number of observed events, B is the number of accidentally selected background events, and ϵ is the efficiency for selecting signal events that corrects the number of observed events to account for the number of interactions that occurred but were not observed.

1.4.3 Differential Cross Section

When the cross section is measured as a function of some event property, the measurement is no longer a total cross section but is a differential cross section. In the case of a differential cross section, the total cross section has been split into a number of separate cross section measurements, each for a specific value or range of values of the given event property. For neutrino cross sections, there are a few different common event properties used to measure differential cross sections. One of the most common event properties to use for measuring a neutrino cross section is the incident neutrino energy which would result in different cross section measurements for different ranges of neutrino energy. Additional parameters used in differential measurements are the different kinematic properties of the outgoing particles in the neutrino interactions. The cross section equation for a differential measurement is then calculated per bin:

$$\sigma_i = \frac{N_i^{obs} - B_i}{\epsilon_i \Phi T} \tag{1.9}$$

with the number of observed events, background events, and efficiencies also calculated per bin.

The CC $1\pi^+$ measurement in this thesis is a differential measurement in two different variables: the outgoing muon momentum and muon angle. The resulting measurement will be the cross section broken down as a function of each of these variables. Measuring the cross section as a function of these variables is a way to test the different interaction models which predict the rate of interactions with different kinematic properties. The benefit of working in the phase space defined by the momentum and angle of the outgoing muon is that this is a directly observed property. While a differential measurement as a function of neutrino energy relies on reconstructing the neutrino energy from physics assumptions combined with observed properties, the outgoing particle properties are directly observed and thus are limited only by the understanding of the ability of a detector to observe them.

1.4.4 Previous Measurements

PØD Measurements The analysis described in this document is the second measurement of CC $1\pi^+$ in the PØD, and builds on a previous measurement which was a single bin measurement that integrated over the muon kinematics. The previous measurement is detailed in [7] with the final measurement presented in Figure 1.9.

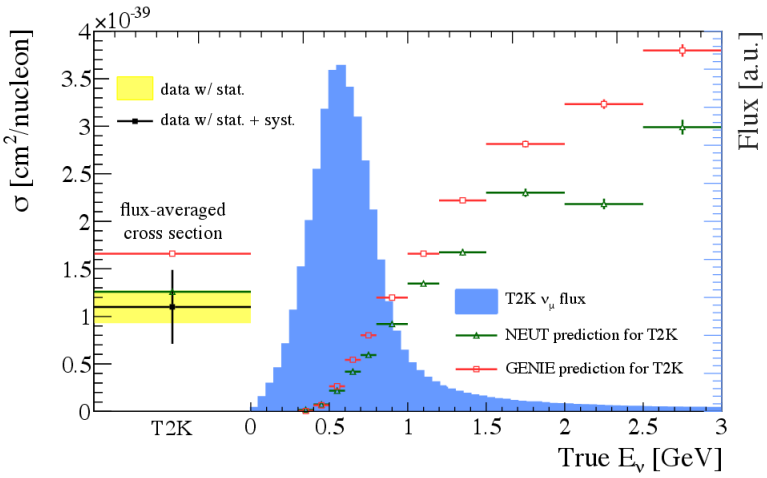

Figure 1.9: The 2015 single bin CC $1\pi^+$ cross section on water PØD-based measurement [7] compared with NEUT [8] and GENIE [9] predictions, overlayed on the T2K flux.

The single bin measurement provided a good start, but to compare with new theoretical models for CC $1\pi^+$ a differential measurement was the clear next step. In addition to expanding the measurement to muon kinematics, new analysis techniques were implemented to increase the statistics, efficiency, and purity of the past measurement.

T2K Measurements Measurement of the CC $1\pi^+$ cross section has also been made by other subdetectors in the T2K experiment, most notably being those made using the Tracker - a combination of the TPCs and the smaller fine grain detectors sandwiched between them. The PØD offers some advantages to the measurements in the Tracker mainly due to the large amount of target material which increases the number of events, and also in the angular acceptance. For events to travel within the TPC, the angle of individual particles must be closer to that of the direction of

the beam. The PØD also offers the opportunity to make a water subtraction measurement to get the cross section on a single target, water, which is much more challenging to do with the Tracker region of the TPC. For these reasons the PØD measurement is a nice complement to measurements already in progress or complete in other subdetectors.

Chapter 2

Event Simulation

2.1 Introduction

Neutrino interactions are inherently difficult to study due to the fact that neutrinos are difficult to produce at specific energies. This one fact introduces a large amount of uncertainty in the measurements that are made and requires extensive work to be done to understand the interactions that occur and the measurements that are made. Being able to accurately simulate events for a range of energies becomes extremely important for making measurements and understanding the abilities and limitations of the detectors being used. In this analysis, the main event simulation software that is used is the NEUT Monte Carlo event simulator developed by and for T2K and its predecessors [8].

2.2 Interaction Simulation

The current neutrino simulations involve a number of different physics models combined to best reflect the community's understanding of the physics involved, tempered by the feasibility of implementing that physics in a piece of software that can run quickly enough to generate sufficiently large data sets to be useful to experimentalists. Combining different models is a challenge because there is not always 100% consistency between the models in place, but this is a feature of simulation packages that cannot be avoided. Understanding the limitations and inherent inconsistencies in the models as implemented is important for every analysis using simulation software, and to that end extensive tools for evaluating errors, both due to the implementation and the limits and uncertainties in the model, have been developed.

The models included in simulation software are usually factorized by the type of interaction (cross section models), the material being interacted with (the nuclear model), and then what happens to the particles after the interaction (the propagation of particles through the nucleus and the

rest of the detector). The ideal case is a fully consistent theoretical understanding of all these pieces together for all energy regions, but the current understanding of neutrino and nuclear physics is not so ideal. There are further factorizations within these categories for different particles, interaction types, and energy regions. Additionally, in correct treatment, different cross section and nuclear models need to be studied together because there can be overlaps and cross terms that arise due to the physics and phase spaces of the interactions. The fact that these are factorized in the simulations means that special care needs to be taken to keep track of the overlaps and cross terms and add them into the models as best as possible.

Despite all the caveats, neutrino event simulation packages are extremely powerful tools that have been developed to do a very good job at simulating neutrino interactions.

2.2.1 Nuclear Model

A nuclear model simulates the conditions within a nucleus, specifically providing the target nuclei with an initial momentum or the target nucleon with an initial momentum and position within the nucleus. Also a part of the nuclear model is the binding energy of a given target nucleon, which represents the energy required to separate a nucleon from its nucleus.

The nuclear model used to develop most of the interaction models in NEUT is the relativistic Fermi gas model (RFG) [10]. A notable feature of the RFG model is that all nucleons within a nucleus have the same binding energy that is only dependent on the type of nucleus. Until recently this was the primary nuclear model implemented, but recently this was replaced with the Spectral Function [11], but only for use with some interaction models. The Spectral Function model provides a range of binding energies to nucleons within a nucleus as a function of the nucleon momentum, and also allows nucleons within a nucleus to have a larger momentum than the RFG model by pairing nucleons into pairs of bound states. Because this model has only recently been updated, the only cross section models that use the new Spectral function are CCQE [11] and MEC [2](an interaction mode similar to CCQE but in which a correlated pair of nucleons

are interacted with, and subsequently ejected from the initial interaction), while most of the other models are still built on top of the RFG model.

2.2.2 Interaction Models

The interaction models are the heart of the physics cross section models, and these dictate how often any type of interaction will occur, as well as determining what particles will be created by the interaction and what their trajectories and momenta will be. This is where the specifics of the Rein-Sehgal [12] model are incorporated to ensure that the CC resonant events occur at the right energies and result in the right particles, according to the theory. There are many models included, and those most relevant to this analysis are:

- Benhar CCQE [11]

  This model uses the spectral function for the nuclear modeling, and includes more interference terms than the previous Llewellyn-Smith CCQE model that is built on the RFG [13]. These changes allow the outgoing particles to span a greater range of phase space by providing a greater range of initial conditions inside the nucleus.

- Nieves MEC [2]

  This model is a new addition that adds in the effect of CCQE interactions on correlated pairs of nucleons instead of on single nucleons. In addition to producing extra nucleons in the final state, this interaction mode allows for a slightly larger range in allowed muon kinematics. Also included in this implementation are the cross terms that arise between this interaction and CCQE interaction.

- Rein-Sehgal CC-Res [12]

  The Rein-Sehgal models the delta resonances for neutrino interactions with W(transferred four momentum squared) less than 1.2 GeV. There is a new model (called the Minoo model in this thesis) recently developed by Monireh Kabirnezhad that improves on the Rein-Sehgal model by including the mass of the leptons (which was left out of the Rein-Sehgal calculation), including resonances up to W=2 GeV, and including the mechanism for non-resonant

pion production in this same energy range [14]. The original Rein-Sehgal model produces a wide range of muon and pion kinematics, while the new model has an adjusted range of kinematics, but is extended to higher neutrino energy (due to the increase in allowed W).

- Rein-Sehgal CC-Coh [15]

  Coherent interactions are defined by the interaction leaving the nucleus in an unchanged state, and the Rein-Sehgal model uses this requirement to suppress a large part of the possible interaction phase space, resulting in very forward going muons and pions in the final state of interactions. There is another model by Berger and Sehgal [16] that is based not on the modeling of nuclear processes inside a nucleus, but instead on experimental data, which finds that there is also a suppression of the coherent cross section in the region where neutrino energies can excite resonances in a nucleus.

- Bodek-Yang DIS [17]

  The T2K neutrino beam is mostly made up of neutrinos too low in energy to experience DIS events, it is only in the high energy tail (neutrinos of energy greater than 3 GeV). that these occur, which is overall not a large fraction of events.

Of the models included above, the Rein-Sehgal CC resonant and CC coherent models are the ones being tested in this analysis. The CCQE model by Benhar and Llewellyn-Smith is the model for the main background, producing events that the analysis confuses with signal CC $1\pi^+$ events.

2.2.3 Particle Propagation

After the appropriate neutrino interaction model has been called, the simulation has a list of particles that have been created by the interaction. These particles have directions and momenta, but are in the same location where the interaction took place. From the interaction location the particles need to escape the nucleus, if they occurred on a nucleon, and for this another set of models comes into play. The interactions that occur here are referred to as final state interactions (FSI), as they will determine the final particles that exit the nucleus and will travel through the detector.

2.2.4 Detector Effects

The last part of the simulation is the modeling of the detectors and propagation of particles through them. The software package GEANT4 [18] is used both to model the composition and geometry of the ND280 subdetectors, as well as to model how energy is deposited in the different materials that make the subdetectors by passing particles. The most relevant physics processes for the analysis presented in this thesis that are modeled by GEANT4 are:

- Electromagnetic

  Both the curvature of particles as they move through the magnetic filed and some of the interactions with matter are covered by electromagnetic interactions. Compton scattering changes the energy and trajectory of particles, while ionization slows passing particles as well as creating optical photons that make up the output light in scintillation detectors.

- Optical

  The simulation of photons with a wavelength much greater than the typical atomic spacing are of too low energy to need to be modeled with the electromagnetic processes, and are instead the focus of optical modeling. The optical modeling focuses on reflection and refraction, the absorption and emission spectra of different scintillators, and the propagation of the optical photons to the light collectors within the detectors.

- Hadronic

  The interaction of hadrons within the detectors is determined by the interaction cross sections for different particles, both through elastic and inelastic scattering, on the variety of targets available within the detector. Included in these simulations are the resulting particles from the interactions that are then propagated through the detectors in turn.

- Decay

  The lifetime of a particle together with the particle's velocity and material being traversed impact the mean free path of a particle. The probability of a particle decaying is then charac-

terized by the mean free path, which is modeled within the detector together with the decay products that result from a given decay.

GEANT4 has been used for many years and for many experiments, and as such its agreement to data is very good, making it a very reliable tool for use in analyses. Because these simulations directly affect the measurements being made, they are still checked against the data throughout this analysis and any deviations are characterized as systematic errors on the models and handled with care.

2.2.5 Neutrino Flux

The generation of neutrinos from proton beams is simulated to study the production of neutrinos and gain a better understanding of how many neutrinos as a function of energy are created by these accelerators. These simulations are done using FLUKA [19] and GEANT4 [20] to model the interaction of protons with the graphite target that create hadrons and muons, and also the decay of these particles into the neutrinos that make up the neutrino beam. The simulations are also reweighted using measurements from the T2K beam monitoring equipment as well as other charged pion and kaon experiments, all of which is documented in [21].

For the neutrino event generators used to simulate neutrino interactions in the neutrino detectors, this step is not necessary, but what is necessary is a way to characterize the number and energy of neutrinos incident on the detector. The neutrino energy is often the first piece of the simulation, as the probability of each neutrino interaction type is strongly dependent on the energy of incident neutrino.

2.3 Monte Carlo Method

With all the physics encapsulated in the different physics models, all that is left is to produce high statistic samples of events that span the available phase space of what events are possible from a given neutrino beam. The most effective way to do this is to create events by randomly sampling from probability distribution functions, and doing this random sampling many times is called a

Monte Carlo (MC) method. This method allows for the correct physics to be observed, by having all the physics models implemented as probability distribution functions, but letting the results have a random distribution within the given probabilities. The randomness is carried through the event, starting with the assignment of what type of interaction will occur, what target it will occur on, and what particles will exit the interaction and with what energy and momenta.

The implementation of the models within the simulation package are built on this randomness, defining the properties of each physical model by the probability of every property. This form of modeling allows for many hundreds of thousands of unique events to be created while keeping all these events consistent with the physics models implemented. This also means that different samples of generated events will have different statistics and thus slightly different distributions, which is just another way they are similar to real data. The Monte Carlo Method is so vital a part of how neutrino event generators work that the simulations are often just referred to as MC, a practice that is used in this document as well.

2.4 MC Productions Used In This Analysis

The simulated events used for this analysis is predominantly production 6b Run4 MC. This production simulates neutrino events equivalent to 3.5×10^{20} protons on target. The sample was subdivided into thirds for use in this analysis, with one third used to test and train the tools used throughout the analysis, and the other two thirds used within the analysis itself to evaluate systematics and calculate efficiencies.

In addition to the official MC, there are additional methods and reasons to generate events. There is a simulation package called a particle gun that allows the user to put a particle at any position in the detectors with any angle and momentum, and this package is useful for testing the detector response and reconstruction on individual particles without relying on the full MC. Also there are additional MC generations done with different models in place, or using entirely different event generators, most notably the GENIE [9] Run4 MC used for validation within this analysis.

Chapter 3

Track Reconstruction

3.1 Introduction

Particles that pass through the detectors create tracks that are saved as the amount of electrical charge collected at specific positions and times. The task of turning a collection of charge distributed across the PØD into a three dimensional track is done by a large software suite. The tools in this software package perform tasks that include: conversions between the amount of charge collected to the amount of charge deposited, corrections for detector materials and geometries, and characterizing charge collected in the PØD as different reconstruction objects that can be used as part of an analysis.

3.2 Reconstruction Objects

The reconstruction package of most use in this analysis is the one developed to reconstruct objects in the PØD known as pØdRecon. This package is documented in [22] with the relevant pieces to this analysis described below.

3.2.1 2D and 3D

The detection planes in the PØD are divided into two projections: XZ and YZ. The detection planes with vertical bars give resolution in the X axis, and multiple sets of these planes stacked in the Z direction gives the second coordinate, making the XZ Plane. The same is done for the horizontally stacked bars in the Y layer to give a YZ readout plane. Reconstruction of an event is done first in these XZ and YZ projections, then the projections are combined to develop three dimensional objects.

3.2.2 Hits

For each electronic readout, the signal collected is calibrated and corrected for electronic variations throughout the data collection period, as well as for any variations in the material the signal had to pass through. What is left is a calibrated hit, or collection of energy at a specific position and time. These hits are used to make all the following objects. Hits are also collected into nodes, which are a collection of all the hits in one XZ or YZ layer, stored as a single object: the total charge and the charge weighted average position of that charge.

3.2.3 Clusters

One of the biggest tasks for pØdRecon is to collect the hits in an event and group them together into separate objects that represent separate particles. Clusters are these groups of hits that have not yet been classified as a more advanced reconstruction object, but are identified as coming from the same passing particle.

3.2.4 Tracks

This analysis specifically looks for the signature of charged particles passing in relatively straight trajectories as they travel through the PØD. Objects with this trajectory will deposit energy in a straight line that can be characterized by the length, angle, start point, and the amount of charge deposited at every point along the path. Objects with these properties are called tracks, and are reconstructed by an algorithm called a Kalman filter that is specifically designed to reconstruct straight tracks [23].

3.2.5 Kalman Tracks

In pØdRecon a track object has a start and end point, a direction, and a number of nodes containing the energy deposited as the track crossed each layer of the PØD. The requirements for an object to be reconstructed as a Kalman track are:

- A track must have at least five nodes.

- Each node must be within a range of solid angle determined from the direction of the previous node.
- There must be no gaps between nodes greater in size than one PØDule.

3.2.6 Showers

The design of the PØD and pØdRecon is to optimize the identification of electromagnetic showers. Electromagnetic showers do not appear as straight lines in the detector, but instead appear as charge radiating from a point and spreading out as it travels. These objects are characterized as a start position and average direction, as well as a width to characterize the spread in hits.

3.2.7 Vertices

The point of origin of a track or shower is the vertex of the event, the location at which the initial neutrino interaction occurred and created the subsequent particles. The vertex is reconstructed after the other objects have been reconstructed, using the path of the track(s) and/or shower(s) to extrapolate where the objects must have originated from.

3.2.8 PØdRecon and Track Based Analyses

A challenge this analysis faced is that pØdRecon was optimized as a shower reconstruction tool. What this means is that any object that can be reconstructed as a shower often is because the software was optimized for the π^0 analyses that were specifically looking for shower objects. When performing a track-based analysis, this feature becomes problematic as it preferentially reconstructs objects as showers instead of as tracks, effectively removing them from the track sample. One feature to alleviate this problem is that all reconstruction objects retain each of their fit properties, so an object that was first reconstructed as a Kalman track, then later as a shower, still retains the information from the Kalman fit. The downside is that if this track was later reconstructed as a shower, it is treated as a shower for further reconstruction steps, notably when determining

the vertex position of an event. This means that even though the track-like properties have been retained, the shower assumption is still used to make other reconstruction decisions.

Another property of pØdRecon is that an object that cannot be fit by the Kalman filter is reconstructed as a shower or is not reconstructed at all. This would be fine if the Kalman filter was able to fit all tracks, but instead it is tuned to fit well behaved tracks and fails on objects that are not long enough for the filter to function. This feature ensures that tracks fit by the Kalman filter are well behaved and well understood, but it does leave a number of short or high angle tracks unreconstructed.

3.3 Cluster Track Fitter

For a track based analysis, a reconstruction package would be most useful if it fit all objects as tracks and reported a quality of fit for each track. This would allow the analysis to decide which tracks should be included in the reconstruction, instead of letting the reconstruction algorithm make that determination. To that end a new reconstruction tool was created that could fit any collection of hits to a simple track. This tool is called the Cluster Track Fitter and it was used to reconstruct any object that was not fit as a Kalman track.

3.3.1 Objects Reconstructed as Cluster Tracks

The class of objects that are not fit as Kalman tracks are predominantly tracks that fail the five detection plane limit required by the Kalman Filter. This means that these objects are either short, traveling across the PØD only far enough to cross a few detection planes, or are high angled, traveling a great distance across the PØD but at a high enough angle that they only cross a few detection planes. Only crossing a few detection planes means that objects reconstructed as cluster tracks have fewer data points to assist in a fit, so a number of assumptions were made about these objects in order to assist in fitting them.

The true kinematics of muons and pions are plotted in Figure 3.1 with all particles shown in the top two plots and the other four plots depicting the breakdown of tracks by reconstruction

algorithm. Figure 3.1c contains all the muons fit as Kalman tracks, while Figure 3.1e contains all the muons fit as cluster tracks. From these two figures it can be seen that most muons are fit as Kalman tracks, with only 14% being reconstructed as cluster tracks. As described, the particles fit with the Cluster Track Fitter are almost exclusively high angle (when $1 - \cos(\theta)$ goes to 1) and low momentum. This behavior can be seen for pions as well in Figure 3.1d for Kalman tracks and Figure 3.1f for cluster tracks. The percentage of pions that are reconstructed as cluster tracks is higher than that for muons, reaching almost 29%.

3.3.2 Cluster Track Fitting Method

The underlying method used by the Cluster Track Fitter is a line sweep technique that picks a point and creates a straight line emanating from that point and evaluates how well that line corresponds to the distribution of charge in an event. For simplicity, the origin of the line is chosen to be the reconstructed vertex of an event. The method for evaluating the quality of fit of the line to the hits is a sum of the perpendicular distance between each hit and the fit line. The procedure is then repeated for test lines at a number of different angles and the test line with the best quality - the line that minimizes the distance between all hits and the test line, is chosen as the best fit line.

In practice, the Cluster Track Fitter follows the above procedure in two dimensional projections (XZ and YZ), obtaining 2D cluster tracks that can then be stitched together into a 3D cluster track. Once the 3D cluster track has been created it is characterized in the same way as a Kalman track: start position, track angle and length, and a list of nodes. This is particularly important as it allows an analysis to treat cluster tracks and Kalman tracks the same way.

3.3.3 Cluster Track Fitting Assumptions

A number of assumptions are made when making a cluster track. These assumptions are necessary for the method described above, and are not a problem as long as they are understood and accounted for within an analysis.

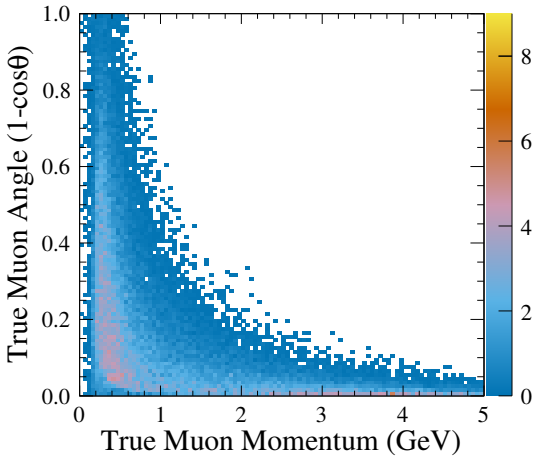

(a) Total Muons

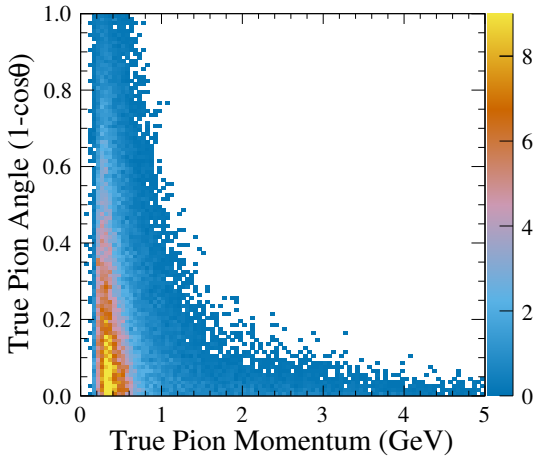

(b) Total Pions

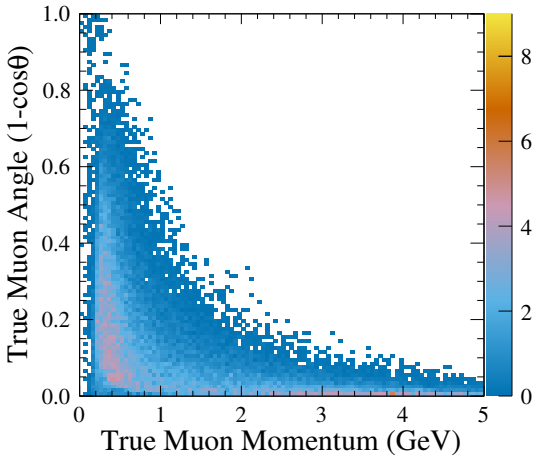

(c) Kalman Muons

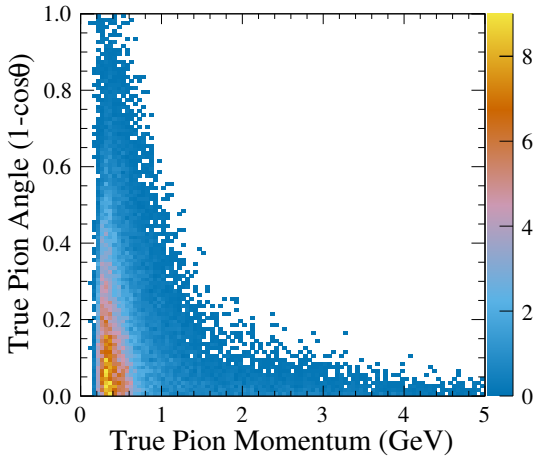

(d) Kalman Pions

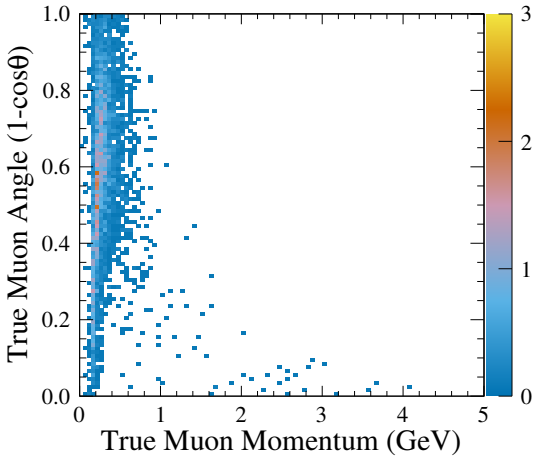

(e) Cluster Muons

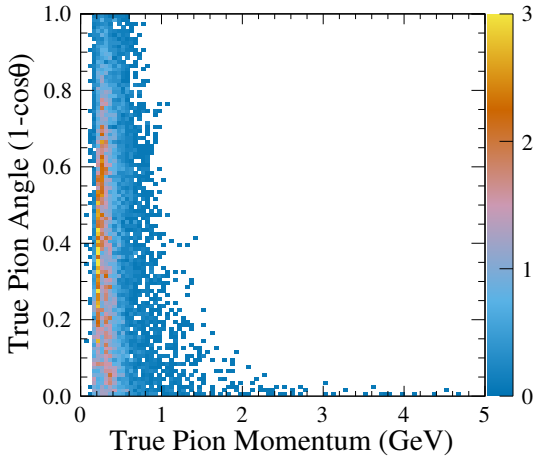

(f) Cluster Pions

Figure 3.1: The true particle momentum in GeV and angle in $1 - \cos(\theta)$ broken down by reconstruction algorithm and particle.

PØdRecon Cluster Object

PØdRecon uses a number of techniques to identify which hits in the PØD should be grouped together into one cluster. These methods depend primarily on the proximity of hits to one another and are described in [22]. The assumption the Cluster Track Fitter (and all the reconstruction algorithms) makes is that the hits in the cluster object are correctly associated with all the charge deposited by a single particle. There is always a chance that the cluster object is, in actuality, the charge deposited by multiple particles that are very close to one another, or that one particle moved in such a way inside the detector that its charge was split into two cluster objects. There is also the possibility that the cluster object is just a collection of noisy hits that happened to occur near one another, or that one noisy hit was grouped together with the hits of a passing particle.

All the cases above are possible, but ultimately these are a feature of a reconstruction package that cannot be avoided. The occurrences of the reconstruction failures given above lead to mistakes in the reconstructed angle and momentum of a particle, and are taken into account when the accuracy of the momentum and angle reconstruction is studied (Chapter 3.4).

PØdRecon Vertex

The Cluster Track Fitter is not an official part of pØdRecon, and as such it is used to analyze objects after pØdRecon has finished reconstructing an event. The concern that arises is that the Cluster Track Fitter uses information from different stages of pØdRecon. The cluster object that is the input to the Cluster Track Fitter is an object that failed the Kalman track fitter, but has not yet been fit by the shower fitter. The vertex, however, is an object that is created after pØdRecon has finished classifying all the objects in the event with the Kalman filter and shower filter. This means that for events where pØdRecon used an object's shower information to reconstruct a vertex, the Cluster Track Fitter is disregarding the reconstructed shower and re-fitting that object as a cluster track, but using the vertex that depends on the shower object.

This procedure is not ideal and is the main reason that the cluster track fitter has not been implemented into pØdRecon. The reason the implementation was done this way is a practical one:

cluster tracks are inherently difficult to fit (that's why they weren't fit by the Kalman filter) and identifying their track start or direction independently would require an extensive amount of work.

The cluster track must therefore be used carefully. For this analysis the vertex issue was accounted for by virtue of requiring multiple tracks to be in an event. This analysis requires that an event have two tracks, and it was found that more than 99% of cluster tracks in two track events are paired with a Kalman track. For individual cluster objects, the pØdRecon vertex is entirely dependent on the shower fitter's results and thus suspect as the shower fit is the information discarded by the Cluster Track Fitter. For events with multiple objects, especially at least one track fit by the Kalman track filter, the reconstructed vertex is much less dependent on the cluster track information as a Kalman track has a very well reconstructed start position.

In addition to taking advantage of the Kalman track of a two track event, a number of validation variables were created to test the quality of a reconstructed vertex. One such variable was created by fitting a cluster track to an object, then selecting a point in the middle of the cluster track and using that point as the vertex and running the cluster track fitter again. If the track was well fit the first time, the new fit should have the same angle best fit line as the first fit, indicating that the first track angle and track vertex are of good quality. If an event had a poor vertex and formed a fit line at a significantly different angle, this could be an indication that the vertex and/or the angle of the track were not a particularly good fit, or that the track is not particularly track-like in energy deposition. This variable is described in Appendix A and is used to help determine if tracks should be used in this analysis.

Straight Line Assumption

Cluster tracks are fit with a single straight line. This is an assumption that the particle depositing energy traveled in a straight line and didn't deviate through additional interactions in the detector or curve due to the presence of the magnetic field.

In general cluster tracks are short and thus they do not have the opportunity to interact or undergo detectable curvature within the PØD. These short track trajectories are accurately approximated by a straight line, but for longer tracks this assumption may not hold. Longer cluster tracks

are predominantly high angle and thus pass through few detection planes, making any non-linear behavior hard to detect. The problem that could arise through mis-reconstructing the exact path of a particle is that the path a particle travels is used to reconstruct the momentum of that particle, as described in Chapter 3.4. The track length difference between a straight and curved cluster track would lead to a difference in reconstructed momentum, an effect that is handled by understanding the momentum reconstruction accuracy.

Predominantly Forward Going

A feature of pØdRecon is that it preferentially reconstructs tracks as traveling in the direction of the neutrino beam as opposed to traveling against the direction of neutrinos. This assumption is usually safe, as most particles are traveling forward as a result of originating from an interaction with a very energetic neutrino and the requirements of momentum conservation. For isolated tracks there is little information in just the number and position of hits for the reconstruction algorithm to determine a direction. For multiple tracks this problem is often solved since these tracks will meet at a vertex, which clearly determines the start position of a track. In the absence of another track, the direction of a track can sometimes still be verified by studying the energy deposition along the length of a track, as particles will deposit more energy as the slow and at the end of their track. For this analysis the requirement that a track has two events that must come from one vertex makes the likelihood of mis-reconstructing a backwards going track unlikely.

3.4 Momentum Reconstruction

Momentum reconstruction in the PØD is done by assuming that the reason a track slows down as it passes through the detector is that it is losing energy by ionizing particles as it passes through the detector. The amount of energy that is lost is then a function of the current momentum of the particle and the material it is passing through. A reconstructed track in the PØD passes through known material, and the end of a track provides a starting point to reconstruct the momentum as this is where the momentum is known: either the momentum is zero because the track has stopped or the momentum is provided by the TPC at the point where the particle exits the PØD. In either case,

it is possible to take small steps backwards along the track using the current known momentum and the material being traversed, to calculated how much energy the track must have lost at that point, add the lost momentum back into the particle, and take another step back along the track. The reconstruction package developed to do this calculation is the Momentum Tool.

3.4.1 Momentum Tool

As charged particles pass through matter, they interact with that matter and lose energy. For relativistic particles, this energy loss is primarily through the ionization of the material being traversed. The energy loss per distance traveled (proportional to mass stopping power) as a function of particle energy is shown in Figure 3.2 [24]. Most muons reconstructed in the PØD for this analysis have a momentum between 150 MeV and 700 MeV, though muons with momenta up to 5 GeV are included. At these momenta muons fall on the Bethe region of the energy loss curve, and in fact are predominantly in the region of minimum ionization. For this reason, these particles are referred to as Minimum Ionizing Particles (MIPs). From Figure 3.2 the energy loss can be seen to be fairly flat over the region of interest for the muons, allowing them to all be treated as minimum ionizing particles.

The stopping power in the Bethe region for other materials and particles is shown in Figure 3.3 [24], where it can be seen that pions of similar energies as muons also fall in the same MIP region, but protons have to have much higher momentum (on the order of 10 GeV) to deposit energy as MIPs. In this analysis, pions have similar momenta as muons (250 MeV - 700 MeV), while protons generally have momenta less than 300 MeV putting them firmly outside the MIP region.

The momentum tool used in the PØD uses these curves to take small steps in distance along a track, starting at the end of the track and working back towards the start. The method uses the known momentum at each point, and the material being traversed, to calculate the amount of energy that was lost. This lost energy is added to the particle's momentum, and the procedure is repeated, taking another step back along the particle's trajectory, eventually adding up all the energy the particle lost and arriving at the vertex with the initial energy of the particle.

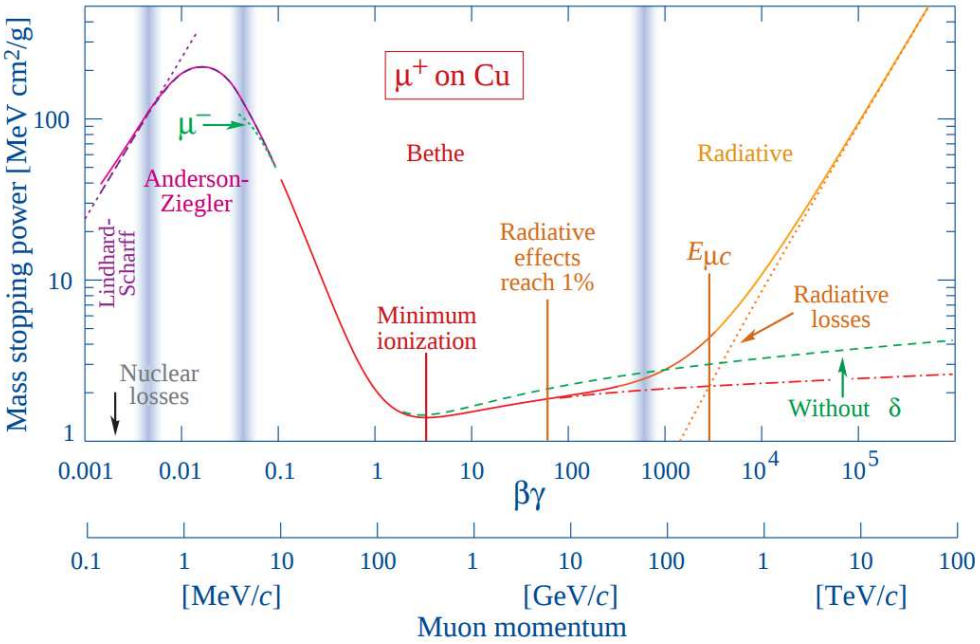

Figure 3.2: Mass stopping power for positive muons in copper as a function of $\beta\gamma$ = momentum/(Mass $\times$ c). Solid curves represent the total stopping power, vertical bands represent boundaries between regions characterized by different approximations.

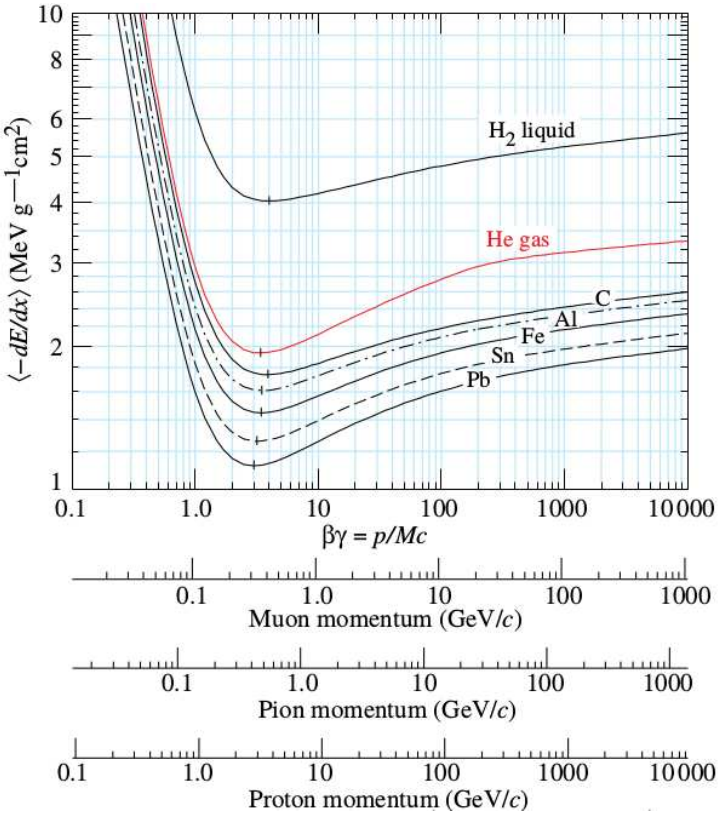

Figure 3.3: Mass stopping power in the Bethe region for different target materials and transiting particles.

For tracks that have lost all their energy by traversing the detector, the momentum tool uses an arbitrarily small track-end momentum in place of zero in order to be able to start the energy loss calculation. Tracks that exit the PØD and are matched to TPC tracks can use the momentum reconstructed by the TPC as the starting momentum, which is reconstructed using the curvature of the charged particles in the magnetic field.

One important note is that when the momentum is calculated, the mass and charge of the particle is part of the equation, and thus requires knowing the identity of the particle. However, at this stage of the reconstruction the particle identity is not known. To account for the unknown identity of the particle, for each track the momentum is simultaneously calculated for three different particle assumptions: muon, pion, and proton. The momentum tool saves the final momentum for a particle for each of the three particle assumptions, and it is up to the analysis to assign a particle identification to a given track and thus determine which momentum is the correct one to use.

3.4.2 Momentum Resolution

Extensive work was recently done to improve the momentum tool, which is documented in [25]. The calibrations were done for this analysis, so the muon and pion were the primary particles calibrated (though some work was also done to update the proton calibration, it is not reported here). The calibrations for the pions were performed only for pions that did not undergo hadronic interactions at their end point - these particles lost energy by non-ionization interactions and thus the momentum reconstruction is not seeded with the proper end of track energy (it assumes zero when in fact there was energy carried away through other processes). Additionally, the majority of cluster track objects were pions, not muons, so the calibration was done for only pions and applied to the muons. The calibrations were done separately for tracks contained within the PØD and for tracks that exit the PØD and enter the TPC and are thus seeded their initial momentum from the TPC.

The results of the momentum calibration are provided in Table 3.1, where the bias and width of the resolution (reco - true / true) are reported as percentages.

Table 3.1: The reconstructed momentum resolution (%) from the Momentum Tool.

		Kalman Contained		Kalman Exiting		Cluster	
		μ	pi^+	μ	pi^+	μ	pi^+
water	bias	0.0	1.0	1.0	0.02	-0.5	
	width	5.4	6.8	12.5	10.8	15.0	
air	bias	1.9	1.6	0.9	0.0	-1.4	
	width	4.4	5.0	11.9	10.0	14.8	

3.5 Angle Reconstruction

Angle reconstruction is done as a part of the track reconstruction, and as such is dependent on which reconstruction algorithm was used to reconstruct the track and not on the actual identity of the particle. Similarly the presence of water in the detector does not affect the angle of the track, it simply provides more mass for particles to interact with and changes the length of a track for a given momentum. In considering the angle of a reconstructed track, the presence or absence of water only changes the proportion of tracks reconstructed as Kalman or cluster tracks, but does not affect the accuracy of the angular reconstruction. The results studied are for water-in tracks, with both true muons and true pions considered together.

3.5.1 Angle Residual

Table 3.2 includes the bias and the residual (reco angle - true angle) for the different track categories reported in degrees. In this case the contained and exiting tracks do not depend on the TPC, but as the two samples have different angular acceptances they are still considered separately.

Table 3.2: The reconstructed angle resolution (%) from the Momentum Tool.

	Kalman Contained μ & π^+	Kalman Exiting μ & π^+	Cluster μ & π^+
bias	0.8	-1.7	-1.2
width	6.7	4.9	9.6

Chapter 4

Particle Identification

4.1 Introduction

After events have been reconstructed as collections of tracks, the next task becomes assigning an particle identity (muon, pion, other) to each track to determine if or how it can be used in this analysis. For the PØD, assigning identity to a particle is difficult as there is no standard tool to use for this task. For this CC $1\pi^+$ analysis, the particles leaving the signal interaction (CC resonant and CC coherent) are a muon, a single pion, and a proton or neutron. In the PØD a neutron is undetectable, and for the majority of CC $1\pi^+$ interactions induced by the T2K beam, the proton in the interaction has a momentum of less that 250 MeV putting it below the detection efficiency.

The inability to detect the protons in the CC $1\pi^+$ event, in most cases, then dictated the topology of events that could be detected: events with two tracks, one a muon and one a pion. Working with only two track events allowed this analysis to make use of this topology when assigning track identities. The approach taken was to first identify events where both tracks deposited energy in a way consistent with a minimum ionizing particle (MIP). Once events with two MIP-like tracks were identified, the next goal was to assign identity to the particles, requiring one to be a muon and one to be a pion. This chapter details the multivariate analysis used to first identify MIP-like particles and second to separate the MIPs into muons and pions. The final particle identities are assigned using a log-likelihood function to combine multiple sources of information about each particle.

4.2 Classifying Events with an MVA

4.2.1 Introduction to an MVA

A Multivariate Analysis (MVA) is a general name for a family of analysis algorithms built on machine learning techniques that are particularly suited to classification problems. As the goal of a

PID is to separate different types of particles from one another, the problem of identifying particles can be well adapted to an MVA. The class of MVA used in this analysis is that of "supervised learning" algorithms, meaning that a training data set with a known output is provided to the MVA, and is used to train the MVA to be effective at classifying data similar to those used to train it. The data an MVA is trained on are a collection of variables that represent different information about each datum that can be used to separate the different classifications. The power of the MVA is the different algorithms that can analyze the provided data in a multidimensional space with a dimensionality determined by the number of provided variables.

4.2.2 Boosted Decision Trees

The specific MVA method used in this analysis is a Boosted Decision Tree (BDT) implemented in ROOT's TMVA package [26] [27]. This method was chosen because it is particularly well suited to classification problems that need to separate two different samples. Also the BDT performed better (with default parameters) than the other classification MVA's included in TMVA. Finally, of all the MVA techniques available, the BDT is one of the most straight forward in application, making it easier to understand and present to a collaboration not yet accustomed to using multivariate analyses.

Decision Trees

A decision tree is a straightforward process that takes in a training set and makes subsequent cuts on that set to achieve a desired result. The method starts with all the training events, then chooses a variable and cut value that most efficiently splits the signal and background events. The method is repeated with different variables on the different sets, resulting in smaller and smaller groups of events with hopefully more pure signal or background samples.

Boosting

Boosting is a term used to describe a method of doing numerous MVA optimizations by re-weighting the input training sample. What this means is that different elements of the provided data

are made more important or less, changing the way the MVA attempts to optimize its separation of signal and background. This method is useful for a number of reasons. Boosting helps overcome statistical effects that may influence a simple sequence of cuts, reducing the dependence on random statistical fluctuations in training samples. Boosting also allows for the combination of different variables with different cut values, allowing the MVA to more fully explore the multidimensional space made by the different variable options. Perhaps most importantly, boosting can greatly improve the effectiveness of a decision tree by selectively weighting events that were incorrectly classified in previous iterations of the decision tree. This method ensures that events that were incorrectly classified are treated more carefully, greatly increasing the performance of the decision tree in subsequent iterations. Boosting allows for hundreds or thousands of different combinations of variables and cut values, and the weighted average of the results of each of these boosted trees is what is finally used to determine a function that can be used to classify any event.

4.2.3 Training and Testing Samples

An MVA takes in three classes of information: training data to classify, classification results for the given data, and information about the data that the MVA will use to perform the classification. In the context of this analysis, the training data and classification information are provided as a set of MC tracks for which the particle that created the track is known. Because the classification works best with binary decisions, the identification of particles is done in two steps. The first step is to classify MIP-like particles from not-MIP-like particles. Both the particles for this analysis are MIP-like, so this step is separating wanted particles from not wanted particles. The second step is to separate the muons from the pions, a much more challenging prospect. For both of these classification problems, the properties of the tracks are all the the MVA has to work with to perform the classification, so it is important to provide the most useful track information possible.

4.2.4 Variables

With the goal of providing ways to describe tracks, a number of different observables were created so as to provide the MVA as much information about each track as possible. Some of

these observables were simple track properties: track length, track angle, total energy deposited, while others were more complex, looking at the transverse or longitudinal energy deposition of a track. The motivation for the more complex variables was first to identify non-MIP-like tracks, so studying the energy deposition and seeing if it was not consistent with a MIP-like track was a good indicator of whether or not the MVA would be able to use the variable effectively to classify the events. Later the goal became to separate the muon and pion, a more challenging task, where variables were created to search for any potential curvature in the P∅D, utilizing the fact the muons and pions have different charge, or looking for energy deposition indicative of hadronic interactions, a feature of pions that sets them apart from muons. With both goals in mind, individual variables were created and studied in their own right in addition to their performance within the MVA. Lastly, a class of variables was developed to ensure the quality of events selected, which involved looking for particles with poor reconstruction, particularly for events reconstructed with the Cluster Track Fitter.

Just developing possibly useful variables to provide the MVA wasn't enough, so the variables developed were all studied to ensure they could be good inputs to the MVA. For this analysis the inputs to the MVA had to be observable (reconstructed) quantities that could be compared between tracks for both data and MC. Variables were evaluated on a number of criteria, including: their effectiveness at classifying events outside the MVA, good agreement between data and Monte Carlo, and effectiveness within the MVA. In addition to finding good variables, one of the goals was to narrow down the list of variables used in the MVA, as a smaller set of variables reduces the processing time, improves MVA performance, reduces the impact of limited MC statistics, and reduces the amount of introduced systematic error. Once a subset of variables was chosen to be evaluated in the MVA, the goal became to optimize the MVA by selecting the fewest number of variables that gave the best MVA result.

The variables used in the different MVA stages are listed in Table 4.1 and Table 4.2, and descriptions of each variable are included in Appendix A.

Effectiveness outside the MVA

The first step to studying each variable was to determine if the two classifications of track (MIP-like and not-MIP-like or muon and pion) distributed differently. This is referred to as 'separation'. This meant plotting the different particle types as a function of a variable and determining if there was any separation. A variable that demonstrated visible separation was likely to be useful within the MVA. Studies were also done plotting pairs of variables against each other to see if separation could be found in the 2D space. For efficiency, not all possible combinations were considered. Instead a list of core variables were identified, and all other variables were compared with that list. Plotted in Appendix A are the distributions of each event plotted for signal and background events to demonstrate the separation each variable provided on its own outside the framework of the MVA.

Data/MC agreement

The variables chosen for the MVA were required to be well modeled. This meant that they should be demonstratively similar between the data and the Monte Carlo. Because data is unclassified one cannot check that the features utilized by the MVA, specifically the separation of the classifications, was well modeled by the MC. However if the full distributions match well, it can be assumed that the MC does a good job of representing the data.

A challenging part of this study was to make the data/MC comparison without unblinding the analysis (i.e. looking at data in regions of parameter space with high concentrations of signal events). To accomplish this the study was limited to plotting the data/MC comparison in areas of low signal purity. In order to check that the variables were well behaved in the areas that were not visualized, a χ^2 value was computed comparing the data and MC distributions. A variable was said to have good data/MC agreement if the χ^2 per degree of freedom was within 0.5 of 1.0 and also a good visual agreement between data and Monte Carlo in regions where the purity was less than 20%. Appendix A displays the data/MC agreement for each variable selected for the MVA.

Effectiveness within the MVA

ROC Curves A tool for evaluating the performance of an MVA is the ROC (Receiver Operating Characteristic) curve. This curve, shown in the bottom plot of Figure 4.1, is a plot of the signal acceptance for desired tracks vs the rejection rate for undesired tracks. Each point in the plots represents a cut value on the MVA-discriminant for the testing sub-sample. Increasing the MIP-like track efficiency decreases the non-MIP-like track rejection, and vice-versa. The goal in developing an MVA is to maximize both signal acceptance and background rejection, which amounts to pushing the ROC curve towards the upper right corner, increasing the area beneath the curve. When testing different combinations of variables, the set of variables that maximized the area underneath the ROC curve in the region of acceptable efficiency was considered the optimal set.

N-1 Studies These studies consisted of providing the MVA with a set of variables, then training and testing the MVA for that set repeatedly, each time removing a different variable. The variables whose removal caused the biggest reduction in performance (reduced area under the ROC curve) were identified as being the most important to include for future tests. In Figure 4.2 the ROC curves for an ensemble of N-1 studies are plotted, each labeled by the variable that has been removed for that study. In this instance, because the goal is to see which variable has the biggest effect on the MVA, it is the variable whose curve provides the worst performance that is identified as the most important. One note about these studies is that they were performed for many different combinations of the same variables to ensure that the performance of a single variable could be understood independent of the variables it was being tested against. Subsets of variables were used (rather than all possibilities at once) since there was a large set of possible variables to choose from, and high dimensionality (a large number of variables) can degrade performance.

Effectiveness within the MVA: Variable Ranking When TMVA trains on a set of variables the variables are ranked against each other based on how often each variable was used effectively (because to reach the desired separation between classifications a different number of subsequent variables can be used in each iteration). This ranking was used to identify which variables were

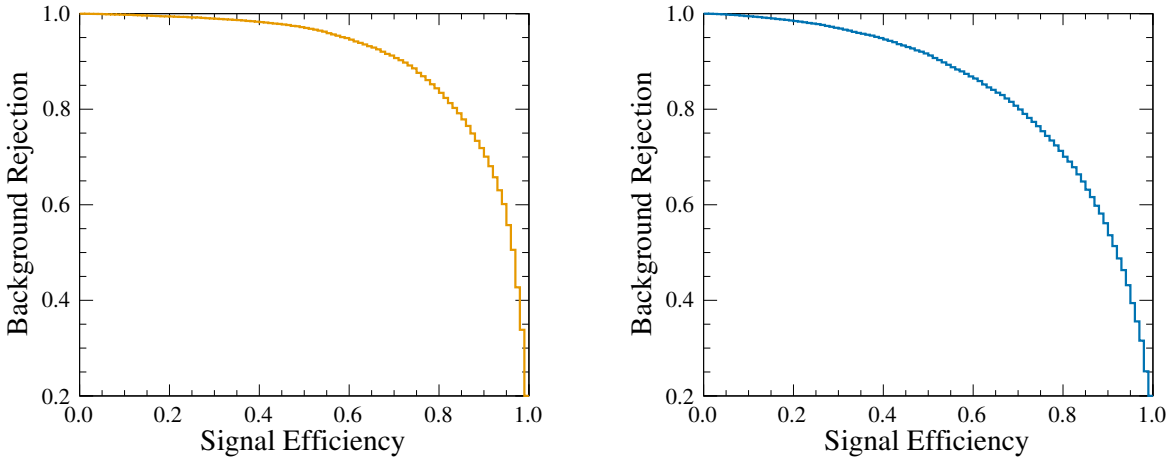

(a) MIP Kalman

(b) MIP Cluster

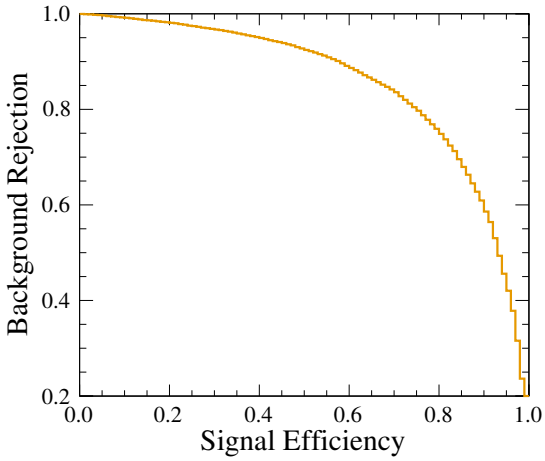

(c) MuPi Kalman

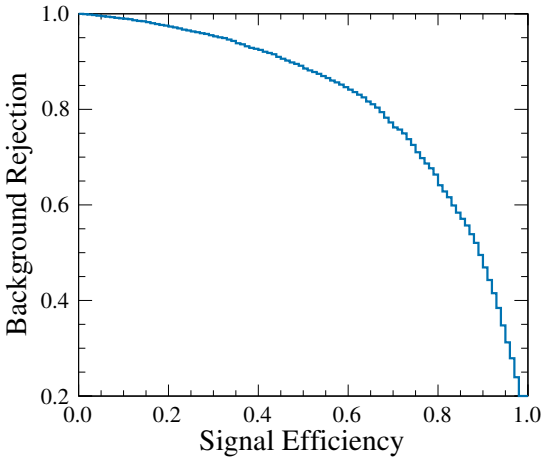

(d) MuPi Cluster

Figure 4.1: ROC curves used to characterize the selection efficiency and background rejection of the final trained MVA.

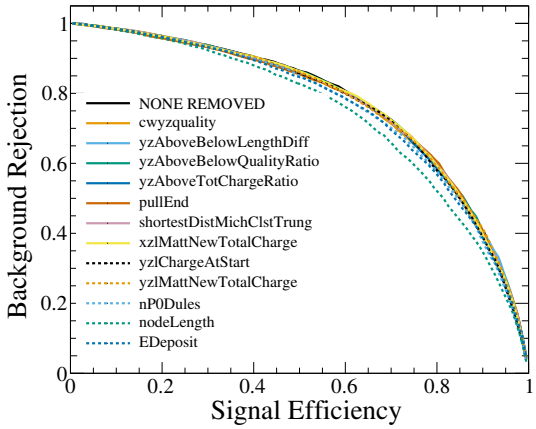

Figure 4.2: ROC curves used to characterize the selection efficiency and background rejection of a trained MVA for all variables except one, with curves labeled by the variable they are missing.

not often being used and if it was found that a variable was not often used and also that its removal in the N-1 study caused little change, it was safe to assume that discarding this variable would not degrade performance.

Correlations Another output of the MVA that was studied for each set of variables was the correlation matrix. Correlations between input variables indicate that they contain redundant information. Their use allowed for the identification of variables whose affects were highly correlated, suggesting that they were not both necessary in the MVA.

The correlation matrices provided by TMVA give the correlations between the variables for both classifications. These are plotted for the MVA to classify MIP-like Kalman tracks and the MVA to classify MIP-like cluster tracks in Figure 4.3. In this figure the 'signal' distribution on the top are the reclassified MIP-like tracks, and the 'background' on the bottom is the non-MIP-like tracks. The correlation between node length (nodeLength) and number of P∅Dules (nP0Dules) is clear (86 in the top left plot of Figure 4.3), as are the relations between XZ and YZ components of the same variables (which make up the pairs of correlated variables particularly notable in the 'background' correlations: 50, 51, and 52 in the bottom left plot of Figure 4.3). These correlations are not surprising as an increase in node length should correspond with an increase in the number of P∅Dules crossed and XZ and YZ variables will often pick up the same features, but the inclusion

of all variables was shown to greatly improve the performance of the MVA. The usefulness of these correlations is not in the events for which the correlation hold true, but for the few cases where the correlation does not hold, implying that the tracks where the variables do not show correlated behavior provides information able to distinguish MIP-like from non-MIP-like tracks. The low number of correlations in the cluster plots are one of the reasons more variables were used to characterize these tracks.

Correlation matrices for the μ/π ID MVAs are shown in Figure 4.4.

Response Function

The result of training an MVA is a function that takes the chosen variables of each datum as inputs and proceeds to output a discriminant value for that datum. That discriminant value in this analysis indicates how MIP-like a track is, or how pion-like a track is, depending on which MVA function is used. Cuts on the discriminant values are used to select samples and ID tracks in this analysis. The performance of the MVAs for selecting and correctly ID'ing tracks can be seen in the discriminant value distribution as plotted in Figure 4.5 for the MIP-like MVA. The left plot contains the discriminant distribution for Kalman tracks, while the right contains the discriminant distribution for cluster tracks. For these plots, all tracks that pass the set of preselection cuts (see Chapter 5.3.1) are evaluated and plotted. The effectiveness of the MIP-like MVA can be seen in the separation of the muon and pion tracks from the tracks of proton and other particles. In the cluster track MVA this separation is less clear, which was expected due to the fact these objects are less well-defined compared to Kalman tracks. The decision on where to place the cuts on this distribution to separate MIP-like particles from non-MIP-like particles will be discussed in Chapter 5. The particle breakdown for the μ/π ID MVA is plotted in Figure 4.7, where the tracks included are all tracks that are selected (see Chapter 5) for the "two MIP-like tracks" sample.

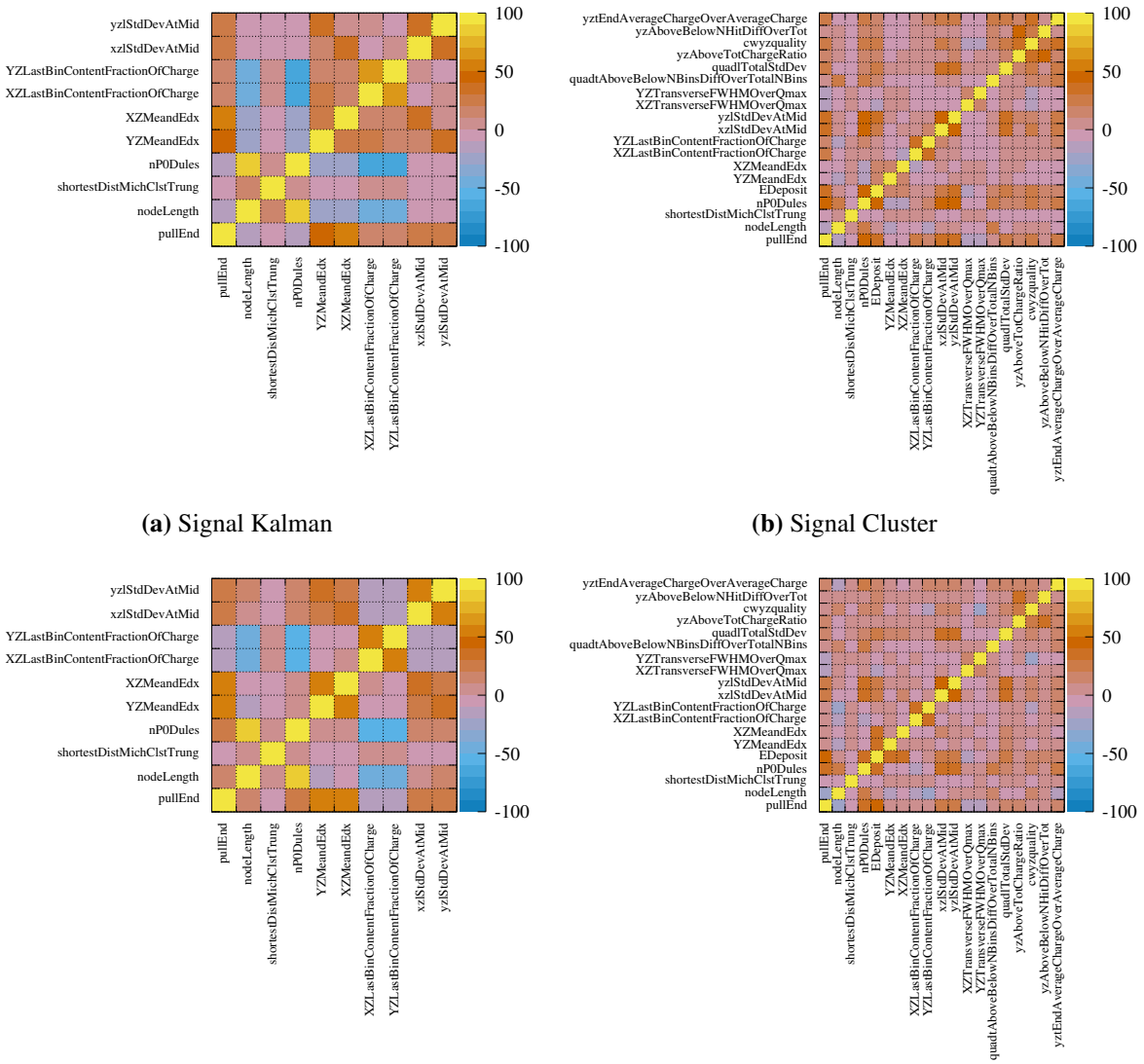

(a) Signal Kalman

(b) Signal Cluster

(c) Background Kalman

(d) Background Cluster

Figure 4.3: Correlation Matrices for the signal and background samples for the MIP Kalman MVA and the MIP cluster MVA.

4.3 Selecting MIP-like Particles

Selecting MIP-like particles is the first step in identifying the particles in this analysis. As the desired particles are muons and pions, the MIP energy deposition is a way to set these apart from any other particles (mostly protons) that deposit energy in the detector.

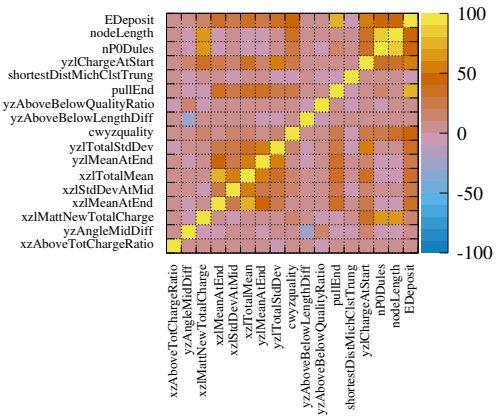

(a) Signal Kalman

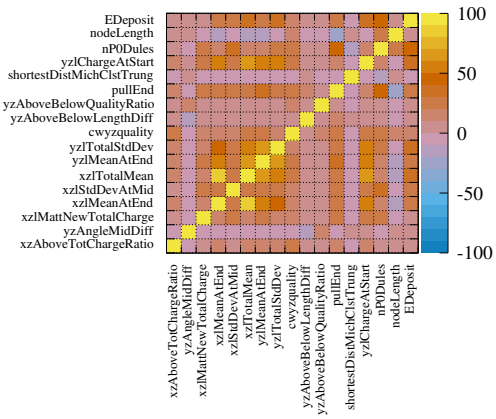

(b) Signal Cluster

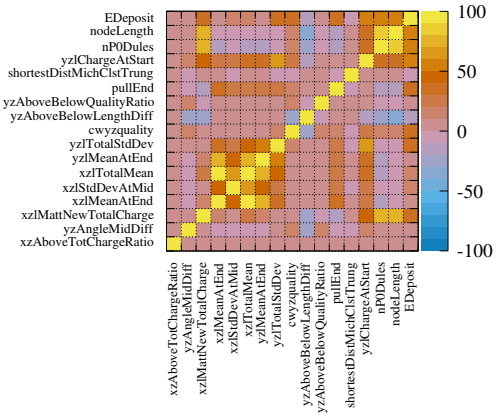

(c) Background Kalman

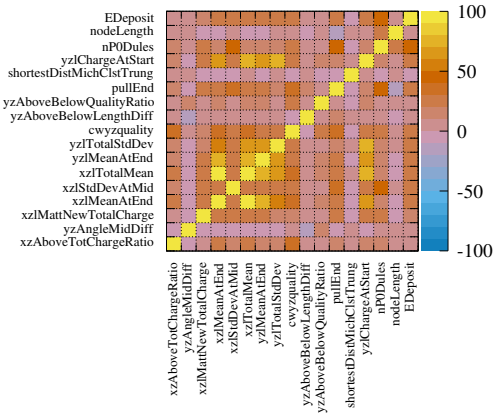

(d) Background Cluster

Figure 4.4: Correlation Matrices for the signal and background samples for the MuPi Kalman MVA and MuPi cluster MVA variable lists.

4.3.1 Training Events

The definition of signal and background for the MIP MVA training was to look at all tracks from two track events as individual inputs to the MVA. Each track that was a muon or a pion was labeled as signal, while the rest of the tracks were labeled as background. Using only tracks from two track events ensured that the events training the MVA were all events that could be included in the analysis, and evaluating the tracks individually, instead of as a whole event, kept the analysis

model independent. Studying the tracks independently meant that the relationship between the muon and the pion, which is determined by the physics model, doesn't come into the training.

4.3.2 Variable Selection

The variables that were found to be most effective at separating MIP-like particles from not-MIP-like particles are listed in Table 4.1, and described in Appendix A. Separate MVAs were trained for Kalman and cluster tracks, since the properties of these tracks - both kinematic and reconstruction - led to them being better separated by different variables. Also of note in the table is that some variables were calculated in the 2D projections, and it was found that different combinations of the 2D information were more effective at sorting events than others.

4.3.3 MIP MVA Response Value

The result of training the MIP MVA is a separation of particles by type, as plotted in Figure 4.5.

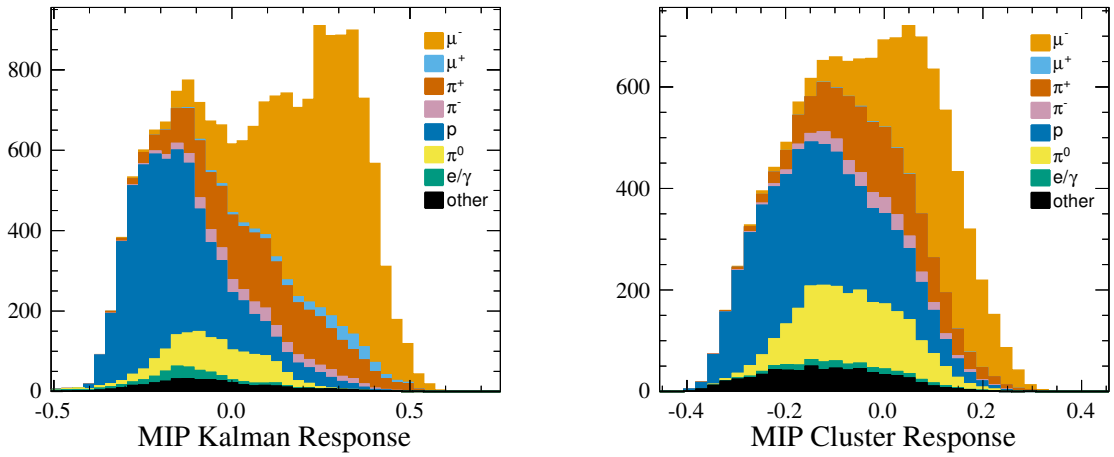

(a) Kalman **(b)** Cluster

Figure 4.5: Response values for the Monte Carlo using the trained MIP MVA broken down by particle for Kalman and cluster tracks.

Table 4.1: MIP MVA Variables

Variable Name	Variable Description	Kalman/ Cluster	Projection
	General and 3D Variables		
nodeLength	Track Length	K, C	
EDeposit	Total Charge Detected	C	
nP0Dules	Number of PØDules Crossed	K, C	
shortestDistMichClstTrung	Distance to Michel Cluster	K, C	
pullEnd	dE/dX Pull at Track End	K, C	
	2D Longitudinal Variables		
LastBinContentFractionOfCharge	Fraction of total charge in Last PØDule	K, C	XZ,YZ
quadlTotalStdDev	Standard deviation of charge per PØDule for whole track	C	XZ+YZ
lStdDevAtMid	Standard deviation of charge per PØDule for middle of track	K, C	XZ, YZ
MeandEdx	Average charge per PØDule	K, C	XZ, YZ
	2D Transverse Variables		
TransverseFWHMOverQmax	FWHM / Total Charge	C	XZ, YZ
AboveTotChargeRatio	Charge Asymmetry	C	YZ
cwquality	Track Width	C	YZ
AboveBelowNHitDiffOverTot	N Hit Asymmetry	C	YZ
tEndAverageChargeOver-AverageCharge	Track End Average Charge / Whole Track Average Charge	C	YZ
quadtAboveBelowNBinsDiffOver-TotalNBins	Width Asymmetry	C	XZ+YZ

Full descriptions of these variables are provided in Appendix A

MIP MVA Validation

The next step is to ensure the MVA is not over-trained, which can be evaluated by comparing the MVA discriminant distribution for training and testing sub-samples. Over-training occurs when an MVA trains on attributes of the training sample that occur due to statistical fluctuations in the training sample, not present in or representative of the total population of events. This is a problem because the goal is to train for use on other samples, specifically the data, and not the random fluctuations on top of that training sample which will be different for different samples. An over trained MVA would return poor agreement when run on a test sample due to the focus on statistical noise instead of general characteristics.

One of the outputs of TMVA is the plots in Figure 4.6, where the testing and training samples are plotted together. From these plots we can see good agreement between the training and testing samples, and thus no sign of overtraining.

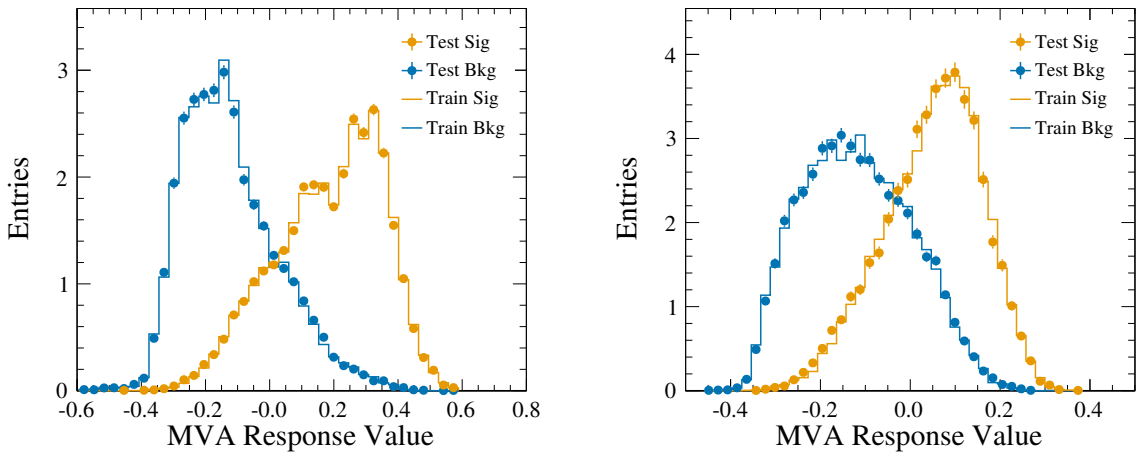

(a) Kalman **(b)** Cluster

Figure 4.6: Overtraining validation plots for the MIP MVA for Kalman and cluster tracks. The signal and background distribution responses plotted for both the training and testing samples.

4.4 Identifying Muons and Pions

Once events could be selected to contain two MIP-like tracks, the next step is to determine which track was a muon and which track was a pion.

4.4.1 Training Events

The events used in training this MVA were any two track event that contained a muon and a pion. Though it was understood that not all events identified as containing two MIP-like tracks would indeed contain a muon and a pion, the training of this stage only looked at separating the events that would be correctly identified by the previous two MIP-like track requirement. Again, the events with only a muon and a pion had the tracks separated and analyzed independently, ensuring that any model dependence wouldn't be able to enter the MVA training. For this stage, pions were labeled as signal, while muons were labeled as background.

4.4.2 Variable Selection

The variables to separate muons and pions are listed in Table 4.2 and described in Appendix A. For this MVA it was found that the list of variables used for the Kalman MVA and the cluster MVA were effectively the same, so they were combined to make one list so as to reduce the complication of the situation. Again two MVAs were trained, to account for the differences between Kalman and cluster events, but both MVAs used the same variable list.

4.4.3 MuPi MVA Response Value

The resulting MuPi MVA Response values for all two track events are plotted in Figure 4.7. From the figure it can be seen that while the Kalman MVA has done a good job separating the muons and pions, the cluster MVA's performance is more subtle, though there are more muons below a response value of zero, than above, showing that the MVA did have an effect. It is important to note that the cluster MVA has very few muons, and from the discussion of the cluster track fitter, muons not reconstructed as Kalman tracks are likely to be short, making them hard to distinguish from other particles.

Table 4.2: MuPi MVA Variables

Variable Name	Variable Description	Projection
	General and 3D Variables	
nodeLength	Track Length	
EDeposit	Total Charge Detected	
nP0Dules	Number of PØDules Crossed	
shortestDistMichClstTrung	Distance to Michel Cluster	
pullEnd	dE/dX Pull at Track End	
	2D Longitudinal Variables	
lMattNewTotalCharge	Total Charge after Removing Bins with charge less than 2sigma from mean	XZ
lMeanAtEnd	Average charge per PØDule for end of track	XZ, YZ
lStdDevAtMid	Standard deviation of charge per PØDule for middle of track	XZ
lTotalMean	Average charge per PØDule	XZ
lTotalStdDev	Standard deviation of charge per PØDule for the whole track	YZ
lChargeAtStart	Total charge for start of track	YZ
	2D Transverse Variables	
AboveTotChargeRatio	Charge asymmetry	XZ
AngleMidDiff	Vertex quality	YZ
cwquality	Track width	YZ
AboveBelowLengthDiff	Track end hit asymmetry	YZ
AboveBelowQualityRatio	Track width asymmetry 2	YZ

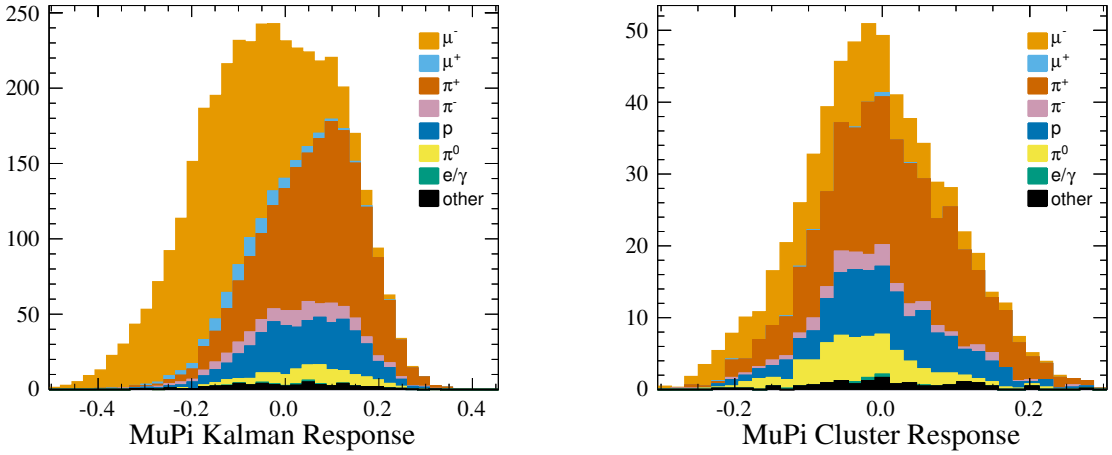

(a) Kalman **(b)** Cluster

Figure 4.7: Response values for the Monte Carlo using the trained MuPi MVA broken down by particle for Kalman [left] and cluster [right] tracks.

MuPi MVA Validation

As before, the quality of the MVA training was checked to ensure there was no evidence of overtraining, and again the agreement between the testing and training samples in Figure 4.8 is evidence of successful training.

4.4.4 Log-Likelihood Particle Identification

The selected and sideband samples of this analysis are made up of two track events where one track is assumed to be a muon and the other track is assumed to be a π^+. The previous section outlines two BDT MVAs, the first of which is used to select MIP-like tracks consistent with muons and charged pions. As will be explained in Chapter 5, all signal and sideband events have one track with a very high MIP-like MVA discriminant value. The MIP-like MVA discriminant score for the second track determines if the event is in the signal or sideband sample. The second MVA helps determine which of the tracks is to be considered the muon and which is to be considered the pion.

Application of the μ/π ID MVA is a bit different than the MIP-like MVA, since there are already two selected tracks to work with. One track will be assigned the muon ID, and the other one the pion ID, so there is no single cut value. This is made even more complex by the fact

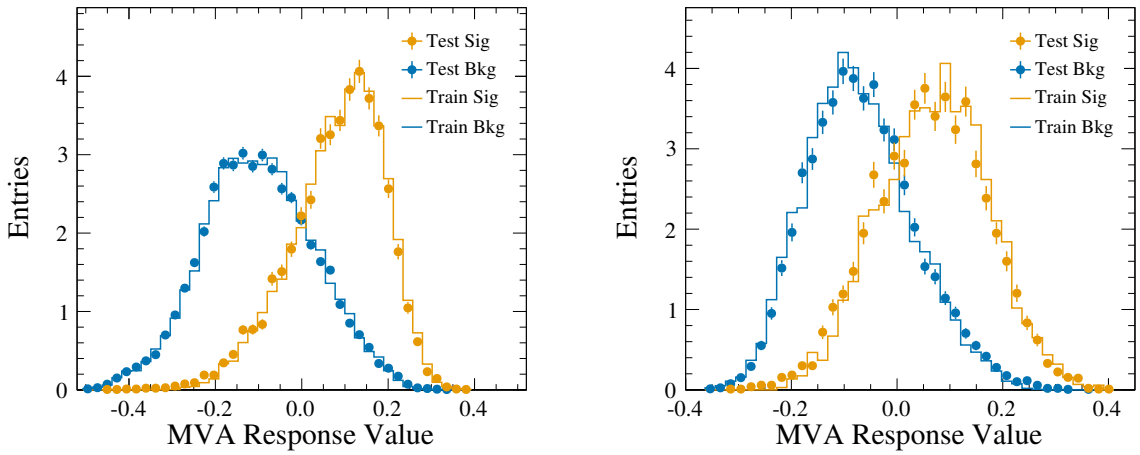

(a) Kalman **(b)** Cluster

Figure 4.8: Validation plots for the MuPi MVA for (a) Kalman and (b) cluster tracks. The signal and background distribution responses plotted for both the training and testing samples.

that we have TPC charge ID information, but only for some of the tracks (those that enter the TPC). This means that to create a standard way to separate muons and pions will require a way to combine different amounts of information for different tracks in such a way that all events can still be compared. Also to consider is that comparing tracks reconstructed with different reconstruction algorithms, the MVA used to classify the tracks are not the same, removing the ability to directly compare MVA response values.

To provide a way to compare events containing tracks with different properties, a log-likelihood function that considers the cluster track MVA discriminant value, Kalman track MVA discriminant value, and the TPC track charge was created. The log-likelihood function returns a value that can be cut on, with track pairs above the cut have track one as the muon, and those below the cut have track two as the muon.

Inputs

The three inputs to the log-likelihood PID are:

1. the reconstruction algorithm used to reconstruct the track,

2. the charge information for the track if it entered the TPC,

3. and the MVA response value for the track.

Reconstruction Algorithm Muons on average share a large fraction of the incoming neutrino momentum, and do not interact hadronically, so are likely to fit by the Kalman track reconstruction algorithm, with only 14% are fit by the cluster track fitter. Pions, with their lower momenta and hadronic interactions, are much more likely to be reconstructed by the cluster track fitter, 29% of the time.

The fraction of Kalman (cluster) tracks that are true muons or pions is calculated by looking at a subset of the Monte Carlo, thus any track has a probability of being a muon based on which reconstruction algorithm was used to reconstruct it.

TPC Charge (TPCC) For the subset of tracks that make it to the TPC, the curvature of the track can be measured. This measurement is binary, either positive or negative, thus for the determination between a negatively charged muon and positively charged pion that binary information is extremely useful. Because not all tracks make it to the TPC, this input can take on one of three values:

- -1: Negatively charged track
- 0: No TPC charge information
- +1: Positively charged track

The MuPi MVA The MuPi MVA described in Chapter 4.2 is designed to classify tracks as either muons or pions based on their energy deposition patterns as reconstructed in the PØD. Every track evaluated by the MVA is given a discriminant value between -1.0 and 1.0, where tracks with a discriminant value closer to one are more likely to be pions. The distributions in Figure 4.7 show the distribution of MVA discriminant values for a sample of true muons and pions as well as other particles. For the likelihood function the discriminant value for other particles is inconsequential, since these events are considered background by the analysis.

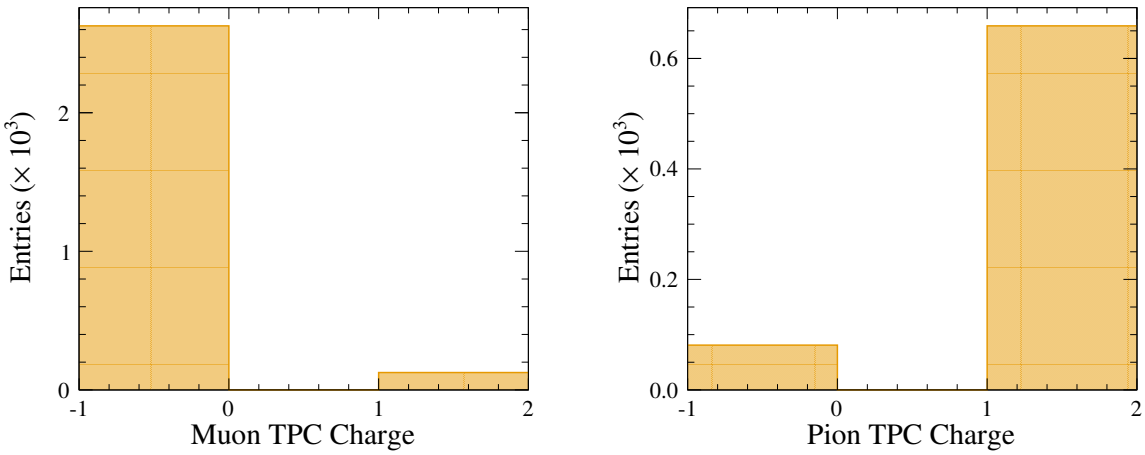

(a) Muons **(b)** Pions

Figure 4.9: TPC Charge for (a) muons and (b) pions for Kalman tracks that enter the TPC. These distributions are used to make the TPC charge likelihood functions.

Building Likelihood Functions

A subset of the MC is used to build likelihood functions for each of the variables above. For these functions, only selected signal events (which by definition contain one reconstructed muon and one reconstructed pion) are used. For the discrete observables, building the likelihood functions is simply evaluating the probabilities of the discrete cases.

For the Reconstruction algorithm, likelihoods for each case are given by (4.8) and (4.2).

$$\mathcal{L}(\mu|\text{RecoAlg} = \text{Kalman}) = (N_{\text{Kalman},\mu})/(N_{\text{Kalman},\mu} + N_{\text{Kalman},\pi}) \tag{4.1}$$

$$\mathcal{L}(\mu|\text{RecoAlg} = \text{Cluster}) = (N_{\text{Cluster},\mu})/(N_{\text{Cluster},\mu} + N_{\text{Cluster},\pi}) \tag{4.2}$$

The TPC Charge has three options, and thus three likelihood functions given by (4.3), (4.4), and (4.5).

$$\mathcal{L}(\mu|\text{TPCC} = -1) = (N_{-1,\mu})/(N_{-1,\mu} + N_{-1,\pi}) \tag{4.3}$$

$$\mathcal{L}(\mu|\text{TPCC} = 0) = (N_{0,\mu})/(N_{0,\mu} + N_{0,\pi}) \tag{4.4}$$

$$\mathcal{L}(\mu|\text{TPCC} = +1) = (N_{+1,\mu})/(N_{+1,\mu} + N_{+1,\pi}) \tag{4.5}$$

This same procedure is used for the MVA response, but because the MVA response is continuous, special care has to be taken. First the Likelihood is calculated per MVA response bin as shown in (4.6), following the same procedure as above.

$$\mathcal{L}(\mu|\text{MVA}_i) = (N_{\text{MVA}_i,\mu})/(N_{\text{MVA}_i,\mu} + N_{\text{MVA}_i,\pi}) \tag{4.6}$$

This bin by bin calculation is then cleaned to removing discontinuities and smoothed to remove drastic bin to bin variations (both due to low statistics), then converted into a spline so as to make a continuous likelihood function. The final likelihood function splines for the MVA responses and the TPC charge are given in Figure 4.10, where the likelihood is for the given track being a muon. The likelihood functions for the pion are simply the inverse of the muon likelihood functions.

For all of these cases, the likelihood of a track being a muon is given. Since all considered events include one muon and one pion, the likelihood for the pion case is given by:

$$\mathcal{L}(\pi) = 1 - \mathcal{L}(\mu). \tag{4.7}$$

Calculating Track and Event Likelihoods

Combining Likelihoods The individual likelihoods can be combined to give a single likelihood value for each track. Because the likelihood values are built on probabilities, they can similarly be combined by multiplying the results. This results in the likelihood given in (4.8).

$$\mathcal{L}(\mu|\text{RecoAlg}, \text{TPCC}, \text{MVA}) = \mathcal{L}(\mu|\text{RecoAlg}) * \mathcal{L}(\mu|\text{TPCC}) * \mathcal{L}(\mu|\text{MVA}) \tag{4.8}$$

Defining the Two Track Likelihood Every event in this analysis consists of two tracks with the assumption that one of the tracks is a muon and the other is a pion. Combining the likelihood of the two tracks becomes very powerful, because only one can be a muon and the other must be a pion, thus if neither is very muon like, or if one is very pion like then identifying the two becomes easy.

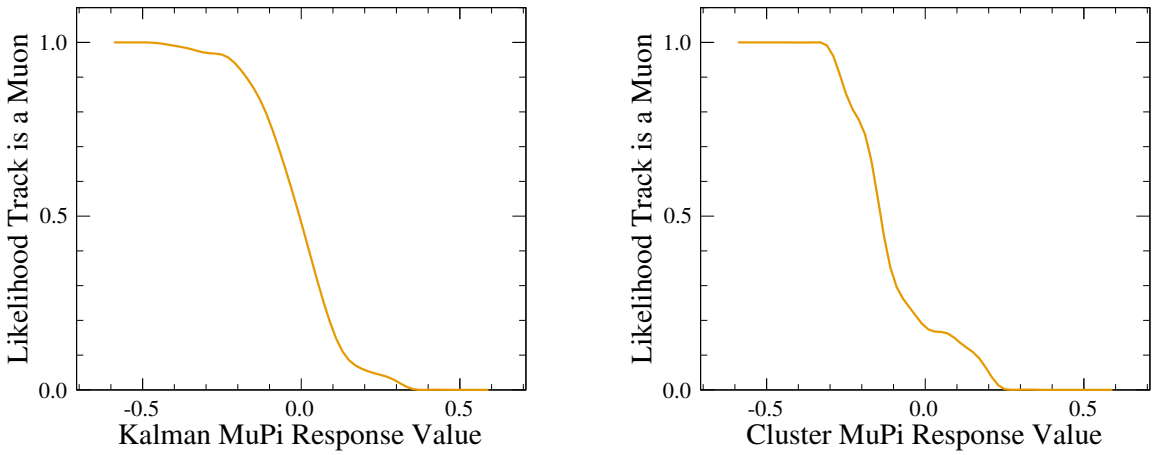

(a) Kalman MVA

(b) Cluster MVA

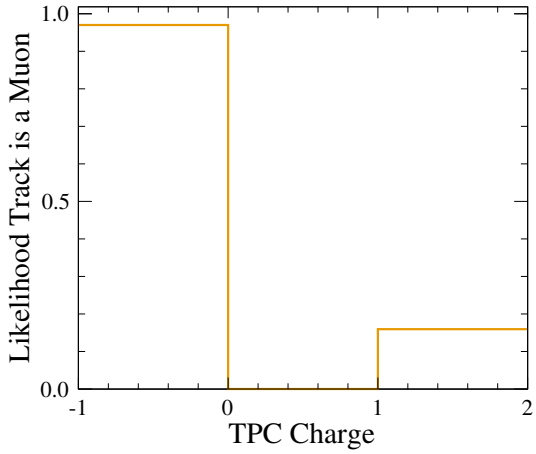

(c) TPC Charge

Figure 4.10: Likelihood PID splines that give the likelihood a track is a muon, using information from the Kalman and cluster MVA responses and the TPC charge.

As there is no initial assumption about which track is which, the tracks are simply identified by which one is first in the list of tracks for that event. The individual track likelihoods are then multiplied to get the event likelihood. Note that instead of evaluating the likelihood that a track is a specific particle, the Likelihood is evaluated for the specific case that the first track is a muon, and the second track is a pion.

$$\mathcal{L}(\text{Track}_1 = \mu, \text{Track}_2 = \pi) = \mathcal{L}(\text{Track}_1 = \mu) * \mathcal{L}(\text{Track}_2 = \pi) \tag{4.9}$$

The complementary likelihood for the case where the identity of the particles is switched is then:

$$\mathcal{L}(\text{Track}_1 = \pi, \text{Track}_2 = \mu) = \mathcal{L}(\text{Track}_1 = \pi) * \mathcal{L}(\text{Track}_2 = \mu) \tag{4.10}$$

Log-Likelihood and Log-Likelihood Ratio The resulting likelihood values are more easily studied when their logarithm has been taken. This results in the Log-likelihood, and when calculated for the ($\mu\pi$) case and the ($\pi\mu$) case, the results can be compared by looking at the log-likelihood ratio:

$$\text{Log-Likelihood ratio} = \log \frac{\mathcal{L}(\mu\pi)}{\mathcal{L}(\pi\mu)} \tag{4.11}$$

Plotting this ratio results in the desired separation between events in which the first particle is a muon and the second is a pion (MuPi), and events in which the first particle is a pion and the second particle is a muon (PiMu), as seen in Figure 4.11.

Using the Log-Likelihood to Identify Particles

Using the distribution in Figure 4.11 cut values are determined by selecting the cut value that gives the largest fraction of correctly identified track pairs. For Kalman-Kalman events the optimal cut value is 0.43 which results in the correct identification of the particles in 92% of signal events, and for Kalman-cluster Events the cut value is the same 0.43 which results in the correct identification of the particles in 88% of signal events.

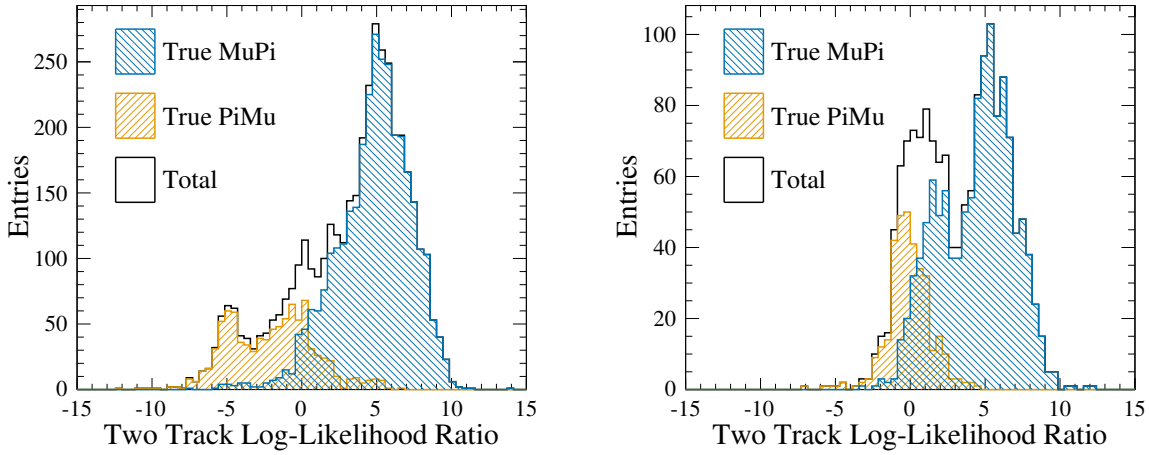

(a) Two Kalman Tracks

(b) One Kalman and One Cluster Track

Figure 4.11: The log-likelihood ratio for events with (a) two Kalman tracks, and (b) one Kalman and one cluster track.

In practice, an event that has a log-likelihood ratio above the cut value mentioned above is identified as a ($\mu\pi$) event, meaning that the first track is a muon and the second track is a pion, or if the log-likelihood ratio is below the cut value the first track is identified as a pion and the second track is a muon (e.g. a $\pi\mu$ event).

Chapter 5

Event Selections

5.1 Introduction

The difficulty in measuring neutrino interaction cross sections is introduced when it is time to select which events are signal, and which events are background. The previous chapters have described the challenges associated with reconstructing and identifying events, but in the end a set of events defined as signal have to be selected. This process is complicated by the fact that there will always be events that are not signal that an analysis cannot avoid selecting along with the signal events. These events are backgrounds and need to be accounted for in an analysis, one method of which involves creating specific samples that contain only background events so that their properties and numbers can be measured from the data. Whether selecting signal or background events, the first step is clearly defining what makes an event signal or background, as even this definition is not as simple as it sounds. This chapter describes the different definitions for signal that were used in this analysis and goes on to describe how events that meet these signal definitions were selected. In addition to selecting signal, the method for selecting background events is also described. Lastly is the procedure used to determine the analysis binning in muon kinematics that was used throughout the rest of the analysis.

From this point forward, all MC is scaled to the T2K Run 4 water-in data sample, which is 1.63×10^{20} protons on target.

5.2 Signal Definitions

One of the goals of this analysis was to be clear what was being measured and what assumptions were being made at every analysis step. The desire was that this attention would keep the analysis as model independent as possible. Throughout the analysis special attention was paid to

the difference between what measurements were trying to be made and what was actually being measured.

To that end, three different signal definitions were used in this analysis. The primary signal definition used in this analysis was based entirely on observed (reconstructed) quantities, as this definition best reflected the realities of detecting events with the PØD. Second is the signal definition generally accepted by the community as categorizing a CC $1\pi^+$ interaction, which is based on the number and identity of final state particles present after a neutrino interaction. Last is the signal definition based on the single pion production models (resonant and coherent) that described the primary physics interactions.

5.2.1 Reconstructed $1\mu\ 1\pi$

This signal definition requires that any signal event have only two reconstructed tracks with a common vertex: one a muon and the other a positively charged pion. Note that this definition did not include nucleons and thus an additional requirement could be added: the nucleon from the event must be a neutron (which was unlikely to be detected in the PØD) or a proton that was of low enough energy that it was not detected in the PØD (it was seen that most protons did meet this requirement).

Events in this definition represented the best that this analysis could do in identifying CC $1\pi^+$ events, as an event must have been reconstructed in order to have been selected by the analysis. This definition introduced detector and reconstruction restrictions on the selection (and thus detector and reconstruction model dependencies), as the acceptance of the detector and the reconstruction efficiency both determined which particles were and were not reconstructable. This definition is physics model independent because it does not depend on what physics model created the two track event, only that two tracks were reconstructed.

The majority of this analysis was done with the reconstructed $1\mu\ 1\pi$ signal definition, including the development of the signal extraction tools and subsequent measurement of the number of signal events observed in the detector. This decision was made because with this definition the efficiency

of selecting events depends only on the ability to identify signal events from all the observed and reconstructed two track events.

In Figure 5.1 the true muon and pion kinematics for all events with the reconstructed 1μ 1π signal definition are plotted. For this and all following plots, "true" refers to event or track properties extracted from the MC and not reconstructed by the analysis. Because this signal definition requires events to be reconstructed, both figures show fewer events at the lowest muon momenta, as particles with momenta below 200 MeV unlikely to be reconstructed. Similarly the number of events with high angle is affected by the difficulty in reconstructing these events. Another feature to the muon and pion distributions is that while the muon distribution is spread across the momentum and angle spectra, the pions are predominantly distributed below 500 MeV, a feature that was discussed when reconstructing these particles.

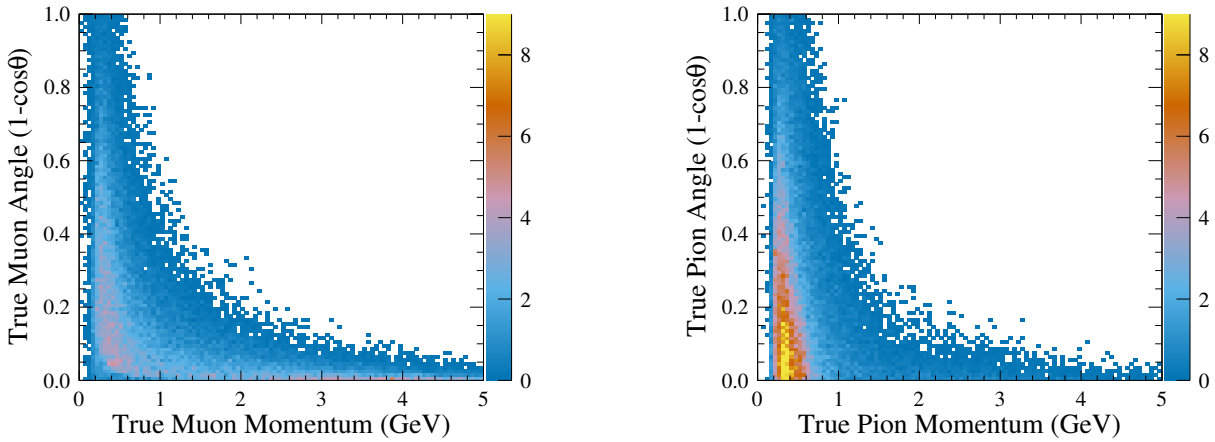

(a) Muon **(b)** Pion

Figure 5.1: True p-theta distributions for the reconstructed 1μ 1π signal definition. Plotted are the muon and pion from signal events with a true vertex within the fiducial volume. The MC is scaled to the expected data.

5.2.2 After Final State Interaction CC $1\pi^+$

This definition is expressed in terms of which particle type leave the nucleus after the initial neutrino interaction and reflect any subsequent interactions that occurred before detection, so-called final state interactions (FSI). The definition requires that a signal event have:

- only one muon
- only one pion
- any number of nucleons (protons or neutrons)
- no other particles.

The *After FSI* signal definition is the generally accepted definition of CC $1\pi^+$ in the theoretical and experimental community and is used to report the final measurement of this analysis. The difference between this definition and the reconstructed 1μ 1π definition is entirely detector and reconstruction based: the correct particles (1μ and 1π) exit the nuclei, but there is no requirement that any of the particles be reconstructable. Converting between the previous reconstructed 1μ 1π definition to this after FSI CC $1\pi^+$ definition required a good understanding of the P∅D acceptance and reconstruction efficiency. Again, this is a model independent signal definition because there is no requirement on what physics interactions created the final state particles.

In Figure 5.2 the true muon and pion kinematics are plotted for this signal definition. In addition to gaining almost four times more events, the distribution of events for the After FSI signal definition also differs from the reconstructed 1μ 1π definition in that the regions where reconstruction was difficult have been filled in with more events, both at low momentum and high angle.

5.2.3 Primary Interaction CC $1\pi^+$

A Primary Interaction CC $1\pi^+$ definition requires that the interaction of the neutrino be a single-pion charge-current resonant event, a coherent event, or a DIS interaction resulting in one muon and one pion (and any number of nucleons) exiting the primary interaction, before final state interactions. This definition has no dependence on reconstructed quantities and also does not require

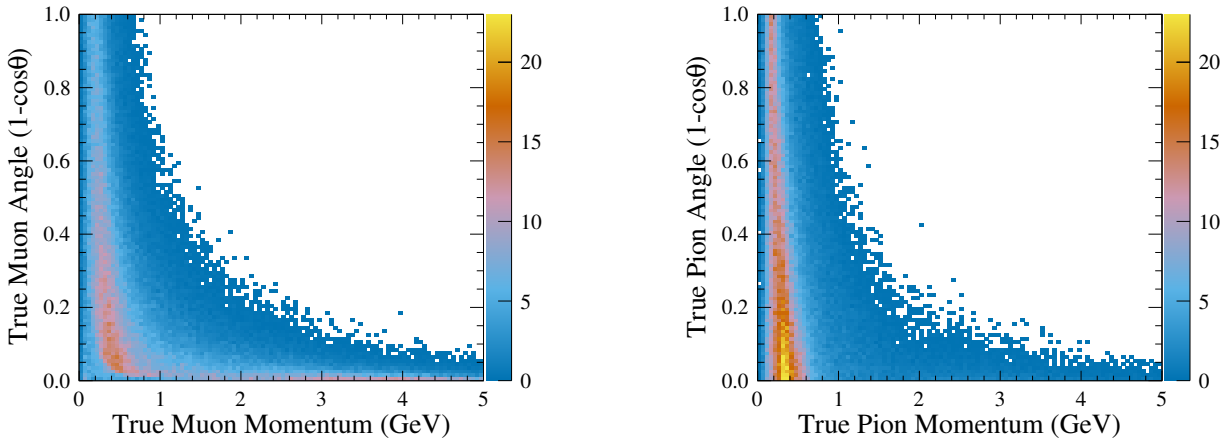

(a) Muon **(b)** Pion

Figure 5.2: True p-theta distributions for the after FSI CC $1\pi^+$ signal definition. Plotted are the muon and pion from signal events with a true vertex within the fiducial volume. The number of events is scaled to match expected data.

that the muon and pion still exist outside the nucleus after FSI. This definition is impractical to use when making a measurement because there are numerous final state topologies consisting of a wide range of types and numbers of particles that it may not be possible to separate from other interaction modes in a realisable detector.

Additionally, the existence of events that cannot be identified correctly means that converting the measured result to this signal definition would require using physics models to estimate the efficiency, and thus this signal definition is completely model dependent.

This signal definition does have a use in that if the result of this analysis is to be studied as it pertains to underlying physics models, the measurement obtained can be corrected by applying these models to the data. This correction is inherently model dependent, and thus must be handled carefully wherever it is used.

In Figure 5.3 the true muon and pion kinematics are plotted for this signal definition. Note that the models plotted here are the default models in NEUT 5.3.3. This distribution differs from the distribution of After FSI events in that there is an overall increase in the number of events of about 25% and there are fewer events with true pion momentum above 2 GeV.

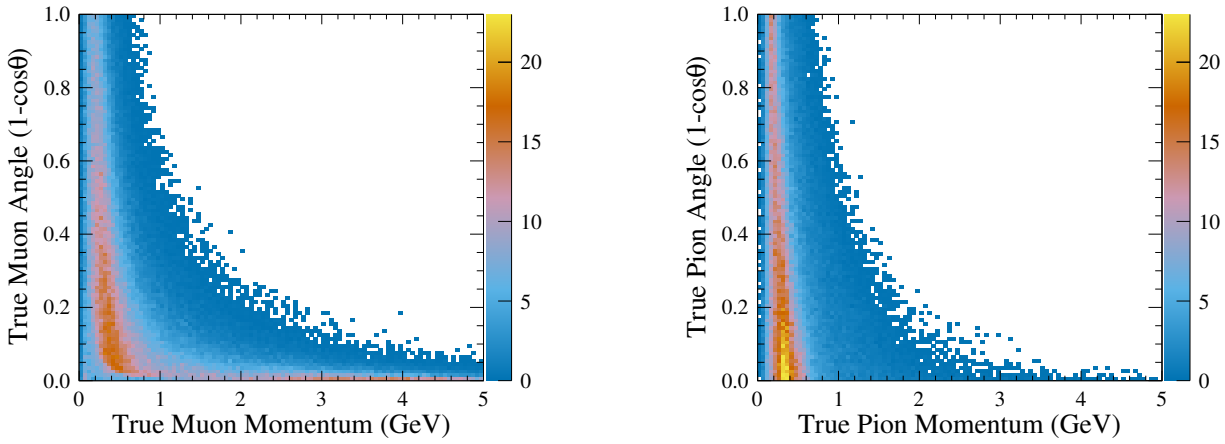

(a) Muon **(b)** Pion

Figure 5.3: True p-theta distributions for the Primary Interaction CC $1\pi^+$ signal definition. Plotted are the muon and pion from signal events with a true vertex within the fiducial volume. The number of events is scaled to the expected data.

5.3 Analysis Event Samples

With the definition of what is signal clearly-defined, it was time to attempt to isolate these events as well as possible. The method for doing this was to apply "cuts" to all the events measured by the PØD: looking at specific event or track features and deciding what range of values were acceptable for events to be kept as part of a selection.

A series of cuts was used to identify event samples for this analysis. These cuts were designed to select well reconstructed signal-like events based on the properties of the tracks. Additionally background-like events were selected in a similar fashion to develop samples called "sidebands" that could be used to characterize the background events that inevitably contaminated the signal sample. Finally, the selected and sideband samples were broken down into different categories based on the muon reconstruction algorithm and trajectory.

The selection cuts described in this section were applied to both MC and data, with the exception of the first Pre-Cut (the data quality cut is not necessary for MC). The plots and numbers of events in this section are all for MC events scaled to the expected number of data events (scaled by exposure), either all events or only signal events, as labeled for each plot.

5.3.1 Pre-selection Cuts

All the selected events were required to pass a series of precuts that ensured the events were well reconstructed and that the interaction took place within the PØD fiducial volume. The specific cuts were as follows:

1. Data Quality

   The data was taken when all of ND280 and the neutrino beam line were operating correctly. Every event collected has an associated flag that indicates if any part of the experiment was not operating within defined boundaries to ensure that only good data is used in analyses. (This is the only precut that is not relevant to MC)

2. Fiducial Vertex

   The vertex of the event was reconstructed within the fiducial volume of the PØD, as defined in Table 1.1.

3. Two tracks

   Exactly two reconstructed track objects were associated with the vertex.

4. 3D Vertex

   The vertex created by pØdRecon combines 2D vertex information from the XZ and YZ planes to create a 3D vertex. Sometimes this process fails, which is indicative of a poorly reconstructed vertex. Events without a 3D vertex were excluded from the analysis.

5. 3D Tracks

   Tracks created by pØdRecon combine 2D track information from the XZ and YZ planes to create a 3D track. When one of the 2D projections is missing, or does not have enough information, this process can fail. Events without two 3D tracks were excluded from the analysis.

6. Track Start - Vertex Distance

   In a well reconstructed event the start position of the first track (the location of the first node) is consistent with the reconstructed vertex position. This analysis employed a cut that required that the distance between vertex and track start be less than 80 mm based on studies in the previous PØD CC $1\pi^+$ analysis. [7]

7. Containment

   Tracks whose end point is poorly-defined do not have a well reconstructed momentum, as this end point is essential in calculating the momentum (as described in Chapter 3.4). To ensure the endpoint of a track is known, any tracks that exit the PØD through the sides or the upstream face are excluded from the analysis. Side exiting tracks were defined as any tracks with hits in the outermost four scintillator bars of the PØD. Additionally any tracks that exited the downstream face of the PØD but were not matched with a TPC track were also excluded for the same reason.

8. Muon Kinematic Range Cut

   The signal extraction method used in this analysis employed a template fit that used two dimensional histograms binned in muon momentum and angle. These histograms were plotted with ranges of $0 < (1 - \cos\theta_\mu) < 1$ and 0 GeV < P_μ < 5 GeV. This imposed a cut on the reconstructed muon kinematics to exclude backward reconstructed tracks or tracks with momentum greater than 5 GeV. Both of these cases were uncommon and lacked sufficient statistics to be included in the analysis.

Plotted in Figure 5.4 is the muon and pion momentum versus angle distributions both before ((a) and (b)) and after ((c) and (d)) precuts. For plots (a) and (b), all fiducial signal (Reconstructed 1μ 1π) events were included. Plots (c) and (d) contain all signal events that passed the precuts. The numbers of events after each precut are listed in Table 5.1, generated by looking at the Monte Carlo scaled to the expected data. Also included in the table is the signal purity of the sample after each cut given in Equation 5.1 and the selection efficiency given in Equation 5.2.

$$\text{Purity} = \frac{\text{Selected Signal Events}}{\text{All Selected Events}} \tag{5.1}$$

$$\text{Efficiency} = \frac{\text{Selected Signal Events}}{\text{All Signal Events}} \tag{5.2}$$

The after precut phase space plots do not differ in distribution much other than the large decrease in the number of events. The one exception would be the removal of very low momentum particles (less than 100 MeV), as these events are not well reconstructed.

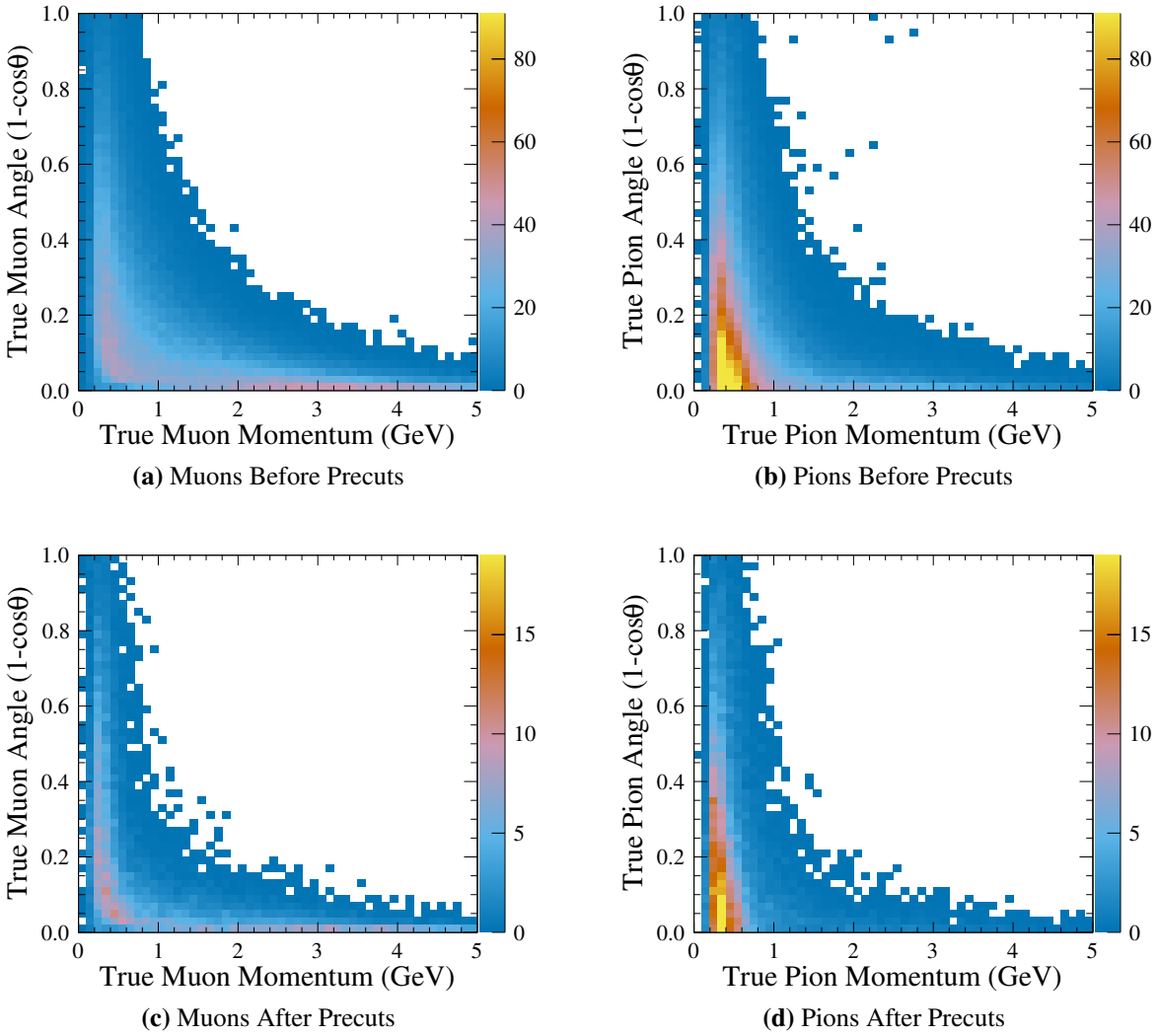

(a) Muons Before Precuts

(b) Pions Before Precuts

(c) Muons After Precuts

(d) Pions After Precuts

Figure 5.4: True p-theta distribution before and after precuts for both muons and pions. The number of MC events is scaled to the expected data.

Table 5.1: Precut Progression: Events, Purities, and Efficiencies

Cut	Total Events	Signal Events	Purity	Efficiency
Reco Vertex	373184	11659.2	0.0312	1
Fiducial Vertex	91961.3	4704.31	0.0512	0.403
Two Tracks	19540.1	3157.79	0.162	0.271
3D Vertex	18876.2	3149.54	0.167	0.270
3D Tracks	18049.6	3145.41	0.174	0.270
Track-Vertex Distance	12291.1	2344.71	0.191	0.201
Containment	7115.36	1419.0	0.199	0.122
Muon Kinematics	6747.56	1319.94	0.196	0.113

5.3.2 Sample Selections

After events passed precuts, the primary goal was to identify the signal events that would populate the selected sample. The MIP-MVA discussed in Chapter 4.3 worked well at dividing MIP-like tracks from non-MIP-like tracks, so well in fact that it also separated the muons - which are very MIP-like - from the pions that, though MIP-like, can also undergo hadronic interactions and deposit energy in non-MIP-like ways. What this meant for selecting events is that the more strict a cut applied to the MIP-MVA discriminant value the more likely the particle would be a muon. Specifically, the MVA predicted that almost all tracks with a MIP-MVA discriminant value above 0.1 were muon tracks, and similarly that the vast majority of muon tracks had a MIP-MVA discriminant value above 0.1. Relaxing the cut brought in more pions, and relaxing it brought in more not-MIP-like particles like protons. All events chosen for this analysis were required to have one track that passed the strict cut on the MIP-MVA discriminant value of being greater than 0.1, almost ensuring that one particle would be a muon. The cut on the second track in an event was used to separate selected signal events from the background samples that would make up the sidebands.

The Selected Sample

With the first track required to pass the strict MIP-MVA Discriminant cut (> 0.1), the best selection of signal events was made by requiring the second track to also be very MIP-like and pass a MIP-MVA discriminant cut of 0.0 for Kalman tracks, and 0.04 for cluster tracks. These values were chosen to give good signal efficiency and purity, but were not strictly optimized so as to avoid introducing too much dependency on the MVA discriminant values.

The result of the two MIP-MVA cuts are plotted in Figure 5.5 where the true muon and pion kinematics for selected signal events are shown. The selected sample again has fewer events than the previous sample, this time losing a lot of the high angle tracks for both muons and pions.

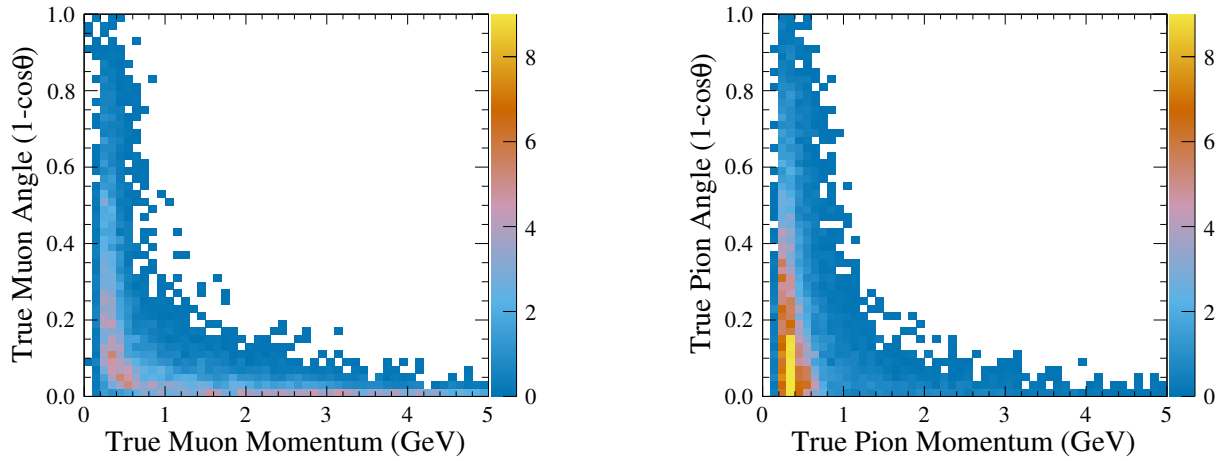

(a) Muon **(b)** Pion

Figure 5.5: True p-theta distribution of muons and pions for events with two selected tracks. The number of MC events is scaled to the expected data.

Sidebands

The sideband regions serve the analysis by giving a data-driven way to characterize the backgrounds, and thus understand the shape and amplitude of backgrounds that contaminate the selected signal sample. The sidebands for this analysis were chosen as events that passed the same precuts and single MIP-like track cut, but failed the second MIP-like track cut, indicating that the

sideband region was much more likely to contain a muon and a proton instead of a muon and a pion.

Far Sideband To make the best measurement of the background events, a sample with a high background purity was required. Starting with the two track sample, with one track passing the MIP MVA Discriminant cut of > 0.1, the next goal was to make a cut on the second track such that the majority of the evens were NOT signal. The cut chosen for the second track was that the MIP MVA Discriminant be less than -0.1. The muon and pion p-theta distributions for the few signal events that make it into the far sideband are plotted in Figure 5.6. As this region has very few signal events, the plot of signal events does not have many entries, but the ones it does have still cover the same phase space as the selected sample.

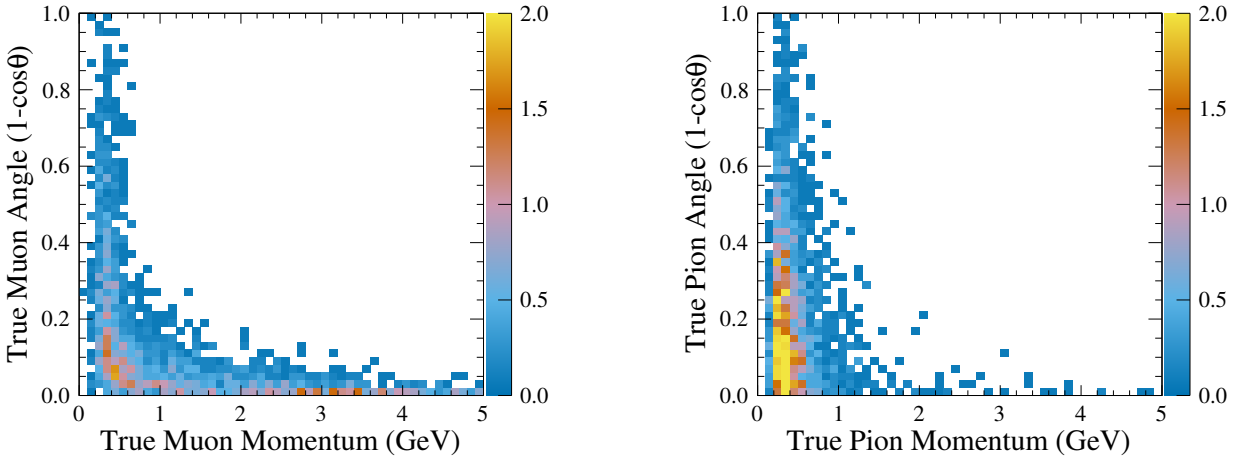

(a) Muon **(b)** Pion

Figure 5.6: True p-theta distribution of muons and pions for events in the far sideband (one selected track, the other track in the far sideband cut). The number of MC events is scaled to the expected data.

Near Sideband With the definition of the selected signal region and the far sideband, there remained a number of events left in between the two. These are events that still have one track that passed the MIP-MVA Discriminant cut of >0.1, but the second track has a MIP-MVA Discriminant value between -1.0 and 0.0 (0.04 for cluster tracks). All the events in this region were collected

into a sample called the near sideband. The near sideband does not have the signal purity of the selected region, nor the background purity of the far sideband, but it does provide a region in which both the signal and background contribute and can help constrain both samples.

The muon and pion p-theta distributions for signal events in the near sideband are plotted in Figure 5.7. With more signal events than the far sideband these plots have more entries, but still have events in the same phase space.

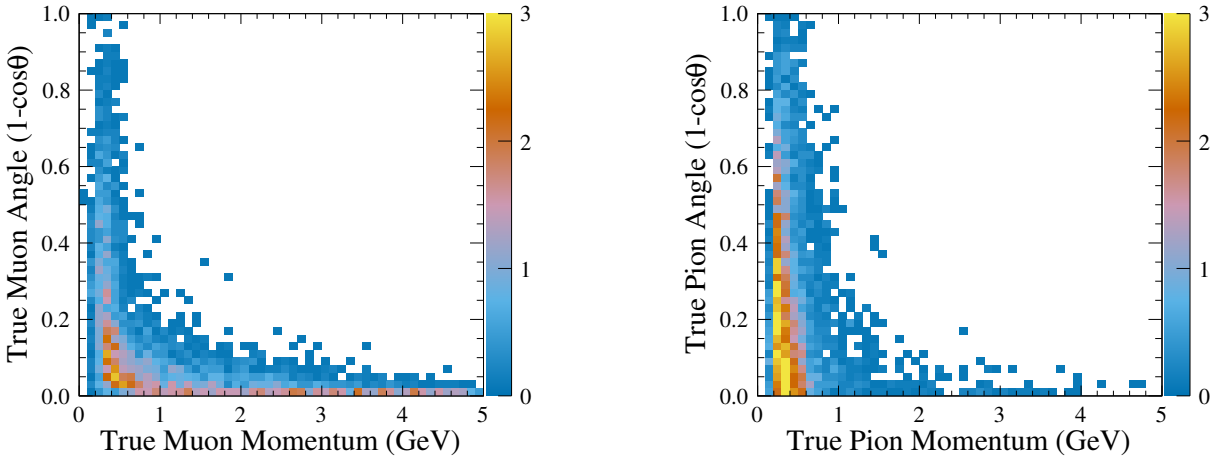

(a) Muon **(b)** Pion

Figure 5.7: True p-theta distribution of muons and pions for events in the near sideband (one selected track, the other track in the near sideband cut). The number of MC events is scaled to the expected data.

Selection and Sideband Summary The events that made it into the selected and sideband samples plotted above are summarized in Table 5.2, with the efficiencies and purities continued from Table 5.1. It is useful to note that the selected sample has a 61% signal purity, and the far sideband has a 92% background purity, making both very useful samples for this analysis.

Signal and Sideband Coverages and Efficiencies

The goal of a sideband is that it gives a handle at understanding the backgrounds that make it into the selected sample. A way to ensure that the sideband is representative of the events it is designed to describe is to compare the distribution of the events in both samples as a function of

Table 5.2: Selection Stats: Events, Purities, and Efficiencies

Selection	Total Events	Signal Events	Purity	Efficiency
After Precuts	6747.6	1319.94	0.196	0.113
One Mu-Like Track	3629.8	1017.29	0.280	0.0873
Selected Sample	990.9	608.79	0.614	0.0522
Near Sideband	783.2	261.12	0.333	0.0224
Far Sideband	1855.8	147.37	0.0794	0.0126

a number of different kinematic variables. To that end, a number of studies were done looking at the distribution of events in the different samples and comparing them in different phase spaces. The goal of the exercise was to show that wherever events existed in the signal region, they also existed in the sideband regions. Also important was confirmation that the selected signal sample had coverage of the full phase spaces for each of these variables. These results are important as they mean that integrating over these kinematic variables in order to report the measured cross section in muon angle and momentum is not hiding any inefficiencies in the phase space sampling.

Validation in 2D: q_0 vs q_3 Comparisons between different selections in two dimensions at once are a little difficult, but for this study the different distributions are simply provided side by side. This study is the total energy (q_0) vs total three momentum (q_3) transferred from the leptonic system (the neutrino and muon) to the hadronic system (the proton or neutron and pion). Plotted in Figure 5.8 is the q_0 vs q_3 distribution for all events used in this analysis, while Figure 5.9 contains just the selected events, Figure 5.10 just near sideband events, and Figure 5.11 just far sideband events. For each plot the distribution is separated by interaction type, representing the different interaction modes present in the different selections. From studying these plots it is apparent that the general shape of each interaction is well represented across all selections, with no glaring holes in coverage between samples.

Phase Space Efficiencies Efficiencies are another way of describing the coverage across the different kinematic variables. Again this efficiency is given by Equation 5.2 and represents the

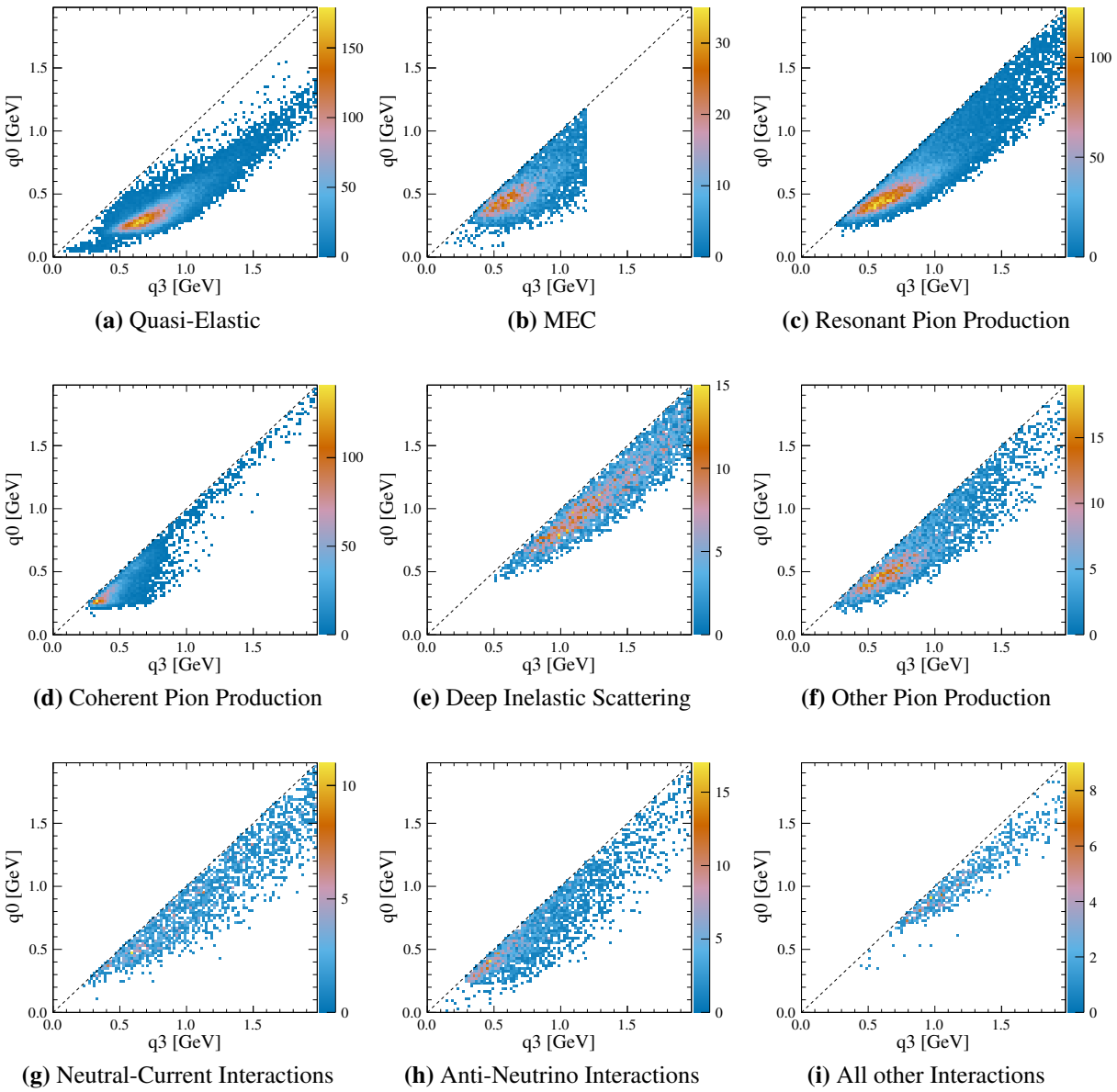

(a) Quasi-Elastic **(b)** MEC **(c)** Resonant Pion Production

(d) Coherent Pion Production **(e)** Deep Inelastic Scattering **(f)** Other Pion Production

(g) Neutral-Current Interactions **(h)** Anti-Neutrino Interactions **(i)** All other Interactions

Figure 5.8: The true q_0 vs. q_3 distribution for all events used in the analysis (selected + sideband samples). Plots are broken out by interaction type.

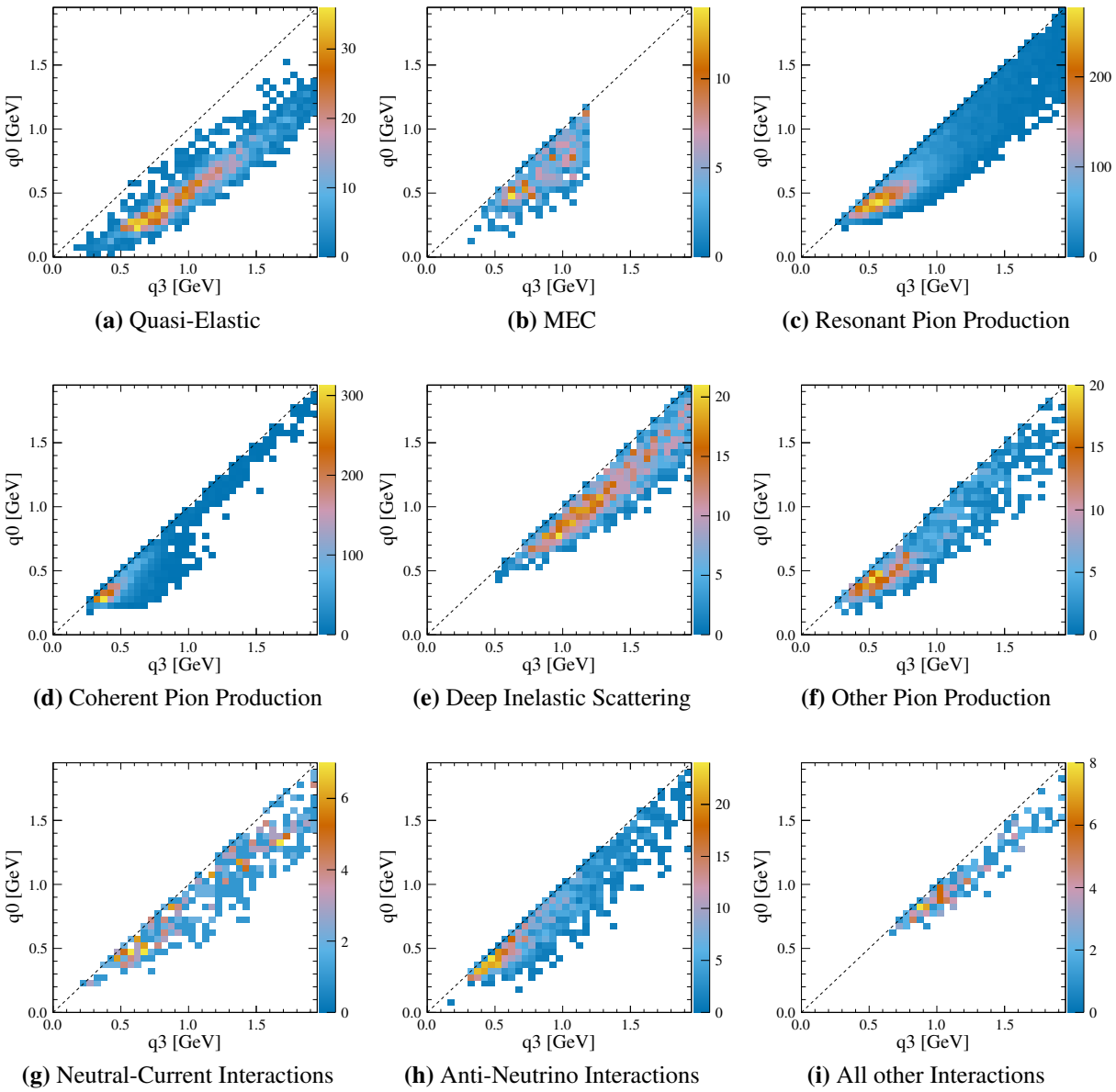

(a) Quasi-Elastic **(b)** MEC **(c)** Resonant Pion Production

(d) Coherent Pion Production **(e)** Deep Inelastic Scattering **(f)** Other Pion Production

(g) Neutral-Current Interactions **(h)** Anti-Neutrino Interactions **(i)** All other Interactions

Figure 5.9: The true q_0 vs. q_3 distribution for the selected event sample. Plots are broken out by interaction type.

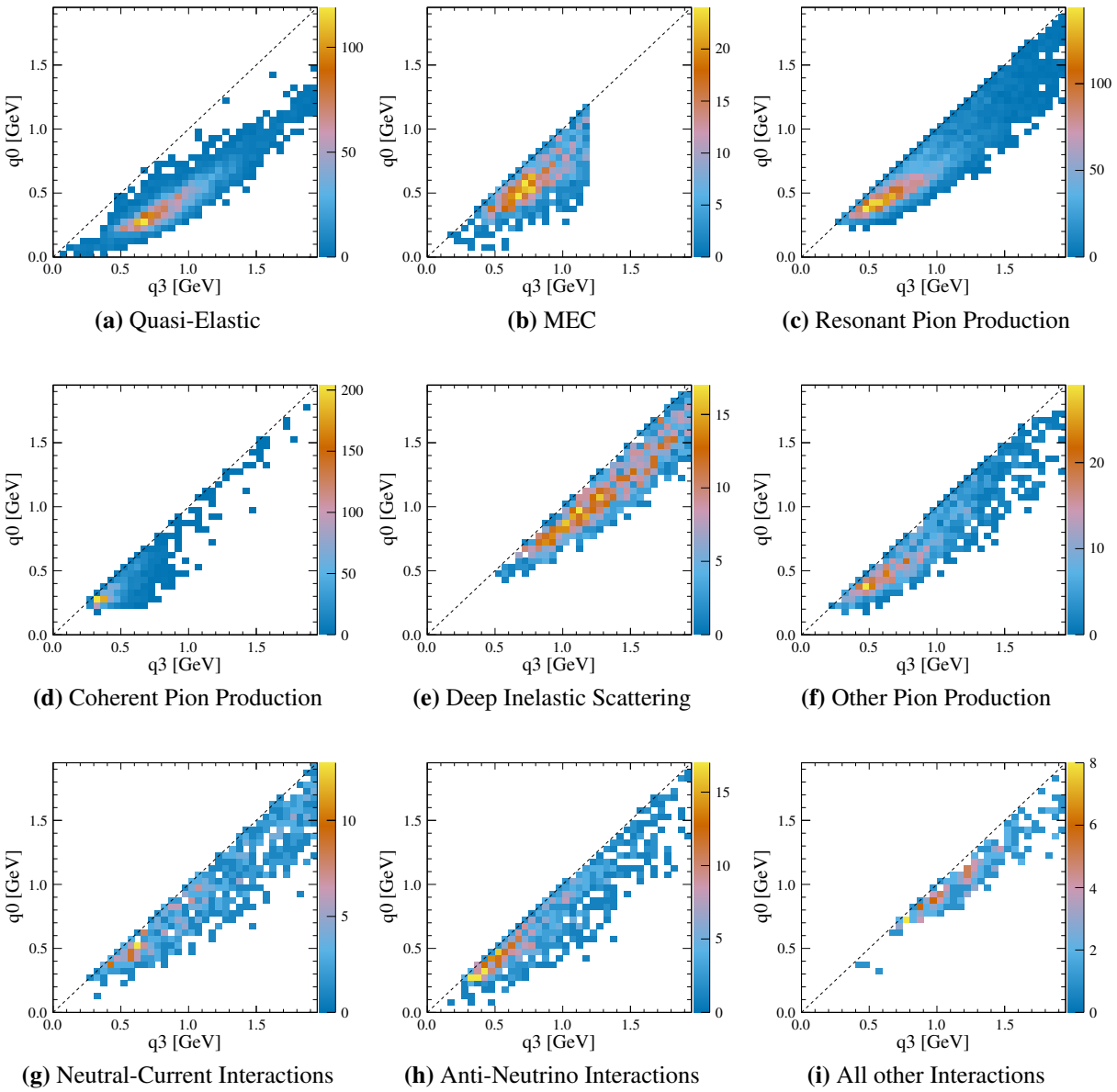

(a) Quasi-Elastic **(b)** MEC **(c)** Resonant Pion Production

(d) Coherent Pion Production **(e)** Deep Inelastic Scattering **(f)** Other Pion Production

(g) Neutral-Current Interactions **(h)** Anti-Neutrino Interactions **(i)** All other Interactions

Figure 5.10: The true q_0 vs. q_3 distribution for the near sideband event sample. Plots are broken out by interaction type.

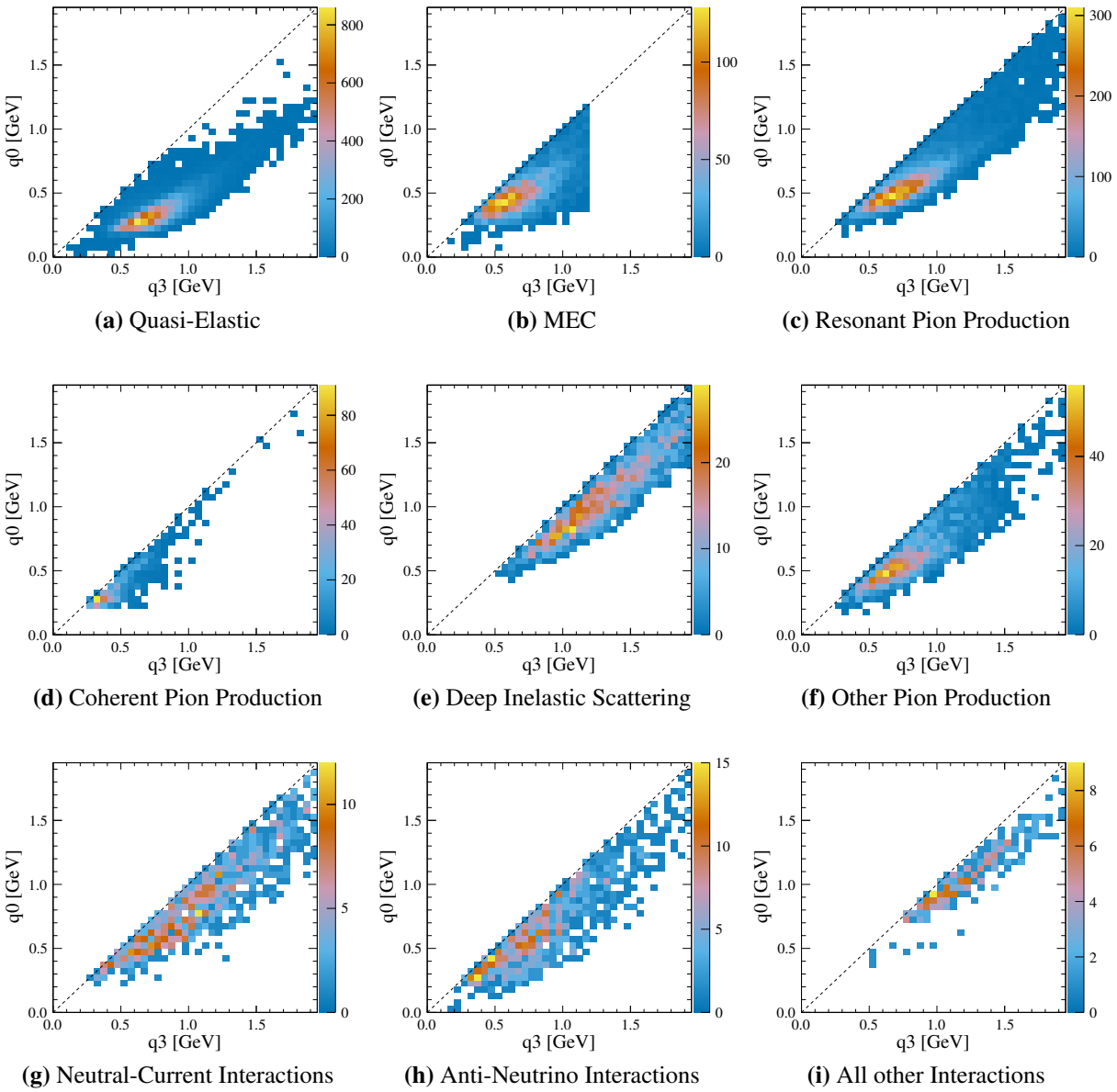

(a) Quasi-Elastic **(b)** MEC **(c)** Resonant Pion Production

(d) Coherent Pion Production **(e)** Deep Inelastic Scattering **(f)** Other Pion Production

(g) Neutral-Current Interactions **(h)** Anti-Neutrino Interactions **(i)** All other Interactions

Figure 5.11: The true q_0 vs. q_3 distribution for the far sideband event sample. Plots are broken out by interaction type.

number of signal events selected as compared to all signal events. The goal is that all selections have some efficiency across the phase space of each variable. A large number of variables were studied to ensure that there were good efficiencies no matter which phase space was considered, four of which are shown in Figure 5.12: Q^2, W^2, Bjorken X, and Bjorken Y:

$$Q^2 = (-(\mathbf{p}_\nu - \mathbf{p}_\mu))^{\mathbf{2}} \tag{5.3}$$

$$W^2 = M_p^2 + 2 * M_p * (E_\nu - E_\mu) - Q^2 \tag{5.4}$$

$$\text{Bjorken } Y = (E_\nu - E_\mu)/E_\nu \tag{5.5}$$

$$\text{Bjorken } X = Q^2/(2 * M_p * (E_\nu - E_\mu)) \tag{5.6}$$

where $\mathbf{p}$ and E are the four momentum and energy for the neutrino or muon and M_p is the mass of the proton.

The plots for these variables include the distribution of all signal events with a vertex inside the P∅D fiducial volume, plotted in grey behind the respective efficiency plots. This gives an indication of over what region it is important to have a good efficiency because this is where the events are. The selection efficiencies are plotted for all events used in the analysis, as well as for each individual sample (selected, near sideband, and far sideband). Again it was found that the samples have good efficiencies where there are events, non-zero efficiencies across the whole range of each variable, and good overlap in efficiency between different samples. These plots show there are no phase space restrictions that need to be considered for this analysis.

5.3.3 Muon Kinematic Samples

All events in the Selected and Sideband samples are further categorized by the reconstruction method of the track identified as the muon. Events reconstructed as Kalman or cluster tracks have different properties from reconstruction efficiencies to uncertainties and kinematic phase spaces. Another separation that was made, for all the same reasons, was splitting the Kalman selection into events that remained within the P∅D and the events that entered the TPC. In order to make these

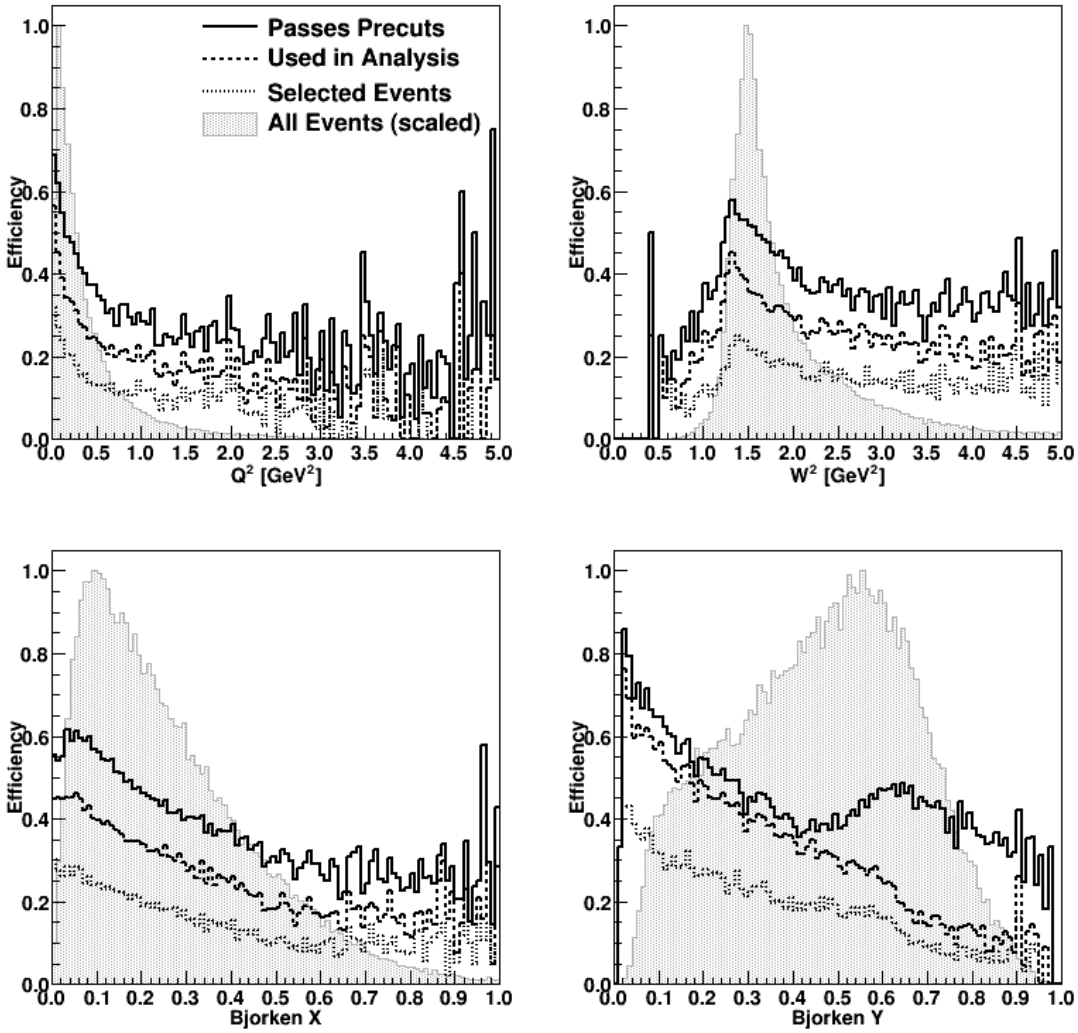

Figure 5.12: The selection efficiencies for events used in the analysis (selected + sideband samples) as a function of Q^2, W^2, Bjorken X, and Bjorken Y. The shaped of the distribution for all signal events with a vertex inside the PØD fiducial volume (gray filled, A.U.), and the efficiencies for precut (solid), analysis (dashed), and Selected (dotted) events are plotted.

divisions it was necessary to apply the particle identification discussed in Chapter 4 to identify the muon to be classified.

Particle Identification

Because the measurement made in this analysis was in terms of muon angle and momentum, it was important not only to select signal events, but also to identify which particle was the muon. The method developed to make this distinction was described in Chapter 4, and is a function of charge information from the TPC, reconstruction algorithm, and the discriminant value from the MuPi MVA. The result is an assignment of muon and pion to all events across all samples. For the Selected sample, these events were assumed to be muon and pion so this assignment made sense. For the Sidebands, the assignment of "pion" to the second track is not assumed to be exactly true for all events, as many of these events are background and do not have a pion, and was instead considered to be "not-muon" in practice.

Misidentified Events For all samples, the signal events present in the sample were characterized as correctly identified or as mis-ID'ed - these mis-ID'ed events being signal events for which the muon was identified as a pion, and the pion as the muon. These events needed to be considered carefully, because they were effectively background events no matter what sample they were a part of. A signal event with the pion reconstructed as a muon populated a plot that was supposed to be muon kinematics, and thus was not the desired signal. The specific treatment of these events is addressed in Chapter 6.3.3.

Kalman Contained

The Kalman Contained sample is defined as events where the muon was reconstructed as a Kalman track and did not enter the TPC. These events have a restricted momentum because they are not allowed to exit the PØD and thus the muon momentum spans the range of 200 MeV - 600 MeV. The angular range for PØD contained tracks has little restriction and thus spans the range of 0° - 80° with respect to the direction of the neutrino beam, with most the events are below

60°. The upper limit on angle is restricted due to the geometry of the PØD that makes it difficult to reconstruct tracks that reach high angles and thus pass through few layers of the PØD. Figure 5.13 contains the muon and pion p-theta space for Kalman PØD contained events.

Kalman Exiting

Events that are part of the Kalman Exiting sample are ones for which the muon was reconstructed as a Kalman track, exited the PØD through the downstream face, and were matched to a TPC track. These events have no upper restriction on their momentum, and only the lower bound on the momentum defined by being reconstructed as Kalman tracks, thus they span the range of 200 MeV to over 5 GeV. The requirement that these tracks start in the fiducial volume of the PØD and still enter into the TPC does impose an angular restriction on these events and most are within 20° of the angle of the neutrino beam, with the highest angles being around 45°. The distribution of these events for muon and pion signal events is plotted in Figure 5.14.

Cluster

The cluster sample contains events for which the muon track was reconstructed using the Cluster Track Fitter. This was not as common of an occurrence, because for most events that contained a cluster track (all events with a cluster track were paired with a Kalman track) the cluster track was chosen as the pion instead of the muon. For the events in this sample, the muon was generally low momentum and/or high angle, which is why it was not reconstructed as a Kalman track. These events have a momentum no greater than 400 MeV and an angle around 70° with respect to the neutrino beam, though they can range from 40° to almost 90°. This sample is the smallest of the three, and the least well reconstructed. These events are kept as part of the sample due to the fact that cluster tracks are the only way to reconstruct very low momentum or high angle tracks. The muon and pion p-theta space for signal events in the cluster selections are plotted in Figure 5.15.

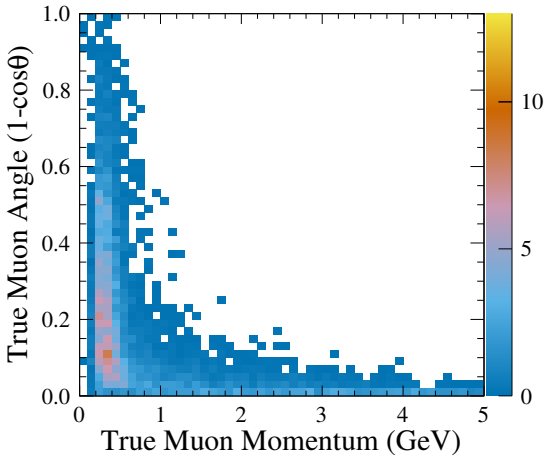

(a) Selected Muons

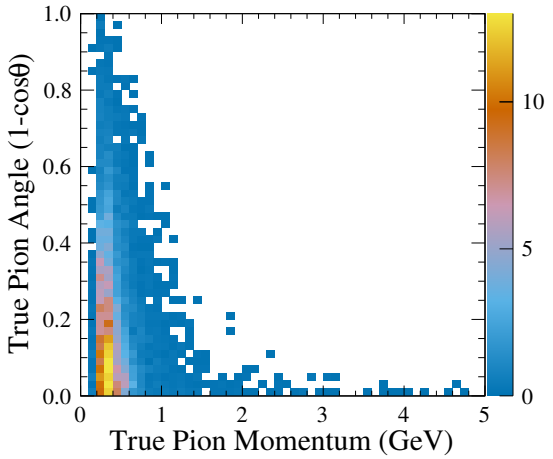

(b) Selected Pions

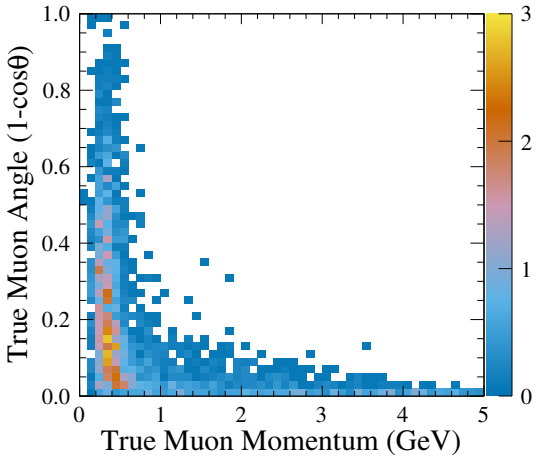

(c) Near Sideband Muons

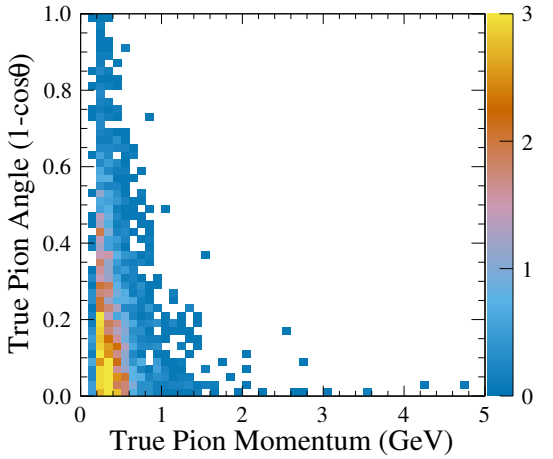

(d) Near Sideband Pions

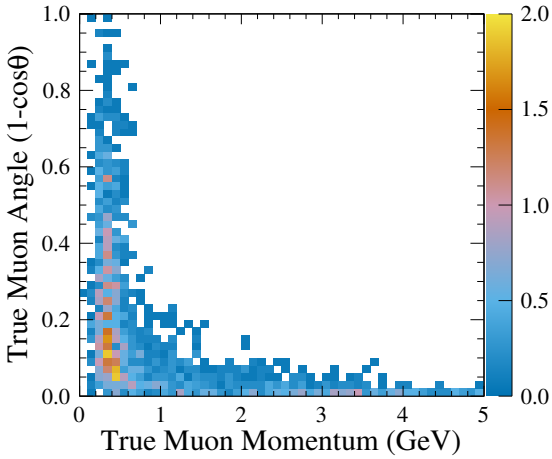

(e) Far Sideband Muons

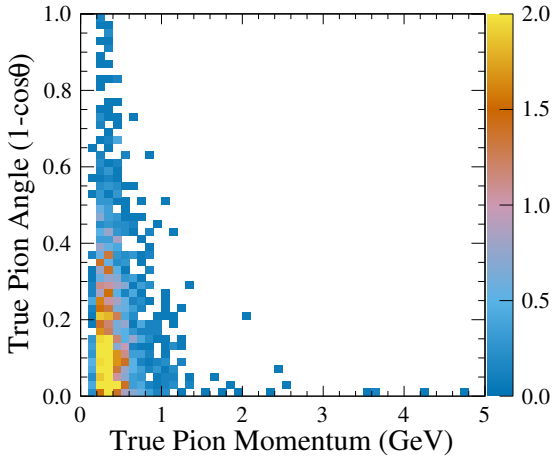

(f) Far Sideband Pions

Figure 5.13: True p-theta distribution for muons and pions in the Kalman contained sample. The number of MC events is scaled to the expected data.

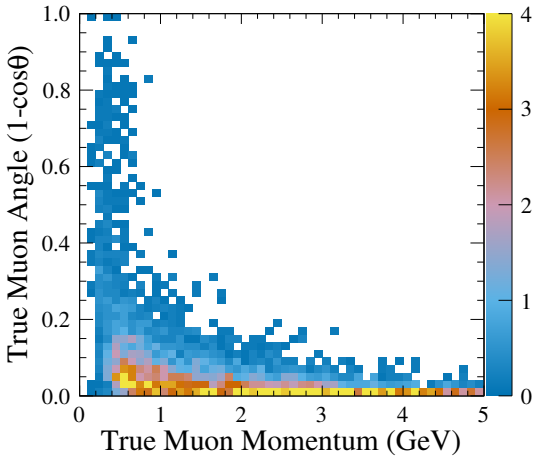

(a) Selected Muons

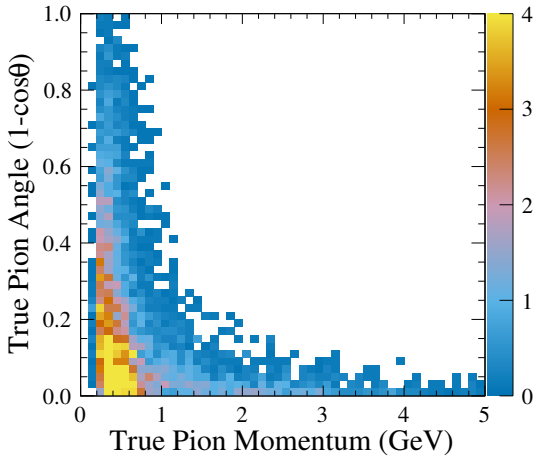

(b) Selected Pions

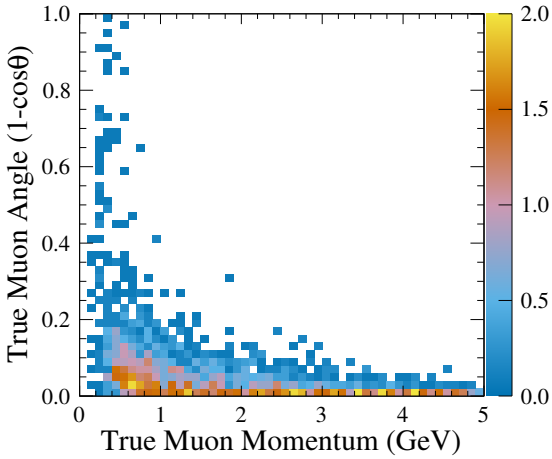

(c) Near Sideband Muons

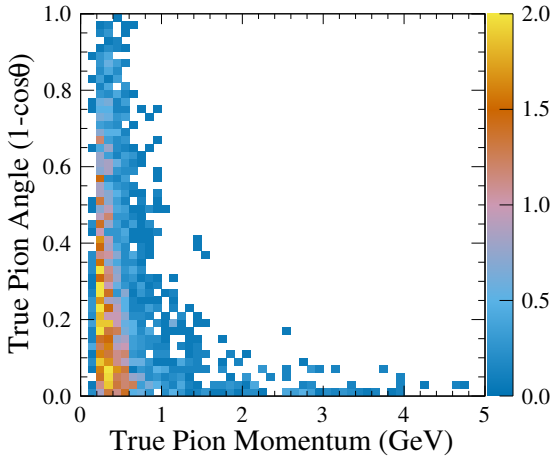

(d) Near Sideband Pions

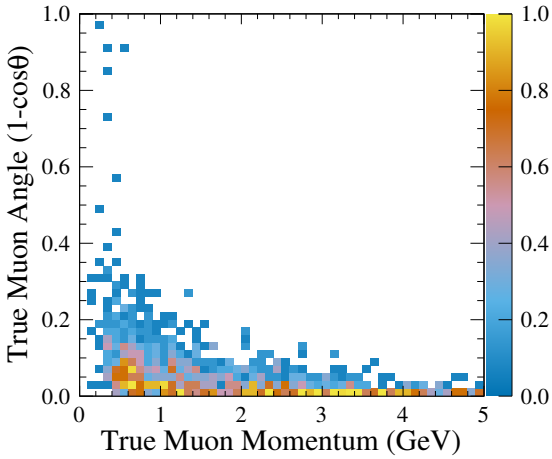

(e) Far Sideband Muons

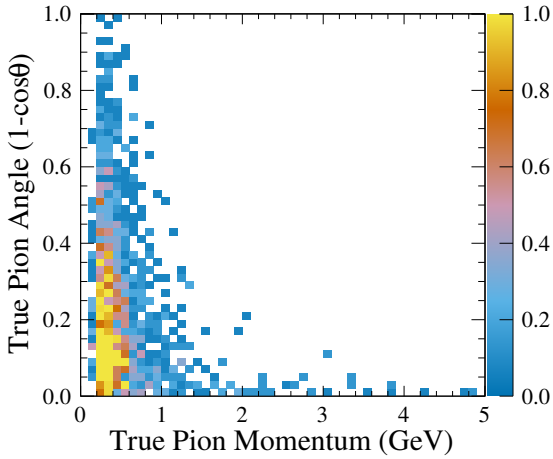

(f) Far Sideband Pions

Figure 5.14: True p-theta distribution for muons and pions in the Kalman exiting sample. The number of MC events is scaled to the expected data.

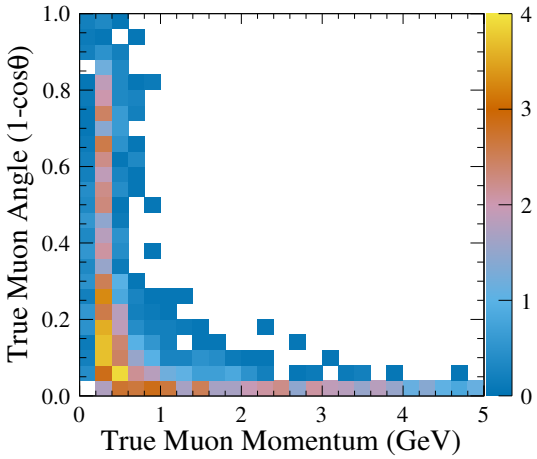

(a) Selected Muons

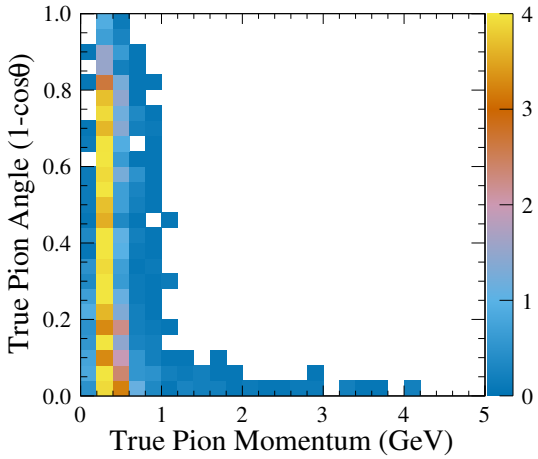

(b) Selected Pions

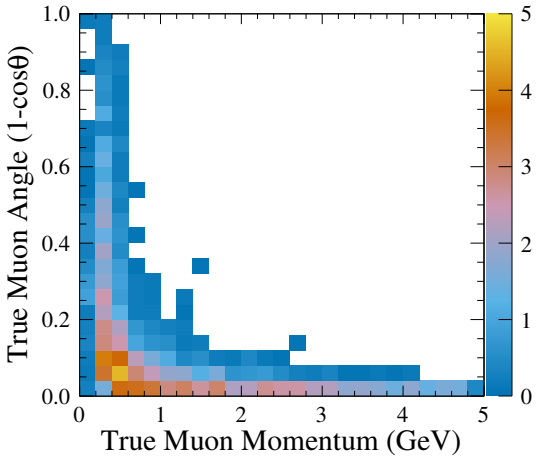

(c) Near Sideband Muons

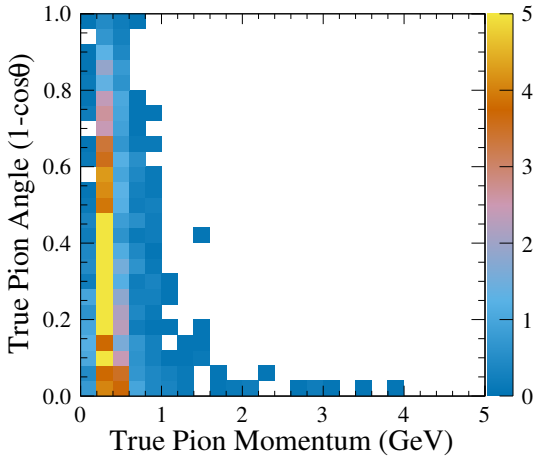

(d) Near Sideband Pions

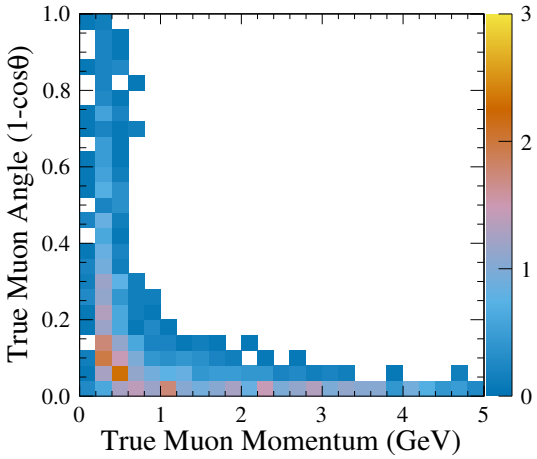

(e) Far Sideband Muons

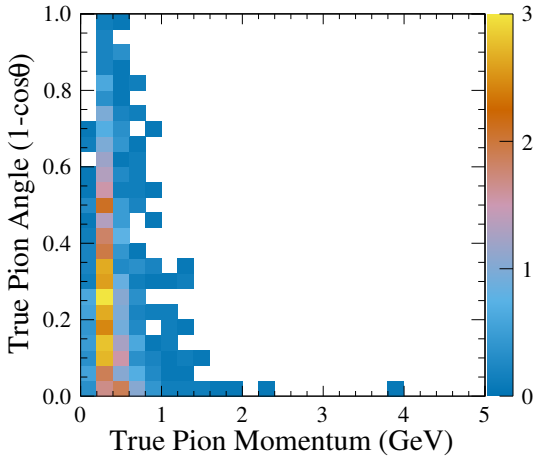

(f) Far Sideband Pions

Figure 5.15: True p-theta distribution for muons and pions in the cluster sample. The number of MC events is scaled to the expected data.

5.3.4 Signal Events in Signal and Background Samples

After making the selections defined above, it is useful to plot the signal and background contained in those selections. The signal definition that is used for studying the selections is the reconstructed $1\mu; 1\pi$ definition described in Chapter 5.2.

Misidentified Tracks

Events with misidentified tracks, discussed earlier, are signal events that were included in one of the selections, but had the two tracks misidentified. For these tracks, the pion was reconstructed as the muon, and thus the wrong particle assumption was used when calculating the momentum. In addition to the particle having the wrong momentum calculation, the inclusion of this particle in the muon kinematic plots would be incorrect as it was not a muon, and thus neither the angle nor momentum applies. These reasons are why even though these events are signal events they had to be treated like backgrounds: studied and understood but ultimately not included in the final signal measurement.

Signal-Background Events

Another special class of events are the events that are the result of signal according to the Primary Interaction CC $1\pi^+$ signal definition but not signal according to the reconstructed 1μ 1π signal definition. These events are defined as background for the analysis because they do not contain the required reconstructed particles, but the underlying physics is what this analysis is trying to measure. These events usually appear as a muon and a proton because the pion did not escape the nucleus due to FSI, or the pion is too low momentum to be reconstructed. Although these events are signal physics, they do not meet this signal definition and thus are be treated as background. Since these events are the result of signal physics means that they must be studied and treated carefully throughout the analysis to ensure that signal models are not used to estimate the contributions of these backgrounds and thus introduce signal model dependence into the measurement.

5.3.5 The Nine Analysis Samples

The final event selections are now defined that produce nine samples used in the analysis:

1. Selected:

   Kalman Contained, Kalman Exiting, Cluster

2. Near Sideband:

   Kalman Contained, Kalman Exiting, Cluster

3. Far Sideband:

   Kalman Contained, Kalman Exiting, Cluster

Correctly Identified Particles

After the identification of the muon in the event, and the separation into muon kinematic categories, the correctly identified and misidentified tracks can be separated. The true muon kinematics for correctly identified tracks are shown in Figure 5.16, with the corresponding pion kinematic distributions shown in Figure 5.17.

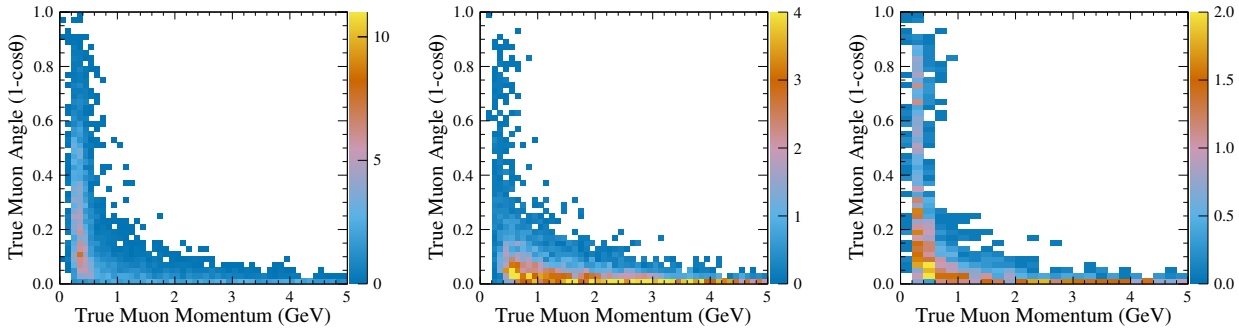

(a) Selected Kalman Contained **(b)** Selected Kalman Exiting **(c)** Selected Cluster

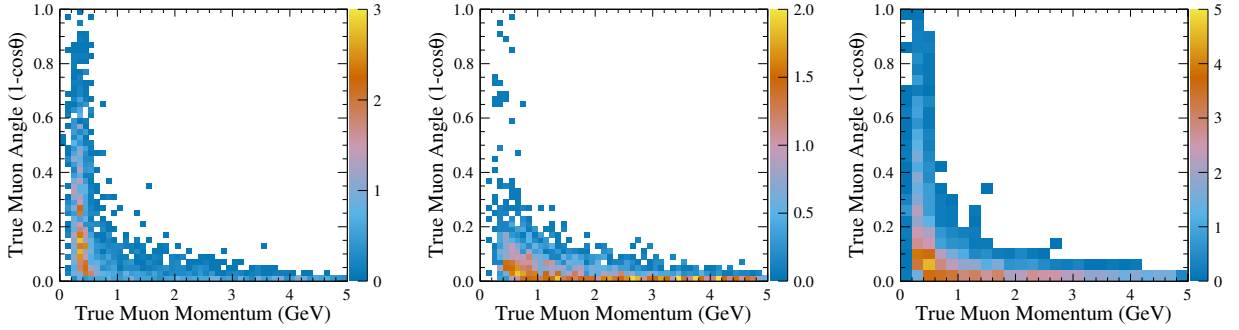

(d) Near Sideband Kalman Contained **(e)** Near Sideband Kalman Exiting **(f)** Near Sideband Cluster

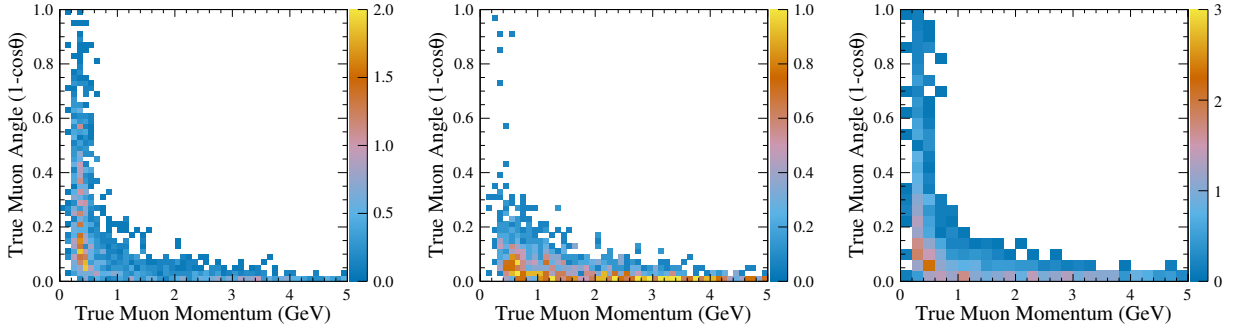

(g) Far Sideband Kalman Contained **(h)** Far Sideband Kalman Exiting **(i)** Far Sideband Cluster

Figure 5.16: True muon P-Theta distribution for events with correctly identified tracks. The number of MC events is scaled to the expected data.

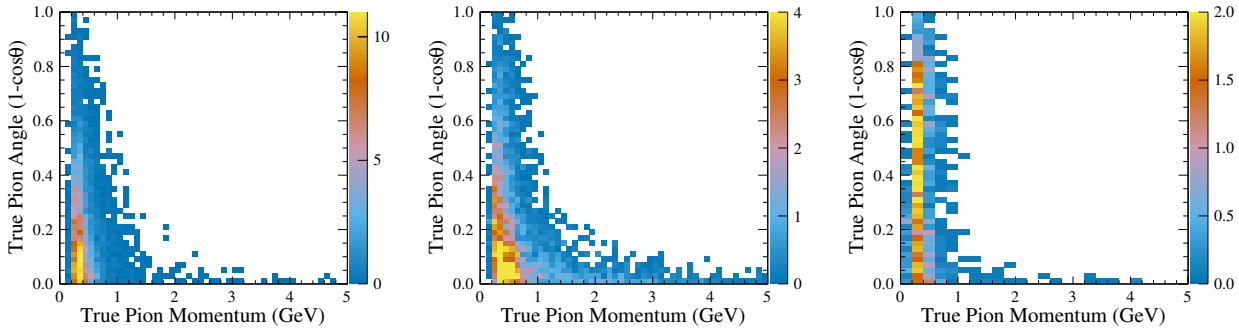

(a) Selected Kalman Contained **(b)** Selected Kalman Exiting **(c)** Selected Cluster

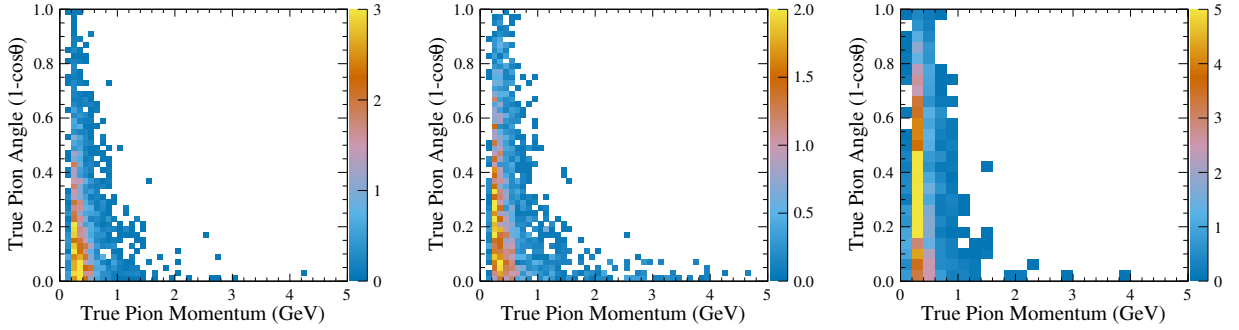

(d) Near Sideband Kalman Contained **(e)** Near Sideband Kalman Exiting **(f)** Near Sideband Cluster

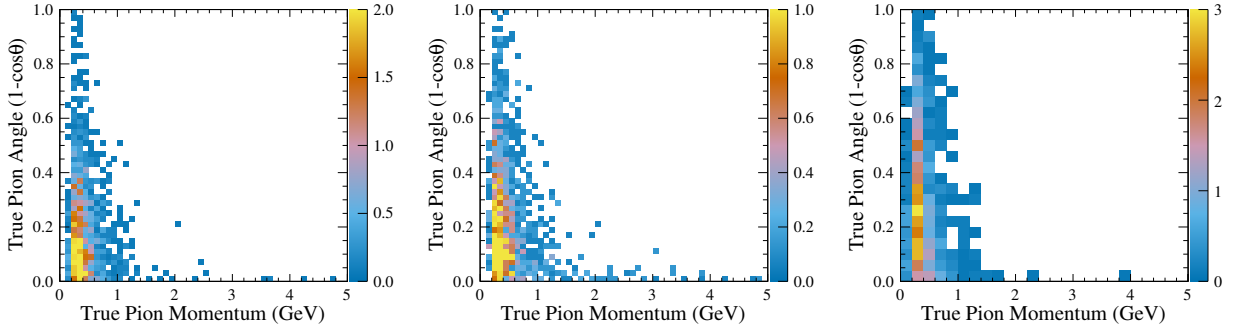

(g) Far Sideband Kalman Contained **(h)** Far Sideband Kalman Exiting **(i)** Far Sideband Cluster

Figure 5.17: True pion P-Theta distribution for events with correctly identified tracks. The number of MC events is scaled to the expected data.

Reconstructed Muon Distributions

This analysis was carried out in the reconstructed muon p-theta space, divided into nine samples, as plotted below using the MC predictions. The plots in Figure 5.18 show the reconstructed muon momentum and angle two dimensional distribution. Though the analysis was done in the two dimensional space, projections of that space can be taken and are much easier understood. Figure 5.19 and Figure 5.21 show the momentum or angle projection of the different samples broken down by signal, misidentified, signal background, and background events. These plots are useful for understanding the purity in the different samples as simulated by the MC, as well as seeing the contribution of signal background to the backgrounds of each sample. Additionally Figure 5.20 and Figure 5.22 break down the signal and background into the primary interaction modes. From these plots the contribution of different channels to the backgrounds and signal as predicted by the MC can be seen. The signal samples, for example, have a wide spread of the different background interaction modes, while the proportion of quasi elastic events increases disproportionately to the other backgrounds in the near and far sidebands. Also the proportion of signal events that are from coherent interactions can be seen to be almost half the signal, as predicted by the MC.

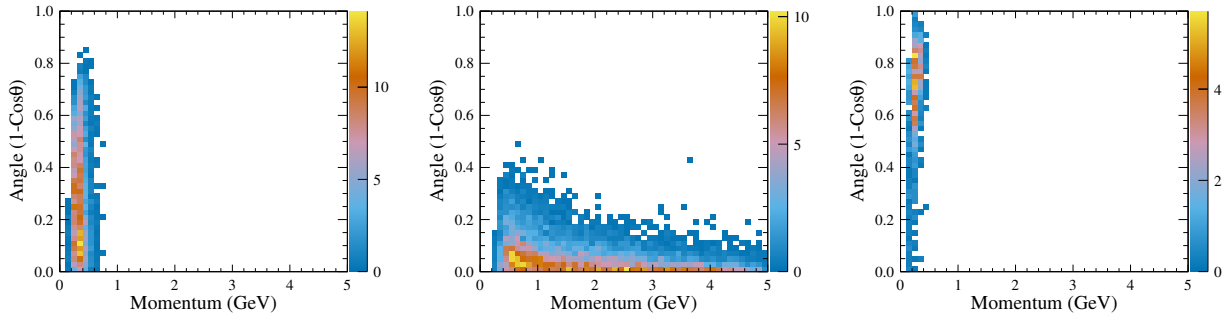

(a) Selected Kalman Contained **(b)** Selected Kalman Exiting **(c)** Selected Cluster

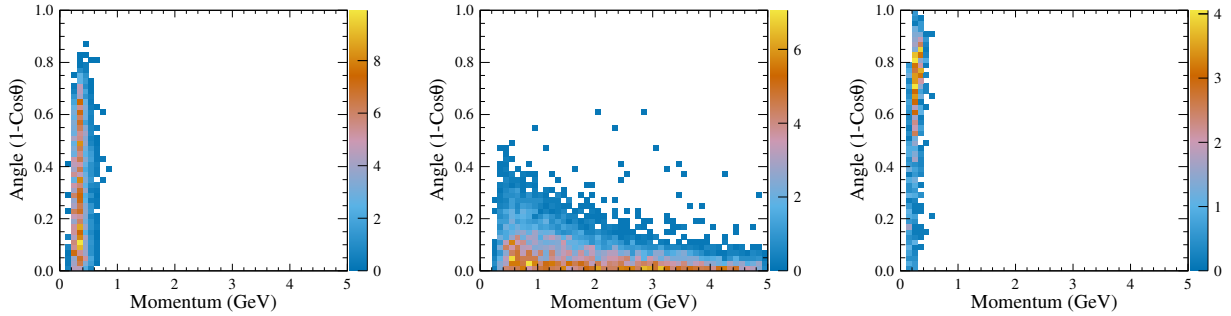

(d) Near Sideband Kalman Contained **(e)** Near Sideband Kalman Exiting **(f)** Near Sideband Cluster

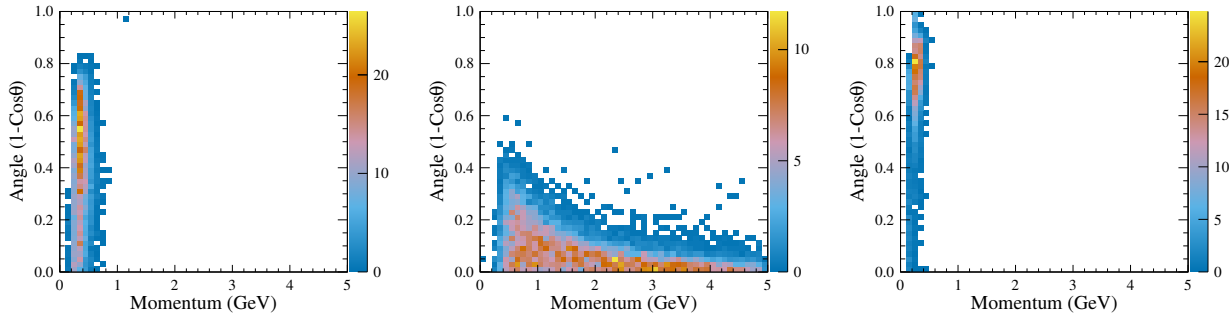

(g) Far Sideband Kalman Contained **(h)** Far Sideband Kalman Exiting **(i)** Far Sideband Cluster

Figure 5.18: Reconstructed muon p-theta distribution in each of the nine samples as predicted by NEUT. The number of MC events is scaled to the expected data.

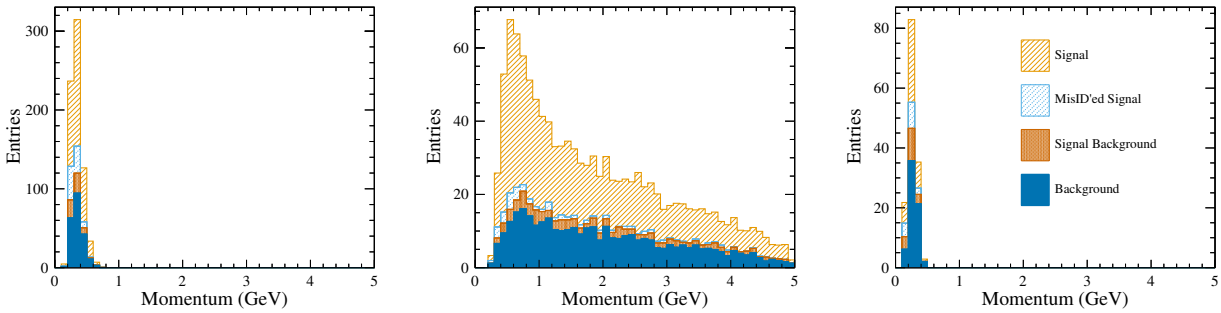

(a) Selected Kalman Contained **(b)** Selected Kalman Exiting **(c)** Selected Cluster

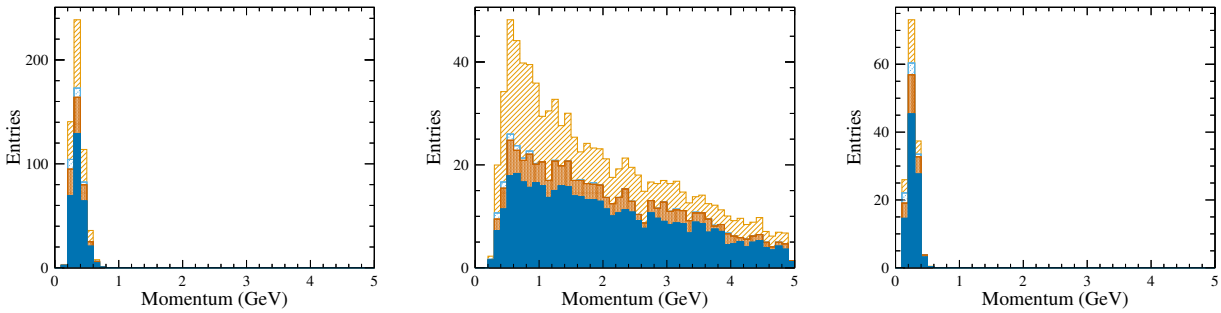

(d) Near Sideband Kalman Contained **(e)** Near Sideband Kalman Exiting **(f)** Near Sideband Cluster

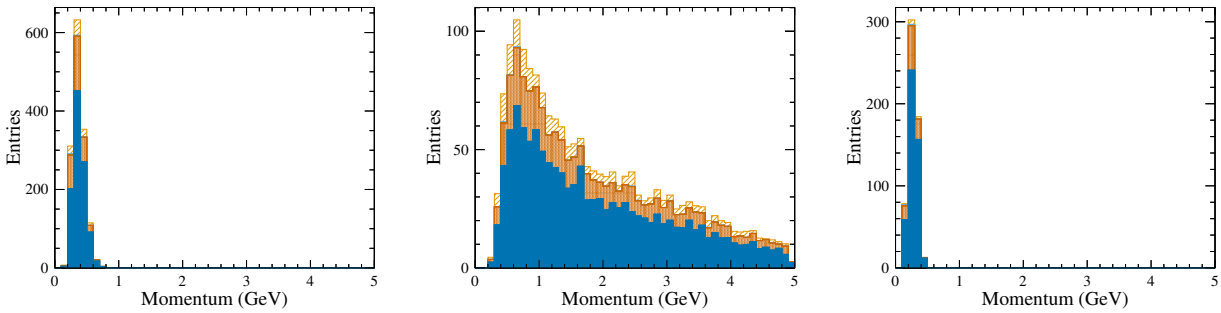

(g) Far Sideband Kalman Contained **(h)** Far Sideband Kalman Exiting **(i)** Far Sideband Cluster

Figure 5.19: Reconstructed muon momentum projection broken down by category as predicted by NEUT. The number of MC events is scaled to the expected data.

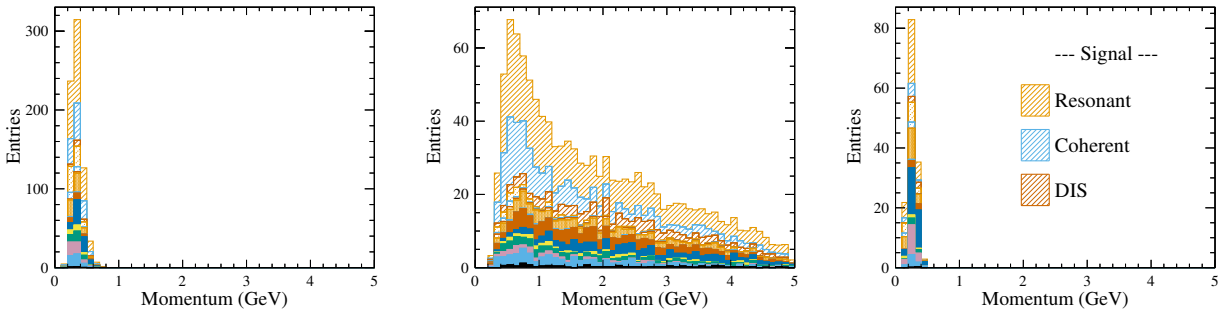

(a) Selected Kalman Contained **(b)** Selected Kalman Exiting **(c)** Selected Cluster

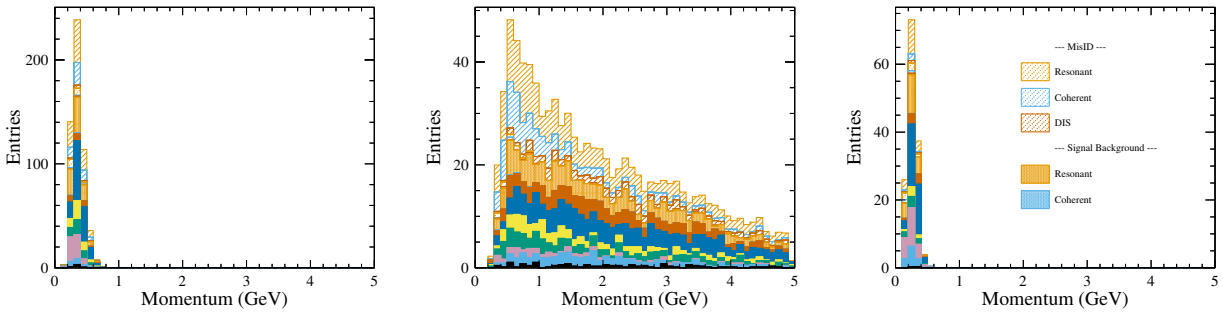

(d) Near Sideband Kalman Contained **(e)** Near Sideband Kalman Exiting **(f)** Near Sideband Cluster

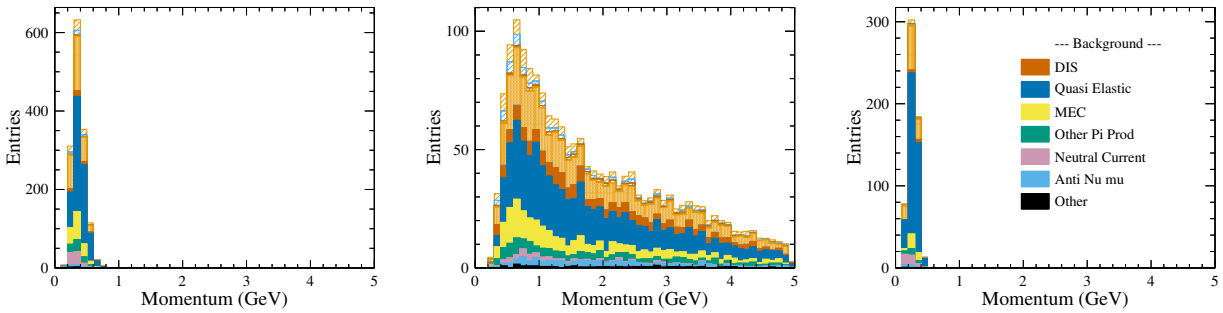

(g) Far Sideband Kalman Contained **(h)** Far Sideband Kalman Exiting **(i)** Far Sideband Cluster

Figure 5.20: Reconstructed Muon Momentum Projection broken down by primary interaction type as predicted by NEUT. The number of MC events is scaled to the expected data.

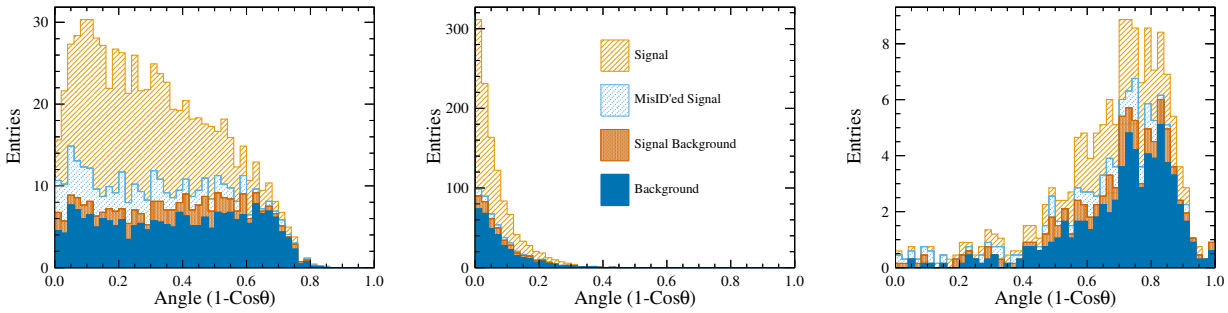

(a) Selected Kalman Contained

(b) Selected Kalman Exiting

(c) Selected Cluster

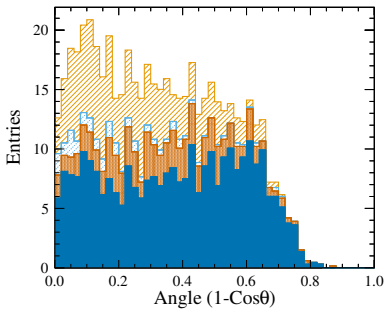

(d) Near Sideband Kalman Contained

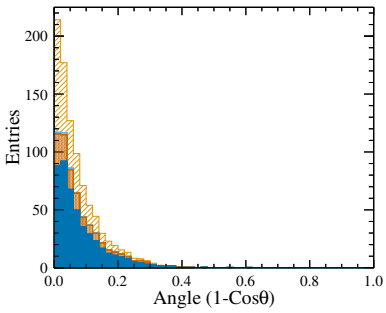

(e) Near Sideband Kalman Exiting

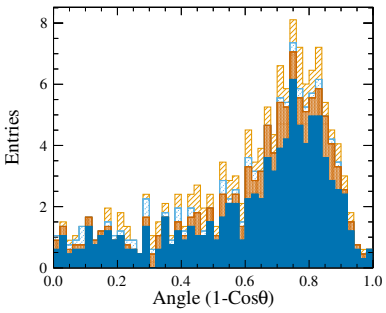

(f) Near Sideband Cluster

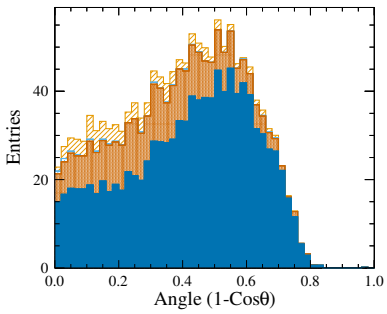

(g) Far Sideband Kalman Contained

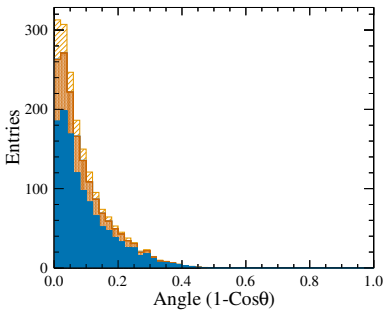

(h) Far Sideband Kalman Exiting

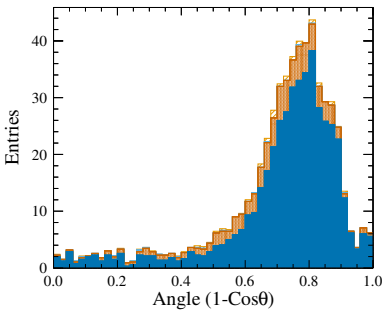

(i) Far Sideband Cluster

Figure 5.21: Reconstructed Muon Angle Projection broken down by event category as predicted by NEUT. The number of MC events is scaled to the expected data.

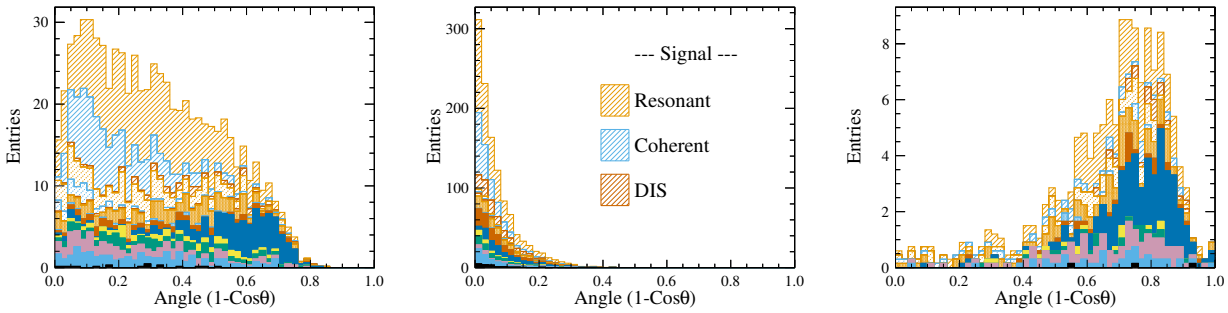

(a) Selected Kalman Contained **(b)** Selected Kalman Exiting **(c)** Selected Cluster

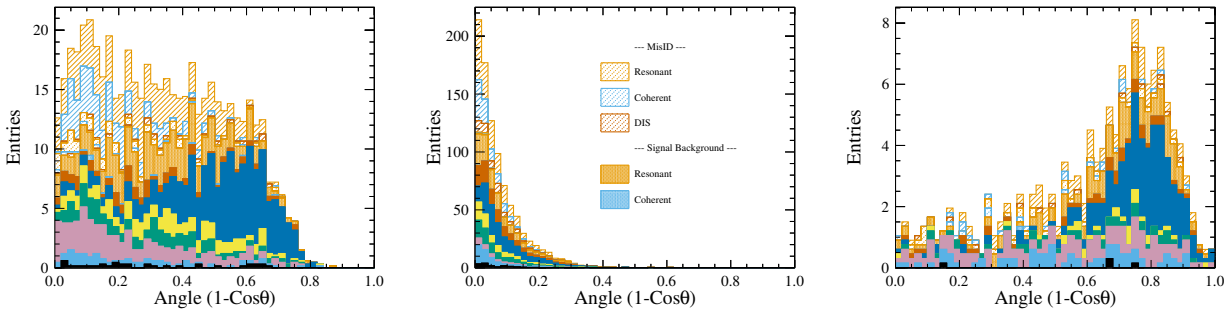

(d) Near Sideband Kalman Contained **(e)** Near Sideband Kalman Exiting **(f)** Near Sideband Cluster

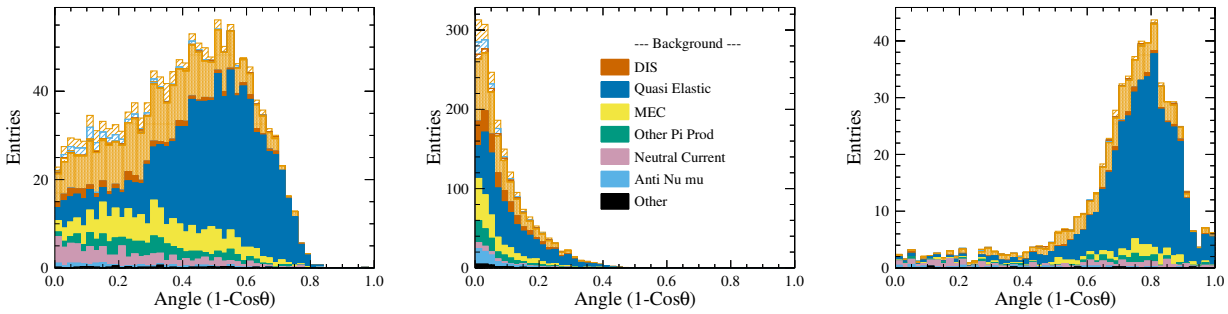

(g) Far Sideband Kalman Contained **(h)** Far Sideband Kalman Exiting **(i)** Far Sideband Cluster

Figure 5.22: Reconstructed Muon Angle Projection broken down by primary interaction type as predicted by NEUT. The number of MC events is scaled to the expected data.

5.4 Analysis Binning

With the samples defined, the breakdown of events was understood well enough to look at the expected statistics in each sample and determine what binning would be most appropriate for analyzing and presenting the results. Choosing the binning for the analysis is a process that involves the balancing of many factors. Bins that are too small do not have sufficient statistics to be useful for a measurement. Additionally if bins are too small the events in those bins may have an uncertainty on their momentum and angle that is very large. The goal is to make the bins large enough that there is a reasonable amount of certainty that the events in the bins belong in the bins. Making bins too large, however, reduces the number of bins in the analysis, making the measurement much more coarse in the given dimension. Lastly, bins that are too wide can span regions of phase space where the behavior of all the events within a single bin can have different properties. This becomes especially problematic when looking at the efficiency across a bin - if the reconstruction efficiency is not flat across the full range of that bin, then correcting the number of events in that bin later will be very difficult to do correctly.

The method this analysis settled on for choosing bins was to balance the uncertainty in reconstructing the momentum and angle with the uncertainty present from the number of events in the bin. The binning was determined in muon angle and momentum independently, starting at the point with the highest number of events and growing the bins from there. This procedure was done separately for all three muon kinematic samples (Kalman Contained, Kalman Exiting, Cluster) using only signal events from the MC, scaled to data. When the bins were determined for each sample, the decision was made to combine them into one global set of bins for all samples to use. At this point a check was also done to ensure that the efficiencies were flat across all the chosen bins, and boundaries were adjusted to improve performance.

The statistical uncertainty is calculated as the square root of the number of events in an analysis bin. The bin migration probability is estimated from the resolution on p_μ and θ_μ as modeled by the MC (as discussed in Chapter 3). The resulting analysis bins are given in Table 5.3, and the signal is plotted with the analysis bins for the nine analysis samples in Figure 5.23, with the full samples

plotted in projections in Figure 5.24 through Figure 5.27. With the new binning the contribution of different interaction modes to the signals and backgrounds are more easily studied without losing any of the large scale structure that was apparent in the previous plots.

Table 5.3: The momentum and angle bins for the analysis.

Momentum [GeV/c]	Angle $[1 - \cos(\theta)]$
0.0-0.15	0.0-0.015
0.15-2.75	0.015-0.06
0.275-0.45	0.060-0.181
0.45-0.7	0.181-0.357
0.7-1.1	0.357-0.5
1.1-1.6	0.5-1.0
1.6-2.6	
2.6-5.0	

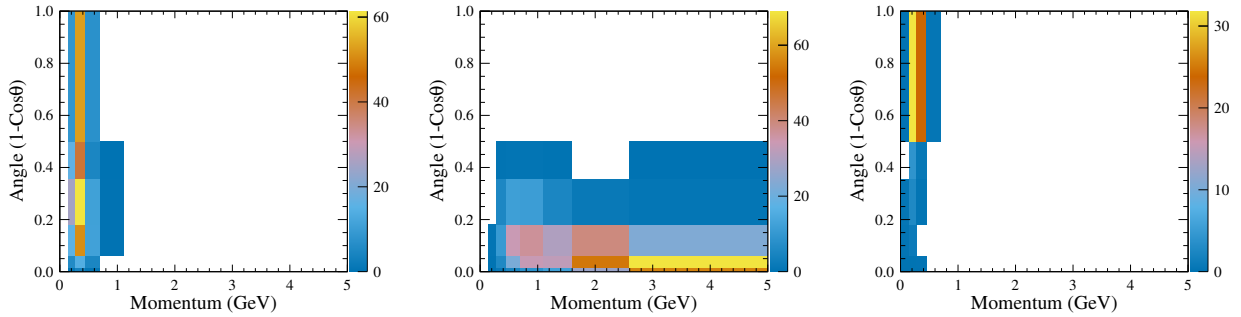

(a) Selected Kalman Contained **(b)** Selected Kalman Exiting **(c)** Selected Cluster

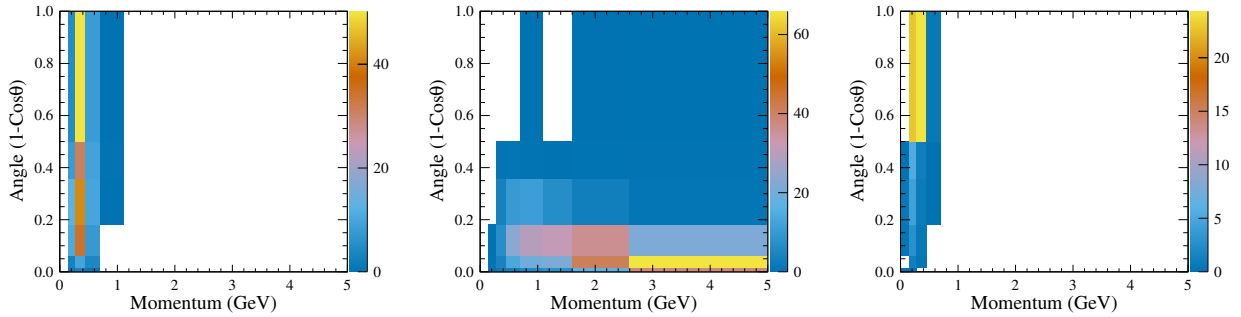

(d) Near Sideband Kalman Contained **(e)** Near Sideband Kalman Exiting **(f)** Near Sideband Cluster

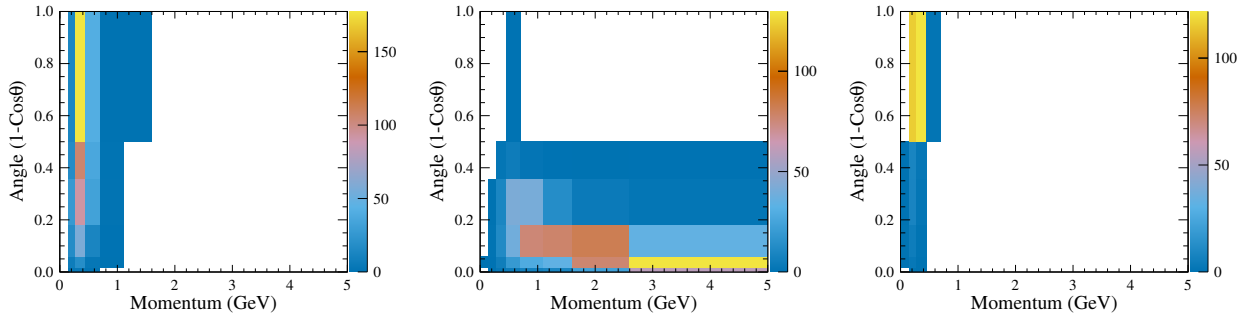

(g) Far Sideband Kalman Contained **(h)** Far Sideband Kalman Exiting **(i)** Far Sideband Cluster

Figure 5.23: Full P-Theta distribution in each of the selections in analysis bins as predicted by NEUT. The number of MC events is scaled to the expected data.

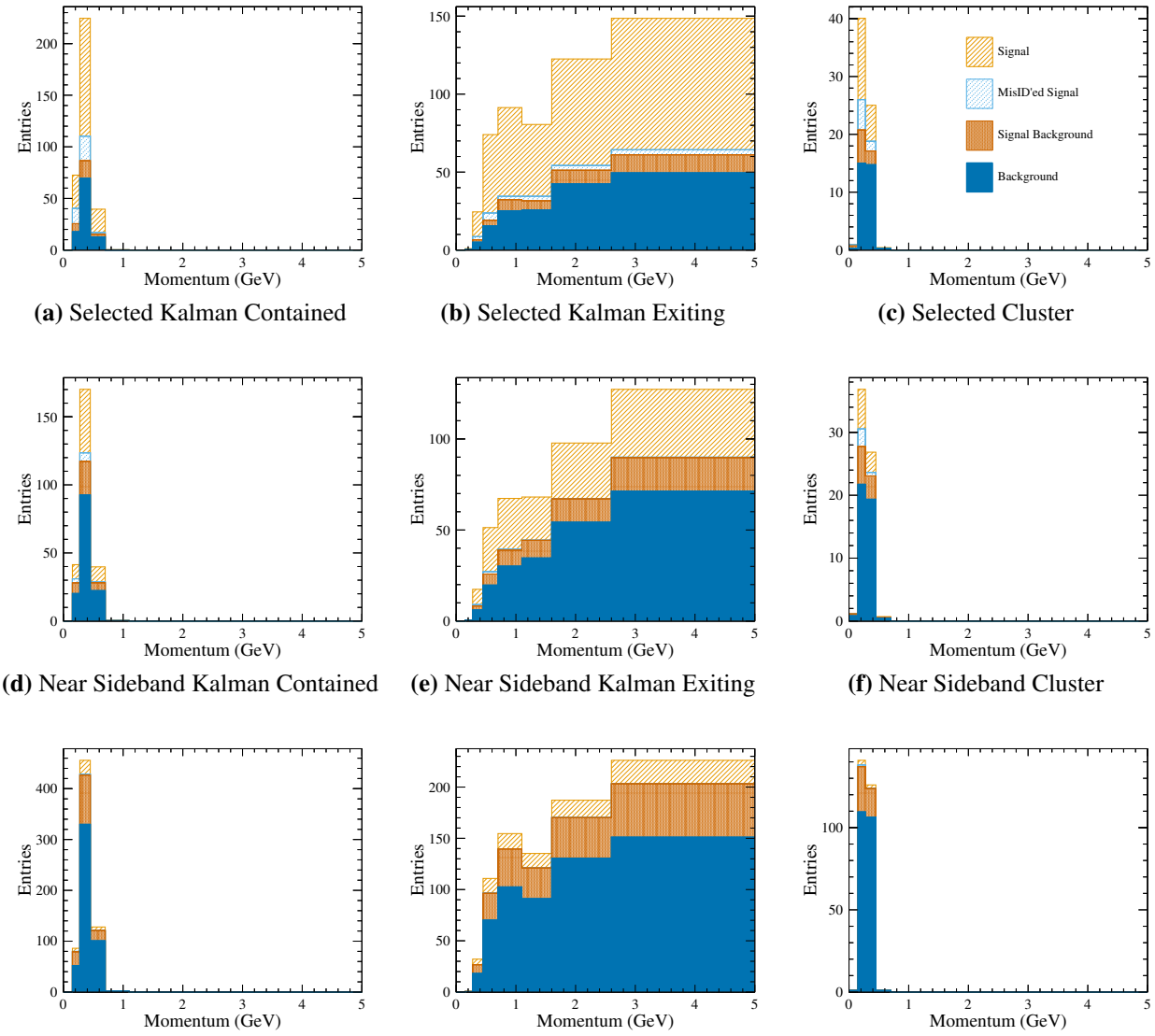

(a) Selected Kalman Contained **(b)** Selected Kalman Exiting **(c)** Selected Cluster

(d) Near Sideband Kalman Contained **(e)** Near Sideband Kalman Exiting **(f)** Near Sideband Cluster

(g) Far Sideband Kalman Contained **(h)** Far Sideband Kalman Exiting **(i)** Far Sideband Cluster

Figure 5.24: Muon momentum projection in analysis bins broken down by event category as predicted by NEUT. The number of MC events is scaled to the expected data.

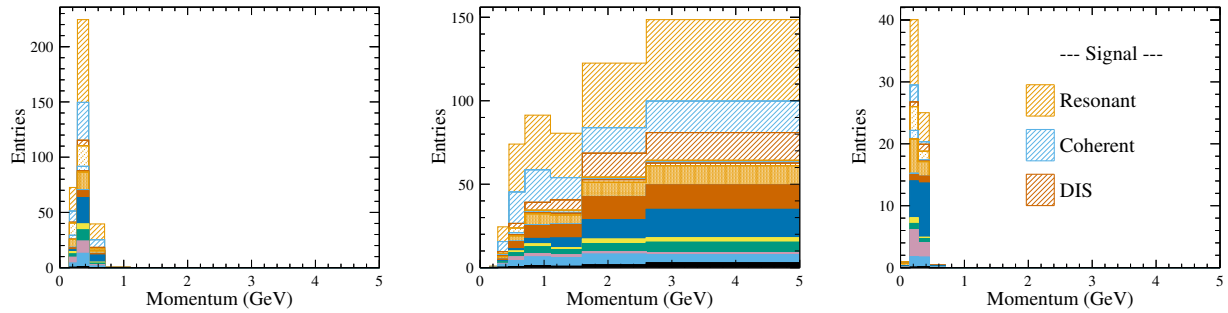

(a) Selected Kalman Contained **(b)** Selected Kalman Exiting **(c)** Selected Cluster

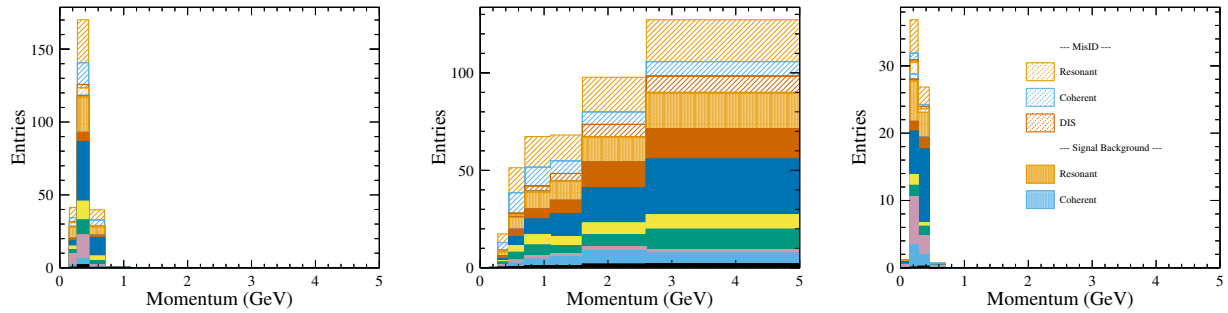

(d) Near Sideband Kalman Contained **(e)** Near Sideband Kalman Exiting **(f)** Near Sideband Cluster

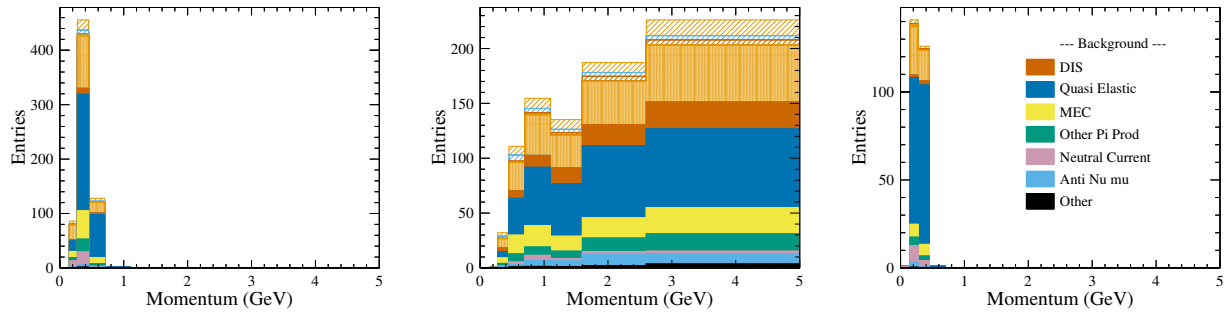

(g) Far Sideband Kalman Contained **(h)** Far Sideband Kalman Exiting **(i)** Far Sideband Cluster

Figure 5.25: Muon momentum projection in analysis bins broken down by primary interaction type as predicted by NEUT. The number of MC events is scaled to the expected data.

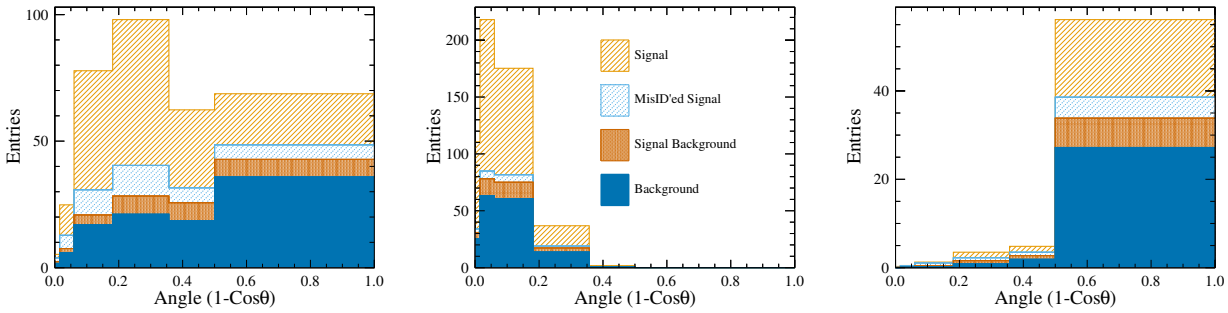

(a) Selected Kalman Contained **(b)** Selected Kalman Exiting **(c)** Selected Cluster

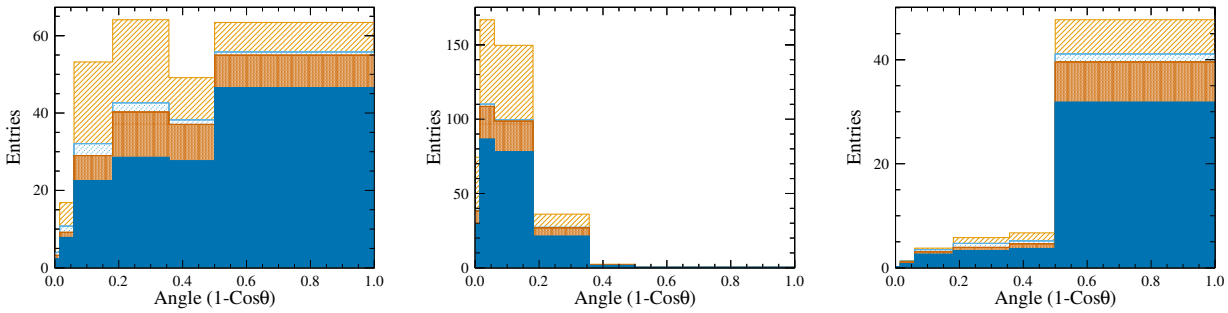

(d) Near Sideband Kalman Contained **(e)** Near Sideband Kalman Exiting **(f)** Near Sideband Cluster

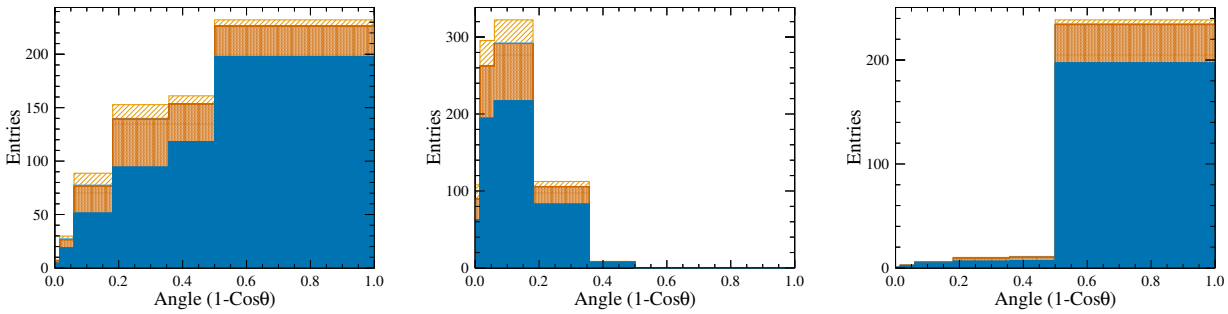

(g) Far Sideband Kalman Contained **(h)** Far Sideband Kalman Exiting **(i)** Far Sideband Cluster

Figure 5.26: Muon angle projection in analysis bins broken down by event category as predicted by NEUT. The number of MC events is scaled to the expected data.

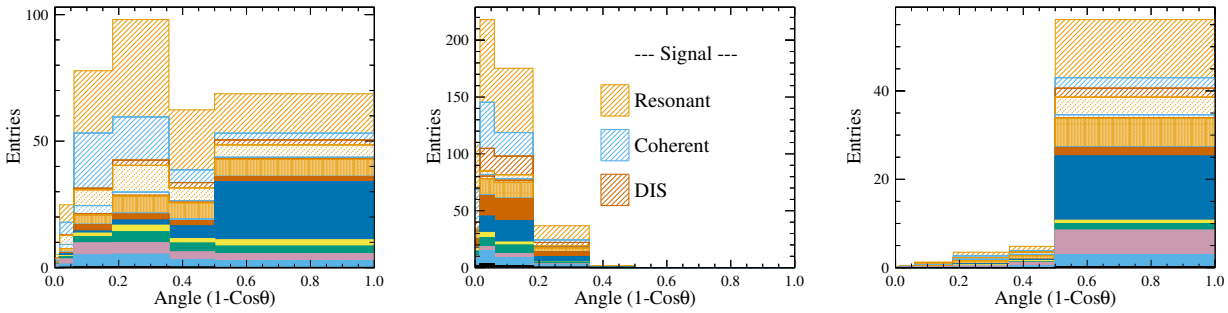

(a) Selected Kalman Contained **(b)** Selected Kalman Exiting **(c)** Selected Cluster

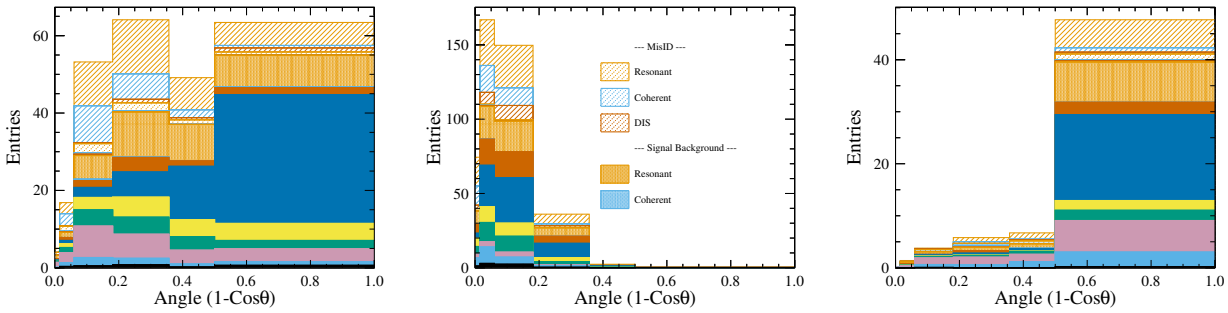

(d) Near Sideband Kalman Contained **(e)** Near Sideband Kalman Exiting **(f)** Near Sideband Cluster

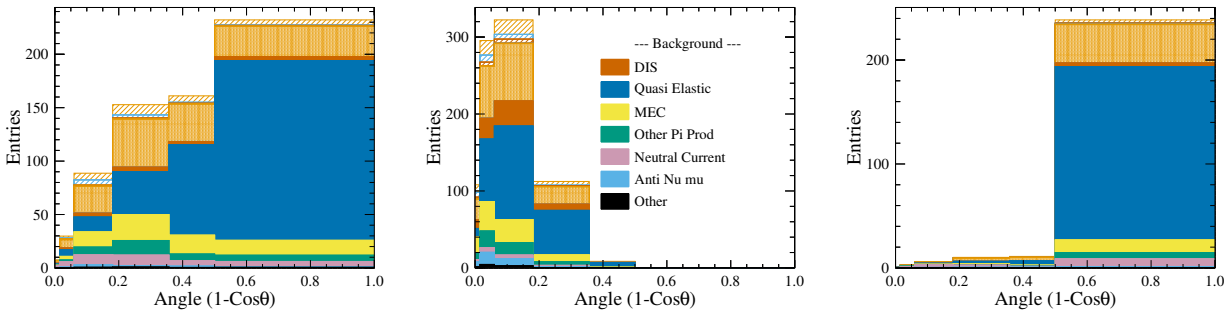

(g) Far Sideband Kalman Contained **(h)** Far Sideband Kalman Exiting **(i)** Far Sideband Cluster

Figure 5.27: Muon angle projection in analysis bins broken down by primary interaction type as predicted by NEUT. The number of MC events is scaled to the expected data.

Chapter 6

Signal Extraction

6.1 Introduction

6.1.1 Measuring the Signal

With the event selections for the analysis defined, the work of creating as pure of a signal region as possible has been done, and the next step is to evaluate the number of signal events within that event selection. An estimate of the amount of background contamination can be made through studying the MC, but relying solely on the MC for that estimate is not ideal, especially when event samples with high background purity have been defined. The strategy used in this analysis is to fit the MC to the sideband samples, adjusting the shape of the models in the MC until they fit the data. With the adjustments made to the background MC models, the prediction of backgrounds in the signal region is also adjusted, and thus better represents the true background in these samples. The amount of signal can then be fit alongside the fit to the backgrounds across all the samples.

6.1.2 Fitting the Signal

Though the method actually employed by the analysis is more complicated than that described above, the overall strategy is still the same. For this analysis a log-likelihood template fitter was built to provide a framework in which adjustments to the MC can be made so as to fit all nine analysis samples at the same time, ensuring that all changes are consistent across all samples. Special care is taken in this fitter to only use MC templates for the background models, allowing the fit to the signal to not be constrained by the MC models at all. A technique was developed for this analysis to allow the signal to be fit across the different samples in a way consistent with the known acceptance and efficiency differences of the different samples, and in this way the signal is fit in the selected and sideband regions at the same time. Another unique method was developed to

fit the background events that result from signal physics, as they could not be fit with MC models as that would introduce a dependence on signal physics models to the analysis.

6.1.3 Systematic Errors as Fit Parameters

The ways in which the MC is adjusted is by changing underlying features of the physics models, detector simulation models, and even reconstruction and analysis assumptions that determine how many events are in each analysis sample and each analysis p-theta bin. This is done by adjusting a parameter and seeing the effect it has on the events included in the sample. These parameters are characterized by the value they are thought to have, and the error on that value as evaluated by the community at large, T2K collaboration, or analyzers of this analysis. These parameters introduce the uncertainty to the measurement being made, and characterize the ways in which this measurement is influenced by the uncertainties. Called systematic errors, or systematics, these parameters represent errors that are introduced to the analysis by inaccuracy or uncertainty inherent to the models and measurements used in this analysis.

6.1.4 Chapter Contents

This chapter will go through the different classes of systematics and explain the motivation behind them as well as how they apply to this analysis. With the free parameters understood, the next section of this chapter will describe the fitter that was built to do the signal extraction, taking particular note of the special features that were included to keep to the goal of a model independent measurement.

6.2 Systematic Errors

6.2.1 Introduction

Systematic errors represent the uncertainty in a measurement or model. The models used to simulate the different physics interactions, the simulation of the detector, the measurement of the momentum of a particle, even the mass of the detector, all of these have an uncertainty on them

that has to be understood in order to make a measurement. These uncertainties can be in the form of measurement error, as is the case with the mass of the detector, or they can be in the form of deviation between model and reality, as it is with the physics models and reconstruction methods. In all of these cases, the uncertainty was characterized so that it could be propagated to the final result of this analysis. In some cases, as with the momentum, this calculation was done within the analysis, while for other situations like the accuracy of the physics models in NEUT, the uncertainty comes from the theoretical and experimental communities working together to make their best estimate of the accuracy of the models at hand.

Systematics as Measurement Errors

The systematics are characterized as errors on measurements, indicating how different a given value may be from its assumed central value. Alternately, especially in the case of physics models, systematics can be characterized as parameters that control the shape and amplitude of simulation models and varying these systematics within their allowed ranges can produce different distributions of events within the event generators. These parameters do still have a central value and error range on them, making them similar to measurement errors. What is important is that adjusting the systematics changes the distribution of events within and across the event selections. Seeing how the changes in a given systematic changes the number of signal events being measured provides a way to quantify the effect of that systematic on the final measurement.

Systematics as Fit Parameters

The effect of adjusting a systematic parameter and having it in turn adjust the number or distribution of events in the selection samples provides the perfect way to adjust the MC templates to match the data in the framework of the log-likelihood fit. Because the events for each of the samples are treated the same, from simulation physics to reconstructed properties, the systematic variations applied in one sample can and should be applied to all samples. Adjusting background parameters to fit background in the sidebands allows these same backgrounds to be estimated in

the selected region. Also, having multiple kinematic ranges to test across provides a cross check to the kinematic variations, as the samples are all fit at the same time.

6.2.2 Physics Model Systematics

The cross section and physics models used to simulate neutrino interactions in NEUT represent an attempt by the neutrino physics community to recreate the physics that has been measured by experiments and modeled by theorists. These models are continually being tested and refined and as such the confidence in these models is directly related to their agreement with available data, and the uncertainties on the free parameters of the models are set to reflect those confidence levels. The best physics models come from the theorists with theory driven ways to adjust the models - parameters that characterize the shape of the distribution of events. Other models have been modified by the experimentalists to provide means of adjusting the theoretical models to suit their purposes and explain the discrepancies found in data. Either way, these systematics represent the best attempt at characterizing the uncertainty in the models included in the event simulators and physics motivated uncertainties that the models can be adjusted within.

Cross Section

Variations of cross section models and parameters are done in the framework of T2KReWeight, a software package built to work with NEUT to reweight previously generated events so that the adjustments to the models can be studied without having to generate new sets of events.

Event weights work by changing the likelihood of a given event: if adjusting a dial means that events with given kinematics are more likely, then the event has more weight, effectively counting as more than one event when studied in the two dimensional histograms used to characterize the event selection. Similarly if an event is less likely to occur for a given systematic parameter value, the event can have a small weight, decreasing the presence of that event in the corresponding kinematic bin. Through this process, the shape of the templates used in the fitter are changed to reflect the new systematic parameter value. The list of parameters available to be adjusted is given in Table 6.1. Additionally there are parameters used to adjust the signal cross sections given in

Table 6.2, but these are not used in the fitter to change the signal templates, and instead are used only for the neutral-current or electron-neutrino-induced versions of the resonant and coherent interactions.

This table includes the names of the T2KReWeight dials, as well as their default values in T2KReWeight, the central value used in this analysis, and the absolute one sigma variation used in this analysis. All the dials used in this analysis are included in this table, however it is important to remember that in the signal extraction procedure there is no influence from the single-charged-pion production models. The dials that do affect the signal model are included only for software validation.

Final State Interaction

As with the cross section models, the models of Final State Interactions (FSI) used in the MC (Table 6.3) have an uncertainty that can be evaluated by using the dials in T2K ReWeight. This time it isn't the physics governing individual cross sections, but instead the physics that determines what interactions occur within a nucleus as particles are propagated from the initial interaction point through the nucleus and outside its influence. Although the FSI dials are not dependent on the signal physics models, they still contain enough interaction model dependence that they were not applied to the signal models within the fitter. That said, studies were done adjusting the signal model with the FSI parameters to ensure that the fitter could fit any variation to the signal models that the uncertainty in the FSI parameters could result in.

6.2.3 Flux Systematics

The number of neutrinos that pass through the PØD fiducial volume is an important component of the cross section measurement. To that end there is a group in the T2K experiment whose job it is to monitor the neutrino beam and characterize the number of neutrinos seen by the experiment. The group in charge of this is appropriately called the Beam group, and they provide not only a measurement of the number of neutrinos as a function of energy with errors for the different neutrino flavors present in the T2K beam, but also a covariance matrix that indicates how the errors

Table 6.1: Cross Section Parameters for Background Models

Parameter Name (analysis)	Parameter Description	T2K ReWeight Dial Name	Fit Central Value [Default Value]	Sigma (absolute)
MaCCQE	Axial Form Factor	kNXSec_MaCCQE	1.15 [1.2]	0.41
pF_C12	Pauli blocking parameter pF on Carbon	kNIWG2014a_pF_C12	223 [217]	31
pF_O16	Pauli blocking parameter pF on Oxygen	kNIWG2014a_pF_O16	223 [225]	31
Eb_C12	Binding Energy Eb for Carbon	kNIWG2014a_Eb_C12	25 [25]	9
Eb_O16	Binding Energy Eb for Oxygen	kNIWG2014a_Eb_O16	27 [27]	9
MEC_Norm_C12	Multi-nucleon component normalization for Carbon	kNIWGMEC_Norm_C12	0.27 [1]	0.29
MEC_Norm_O16	Multi-nucleon component normalization for Carbon	kNIWGMEC_Norm_C12	0.27 [1]	0.35
ccnuE0	Radiative corrections	kNIWG2012a_ccnueE0	1 [1]	0.03
dismpishp	CC other shape uncertainty	kNIWG2012a_dismpishp	0 [0]	0.4
nccohE0	NC coherent normalization	kNIWG2012a_nccohE0	1 [1]	0.3
ncotherE0	NC other normalization	kNIWG2012a_ncotherE0	1 [1]	0.3

Table 6.2: Cross Section Parameters for Signal Models

Parameter Name (analysis)	Parameter Description	T2K ReWeight Dial Name	Central Value	Sigma (absolute)
CA5RES	CA5	kNXSec_CA5RES	1.01	0.12
MaNFFRES	1pi axial form factor	kNXSec_MaNFFRES	0.95	0.15
BgSclRes	Isospin = 1/2 bkrd norm	kNXSec_BgSclRES	1.3	0.2
cccohE0_O16	CC coherent normalization on C, O	kNIWG2012a_cccohE0	1	1

Note: These dials affect signal channels and are not used in the fit, except as applied to some background channels (neutral-current or anti-neutrino-induced events).

Table 6.3: FSI Parameters

Parameter Name (analysis)	Parameter Description	T2K ReWeight Dial Name	Central Value	Sigma (absolute)
FSI_inel_lo	Inelastic scattering at low energy	kNCasc_FrInelLow_pi	1	0.41
FSI_inel_hi	Inelastic scattering at high energy	kNCasc_FrInelHigh_pi	1	0.34
FSI_PiProd	Pion production	kNCasc_FrPiProd_pi	1	0.5
FSI_PiAbs	Pion absorption	kNCasc_FrAbs_pi	1	0.41
FSI_cex_lo	Charge exchange at low energy	kNCasc_FrCExLow_pi	1	0.57
FSI_cex_Hi	Charge exchange at high energy	kNCasc_FrCExHigh_pi	1	0.28

Note: These dials affect signal and background channels and are used in the fit, but are applied only to the background channels.

are correlated between different neutrino energies and flavors. The flux systematics are therefore characterized as the error provided by the Beam group, but when the errors are varied within the framework of the fitter, the correlations are taken into account to ensure that the flux variations attempted by the fitter correspond to physically reasonable situations.

One optimization to the fitter that was done was to study the effect of the different flux systematic parameters to see the effect they have on this analysis. To cover the whole energy range for all the different flavors of neutrinos that make up the T2K neutrino beam, 30 parameters are required. These parameters include the muon neutrinos that create the events this analysis is designed to measure, but also the contamination of muon anti-neutrinos and electron neutrinos and electron anti-neutrinos. The design of this analysis (requiring a muon) is such that the neutrinos other than muon neutrino are not a significant contribution to the analysis, and the number of parameters was able to be greatly reduced.

The requirement for two MIP-like tracks in the analysis excluded the selection of events containing electrons, as well as excluding events that did not have a muon. These two features meant that the component of the neutrino beam made up of electron neutrinos and anti-neutrinos did not have a noticeable affect on this analysis, and all the electron (anti)neutrino flux parameters were not necessary. In their place a single dial was created to adjust the scale of electron neutrinos: NuMu_NuE_xsecRatio.

Though the products of muon anti-neutrinos were not as easily excluded from the analysis as electrons (as positive muons are similar in behavior to negative muons), the small number of muon anti-neutrinos in the neutrino beam were found to a small effect on the analysis and a corresponding normalization dial was created to represent the uncertainty in the ratio of anti muon neutrinos to muon neutrinos: NuMu_NuMuBar_xsecRatio.

The switch to the two new parameters reduced the number of flux systematic parameters from 30 to 13. This reduction in cross section parameters meant that there were fewer fit parameters that needed to be used in the fit, which improved the fit time without degrading the fit performance. The list of flux parameters are included in Table 6.4.

Table 6.4: Flux Parameters

Parameter Name (analysis)	Parameter Description	Sigma (%)	Number of parameters
NDNuModeNumu0-10	ν_μ flux	10	11
NuMu_NuMuBar_xsecRatio	$\nu_\mu/\bar{\nu}_\mu$ cross section ratio	20	1
NuMu_NuE_xsecRatio	$\nu_\mu/(\bar{\nu}_e + \nu_e)$ cross section ratio	24	1

Note: These dials affect signal and background channels and are used in the fit, but are applied only to the background channels.

6.2.4 Detector Systematics

Detector systematics represent the uncertainties inherent in both the physical detector, the modeling of the detector, and the reconstruction designed to measure events in that detector. Because these uncertainties apply to all particles that pass through the detector and are reconstructed, these are uncertainties that are applied to both the signal and background models in the fit. The full list of detector systematics is given in Table 6.5, each of which is detailed below.

Muon Track Angle And Momentum

The reconstruction of the angle and momentum was discussed in Chapter 3.4 and Chapter 3.5. The systematic error on the biases was evaluated using the data/MC studies, while the error on the resolution was taken from TN 238 which studied through going muons in the P∅D [28] to evaluate the momentum resolution. For cluster track resolution a conservative estimate was used to fully cover the uncertainty, based on data/MC studies.

Implementing these errors for biases involved adjusting the momentum of all tracks by the bias and creating a linear spline to adjust the bin content of the analysis spectra accordingly. or the resolution systematic, each event contributed to not only the p-theta bin it was reconstructed in, but also to any bin it might be reconstructed in given the resolution of the different reconstructed parameters. The contribution to each event was weighted by the percentage chance that the event would be in which bin. By adjusting the resolution, the width of possible momentum or angle values each event had would change, changing the percentage chance it was in any given bin, and

Table 6.5: All Detector Parameters

Parameter Name	Description	1 σ error
AngleBias	Reconstructed Angle Bias	0.03%
AngleRes	Reconstructed Angle Resolution	10%
P0DMomBias	PØD Reconstructed Momentum Bias	1.4%
P0DMomRes	PØD Reconstructed Momentum Resolution	7%
TPCMomBias	TPC Reconstructed Momentum Bias	0%
TPCMomRes	TPC Reconstructed Momentum Resolution	8.1
MuSelEff	Muon Selection Efficiency	data/MC ratio
PiSelEff	Pion Selection Efficiency	data/MC ratio
MuPiLike	MuPi PID Efficiency	data/MC ratio
(PDetEff	Proton Detection Efficiency	data/MC ratio
FidMassWater	Total Water Fiducial Mass	2%
FidMassOther	Not Water Fiducial Mass	1.5%
FidMassBags0	Water Layers: 1, 25	50%
FidMassBags1	Water Layers: 2-7	10%
FidMassBags2	Water Layers: 8-13	10%
FidMassBags3	Water Layers: 14-19	10%
FidMassBags4	Water Layers: 20-24	10%
SIelXsecRatio	Secondary Interaction Elastic Cross Section Ratio	10%
SIinelXsecRatio	Secondary Interaction Inelastic Cross Section Ratio	10%
oop_norm	out of PØD	100%

thus adjusting the weights in those bins. Table 6.6 shows the list of parameters considered, and their 1σ uncertainties.

Table 6.6: Reconstruction Parameters

Parameter	Track Property	Uncertainty
angleBias	Kalman Track Angle Bias	0.03%
	Cluster Track Angle Bias	0.03%
angleRes	Kalman Track Angle Resolution	10%
	Cluster Track Angle Resolution	10%
P0DMomBias	Kalman Track Momentum Bias	1.4%
	Cluster Track Momentum Bias	1.4%
P0DMomRes	Kalman Track Momentum Resolution	7%
	Cluster Track Momentum Resolution	7%
TPCMomBias	TPC Track Momentum Bias	0.0%
TPCMomRes	TPC Track Momentum Resolution	8.1%

Proton Detection Efficiency

The signal definition discussed in Chapter 5.2 requires that only two tracks be reconstructed in a CC $1\pi^+$ event: the muon and the pion. This definition requires that if the CC $1\pi^+$ event also had a proton in the final state, that proton had to be not reconstructed. The efficiency for detecting protons therefore must be compared between data and MC, as any mis-modeling in the proton detection efficiency would change the number of events selected by this analysis.

The proton efficiency was studied and found to be correlated with the number of hits the reconstruction associated with the proton. To understand the dependence on the number of hits, the proton tracks were compared directly between data and MC. The MIP-MVA Discriminant was used to develop a relatively pure sample of protons, and the number of hits was compared between the two. The ratio between data and MC was taken as the one sigma error on the proton efficiency, with a function fit to the data used instead of the data itself to remove any dependence on statistical variations specific to the data itself. The proton detection efficiencies for the MC and data are plotted in Figure 6.1.

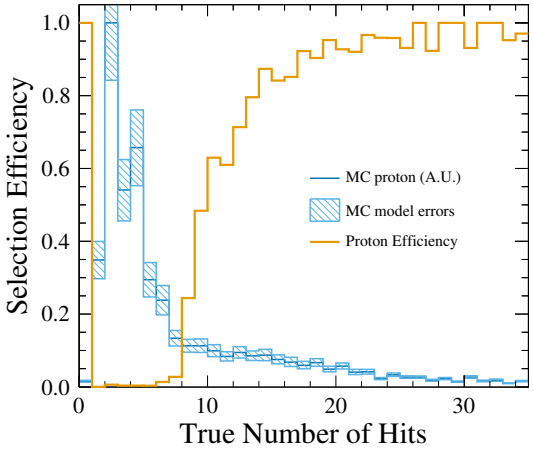

(a) Efficiency vs True Hits Per Bin

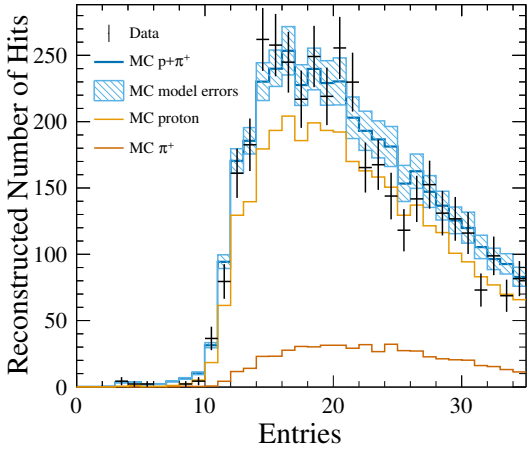

(b) Reconstructed Hits Per Bin

Figure 6.1: Proton detection efficiency as a function of the number of reconstructed hits. (a) The true number of hits per proton track overlaid with the detection efficiency. (b) The reconstructed number of hits per proton track for data and MC.

Muon and Pion Selection Efficiency

The identification and selection of muons and pions is described in Chapter 4.2 and Chapter 5.3.2 respectively. The events that make it into the different samples (selected and sidebands) are determined entirely by cuts on the MIP MVA response value. Evaluating the uncertainty on the MVA is therefore the goal of these systematics.

Assigning error to the MVA response values was done simply by comparing the distribution of the MVA response between data and MC, and assigning the difference to be the one sigma variation. This method was used instead of adjusting all the inputs to the MVA and propagating them through because, by design, the input variables to the MVA have very good data-MC agreement (see Appendix A for individual input data/MC comparisons). For the actual comparison, the shape of the data distribution for all selected events was smoothed so that comparisons could be made to data without being dependent on any statistical fluctuations in the data itself. Events were weighted by the muon or pion MVA response values, with the weights determined by the difference between the MC and the data function such that the plus one sigma variation shifted the MC to match the data function. With the events weighted by the MVA response values, the weighted p-theta dis-

tributions could be plotted, and a linear spline made for each bin to describe how to shift the bin from nominal to the weighted spectra. The value of the spline at the weight matching the data was defined as plus one sigma, with other values of sigma available by interpolating or extrapolating along that line. Plotted in Figure 6.2 is the MIP MVA response value distribution for Kalman and cluster tracks.

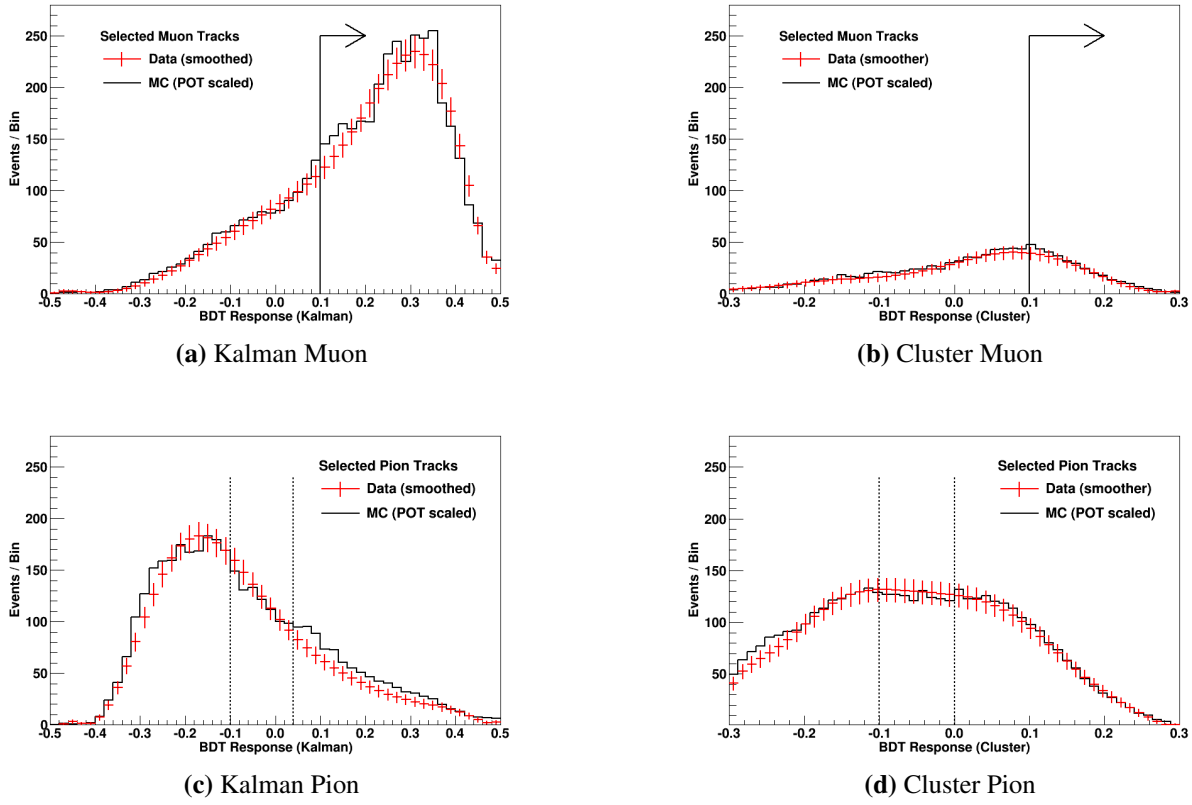

(a) Kalman Muon

(b) Cluster Muon

(c) Kalman Pion

(d) Cluster Pion

Figure 6.2: MIP MVA response values compared to smoothed data. The vertical lines represent the cut values used to define the different samples.

The uncertainty on the MVA response value is applied to muons and pions as two separate dials, to account for the different selection efficiencies for the two particles. The muon selection efficiency is plotted in Figure 6.3 and the pion selection efficiency is plotted in Figure 6.4. For both particles, the efficiency plots show fairly flat efficiency in angle over the region of interest, as well as fairly flat efficiency over the momentum distribution, the exception being the low momen-

tum bins for both particles. This feature was minimized by binning choices, but still exists, and requires careful consideration when it comes time to efficiency correct the final result, which will be discussed in Chapter 7.

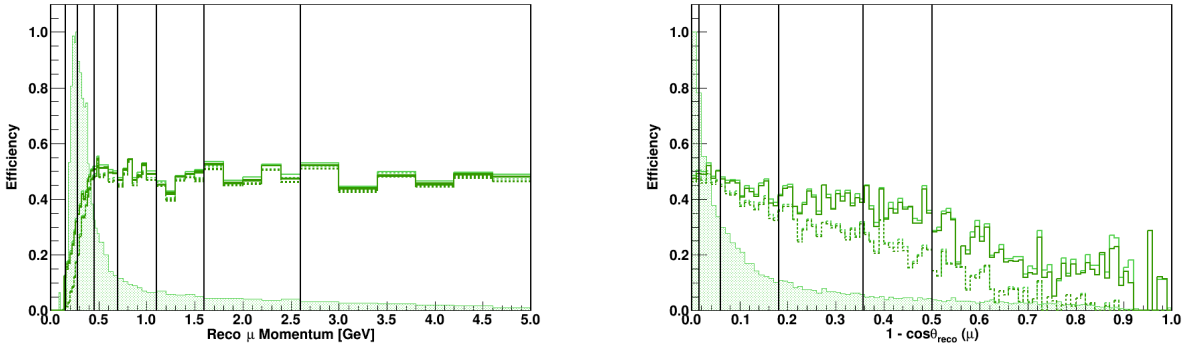

(a) Momentum **(b)** Angle

Figure 6.3: Muon selection efficiency. The solid line is for all selected muons, the dashed line for all correctly identified selected muons, and the solid background histogram is the distribution of events to indicate the region of interest.

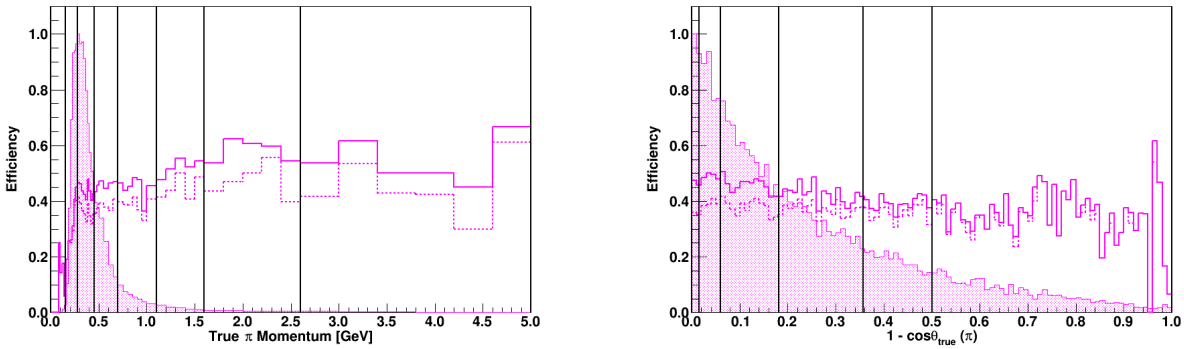

(a) Momentum **(b)** Angle

Figure 6.4: Pion selection efficiency. The solid line is for all selected muons, the dashed line for all correctly identified selected muons, and the solid background histogram is the distribution of events to indicate the region of interest.

TPC Matching When selecting events, tracks that exit the PØD through the downstream face are required to match to a TPC track. Tracks that should have been matched but were not are excluded from the analysis, and corrected for by the efficiency corrections. Both the procedure for carrying out the TPC matching and the analysis of the uncertainty on the TPC matching is done using the procedure from TN208 [29], which found an uncertainty of 0.3%. The propagated effect of the TPC matching uncertainty on this analysis is small, with nearly 100% of events correctly matched, and is thus accounted for with the existing muon selection efficiency and neglected in this analysis.

Particle Identification

The PID method described in Chapter 4 is another place where a complex MVA response value is used in this analysis, this time it is complicated further by the log-likelihood method that combines Kalman and cluster track information together with TPC information to give one PID result for each event. As with the muon and pion selection efficiencies, the PID systematic is also calculated by comparing smoothed data to the MC and using the difference between them to weight events and define the one sigma variation. The data and MC distribution of the PID value is plotted in Figure 6.5.

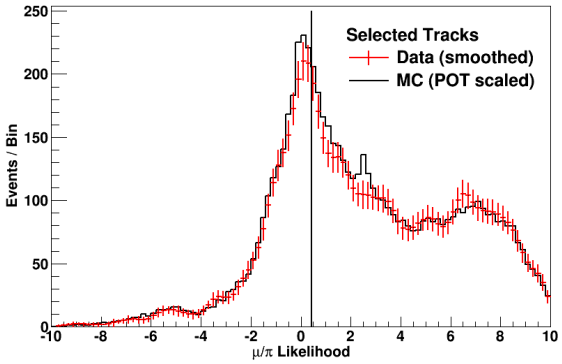

Figure 6.5: PID result for all selected events plotted for data and MC for both water in and water out PØD configurations.

Fiducial Mass

The fiducial mass calculation is discussed in Chapter 1.3.4 and the errors on the total mass are provided in Table 1.3 and Table 1.4, which are used to create the fiducial mass systematics. For this systematic the location in the PØD of the vertex was used to determine which material was being interacted with, allowing the correct weights to be assigned to each event.

For the water target, the systematic was broken into multiple pieces. Initially there was one parameter for each water layer to account for the fact that events in different water layers have different acceptance. For example, the more upstream water layers are more likely to have high momentum contained events than the downstream water layers, and similarly the downstream water layers can have a higher angular distribution for events entering into the TPC than events originating in the upstream layers. Through testing it was found that combining the bags into groups was sufficient to provide the freedom necessary for the acceptance differences, while assisting the fitting by requiring fewer systematic parameters. Large systematics were assigned to cover the combination of multiple bags as well as to account for any other errors related to filling the water bags. Though the systematics are large, they were found to have very little effect on the final measurement.

Table 6.7: Fiducial Water Parameters

Parameter Name	Description	Sigma
FidMassOther	Non-Water Mass	1.5%
FidMassWater	Total Water Mass	2%
FidMassBags1	Water Layers: 1-6	10%
FidMassBags2	Water Layers: 7-12	10%
FidMassBags3	Water Layers: 13-18	10%
FidMassBags4	Water Layers: 19-24	10%
FidMassBags0	Water Layers: 25	50%

Pion Secondary Interactions

As pions travel through the PØD they slow by ionizing the material they travel through or by interacting hadronically. Unlike ionization, hadronic interactions tend to change or end the pion track, which is a feature that makes it difficult to reconstruct the momentum of pions within the PØD. These hadronic interactions are referred to as secondary interactions (SI) due to them occurring well after the primary neutrino interaction that created the pion. The modeling of the secondary interactions was important to the analysis because any uncertainty in that modeling could produce pions that traveled different distances in the simulation than pions in the data, and/or undergo secondary interactions more or less frequently. These variations would propagate to the analysis by affecting the chance of an event to pass precuts, be selected for different samples (signal, near-sideband, or far-sideband), or the chance for the muon and pion to be misidentified. To characterize this uncertainty, weights were adjusted for different events based on the pion kinematics and for different variations in the probability of secondary interactions. The probability for secondary interactions is of course characterized by the cross section for these events to occur, so the cross section was extracted from the simulation and varied.

Pion secondary interactions are modeled by GEANT4, a simulation package designed to propagate particles through matter. The model for simulating pion secondary interactions within GEANT4 is the QGSP_BERT model [30] and the GEANT4 Bertini cascade [20]. To develop a reweight scheme that could account for the uncertainties in these models, the cross section for pions undergoing elastic or inelastic secondary interactions were extracted from the models for a number of different targets. Comparing these cross sections with global data from the DOSSIER data base [31] motivated an error of approximately 10% to be applied to the cross sections. Propagating that error produced a cross section band for the elastic and inelastic cross sections for the different targets that was found to cover the data quite well, and thus was used to calculate the event weights for the systematic parameters.

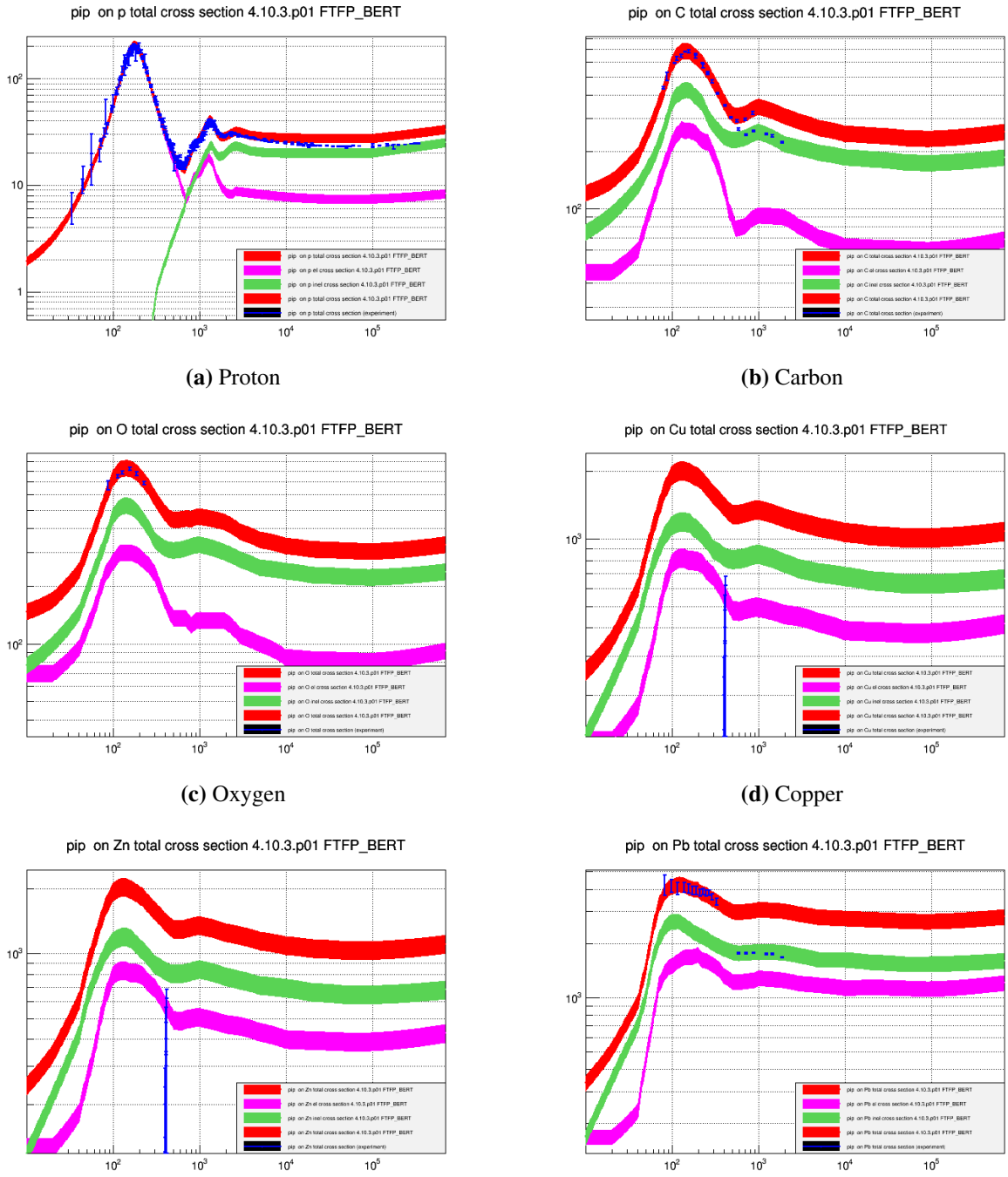

(a) Proton

(b) Carbon

(c) Oxygen

(d) Copper

(e) Zinc

(f) Lead

Figure 6.6: Pion interaction cross section as a function of neutrino energy on different targets for elastic and inelastic processes with a 10% error band and over plotted with data where available. The top (red) curve is the total cross section band, the middle (green) curve is the elastic cross section band, and the bottom (purple) curve is the inelastic cross section band.

Vertex Resolution and External Tracks

Out Of PØD Events with a true interaction outside the PØD that are reconstructed as starting within the fiducial volume of this analysis are exceedingly small. This is due primarily to the fact that to be considered for this analysis an event must have a vertex with two associated tracks within the fiducial volume. An event that originated outside the PØD is very unlikely to have two tracks close enough together by the time they reach the fiducial volume, nor is it likely that one track from outside the PØD will enter the fiducial volume in such a way as to meet up with another unassociated track to look like a pair that started within the PØD. Because of this, the decision was made to implement a simple scaling dial to account for this effect, giving it a 100% range of freedom.

Vertex Resolution and Fiducial Volume The definition of the fiducial volume introduces some error in that an event that is reconstructed within the fiducial volume may have actually originated outside the defined boundary. This mistake occurs when the vertex is incorrect, and thus the error on the vertex position can be used to account for this situation. In addition to the chance that an event reconstructed within the fiducial volume may have truly occurred outside the fiducial volume, there is also the reciprocal case of events reconstructed outside the fiducial volume being reconstructed within it. These two cases have the effect of canceling each other out when looking at the X and Y fiducial boundaries, but the change in acceptance of events at the upstream and downstream edges of the fiducial boundaries means that this argument cannot be applied to the Z direction. However, it was found that applying a 100% error on these events studies showed negligible effect on the analysis. The uncertainty on the fiducial mass of the edge bags, which make up the upstream and downstream boundaries of the fiducial volume, was considered sufficient to cover any effect from events moving through the upstream or downstream Z faces.

6.3 Template Binned Log-Likelihood Fit

6.3.1 Introduction

The binned log-likelihood fitter built for this analysis used the systematic parameters to adjust the different MC templates to get the MC to most closely match the shape and amplitude of data across all nine samples. The MC was broken down into different templates to make plotting and coding easier and more intuitive, with the templates separated by NEUT interaction type. The systematics described above were used to adjust these templates, independently or in groups, to change the shapes and amplitudes of the affected templates across all samples in a consistent manner. Signal bins were also included as part of the fit, independent for each p-theta bin in each of the three muon kinematic samples (Kalman contained, Kalman exiting, cluster all). The amount of signal within one muon kinematic sample was split between the selected and sideband samples in ways determined not by interaction physics but instead by reconstruction and detection efficiencies, so these events were scaled together providing a way to constrain the signal measurement across samples without relying on physics models of the signal. Lastly a method was used to scale the mis-ID'ed and signal background contribution to each sample off of the signal in each sample, allowing these background events to be characterized without relying on the physics model.

The fitter used the Minuit2 minimization algorithm implemented in ROOT [26] to minimize the χ^2 calculated by comparing the entries between data and simulation. Minuit2 works to adjust given parameters to explore the phase space available, always seeking for the minimum then characterizing the space around the minimum to compute the one sigma ranges for each parameter. In the fitter, this algorithm involved iteration, changing the fit parameters to minimize the χ^2 in different combinations and amounts until the best fit was achieved by finding the minimum in χ^2 space. Over hundreds or thousands of iterations the combination of fit parameters was found and reported as the fit result.

The technical details of the fitter are described below, starting with the components that make up the fitter. Once the pieces of the fitter are understood, the binned log-likelihood method used to perform the actual fit is detailed, followed by the propagation of errors that is done within the

fitting framework. Lastly is a selection of fitter validation studies that demonstrate the effectiveness of the template fitter.

6.3.2 Fitter Components

The mock data is stored in the fitter in a number of templates that can each be adjusted by any number of systematic dials. To understand the relation between the systematics and the templates, an explanation of how the mock data is stored and manipulated is presented here.

Samples (Spectra)

This analysis breaks down data samples and Monte Carlo inputs into nine samples, as described in Chapter 5.3. These samples consist of selected and sideband events for the three muon reconstruction categories, binned in muon momentum and angle. The distribution of events in one of the nine samples, plotted as a muon p-theta histogram, is referred to here as a spectra, the contents of which are compared between data and Monte Carlo to calculate the χ^2. The events from one spectra are divided between a number of interaction channels, each of which forms a template that is added to all the other channel templates to make the spectra. The nine spectra are:

- Selected

  Kalman Contained, Kalman Exiting, Cluster

- Near Sideband

  Kalman Contained, Kalman Exiting, Cluster

- Far Sideband

  Kalman Contained, Kalman Exiting, Cluster

Sample Subdivisions (Templates/Channels)

The subdivisions that make up a single spectra are the templates that are adjusted in the fit. For this analysis the templates are interaction channels defined by NEUT interaction codes, as listed in Table 6.8. The templates used in this analysis were chosen to best represent the signals and

backgrounds important to the CC $1\pi^+$ measurement. It is important to note that the functionality of the fitter is not dependent on the specific subdivisions, and would work exactly the same with any number or division of templates, provided that the signal, misidentified signal, signal backgrounds and backgrounds stayed independent.

Table 6.8: Channel Template Definitions

Template Name	Interaction Mode	NEUT Code	Additional Requirements
pipn$*$	resonant pion production	11, 13	signal, correctly ID'ed
coh$*$	coherent pion production	16	signal, correctly ID'ed
dis$*$	DIS single-pion production	21, 26	signal, correctly ID'ed
sig	sum of the above three	11, 13, 16, 21, 26	signal, correctly ID'ed
mpipn$*$	mis id-ed resonant pion production	11, 13	signal, mis ID'ed
mcoh$*$	mis id-ed coherent pion production	16	signal, mis ID'ed
mdis$*$	mid id-ed DIS single-pion production	21, 26	signal, mis ID'ed
msig	sum of the above three	11, 13, 16, 21, 26	signal, mis ID'ed
bpipn$*$	background resonant pion production	11, 13	not signal
bcoh$*$	background coherent pion production	16	not signal
bsig	sum of the above two	11, 13, 16	not signal
bdis	DIS not signal-pion production	21, 26	not signal
bqel	quasi elastic	1	not signal
bmec	multi nucleon	2	not signal
bopp	other pion production	12	not signal
bnnc	neutral-current	> 30	not signal
bbar	anti neutrino	< 0	not signal
both	other	!(11, 13, 16, 1, 2, 12, 21, 26, > 30, < 0)	not signal

$*$ Channels provided for completeness but not used for signal extraction

Fit Parameters (Systematics)

The fit parameters are used to adjust the shape and normalization of the templates which allows the MC prediction to change to improve agreement with the data. In order to apply a parameter shift to a spectra, the splines associated with that parameter are evaluated at the new parameter value to produce a weight for each kinematic bin. The weights from the multiple splines, each associated with a parameter shift, are combined and then applied to the nominal bin content. One fit parameter can affect any number of templates in any number of spectra. A change to a single parameter can affect one or more templates across many spectra, allowing systematic parameters to be constrained by sideband samples.

The systematics used in this analysis are described in Chapter 6.2, and the properties of each systematic (central value, one sigma range, minimum and maximum allowed range) are available to the fitter. The fit parameter properties and current value are used within the fitter for determining subsequent test values for the parameter as the fitter works to best fit the data. The channels affected by each systematic are also associated with each fit parameter as listed in Table 6.9. Because the fit procedure does not apply constrains to the signal, any theory model systematics that would affect signal and background are applied only to the background templates, and not to the signal.

Fit Parameter Splines

Splines are the functional relation between systematics and templates. For each template affected by a systematic, a spline is built for each kinematic bin to represent how the number of events in that bin change as the systematic changes. This allows events to effectively fluctuate between kinematic bins and between analysis samples in an inclusive way, or to scale up or down or simply change shape, depending on the systematic parameter. How the weight of an event changes for a given systematic is described in Chapter 6.2, but the procedure for building the splines remains the same:

1. Determine the central or best value for the parameter.

2. Determine the one sigma variation for the parameter.

Table 6.9: Signal Extraction Systematics and Affected Channels.

Parameter	Affected Channels
Cross Section Dials	
MaCCQE	bqel, bbar
pF_C12, O16	bqel, bbar
Eb_C12, O16	bqel, bbar
MEC_Norm_C12, O16	bmec, bbar
CA5RES	bopp, bnnc, bbar
MaNFFRES	bopp, bnnc, bbar
BgSclRES	bopp, bnnc, bbar
ccnuE0	bdis, bqel, bmec, bopp, bbar
dismpishp	bdis, both, bbar
nccohE0	bnnc, bbar
ncotherE0	bnnc, bbar
FSI Dials	
FSI_inel_lo	bdis, bqel, bmec, bopp, bnnc, bbar, both
FSI_inel_hi	bdis, bqel, bmec, bopp, bnnc, bbar, both
FSI_PiProd	bdis, bqel, bmec, bopp, bnnc, bbar, both
FSI_PiAbs	bdis, bqel, bmec, bopp, bnnc, bbar, both
FSI_cex_lo	bdis, bqel, bmec, bopp, bnnc, bbar, both
FSI_cex_Hi	bdis, bqel, bmec, bopp, bnnc, bbar, both
Flux Dials	
NDNuModeNumu0-10	bdis, bqel, bmec, bopp, bnnc, both
NuMu_NuMuBar_xsecRatio	bbar
NuMu_NuE_xsecRatio	bdis, bqel, bmec, bopp, bnnc, bbar, both
Detector Systematic Dials	
AngleBias	sig, msig, bsig, bdis, bqel, bmec, bopp, bnnc, bbar, both
AngleRes	sig, msig, bsig, bdis, bqel, bmec, bopp, bnnc, bbar, both
P0DMomBias	sig, msig, bsig, bdis, bqel, bmec, bopp, bnnc, bbar, both
P0DMomRes	sig, msig, bsig, bdis, bqel, bmec, bopp, bnnc, bbar, both
TPCMomBias	sig, msig, bsig, bdis, bqel, bmec, bopp, bnnc, bbar, both
TPCMomRes	sig, msig, bsig, bdis, bqel, bmec, bopp, bnnc, bbar, both
MuSelEff	sig, msig, bsig, bdis, bqel, bmec, bopp, bnnc, bbar, both
FidMassWater	sig, msig, bsig, bdis, bqel, bmec, bopp, bnnc, bbar, both
FidMassOther	sig, msig, bsig, bdis, bqel, bmec, bopp, bnnc, bbar, both
FidMassBags	sig, msig, bsig, bdis, bqel, bmec, bopp, bnnc, bbar, both
SIelXsecRatio	sig, msig, bsig, bdis, bqel, bmec, bopp, bnnc, bbar, both
SIinelXsecRatio	sig, msig, bsig, bdis, bqel, bmec, bopp, bnnc, bbar, both
oop_norm	sig, msig, bsig, bdis, bqel, bmec, bopp, bnnc, bbar, both

3. Determine the range of desired values for the parameter.

4. Define step sizes that capture the structure of the event rate variations, with greater resolution around the central value.

5. Evaluate the weight of each event in the Monte Carlo for the parameter at each chosen step.

6. Plot the weighted events with the analysis binning used by the fitter.

7. For each bin, record the weighted number of events in that bin compared to the default number of events in that bin. Do this for every chosen step in parameter value.

8. For each bin, plot the ratio of weighted to the nominal number of events as a function of parameter values in units of σ.

Splines are evaluated via linear interpolation between points. An example of the splines is given in Figure 6.7, where the splines for each individual bin are plotted separately, showing how each bin adjusts independently as the parameter value is changed.

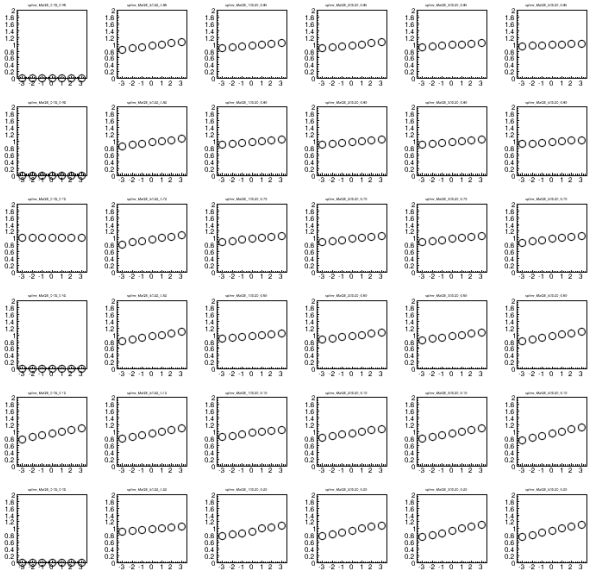

Figure 6.7: An example of splines built to adjust the contents of the bqel template bin by bin for given adjustments of the MaCCQE systematic dial. Each plot represents one p-theta bin, and each point within a plot represents the shift in the number of events in that bin when the systematic has be adjusted a given amount from nominal.

Signal Bin Weights

The signal bin weight normalization parameters are used to adjust the signal Monte Carlo template to fit the data. What is different about signal bin weights, as compared to the other parameters, is that they have no central value, uncertainty range, or pre-defined range of validity and no bin-to-bin correlation. These parameters are permitted to take any value in any bin so as to best fit the data. These bins are constrained within a muon kinematic sample: within the Kalman contained sample, the bin weight applied to bin i in the selected sample is the same weight applied to bin i in the near and far sideband samples as well. Because there are background templates in all spectra, the effect of the signal bin weights is to effectively produce the result of a background subtraction; the number of data events minus the number of background events gives the number of signal events. Thus the default signal model is scaled in that bin to account for the difference between the number of predicted background events and the data.

Because these bin weights are independent across bins (but constrained within muon reconstruction categories), they do not depend on the initial signal model they are scaling. The distribution of signal within these three categories (across the Selected, Near Sideband, and Far Sideband samples) is determined by selection and detection efficiencies, both of which are dependent only on the detector model, and not the physics models. This means that the same signal bin weight can be applied to a bin across the Selected and Sideband regions, as long as they are all within the same muon kinematic category. Using one parameter across three spectra allows that parameter to be constrained, as there are fewer free parameters than bins, while also ensuring that the signal determination is (physics) model independent.

6.3.3 Signal Background Treatment

Signal events where the muon and pion are misidentified (mis-ID'ed events, Chapter 5.3.3), or true resonant or coherent events that make it into the sample without having both a muon and pion reconstructed (signal-background events, Chapter 5.3.4) are handled carefully in this analysis. These events are not by definition signal events, either because the wrong particle is identified as

a muon, or because the two particles are not muon and pion. Unfortunately these events are in all of our samples and therefore must be fit. Because these events are created by signal physics they cannot be fit with physics models because doing so would introduce signal model dependence into the measurement, which this analysis is specifically trying to avoid.

The solution to this problem was to relate the number of mis-ID'ed events and the number of signal-background events to the number of measured signal events. The one thing all these events have in common is that the events do have a true muon, and so they can be related to one another through true muon space. An important caveat to make before continuing, is that there is no fit done in true muon space - it is simply used as a way to relate the number and distribution of mis-ID'ed and signal background events to the number of measured signal events. The primary reason for events to be classified as signal or signal-background is detector acceptance and efficiency. Because the detector response is modeled well in the simulation, the ratio of events with given true muon kinematics ending up in signal and signal-background bins given by the simulation can be trusted. Because this method depends on detector simulation, using this method does not introduce much, if any, signal model dependence to the measurement.

Scaling Signal-Backgrounds from Measured Signal Bins

The following procedure is done for all nine samples.

First, a number of reference muon p-theta templates have to be built:

- SigReco^{ref}

  The reconstructed muon p-theta distribution of the signal

- SigTrue$_i^{ref}$

  The true muon p-theta distribution of the signal for the events in the i'th bin of SigReco^{ref}

- SigTrue^{ref}

  The true muon p-theta distribution of the signal

- BkgTrue^{ref}

  The true muon p-theta distribution of the signal-background

- BkgReco$^{ref}_{j}$

  The reconstructed muon p-theta distribution of the signal-background for the events in the j'th bin of BkgTrue^{ref}

With these templates the procedure for scaling the signal-backgrounds is:

1. Measure the reconstructed signal muon p-theta distribution: SigReco^{data}

2. Compare the measured muon p-theta distribution to the reference reconstructed muon p-theta distribution to get individual bin scale factors b_i:

$$b_i = \frac{\text{SigReco}^{data}_{i}}{\text{SigReco}^{ref}_{i}} \tag{6.1}$$

3. Apply the b_i scale factors to the individual bin true p-theta signal distributions, then add them together to get the total true signal p-theta distribution, weighted by data: SigTrue^{data}.

$$\text{SigTrue}^{data} = \sum_{i} b_i \times \text{SigTrue}^{ref}_{i} \tag{6.2}$$

4. Compare the weighted true muon p=theta distribution to the reference true muon p-theta distribution to get individual bin scale factors c_j

$$c_j = \frac{\text{SigTrue}^{data}_{j}}{\text{SigTrue}^{ref}_{j}} \tag{6.3}$$

5. Apply the c_j scale factors to the individual bin reco p-theta signal-background distributions, then add them together to get the total reco signal-background p-theta distribution, weighted by data: BkgReco^{data}.

$$\text{BkgReco}^{data} = \sum_j c_j \times \text{BkgReco}_j^{ref} \tag{6.4}$$

The final BkgReco^{data} that is returned from this method is an estimate of the number of signal-background (or mis-ID'ed) events given the number of measured signal events. This method allows for shape change of the signal-background and mis-ID'ed templates to reflect the measured signal.

Application within the Fitter

This procedure is carried out at every iteration in the fitter when the unconstrained signal bins change to better fit the data. This means that the signal normalization bins affect not only the shape of the signal, but also the shape of the signal background and mis-ID'ed templates. In practice, the measured signal in the "selected" samples are used to extract the c_j weights for the three muon reconstruction categories (contained, exiting, or cluster). The associated weights are then used to scale the mis-ID'ed and signal-background templates in the associated three samples ("selected", "near sideband", "far sideband"). Although there is some level of signal in all the samples, the "selected" category is used to extract the weights because it is the best measurement of the signal for each muon reconstruction category.

6.3.4 Binned Log-Likelihood Fit

The fitter uses a binned log-likelihood χ^2 minimization. The calculation is a comparison at a particular point in parameter space between the Monte Carlo and the data:

$$\chi^2_{\text{total}} = \sum_i^{\text{bins}} \frac{(N_i^{\text{MC Signal}} + N_i^{\text{MC Background}} - N_i^{\text{Data}})^2}{N_i^{\text{Data}}} \tag{6.5}$$

where N is the number of events in a data or Monte Carlo bin (signal + background) and the total χ^2 is the sum of this quantity across all the kinematic bins.

In practice, a number of parameters are applied to the Monte Carlo to get the simulation to best match the data and thus minimize the χ^2:

$$\chi^2_{\text{total}} = \sum_{i}^{\text{bins}} \left(\frac{(N_i^{\text{MC Signal}} Z_i + N_i^{\text{MC Background}} \sum_m W_m - N_i^{\text{Data}})^2}{N_i^{\text{Data}}} \right) + \sum_n P(W_n) \tag{6.6}$$

where Z_i are the unconstrained weights applied to the MC signal, and W_m are the weights from each systematic spline which are applied to the backgrounds. Because the systematics applied to the background are constrained, there is also a penalty term in the χ^2 calculation of the form:

$$P(\text{systematic}) = \left(\frac{\text{current value} - \text{central value}}{1\sigma \text{ uncertainty}} \right)^2 \tag{6.7}$$

where the central values and 1σ uncertainties are unique to each systematic, as indicated on the tables in Chapter 6.2. The penalty term increases the result of the χ^2 calculation the further from nominal a dial is pushed.

This is still a simplified version of the χ^2 equation. As discussed in Chapter 5.3, in this analysis a number of selections and samples are fit simultaneously. The sidebands provide regions that can constrain the backgrounds, while the contained, exiting (and cluster) samples give access to different regions of muon kinematics. Together with the different samples are the systematics which are applied the same across all samples, or across all selections within a sample. With these complexities added, the χ^2 equation becomes:

$$\chi^2 = \sum_{k}^{\text{samp}} \left\{ \sum_{i}^{\text{bins}} \sum_{j}^{\text{sel}} \left(\frac{(N_{ijk}^{\text{MC Signal}} Z_{ik} + N_{ijk}^{\text{MC Background}} \prod_m X_m - N_{ijk}^{\text{Data}})^2}{N_{ijk}^{\text{Data}}} \right) \right\} + \sum_m P(X_m) \tag{6.8}$$

where X_m replaces the W_m from the previous equation, representing the systematics that are applied across all samples. Note that the index k is for the three samples (contained, exiting, cluster), the index i is for the 48 p-theta bins, and the index j is for the three selections (selected, near sideband, far sideband).

When the χ^2 is minimized, the final number of measured signal events in a bin is then given by the best-fit values of the signal fit parameters:

$$N_{ijk}^{\text{best fit Signal}} = N_{ijk}^{\text{MC Signal}} Z_{ik}^{\text{best fit}} \tag{6.9}$$

Background Error Propagation

The fit is done by minimizing the χ^2 across all samples and selections. Once the best fit value has been found, the minimizer proceeds to explore χ^2 space to find the one sigma error range for each of the fit parameters. The result is a set of best-fit parameter values for each systematic and signal bin as well as one sigma values for each parameter. Applying the one sigma parameter values allows for the calculation of the error on the extracted signal by following the same procedure as extracting the signal itself:

$$N_{ijk}^{\text{Signal}+1\sigma} = N_{ijk}^{\text{MC Signal}} Z_{ik}^{\text{best fit}+1\sigma} \tag{6.10}$$

$$N_{ijk}^{\text{Signal}-1\sigma} = N_{ijk}^{\text{MC Signal}} Z_{ik}^{\text{best fit}-1\sigma} \tag{6.11}$$

The final result is then an extracted signal obtained from (6.9) and errors extracted from (6.10) and (6.11), given below:

$$N_{ijk}^{\text{Signal}} = N_{ijk}^{\text{Signal}} \}^{+N_{ijk}^{\text{Signal}+1\sigma}}_{-N_{ijk}^{\text{Signal}-1\sigma}} \tag{6.12}$$

The fit also produces a covariance matrix that encodes the relationships between the uncertainties on the best-fit fit parameters. This procedure is correct as long as the correlations between the signal bin normalization parameters and the background model parameters is small. If the correlations are large the uncertainties must be profiled (or marginalized) over. The component of the correlation matrix that contains the signal bin normalization parameters is also an essential part of the result, as it encodes the relationship between the uncertainties for each bin.

6.4 Fitter Studies

As part of validating the functionality of the fitter, many studies were done with many different types of mock data and different combinations of the fitter. After fundamental validation was done, the real test was to see how well the fitter performed at fitting mock data that varied from the default templates in different ways. The mock data studies that were done fell into a few categories:

- use systematics to adjust the signal models
- use systematics to adjust the background models
- new signal models
- new background models
- statistical throws

Using the implemented systematics to adjust the default templates to make mock data allowed for quick and varied mock data generation, allowing the analysis to test the fitter extensively. Adjusting multiple systematics made the fitting more complicated, and it was found that large variations to the background models caused the fitter to have a little trouble with the fit - but the background models are ones that are better understood and thus not expected to vary too much outside predictions. Even then, mock data had to be made with ALL background dials adjusted $> 1\sigma$ away from their default values to produce any trouble in the fit, a situation that was very unlikely, and even then the fitter worked, just had larger errors, a result largely due to the penalty terms working to prevent the fit parameters from shifting so far. All other studies using the systematic dials resulted in quality fits.

Mock data generated with new models was a different challenge, and was done by replacing the CCQE model and the coherent and resonant models. These new models were then fit with templates and dials based on old models, as a test of the model dependent nature of the fitter. The results from these studies were very reassuring because the fitter handled them without any problem - especially in the case of signal model changes, which were fit out very well. An additional test in this vein was to use mock data generated by a different event generator, GENIE, which uses some of the same models, but has them implemented in slightly different ways. The fits to the GENIE signal and background dials were within errors, proving that the fitter was well ready to fit any data.

The full array of studies and the resulting plots are included in Appendix B.

6.4.1 Fit Convergence Studies

The final study that was needed before looking at the data was a few hundred mock data statistical and systematic fits designed to evaluate the range of χ^2 values to expect for converged fits. For the systematic fits, the systematic parameters were varied randomly about their central values. Statistical fits were done starting with the default templates and then applying fluctuations to each bin based on the Poisson error associated with the number of entries in that bin: the statistical error. Last was a set of studies combining the statistical and systematic variations. The results of the statistical throws are shown in Figure 6.8, with the three different studies plotted in different colors, and the average χ^2 value for the fits described in Chapter B are listed in Table 6.10.

Studying the χ^2 from the table it can be seen that the mock data studies all converged for values near the systematic throws, which is to be expected as that was how those studies were performed. Even the GENIE studies, which were made from a different generator (and thus different templates) are within the fit ranges of the systematic throws. Adding in the statistical variations provided shapes to the mock data templates that were not able to be perfectly reproduced by the templates and systematic parameters, resulting in higher χ^2 minimum fit values. These statistical variations represent the expected range for the data fits, so are important to have before proceeding to look at data.

Table 6.10: Fit χ^2 for MC and Data Studies

Study	χ^2
Asimov	5.76213
$\pm 1\sigma$ Flux	2.344515
$\pm 1\sigma$ FSI	5.60906
$\pm 1\sigma$ XSec Bkg	5.072575
Coherent Model	5.51621
Resonant Model	5.05494
GENIE Signal	11.8744
GENIE Background	27.8949

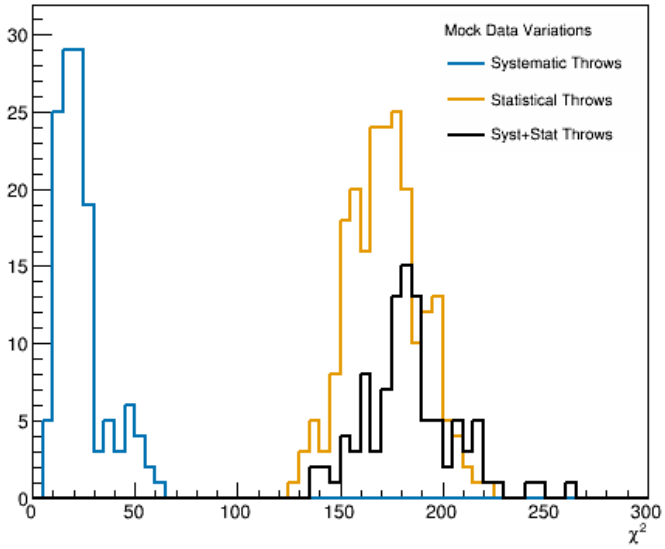

Figure 6.8: Fit χ^2 distribution for systematic and statistical throws.

Chapter 7

Cross Section Measurement

7.1 Introduction

Using the tools described in the previous chapters, the Run 4 water-in data corresponding to 1.63×10^{20} was divided into the nine samples to be analyzed. From Chapter 1.4 the four inputs required to calculate a cross section are:

1. Measured Signal;
2. Signal Efficiency;
3. Neutrino Flux;
4. Number of Targets.

For each of the inputs, not only are the values important but just as vital is the error on these inputs. The flux and number of targets are experiment and detector specific, and thus are available from external efforts. The measured signal is a result of the fitter described in Chapter 6, and the evaluation of the efficiency and the error on the efficiency is presented here. The inputs, errors, and methods for evaluating errors are described in this chapter, along with the final cross section calculations.

7.2 Measured Events

The first input to the cross section calculation is the signal extracted by the fitter discussed in Chapter 6. This is the number of interactions measured in the detector that fit the defined signal definition.

7.2.1 Data Strategy

The data is unveiled in stages by fitting the far sideband first, then adding the near sideband, and lastly the signal region. This staged unveiling is done to test the fitter on real data and ensure the fitting framework is properly handling the data, starting with the region containing the least signal to avoid any bias. Moving in stages allows for confirmation that everything is working correctly in the analysis before looking at the signal region, and also to define what a "good" fit would be when it is time to look at all the data.

7.2.2 Fitter Data Studies

Using the sideband data sets, three studies were done before looking at the full data set. These studies were performed to ensure that the templates and systematic parameters are able to fit real data. The goal is to ensure that the fitter converges to a reasonable χ^2 value, that the fit makes visible progress in matching the input data, and that the fit parameters do not need to take on values more than two standard deviations from their nominal value to achieve that fit.

Far Sideband

The far sideband is the region that contains only 8% signal events, so starting with this sideband when looking at data means there will be less chance for bias if a problem is found and something needs to be fixed. For the far sideband test, only the data in the far sideband is fit, meaning only three of the nine samples are included (Kalman contained, Kalman exiting, and cluster for the far sideband). The signal bins are held constant for this fit, since there is no other signal region to use to constrain the parameters. Since the signal, mis-ID'ed, and signal Background were held constant, this fit is not expected to be perfect, but the post-fit templates should match the data better than the pre-fit templates.

The fit converged with a χ^2 of 71.2, putting it a little lower than the average value of $\chi^2_{\text{syst+stat}}$=180 for a statstically unique sample from Figure 6.8, but as only one third of the samples were considered this is reasonable and considered a good fit. Plotted in Figure 7.1 and Figure 7.2 are the data over the pre-fit NEUT templates, while Figure 7.3 and Figure 7.4 are the data over the post-fit

NEUT templates. For these plots the post-fit templates are visually closer to the data values than the pre-fit, again confirming that the fitter is performing well for the data. Lastly the fit parameter deviations from nominal and error are plotted in Figure 7.5 and all are near their nominal and within the one sigma error band again confirming the fit is a success.

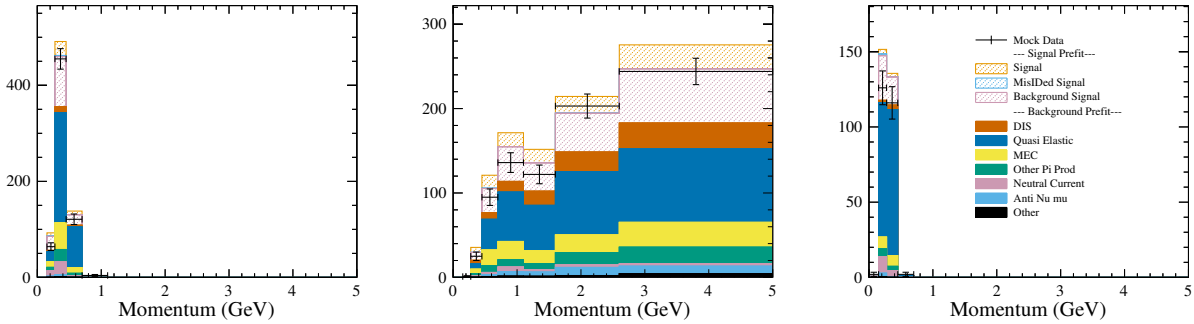

(a) Far Sideband Kalman Contained **(b)** Far Sideband Kalman Exiting **(c)** Far Sideband Cluster

Figure 7.1: Far Sideband Data Fit - Data with Pre-Fit NEUT Templates - Momentum Projection

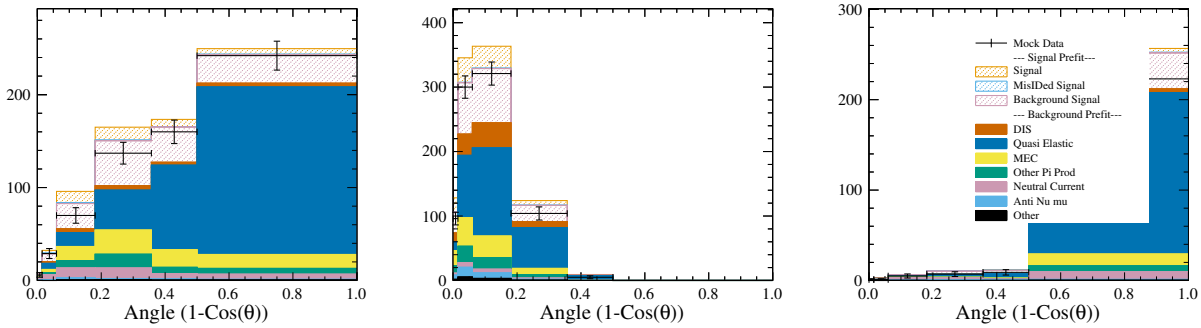

(a) Far Sideband Kalman Contained **(b)** Far Sideband Kalman Exiting **(c)** Far Sideband Cluster

Figure 7.2: Far Sideband Data Fit - Data with Pre-Fit NEUT Templates - Angle Projection

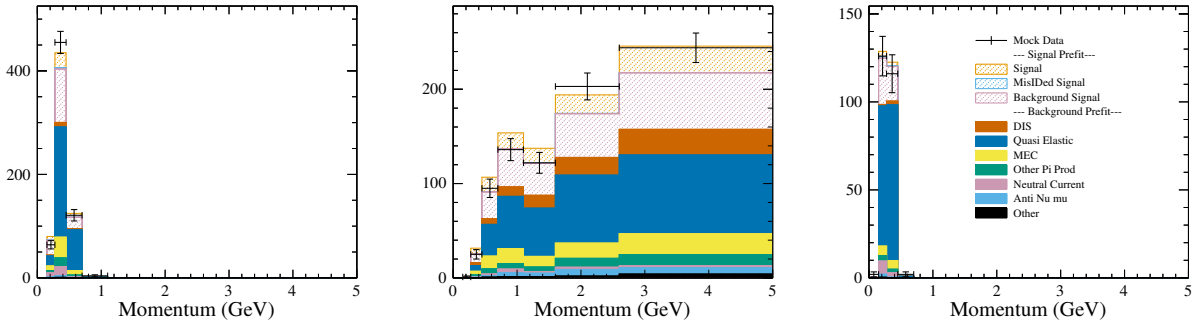

(a) Far Sideband Kalman Contained **(b)** Far Sideband Kalman Exiting **(c)** Far Sideband Cluster

Figure 7.3: Far Sideband Data Fit - Data with Post-Fit NEUT Templates - Momentum Projection

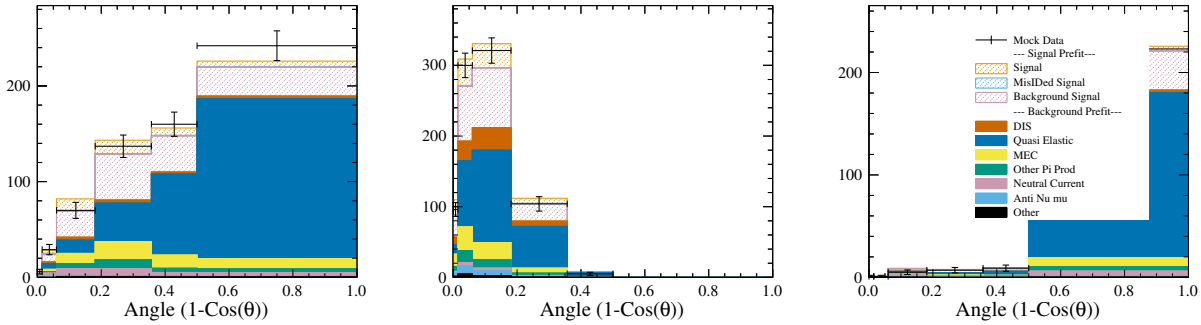

(a) Far Sideband Kalman Contained **(b)** Far Sideband Kalman Exiting **(c)** Far Sideband Cluster

Figure 7.4: Far Sideband Data Fit - Data with Post-Fit NEUT Templates - Angle Projection

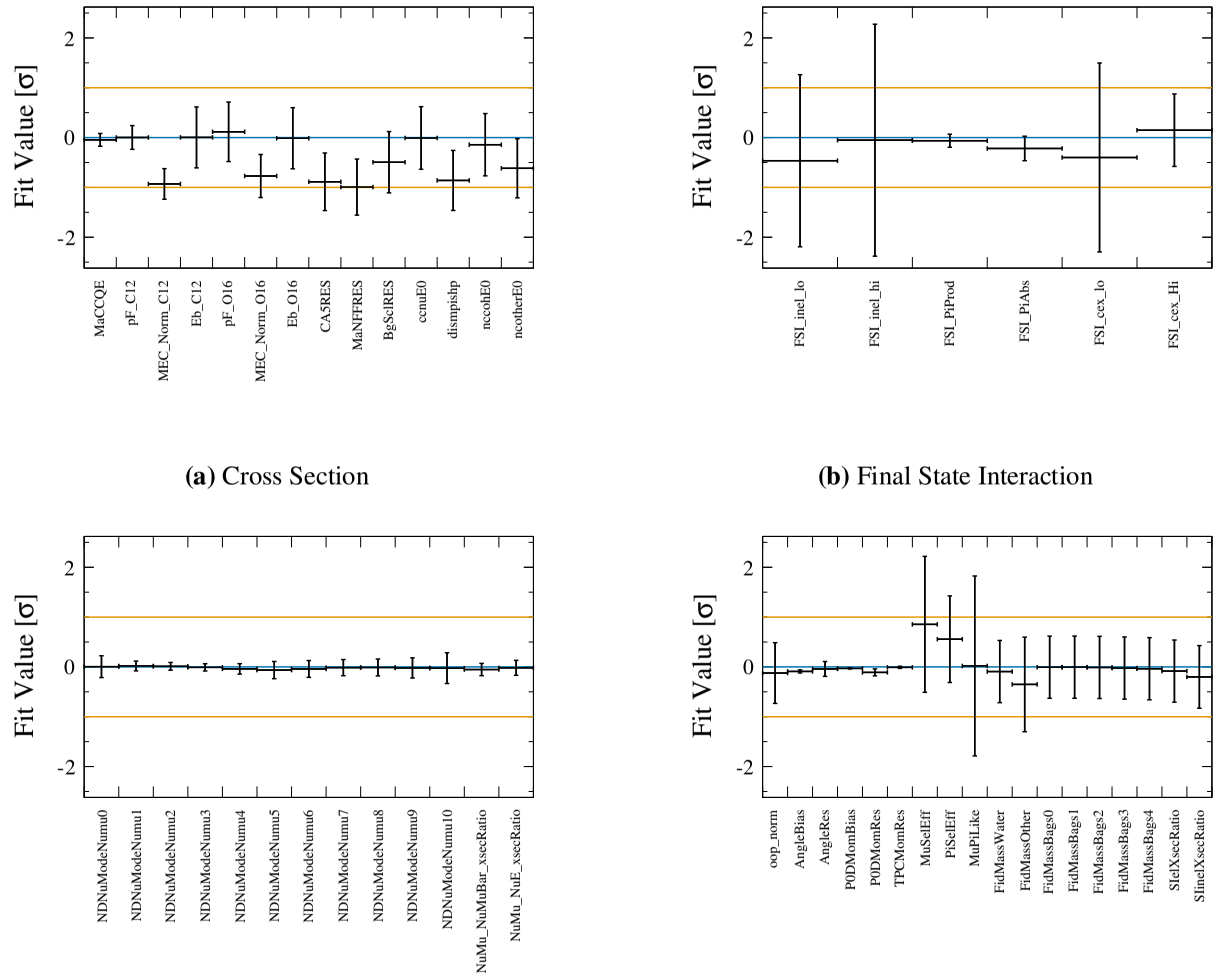

(a) Cross Section

(b) Final State Interaction

(c) Flux

(d) Analysis and Detector

Figure 7.5: Far Sideband Data Fit - Fit parameter deviation from nominal. The points in this plot are the best fit parameter value in units of sigma for each dial. The error bars on the points are the error on that parameter from the fit, while the orange lines at +1 and -1 represent the default one sigma error placed on the variable.

Near and Far Sideband

For the near and far sideband fit, both the sideband regions were included. The near sideband does not have the background purity of the far sideband, but with only 33% signal it is a chance to test more data without the full bias associated with looking at the signal region. The first fit was performed with the same method as the far sideband only fit, and the signal bin parameters were fixed at one and not varied as part of the fit. For the second fit, the signal bin parameters were allowed to move, with the near sideband acting as the signal region for weighting the mis-ID'ed and signal-background contribution in the two sideband regions. Because these fits use both sideband regions, there are six templates as part of the fit (Kalman contained, Kalman exiting, and cluster for both the near sideband and the far sideband).

Without Signal Bin Parameters The near and far sideband fit without signal bin parameters converged with a χ^2 of 179.0, which is nearly the center of the range of acceptable values from the statistical throw study. With only two thirds of the templates, this is actually a little high, but not enough to be a red flag. Plotted in Figure 7.6 and Figure 7.7 are the data over the pre-fit NEUT templates, while Figure 7.8 and Figure 7.9 are the data over the post-fit NEUT templates. Again the templates of the post-fit plots visibly match the data better than that of the pre-fit plots, confirming that the fit performed well. There was more tension in this fit, evident from the higher χ^2 and noticeable mismatches in the fit, particularly the high momentum of the Kalman Exiting bins, but without signal bins to take in this excess, and signal regions to better constrain the signal, this is to be expected. The fit parameter deviations from nominal and error are plotted in Figure 7.10 and again they are well-constrained within the one sigma bounds confirming a well-behaved fit.

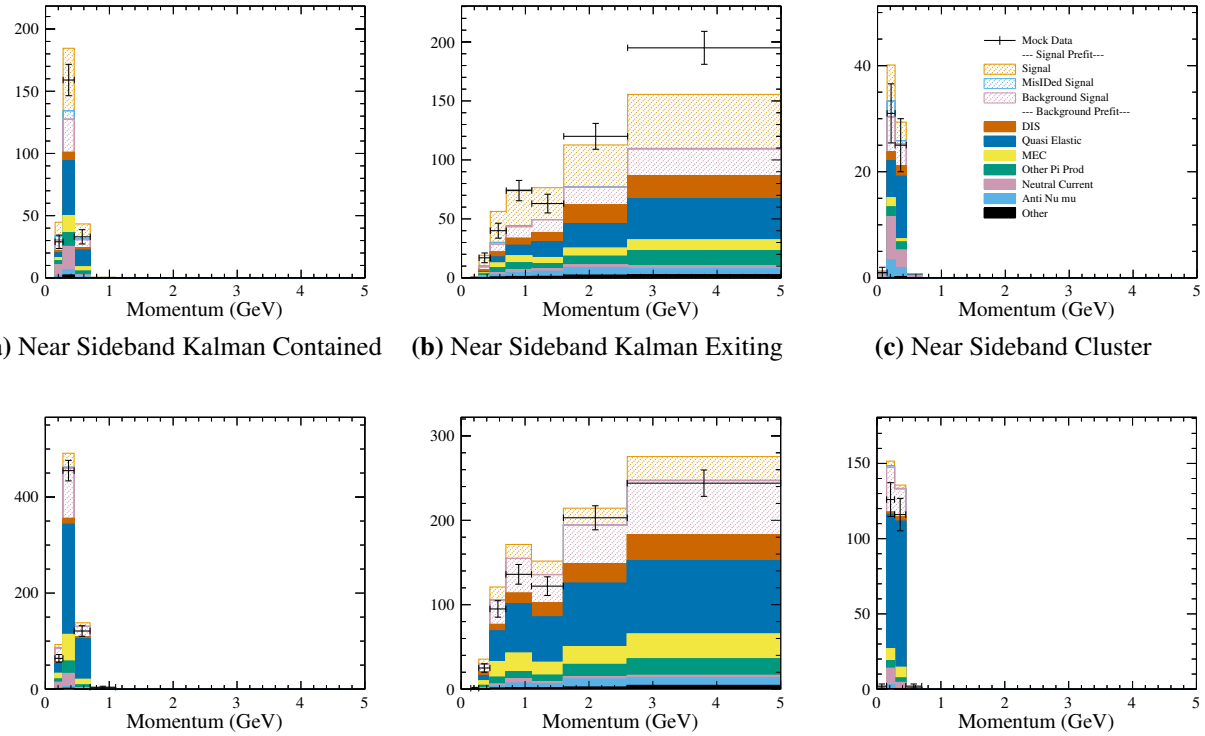

(a) Near Sideband Kalman Contained **(b)** Near Sideband Kalman Exiting **(c)** Near Sideband Cluster

(d) Far Sideband Kalman Contained **(e)** Far Sideband Kalman Exiting **(f)** Far Sideband Cluster

Figure 7.6: Near And Far Sideband Data Fit - Data with Pre-Fit NEUT Templates - Momentum Projection

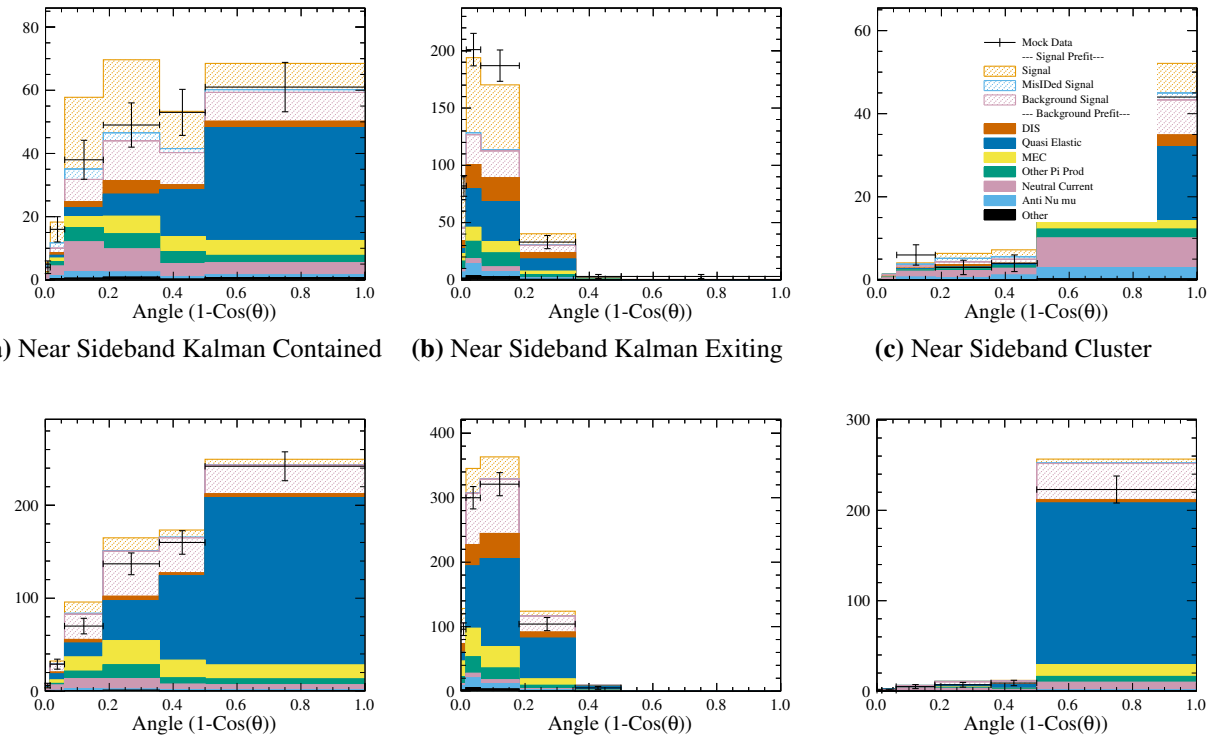

(a) Near Sideband Kalman Contained **(b)** Near Sideband Kalman Exiting **(c)** Near Sideband Cluster

(d) Far Sideband Kalman Contained **(e)** Far Sideband Kalman Exiting **(f)** Far Sideband Cluster

Figure 7.7: Near And Far Sideband Data Fit - Data with Pre-Fit NEUT Templates - Angle Projection

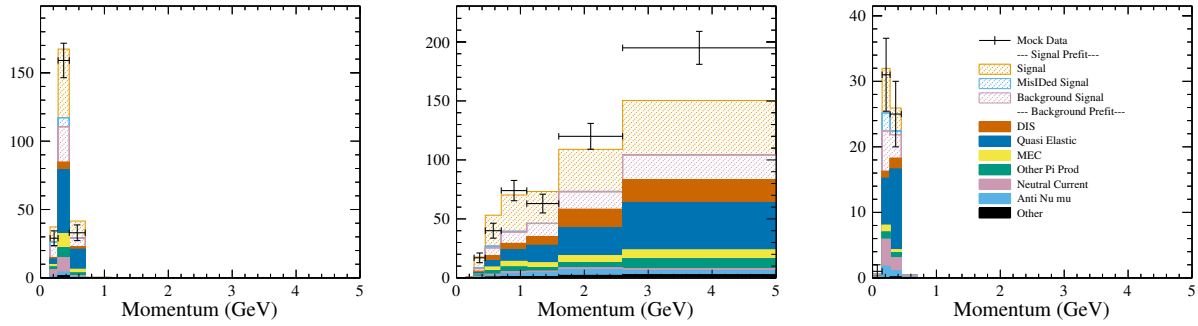

(a) Near Sideband Kalman Contained **(b)** Near Sideband Kalman Exiting **(c)** Near Sideband Cluster

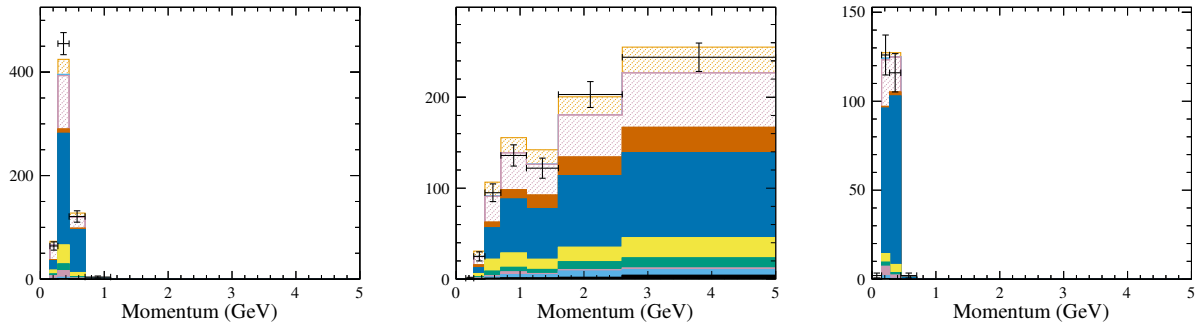

(d) Far Sideband Kalman Contained **(e)** Far Sideband Kalman Exiting **(f)** Far Sideband Cluster

Figure 7.8: Near And Far Sideband Data Fit - Data with Post-Fit NEUT Templates - Momentum Projection

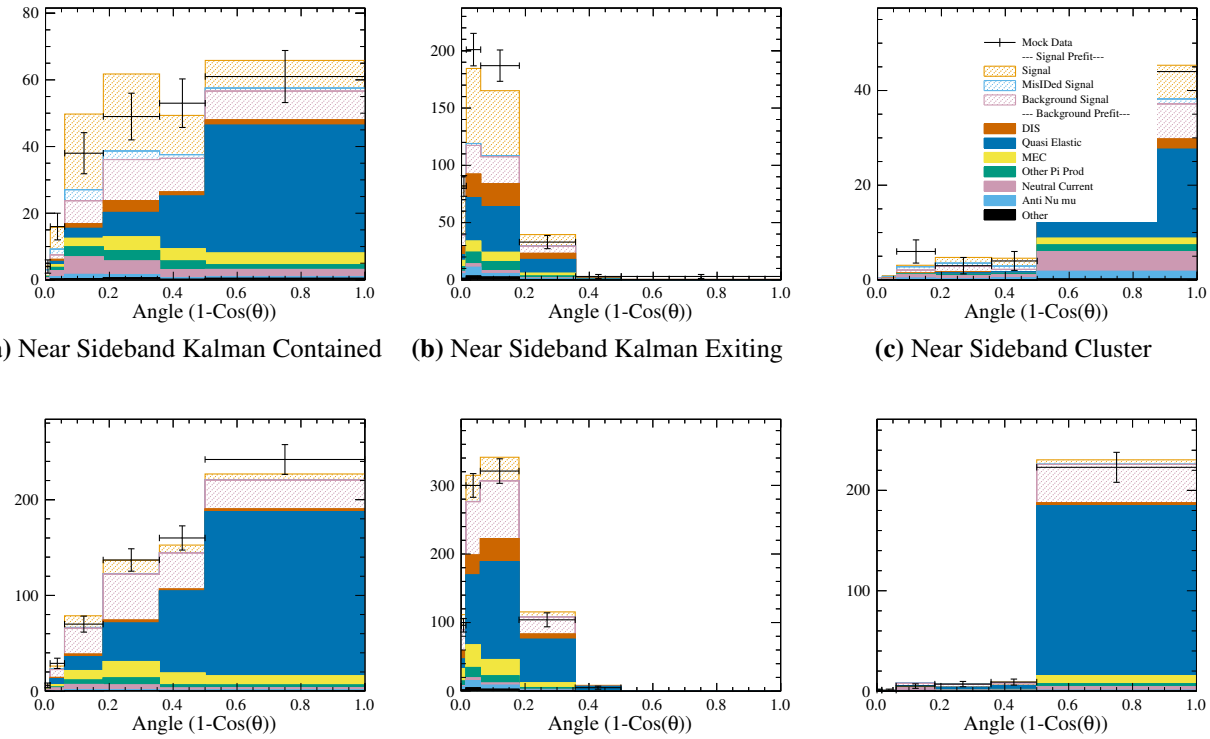

(a) Near Sideband Kalman Contained **(b)** Near Sideband Kalman Exiting **(c)** Near Sideband Cluster

(d) Far Sideband Kalman Contained **(e)** Far Sideband Kalman Exiting **(f)** Far Sideband Cluster

Figure 7.9: Near And Far Sideband Data Fit - Data with Post-Fit NEUT Templates - Angle Projection

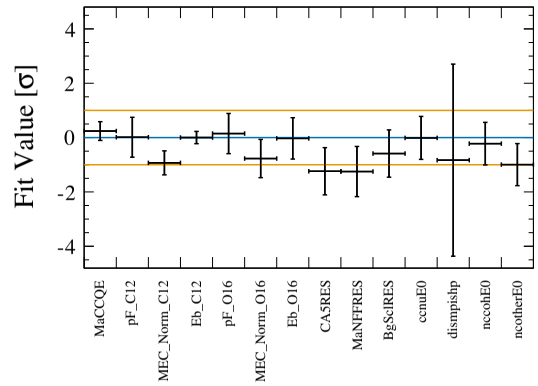

(a) Cross Section

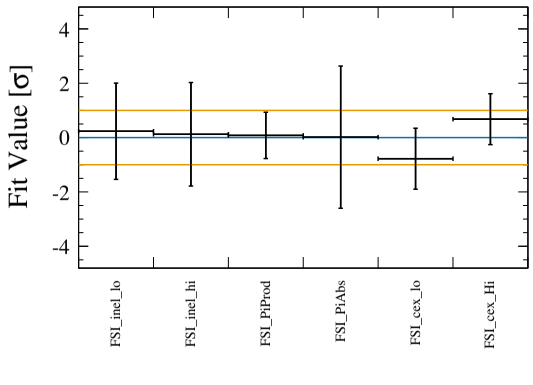

(b) Final State Interaction

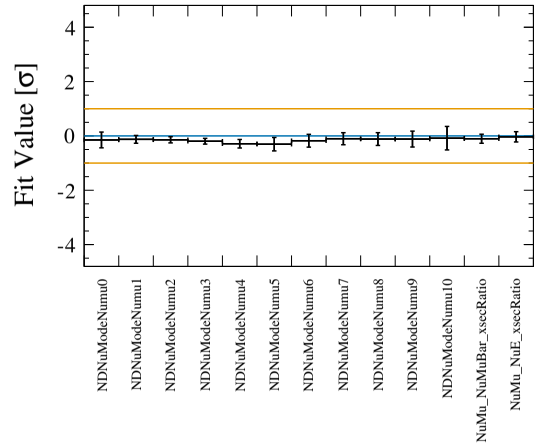

(c) Flux

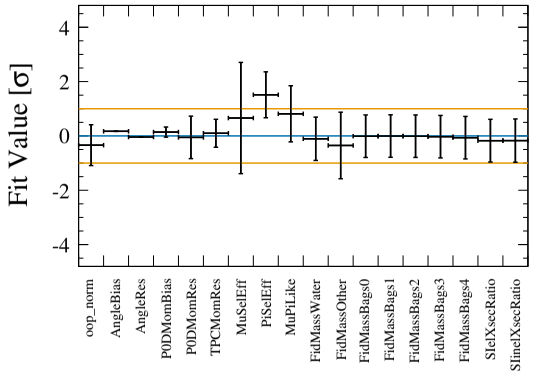

(d) Analysis and Detector

Figure 7.10: Near And Far Sideband Data Fit - Fit parameter deviation from nominal. The points in this plot are the best fit parameter value in units of sigma for each dial. The error bars on the points are the error on that parameter from the fit, while the orange lines at +1 and -1 represent the default one sigma error placed on the variable.

With Signal Bin Parameters Similar to the previous fit but with the signal bin parameters allowed to vary, the same data is fit with all the fit parameters intended to be used on the total data set. This fit converged with a χ^2 of 123.4, the decrease in χ^2 from the previous fit implying that the introduction of the signal bin parameters eased up some freedom in the fit, allowing it to better fit the data. Plotted in Figure 7.11 and Figure 7.12 are the data over the pre-fit NEUT templates, while Figure 7.13 and Figure 7.14 are the data over the post-fit NEUT templates. With these plots the improvement of the post-fit templates to the pre-fit templates in matching the data is again visible, confirming the fit was successful, and actually matches better than the previous fit without the signal bin parameters. The fit parameter deviations from nominal and error are plotted in Figure 7.17 and are again within acceptable ranges.

With the addition of the signal bin parameters comes the ability to extract a measured signal from the fit, the result of which is plotted in Figure 7.15 and Figure 7.16. With only 33% signal, the near sideband is not a great source for signal events, but this functionality is necessary for the full data fit. These plots are also a useful cross check that not only is the signal extraction method working, but also that the fit error plotted with the extracted signal is reasonable. If the errors were too large this could indicate that the analysis should have chosen better binning to reduce statistical error, or done a better job to reduce systematic error. In this case the fit is good and ready to be run on the complete data set.

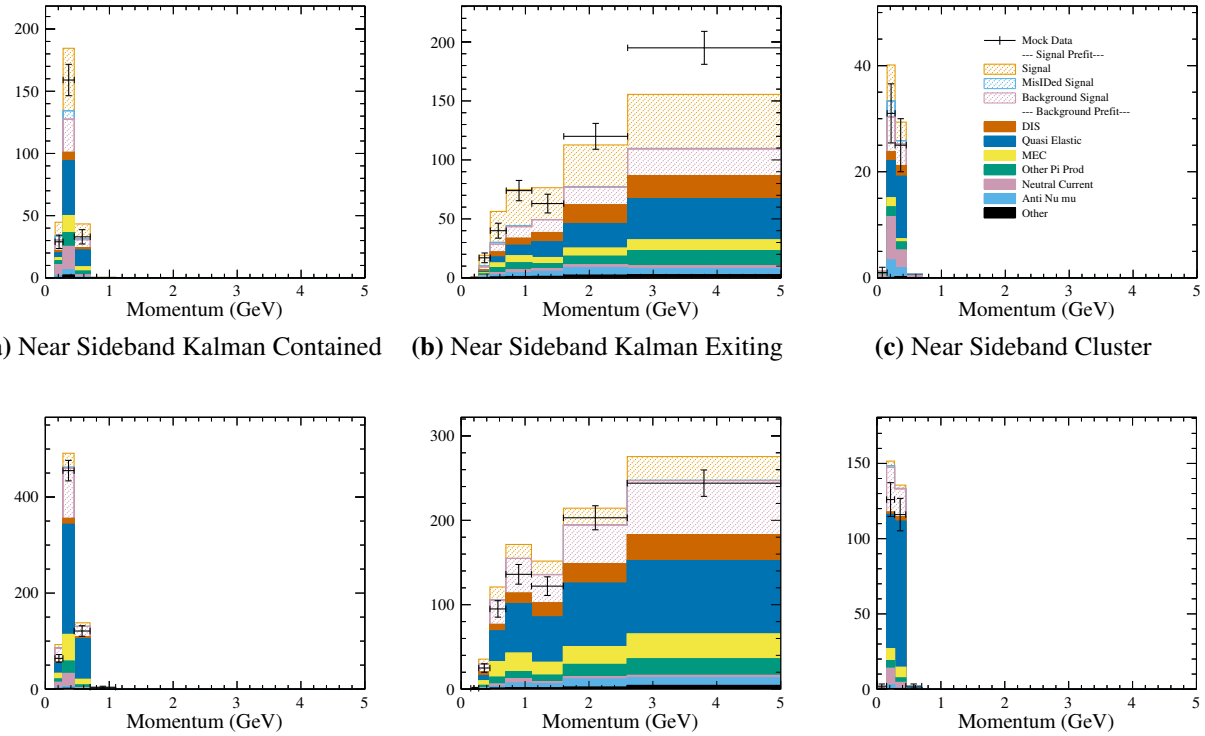

(a) Near Sideband Kalman Contained **(b)** Near Sideband Kalman Exiting **(c)** Near Sideband Cluster

(d) Far Sideband Kalman Contained **(e)** Far Sideband Kalman Exiting **(f)** Far Sideband Cluster

Figure 7.11: Near And Far Sideband Data Fit with Signal Fit - Data with Pre-Fit NEUT Templates - Momentum Projection

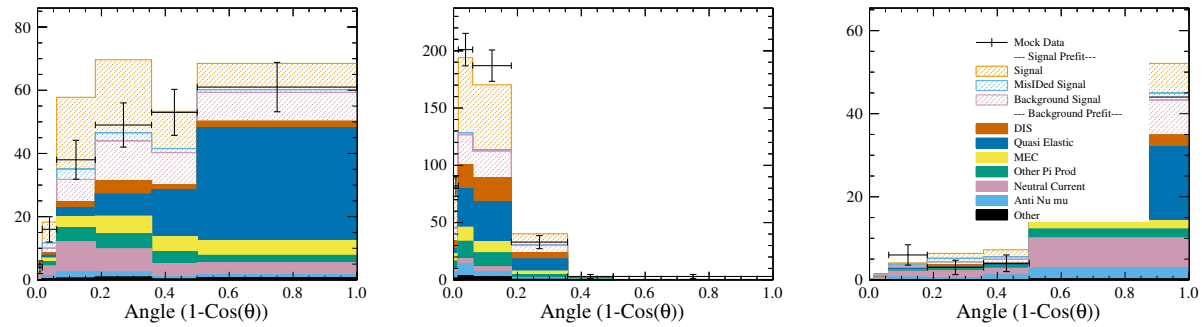

(a) Near Sideband Kalman Contained **(b)** Near Sideband Kalman Exiting **(c)** Near Sideband Cluster

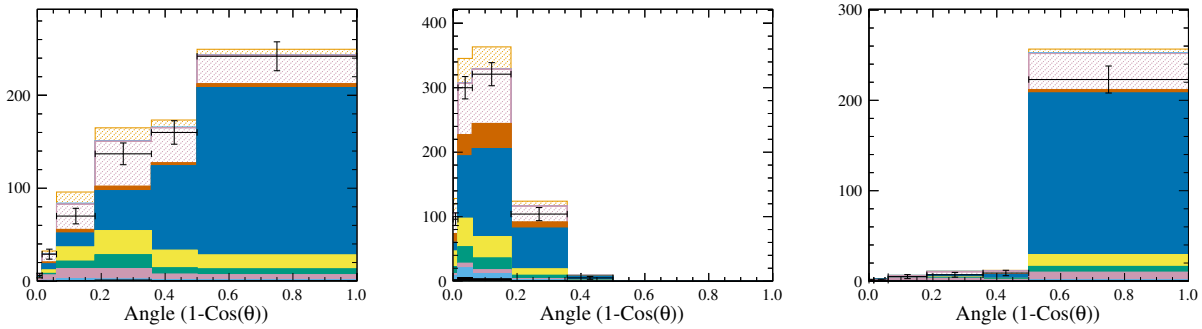

(d) Far Sideband Kalman Contained **(e)** Far Sideband Kalman Exiting **(f)** Far Sideband Cluster

Figure 7.12: Near And Far Sideband Data Fit with Signal Fit - Data with Pre-Fit NEUT Templates - Angle Projection

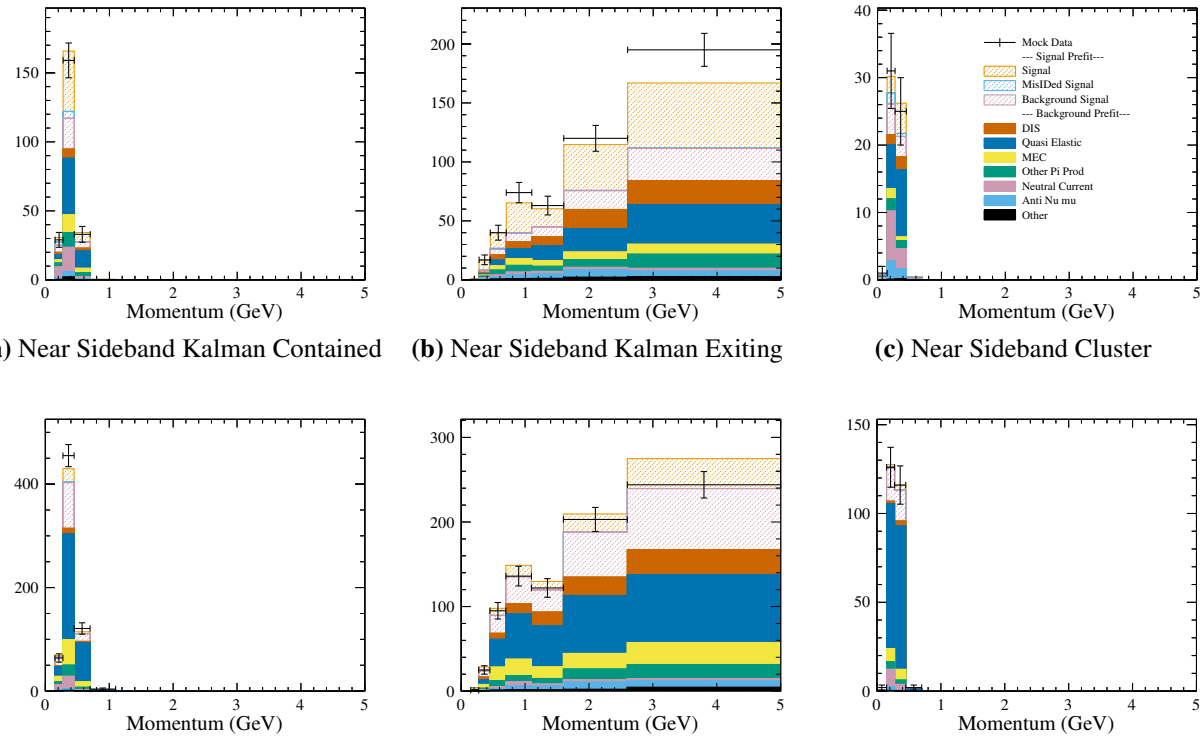

(a) Near Sideband Kalman Contained **(b)** Near Sideband Kalman Exiting **(c)** Near Sideband Cluster

(d) Far Sideband Kalman Contained **(e)** Far Sideband Kalman Exiting **(f)** Far Sideband Cluster

Figure 7.13: Near And Far Sideband Data Fit with Signal Fit - Data with Post-Fit NEUT Templates - Momentum Projection

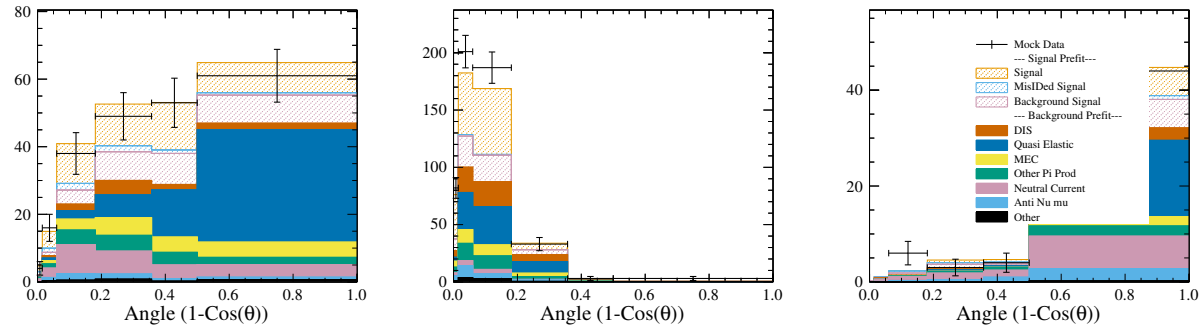

(a) Near Sideband Kalman Contained **(b)** Near Sideband Kalman Exiting **(c)** Near Sideband Cluster

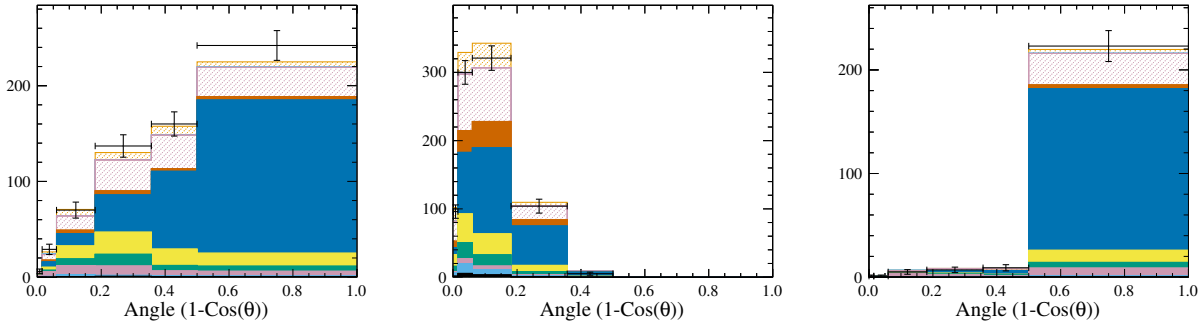

(d) Far Sideband Kalman Contained **(e)** Far Sideband Kalman Exiting **(f)** Far Sideband Cluster

Figure 7.14: Near And Far Sideband Data Fit with Signal Fit - Data with Post-Fit NEUT Templates - Angle Projection

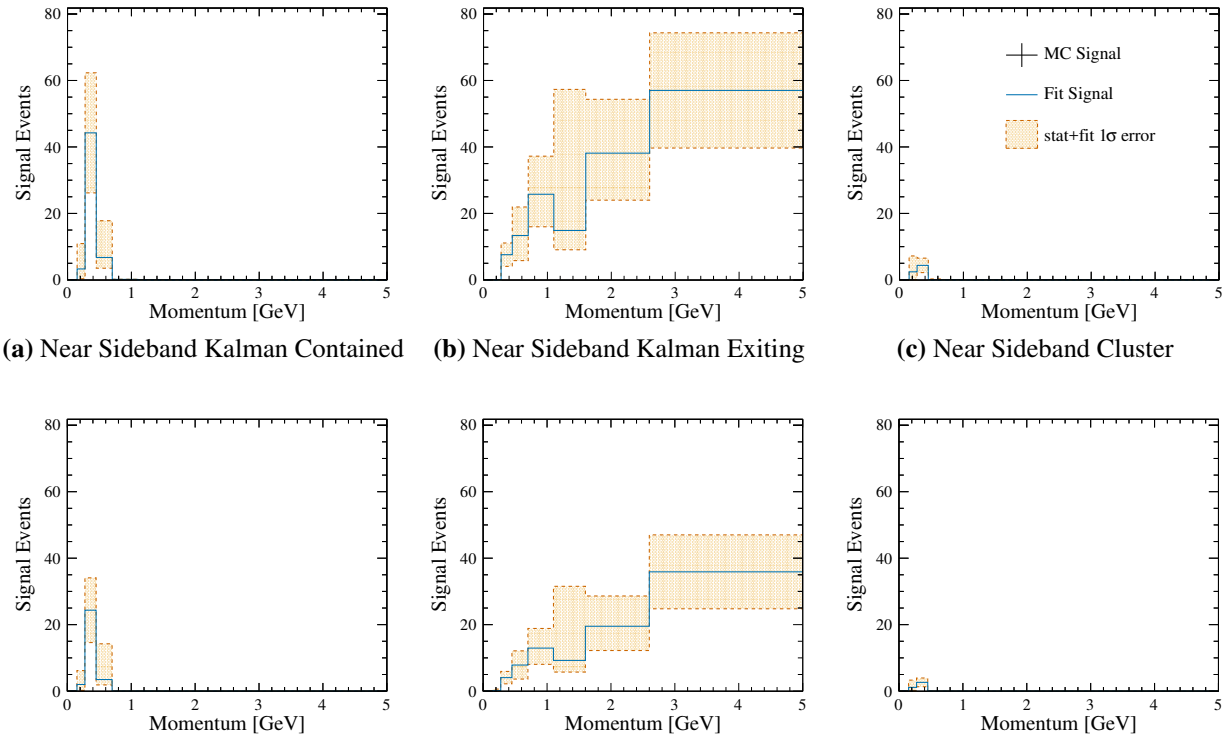

(a) Near Sideband Kalman Contained **(b)** Near Sideband Kalman Exiting **(c)** Near Sideband Cluster

(d) Far Sideband Kalman Contained **(e)** Far Sideband Kalman Exiting **(f)** Far Sideband Cluster

Figure 7.15: Near And Far Sideband Data Fit with Signal Fit - Signal fit in the muon momentum projection. The solid blue line is the best fit and the orange region is the error from the fit. - Momentum projection

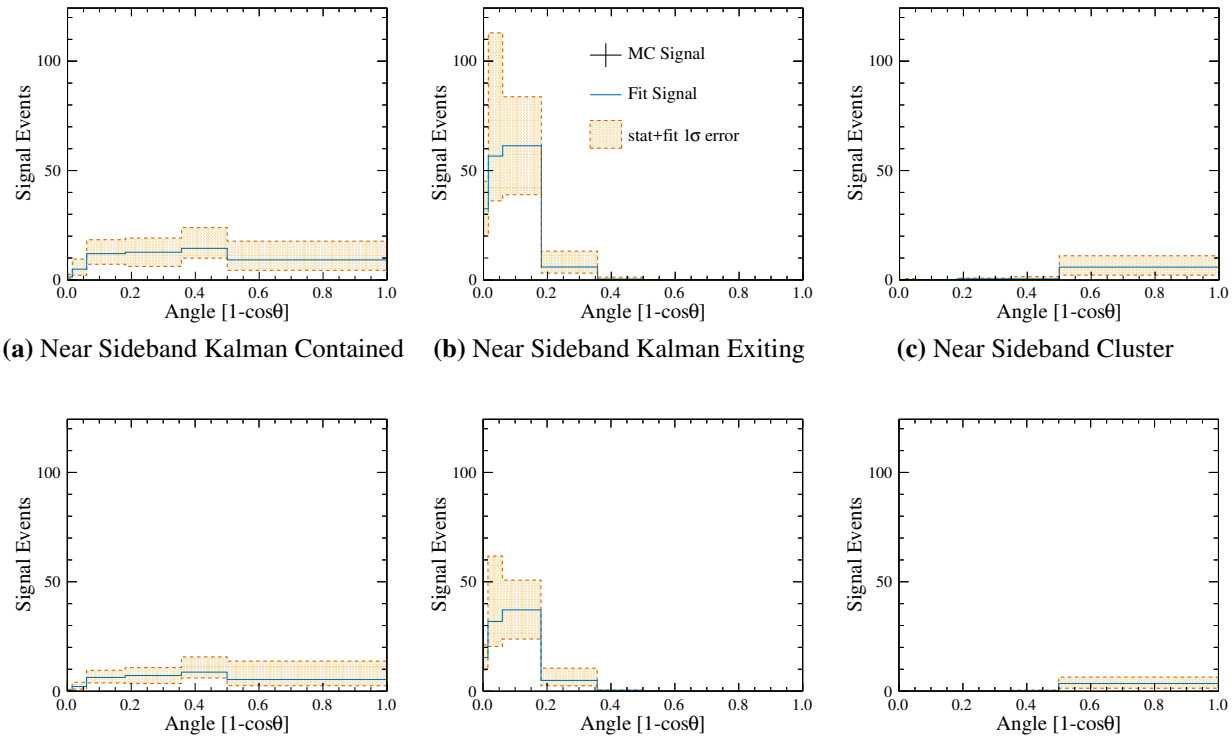

(a) Near Sideband Kalman Contained **(b)** Near Sideband Kalman Exiting **(c)** Near Sideband Cluster

(d) Far Sideband Kalman Contained **(e)** Far Sideband Kalman Exiting **(f)** Far Sideband Cluster

Figure 7.16: Near And Far Sideband Data Fit with Signal Fit - Signal fit in the muon angle projection. The solid blue line is the best fit and the orange region is the error from the fit. - Angle projection

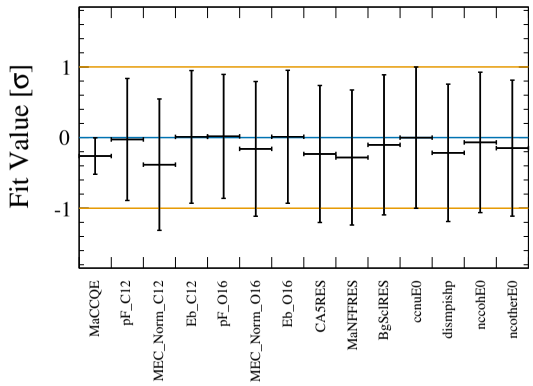

(a) Cross Section

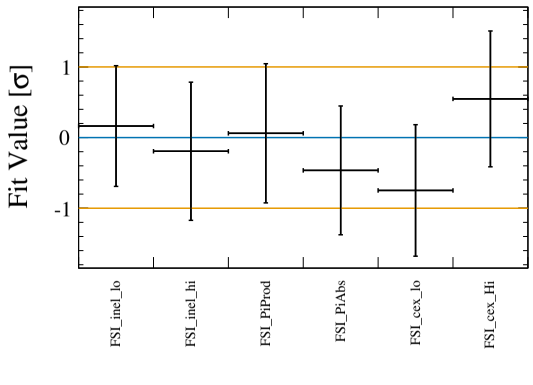

(b) Final State Interaction

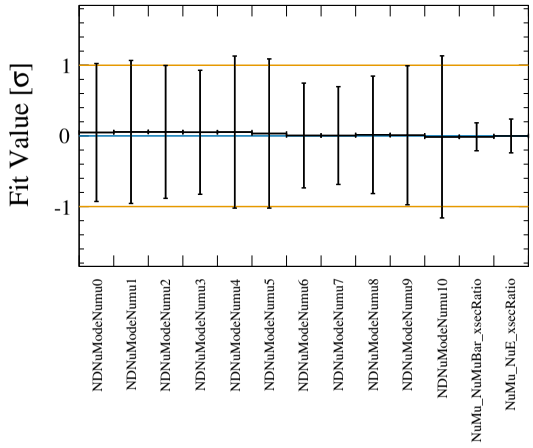

(c) Flux

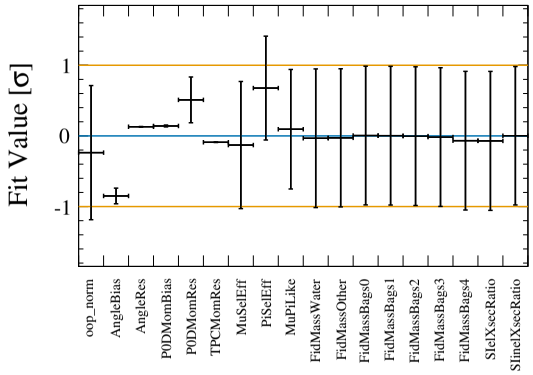

(d) Analysis and Detector

Figure 7.17: Near And Far Sideband Data Fit with Signal Fit - Fit parameter deviation from nominal. The points in this plot are the best fit parameter value in units of sigma for each dial. The error bars on the points are the error on that parameter from the fit, while the orange lines at +1 and -1 represent the default one sigma error placed on the variable.

7.2.3 Data Fit Results

Fitting all nine samples resulted converged with a $\chi^2 = 173.2$, which is right in the middle of the distribution of χ^2 values for the statistical throws shown in Figure 6.8, which means it is consistent with a converged fit for a statistically different sample than the pre-fit templates.

The pre-fit templates with the data overlaid are plotted in Figure 7.18 and Figure 7.19. In these plots the data are seen to be consistently below the pre-fit predictions, with only a few bins containing more events in data than predicted by the Monte Carlo. These bins are not a concern since with 48 bins per sample and nine samples, that results in 432 bins subject to statistical variations. With that many bins at least one should have a three sigma variation from the expected distribution, and 22 should be two sigma different, and it is these variations that caused the higher χ^2 values in the statistical throw study. The general trend of data having fewer events than the MC templates is also expected as the default signal models within the MC for both coherent and resonant pion production have been shown to over estimate pion production at T2K neutrino energies [1].

The post-fit templates with the data overlaid are plotted in Figure 7.20 and Figure 7.21. For most bins in the momentum and angle projections the post-fit templates lie within one sigma of the statistical errors on the data. The bins in which there were more data events than predicted in the pre-fit plots have pulled those bins higher across the signal and sideband regions for those kinematic bins. For the Kalman exiting samples in the momentum projection, the fit shows that not only are the MC predictions too high in general, but the low momentum bins have a greater relative decrease than the higher momentum bins. This means that not only are the default models over estimating the number of events, but they are over estimating the number of events with low muon momenta more than they over estimate events with higher muon momenta. A study of the angle projections shows a similar shape change occurs in the Kalman contained sample, where the signal in the more forward going bins ($1-\cos(\theta)$ is closer to 0) is pulled down more than the signal in the higher angle bins which are sometimes gaining events rather than losing them. This again shows that the default models in NEUT do not represent the data in this analysis well.

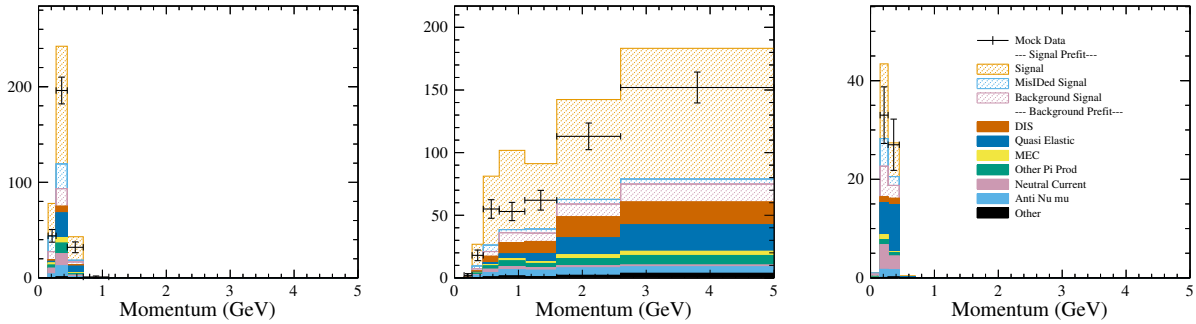

(a) Selected Kalman Contained **(b)** Selected Kalman Exiting **(c)** Selected Cluster

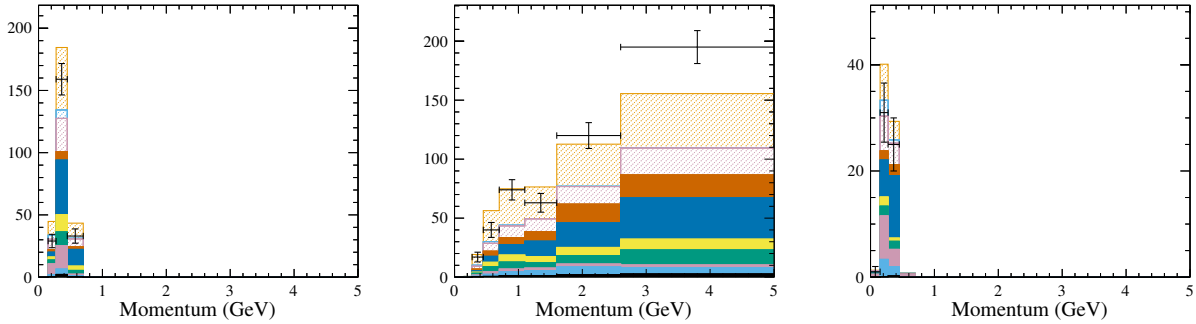

(d) Near Sideband Kalman Contained **(e)** Near Sideband Kalman Exiting **(f)** Near Sideband Cluster

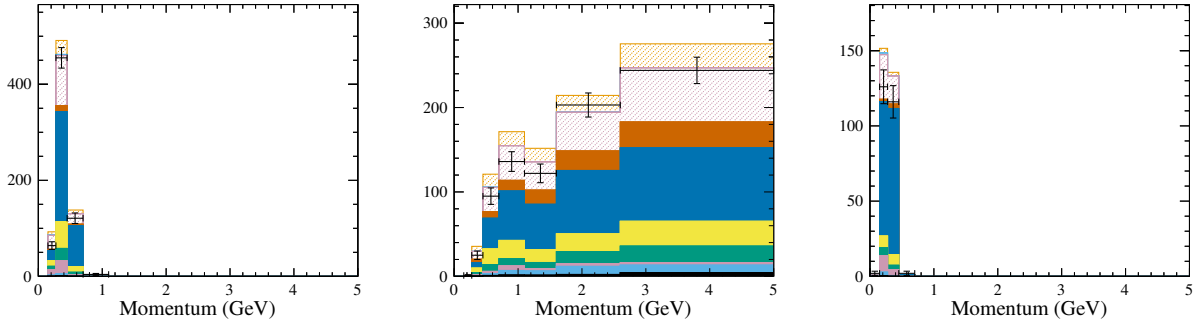

(g) Far Sideband Kalman Contained **(h)** Far Sideband Kalman Exiting **(i)** Far Sideband Cluster

Figure 7.18: Full Data Fit with Pre-Fit NEUT Templates - Momentum Projection

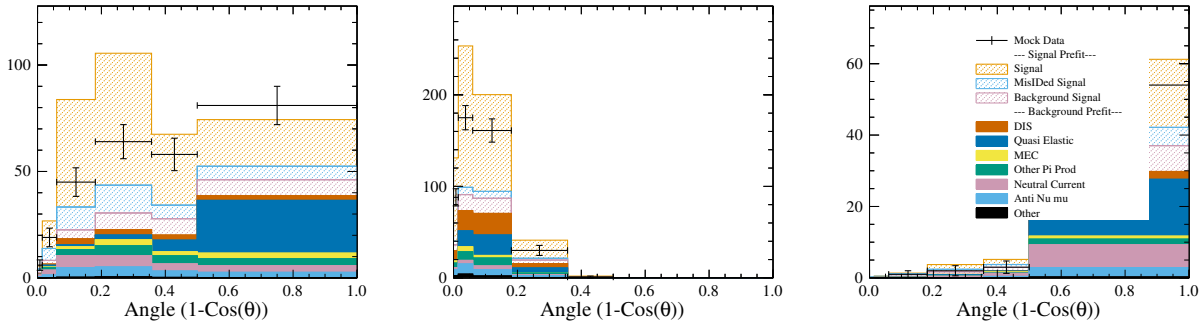

(a) Selected Kalman Contained **(b)** Selected Kalman Exiting **(c)** Selected Cluster

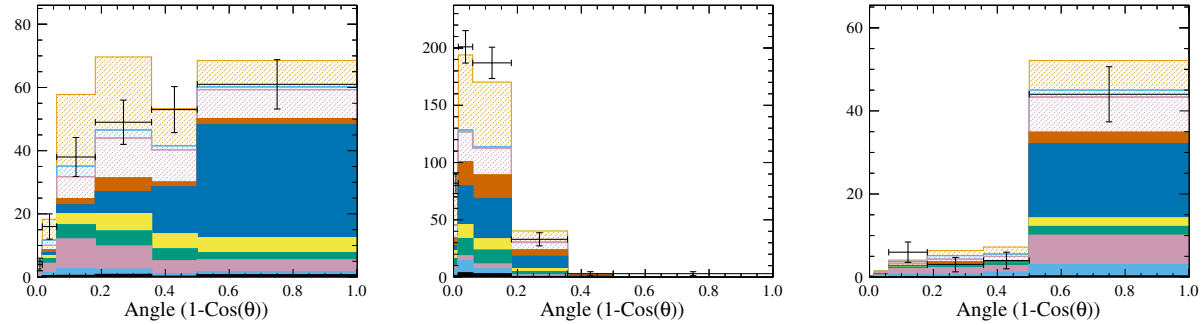

(d) Near Sideband Kalman Contained **(e)** Near Sideband Kalman Exiting **(f)** Near Sideband Cluster

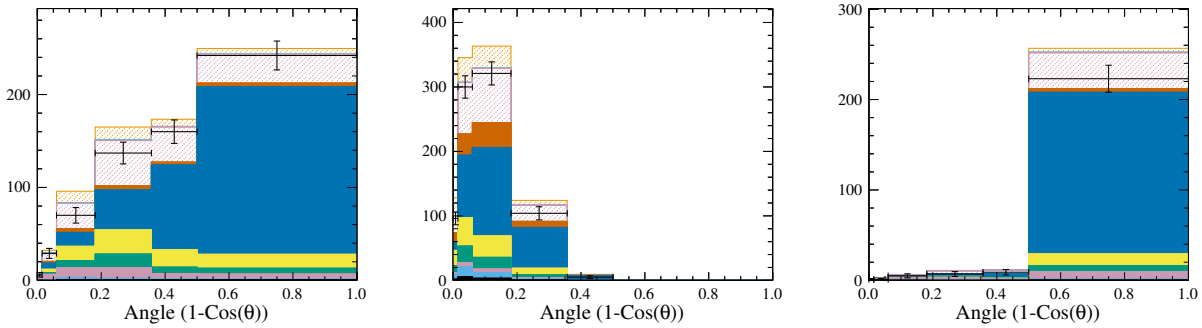

(g) Far Sideband Kalman Contained **(h)** Far Sideband Kalman Exiting **(i)** Far Sideband Cluster

Figure 7.19: Full Data with Pre-Fit NEUT Templates - Angle Projection

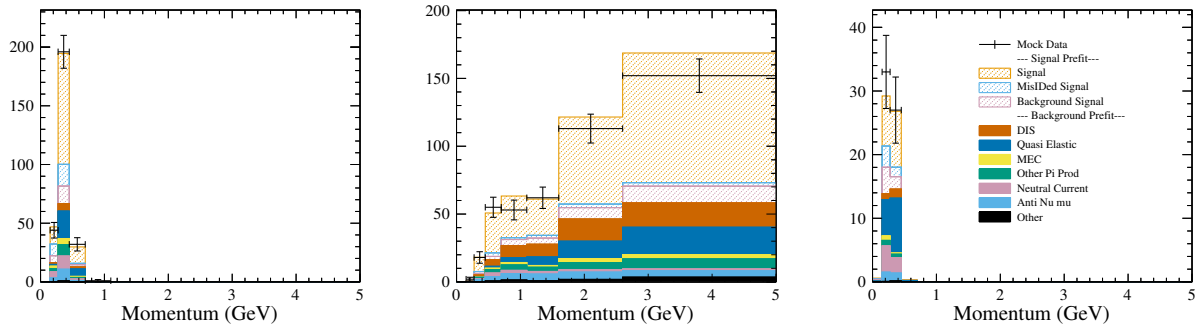

(a) Selected Kalman Contained **(b)** Selected Kalman Exiting **(c)** Selected Cluster

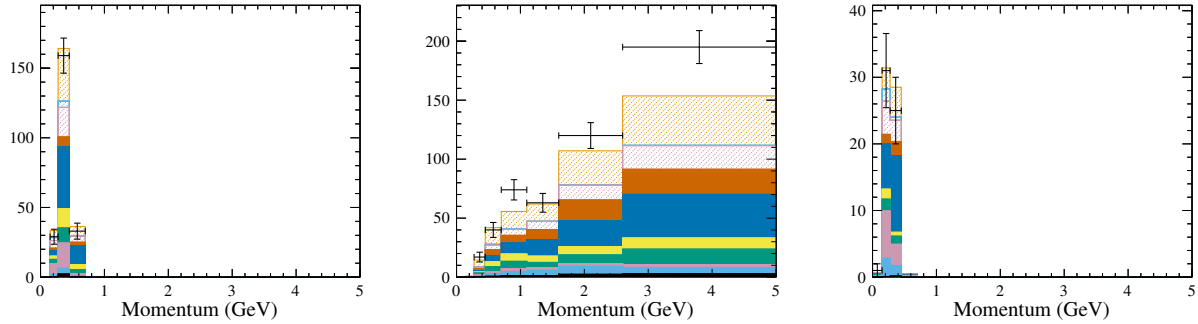

(d) Near Sideband Kalman Contained **(e)** Near Sideband Kalman Exiting **(f)** Near Sideband Cluster

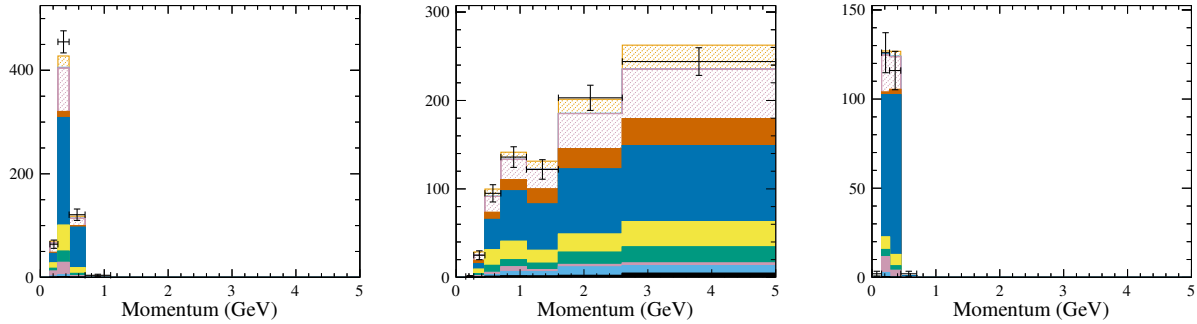

(g) Far Sideband Kalman Contained **(h)** Far Sideband Kalman Exiting **(i)** Far Sideband Cluster

Figure 7.20: Full Data Fit with Post-Fit Neut Templates - Momentum Projection

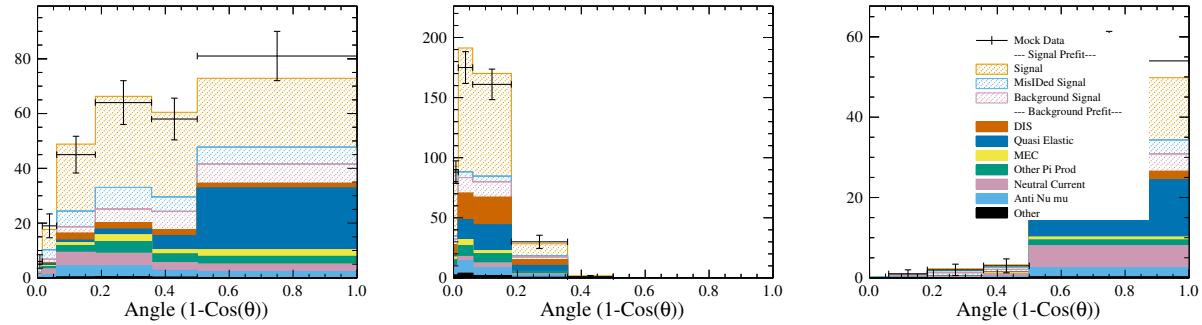

(a) Selected Kalman Contained **(b)** Selected Kalman Exiting **(c)** Selected Cluster

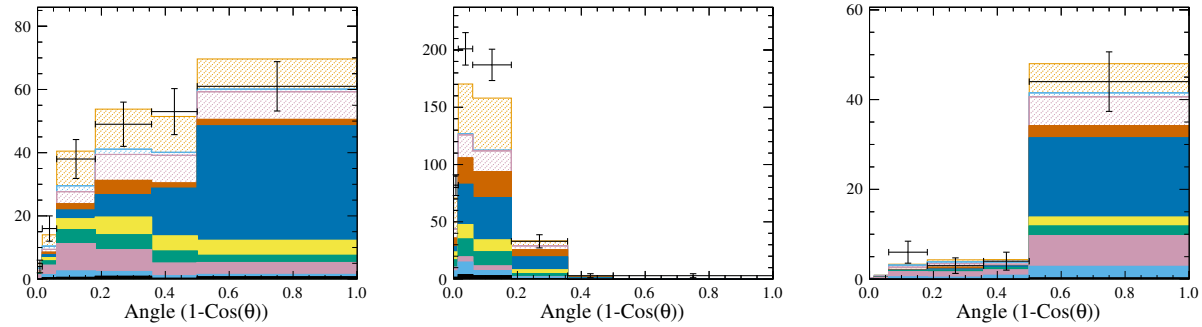

(d) Near Sideband Kalman Contained **(e)** Near Sideband Kalman Exiting **(f)** Near Sideband Cluster

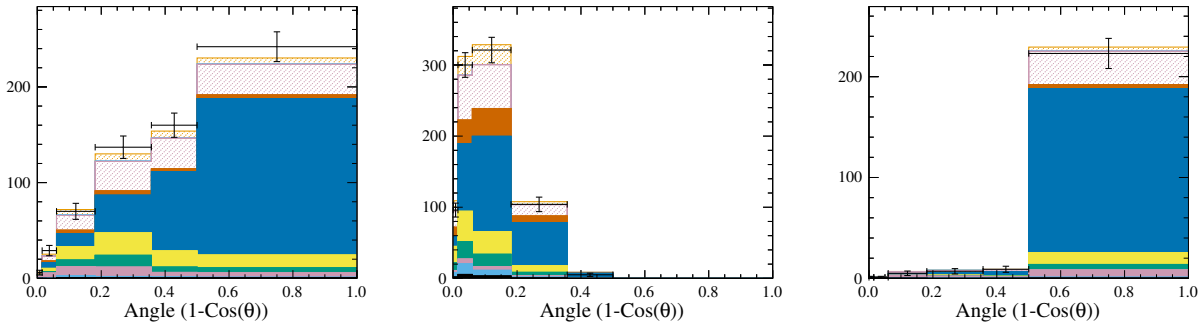

(g) Far Sideband Kalman Contained **(h)** Far Sideband Kalman Exiting **(i)** Far Sideband Cluster

Figure 7.21: Full Data Fit with Post-Fit Neut Templates - Angle Projection

The final extracted signal is plotted in Figure 7.22 and Figure 7.23 with the fit errors colored in around the fit. The signal fit results in the three Selected samples are added together and are the final selected events used in this analysis to calculate the cross section. The total number of events and the error on that total are the numerator in the cross section calculation. The error on this number of events is a combination of the statistical and systematic errors evaluated by the fitter.

To study the systematic errors in more detail, the fit parameter deviations from nominal and error are plotted in Figure 7.24.

Starting with the cross section parameters, all are near the nominal values, with most having errors near their one sigma values. The MaCCQE dial adjusts the amplitude of CCQE, and since that is the largest background in this analysis it is reasonable that this parameter be well constrained, as represented by the smaller error bars. Also well constrained is the Fermi momentum on carbon, which also controls the amplitude of CCQE, though not as strongly as the Ma dial.

The FSI and Flux parameters both show similar fit trends to the previous fitter studies. The final parameter values are close to nominal and the errors are generally on the order of the preliminary one sigma values. The small error bars on the electron neutrino and anti muon neutrino cross section ratios (the right most two bins on the flux plot) show that the fit highly preferred specific values of these parameters. These two parameters were given a 100% error to be sure the error covered the parameters, knowing that the dials had little impact on the fit. The smaller error bands just show that the errors were overestimated and the parameters were able to be constrained by the fit. Additionally these two parameters are centered at the nominal value shows that the percentage of these contaminants in the MC agrees with the fit.

There are a number of interesting bins in the Detector parameter plot. The right half of the bins centered on the nominal and with errors matching the the one sigma range are the errors on the water mass which just confirms that the errors there are were well-modeled and not particularly influential on the final fit. The first bin shows some effect of the out of P∅D contamination parameter, pulling it down, indicating the fit prefers fewer out of P∅D events than the MC indicated. The next five bins show the constraint of the fit on the angle and momentum bias and resolution. These

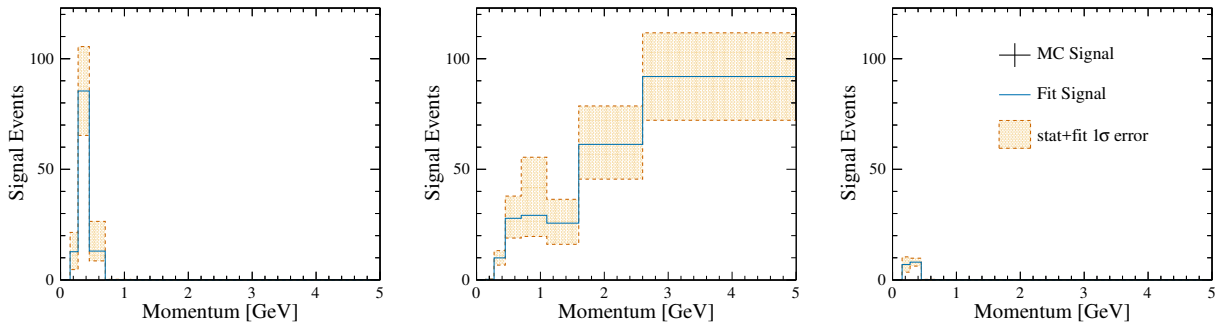

(a) Selected Kalman Contained **(b)** Selected Kalman Exiting **(c)** Selected Cluster

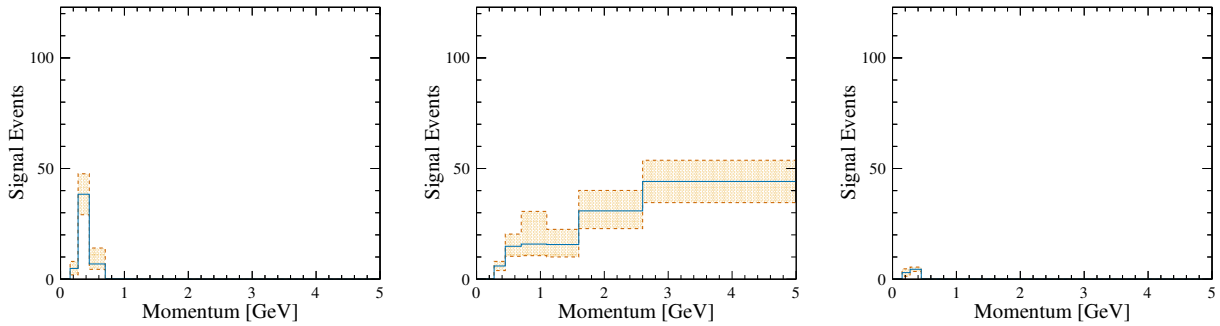

(d) Near Sideband Kalman Contained **(e)** Near Sideband Kalman Exiting **(f)** Near Sideband Cluster

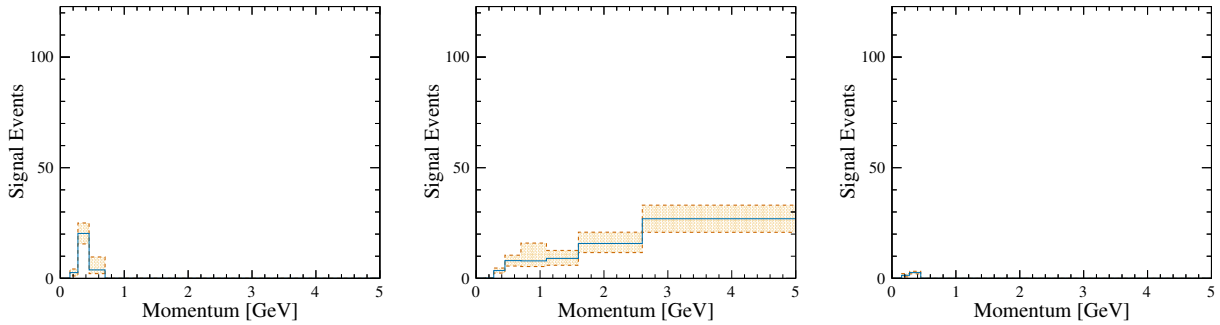

(g) Far Sideband Kalman Contained **(h)** Far Sideband Kalman Exiting **(i)** Far Sideband Cluster

Figure 7.22: Full Data Fit - Extracted signal in the muon momentum projection. The solid blue line is the best fit and the orange region is the error from the fit.

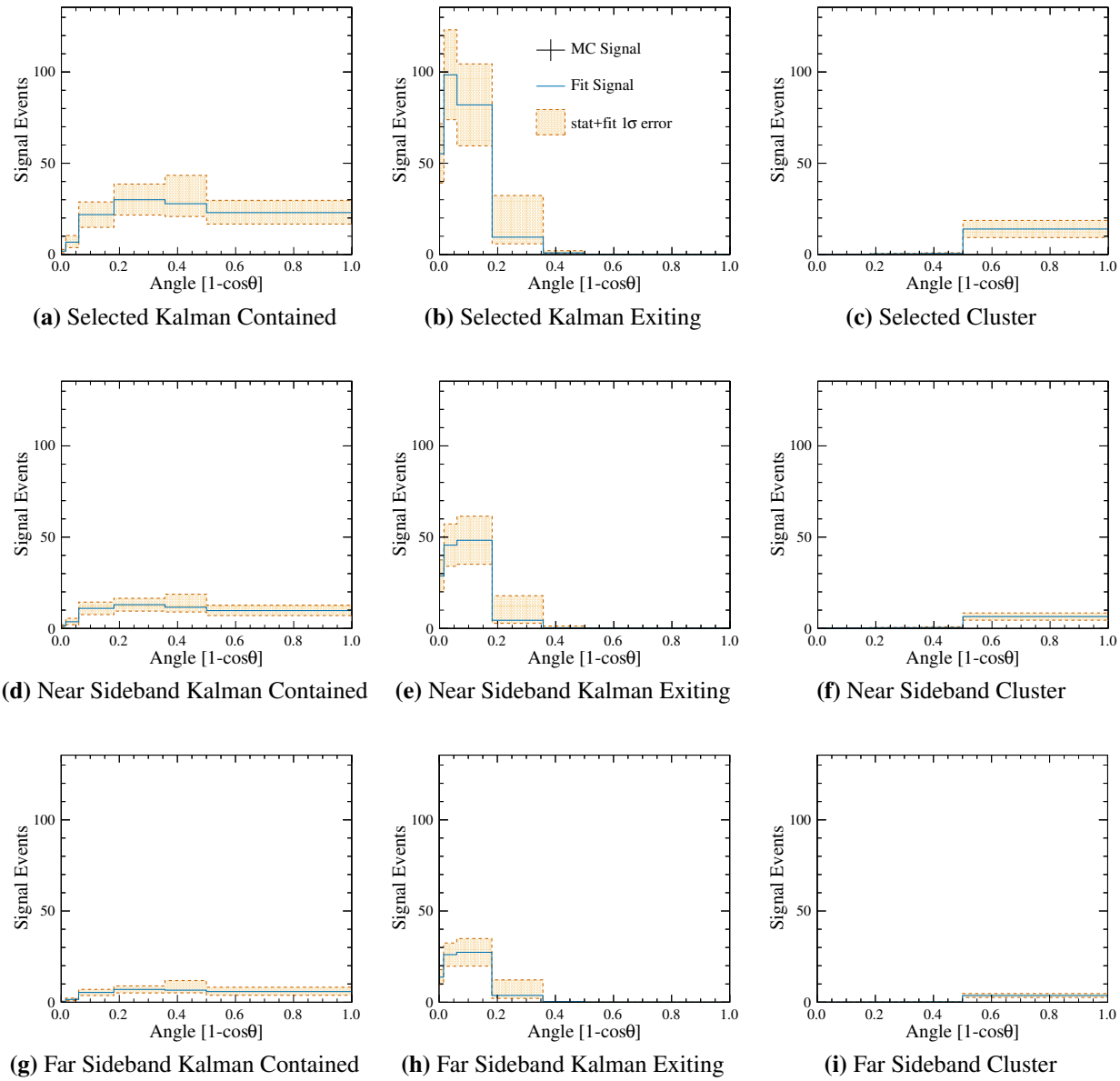

(a) Selected Kalman Contained **(b)** Selected Kalman Exiting **(c)** Selected Cluster

(d) Near Sideband Kalman Contained **(e)** Near Sideband Kalman Exiting **(f)** Near Sideband Cluster

(g) Far Sideband Kalman Contained **(h)** Far Sideband Kalman Exiting **(i)** Far Sideband Cluster

Figure 7.23: Full Data Fit - Extracted signal in the muon angle projection. The solid blue line is the best fit and the orange region is the error from the fit.

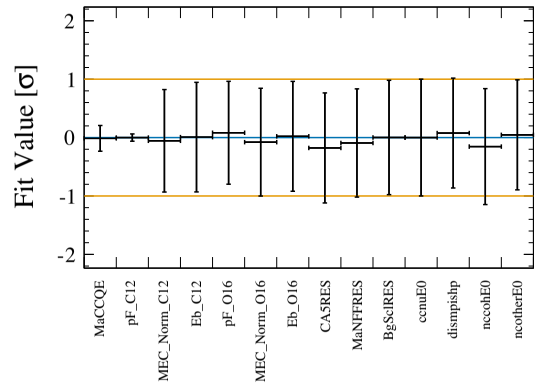

(a) Cross Section

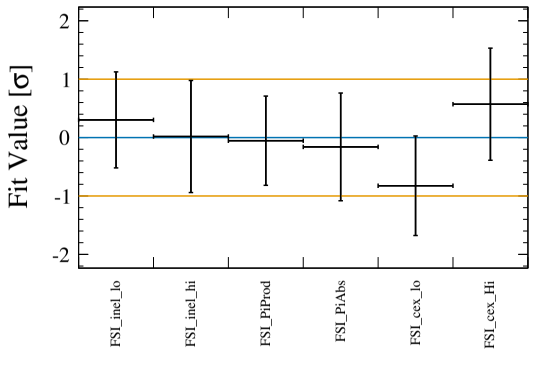

(b) Final State Interaction

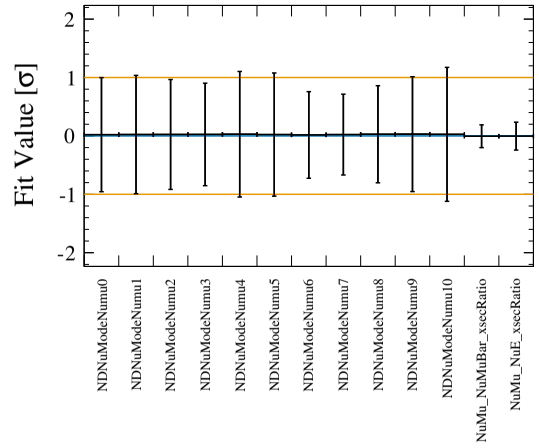

(c) Flux

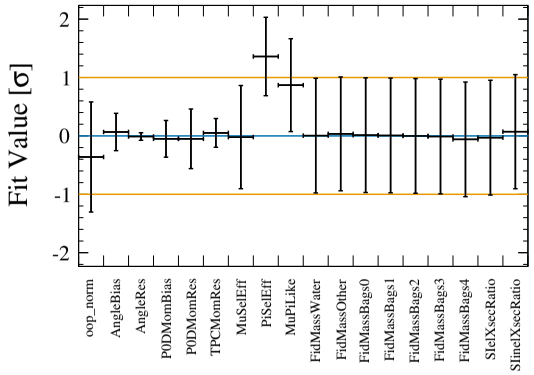

(d) Analysis and Detector

Figure 7.24: Full Data Fit - Fit parameter deviation from nominal. The points in this plot are the best fit parameter value in units of sigma for each dial. The error bars on the points are the error on that parameter from the fit, while the orange lines at +1 and -1 represent the default one sigma error placed on the variable.

parameters adjust the shape of the angle and momentum distributions, so it is expected that the fit would have very preferred values of these parameters. That they are all near nominal nominal indicates that the reconstructed parameters agree with the data and that they are all within the preliminary one sigma error band shows that they are well-covered by their errors. The muon and pion selection efficiencies together with the PID accuracy are three dials that work a little differently than the others in that at their nominal (0) position they represent the default MC, and at $+1\sigma$ they match the data. For these dials the expectation is that they will be pulled up to $+1\sigma$ and as long as they are consistent within their errors of 0 and 1 they are considered to be within the expected range.

7.3 Efficiency

Other than the measured results, the most complicated part of the cross section calculation is the efficiency term. This term serves to correct the measurement to account for any events that would have been seen if the analysis and detector had been perfect at selecting and identifying events. What this means is that a definition of what "should have been seen" has to be made, and the difference between what was seen, and what "should have been seen" must be understood. This is where the signal definitions become important and the care that was taken throughout the analysis to be specific when dealing with different signal definitions will make the calculations easier. Because the efficiency is correcting what was measured to what "should have been" measured, it is very easy for model dependence to enter an analysis with this step, as that is the easiest way to define what "should have been seen".

The procedure for evaluating the efficiency is to first define the signal as what "should have been seen", then to compare that signal with what was measured, bin by bin. The efficiency calculation is simple with only two inputs:

$$\text{Efficiency} = \frac{\text{Selected Signal}}{\text{All Signal}}. \tag{7.1}$$

For working with the binned distribution used in this analysis, the efficiency is calculated bin-by-bin. When defining the selected signal events for the efficiency correction, it is important to be sure that the signal, and thus correction done by applying the efficiency, is not going to be influenced by signal models. Also important to consider is that the events in the Selected and Signal regions should cover the same kinematic phase space for all relevant kinematic variables, not just those the measurement is being presented in. This coverage is important because using the efficiency to correct the selected events into a region where there was no data introduces model dependence, because it is only the signal events that have information about that region, which is entirely model dependent.

7.3.1 Pion Momentum Cut

As was discussed in Chapter 6.2.4, pions with a momentum below 250 MeV are not well-reconstructed within this analysis. Plotted in Figure 7.25 is the pion selection efficiency as a function of true (from the Monte Carlo) and reconstructed pion momentum. When considering efficiency corrections it is important to identify any region of phase space for which there is no data, or over which the efficiency correction is poorly defined. For pions below 250 MeV the selection efficiency is quickly changing, making the efficiency correction dangerous because the correction is not well-defined. This is the reason that a cut on events with a pion momentum less that 250 MeV is included in the selected and total signal definitions throughout this section. It is important to not efficiency correct events into the sample that could not have been detected and for which there is no measured information.

7.3.2 Reconstructed 1μ 1π

The reconstructed signal definition was defined so as to make the efficiency correction straightforward. With this signal definition, the selected signal events extracted by the fitter make up the selected signal, and all events that could have been selected by the analysis as signal make up the denominator. This means that the only reason events do not make it into the selected sample is the analysis cuts themselves. This means that the only effects being adjusted for by the efficiency cor-

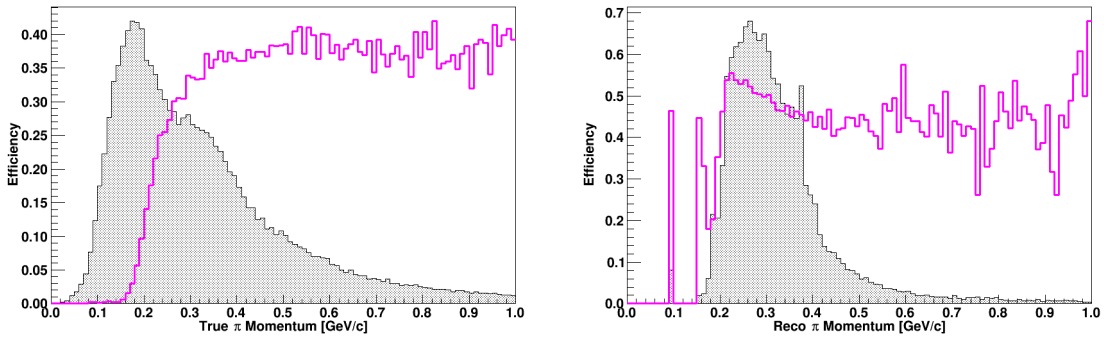

Figure 7.25: Pion efficiency plotted as a function of true pion momentum [left] and reconstructed pion momentum [right]. Overlaid on each plot is the number of After FSI signal pions as a function of the labeled momentum, scaled to arbitrary units.

rection are the analysis particle selection efficiencies and PID which are well understood. This also means that samples pulled from the Monte Carlo can be used without worrying about introducing model dependencies, because it is not model effects that are used to divide the selected signal from the total signal.

The procedure for evaluating the efficiency is to use Equation 7.5, with the following definitions for signal and selected events, defined by the cuts applied to events to be considered in each sample:

$$\begin{aligned} \text{Selected Signal}^{\text{Reco}1\mu1\pi} = &\text{ Passes Precuts \& Is Selected \& PID = } \mu \text{ \& Not mis-ID'ed \&} \\ &\text{Is Reconstructed } 1\mu1\pi \text{ \& } \pi \text{ Momentum} > 250 \text{ MeV}. \end{aligned} \tag{7.2}$$

$$\begin{aligned} \text{All Signal}_1^{\text{Reco}1\mu1\pi} = &\text{ Passes Precuts \& Is Fiducial \& Is True } \mu \text{ \&} \\ &\text{Is Reconstructed } 1\mu1\pi \text{ \& } \pi \text{ Momentum} > 250 \text{ MeV}. \end{aligned} \tag{7.3}$$

$$\begin{aligned} \text{All Signal}_2^{\text{Reco}1\mu1\pi} = &\text{ Does Not Pass Precuts \& Is Fiducial \& Is True } \mu \text{ \&} \\ &\text{Is Reconstructed } 1\mu1\pi \text{ \& } \pi \text{ Momentum} > 250 \text{ MeV}. \end{aligned} \tag{7.4}$$

Here the signal was split into two parts because the events that do not pass pre-cuts generally do not have a reliable muon momentum (largely due to exiting the detector). For these events, the true momentum was smeared to the reconstructed momentum the particles would have been given by using a mapping built by looking at other reconstructed muons and comparing the true

and reconstructed momentum. This method allowed the second signal region to have a reliable reconstructed momentum, and thus it could be added to the first and treated the same. With this, the Signal and Selected samples were plotted in the same muon reconstructed angle and momentum bins as the analysis and the efficiency was calculated for each bin.

$$\text{Efficiency} = \frac{\text{Selected}}{(\text{Signal}_1^{\text{Reco1}\mu 1\pi} + \text{Signal}_2^{\text{Reco1}\mu 1\pi})} \tag{7.5}$$

Efficiency Error

Calculating the error on the efficiency means calculating the error on the inputs to that efficiency calculation. This was done by applying the appropriate systematic errors to the signal and selected samples. The effect of each systematic on the different samples was calculated for each individual kinematic bin as a function of the deviation of the systematic from its nominal value and stored as splines for each systematic, in the same way that parameters are saved and applied within the fitter. The systematics that were applied for the efficiency study are all the detector systematics, the FSI systematics, and the signal model systematics. The background model systematics are all included in the fit, but the signal model systematics have not been incorporated yet. Because the signal model is being used to generate these efficiencies, the uncertainties on the model do need to be included. The incorporation of the signal model parameters, and the use of the signal model to evaluate these efficiencies is unavoidable. The signal definition is still designed to select any events that are reconstructed, and thus is not dependent on the physics model underlying the interactions, which keeps the measurement model independent.

For the error calculation, 5000 ensembles were created. Each ensemble consisted of the default selection and signal distribution, with adjustments made by all the systematics. The systematics applied to each ensemble are evaluated at different values randomly sampled about the central value of the specific systematic. The resulting difference between the distribution of the nominal distribution and the adjusted ensemble were called the *fluctuation* for that ensemble, and the fluctuations were averaged over all ensembles to get the final error:

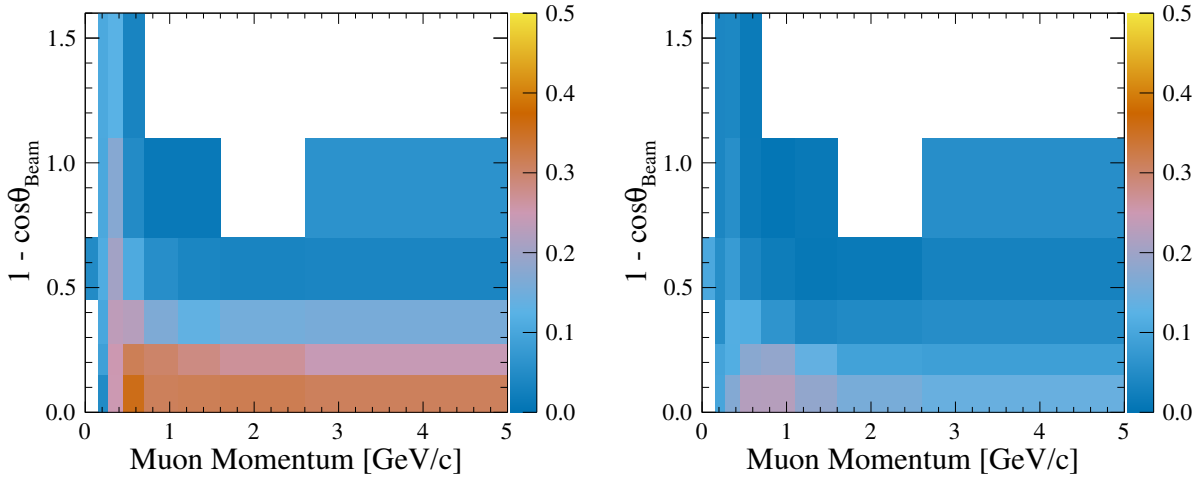

(a) Efficiency **(b)** Error on the Efficiency

Figure 7.26: The selection efficiency used in the cross section calculation for the Reconstructed 1μ 1π signal definition. The efficiency per analysis bin and the error on the efficiency per analysis bin.

$$\text{Selection\_Error}_i = \sqrt{\frac{\sum_n^N (Selection_i^n - Selection_i^0)^2}{/}} N \tag{7.6}$$

This error is the error on analysis bin i and is calculated for $N = 5,000$ ensembles. The error is calculated in the same manner for the Signal distribution.

The total error is then the quadrature sum of the percentage error from both the Signal and Selected sample, evaluated per bin. The efficiency and the error on the efficiency are plotted in Figure 7.26.

The important features in these plots are that there is good coverage of the efficiency, and that the error is not so large as to make the measurement meaningless.

7.3.3 After FSI CC $1\pi^+$

Unlike the reconstructed 1μ 1π signal definition, the after FSI CC $1\pi^+$ definition does not use any information about the reconstructed particles to define the signal, but instead uses the type and number of particles exiting the nucleus after the initial neutrino interaction to define the signal.

To calculate the cross section of after FSI CC $1\pi^+$ events, the efficiency now must correct the number of events observed to the new signal definition. Instead of using the number of measured

events as the selected signal in Equation 7.5, the selected signal is defined as the total number of reconstructed 1μ 1π signal events. This is done because to get the after FSI CC $1\pi^+$ signal definition, the measured events have to be corrected for selection effects (what is corrected for in the reconstructed 1μ 1π efficiency correction) and also for detector reconstruction effects (what is being added). Since this builds on the previous efficiency correction, the corrected reconstructed 1μ 1π signal definition is a good place to start. This leaves two samples:

$$\text{All Selected} = \text{is fiducial \& true } \mu \text{ \& is Reco}1\mu1\pi \text{ \& pi momentum cut} \tag{7.7}$$

$$\text{All Signal}^{\text{FSIcc}1\pi} = \text{is fiducial \& true } \mu \text{ \& is FSI } 1\mu1\pi \text{ \& pi momentum cut} \tag{7.8}$$

Background Subtraction

The challenge with using the data corrected to reconstructed 1μ 1π as the initial selection is that this selection includes both signal and background, whereas the selection for the previous case contained only signal. This selection is all reconstructed 1μ 1π events, which contains both after FSI CC $1\pi^+$ events (signal(after FSI CC $1\pi^+$)) and not after FSI CC $1\pi^+$ events (background or not(after FSI CC $1\pi^+$)). This means that before the efficiency correction can be done, the background events have to be subtracted from the selected events to get the total number of signal events.

$$Signal = Selected - Background \tag{7.9}$$

Calculating the background to subtract off for this correction is simple to do using the MC, but that raises the question of introducing model dependence. Because the background being subtracted is modeled by the background physics processes, as seen in Figure 7.27, there is little signal model dependence being introduced. Additionally, the errors that are used for the background models cover the uncertainty in those models, and so when propagated to the efficiency correction they cover the variation that may exist within the models being used.

The selection broken down into selected signal and selected background are defined below:

$$\text{Selected Signal}^{\text{FSIcc1}\pi} = \text{is fiducial \& true } \mu \text{ \&} \tag{7.10}$$

$$\text{is reco } 1\mu1\pi \text{ \& is FSI } 1\mu1\pi \text{ \& pi momentum cut}$$

$$\text{Selected Background}^{\text{FSIcc1}\pi} = \text{is fiducial \& true } \mu \text{ \&} \tag{7.11}$$

$$\text{is reco } 1\mu1\pi \text{ \& not FSI } 1\mu1\pi \text{ \& pi momentum cut}$$

$$\tag{7.12}$$

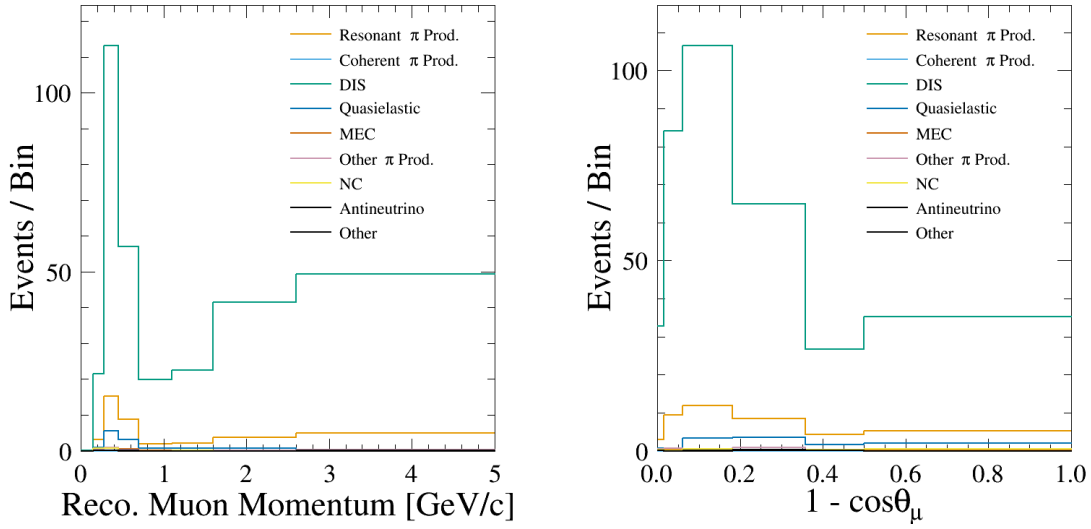

Figure 7.27: Selected Background events for the after FSI CC $1\pi^+$ cross section calculation broken down by interaction type. The left plot is the momentum projection of the Background sample, and right plot is the angle distribution.

The error on this background was calculated using the same method as the error on the inputs to the efficiency correction: many combinations of systematic errors were applied to the samples, and the averages of those errors were used to characterize the error of the background. Specifically, the background was calculated by subtracting the selected signal from the total selected, so those are the two samples that were varied to extract the error on the background.

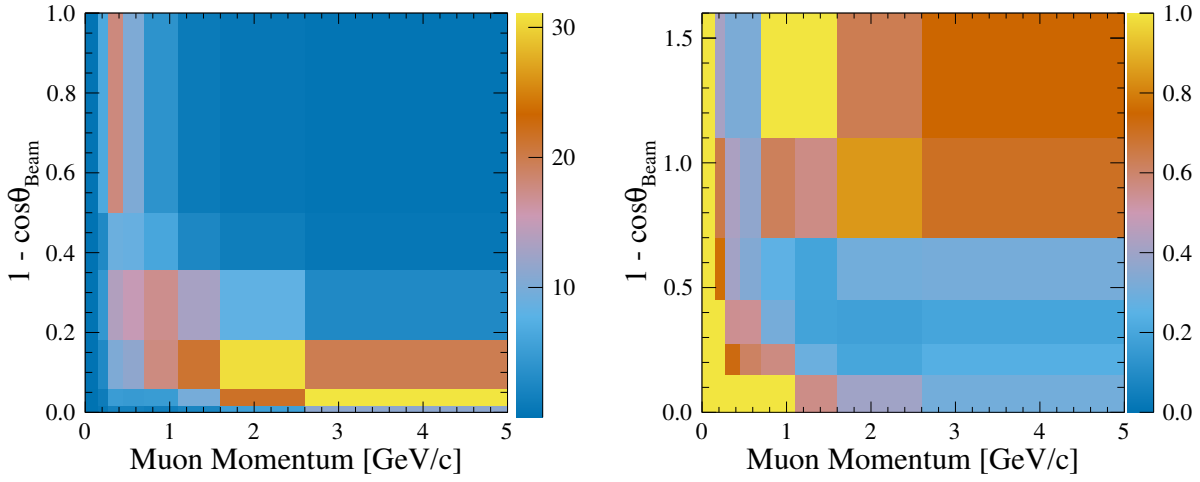

(a) Selected Background

(b) Error on Selected Background

Figure 7.28: Selected Background events and percent error per bin on the selected background events for the after FSI CC $1\pi^+$ cross section calculation.

After FSI CC $1\pi^+$ Efficiency

The efficiency was calculated in the same fashion as before, taking care to clearly define the selected events as selected signal instead of all selected events, because in the cross section calculation the background will be subtracted off before the efficiency is applied.

$$\text{Efficiency}^{\text{FSIcc1}\pi} = \frac{\text{Selected Signal}}{\text{All Signal}^{\text{FSIcc1}\pi}} \tag{7.13}$$

After FSI 1μ 1π Error

The error for the after FSI CC $1\pi^+$ efficiency was calculated in the same fashion as the reconstructed 1μ 1π efficiency described in Section 7.3.2. The samples used in the efficiency calculation in (7.13) are the same ones used to evaluate the error on that efficiency. The final efficiency and error per bin are plotted in Figure 7.29. The efficiency in the region of phase space where the majority of the events are is around 30%, falling to around 17% in the region with only a few events. The error on the efficiency is up at 25% only in the lowest momentum bins where there are almost no events, with the error for the rest of the phase space between 10% and 15%. These selection efficiencies and errors are as good as the analysis could make them, as they are dependent on the

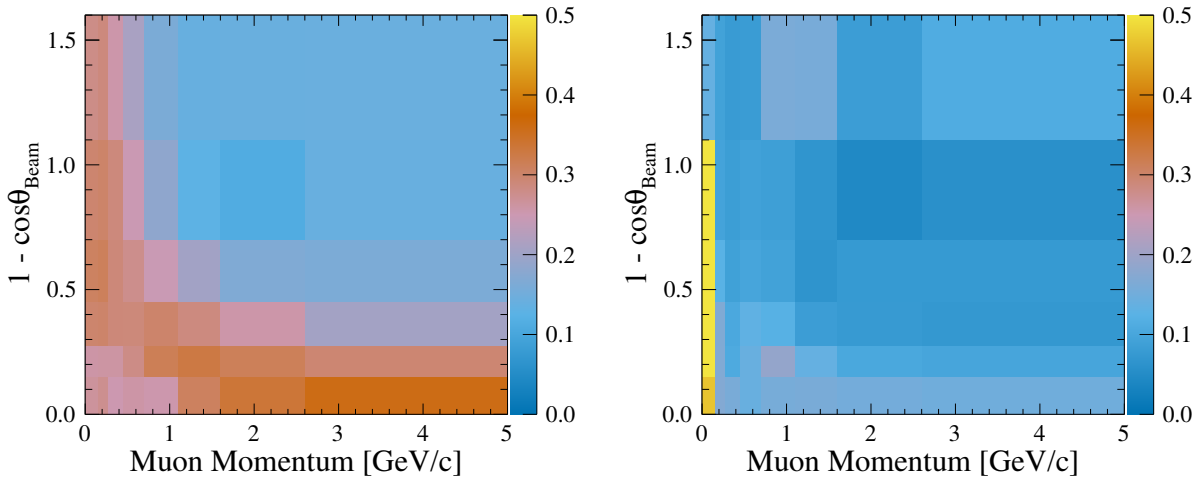

(a) Efficiency

(b) Error on the Efficiency

Figure 7.29: The selection efficiency used in the cross section calculation for the after FSI CC $1\pi^+$ signal definition. The efficiency per analysis bin and the error on the efficiency per analysis bin.

detector acceptance and reconstruction efficiencies. The effort made to improve the momentum reconstruction for this analysis also contributes to the low errors.

7.4 Neutrino Flux

The neutrino flux is monitored by a dedicated group within T2K that releases the flux for each run period, as well as the errors on that flux. For the Run 4 water in period, the integrated flux incident on the fiducial volume is 3.16×10^{12} neutrinos/cm^2 with an error of 7.75%. This number is not dependent on muon angle or momentum and thus is a constant in the cross section calculation for all bins. It is important to remember that this measurement is specific to the T2K neutrino flux, and thus is not directly comparable to similar measurements made by different experiments with different neutrino spectra.

7.5 Target Nucleons

The number of target nucleons within the fiducial volume of the P∅D was calculated in Chapter 1.3.4 along with the error on that number. For this measurement, because resonant interactions can occur on protons and neutrons, the cross section is presented as the cross section per nucleon:

each neutron and proton within the fiducial volume. The number of targets is also not dependent on the kinematic bins and thus the total number of nucleons of 2.80×10^{30} nucleons with an error of 3.0% is used for each bin in the differential cross section calculation.

7.6 Cross Section Measurement

In this section two variations of the cross section measurement are presented. The final cross section is calculated following the Equation 1.9. The first cross section presented is that calculated using the reconstructed 1μ 1π signal definition. While this is a useful definition within the analysis, this measurement is not easily compared to other measurements due to its dependence on the PØD acceptance and reconstruction efficiencies. The second cross section is that for the after FSI CC $1\pi^+$ definition, and as such is more easily compared to other results, though it does integrate over the T2K neutrino flux.

7.6.1 Reconstructed 1μ 1π

The cross section calculation in Equation 7.14 provides the cross section per nucleon per analysis bin i. The terms in the equation have described previously: the number of selected signal events extracted by the fitter per bin N_i, the efficiency per bin ϵ_i, the flux incident on the fiducial volume Φ and the number of target nucleons within the fiducial volume T.

$$\sigma_i = \frac{N_i}{\epsilon_i^{reco1\mu1\pi}\Phi T} \tag{7.14}$$

The error on the cross section is also calculated per bin and is simply the error on all the components added in quadrature. Plotted in figure Figure 7.30 is the measured cross section in momentum and angle projections with double error bars depicting the total error and the error from just the fit which includes statistical and systematic error.

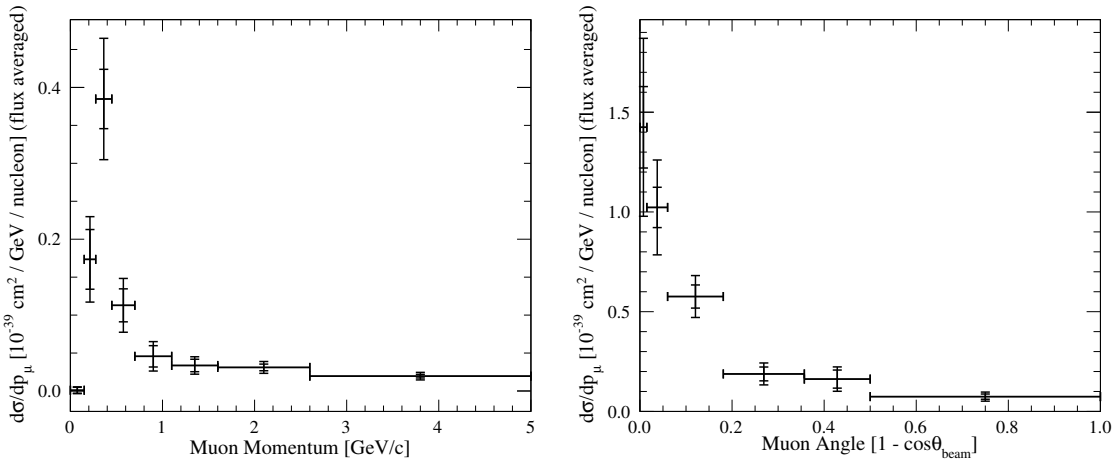

(a) Muon Momentum **(b)** Muon Angle

Figure 7.30: reconstructed 1μ 1π Cross Section Results.

7.6.2 After FSI CC $1\pi^+$

The cross section calculation that is the most directly comparable to other measurements is the after FSI CC $1\pi^+$ cross section. This cross section requires two stages of efficiency correction, first adjusting the number of events measured to be the efficiency corrected number of Reconstructed $1\mu1\pi$ events, then correcting to the full after FSI CC $1\pi^+$ measurement.

$$\sigma_i = \frac{(N_i/\epsilon_i^{reco1\mu1\pi}) - B_i}{\epsilon_i^{AFSIcc1\pi}\Phi T} \tag{7.15}$$

The error on the cross section is also calculated per bin and is again the error on all the components added in quadrature. Here it is important to note that a pion momentum cut of 250 MeV is applied to this calculation, and that the measurement is integrated over the T2K flux.

Plotted in figure Figure 7.31 is the measured after FSI CC $1\pi^+$ cross section calculation, and the momentum and angle projections with errors. For the errors plotted, the outer error bar is the total error, and the inner error bar is the propagated error from the fit.

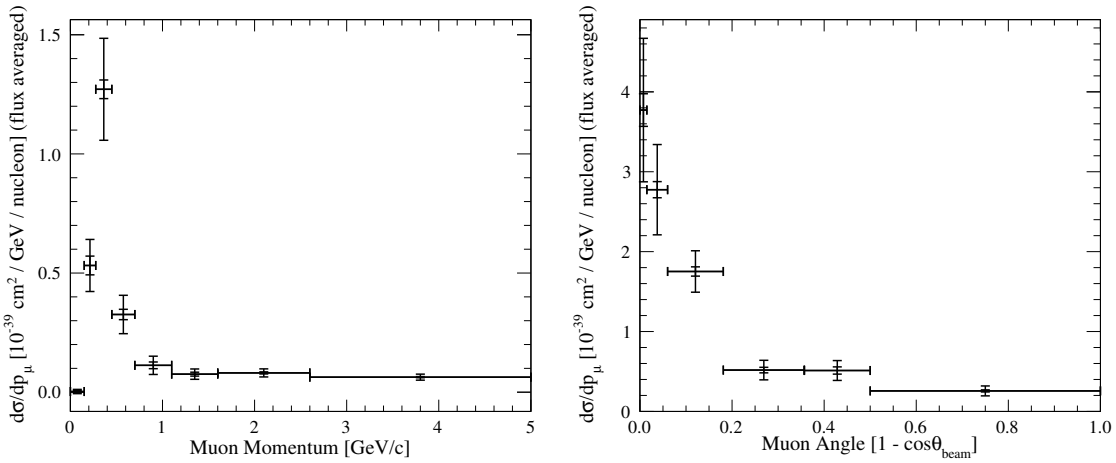

(a) Muon Momentum **(b)** Muon Angle

Figure 7.31: after FSI CC $1\pi^+$ Cross Section Results.

7.6.3 Model Comparisons

To compare a measurement with a theoretical model, either the results of the measurement need to be adjusted for all the reconstruction and detector effects so that they are in terms of true particle kinematics, or the theoretical model needs to be subject to the same reconstruction and detector effects such that the now reconstructed kinematics can be compared to the measured data. The process of relating the phase space of the model to that of the measurement is called folding, and this is effectively what is done in the the Monte Carlo event generators. Folding can work in two directions, either mapping true kinematics (from theoretical models) to reconstructed kinematics, called forward folding, or doing the opposite and mapping reconstructed kinematics back to the true kinematics that created the event, called unfolding.

For comparing with external data sets, *unfolding* can be very useful since it produces a cross section in true kinematics. The method does produce a number of challenges, one of the largest being that determining the true kinematics from the reconstructed measurement is not a one-to-one problem. While an event with known true kinematics has well-defined reconstructed kinematics (which is the basis for using Monte Carlo event generators), a reconstructed event can result from a number of different true events, and the methods for breaking this degeneracy are still being studied in the research community. The methods used to break the true-to-reconstructed degeneracy are

an avenue for model dependence to be incorporated back into the measurement unless extra care is taken. Additionally, the presentation of results in "true" kinematics does not make them directly comparable to all theoretical models: the measurements are still specific to the analysis being performed as the detector acceptance, efficiencies, and neutrino beam are all folded into the final result. This last point means that though these final results are in the "true" phase space, they are not automatically comparable to any model without taking these other inputs into account.

Forward folding requires that the analyzers do the model comparisons as part of the analysis, which ensures that all effects unique to that analysis are applied to the model in the same fashion that the were applied to the data. The simplest way to forward fold a model is to have Monte Carlo files generated using the model, which will allow for the events to be processed in the same fashion as any other simulated events. Forward folding is the method chosen by this analysis, so as to avoid any chance that model dependence enter into the result through the unfolding process. Additionally there are already new signal models available to compare the measurement with and thus the comparison can be done within the framework of the analysis. The Minoo model [14] was added to a special release of NEUT from which a re-weight function based on true muon and true pion kinematics was developed that could be applied to the default NEUT resonant signal used in this analysis to convert the already generated events into the new Minoo model phase space. For the Berger-Sehgal model [16] a simple re-weighting scheme based on true pion kinetic energy was used to scale the NEUT coherent signal, as provided in Table 7.1. Four sets of Monte Carlo were processed as signal events through to cross section extraction following the same procedure described above for data: Default NEUT 5.3.3 [8], default NEUT with the resonant model scaled to the Minoo resonant model, default NEUT with the coherent model scaled to the Berger-Sehgal coherent model, and default NEUT with both the resonant and coherent models scaled to the Minoo and Berger-Sehgal models respectively. The resulting after FSI CC $1\pi^+$ cross sections are plotted in Figure 7.32.

The updated coherent model present by Berger and Sehgal adjusts the coherent cross section and reduces the probability of events at low pion kinetic energy, as discussed in Chapter 2.2.2. As

Table 7.1: Berger-Sehgal Reweighting

Pion KE [GeV]	Weight
0 - 0.25	0.135
0.25 - 0.5	0.40
0.5 - 0.75	0.294
0.75 - 1.0	1.206
> 1.0	1

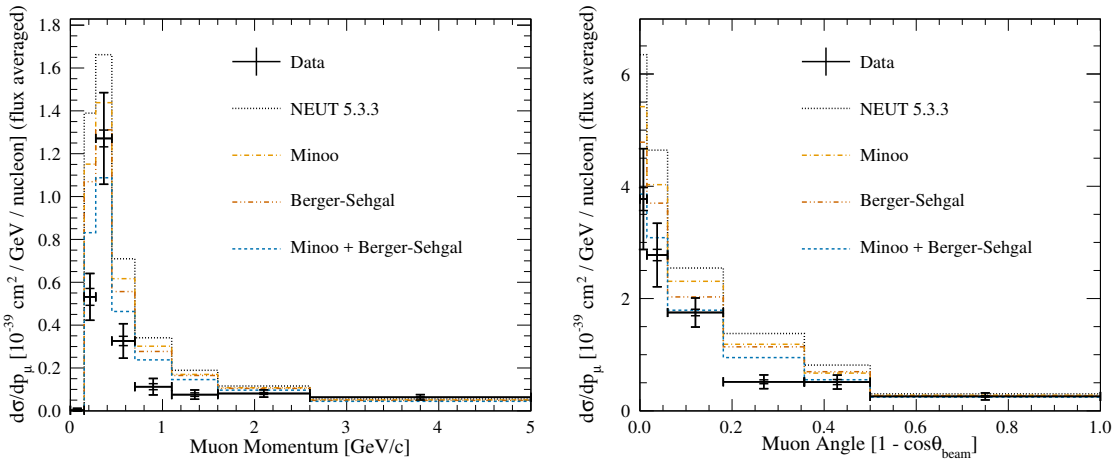

(a) Muon Momentum **(b)** Muon Angle

Figure 7.32: The after FSI CC $1\pi^+$ cross section compared to different model predictions.

most the pions in this analysis are in the lowest kinetic energy region, the coherent fraction of this sample has almost half the cross section of the default NEUT coherent sample, and in Figure 7.32 the effect of this model can be seen to decrease the total CC $1\pi^+$ (coherent+resonant) cross section by almost 20%. Additionally, the Minoo model also described in Chapter 2.2.2 decreases the number of events expected in this analysis, though for this model it is not that the Minoo model predicts fewer events, but instead the model predicts that events will produce pions with lower momentum than the previous models. The change of pion momentum then moves events out of the reconstructed sample, which effectively decreases the number of events expected to be seen in this analysis. The Minoo model predicts around a 10% decrease in the total CC $1\pi^+$ cross section. The result of both of these effects is around a 30% decrease in the predicted CC $1\pi^+$ cross section.

The data is not consistent with any of the models in Figure 7.32, which serves to motivate the need for more measurements of this interaction in this neutrino energy region for a variety of different event kinematics, and also the need for more development of the models currently used to describe the CC $1\pi^+$ interaction. The new models are closer to agreement with the data than the default NEUT models, which implies that the new models are moving in the right direction to describe the physics that is measured correctly.

7.6.4 Comparison to Other Measurements

Previous PØD measurement

The measurement made here was the second time the PØD was used to measure the CC $1\pi^+$ cross section. The first measurement was an integrated cross section measurement that reported the CC $1\pi^+$ cross section per water nucleon as a single number: $(1.10\ ^{+0.39}_{-0.36}) \times 10^{-39}$ cm^2/nucleon [7]. The most comparable measurement by this analysis would be the final after FSI CC $1\pi^+$ cross section calculation. Adding the bins together and calculating the final cross section and error gives an integrated cross section per nucleon from this analysis as $(0.686 \pm 0.21) \times 10^{-39}$ cm^2/nucleon.

The measurement in this analysis is within two sigma of the previous measurement, while the previous measurement is within three sigma of the new measurement. These two results overlap

only at the upper and lower most extent of the error bars, but the difference in the analyses makes this expected.

First is the fact that the two measurements are of different cross sections: the previous measurement was made on water only while the new measurement is for all materials within the fiducial volume. Also the previous measurement efficiency corrects to the full muon momentum spectrum while the new measurement does not include events with pion momenta below 250 MeV. After those fundamental differences are the different approaches used to make the measurements. The previous analysis used a background subtraction method to extract the signal and had a different signal definition throughout the analysis. Both of these would make a signal model dependence possible, and could explain why the previous measurement agreed better with the simulation than the current analysis. These two measurements represent the progression of cross section measurements, and should be seen as progressive steps towards better measurements.

Tracker Measurement

In the ND280 detector, analyses have been done using different parts of the detector. One such measurement is that made using the tracker region to measure the cross section of after FSI CC $1\pi^+$ as a function of a number of different muon and pion kinematics [32]. The tracker measurement reports an integrated cross section of $(1.176\pm0.283) \times 10^{-39}$ cm^2/nucleon, which is consistent with the default NEUT cross section prediction. Throughout the tracker's differential measurements, all are consistent with the NEUT predictions.

Again a direct comparison between the tracker measurement and the measurement described in this thesis can not be done as there are many differences between the analyses, from target to reconstruction to analysis technique. The tracker analysis used an unfolding method to convert the extracted signal into true kinematics, a method that has the potential to introduce model dependence and may point to why the results match the MC so closely. Another unique feature to the tracker measurement was the use of pion decay products, specifically Michel electrons, to identify low-energy pions for some of the samples used in that analysis. This allowed the tracker to reconstruct events with low-momentum pions that were not included in the measurement in this

thesis. Another restriction on some samples in the tracker analysis is events with a muon or pion at high angle (with a $\cos\theta > 0.2$). While the high angle region is one of the less populated regions in the analysis in this thesis and thus contained in the large high angle bin, the contained and cluster samples of the analysis in this thesis do cover these events.

With all the differences between the two analyses, direct comparisons are not valid so no concrete statements can be made. What is certain is that more measurements are needed in this region and that continued care needs to be taken to ensure that measurements are as independent of the signal models as possible.

7.7 Conclusion

The focus of the analysis described in this thesis was to make a model independent measurement of the CC $1\pi^+$ cross section and compare that measurement with the available theoretical models. Careful definition of the reconstructed signal allowed the signal extraction tools to depend on detector, reconstruction, and analysis models and efficiencies for individual reconstructed tracks instead of for model dependent events. The two stage efficiency correction that was used to convert the reconstructed signal to the after FSI CC $1\pi^+$ signal definition was done independent of the signal extraction and as such was carefully studied to ensure as little model dependence entered the correction as possible. The final comparisons to external models was done with forward folded signal models that applied the detector and reconstruction effects to the new models instead of risking the application of model dependence to compare in the true kinematic space. These precautions resulted in a measurement with little signal model dependence, and carefully considered error estimation to complement that measurement. In addition, the phase space of this measurement was studied extensively to make sure that no gaps in efficiency were artificially filled with the efficiency correction, which ensured the result would be accurate and model independent. These precautions together with the improved reconstruction objects allowed this analysis to make a differential measurement that has proven a useful test for the new resonant and coherent models.

Bibliography

[1] J. A. Formaggio and G. P. Zeller. From eV to EeV: Neutrino Cross Sections Across Energy Scales. *Reviews of Modern Physics*, 84:1307–1341, 2012.

[2] J. Nieves, I. Ruiz Simo, and M. J. Vicente Vacas. Inclusive Charged–Current Neutrino–Nucleus Reactions. *Phys. Rev.*, C83:045501, 2011.

[3] K. Abe et al. The T2K Experiment. *Nucl. Instrum. Meth.*, A659:106–135, 2011.

[4] S. Assylbekov et al. The T2K ND280 Off-Axis Pi-Zero Detector. *Nucl. Instrum. Meth.*, A686:48–63, 2012.

[5] Karin Gilje. Geometry and Mass of the π^0 Detector in the ND280 Basket. *T2K Technical Note*, TN73, 2012.

[6] N. Abgrall et al. Time Projection Chambers for the T2K Near Detectors. *Nucl. Instrum. Meth.*, A637:25–46, 2011.

[7] Shamil M. Assylbekov. Measurement of ν_{mu}-induced Charged-Current Single π^+ Production on H_2O. *Colorado State University*, 2015.

[8] Yoshinari Hayato. A neutrino interaction simulation program library NEUT. *Acta Phys. Polon.*, B40:2477–2489, 2009.

[9] Costas Andreopoulos, Christopher Barry, Steve Dytman, Hugh Gallagher, Tomasz Golan, Robert Hatcher, Gabriel Perdue, and Julia Yarba. The GENIE Neutrino Monte Carlo Generator: Physics and User Manual. 2015.

[10] R. A. Smith and E. J. Moniz. Neutrino Reactions on Nuclear Targets. *Nuclear Physics B*, 43:605–622, 1972.

[11] Omar Benhar and Adelchi Fabrocini. Two nucleon spectral function in infinite nuclear matter. *Phys. Rev.*, C62:034304, 2000.

[12] Dieter Rein and Lalit M. Sehgal. Neutrino-Excitation of Baryon Resonances and Single Pion Production. *Annals of Physics*, 133:79–153, 1981.

[13] C. H Llewellyn Smith. Neutrino Interactions at Accelerator Energies. *Physics Reports*, 3:261–379, 1972.

[14] Monireh Kabirnezhad. Single pion production in neutrino-nucleon Interactions. *Phys. Rev.*, D97(1):013002, 2018.

[15] Dieter Rein and Lalit M. Sehgal. Coherent π^0 production in neutrino reactions. *Nuclear Physics B*, 223:29–44, 1983.

[16] Ch. Berger and L. M. Sehgal. PCAC and coherent pion production by low energy neutrinos. *Phys. Rev.*, D79:053003, 2009.

[17] Arie Bodek and Un-ki Yang. Axial and Vector Structure Functions for Electron- and Neutrino- Nucleon Scattering Cross Sections at all Q^2 using Effective Leading order Parton Distribution Functions. *arXiv*, 1011.6592[hep-ph], 2010.

[18] S. Agostinelli et al. GEANT4: A simulation toolkit. *Nucl. Instrum. Meth.*, A506:250–303, 2003.

[19] Giuseppe Battistoni, S. Muraro, Paola R. Sala, Fabio Cerutti, A. Ferrari, Stefan Roesler, A. Fasso, and J. Ranft. The FLUKA code: Description and benchmarking. *AIP Conf. Proc.*, 896:31–49, 2007.

[20] D. H. Wright and M. H. Kelsey. The Geant4 Bertini Cascade. *Nucl. Instrum. Meth.*, A804:175–188, 2015.

[21] K. Abe et al. T2K neutrino flux prediction. *Phys. Rev.*, D87(1):012001, 2013.

[22] Glen Lopez. Measurement of the Single Neutral Pion Production Cross Section in Neutral-Current Neutrino Interactions in the T2K Pi-zero Detector. *Stony Brook University*, 2012.

[23] Greg Welch and Gary Bishop. An Introduction to the Kalman Filter. March 2007.

[24] C. Patrignani and others (Particle Data Group). Review of Particle Physics. *Chin. Phys.*, C40(10):100001, 2016.

[25] Jaclyn Schwehr, Daniel Cherdack, and Matthew Hogan. Measurement of the ν_μ CC $1\pi^+$ Double Differential Cross Section on Water in the P0D. *T2K Technical Note*, TN333, 2018.

[26] R. Brun and F. Rademakers. ROOT: An object oriented data analysis framework. *Nucl. Instrum. Meth.*, A389:81–86, 1997.

[27] Andreas Hocker et al. TMVA - Toolkit for Multivariate Data Analysis. *PoS*, ACAT:040, 2007.

[28] Tianlu Yuan, Jeremy Lopez, and Alysia Marino. A Double Differential Measurement of the Flux Averaged ν_μ CC0π Cross Section on Water. *T2K Technical Note*, TN258, 2016.

[29] Thomas Campbell, Erez Reinherz-Aronis, and Walter Toki. The $\bar{\nu}_\mu/\nu_\mu$ Cross Section Ratio with the P0D+TPC1 Samples. *T2K Technical Note*, TN208, 2017.

[30] Julia Yarba. Recent developments and validation of Geant4 hadronic physics. *J. Phys. Conf. Ser.*, 396:022060, 2012.

[31] M. R. Whalley. A New neutrino cross section data resource. *Nucl. Phys. Proc. Suppl.*, 139:241–246, 2005.

[32] K Abe et al. Measurement of the muon neutrino charged-current single π^+ production on C_8H_8 using the T2K off-axis beam. *not yet submitted*, 2018.

[33] Lee Trung. Event reconstruction and energy calibration using cosmic muons for the T2K pizero detector. *Stony Brook University*, 2009.

[34] Daniel Ruterbories. Measurement of the Total Flux Averaged Neutrino Induced Neutral Current Elastic Scattering Cross Section with the T2K Pi-Zero Detector. *Colorado State University*, 2014.

Appendix A

MVA Variables

This section contains details on all the variables used in the two multivariate analyses (MVAs) used in this analysis. For each variable there is a brief description of what the variable is and how it was calculated, as well as a number of plots. The plots include the distribution of the variable for the given reconstruction algorithm, as well as a data/Monte Carlo comparison. Additionally there are plots showing the individual separation power of each variable for whichever MVA it was used in. If a variable is missing one of the MVA plots, that is an indication that the variable is not used in that MVA.

A.1 General Variables

General variables are those that represent basic track or event properties that are direct outputs of the track fitters.

Track Length

The track length is the length of the reconstructed track. When a track was reconstructed with pØdRecon, it was saved as a series of nodes, where each node represented the charge and position within a single PØDule where the track crossed that PØDule. The track length was calculated by adding up the distance between these nodes.

The track length is a basic track property that is provided to the MVA because many other variables depend on it. This means that the track length is not included to provide separation power, but rather to provide a variable to use in conjunction with other variables.

This variable was used in both the MIP MVA and the MuPi MVA, for both Kalman and Cluster tracks.

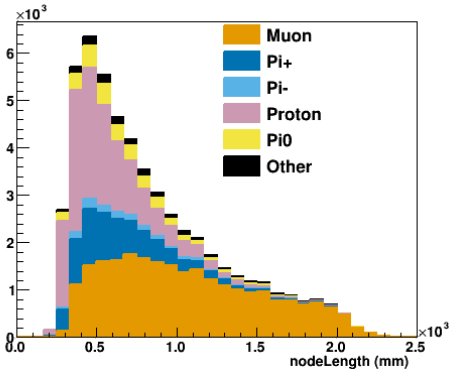

(a) Particle Breakdown

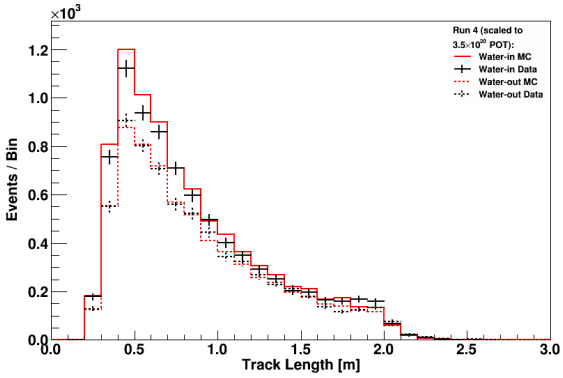

(b) Data MC Comparison

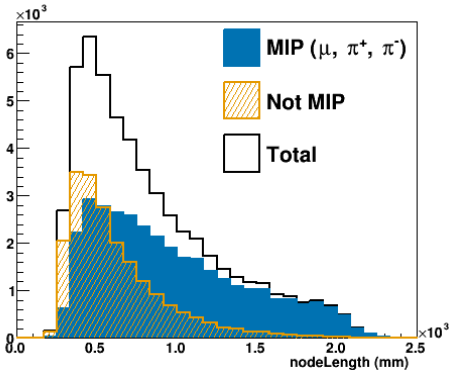

(c) MIP Signal Background Comparison

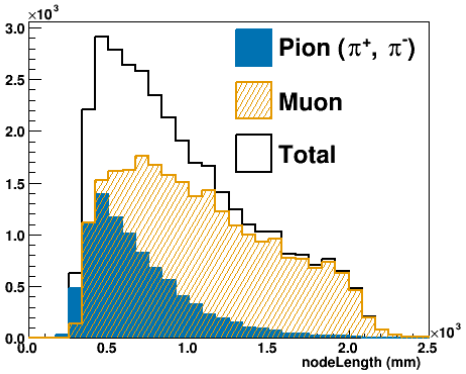

(d) MuPi Signal Background Comparison

Figure A.1: Track Length - Kalman

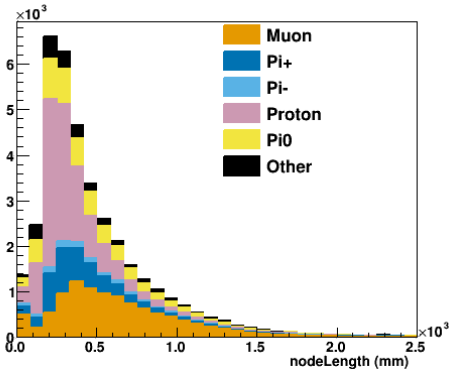

(a) Particle Breakdown

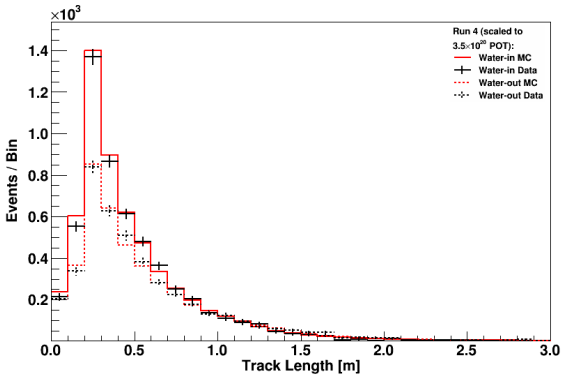

(b) Data MC Comparison

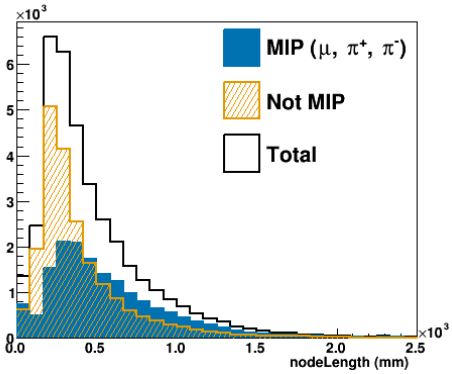

(c) MIP Signal Background Comparison

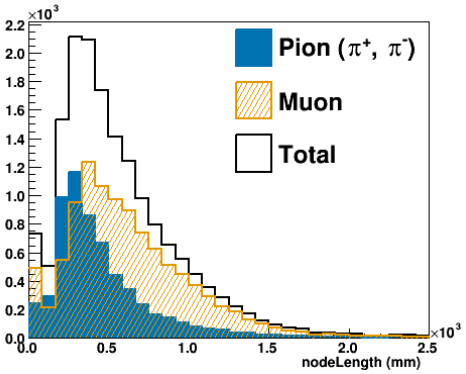

(d) MuPi Signal Background Comparison

Figure A.2: Track Length - Cluster

Total Charge Detected

Any charge seen by the PØD that pØdRecon associated with the track is summed together and stored in this variable. This charge has been calibrated for attenuation and is in units of PEU's (photo electron units).

The total charge is a useful property of a track, especially when used in conjunction with other variables. On its own this variable does not provide much separation, but it is a basic property to compare other variables against.

This variable was used in the MIP MVA for cluster tracks, while in the MuPi MVA it was used for both Cluster and Kalman tracks.

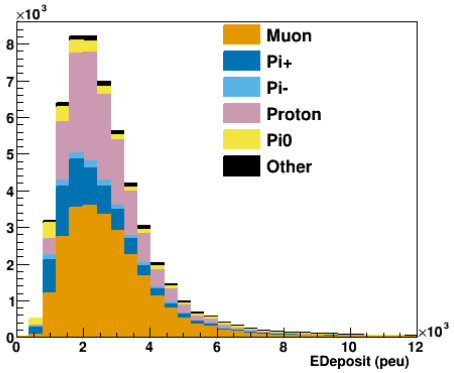

(a) Particle Breakdown

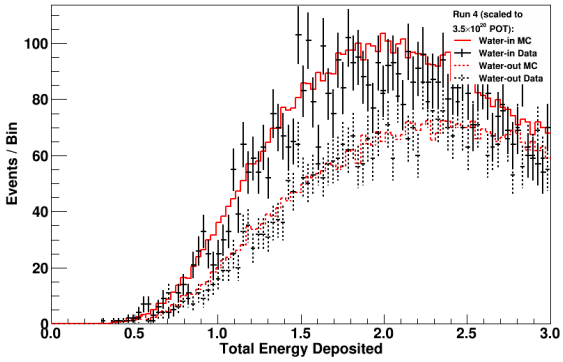

(b) Data MC Comparison

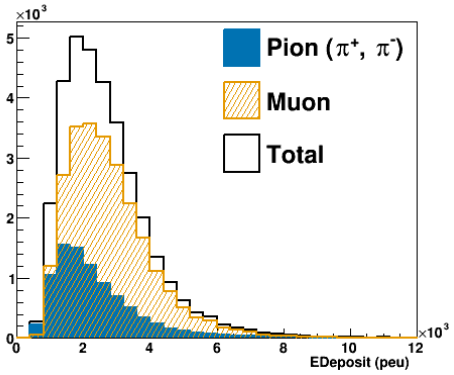

(c) MuPi Signal Background Comparison

Figure A.3: Total Charge Detected - Kalman

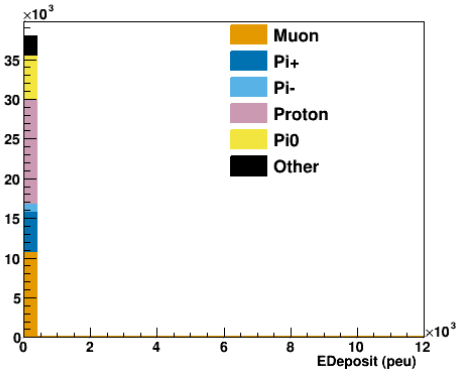

(a) Particle Breakdown

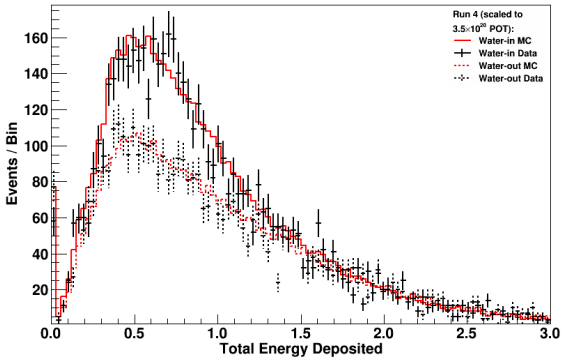

(b) Data MC Comparison

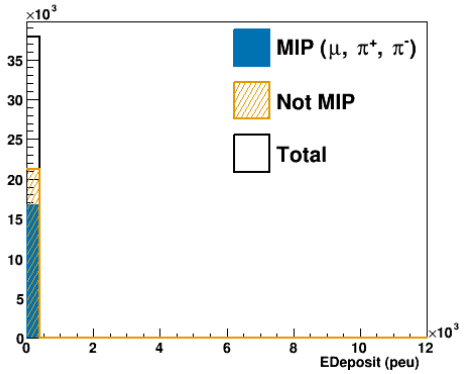

(c) MIP Signal Background Comparison

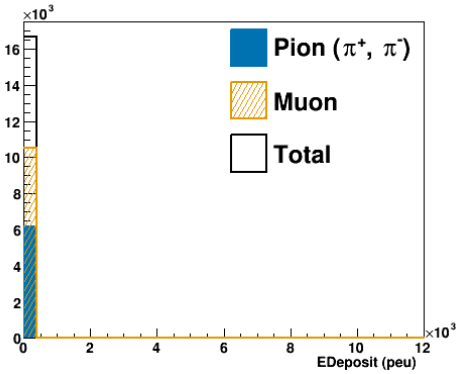

(d) MuPi Signal Background Comparison

Figure A.4: Total Charge Detected - Cluster

Number of PØDules Crossed

The number of PØDules crossed is simply a count of how many PØDules the track traversed.

In conjunction with the track length above, the number of PØDules crossed gives a rough approximation of the angle of a track. Because the measurement is being made in units of the track angle, it was best to not use the reconstructed angle as a direct input to the MVA. This variable allows the MVA to extract angle information and use it to separate other variables.

This variable was used in both the MIP MVA and the MuPi MVA, for both Kalman and Cluster tracks.

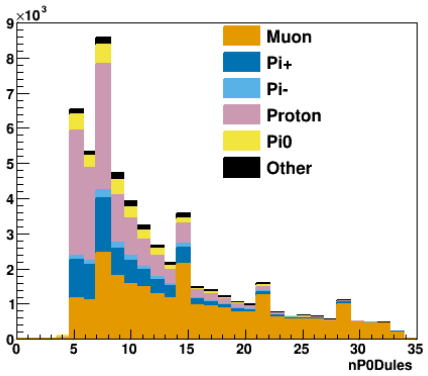

(a) Particle Breakdown

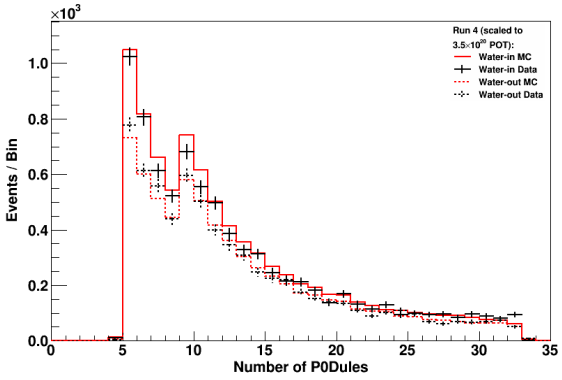

(b) Data MC Comparison

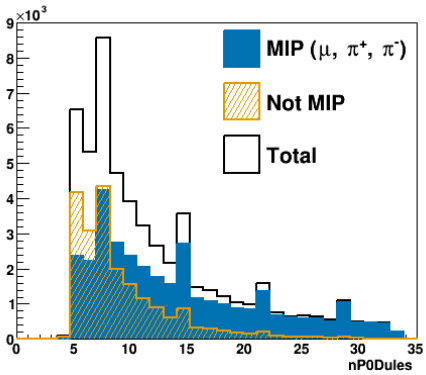

(c) MIP Signal Background Comparison

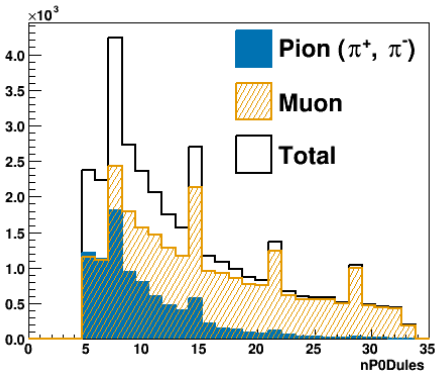

(d) MuPi Signal Background Comparison

Figure A.5: Number of PØDules Crossed - Kalman

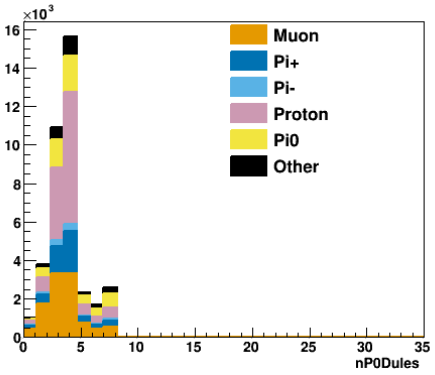

(a) Particle Breakdown

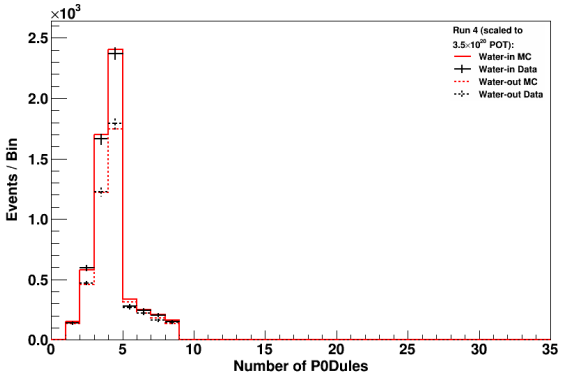

(b) Data MC Comparison

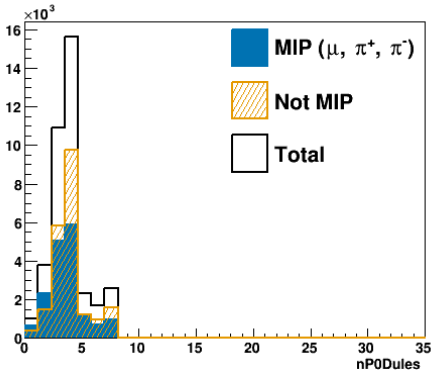

(c) MIP Signal Background Comparison

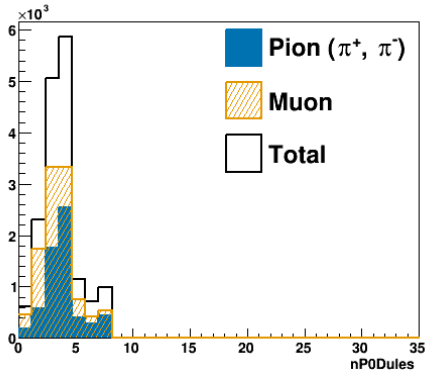

(d) MuPi Signal Background Comparison

Figure A.6: Number of P∅Dules Crossed - Cluster

Distance to Michel Cluster

PØdRecon has an algorithm that studies clusters of energy in the PØD to see if they may have been caused by an electron from a muon decay (a Michel electron). The algorithm this analysis used was developed by Le Trung [33], and after that algorithm identified a cluster as being possibly formed by a Michel electron, the distance between the end of our track and the Michel Cluster was calculated.

Not all events had prospective Michel Clusters, but for the events that did, if the Michel cluster was close enough to a track it was a very good indication that the track was a muon.

This variable was used in both the MIP MVA and the MuPi MVA, for both Kalman and Cluster tracks.

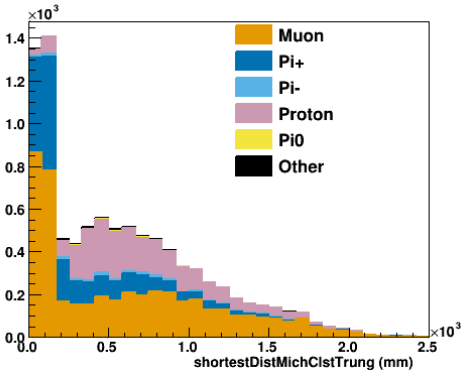

(a) Particle Breakdown

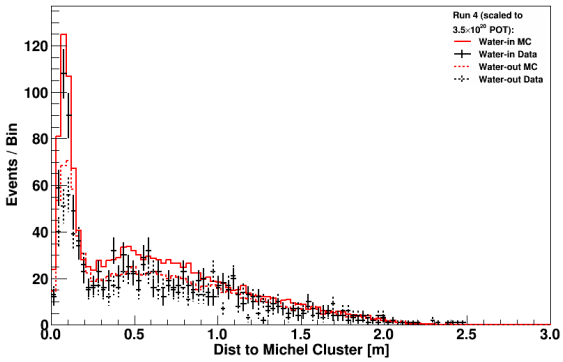

(b) Data MC Comparison

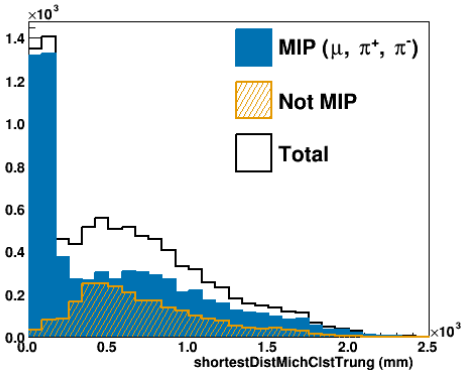

(c) MIP Signal Background Comparison

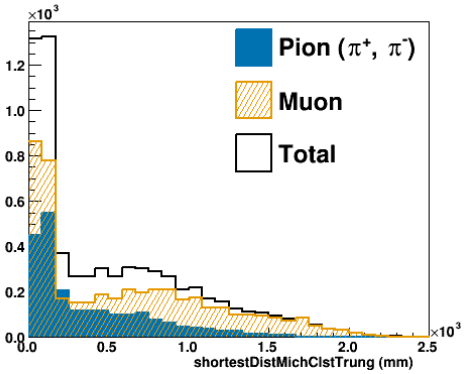

(d) MuPi Signal Background Comparison

Figure A.7: Distance to Michel Cluster - Kalman

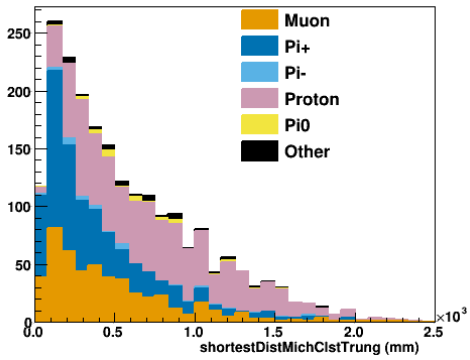

(a) Particle Breakdown

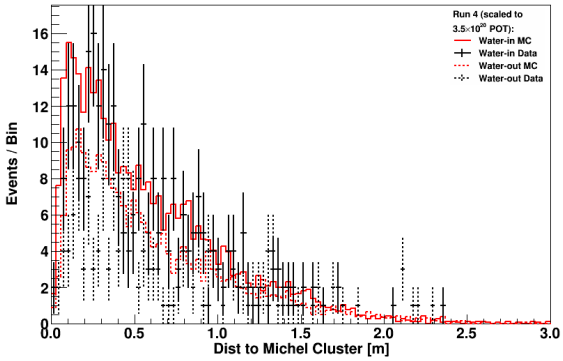

(b) Data MC Comparison

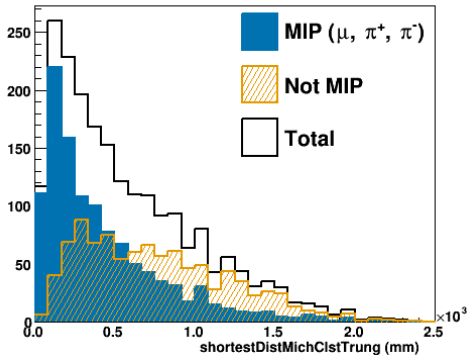

(c) MIP Signal Background Comparison

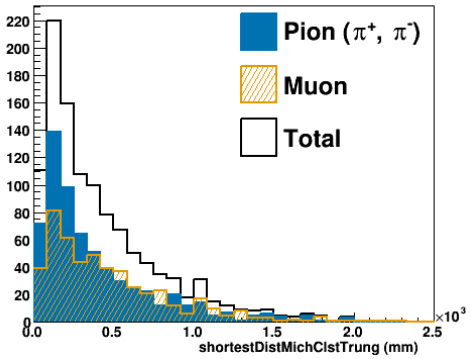

(d) MuPi Signal Background Comparison

Figure A.8: Distance to Michel Cluster - Cluster

dE/dX Pull at Track End

In the PØD NCE analysis done by Daniel Ruterbories [34], a PID was developed to identify protons by looking at the energy deposited at the end of a track. This algorithm energy corrects an angled track so that it can be compared with a perfectly forward going track, matching up the end of the track to the template it is compared to. A pull is calculated based on the energy in each PØDule, stepping back from the end of the track, comparing the track to the template to identify how not-muon-like a track is.

This pull value is computed for both the Kalman and Cluster tracks.

This variable was used in both the MIP MVA and the MuPi MVA, for both Kalman and Cluster tracks.

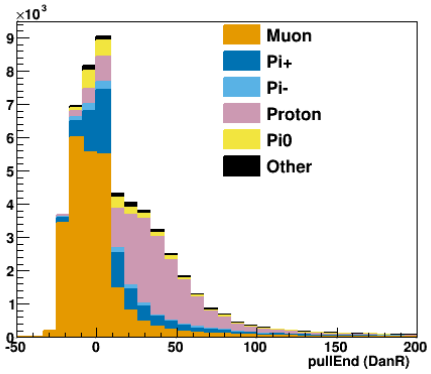

(a) Particle Breakdown

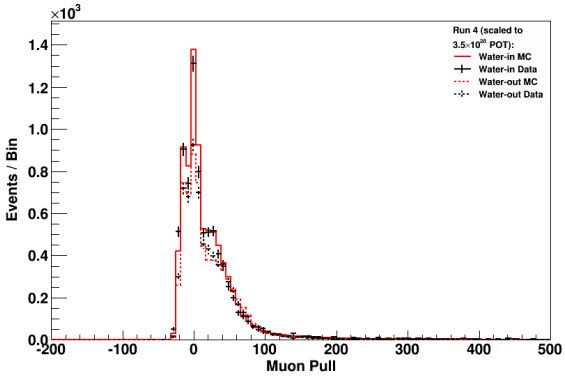

(b) Data MC Comparison

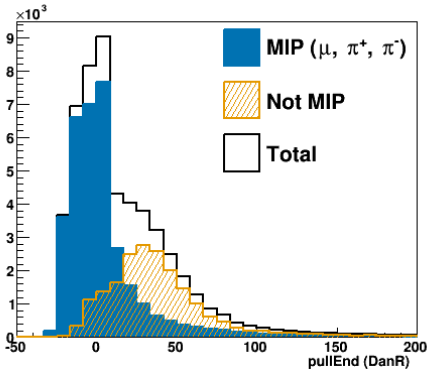

(c) MIP Signal Background Comparison

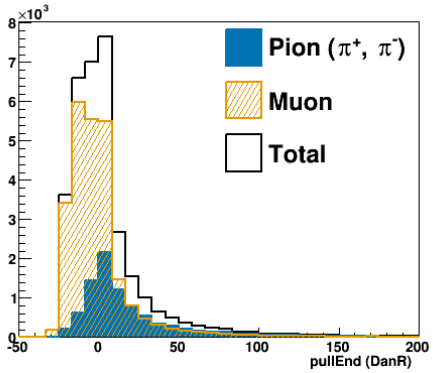

(d) MuPi Signal Background Comparison

Figure A.9: dE/dX Pull at Track End - Kalman

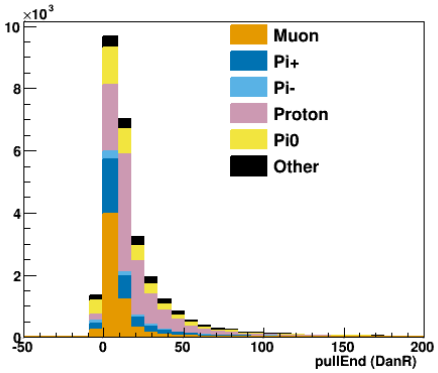

(a) Particle Breakdown

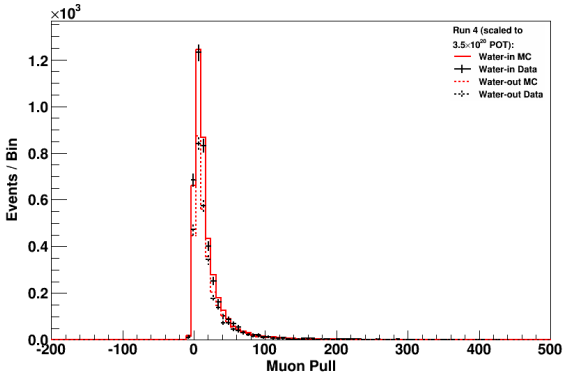

(b) Data MC Comparison

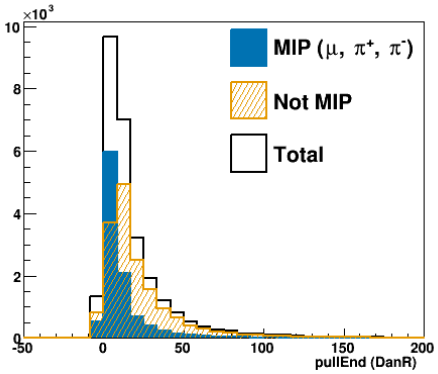

(c) MIP Signal Background Comparison

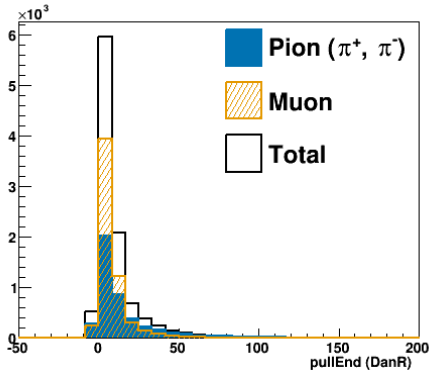

(d) MuPi Signal Background Comparison

Figure A.10: dE/dX Pull at Track End - Cluster

A.2 2D Longitudinal Variables

The energy deposition at different stages along the path of a particle can be helpful in determining its identity, because different particles have different energy depositions. The variables in this section look at deposition of energy in the track binned along the length of the track. The bins are defined such that each bin represents the energy in a single PØDule, with the width of bins adjusting to account for the distance a track has to travel to traverse a bin given the angle at which it is traveling.

Because the tracks being studied are three dimensional, there are two perpendicular planes that can be studied independently to look at the longitudinal projection. The geometry of the PØD gives us XZ and YZ projections to work in. The projections are taken from the original 3D object. In the PØD, there is very little difference between X and Y, with the one main exception being a magnetic field in the Y direction. Other than the magnetic field, it is expected that the XZ and YZ projections should behave very similarly. In some cases, the results from the XZ and YZ projections can be added together in quadrature to form one variable, while in others one or both projections are used in the MVA independently. Which treatment was best was determined for each variable by looking at the effectiveness of each projection independently and combined and then determining what worked best in the MVA.

One last distinction that is used in the longitudinal variables is that some of the variables described below apply to the whole track, while others refer to different thirds of the track. When the track end, track start, or track middle are referenced, they are referring to variables extracted from one third of the bins for the track, with the middle section taking the irregular number of bins if they do not divide evenly.

Sum of Charge in Low Charge PØDules

For this variable, low charge PØDules are defined as PØDules with charge less than two sigma from the average charge per bin of the track. The charge from any bin that meets this criteria is summed for this variable.

For a minimally ionizing particle, the bins with high charge content are usually at the end or beginning of the track. For the majority of the track there is little energy deposited, and this energy deposit reflects the energy of the particle, if it is indeed a MIP. Because this is a feature of the MIPs the MVA is trying to identify, this variable is useful.

The XZ projection of this variable is used in the MuPi MVA for both Kalman and Cluster tracks.

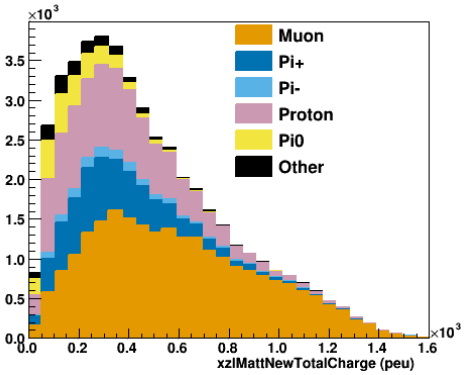

(a) Particle Breakdown

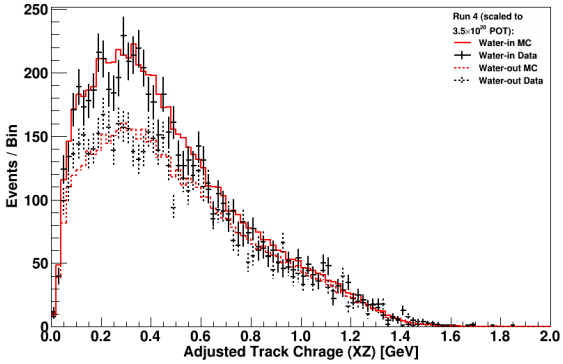

(b) Data MC Comparison

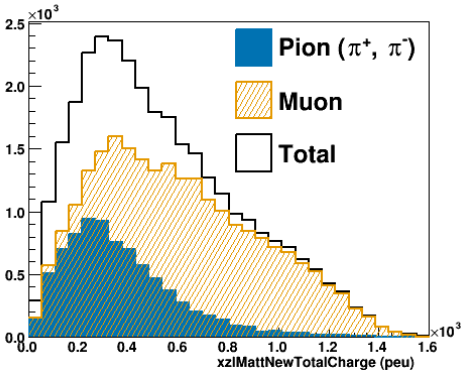

(c) MuPi Signal Background Comparison

Figure A.11: Sum of Charge in Low Charge PØDules - Kalman

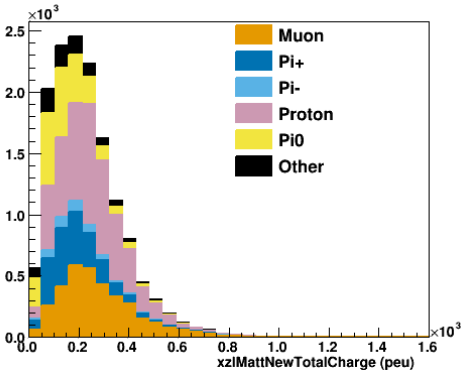

(a) Particle Breakdown

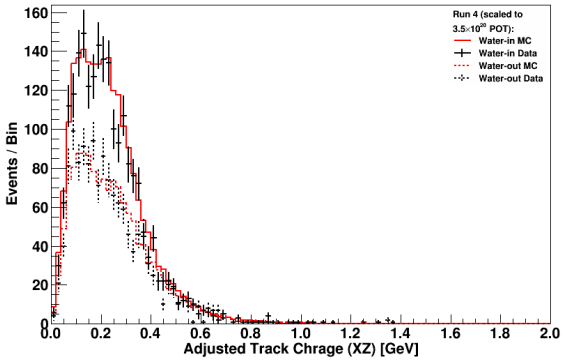

(b) Data MC Comparison

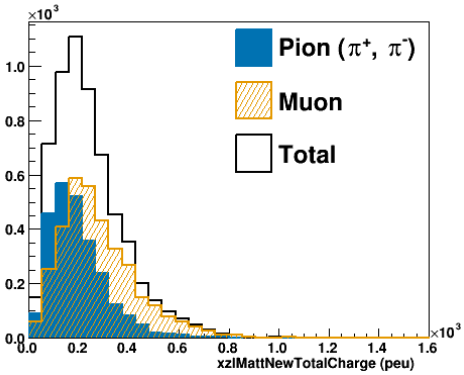

(c) MuPi Signal Background Comparison

Figure A.12: Sum of Charge in Low Charge PØDules - Cluster

Average Charge Per PØDule 1

The average charge per PØDule is calculated for the entire track. This calculation used variable width bins to account for the different distance traveled in a PØDule due to the angle of the track to weight the average.

The average charge is useful especially when compared with other variables. If the average charge for the track end is high, but the average charge for the whole track is low, then the relation between the two can be very informative about the energy deposition of the track. This average will also be dependent on track length, as a shorter track has fewer PØDules to average out the energy spikes that are normally seen at the beginning and end of tracks.

The XZ and YZ projections of this variable were used in the MIP MVA for both Kalman and Cluster Tracks.

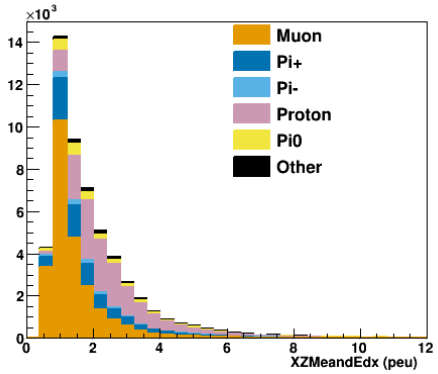

(a) Particle Breakdown

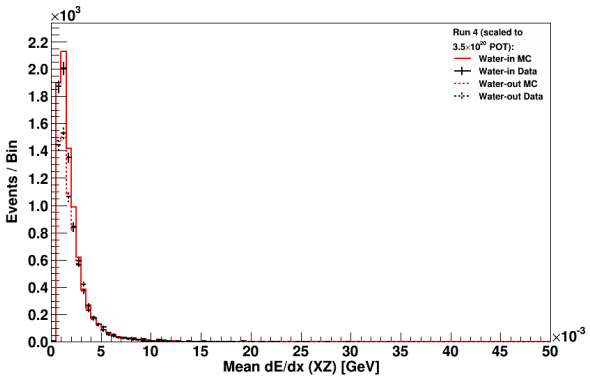

(b) Data MC Comparison

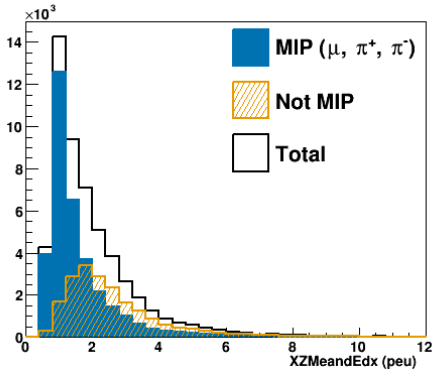

(c) MIP Signal Background Comparison

Figure A.13: Average Charge Per PØDule 1 - XZ - Kalman

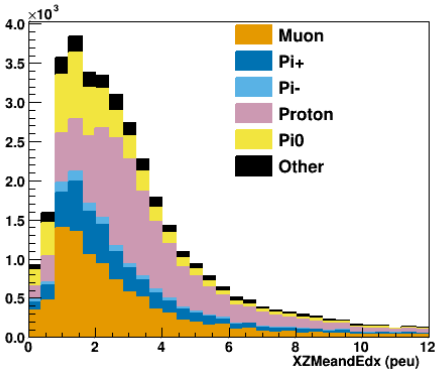

(a) Particle Breakdown

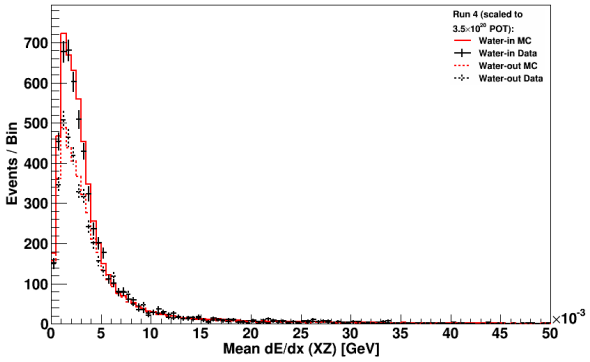

(b) Data MC Comparison

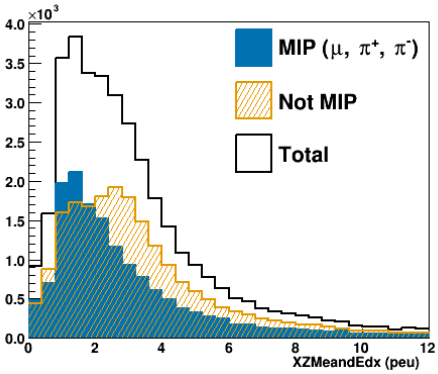

(c) MIP Signal Background Comparison

Figure A.14: Average Charge Per PØDule 1 - XZ - Cluster

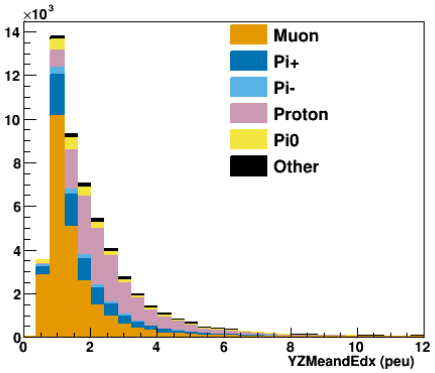

(a) Particle Breakdown

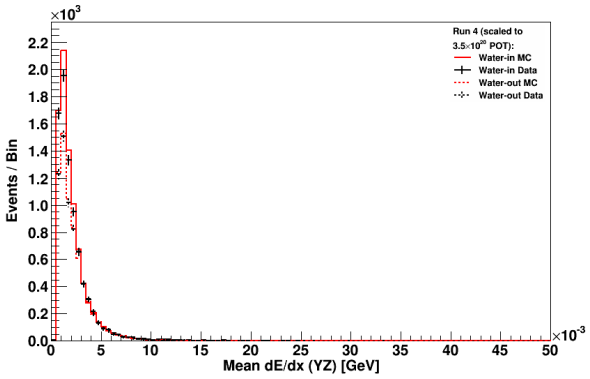

(b) Data MC Comparison

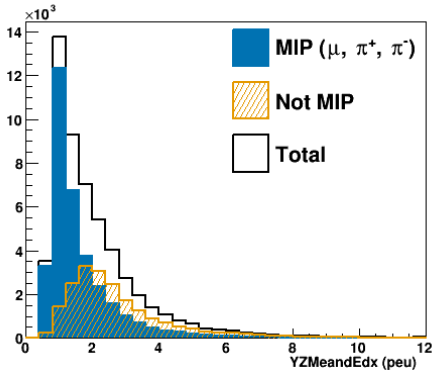

(c) MIP Signal Background Comparison

Figure A.15: Average Charge Per PØDule 1 - YZ - Kalman

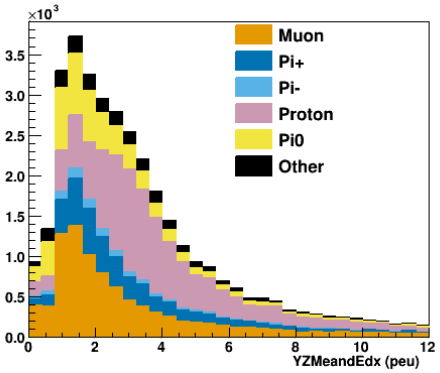

(a) Particle Breakdown

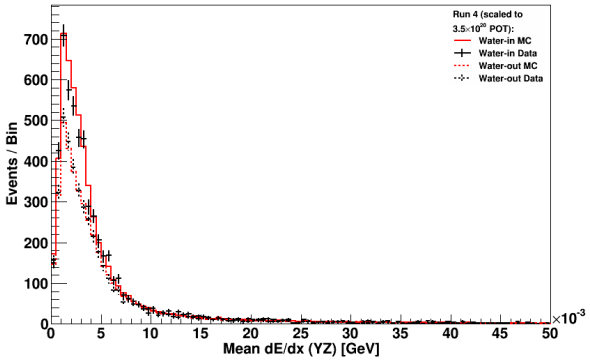

(b) Data MC Comparison

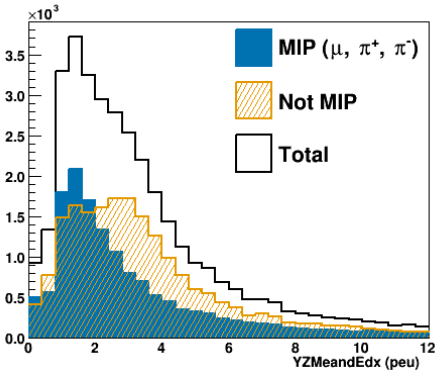

(c) MIP Signal Background Comparison

Figure A.16: Average Charge Per PØDule 1 - YZ - Cluster

Average Charge Per PØDule 2

The average charge per PØDule is calculated for the entire track. This calculation projected angled tracks to the z axis of the detector to bin by PØDule, weighting the charge to account for the difference in track length through scintilator.

The usefulness of the Average charge described above still holds. The inclusion of another form of calculating this average charge was shown to work better in the MuPi MVA than the previous definition, while the previous definition worked better in the MIP MVA.

The XZ projection of this variable is used in the MuPi MVA for both Kalman and Cluster tracks.

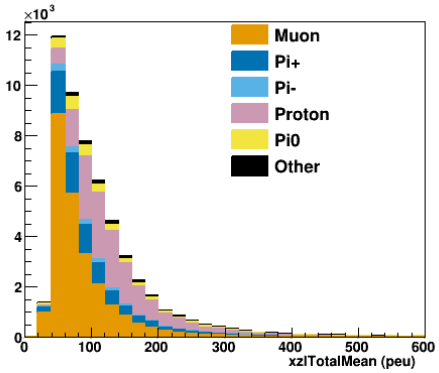

(a) Particle Breakdown

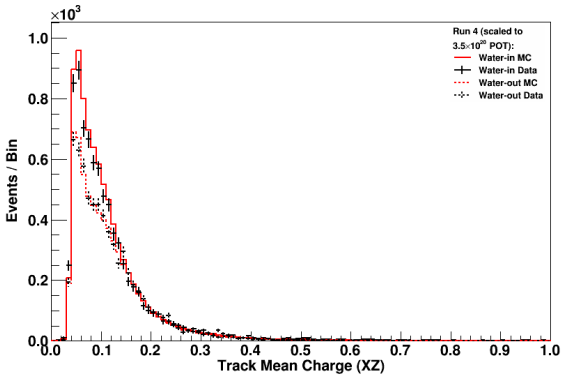

(b) Data MC Comparison

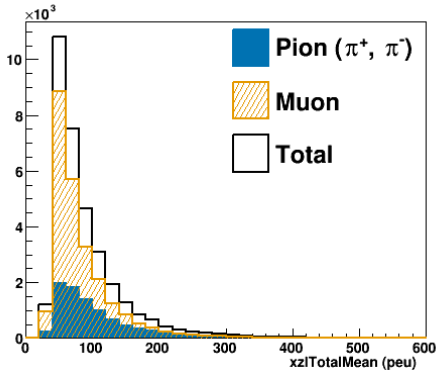

(c) MuPi Signal Background Comparison

Figure A.17: Average Charge Per PØDule 2 - Kalman

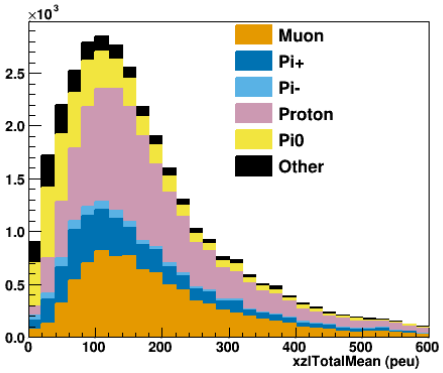

(a) Particle Breakdown

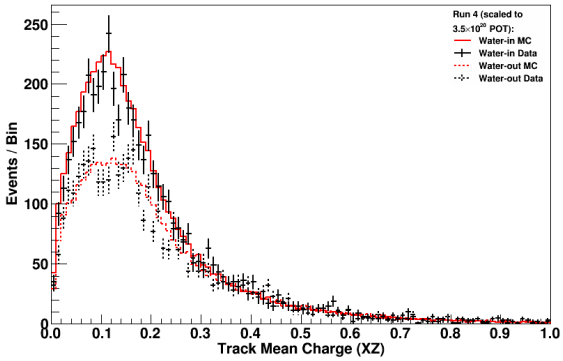

(b) Data MC Comparison

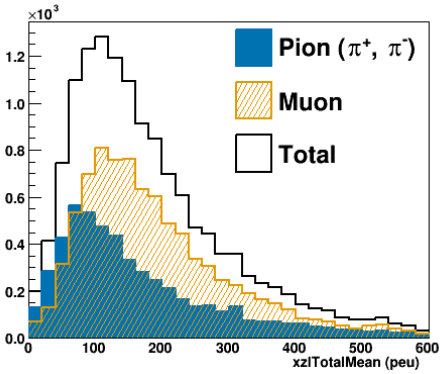

(c) MuPi Signal Background Comparison

Figure A.18: Average Charge Per PØDule 2 - Cluster

Average Charge Per PØDule for Track End

This variable is simply the average charge per PØDule for the last third of the track.

The amount of energy that a track leaves in the PØD at its death can be useful in identifying what type of particle it is. This variable is one way to quantify that particle death energy dump, but it is also scaled by the length of the track, as a longer track will have a longer section of the last third that is not as energetic as the last PØDule or two.

The XZ and YZ projections of this variable were used independently in the MuPi MVA for both Kalman and Cluster tracks.

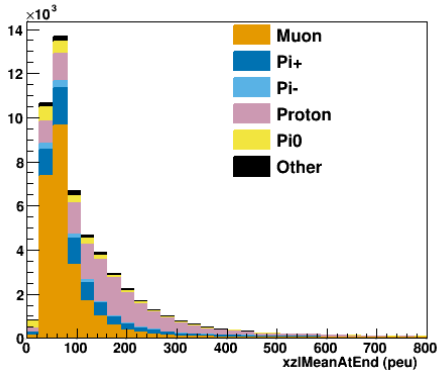

(a) Particle Breakdown

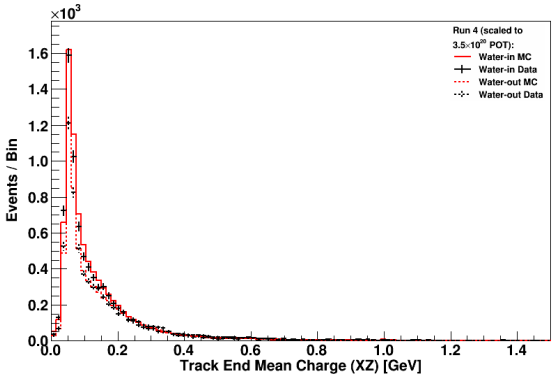

(b) Data MC Comparison

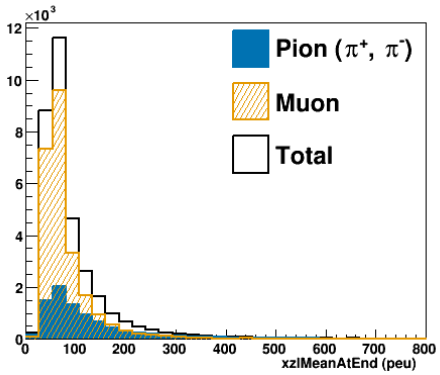

(c) MuPi Signal Background Comparison

Figure A.19: Average Charge Per PØDule for Track End - XZ - Kalman

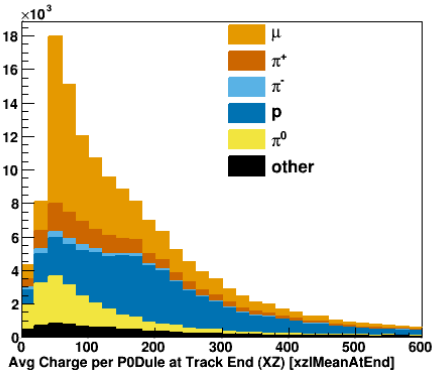

(a) Particle Breakdown

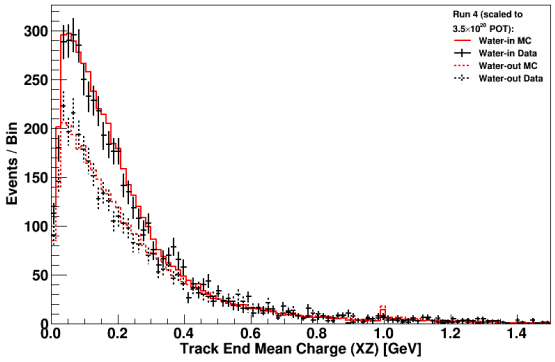

(b) Data MC Comparison

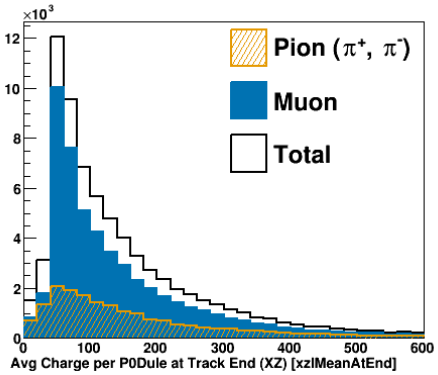

(c) MuPi Signal Background Comparison

Figure A.20: Average Charge Per PØDule for Track End - XZ - Cluster

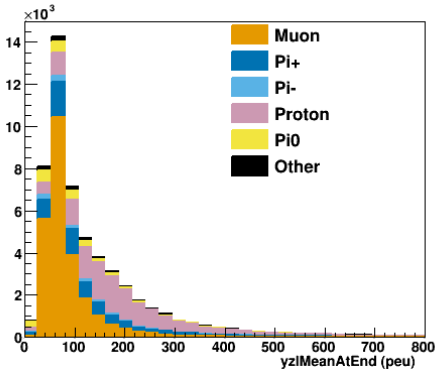

(a) Particle Breakdown

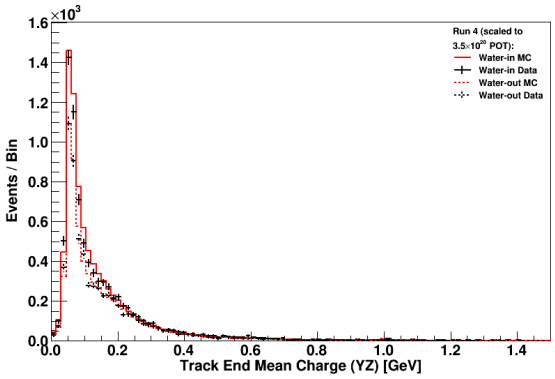

(b) Data MC Comparison

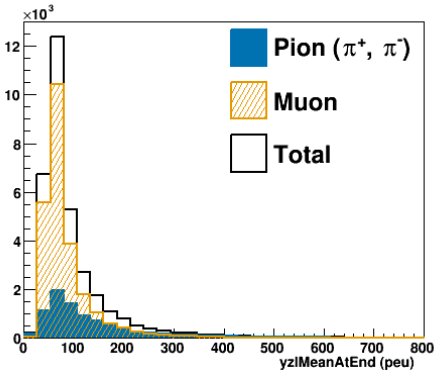

(c) MuPi Signal Background Comparison

Figure A.21: Average Charge Per PØDule for Track End - YZ - Kalman

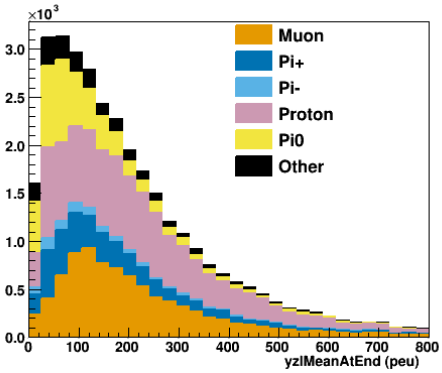

(a) Particle Breakdown

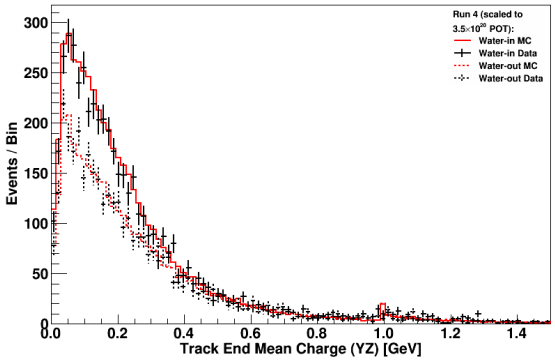

(b) Data MC Comparison

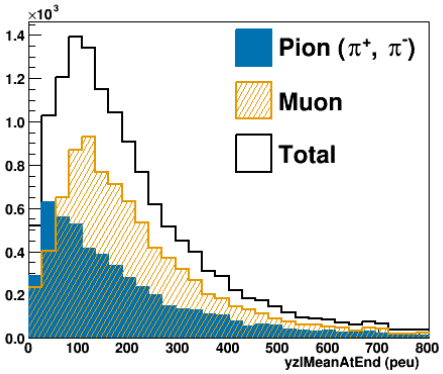

(c) MuPi Signal Background Comparison

Figure A.22: Average Charge Per P∅Dule for Track End - YZ - Cluster

Standard Deviation of Charge Per PØDule

The standard deviation of charge per PØDule is calculated for the entire track.

As with the Average Charge, the Standard Deviation of the charge per PØDule for the whole track is useful especially when compared with other variables. Comparing the standard deviation of the whole track to the standard deviation of just the middle of the track gives another handle on the variations in energy at the end and start of the track which can be useful in differentiating particles that have different types of energetic deaths in the PØD.

The XZ and YZ projections for this variable added in quadrature were used in the MIP MVA for both Kalman and Cluster tracks, while the YZ projection of this variable was used in the MuPi MVA for both Kalman and Cluster tracks.

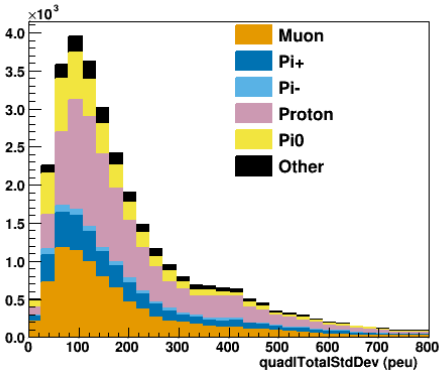

(a) Particle Breakdown

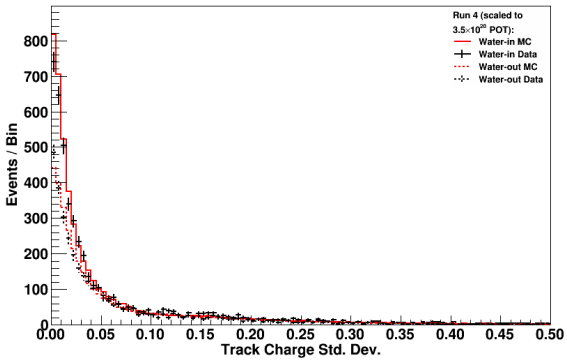

(b) Data MC Comparison

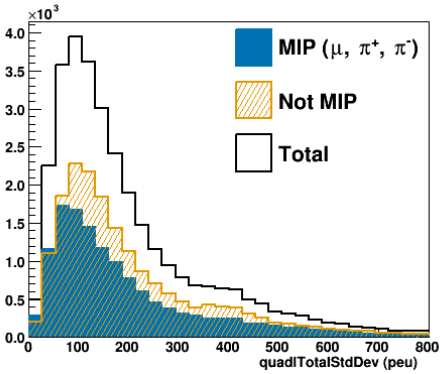

(c) MIP Signal Background Comparison

Figure A.23: Standard Deviation of Charge Per PØDule - XZ+YZ - Cluster

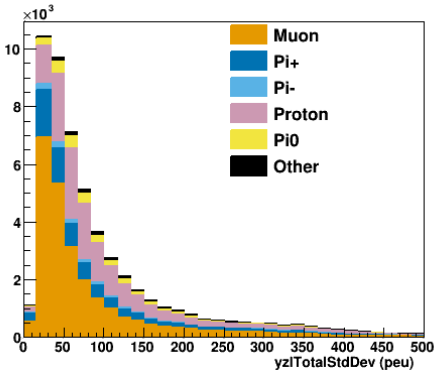

(a) Particle Breakdown

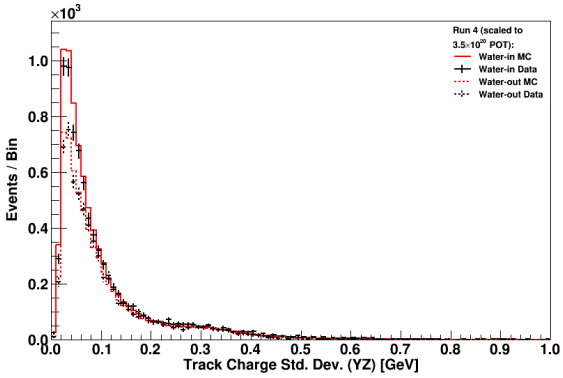

(b) Data MC Comparison

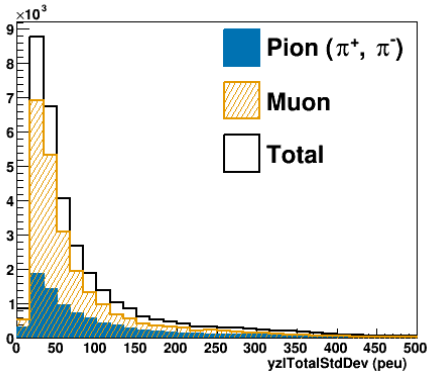

(c) MuPi Signal Background Comparison

Figure A.24: Standard Deviation of Charge Per PØDule - XZ+YZ - Kalman

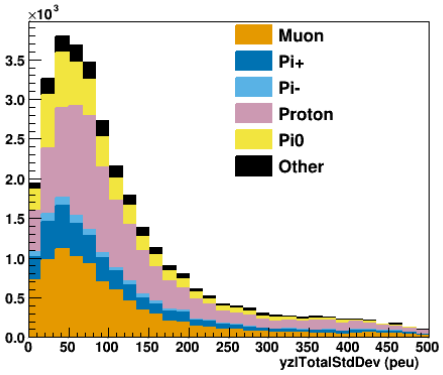

(a) Particle Breakdown

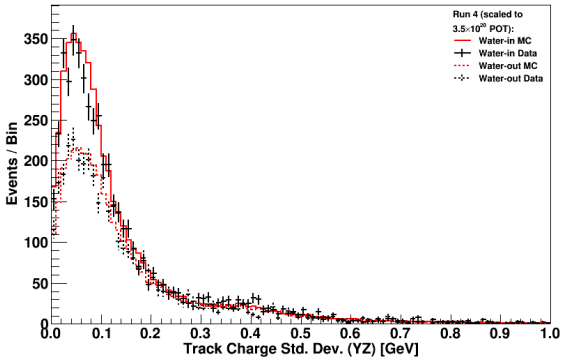

(b) Data MC Comparison

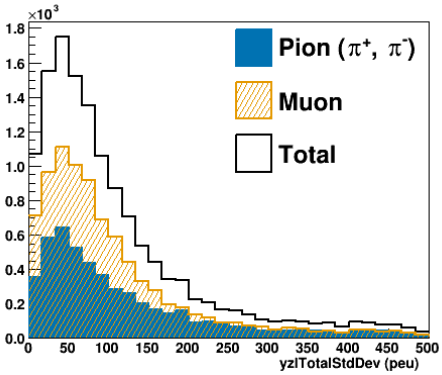

(c) MuPi Signal Background Comparison

Figure A.25: Standard Deviation of Charge Per PØDule - YZ - Cluster

Standard Deviation of Charge Per PØDule for Track Middle

The standard deviation of charge per PØDule is calculated for the middle third of the track.

The middle region of a MIP-like track should be fairly constant in energy deposition, with the energy deposited a good indication of the energy of the track. The standard deviation of the charge per PØDule in this region should then be small for MIP-like tracks.

The XZ and YZ projections of this variable were used in the MIP MVA for both Kalman and Cluster tracks. For the MuPi MVA only the XZ projection was used for both Kalman and Cluster tracks.

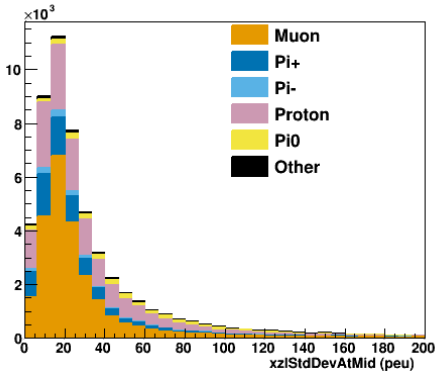

(a) Particle Breakdown

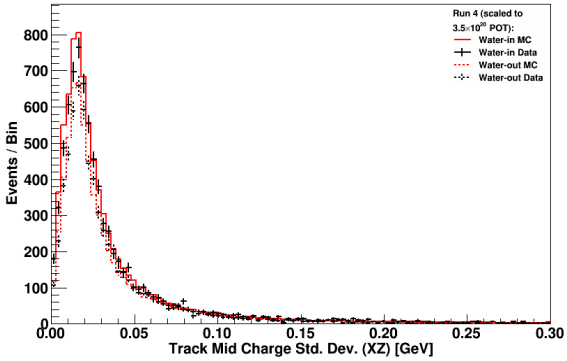

(b) Data MC Comparison

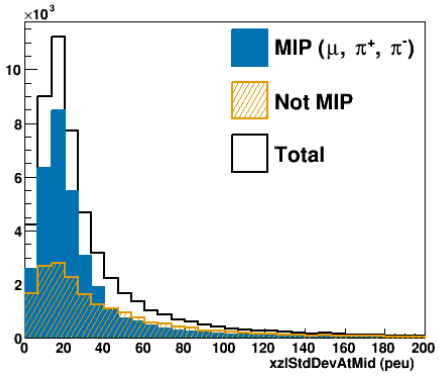

(c) MIP Signal Background Comparison

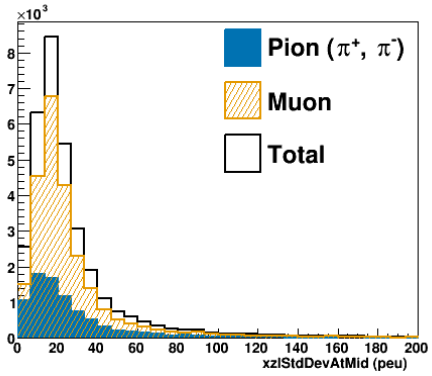

(d) MuPi Signal Background Comparison

Figure A.26: Standard Deviation of Charge Per PØDule for Track Middle - XZ - Kalman

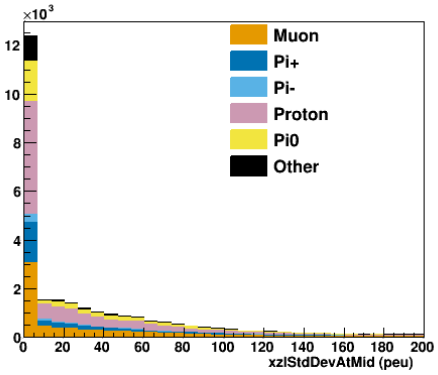

(a) Particle Breakdown

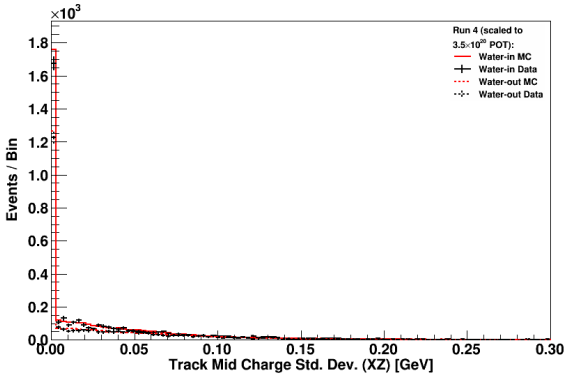

(b) Data MC Comparison

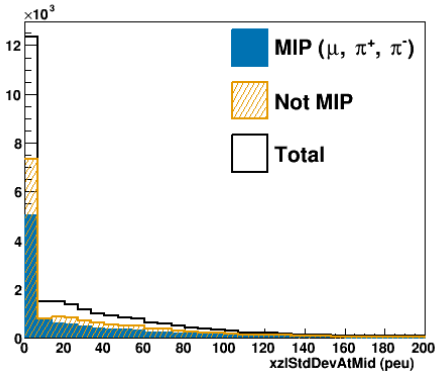

(c) MIP Signal Background Comparison

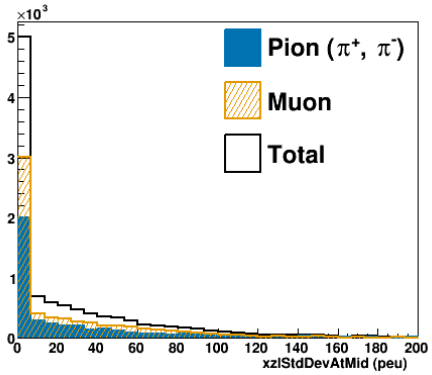

(d) MuPi Signal Background Comparison

Figure A.27: Standard Deviation of Charge Per PØDule for Track Middle - XZ - Cluster

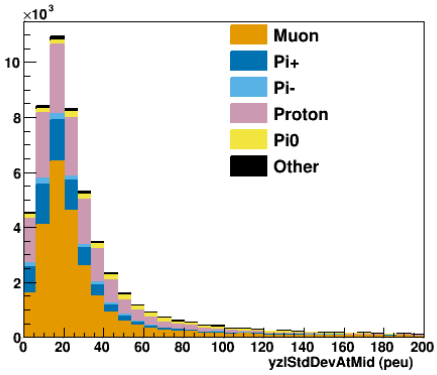

(a) Particle Breakdown

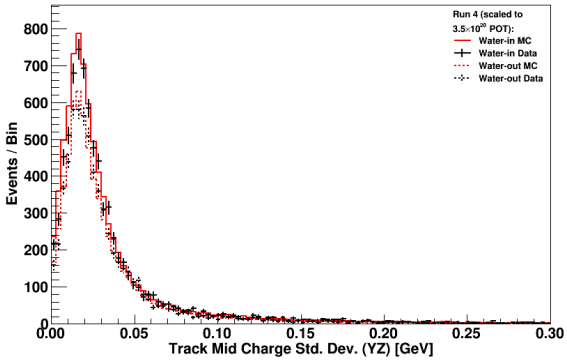

(b) Data MC Comparison

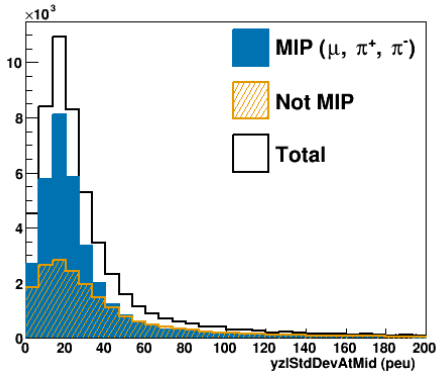

(c) MIP Signal Background Comparison

Figure A.28: Standard Deviation of Charge Per PØDule for Track Middle - YZ - Kalman

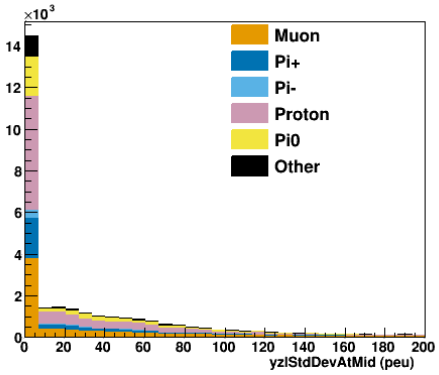

(a) Particle Breakdown

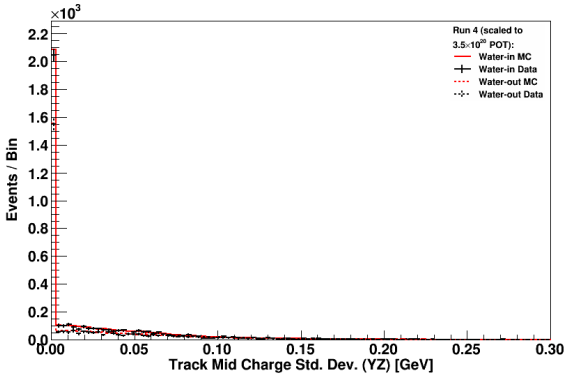

(b) Data MC Comparison

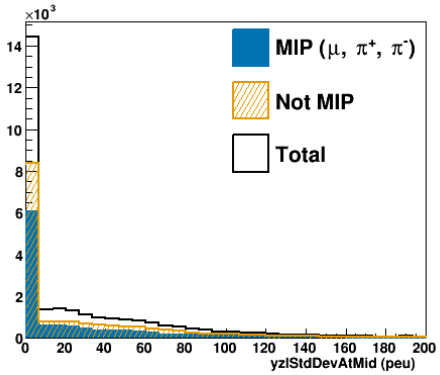

(c) MIP Signal Background Comparison

Figure A.29: Standard Deviation of Charge Per PØDule for Track Middle - YZ - Cluster

Total Charge Detected for Track Start

All the charge detected in the first third of the PØDules traversed by a track was summed for this variable.

Similar to the above variables, the total charge detected at the track start was useful in conjunction with other variables, specifically the total charge as well as some of the averages and standard deviations.

The YZ projection of this variable was used in the MuPi MVA for both Kalman and Cluster tracks.

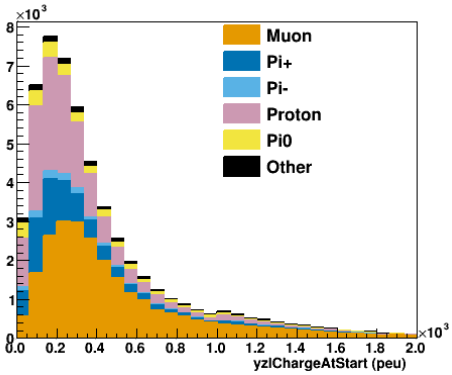

(a) Particle Breakdown

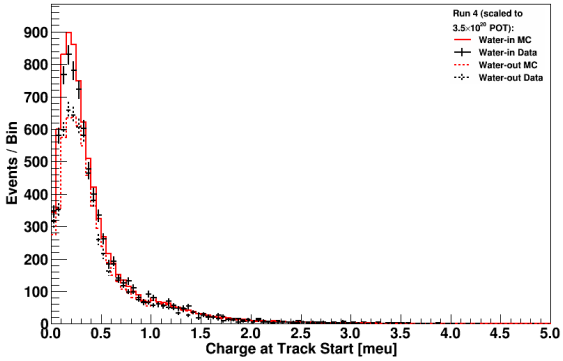

(b) Data MC Comparison

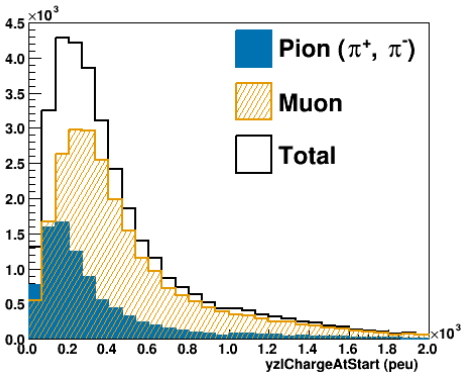

(c) MuPi Signal Background Comparison

Figure A.30: Total Charge Detected for Track Start - Kalman

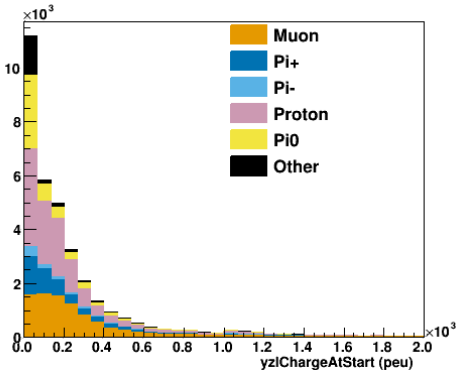

(a) Particle Breakdown

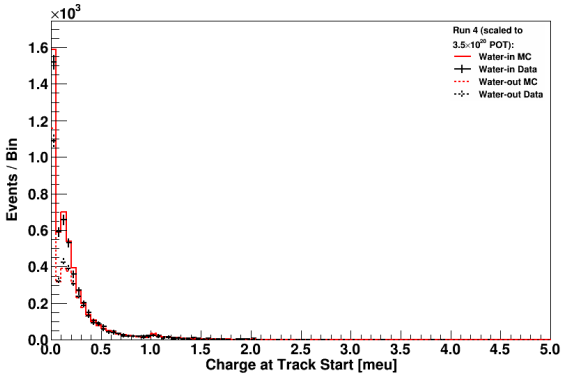

(b) Data MC Comparison

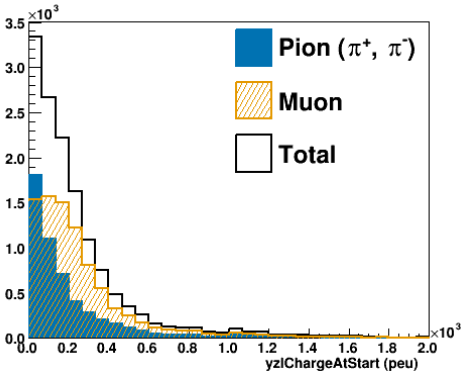

(c) MuPi Signal Background Comparison

Figure A.31: Total Charge Detected for Track Start - Cluster

Fraction of Total Charge Detected in Last PØDule

The fraction of total charge detected in the last PØDule was calculated by dividing charge in the last PØDule by the total charge of the track.

Different particles have different energetic deaths. The amount of energy the particle deposits at the end of the track as a function of the total energy that particle deposited over the length of the track is useful in determining the identity of that particle.

The XZ and YZ projections of this variable are used in the MIP MVA for both Kalman and Cluster tracks.

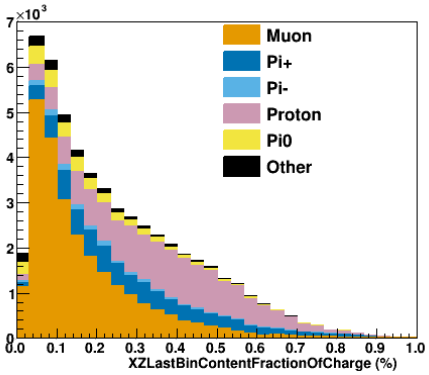

(a) Particle Breakdown

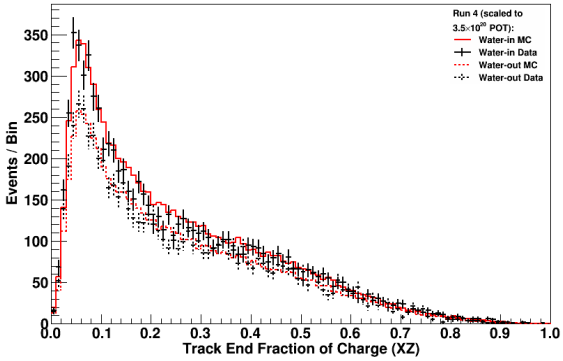

(b) Data MC Comparison

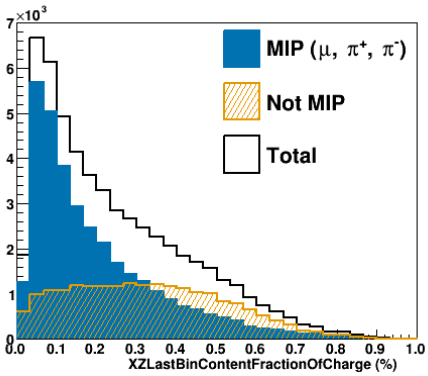

(c) MIP Signal Background Comparison

Figure A.32: Fraction of Total Charge Detected in Last PØDule - XZ - Kalman

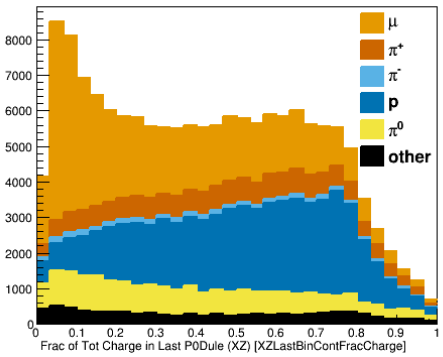

(a) Particle Breakdown

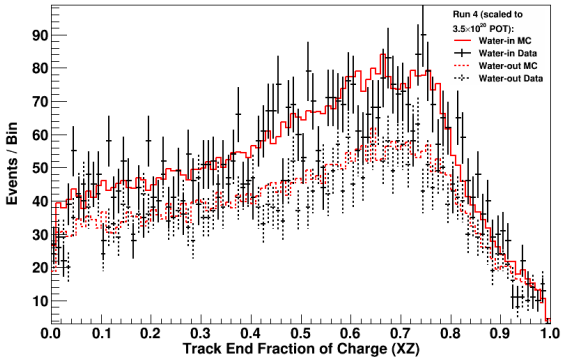

(b) Data MC Comparison

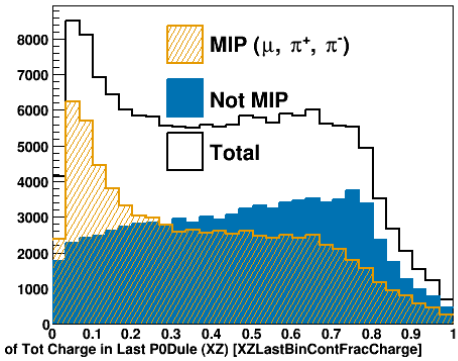

(c) MIP Signal Background Comparison

Figure A.33: Fraction of Total Charge Detected in Last PØDule - XZ - Cluster

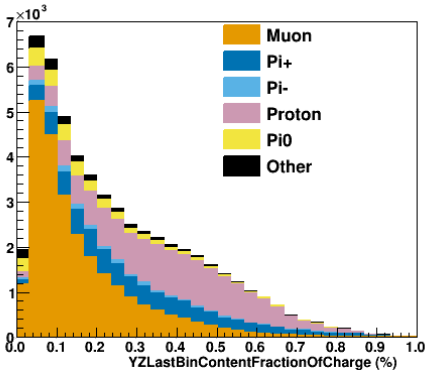

(a) Particle Breakdown

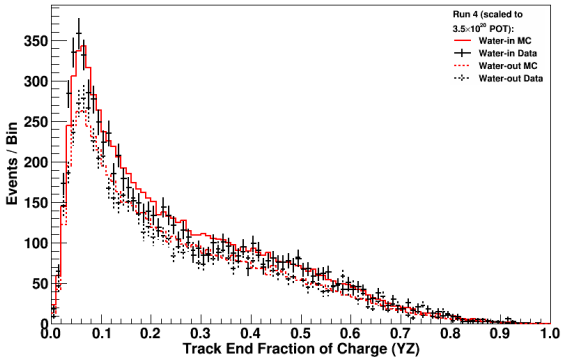

(b) Data MC Comparison

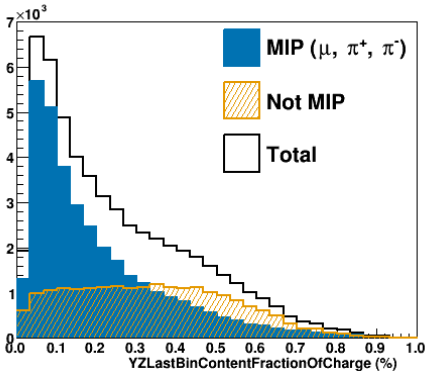

(c) MIP Signal Background Comparison

Figure A.34: Fraction of Total Charge Detected in Last P∅Dule - YZ - Kalman

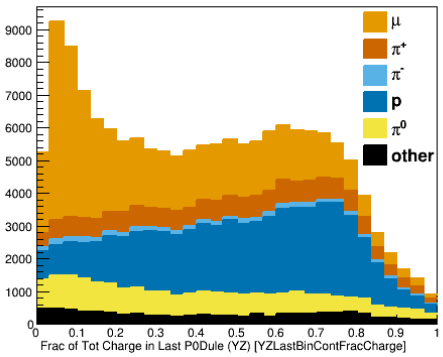

(a) Particle Breakdown

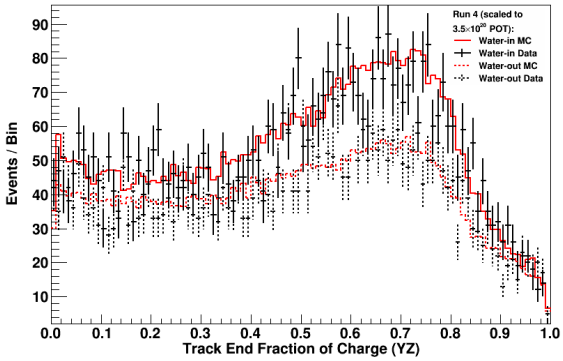

(b) Data MC Comparison

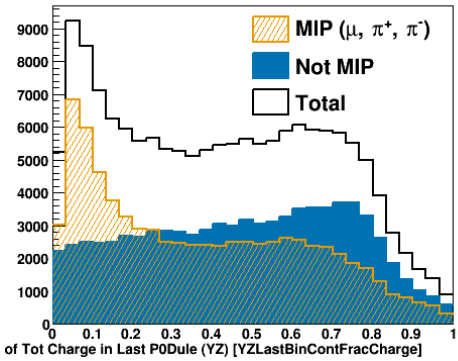

(c) MIP Signal Background Comparison

Figure A.35: Fraction of Total Charge Detected in Last P∅Dule - YZ - Cluster

A.3 2D Transverse Variables

While the longitudinal properties of a track are useful in tracking the behavior of a track over time, the transverse properties of a track give a sense of the smaller scale movement the particle had perpendicular to the main direction of travel, as well as indicate how wide the energy deposit was. In general the transverse properties are related to the spread of energy in the detector, and are averaged over the length of the track, but as with the longitudinal variables some of these variables apply to different thirds of the track. For the instances here where variables refer to start, middle, or end, the position they refer to is the longitudinal start middle or end, but the variable being looked at is the transverse properties of the hits only from the specified third of the longitudinal track.

For the transverse projections, the obvious binning for a forward going track will be dependent on the PØD geometry, which means using the scintilator bars which have central fibers that are approximately 17 mm apart. Because of the triangular shape of the bars, moving away from the center of the track does not correspond to moving through sequential bars, but through overlapping bars. For that reason instead of talking about charge in bars, the transverse variables are binned purely by distance away from the track. The binning is still based on the 17 mm, but it is not assumed that each bin corresponds to a single bar of scintilator.

As with the longitudinal variables, the transverse variables are also calculated in XZ and YZ projections, and different combinations of these projections are used for different variables.

Percent of Average Charge Per Bin at Track End

Using only the hits from the last third of a track (as defined by the longitudinal projection), the average charge per transverse bin was calculated and then divided by the average charge per transverse bin calculated using all the hits in the track.

This ratio compares the transverse charge distribution at the end of the track to the whole track, which helps to identify tracks that were fairly uniform along their length as opposed to tracks that ended in dramatically different fashion than most of their travel through the PØD.

The YZ Projection of this variable was used in the MIP MVA for Cluster tracks.

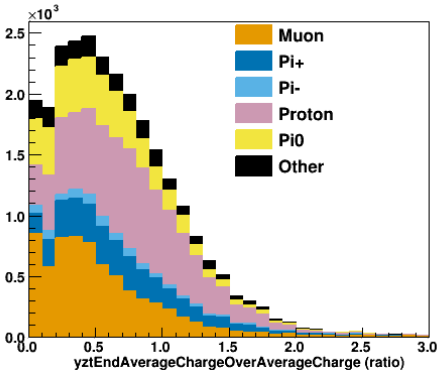

(a) Particle Breakdown

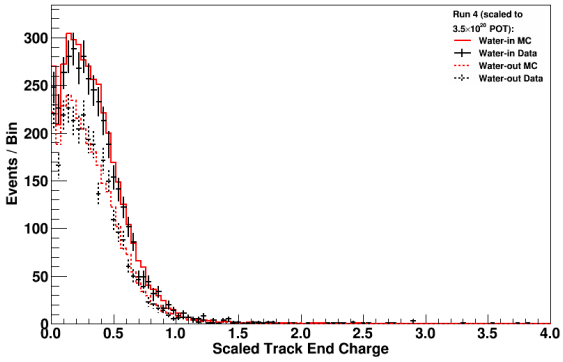

(b) Data MC Comparison

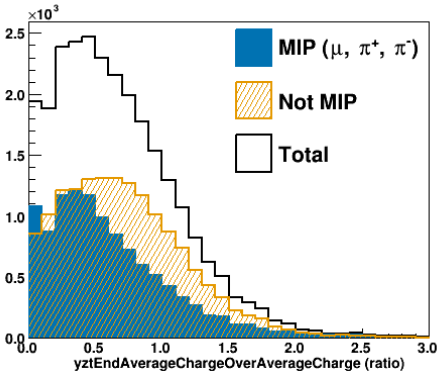

(c) MIP Signal Background Comparison

Figure A.36: Percent of Average Charge Per Bin at Track End - Cluster

Charge Distribution

The Charge distribution variable was defined as the full with half max of the transverse charge distribution divided by the maximum charge in that distribution. The full width half max was found by identifying the two furthest bins from the center of the distribution (one to the left of center, the other to the right) that had a charge greater than half of the maximum charge bin. Once these two bins were identified, the distance between their outer boundaries was taken as the full width half max.

This variable gives a very useful description of the charge distribution perpendicular to the direction of the track. As the expectation that the most charge is in the center, and tapering off to either side, this nicely characterizes that shape and distinguishes between diffuse tracks with a weak central peak and tight tracks with all their charge clustered around the center of the track.

The XZ and YZ projections of this variable were used in the MIP MVA for both Kalman and Cluster tracks.

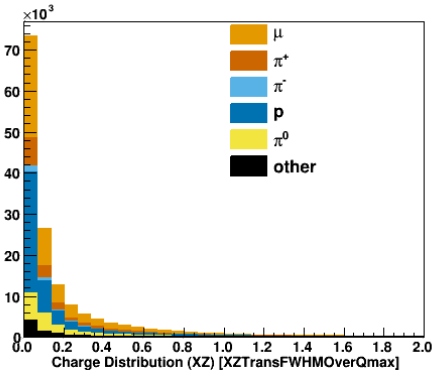

(a) Particle Breakdown

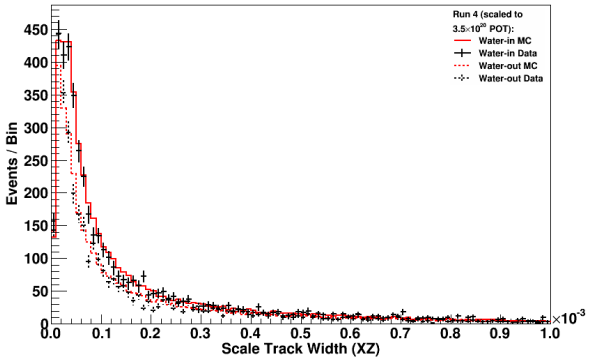

(b) Data MC Comparison

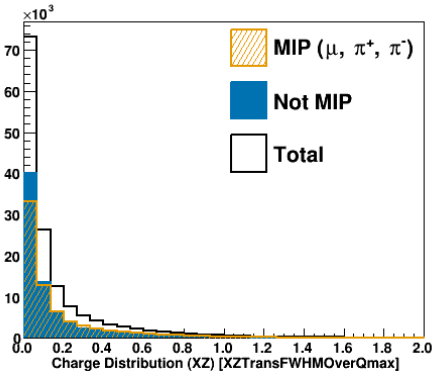

(c) MIP Signal Background Comparison

Figure A.37: Charge Distribution - XZ - Cluster

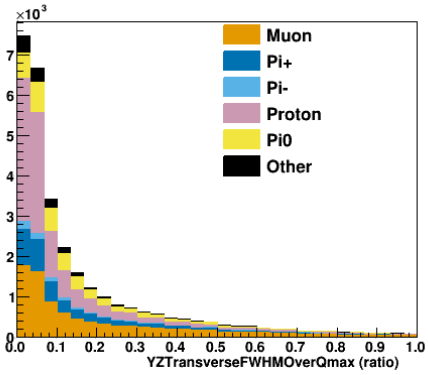

(a) Particle Breakdown

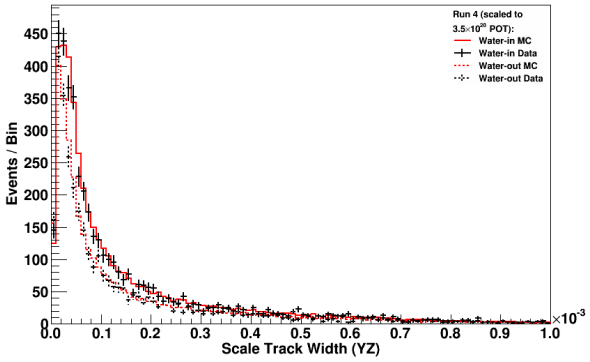

(b) Data MC Comparison

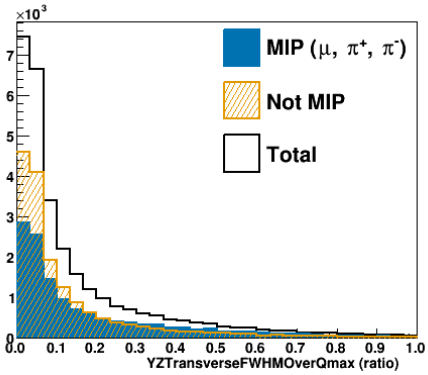

(c) MIP Signal Background Comparison

Figure A.38: Charge Distribution - YZ - Cluster

A.4 2D Line Sweep Variables

A combination of Longitudinal and Transverse variables, the following variables are all based on line fitting methods developed for the cluster track fitter described in Chapter 3.3, specifically the line sweep method described in Chapter 3.3.2. In brief, the line sweep method picks a starting point (usually the vertex) and then finds the angle for a line that minimizes the distance between all the hits and the line. For the following variables, this fitting method is used to get the primary best fit straight line, then a variety of different quantities are studied with respect to that fit, or compared with subsequent fits using the same method.

Some of these variables were originally developed to understand and study the Cluster Track Fitter, and were later found to be useful in the MVA.

As with the transverse and longitudinal variables, these studies are done in XZ and YZ projections, with the results either used together or independently.

Track Width

One of the basic parameters of the line sweep fit is the sum of the charge weighted distance of each point to the best fit line. This is the value that is minimized to chose the best fit line, and is what this analysis calls the track width.

The track width is useful in characterizing the spread of the hits in the track, and is dependent on the number of hits in the track. A particle that bounces around as it travels, or has large kinks in its travel, will have a large track width. A muon, however, would be expected to travel in a straight line and thus have a very small track width.

The YZ Projection of this variable is used in the MIP MVA for Cluster tracks, and in the MuPi MVA for both Kalman and Cluster tracks.

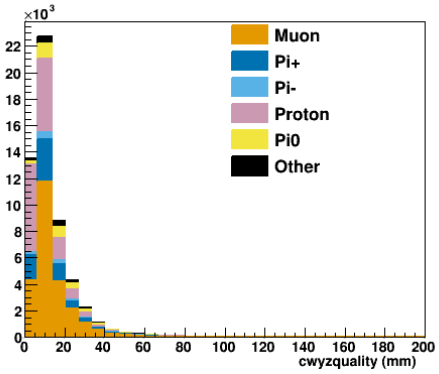

(a) Particle Breakdown

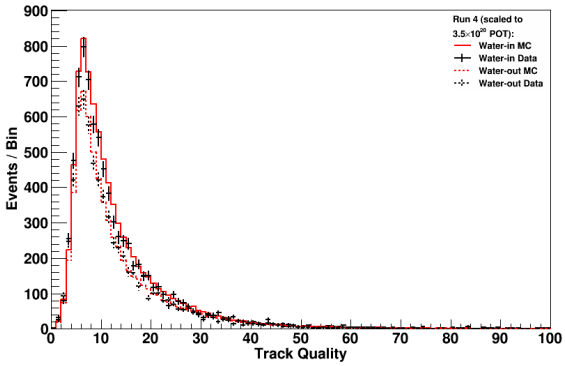

(b) Data MC Comparison

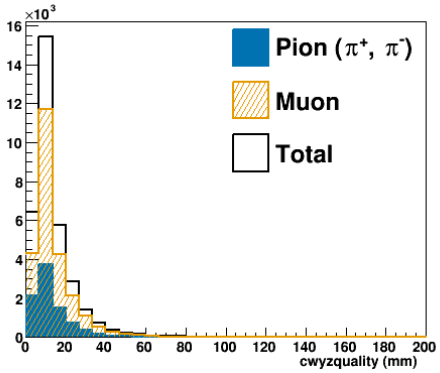

(c) MuPi Signal Background Comparison

Figure A.39: Track Width - Kalman

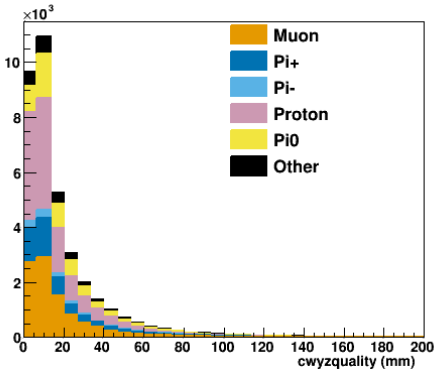

(a) Particle Breakdown

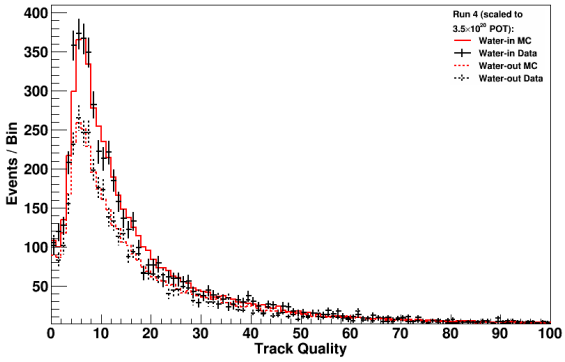

(b) Data MC Comparison

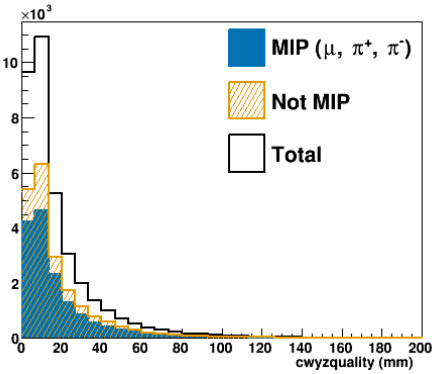

(c) MIP Signal Background Comparison

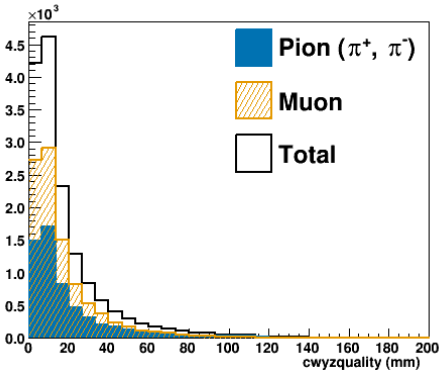

(d) MuPi Signal Background Comparison

Figure A.40: Track Width - Cluster

Vertex Quality

Built as a check on how well the cluster reconstruction was able to fit a track, the vertex quality variable was found to provide help in separating muons and pions. The cluster reconstruction described in Section 3.3 creates a line starting at the reconstructed vertex, then finds the angle of a straight line through the vertex that minimizes the sum of the distance of each hit to that line. As a quality check, this variable was created to do the same fit, but instead of using the vertex as the pivot point of the best fit line a new pivot is chosen at the center of the previously reconstructed track. The idea of this variable is that if the best fit angle using the vertex is drastically different than the best fit angle using a point in the center of the track, then the vertex is probably not accurate for the track. The difference between these two fit angles (in radians) is what is called the Vertex Quality.

While this variable was useful in studying the cluster track fitter, it was found that it was also useful in the MVA. Muons tend to be very straight and simple tracks, while pions have a greater chance of interacting along their flight, which is one thing this variable is able to pick up on.

The YZ projection of this variable is used in the MuPi MVA for both Kalman and Cluster tracks.

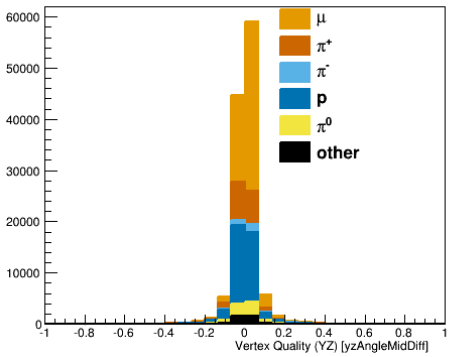

(a) Particle Breakdown

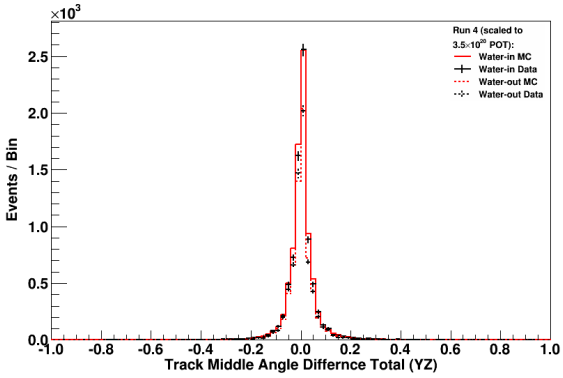

(b) Data MC Comparison

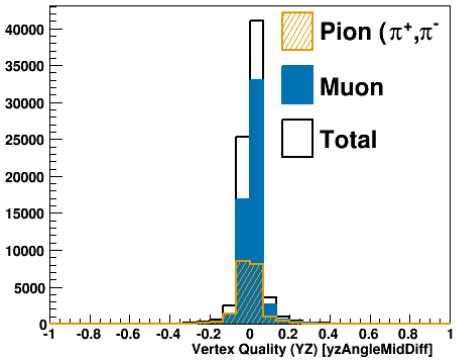

(c) MuPi Signal Background Comparison

Figure A.41: Vertex Quality - Kalman

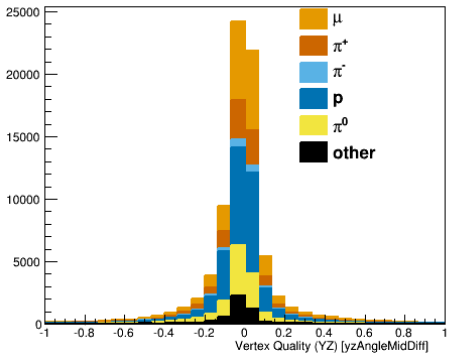

(a) Particle Breakdown

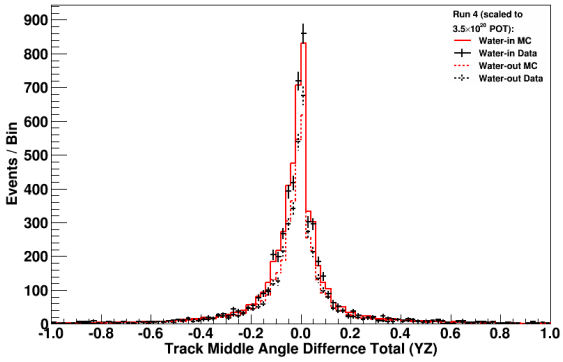

(b) Data MC Comparison

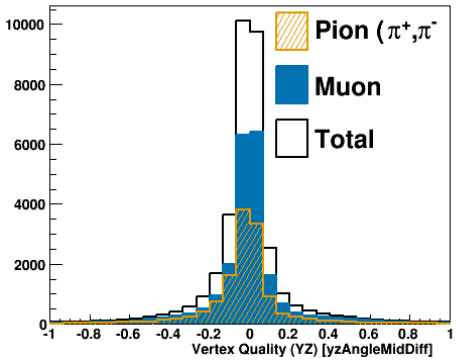

(c) MuPi Signal Background Comparison

Figure A.42: Vertex Quality - Cluster

Track Width Asymmetry 1

The first track width asymmetry uses the track width defined above, but evaluates it separately for hits above the best fit line and hits below the best fit line. The track width for these two subsets of hits are then divided (above / below) to get this ratio.

This kind of comparison can give a better description of the distribution of hits than the single track width variable, as it allows for different behavior in different transverse sections of the track.

The YZ projection of this variable is used in the MuPi MVA for both Kalman and Cluster tracks.

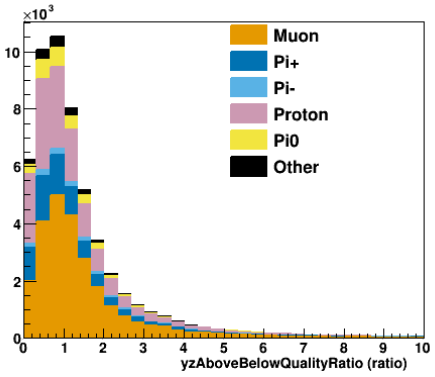

(a) Particle Breakdown

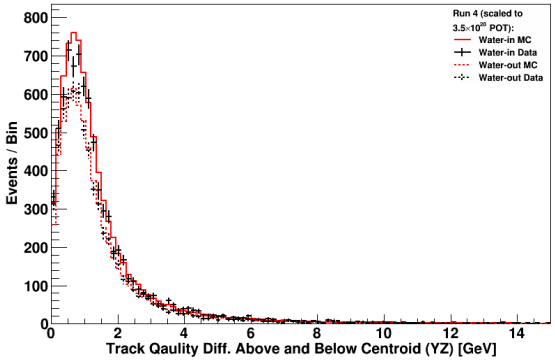

(b) Data MC Comparison

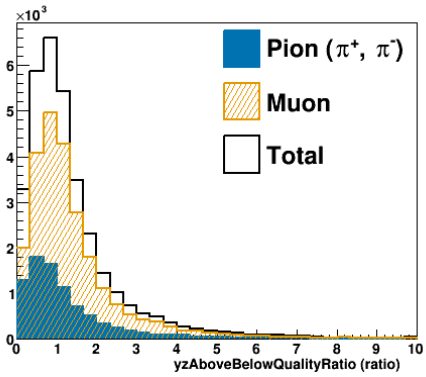

(c) MuPi Signal Background Comparison

Figure A.43: Track Width Asymmetry 1 - Kalman

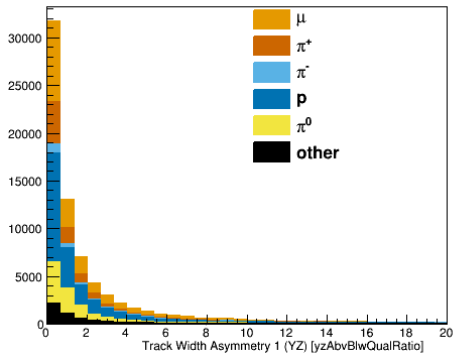

(a) Particle Breakdown

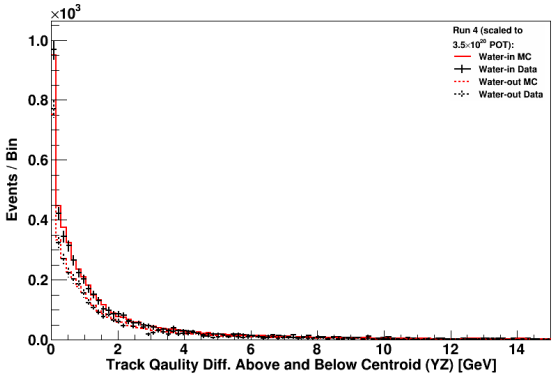

(b) Data MC Comparison

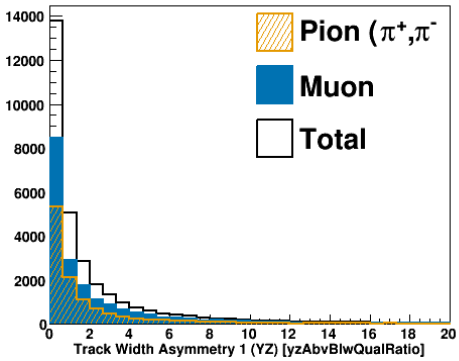

(c) MuPi Signal Background Comparison

Figure A.44: Track Width Asymmetry 1 - Cluster

Track Width Asymmetry 2

This is the second track width asymmetry variable, and it also uses the best fit line to define the above and below regions. What is different is that the transverse projection is made for each of the above and below regions, and the number of bins of each of those distributions is compared. Specifically, this variable is the number of transverse bins above the best fit line, minus the number of bins below the best fit line, divided by the number of bins if you use the transverse projection of the whole track.

This results in a track width asymmetry that is given as a fraction of the total track width, with a granularity of the size of the bins used to make the Transverse projections. But as with the previous track width variable, this is still a very useful property to study when trying to separate the straight track of a MIP from other scattered or kinked tracks.

The XZ and YZ projections for this variable added in quadrature were used in the MIP MVA for Cluster tracks.

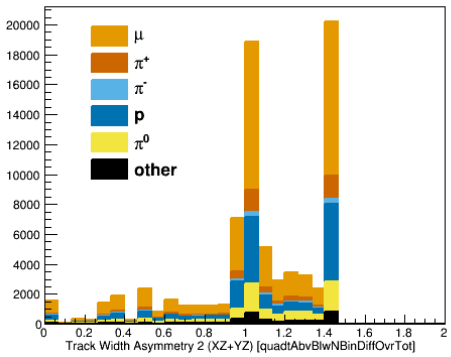

(a) Particle Breakdown

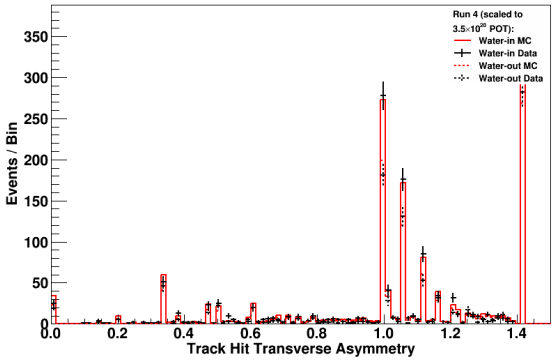

(b) Data MC Comparison

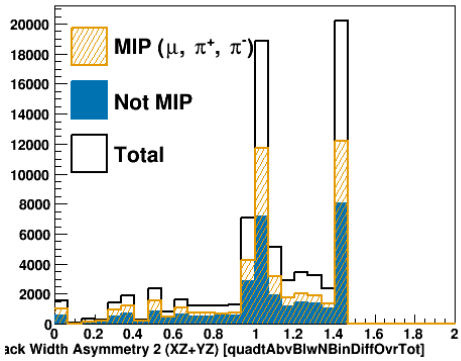

(c) MIP Signal Background Comparison

Figure A.45: Track Width Asymmetry 2 - Cluster

N Hit Asymmetry

The Asymmetry in the number of hits is the number of hits above the best fit line minus the number of hits below the best fit line, divided by the total number of hits.

Looking at the number of hits is one way to get a transverse property that isn't influenced by the charge of the hits, and thus is sensitive to track behavior not focused on the highest charged hits.

The YZ projection of this variable is used in the MIP MVA for Cluster Tracks.

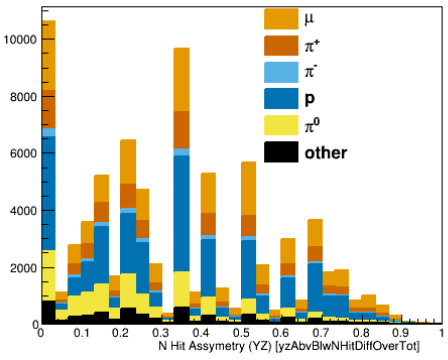

(a) Particle Breakdown

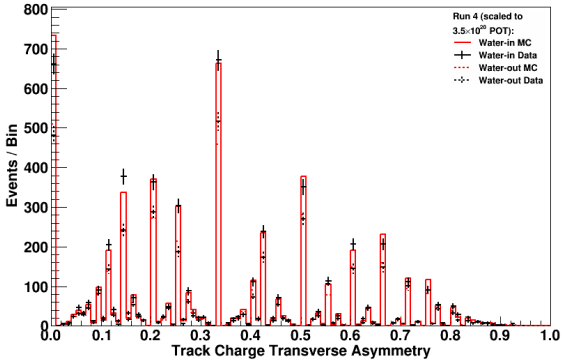

(b) Data MC Comparison

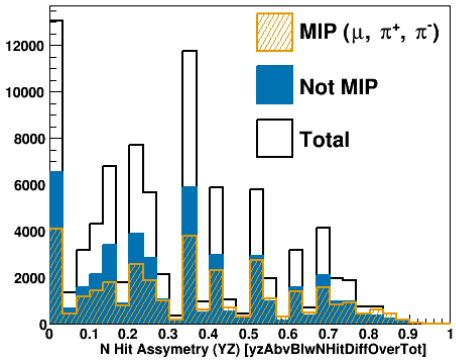

(c) MIP Signal Background Comparison

Figure A.46: N Hit Asymmetry - Cluster

Track End Hit Asymmetry

The track end hit asymmetry is calculated by doing a fit to the hits above the best fit line, as well as a fit to the events below the best fit line, and then taking the difference between the results (above - below).

This variable is used to identify if the best fit line separates not only the transverse distribution of hits, but also the longitudinal distribution. If the fit to the hits above the best fit line results in a much shorter track length than the fit to the hits below the best fit line, then that is indicative of curvature or a kink in the track.

The YZ Projection of this variable is used in the MuPi MVA for both Kalman and Cluster tracks.

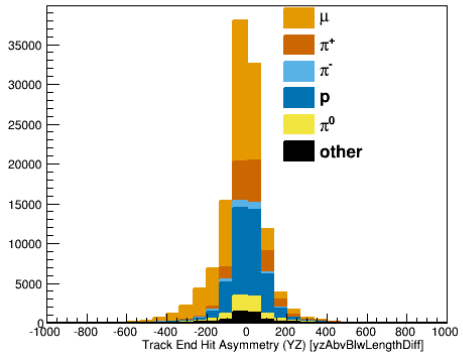

(a) Particle Breakdown

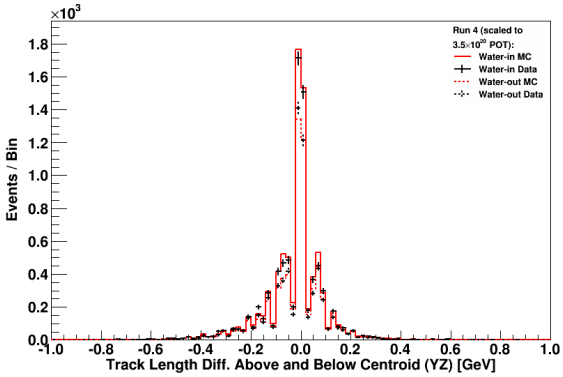

(b) Data MC Comparison

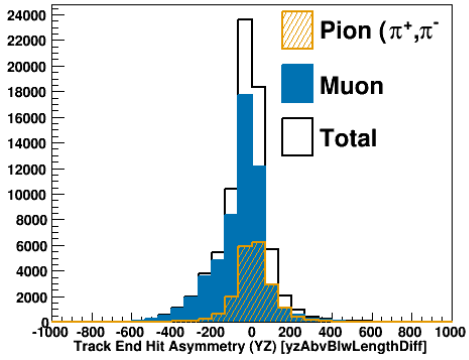

(c) MuPi Signal Background Comparison

Figure A.47: Track End Hit Asymmetry - Kalman

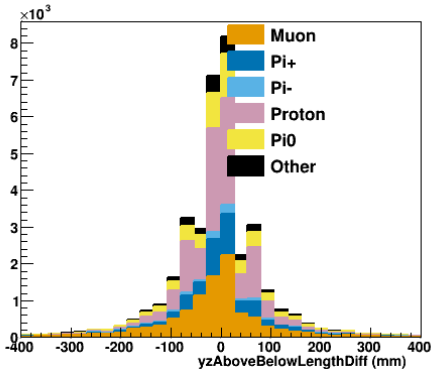

(a) Particle Breakdown

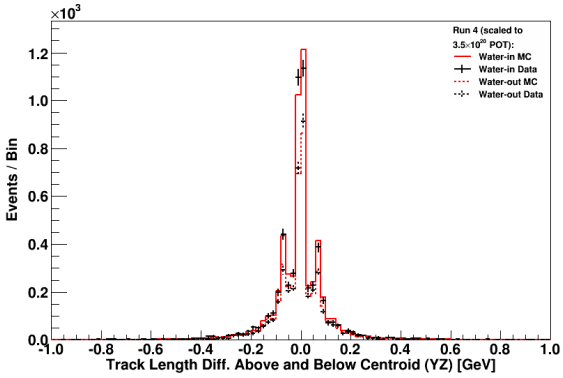

(b) Data MC Comparison

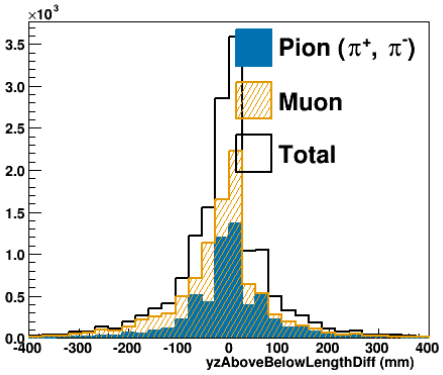

(c) MuPi Signal Background Comparison

Figure A.48: Track End Hit Asymmetry - Cluster

Charge Asymmetry

The ratio of the charge above the best fit line to the total charge in the whole track is stored in the Charge Asymmetry variable.

This variable is a good partner to the hit asymmetry, because though they are similar - more hits usually means more charge - they can be combined to identify events where a few high charge hits are overshadowing other information in the track.

The YZ projection of this variable is used in the MIP MVA for Cluster tracks and the XZ projection is used in the MuPi MVA for both Kalman and Cluster tracks.

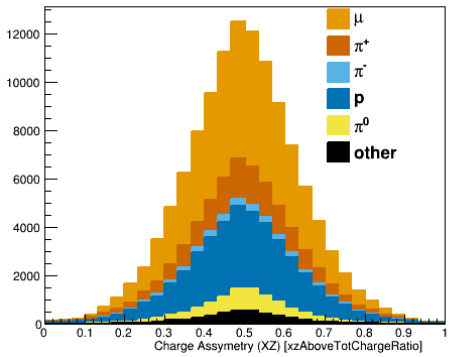

(a) Particle Breakdown

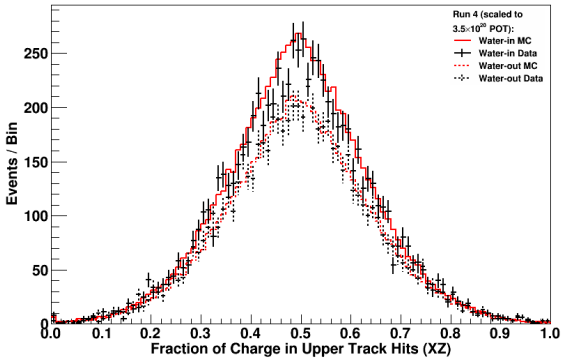

(b) Data MC Comparison

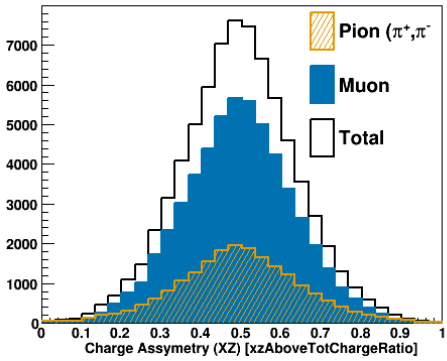

(c) MuPi Signal Background Comparison

Figure A.49: Charge Asymmetry - XZ - Kalman

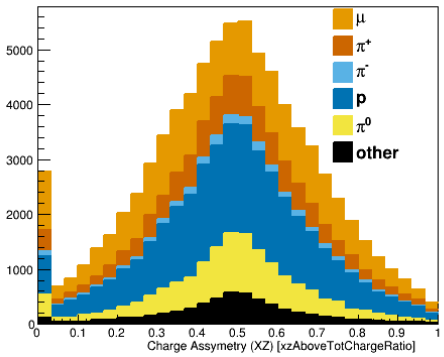

(a) Particle Breakdown

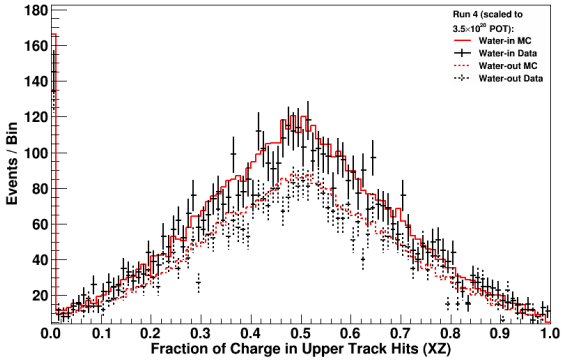

(b) Data MC Comparison

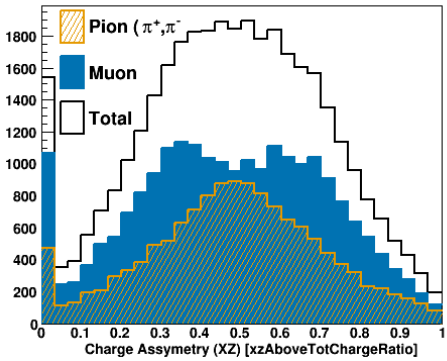

(c) MuPi Signal Background Comparison

Figure A.50: Charge Asymmetry - XZ - Cluster

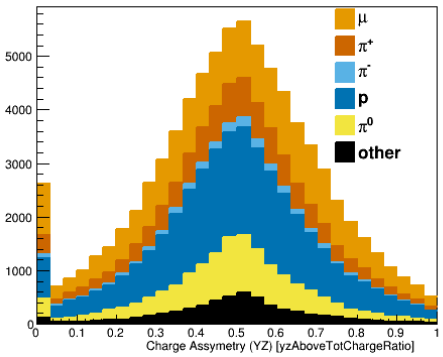

(a) Particle Breakdown

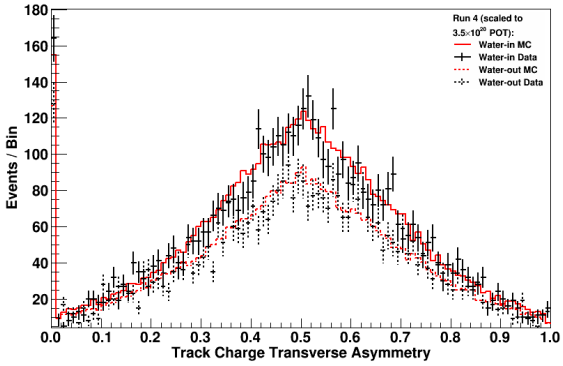

(b) Data MC Comparison

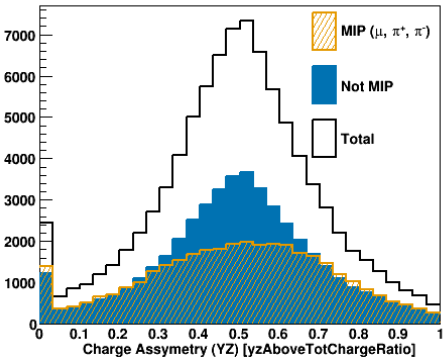

(c) MIP Signal Background Comparison

Figure A.51: Charge Asymmetry - YZ - Cluster

Appendix B

Fitter Studies

B.1 Generating Mock Data

Mock data is generated within the fitter in the same manner that fits are done. The default NEUT templates are adjusted by applying a number of systematics to the templates for a specific sigma. In addition to applying the same parameters that are used in the fits, a number of other adjustments have been implemented, including model updates for signal and background processes as well as systematics that completely change the spectra to represent other event generators. Descriptions of these dials are given below, together with the results of the fitter studies.

All the studies are done with the same fit parameters that will be used for the analysis and are listed in Table 6.9.

Plots for Each Study For each fit four different sets of plots are presented. The first set of plots is the mock data overlaid on the stack of pre-fit templates which shows how different the mock data is from the starting point of the fitter. Next are post fit plots to match the pre-fit ones, with the mock data overlaid on the templates that have now been adjusted to the best fit parameter values. Third are plots of the extracted signal with the fit errors (which are a combination of fit parameter errors as well as statistical errors) as well as the mock data overlaid with the statistical error from the number of mock data events. Last are plots of the fit parameters given as their deviation from nominal in units of sigma for each parameter.

B.2 Mock Data Test With No Variations

B.2.1 Asimov Fit

For this fit, the default Monte Carlo is used as mock data as an exercise of the fitter to ensure it is behaving in a reasonable manner. The expectation is that the fit will be nearly identical to the mock data, with the parameters close to their nominal values.

Plotted in Figures B.1 and B.2 are the mock data over the pre-fit NEUT templates, while Figures B.3 and B.4 are the mock data over the post-fit NEUT templates. The extracted signal is plotted in figures B.5 and B.6. The fit parameter deviations from nominal and error are plotted in figure B.7.

B.3 Mock Data Tests Varying Background Model Parameters

The fitter uses background model parameters to conduct the fit. Making mock data with these parameters should create data that is not too difficult for the fitter to fit. The only difficulty is that the mock data is made in regions where the penalty terms on the parameters will try to pull the fit away from the mock data. The goal is to see that the fitter still performs well fitting the mock data or that any deviations are understood.

B.3.1 Flux Fits

For the flux studies, the flux parameters were adjusted by plus and minus one sigma and applied to all templates (both signal and background).

$+1\sigma$ Flux Parameters

Plotted in Figures B.8 and B.9 are the mock data over the pre-fit NEUT templates, while Figures B.10 and B.11 are the mock data over the post-fit NEUT templates. The extracted signal is plotted in figures B.12 and B.13. The fit parameter deviations from nominal and error are plotted in figure B.14.

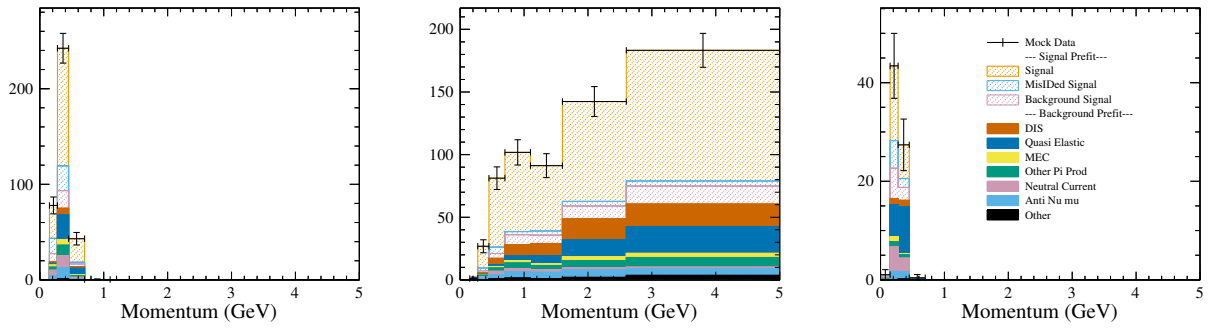

(a) Selected Kalman Contained **(b)** Selected Kalman Exiting **(c)** Selected Cluster

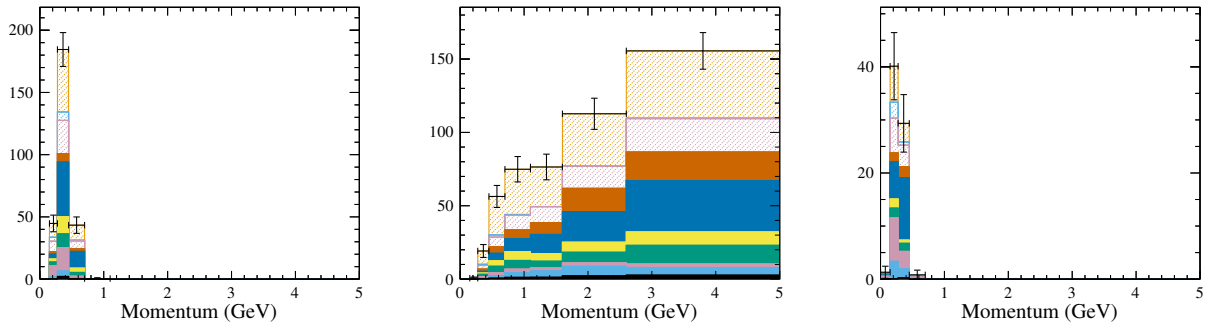

(d) Near Sideband Kalman Contained **(e)** Near Sideband Kalman Exiting **(f)** Near Sideband Cluster

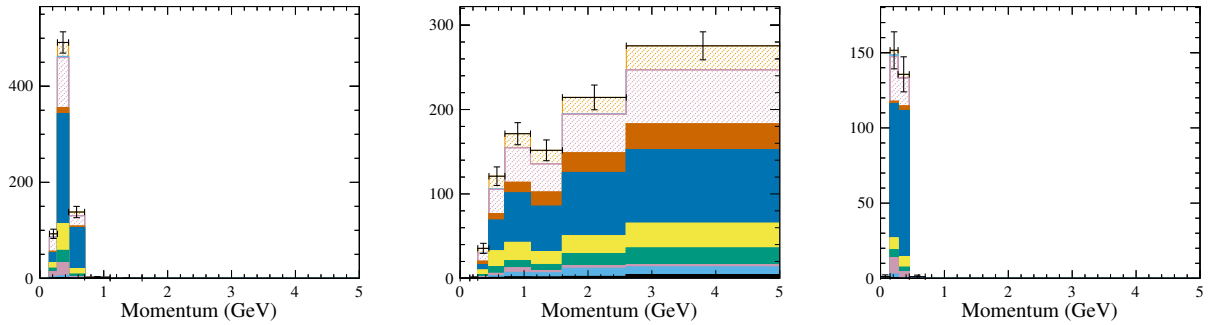

(g) Far Sideband Kalman Contained **(h)** Far Sideband Kalman Exiting **(i)** Far Sideband Cluster

Figure B.1: Asimov Study - Mock Data with Pre-Fit NEUT Templates - Momentum Projection

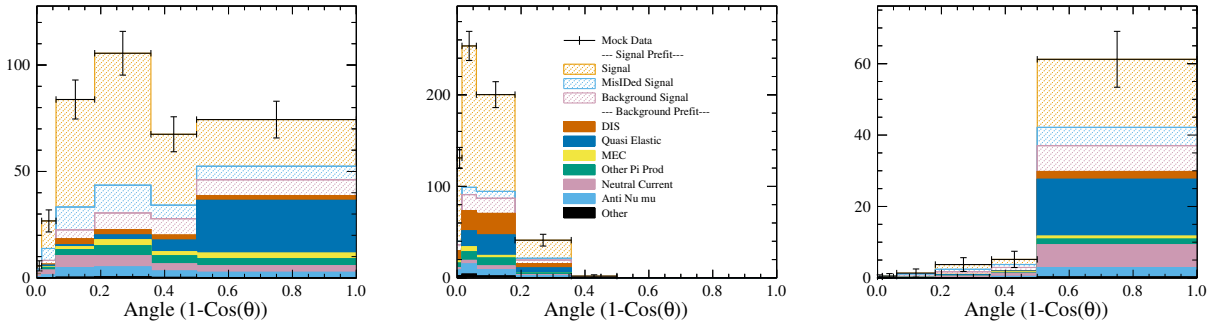

(a) Selected Kalman Contained **(b)** Selected Kalman Exiting **(c)** Selected Cluster

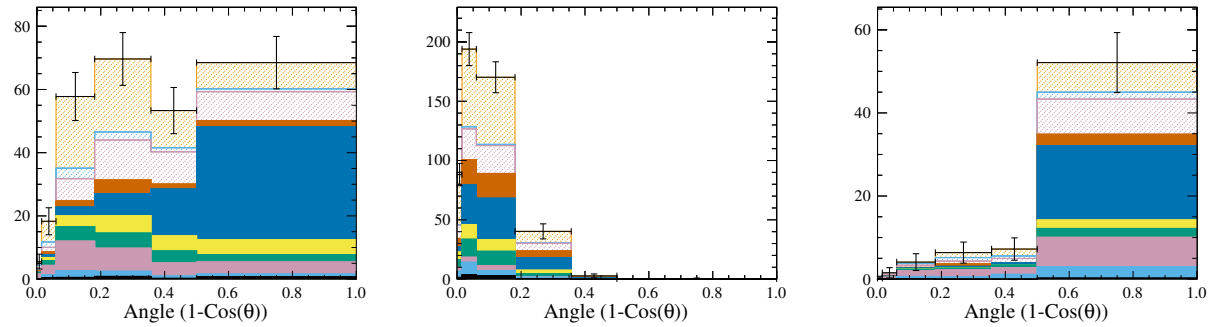

(d) Near Sideband Kalman Contained **(e)** Near Sideband Kalman Exiting **(f)** Near Sideband Cluster

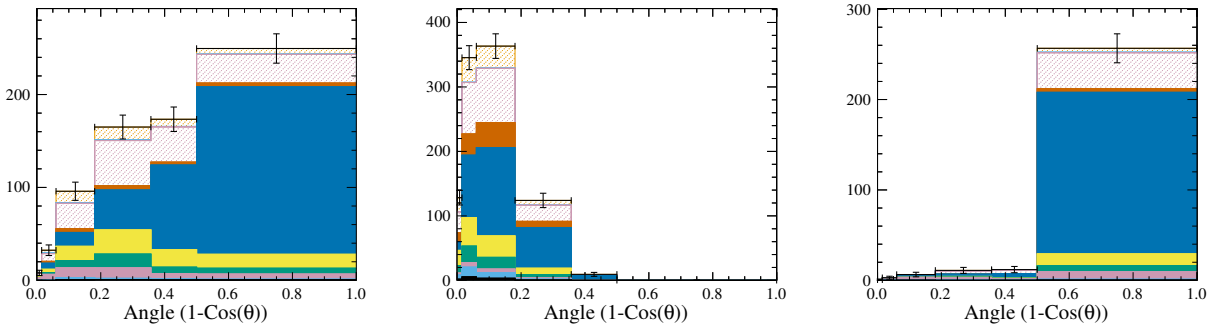

(g) Far Sideband Kalman Contained **(h)** Far Sideband Kalman Exiting **(i)** Far Sideband Cluster

Figure B.2: Asimov Study - Mock Data with Pre-Fit NEUT Templates - Angle Projection

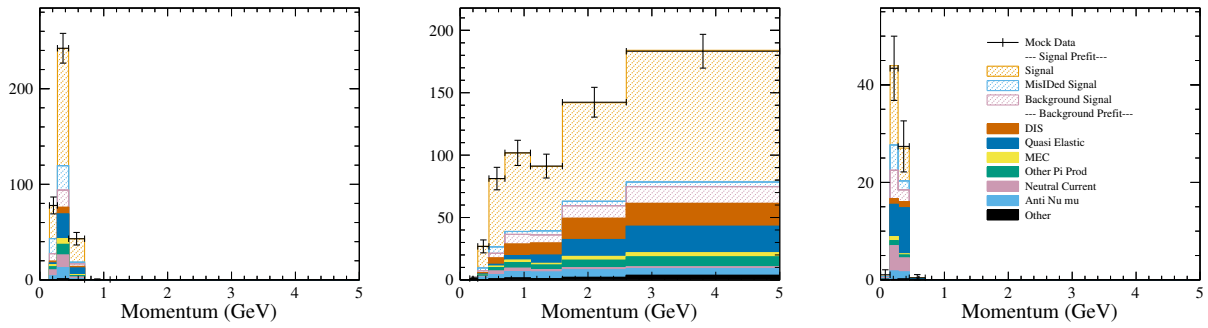

(a) Selected Kalman Contained **(b)** Selected Kalman Exiting **(c)** Selected Cluster

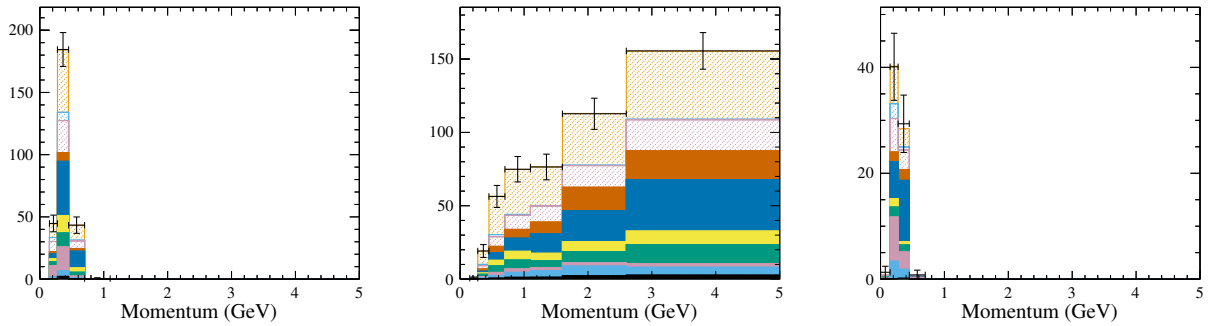

(d) Near Sideband Kalman Contained **(e)** Near Sideband Kalman Exiting **(f)** Near Sideband Cluster

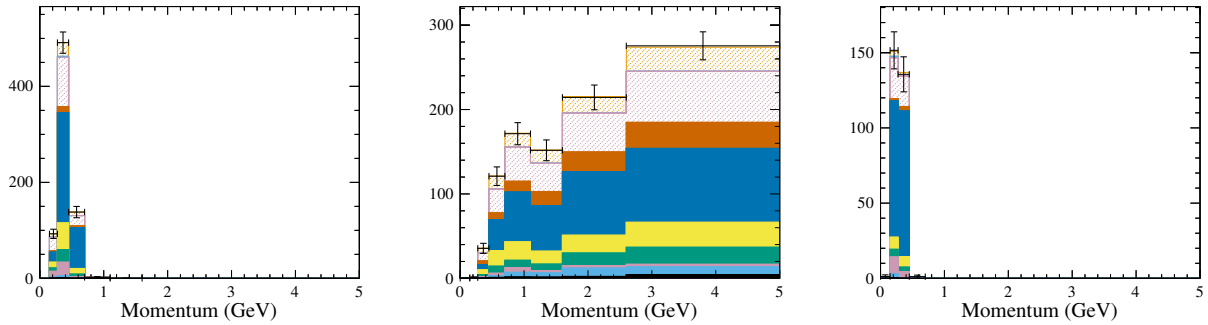

(g) Far Sideband Kalman Contained **(h)** Far Sideband Kalman Exiting **(i)** Far Sideband Cluster

Figure B.3: Asimov Study - Mock Data with Post-Fit NEUT Templates - Momentum Projection

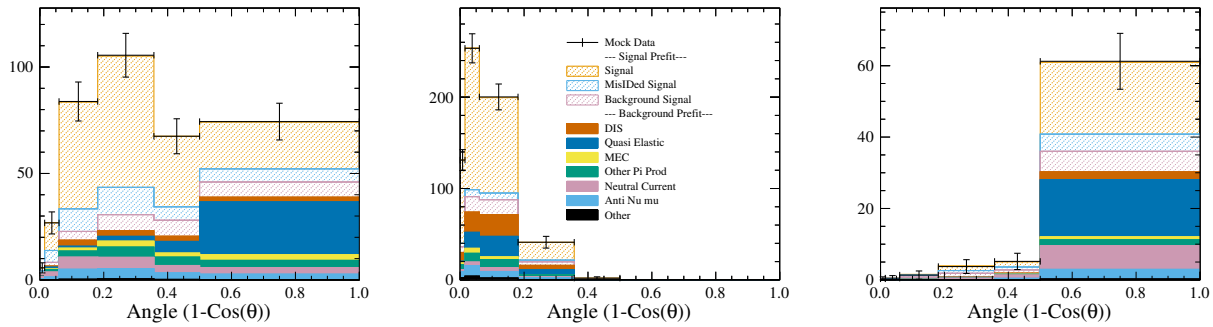

(a) Selected Kalman Contained **(b)** Selected Kalman Exiting **(c)** Selected Cluster

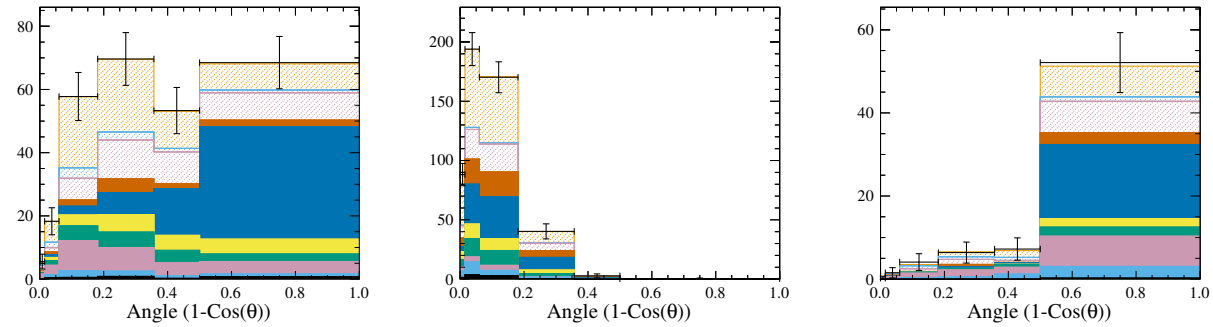

(d) Near Sideband Kalman Contained **(e)** Near Sideband Kalman Exiting **(f)** Near Sideband Cluster

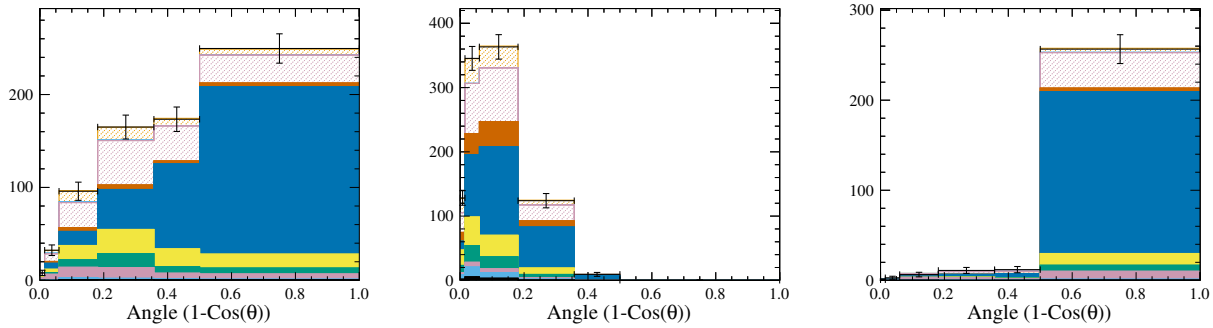

(g) Far Sideband Kalman Contained **(h)** Far Sideband Kalman Exiting **(i)** Far Sideband Cluster

Figure B.4: Asimov Study - Mock Data with Post-Fit NEUT Templates - Angle Projection

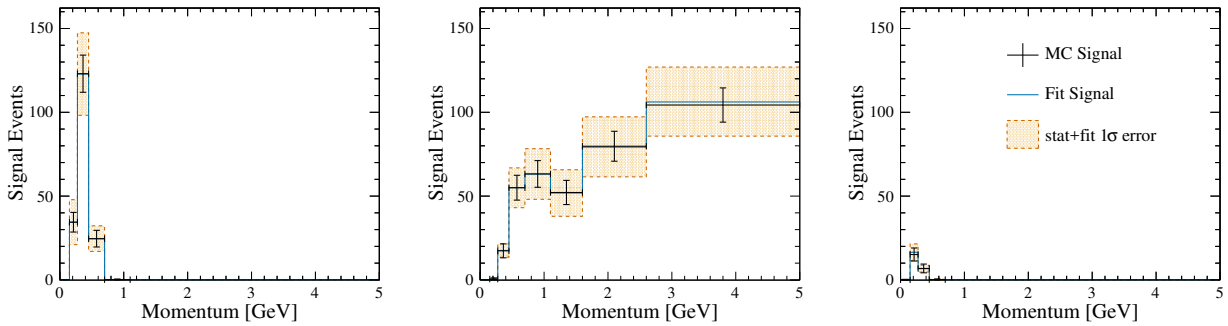

(a) Selected Kalman Contained **(b)** Selected Kalman Exiting **(c)** Selected Cluster

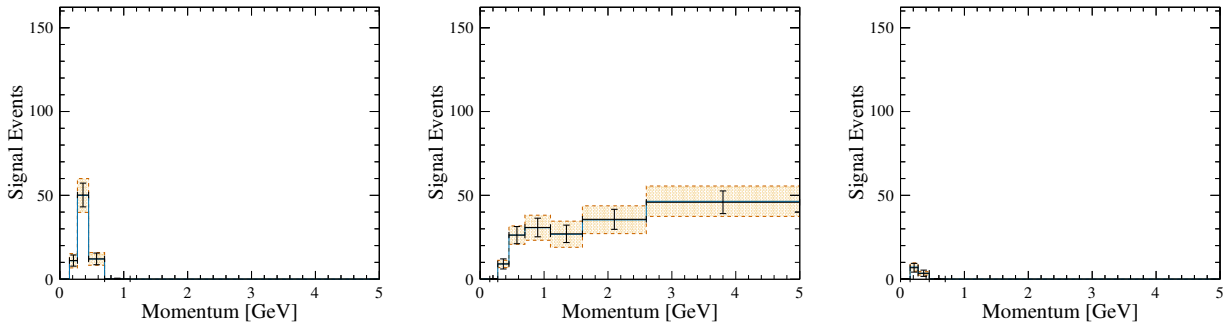

(d) Near Sideband Kalman Contained **(e)** Near Sideband Kalman Exiting **(f)** Near Sideband Cluster

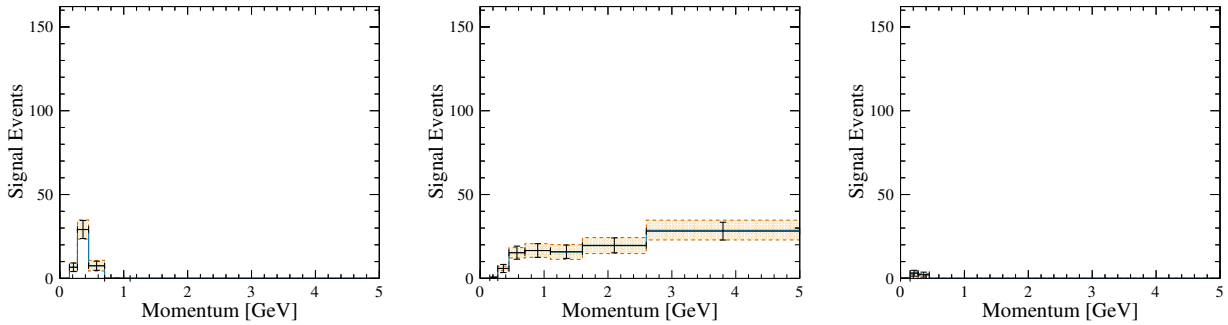

(g) Far Sideband Kalman Contained **(h)** Far Sideband Kalman Exiting **(i)** Far Sideband Cluster

Figure B.5: Asimov Study - Signal fit in the muon momentum projection. Black crosses represent the mock data with statistical error bars. The solid blue line is the best fit and the orange region is the error from the fit. - Momentum projection

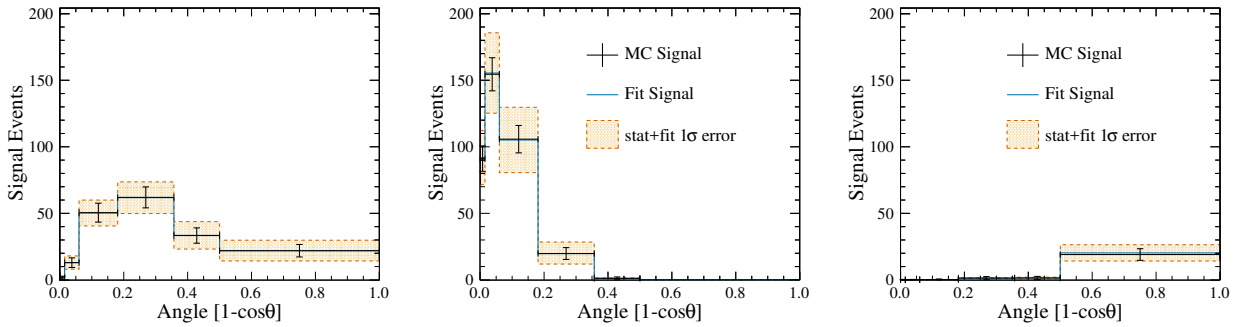

(a) Selected Kalman Contained **(b)** Selected Kalman Exiting **(c)** Selected Cluster

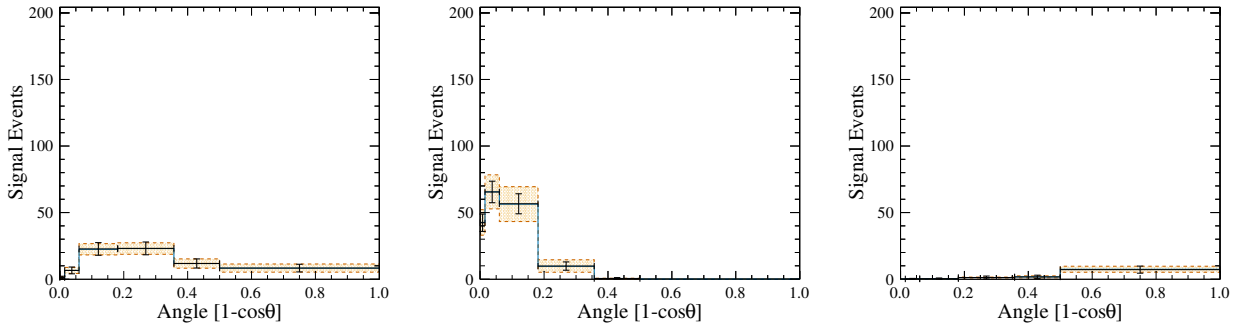

(d) Near Sideband Kalman Contained **(e)** Near Sideband Kalman Exiting **(f)** Near Sideband Cluster

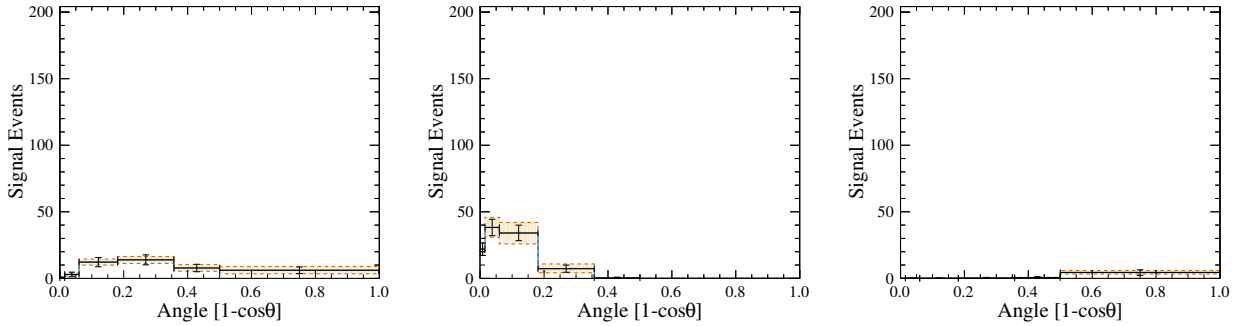

(g) Far Sideband Kalman Contained **(h)** Far Sideband Kalman Exiting **(i)** Far Sideband Cluster

Figure B.6: Asimov Study - Signal fit in the muon angle projection. Black crosses represent the mock data with statistical error bars. The solid blue line is the best fit and the orange region is the error from the fit. - Angle projection

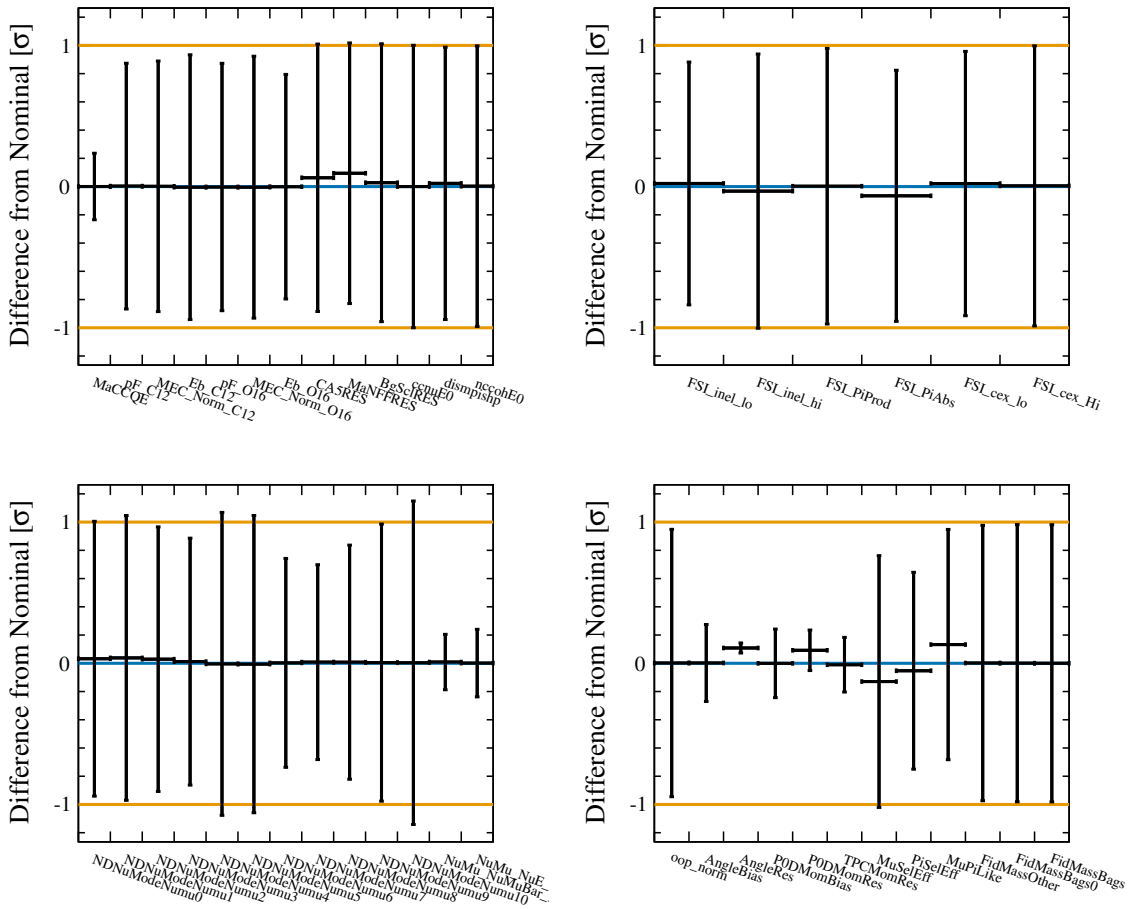

Figure B.7: Asimov Study - Fit parameter deviation from nominal. The points in this plot are the best fit parameter value in units of sigma for each dial. The error bars on the points are the error on that parameter from the fit, while the orange lines at +1 and -1 represent the default one sigma error placed on the variable.

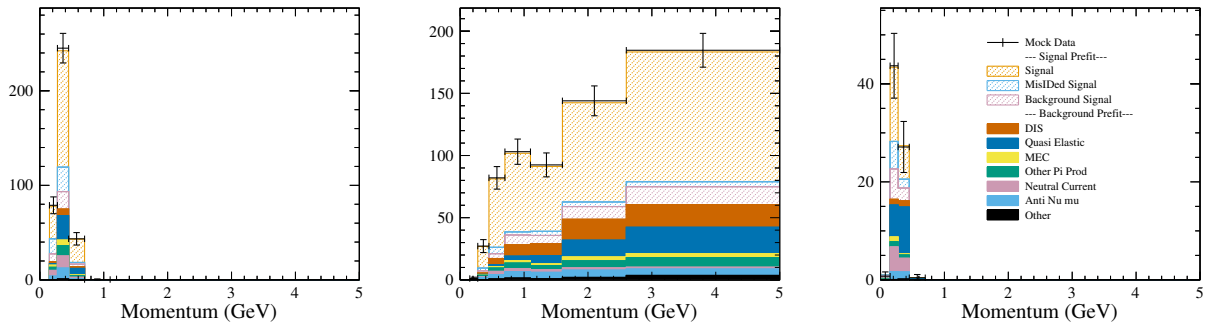

(a) Selected Kalman Contained **(b)** Selected Kalman Exiting **(c)** Selected Cluster

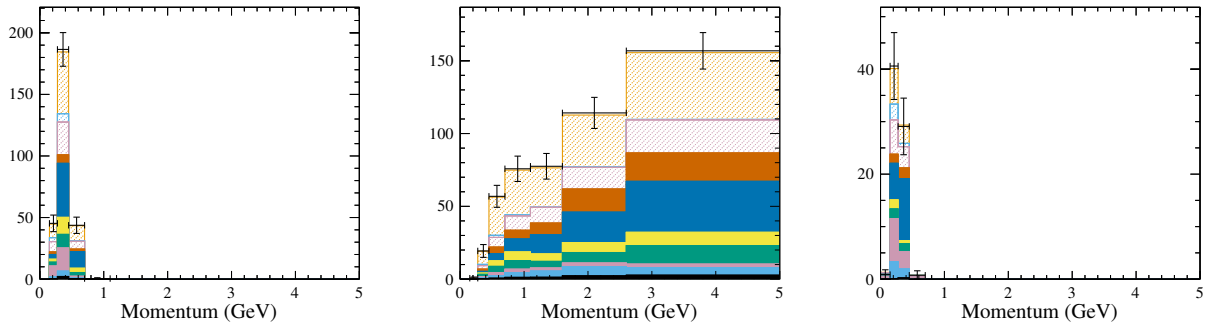

(d) Near Sideband Kalman Contained **(e)** Near Sideband Kalman Exiting **(f)** Near Sideband Cluster

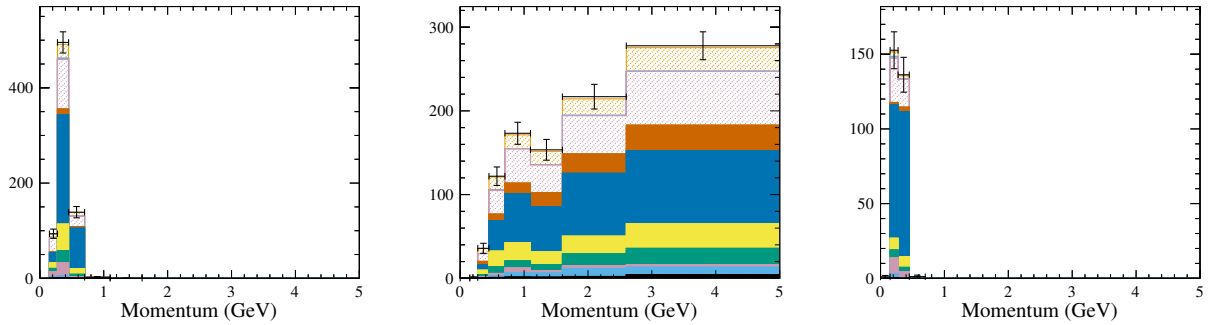

(g) Far Sideband Kalman Contained **(h)** Far Sideband Kalman Exiting **(i)** Far Sideband Cluster

Figure B.8: $+1\sigma$ Flux Parameters Study - Mock Data with Pre-Fit NEUT Templates - Momentum Projection

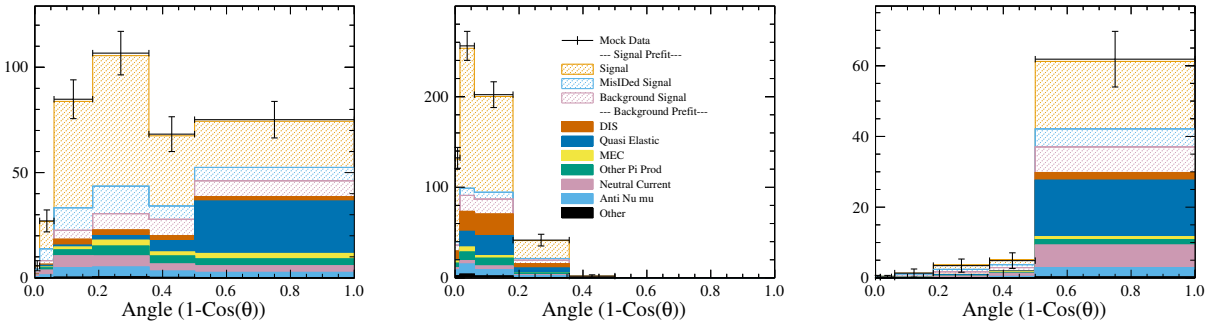

(a) Selected Kalman Contained **(b)** Selected Kalman Exiting **(c)** Selected Cluster

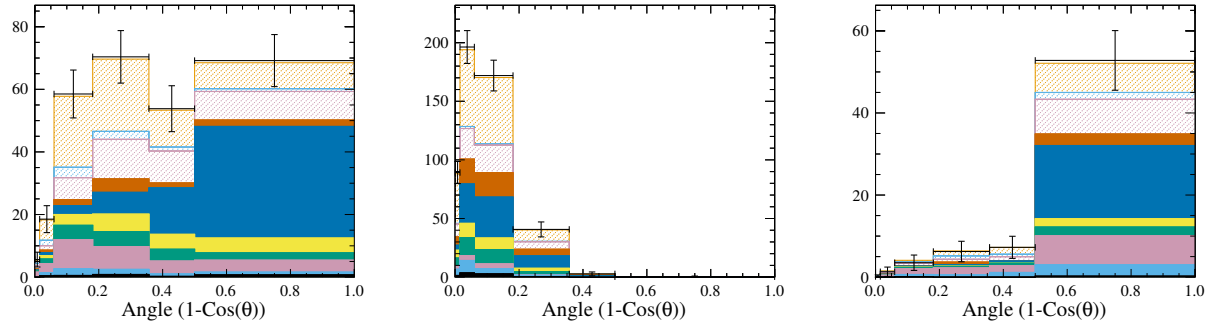

(d) Near Sideband Kalman Contained **(e)** Near Sideband Kalman Exiting **(f)** Near Sideband Cluster

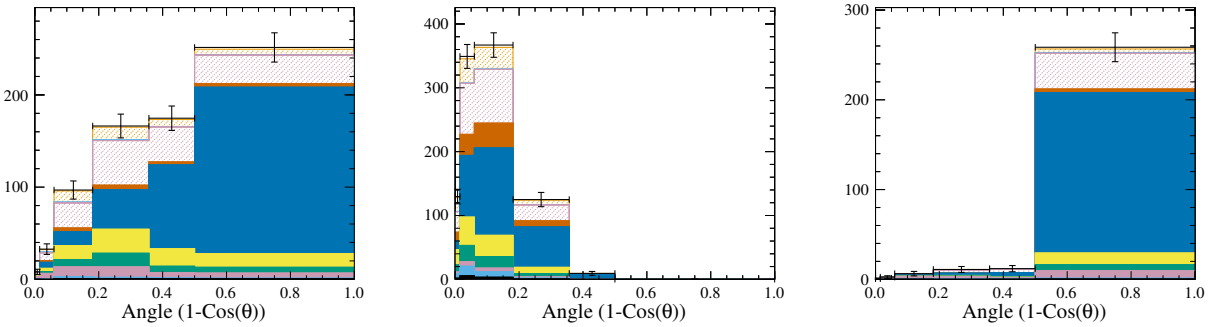

(g) Far Sideband Kalman Contained **(h)** Far Sideband Kalman Exiting **(i)** Far Sideband Cluster

Figure B.9: $+1\sigma$ Flux Parameters Study - Mock Data with Pre-Fit NEUT Templates - Angle Projection

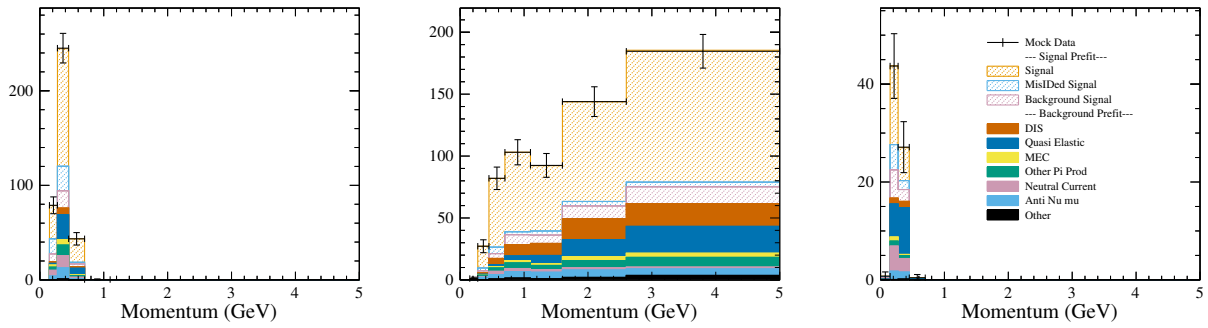

(a) Selected Kalman Contained **(b)** Selected Kalman Exiting **(c)** Selected Cluster

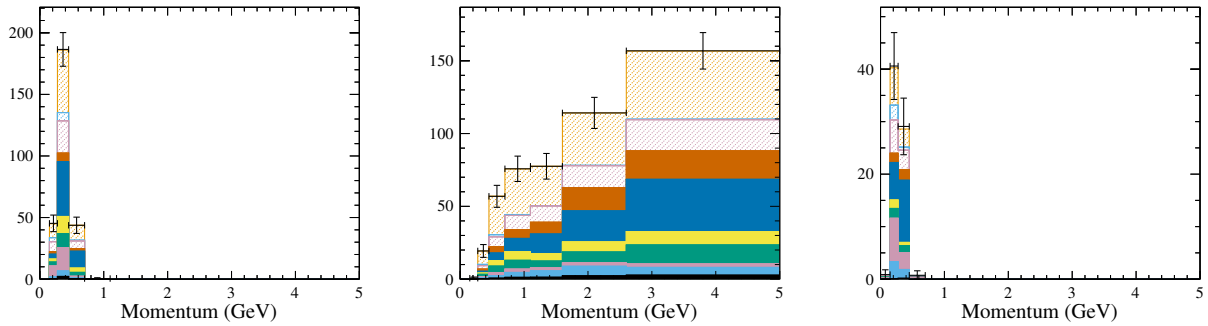

(d) Near Sideband Kalman Contained **(e)** Near Sideband Kalman Exiting **(f)** Near Sideband Cluster

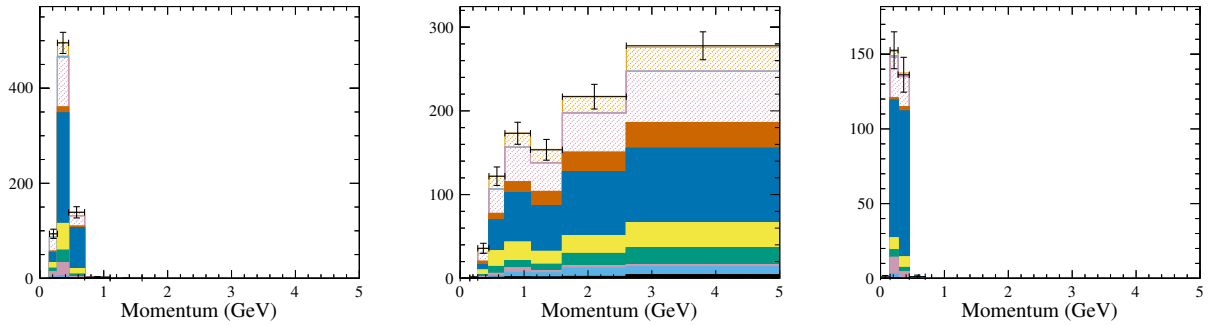

(g) Far Sideband Kalman Contained **(h)** Far Sideband Kalman Exiting **(i)** Far Sideband Cluster

Figure B.10: $+1\sigma$ Flux Parameters Study - Mock Data with Post-Fit NEUT Templates - Momentum Projection

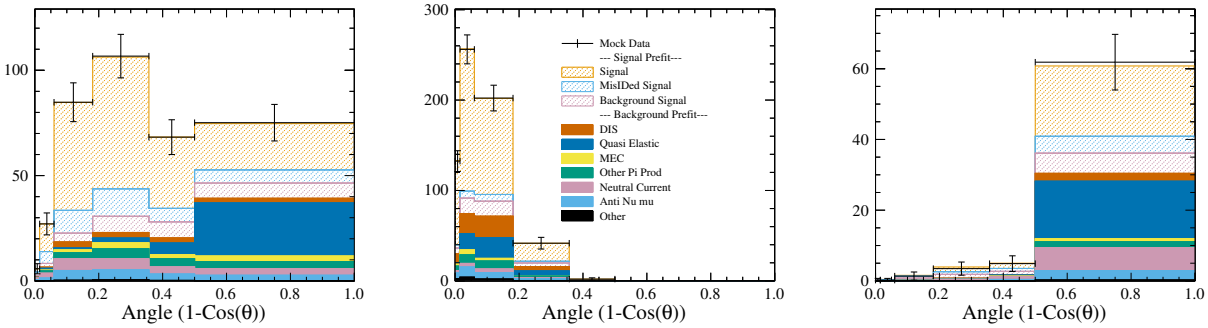

(a) Selected Kalman Contained **(b)** Selected Kalman Exiting **(c)** Selected Cluster

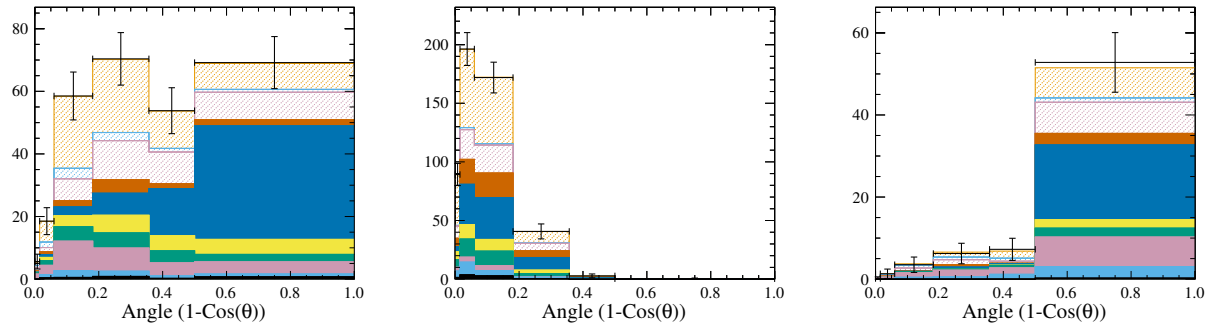

(d) Near Sideband Kalman Contained **(e)** Near Sideband Kalman Exiting **(f)** Near Sideband Cluster

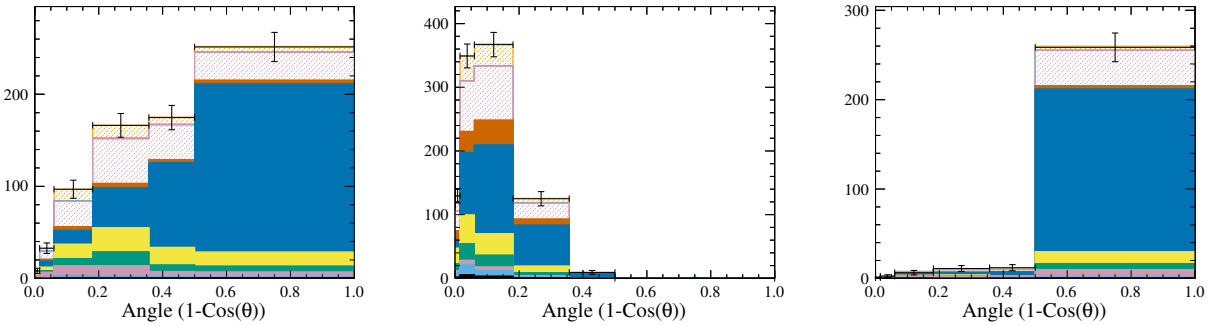

(g) Far Sideband Kalman Contained **(h)** Far Sideband Kalman Exiting **(i)** Far Sideband Cluster

Figure B.11: $+1\sigma$ Flux Parameters Study - Mock Data with Post-Fit NEUT Templates - Angle Projection

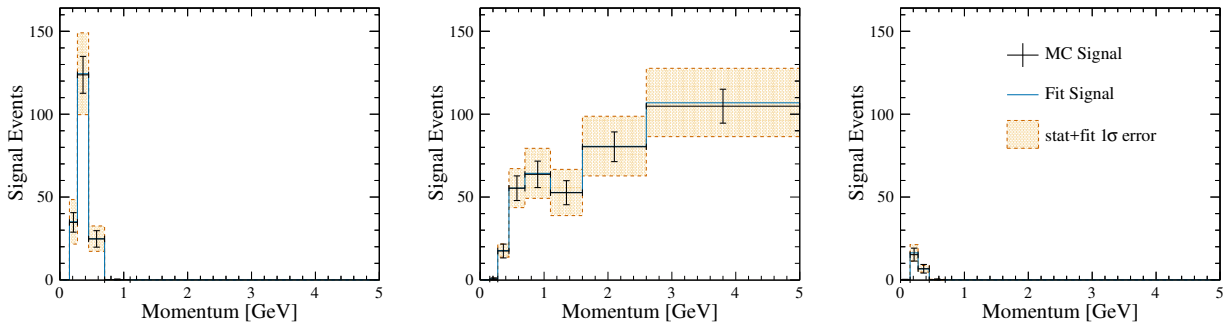

(a) Selected Kalman Contained **(b)** Selected Kalman Exiting **(c)** Selected Cluster

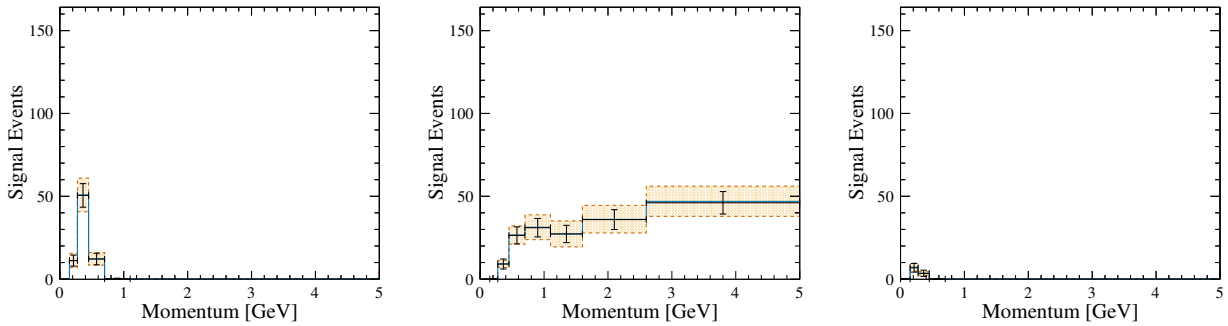

(d) Near Sideband Kalman Contained **(e)** Near Sideband Kalman Exiting **(f)** Near Sideband Cluster

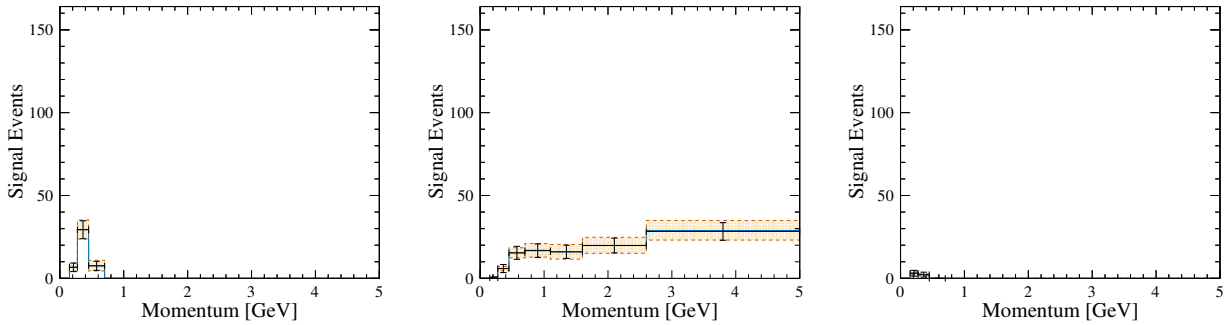

(g) Far Sideband Kalman Contained **(h)** Far Sideband Kalman Exiting **(i)** Far Sideband Cluster

Figure B.12: $+1\sigma$ Flux Parameters Study - Signal fit in the muon momentum projection. Black crosses represent the mock data with statistical error bars. The solid blue line is the best fit and the orange region is the error from the fit. - Momentum projection

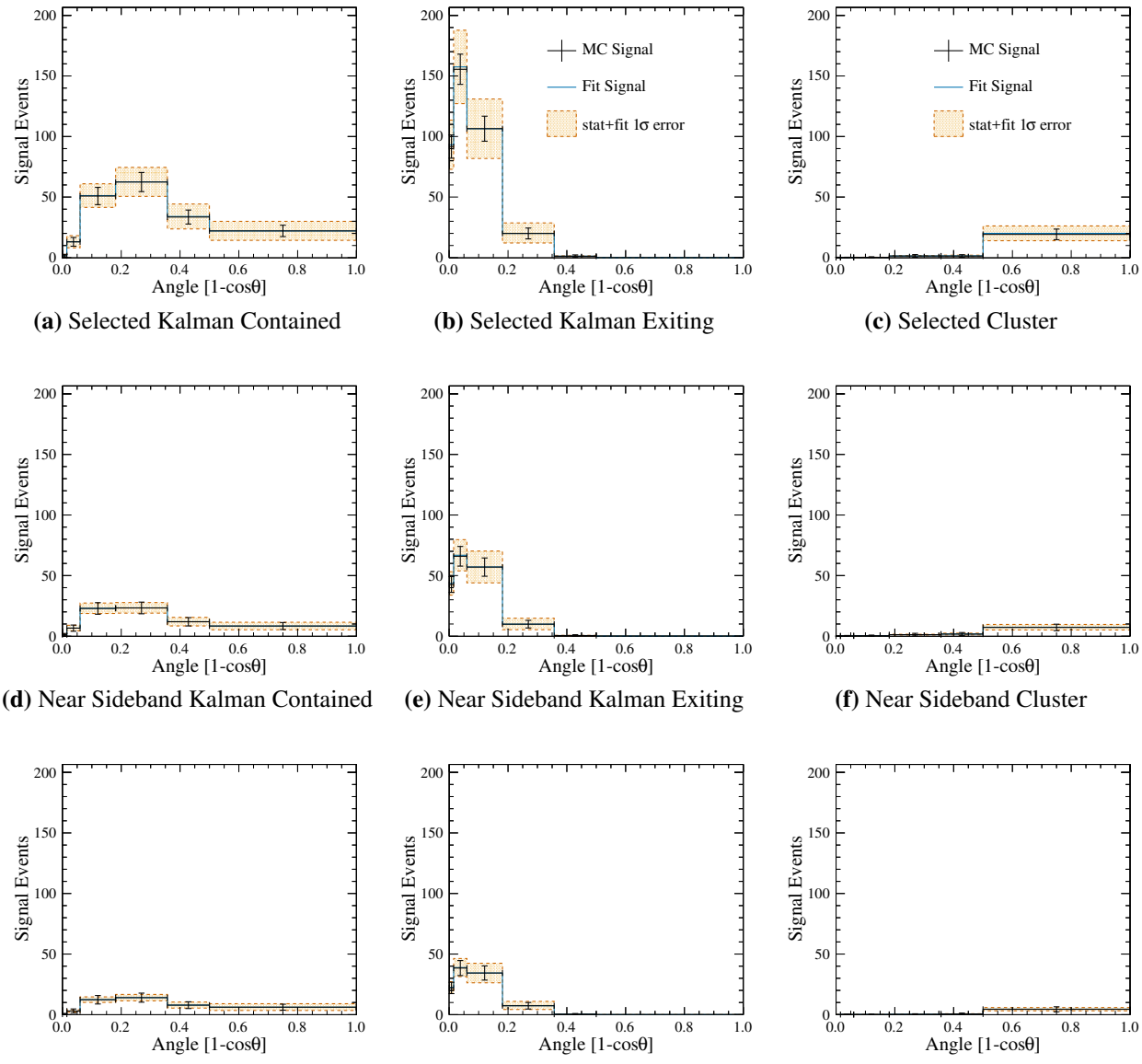

(a) Selected Kalman Contained **(b)** Selected Kalman Exiting **(c)** Selected Cluster

(d) Near Sideband Kalman Contained **(e)** Near Sideband Kalman Exiting **(f)** Near Sideband Cluster

(g) Far Sideband Kalman Contained **(h)** Far Sideband Kalman Exiting **(i)** Far Sideband Cluster

Figure B.13: $+1\sigma$ Flux Parameters Study - Signal fit in the muon angle projection. Black crosses represent the mock data with statistical error bars. The solid blue line is the best fit and the orange region is the error from the fit. - Angle projection

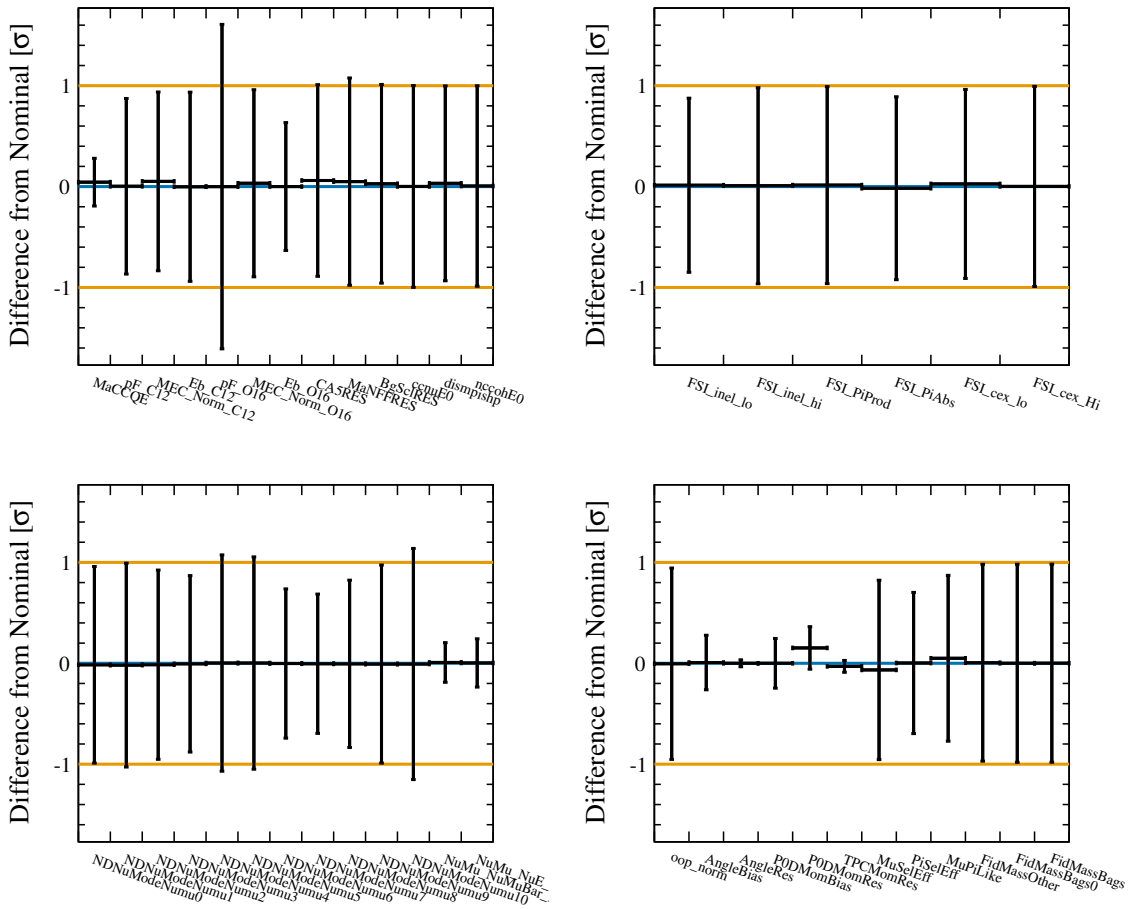

Figure B.14: $+1\sigma$ Flux Parameters Study - Fit parameter deviation from nominal. The points in this plot are the best fit parameter value in units of sigma for each dial. The error bars on the points are the error on that parameter from the fit, while the orange lines at +1 and -1 represent the default one sigma error placed on the variable.

-1σ Flux Parameters

Plotted in Figures B.15 and B.16 are the mock data over the pre-fit NEUT templates, while Figures B.17 and B.18 are the mock data over the post-fit NEUT templates. The extracted signal is plotted in figures B.19 and B.20. The fit parameter deviations from nominal and error are plotted in figure B.21.

B.3.2 FSI Fits

For these studies all the FSI dials were adjusted at the same time, plus or minus one sigma. These dials have the response functions that are the least linear of any of the re-weight dials, and thus produce a more complex mock data set for the fitter to work with.

$+1\sigma$ FSI Parameters

Plotted in Figures B.22 and B.23 are the mock data over the pre-fit NEUT templates, while Figures B.24 and B.25 are the mock data over the post-fit NEUT templates. The extracted signal is plotted in figures B.26 and B.27. The fit parameter deviations from nominal and error are plotted in figure B.28.

-1σ FSI Parameters

Plotted in Figures B.29 and B.30 are the mock data over the pre-fit NEUT templates, while Figures B.31 and B.32 are the mock data over the post-fit NEUT templates. The extracted signal is plotted in figures B.33 and B.34. The fit parameter deviations from nominal and error are plotted in figure B.35.

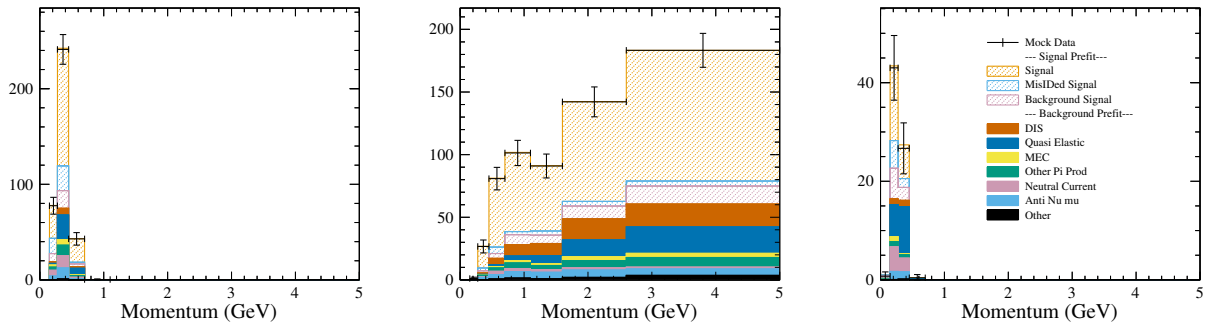

(a) Selected Kalman Contained **(b)** Selected Kalman Exiting **(c)** Selected Cluster

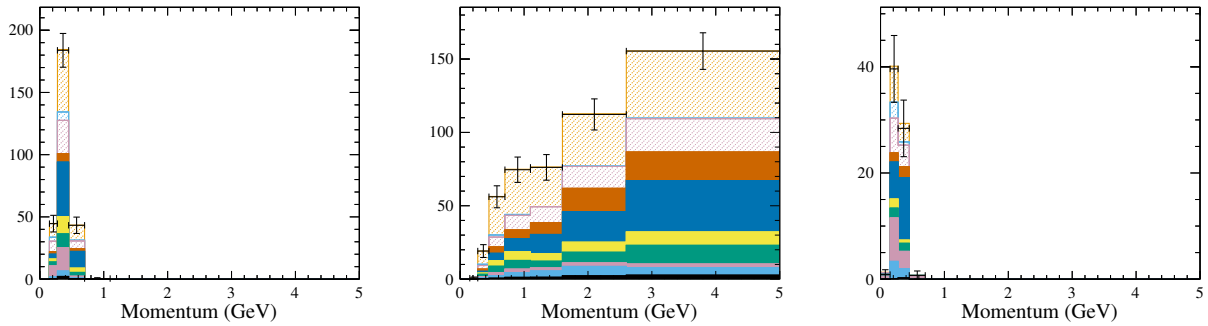

(d) Near Sideband Kalman Contained **(e)** Near Sideband Kalman Exiting **(f)** Near Sideband Cluster

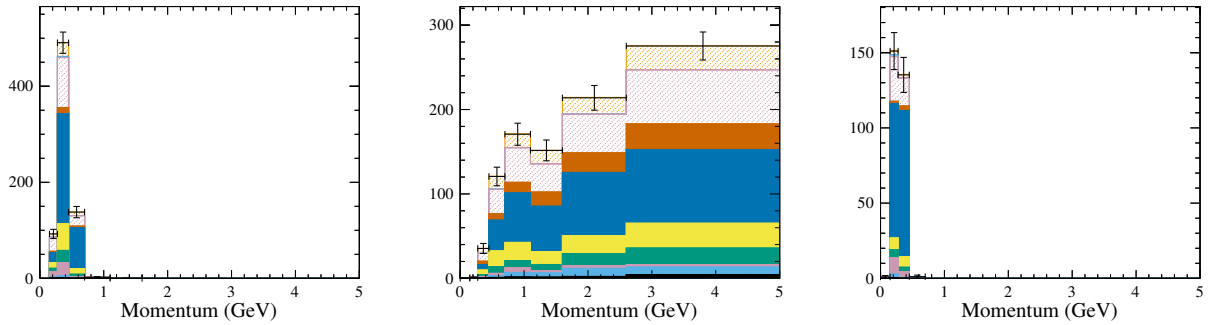

(g) Far Sideband Kalman Contained **(h)** Far Sideband Kalman Exiting **(i)** Far Sideband Cluster

Figure B.15: -1σ Flux Parameters Study- Mock Data with Pre-Fit NEUT Templates - Momentum Projection

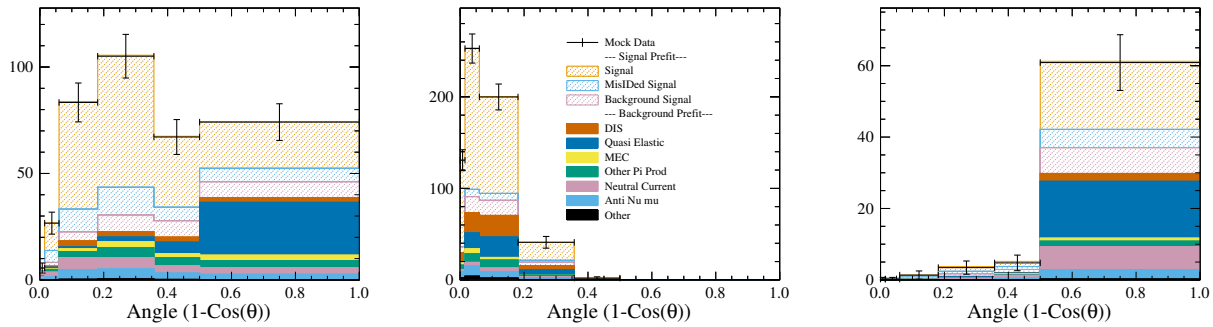

(a) Selected Kalman Contained **(b)** Selected Kalman Exiting **(c)** Selected Cluster

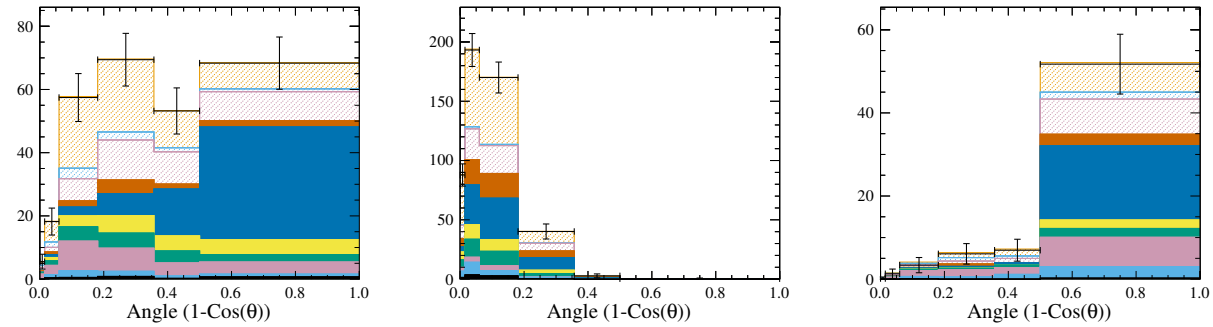

(d) Near Sideband Kalman Contained **(e)** Near Sideband Kalman Exiting **(f)** Near Sideband Cluster

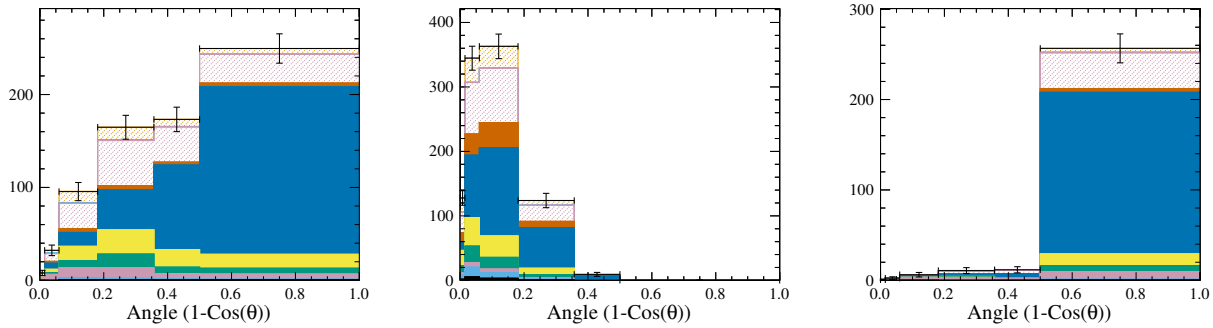

(g) Far Sideband Kalman Contained **(h)** Far Sideband Kalman Exiting **(i)** Far Sideband Cluster

Figure B.16: -1σ Flux Parameters Study - Mock Data with Pre-Fit NEUT Templates - Angle Projection

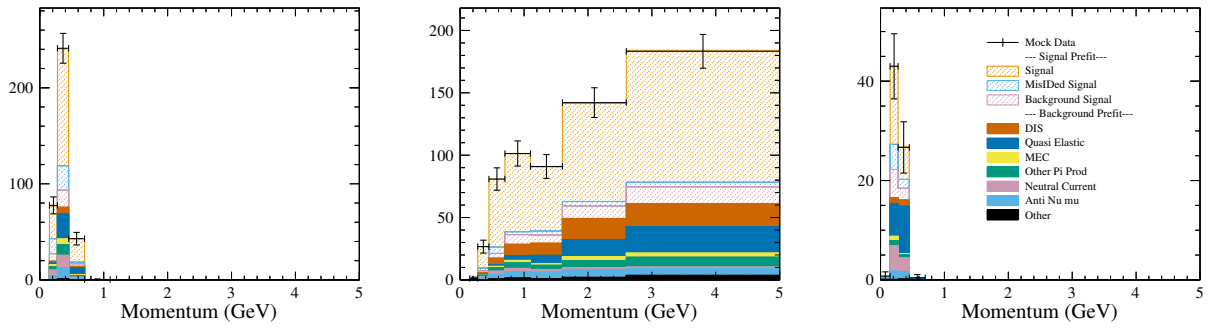

(a) Selected Kalman Contained **(b)** Selected Kalman Exiting **(c)** Selected Cluster

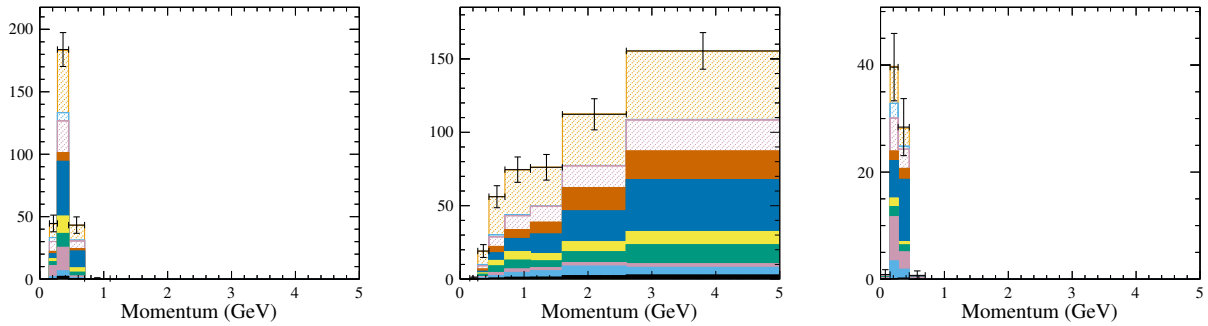

(d) Near Sideband Kalman Contained **(e)** Near Sideband Kalman Exiting **(f)** Near Sideband Cluster

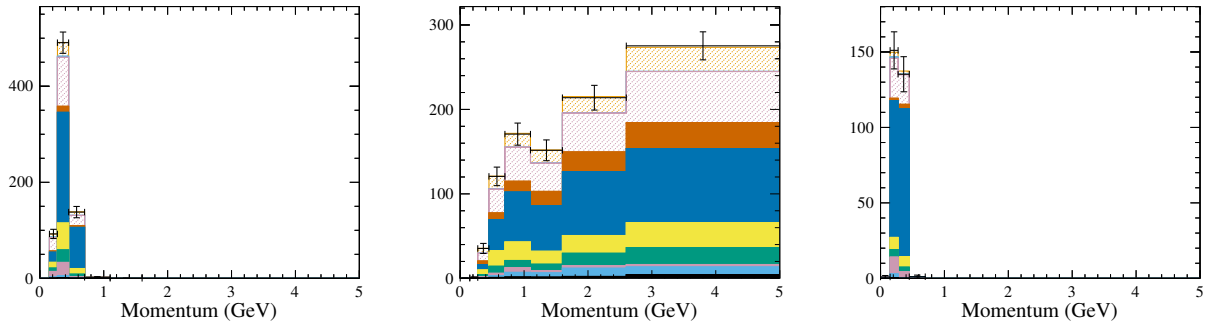

(g) Far Sideband Kalman Contained **(h)** Far Sideband Kalman Exiting **(i)** Far Sideband Cluster

Figure B.17: -1σ Flux Parameters Study- Mock Data with Post-Fit NEUT Templates - Momentum Projection

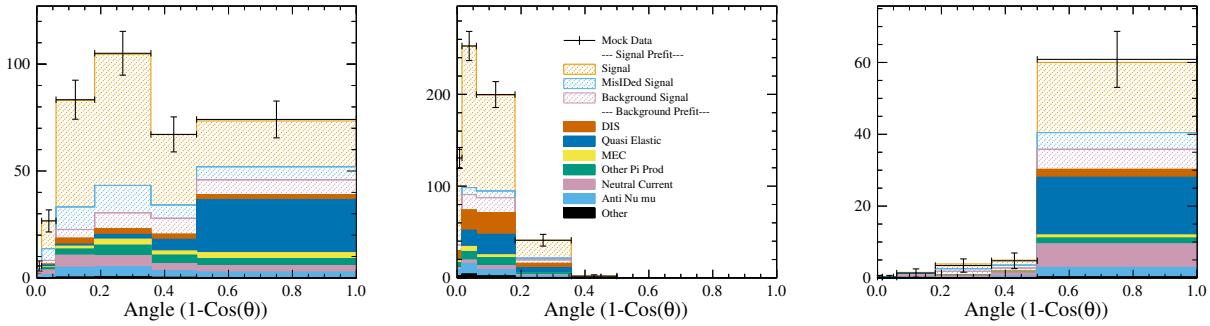

(a) Selected Kalman Contained **(b)** Selected Kalman Exiting **(c)** Selected Cluster

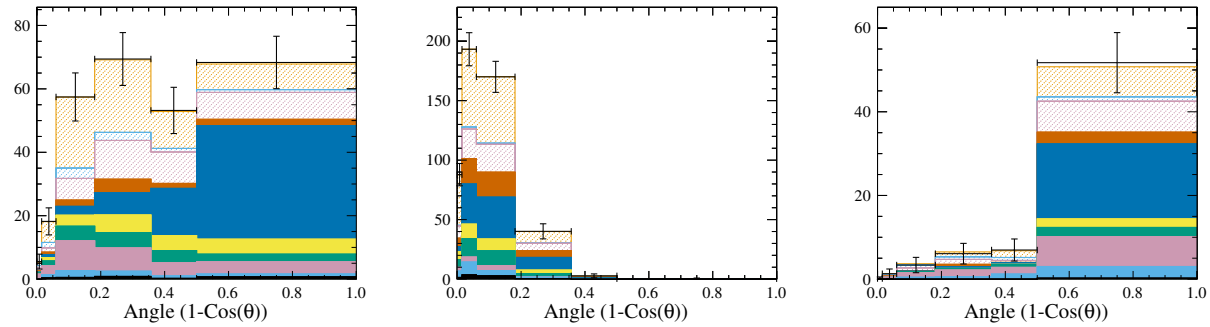

(d) Near Sideband Kalman Contained **(e)** Near Sideband Kalman Exiting **(f)** Near Sideband Cluster

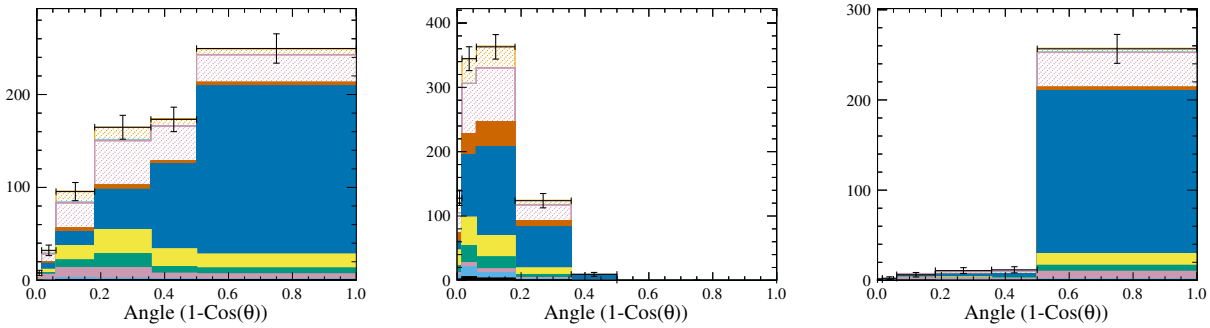

(g) Far Sideband Kalman Contained **(h)** Far Sideband Kalman Exiting **(i)** Far Sideband Cluster

Figure B.18: -1σ Flux Parameters Study - Mock Data with Post-Fit NEUT Templates - Angle Projection

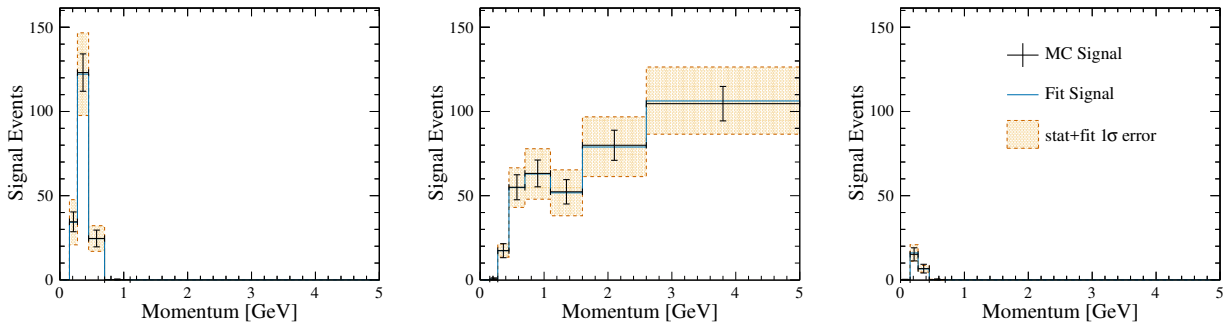

(a) Selected Kalman Contained **(b)** Selected Kalman Exiting **(c)** Selected Cluster

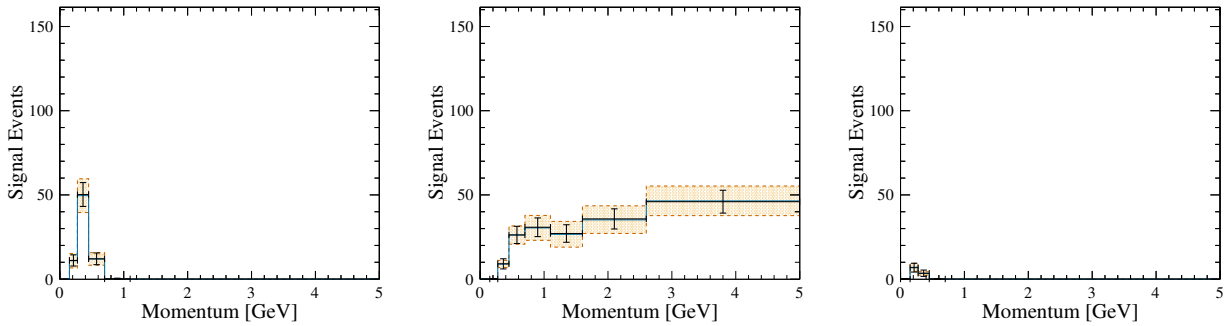

(d) Near Sideband Kalman Contained **(e)** Near Sideband Kalman Exiting **(f)** Near Sideband Cluster

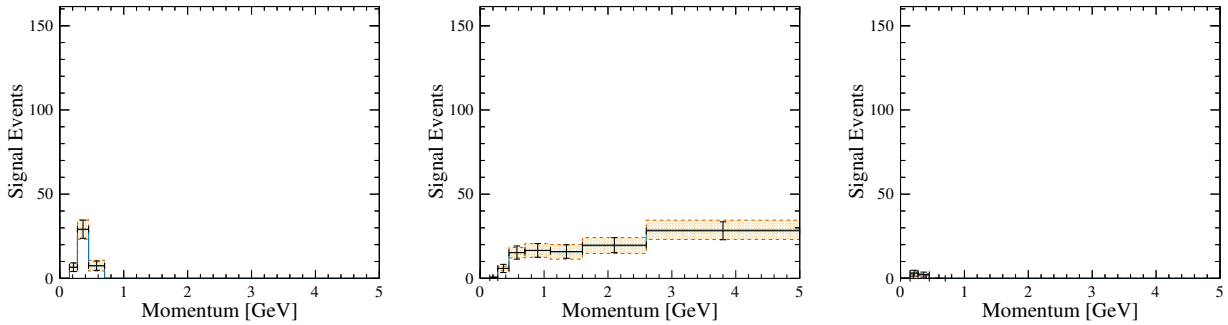

(g) Far Sideband Kalman Contained **(h)** Far Sideband Kalman Exiting **(i)** Far Sideband Cluster

Figure B.19: -1σ Flux Parameters Study - Signal fit in the muon momentum projection. Black crosses represent the mock data with statistical error bars. The solid blue line is the best fit and the orange region is the error from the fit. - Momentum projection

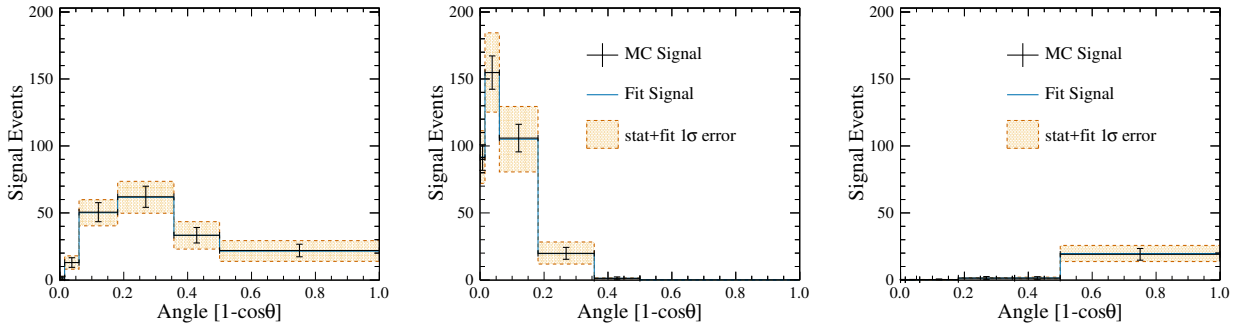

(a) Selected Kalman Contained **(b)** Selected Kalman Exiting **(c)** Selected Cluster

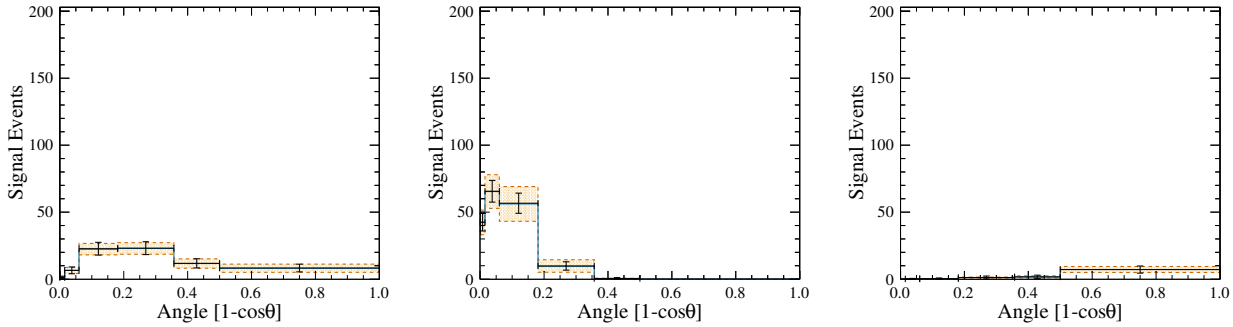

(d) Near Sideband Kalman Contained **(e)** Near Sideband Kalman Exiting **(f)** Near Sideband Cluster

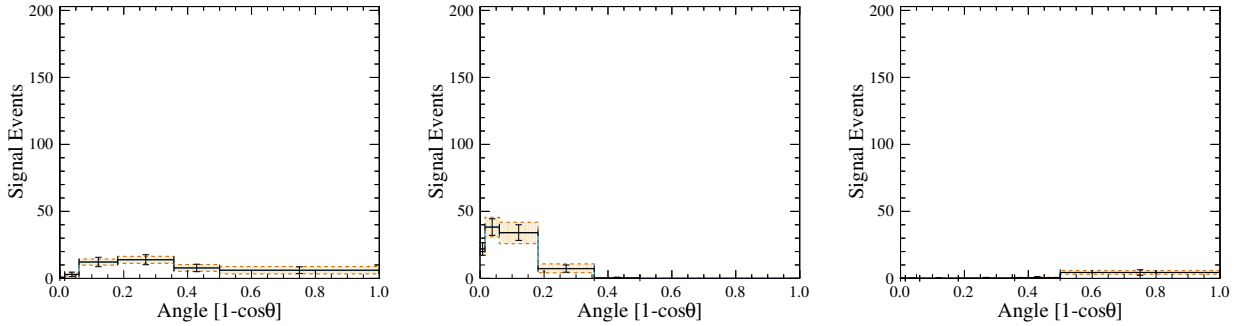

(g) Far Sideband Kalman Contained **(h)** Far Sideband Kalman Exiting **(i)** Far Sideband Cluster

Figure B.20: -1σ Flux Parameters Study - Signal fit in the muon angle projection. Black crosses represent the mock data with statistical error bars. The solid blue line is the best fit and the orange region is the error from the fit. - Angle projection

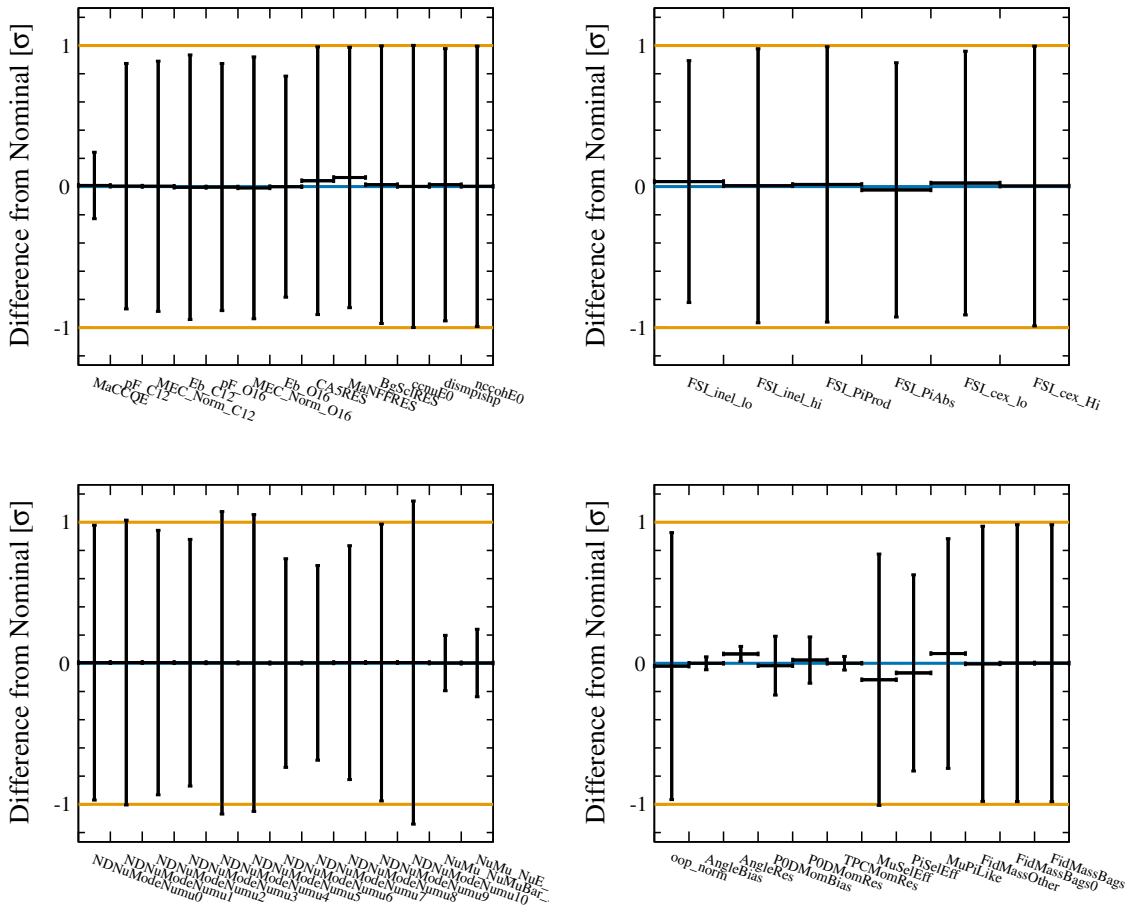

Figure B.21: -1σ Flux Parameters Study - Fit parameter deviation from nominal. The points in this plot are the best fit parameter value in units of sigma for each dial. The error bars on the points are the error on that parameter from the fit, while the orange lines at +1 and -1 represent the default one sigma error placed on the variable.

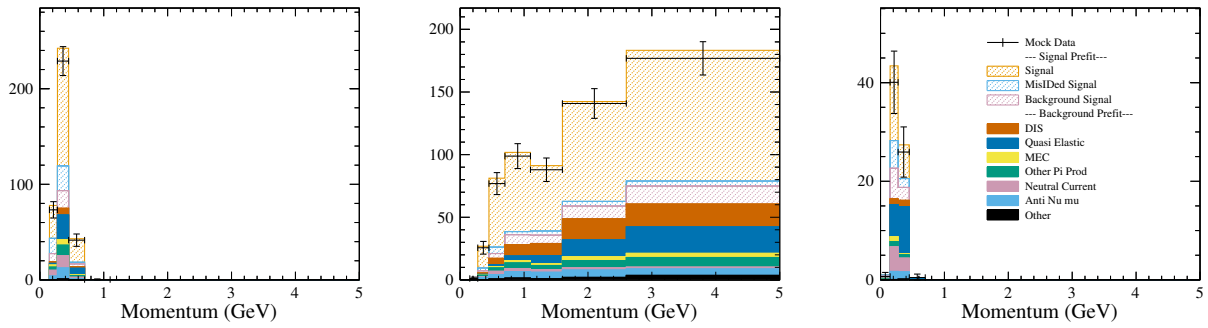

(a) Selected Kalman Contained **(b)** Selected Kalman Exiting **(c)** Selected Cluster

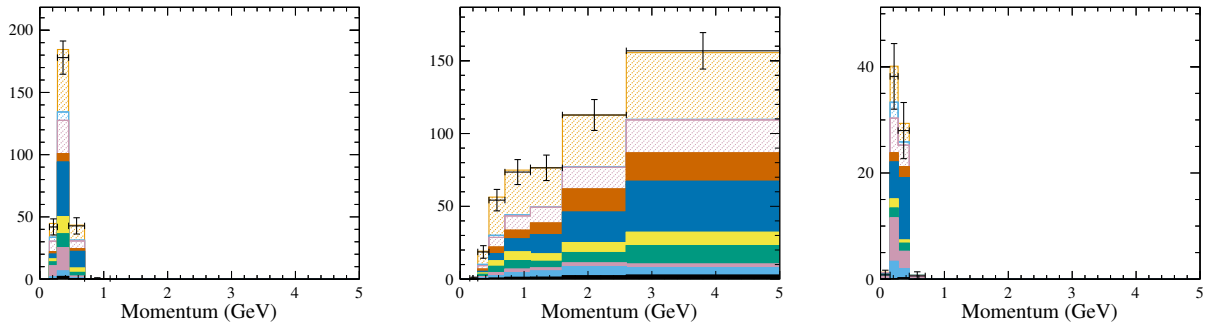

(d) Near Sideband Kalman Contained **(e)** Near Sideband Kalman Exiting **(f)** Near Sideband Cluster

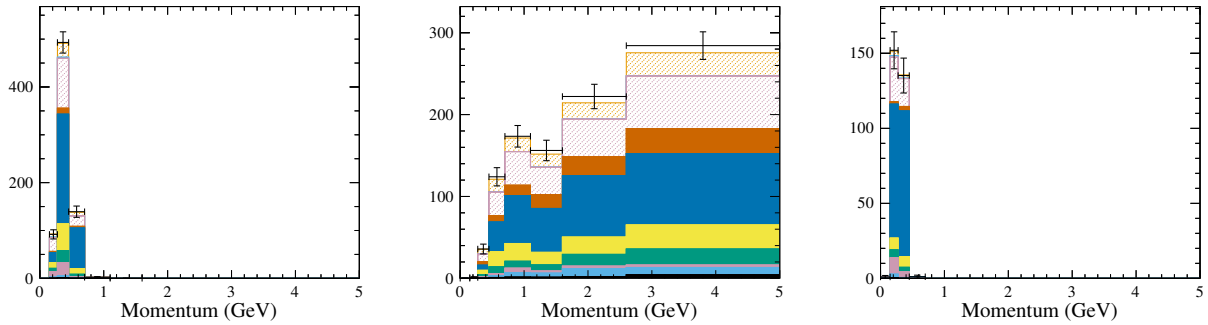

(g) Far Sideband Kalman Contained **(h)** Far Sideband Kalman Exiting **(i)** Far Sideband Cluster

Figure B.22: $+1\sigma$ FSI Parameters Study - Mock Data with Pre-Fit NEUT Templates - Momentum Projection

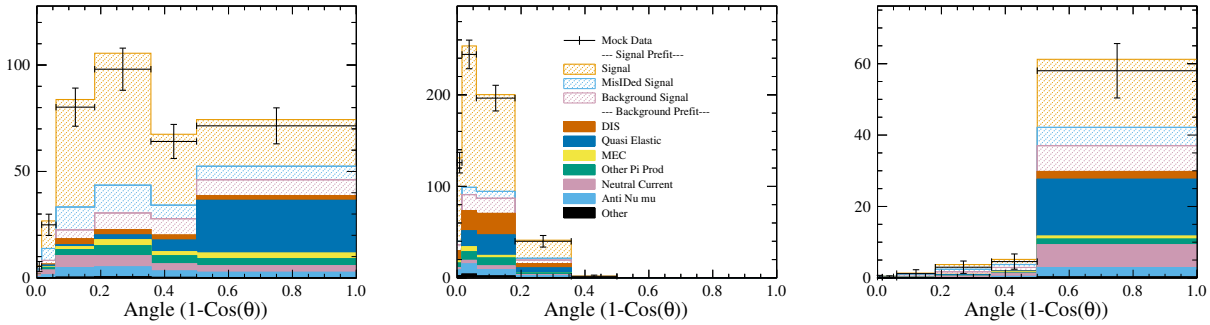

(a) Selected Kalman Contained **(b)** Selected Kalman Exiting **(c)** Selected Cluster

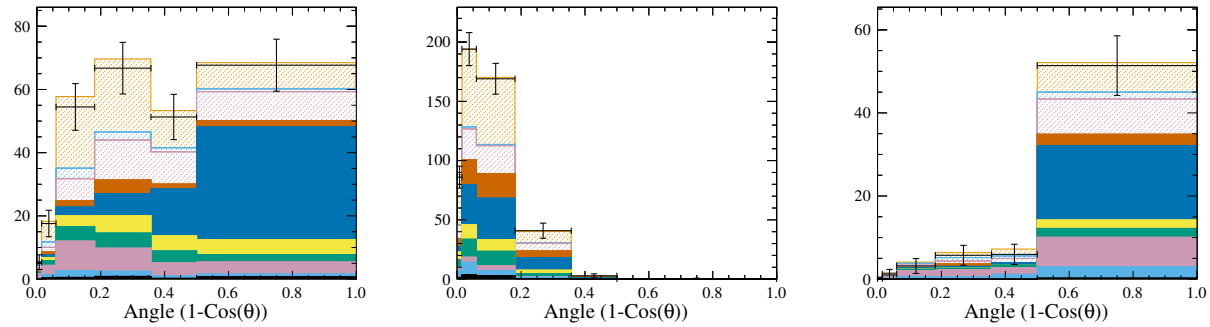

(d) Near Sideband Kalman Contained **(e)** Near Sideband Kalman Exiting **(f)** Near Sideband Cluster

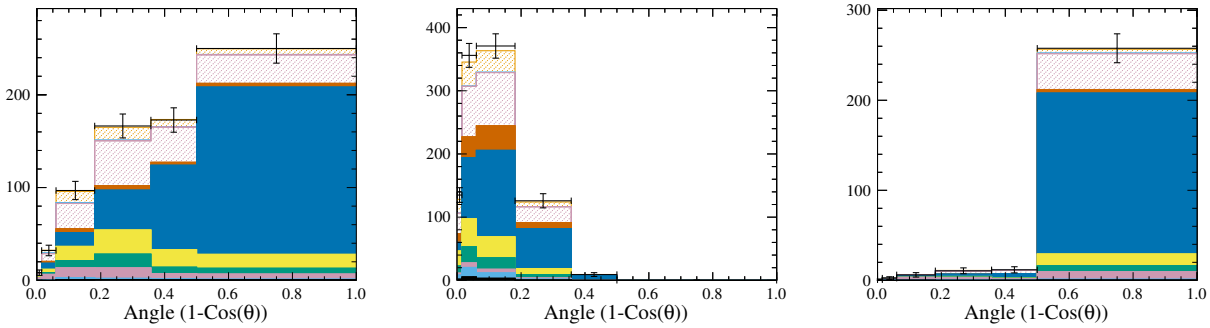

(g) Far Sideband Kalman Contained **(h)** Far Sideband Kalman Exiting **(i)** Far Sideband Cluster

Figure B.23: $+1\sigma$ FSI Parameters - Mock Data with Pre-Fit NEUT Templates - Angle Projection

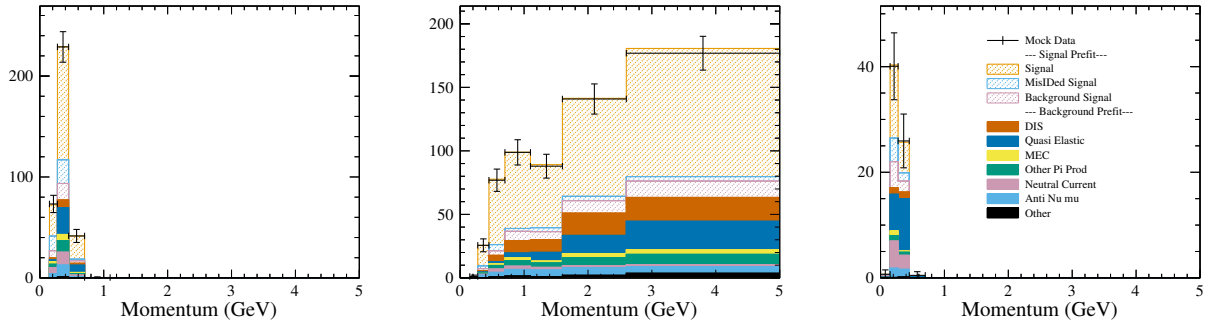

(a) Selected Kalman Contained **(b)** Selected Kalman Exiting **(c)** Selected Cluster

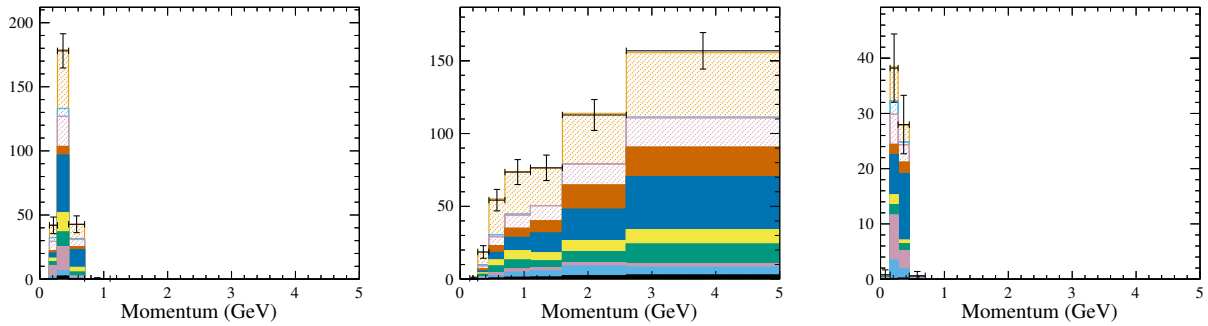

(d) Near Sideband Kalman Contained **(e)** Near Sideband Kalman Exiting **(f)** Near Sideband Cluster

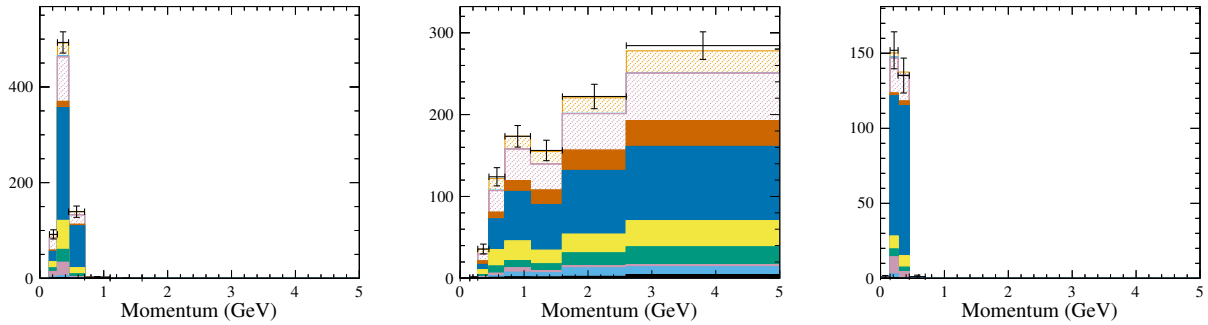

(g) Far Sideband Kalman Contained **(h)** Far Sideband Kalman Exiting **(i)** Far Sideband Cluster

Figure B.24: $+1\sigma$ FSI Parameters - Mock Data with Post-Fit NEUT Templates - Momentum Projection

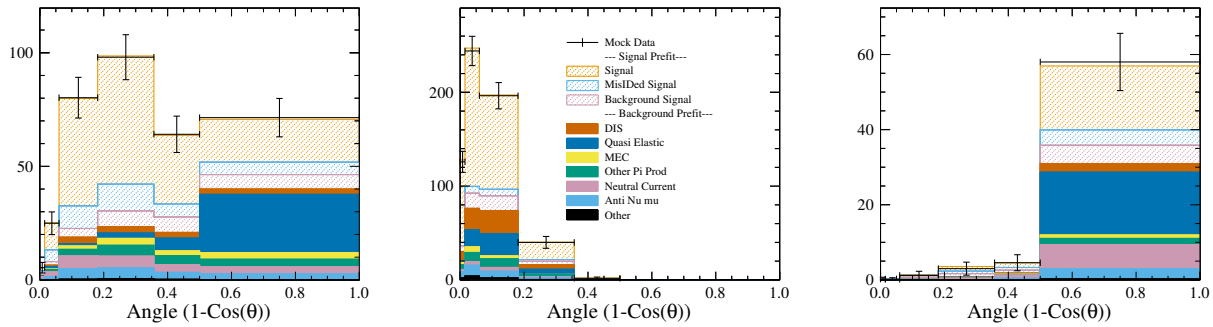

(a) Selected Kalman Contained **(b)** Selected Kalman Exiting **(c)** Selected Cluster

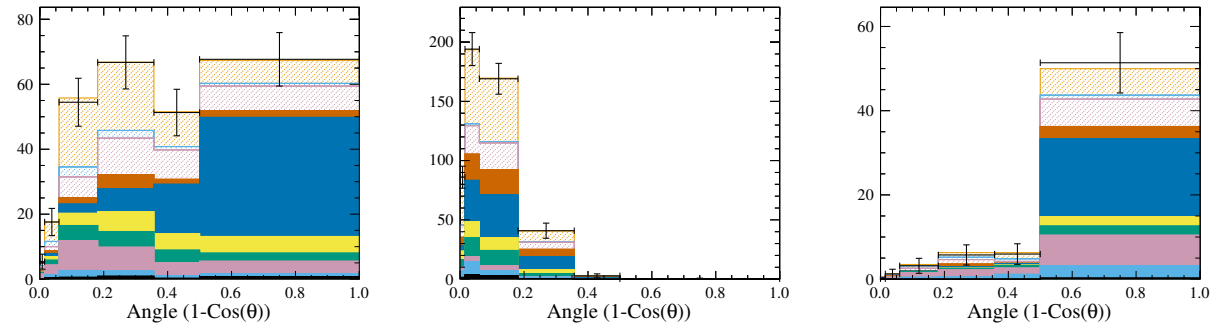

(d) Near Sideband Kalman Contained **(e)** Near Sideband Kalman Exiting **(f)** Near Sideband Cluster

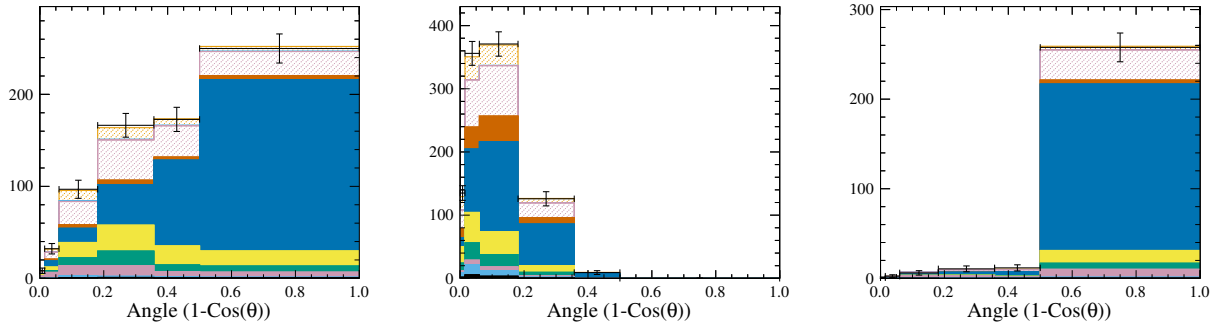

(g) Far Sideband Kalman Contained **(h)** Far Sideband Kalman Exiting **(i)** Far Sideband Cluster

Figure B.25: $+1\sigma$ FSI Parameters - Mock Data with Post-Fit NEUT Templates - Angle Projection

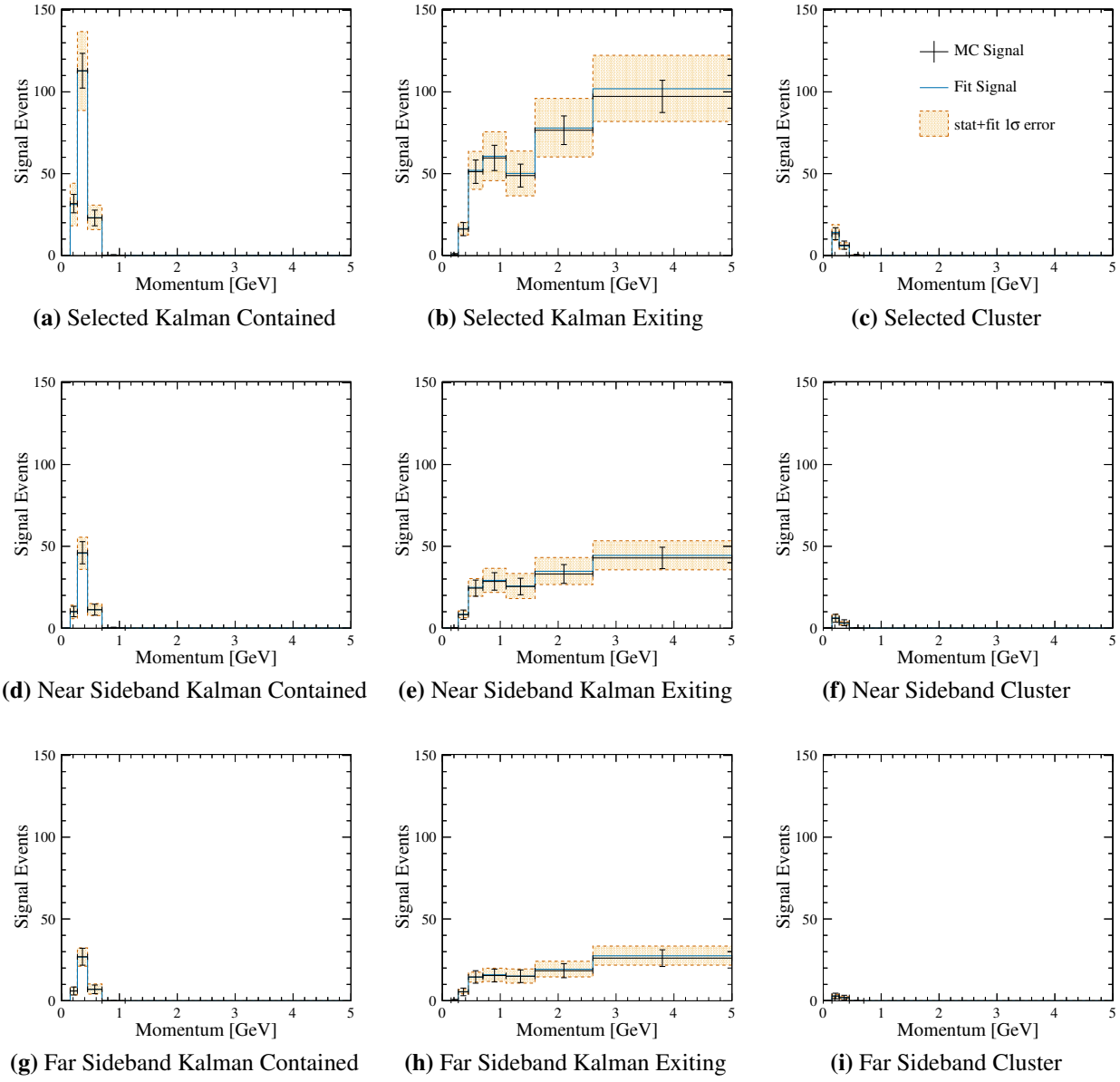

(a) Selected Kalman Contained **(b)** Selected Kalman Exiting **(c)** Selected Cluster

(d) Near Sideband Kalman Contained **(e)** Near Sideband Kalman Exiting **(f)** Near Sideband Cluster

(g) Far Sideband Kalman Contained **(h)** Far Sideband Kalman Exiting **(i)** Far Sideband Cluster

Figure B.26: $+1\sigma$ FSI Parameters Study - Signal fit in the muon momentum projection. Black crosses represent the mock data with statistical error bars. The solid blue line is the best fit and the orange region is the error from the fit. - Momentum projection

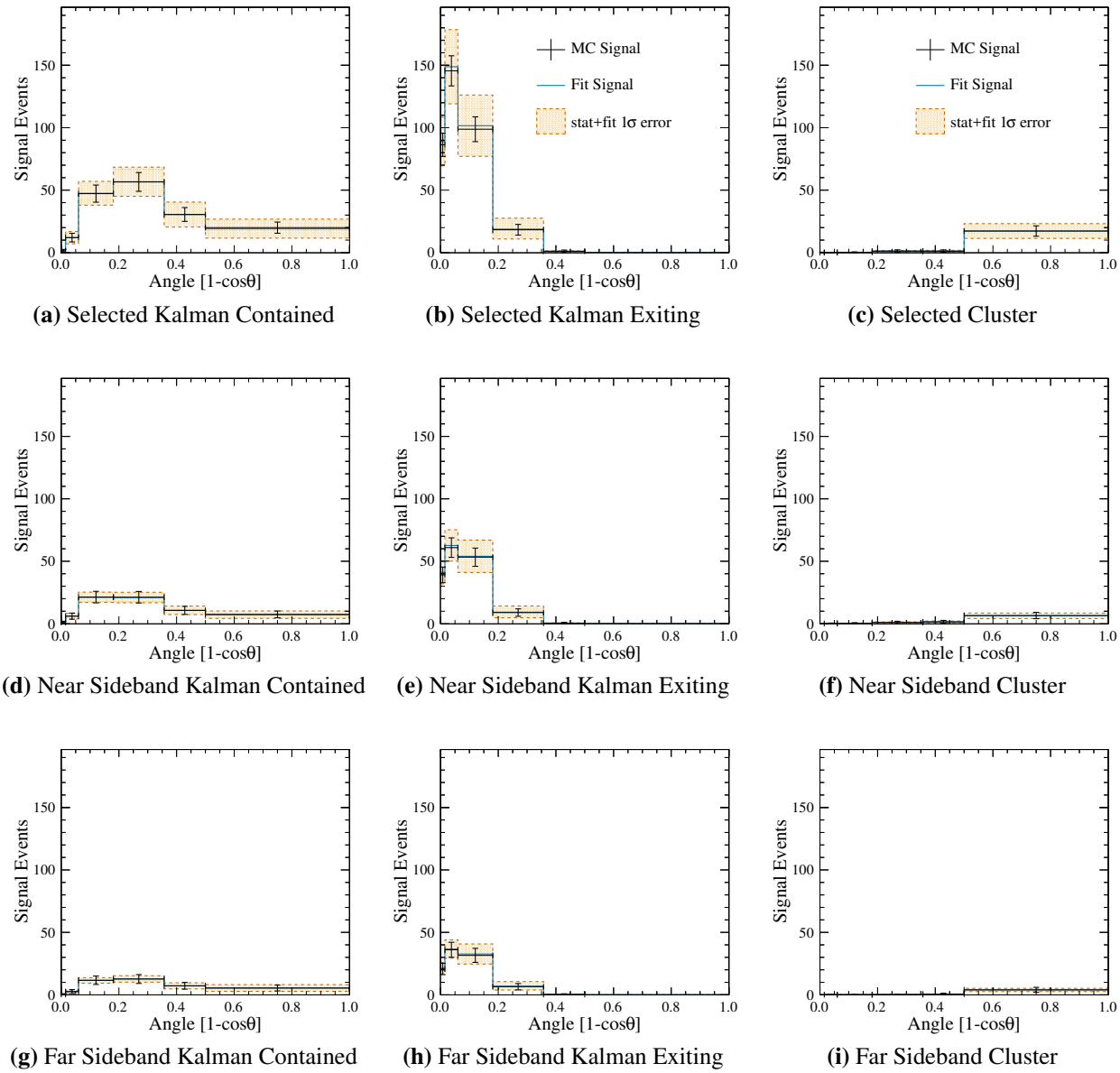

(a) Selected Kalman Contained **(b)** Selected Kalman Exiting **(c)** Selected Cluster

(d) Near Sideband Kalman Contained **(e)** Near Sideband Kalman Exiting **(f)** Near Sideband Cluster

(g) Far Sideband Kalman Contained **(h)** Far Sideband Kalman Exiting **(i)** Far Sideband Cluster

Figure B.27: $+1\sigma$ FSI Parameters Study - Signal fit in the muon angle projection. Black crosses represent the mock data with statistical error bars. The solid blue line is the best fit and the orange region is the error from the fit. - Angle projection

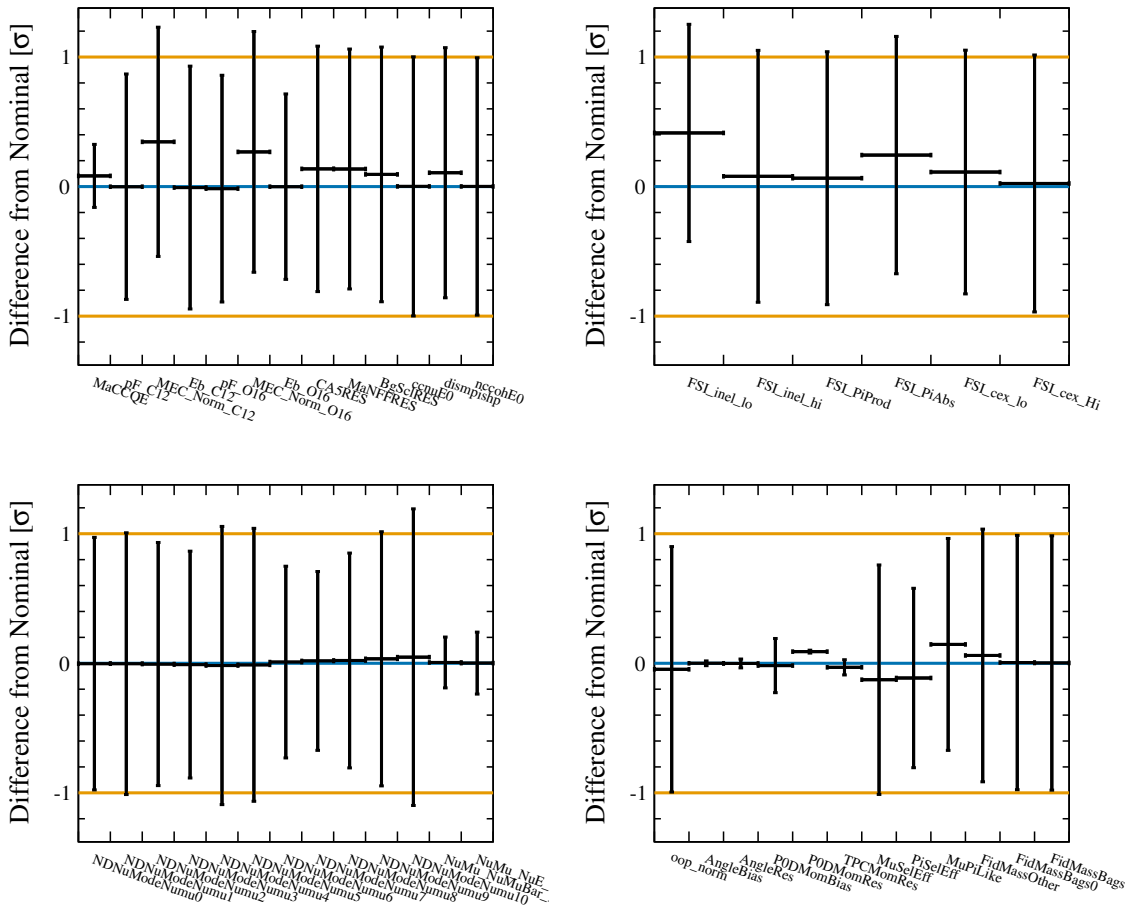

Figure B.28: $+1\sigma$ FSI Parameters Study - Fit parameter deviation from nominal. The points in this plot are the best fit parameter value in units of sigma for each dial. The error bars on the points are the error on that parameter from the fit, while the orange lines at +1 and -1 represent the default one sigma error placed on the variable.

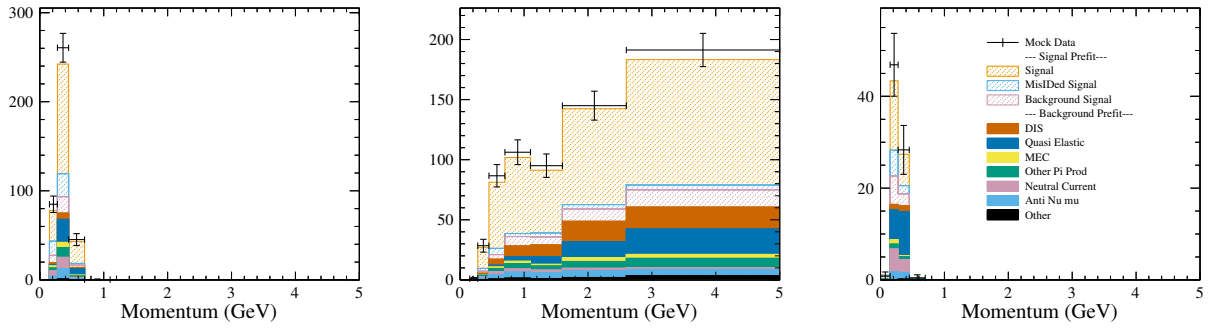

(a) Selected Kalman Contained **(b)** Selected Kalman Exiting **(c)** Selected Cluster

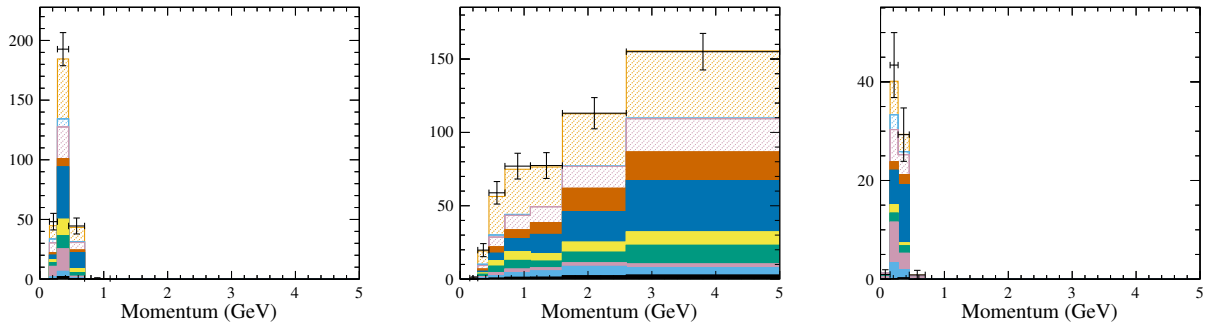

(d) Near Sideband Kalman Contained **(e)** Near Sideband Kalman Exiting **(f)** Near Sideband Cluster

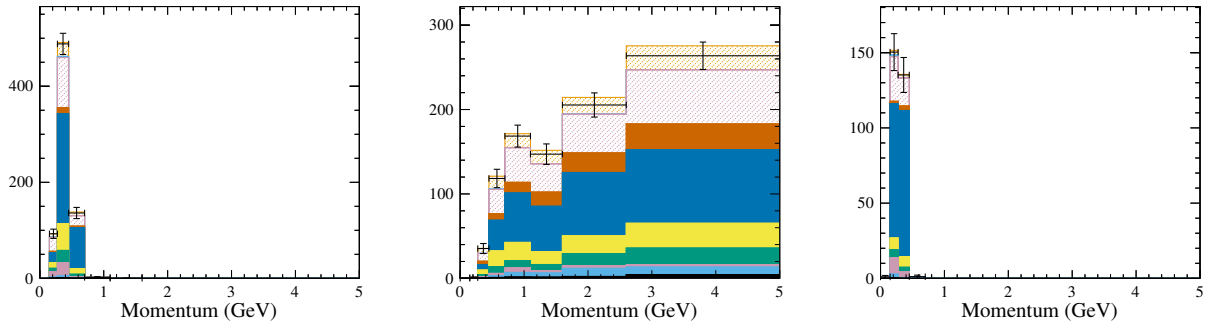

(g) Far Sideband Kalman Contained **(h)** Far Sideband Kalman Exiting **(i)** Far Sideband Cluster

Figure B.29: -1σ FSI Parameters Study - Mock Data with Pre-Fit NEUT Templates - Momentum Projection

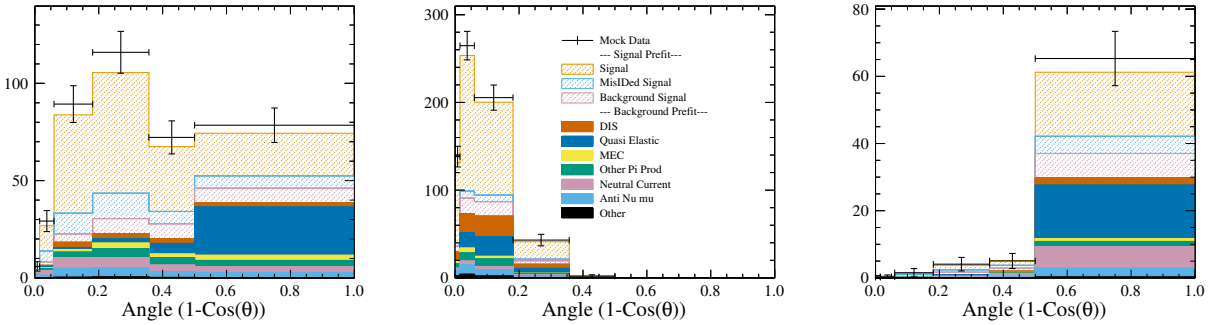

(a) Selected Kalman Contained **(b)** Selected Kalman Exiting **(c)** Selected Cluster

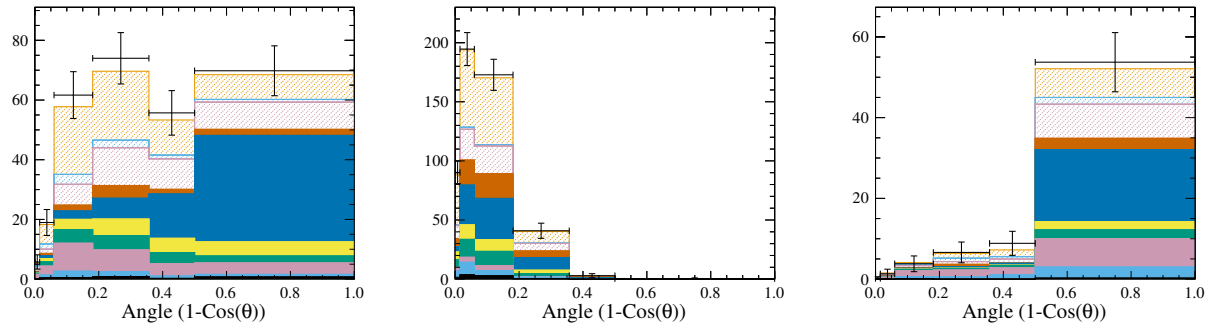

(d) Near Sideband Kalman Contained **(e)** Near Sideband Kalman Exiting **(f)** Near Sideband Cluster

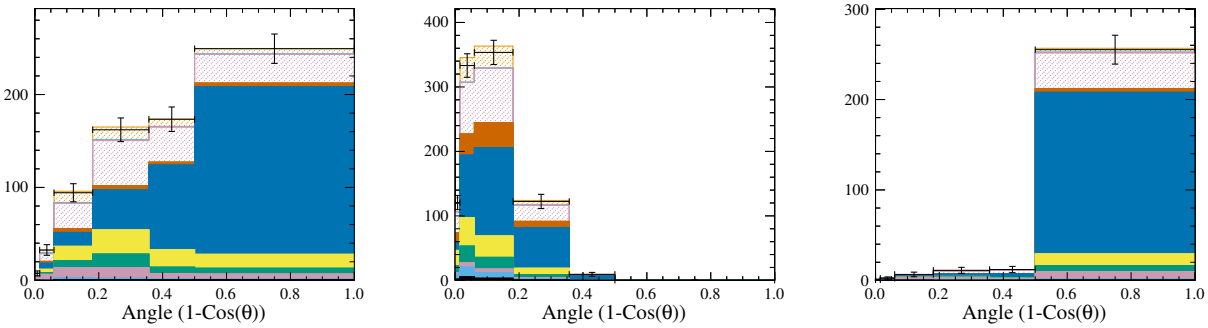

(g) Far Sideband Kalman Contained **(h)** Far Sideband Kalman Exiting **(i)** Far Sideband Cluster

Figure B.30: -1σ FSI Parameters - Mock Data with Pre-Fit NEUT Templates - Angle Projection

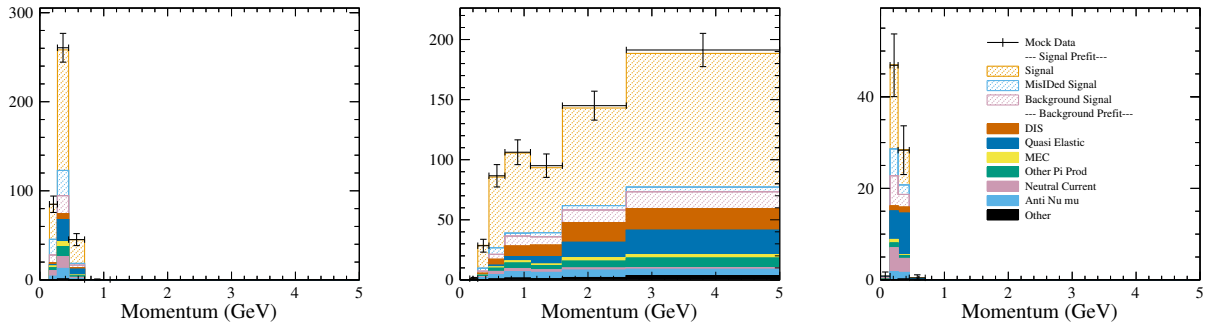

(a) Selected Kalman Contained **(b)** Selected Kalman Exiting **(c)** Selected Cluster

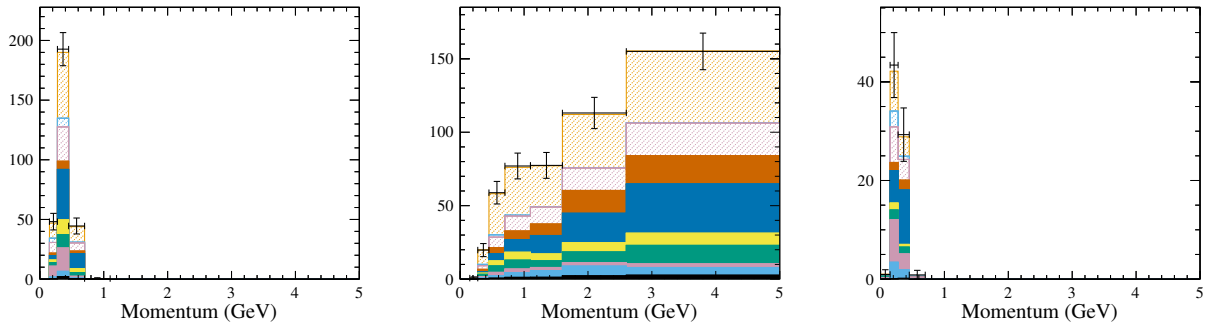

(d) Near Sideband Kalman Contained **(e)** Near Sideband Kalman Exiting **(f)** Near Sideband Cluster

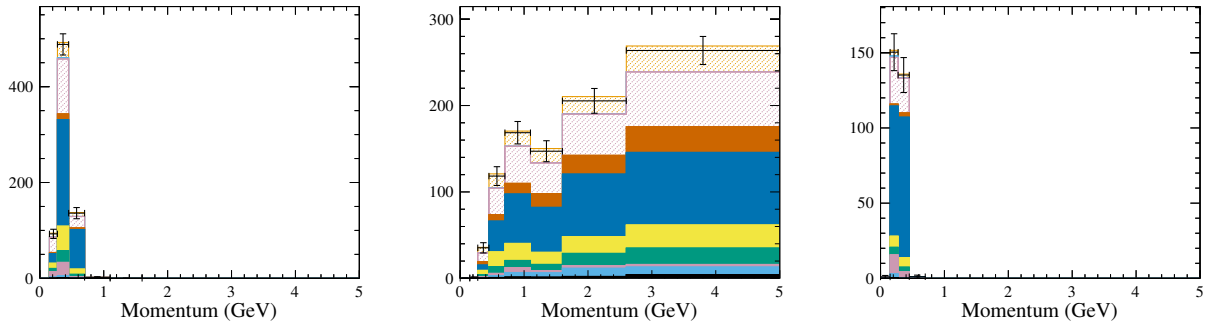

(g) Far Sideband Kalman Contained **(h)** Far Sideband Kalman Exiting **(i)** Far Sideband Cluster

Figure B.31: -1σ FSI Parameters - Mock Data with Post-Fit NEUT Templates - Momentum Projection

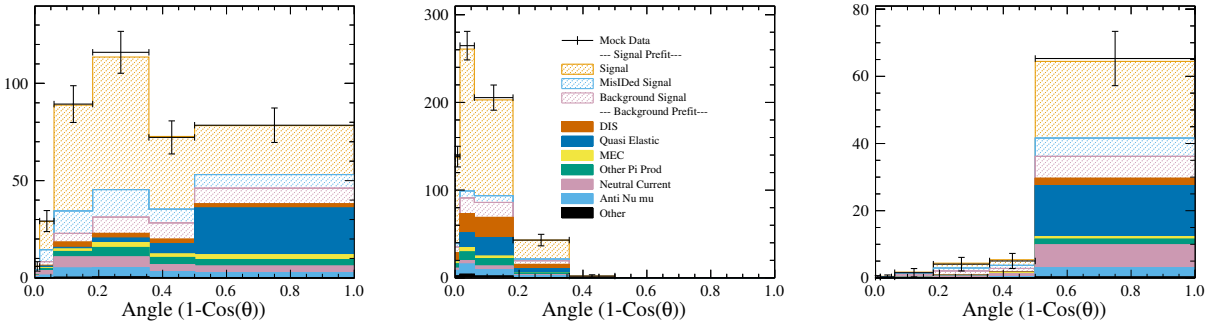

(a) Selected Kalman Contained **(b)** Selected Kalman Exiting **(c)** Selected Cluster

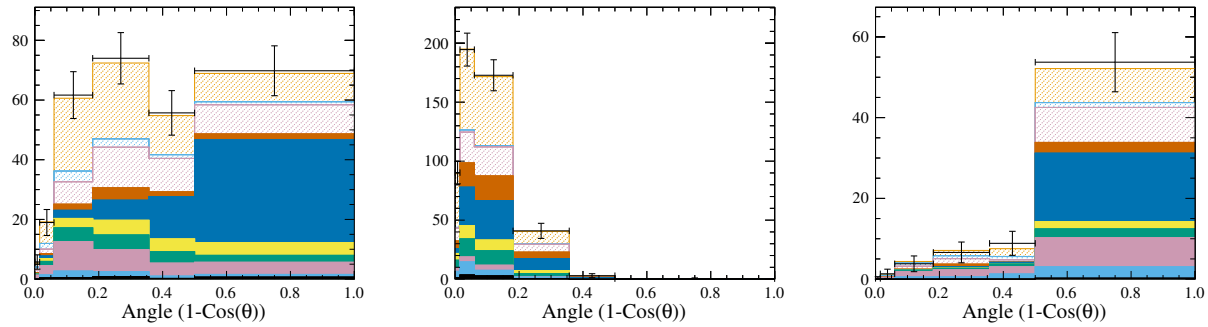

(d) Near Sideband Kalman Contained **(e)** Near Sideband Kalman Exiting **(f)** Near Sideband Cluster

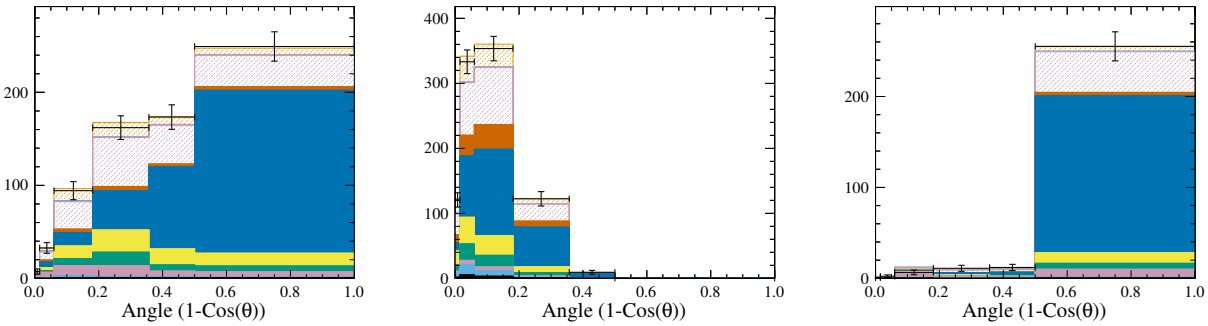

(g) Far Sideband Kalman Contained **(h)** Far Sideband Kalman Exiting **(i)** Far Sideband Cluster

Figure B.32: -1σ FSI Parameters - Mock Data with Post-Fit NEUT Templates - Angle Projection

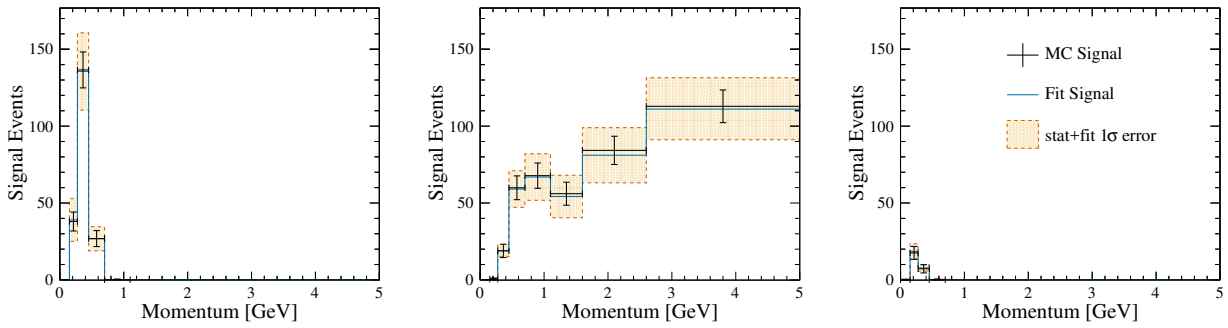

(a) Selected Kalman Contained **(b)** Selected Kalman Exiting **(c)** Selected Cluster

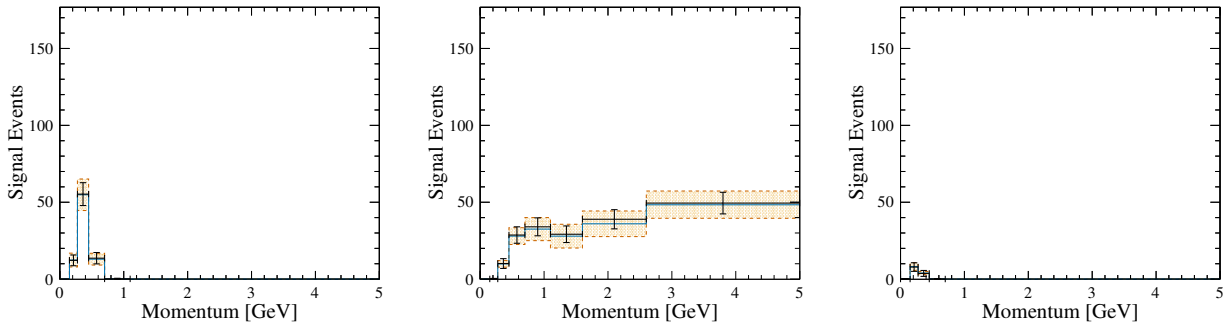

(d) Near Sideband Kalman Contained **(e)** Near Sideband Kalman Exiting **(f)** Near Sideband Cluster

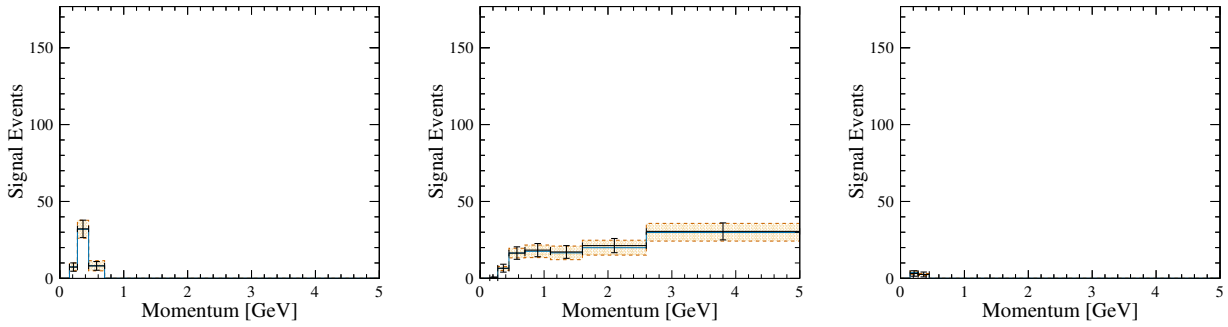

(g) Far Sideband Kalman Contained **(h)** Far Sideband Kalman Exiting **(i)** Far Sideband Cluster

Figure B.33: -1σ FSI Parameters Study - Signal fit in the muon momentum projection. Black crosses represent the mock data with statistical error bars. The solid blue line is the best fit and the orange region is the error from the fit. - Momentum projection

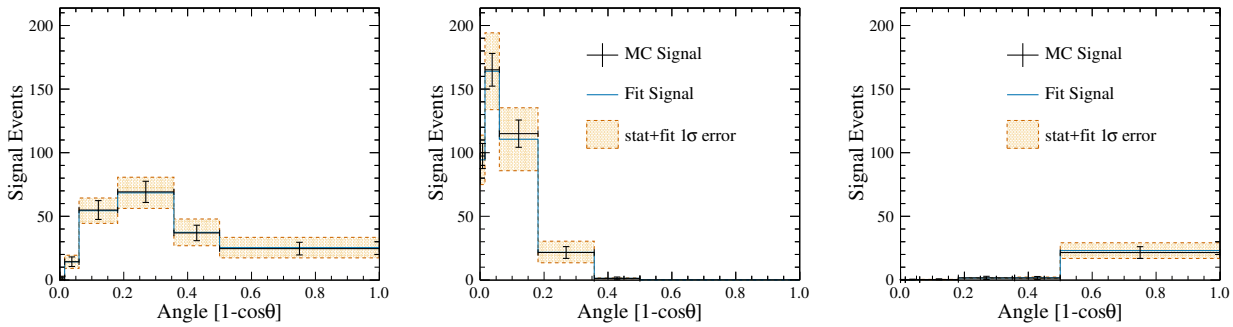

(a) Selected Kalman Contained **(b)** Selected Kalman Exiting **(c)** Selected Cluster

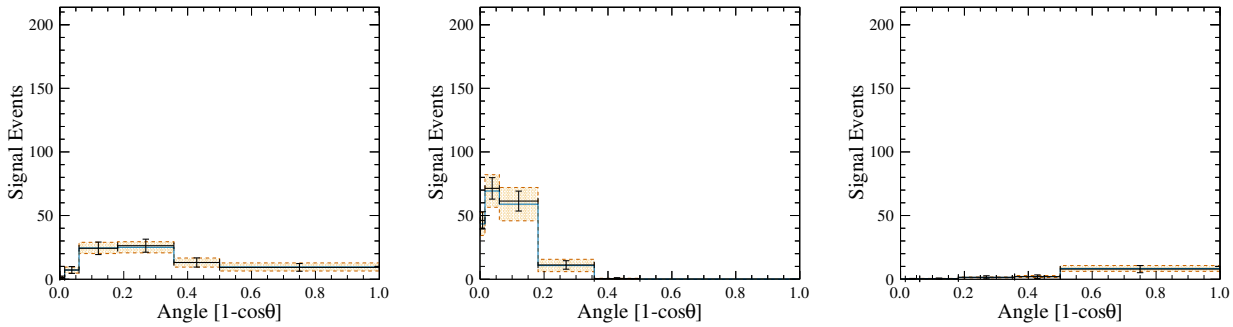

(d) Near Sideband Kalman Contained **(e)** Near Sideband Kalman Exiting **(f)** Near Sideband Cluster

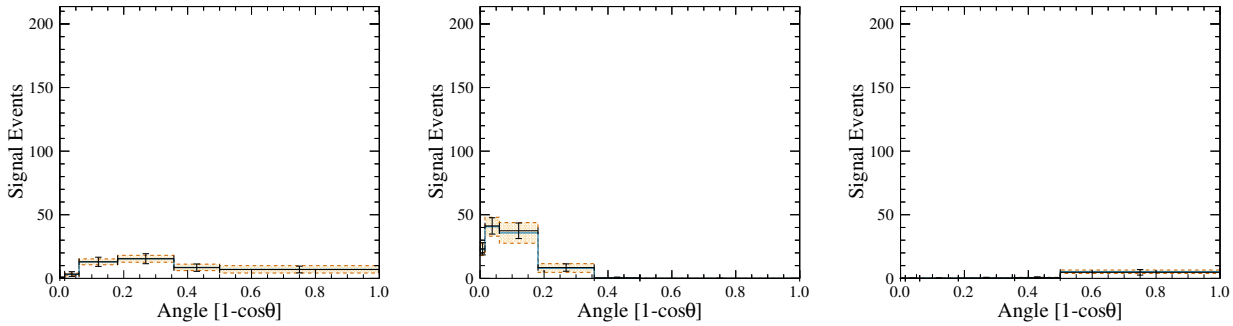

(g) Far Sideband Kalman Contained **(h)** Far Sideband Kalman Exiting **(i)** Far Sideband Cluster

Figure B.34: -1σ FSI Parameters Study - Signal fit in the muon angle projection. Black crosses represent the mock data with statistical error bars. The solid blue line is the best fit and the orange region is the error from the fit. - Angle projection

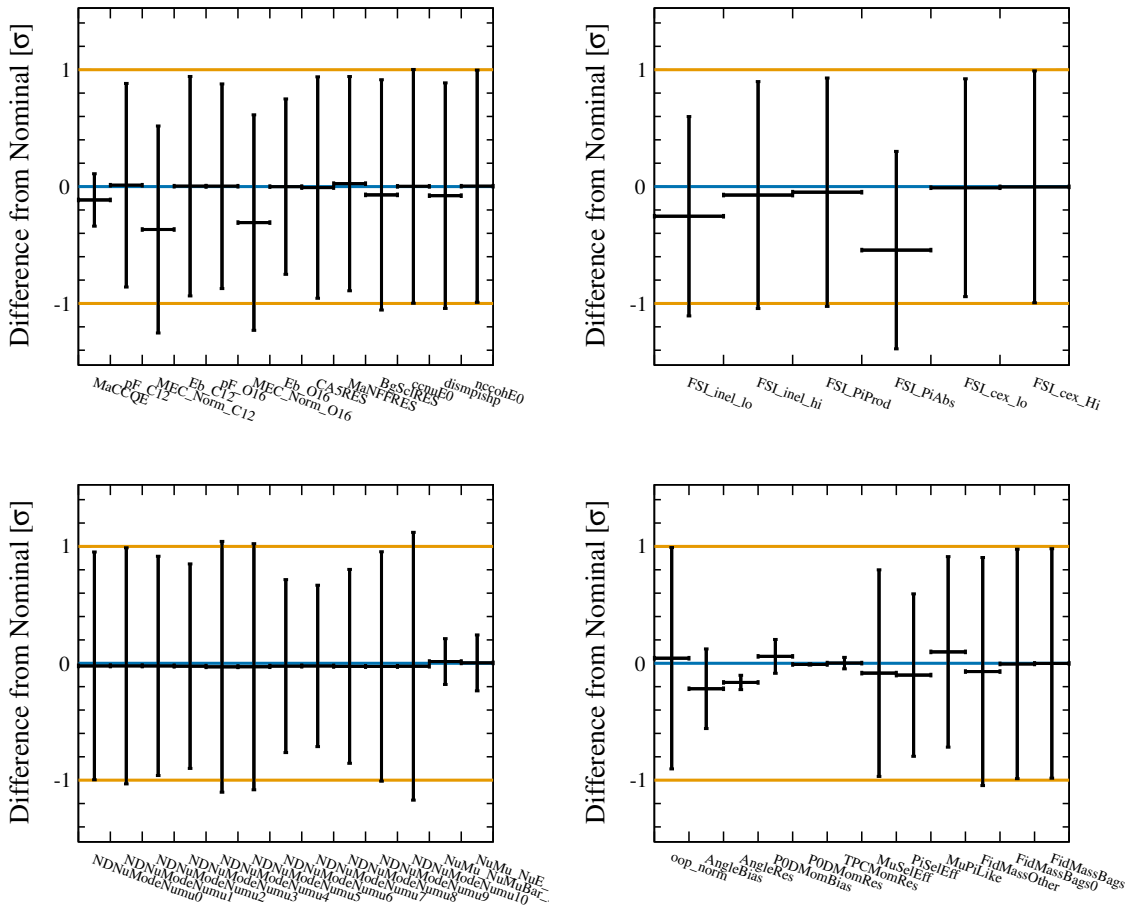

Figure B.35: -1σ FSI Parameters Study - Fit parameter deviation from nominal. The points in this plot are the best fit parameter value in units of sigma for each dial. The error bars on the points are the error on that parameter from the fit, while the orange lines at +1 and -1 represent the default one sigma error placed on the variable.

B.3.3 Background Cross Section Parameter Fits

These parameters are all the cross section dials that apply to background parameters. These are the dials that are used as fit parameters, thus should be well fit by the fitter.

$+1\sigma$ Background Cross Section Parameters

Plotted in Figures B.36 and B.37 are the mock data over the pre-fit NEUT templates, while Figures B.38 and B.39 are the mock data over the post-fit NEUT templates. The extracted signal is plotted in figures B.40 and B.41. The fit parameter deviations from nominal and error are plotted in figure B.42.

-1σ Background Cross Section Parameters

Plotted in Figures B.43 and B.44 are the mock data over the pre-fit NEUT templates, while Figures B.45 and B.46 are the mock data over the post-fit NEUT templates. The extracted signal is plotted in figures B.47 and B.48. The fit parameter deviations from nominal and error are plotted in figure B.49.

B.4 Mock Data Tests With New Signal Physics Models

These studies are done to ensure that this fitter can measure any kind of signal, and thus is not constrained by the default NEUT models. The signal is fit with unconstrained bins on top of the background template fit and has been seen to do a very good job at fitting any variation in the signal models. For these studies, the backgrounds are the nominal NEUT templates.

B.4.1 Rein Sehgal to Berger Sehgal CC Coherent Model

This dial adjusts the default NEUT charge-current coherent model to the tuning based on MINERvA data and updated Berger-Sehgal model. The tuning is simple, merely adjusting the event weight based on the pion energy per Table 7.1 from Chapter 7.6.3. This tests the performance of

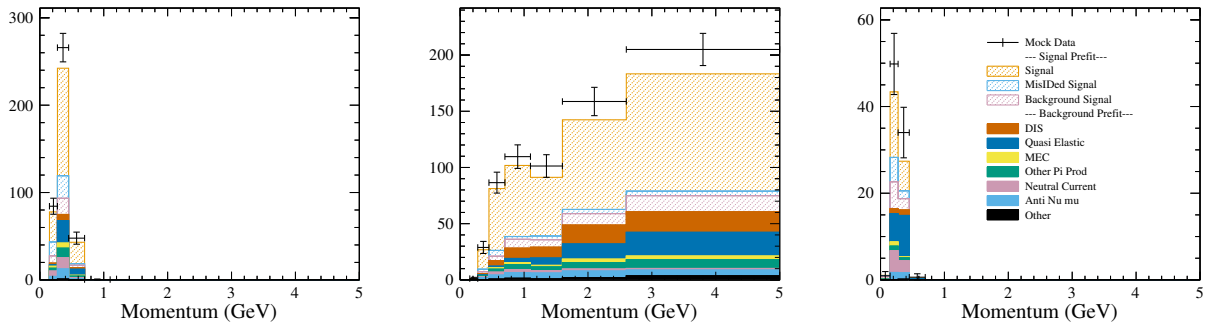

(a) Selected Kalman Contained **(b)** Selected Kalman Exiting **(c)** Selected Cluster

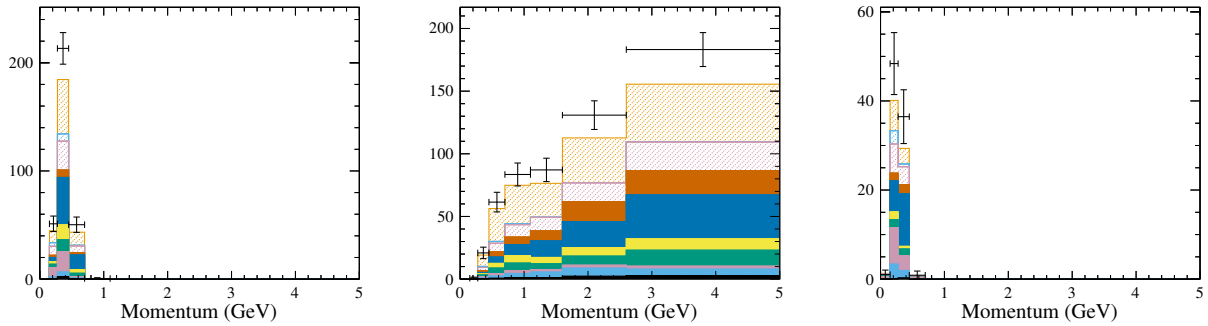

(d) Near Sideband Kalman Contained **(e)** Near Sideband Kalman Exiting **(f)** Near Sideband Cluster

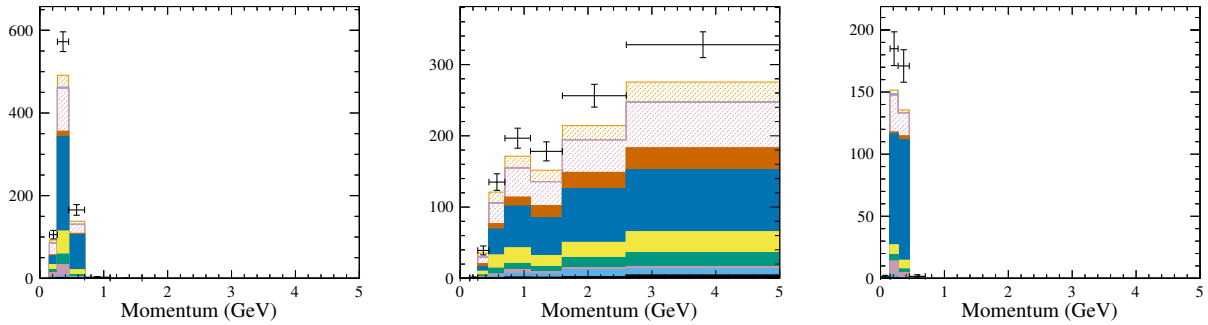

(g) Far Sideband Kalman Contained **(h)** Far Sideband Kalman Exiting **(i)** Far Sideband Cluster

Figure B.36: $+1\sigma$ Background Cross Section Parameters - Mock Data with Pre-Fit NEUT Templates - Momentum Projection

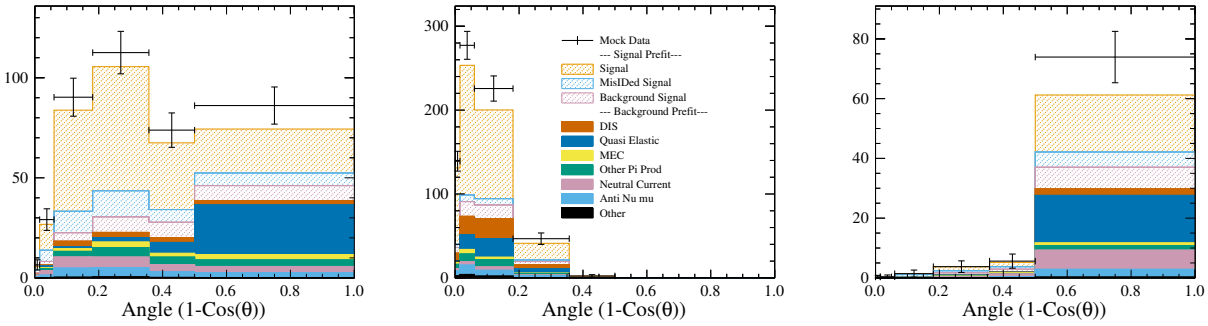

(a) Selected Kalman Contained **(b)** Selected Kalman Exiting **(c)** Selected Cluster

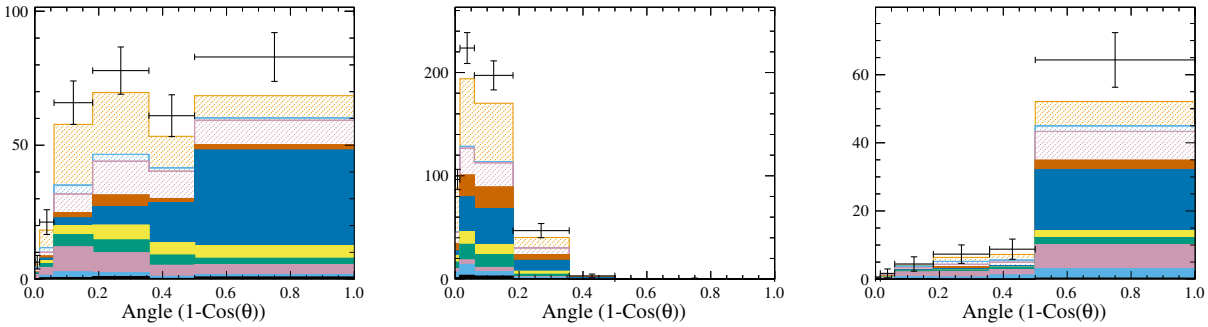

(d) Near Sideband Kalman Contained **(e)** Near Sideband Kalman Exiting **(f)** Near Sideband Cluster

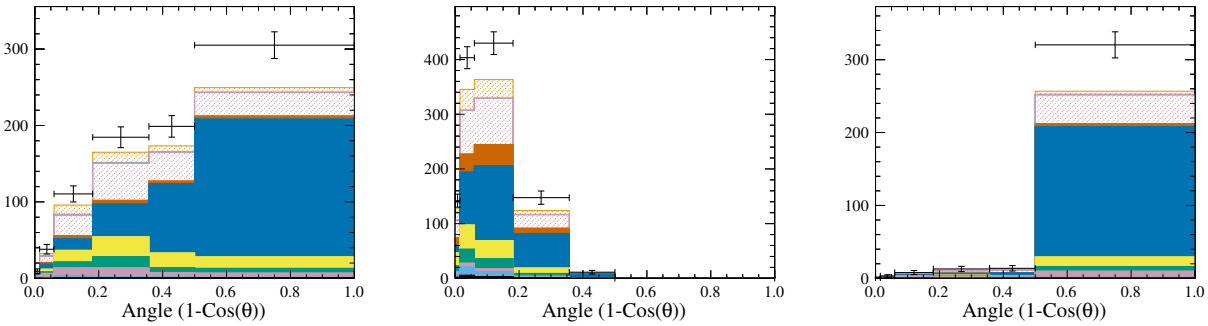

(g) Far Sideband Kalman Contained **(h)** Far Sideband Kalman Exiting **(i)** Far Sideband Cluster

Figure B.37: $+1\sigma$ Background Cross Section Parameters - Mock Data with Pre-Fit NEUT Templates - Angle Projection

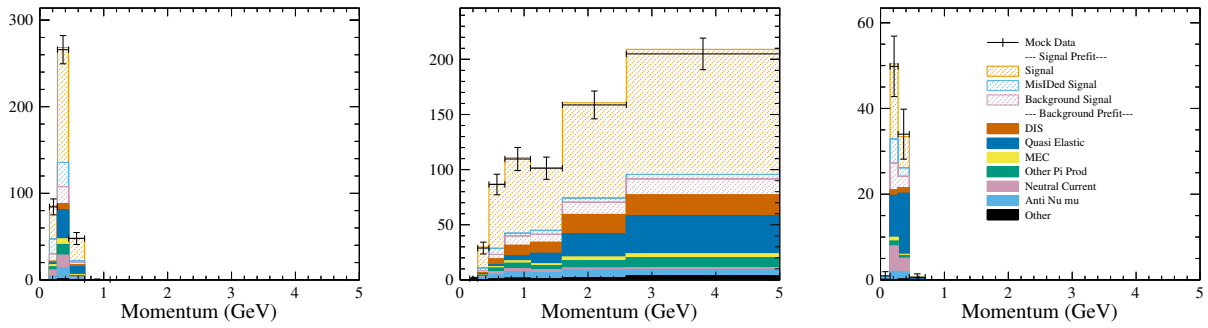

(a) Selected Kalman Contained **(b)** Selected Kalman Exiting **(c)** Selected Cluster

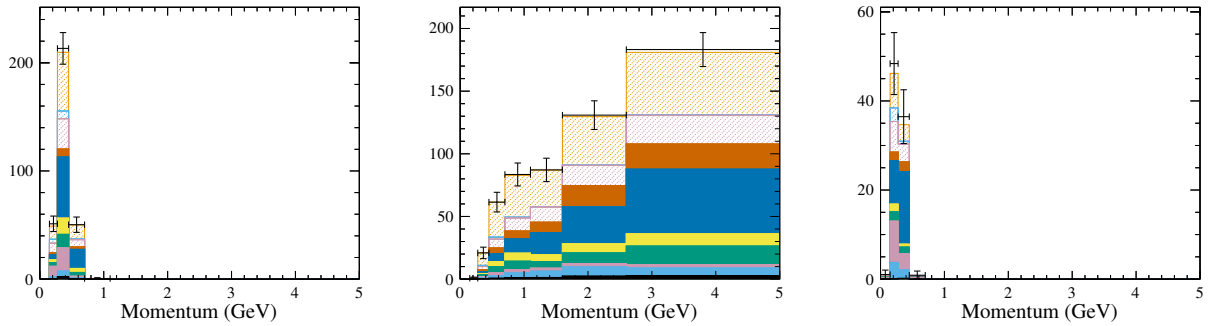

(d) Near Sideband Kalman Contained **(e)** Near Sideband Kalman Exiting **(f)** Near Sideband Cluster

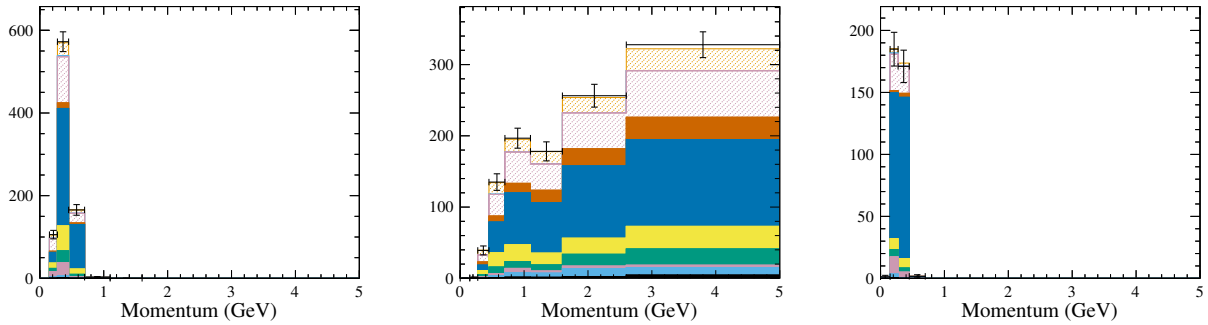

(g) Far Sideband Kalman Contained **(h)** Far Sideband Kalman Exiting **(i)** Far Sideband Cluster

Figure B.38: $+1\sigma$ Background Cross Section Parameters - Mock Data with Post-Fit NEUT Templates - Momentum Projection

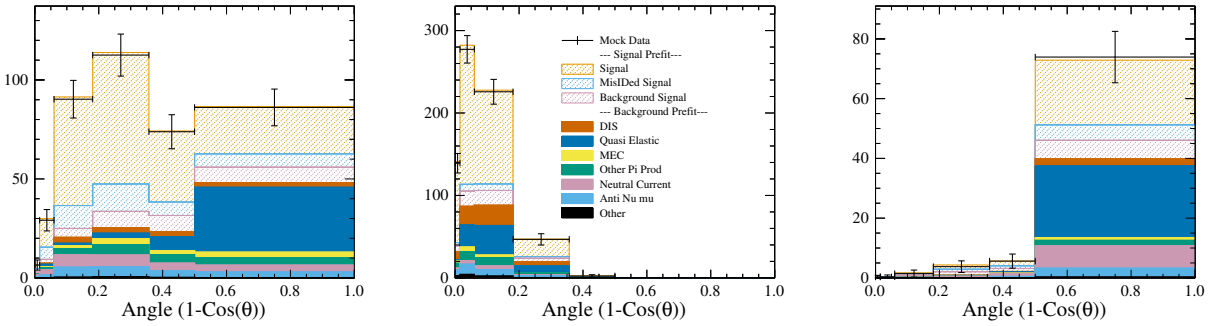

(a) Selected Kalman Contained **(b)** Selected Kalman Exiting **(c)** Selected Cluster

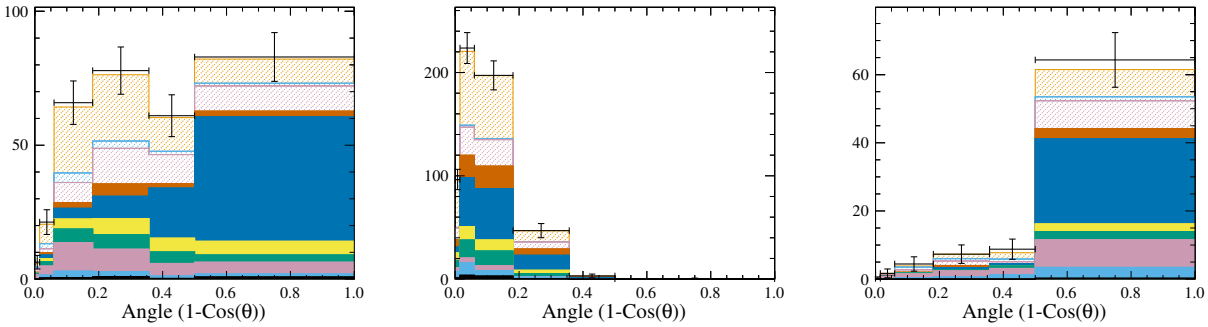

(d) Near Sideband Kalman Contained **(e)** Near Sideband Kalman Exiting **(f)** Near Sideband Cluster

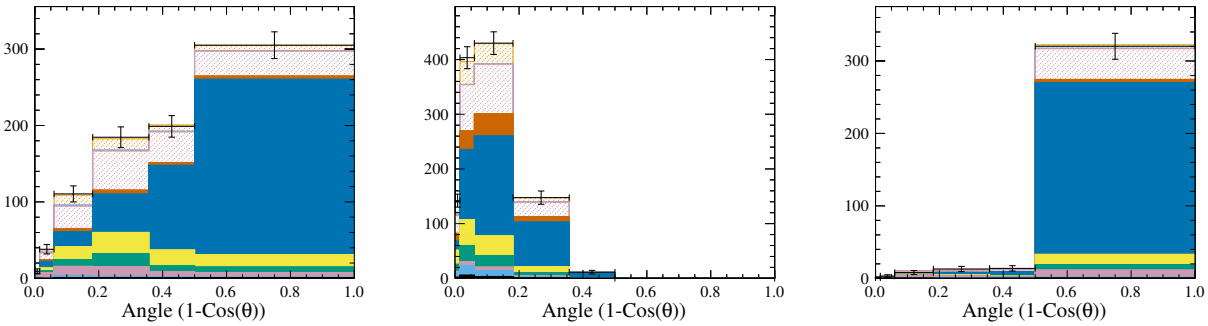

(g) Far Sideband Kalman Contained **(h)** Far Sideband Kalman Exiting **(i)** Far Sideband Cluster

Figure B.39: $+1\sigma$ Background Cross Section Parameters - Mock Data with Post-Fit NEUT Templates - Angle Projection

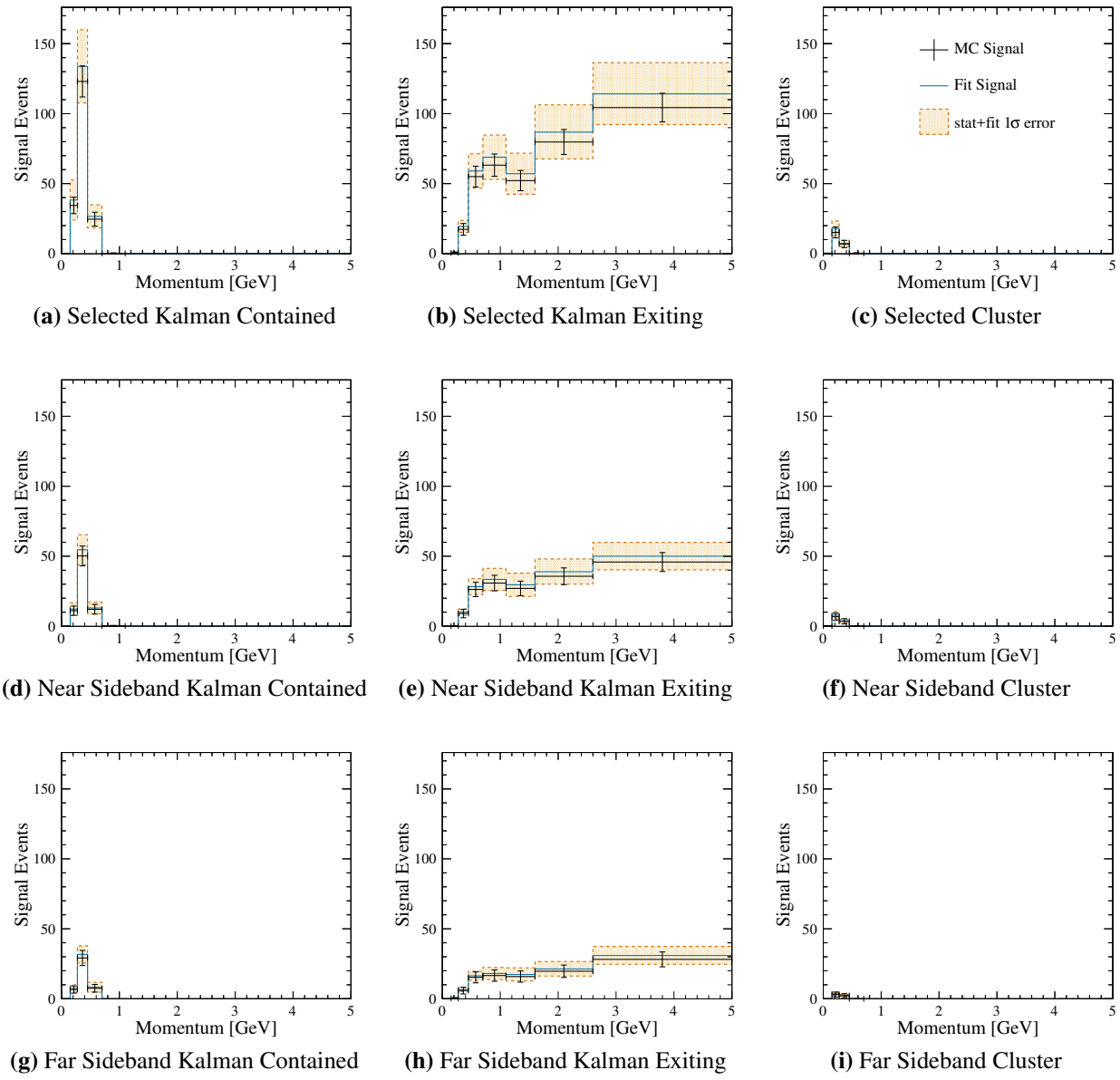

(a) Selected Kalman Contained **(b)** Selected Kalman Exiting **(c)** Selected Cluster

(d) Near Sideband Kalman Contained **(e)** Near Sideband Kalman Exiting **(f)** Near Sideband Cluster

(g) Far Sideband Kalman Contained **(h)** Far Sideband Kalman Exiting **(i)** Far Sideband Cluster

Figure B.40: $+1\sigma$ Background Cross Section Parameters Study - Signal fit in the muon momentum projection. Black crosses represent the mock data with statistical error bars. The solid blue line is the best fit and the orange region is the error from the fit. - Momentum projection

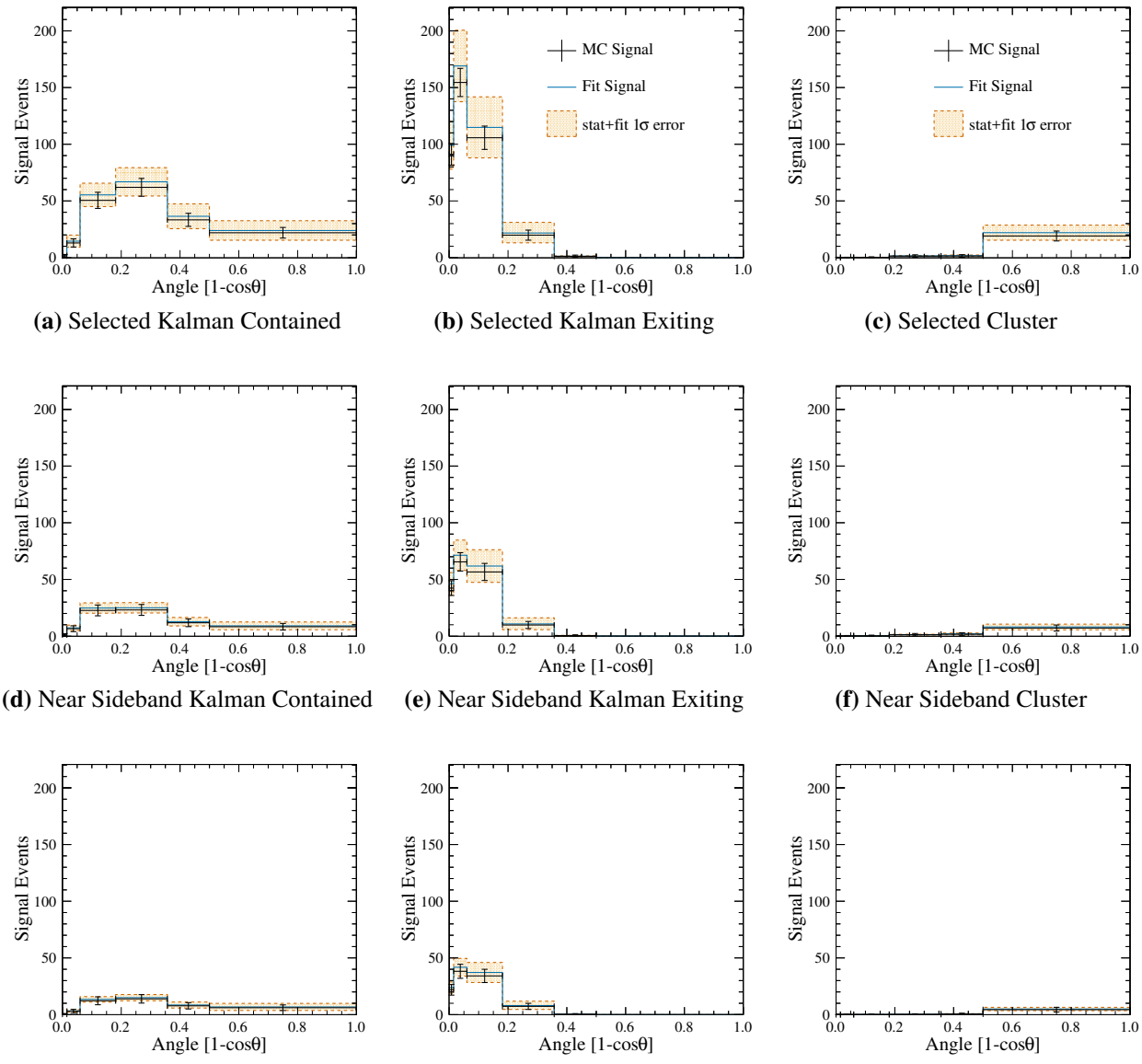

(a) Selected Kalman Contained **(b)** Selected Kalman Exiting **(c)** Selected Cluster

(d) Near Sideband Kalman Contained **(e)** Near Sideband Kalman Exiting **(f)** Near Sideband Cluster

(g) Far Sideband Kalman Contained **(h)** Far Sideband Kalman Exiting **(i)** Far Sideband Cluster

Figure B.41: $+1\sigma$ Background Cross Section Parameters Study - Signal fit in the muon angle projection. Black crosses represent the mock data with statistical error bars. The solid blue line is the best fit and the orange region is the error from the fit. - Angle projection

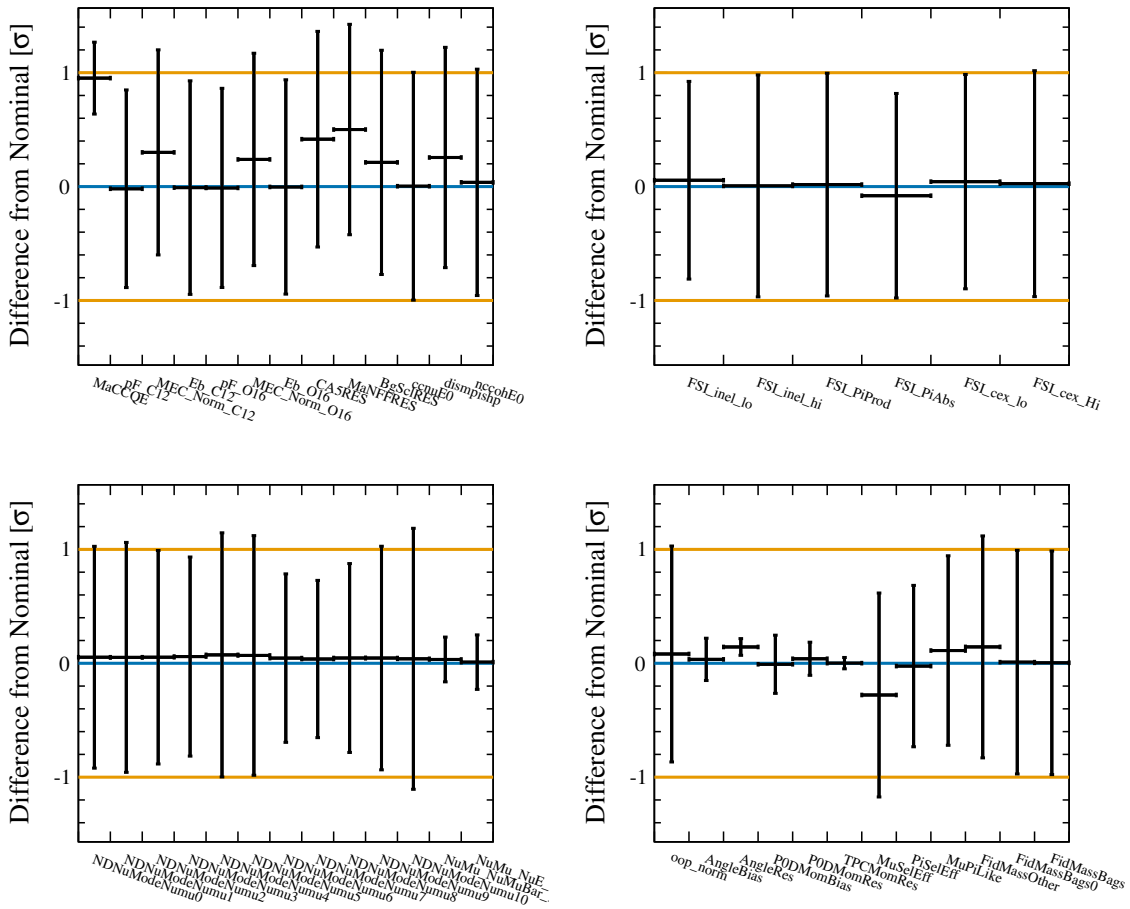

Figure B.42: $+1\sigma$ Background Cross Section Parameters Study - Fit parameter deviation from nominal. The points in this plot are the best fit parameter value in units of sigma for each dial. The error bars on the points are the error on that parameter from the fit, while the orange lines at +1 and -1 represent the default one sigma error placed on the variable.

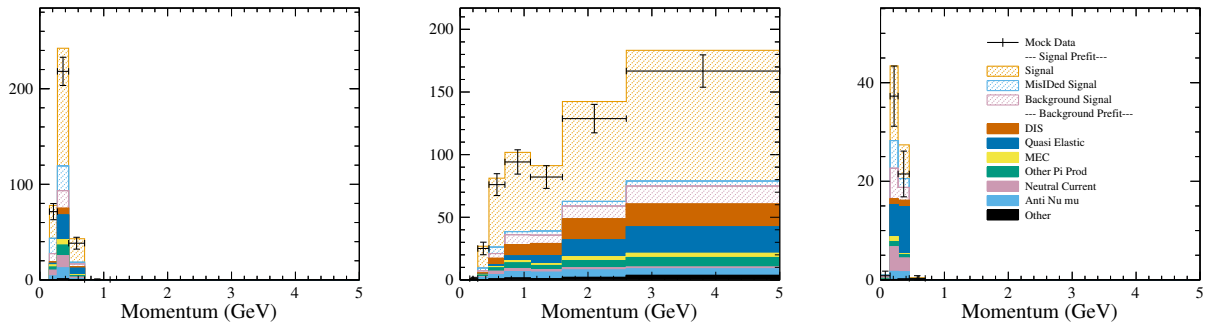

(a) Selected Kalman Contained **(b)** Selected Kalman Exiting **(c)** Selected Cluster

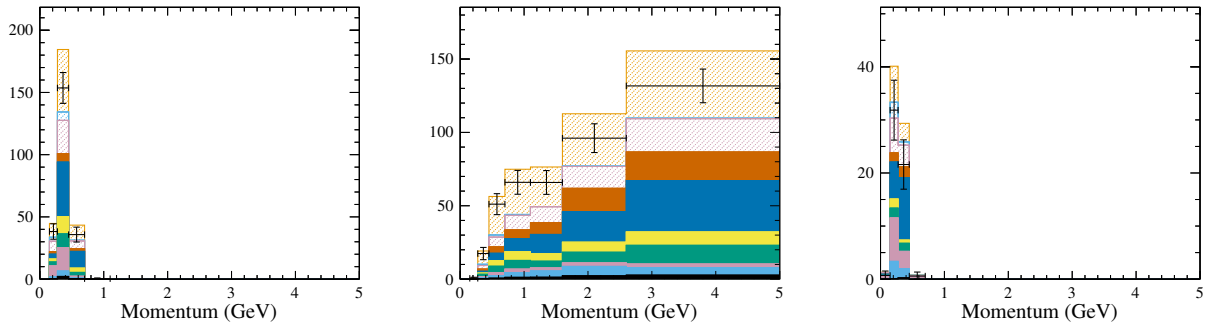

(d) Near Sideband Kalman Contained **(e)** Near Sideband Kalman Exiting **(f)** Near Sideband Cluster

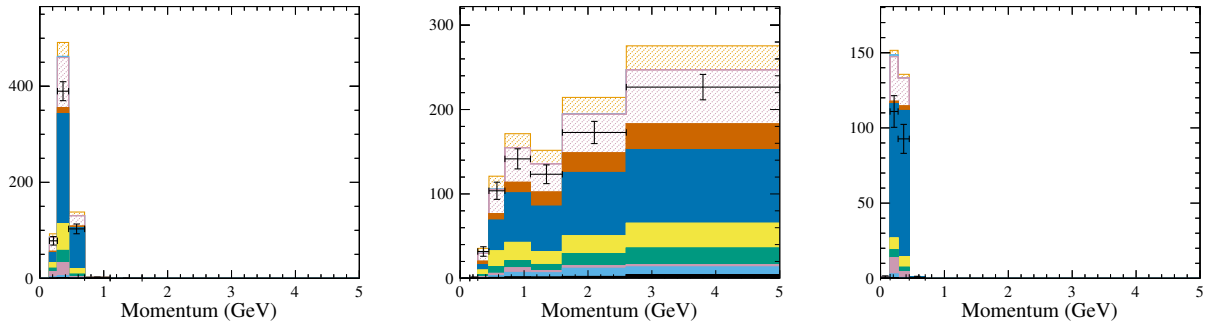

(g) Far Sideband Kalman Contained **(h)** Far Sideband Kalman Exiting **(i)** Far Sideband Cluster

Figure B.43: -1σ Background Cross Section Parameters - Mock Data with Pre-Fit NEUT Templates - Momentum Projection

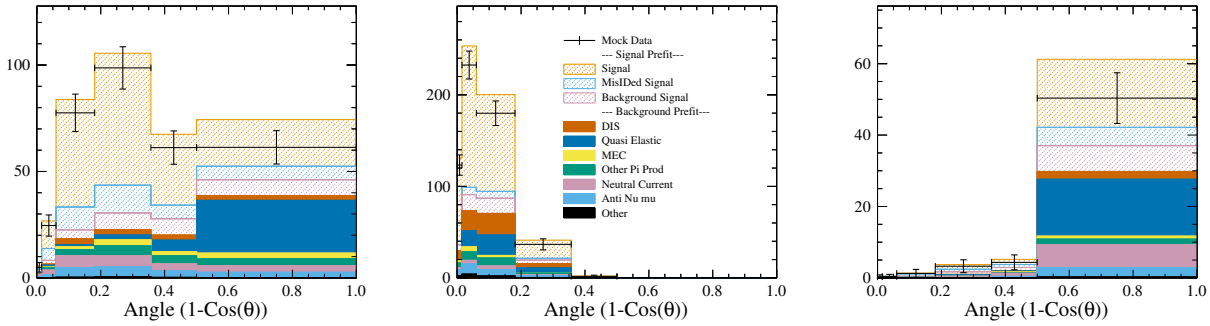

(a) Selected Kalman Contained **(b)** Selected Kalman Exiting **(c)** Selected Cluster

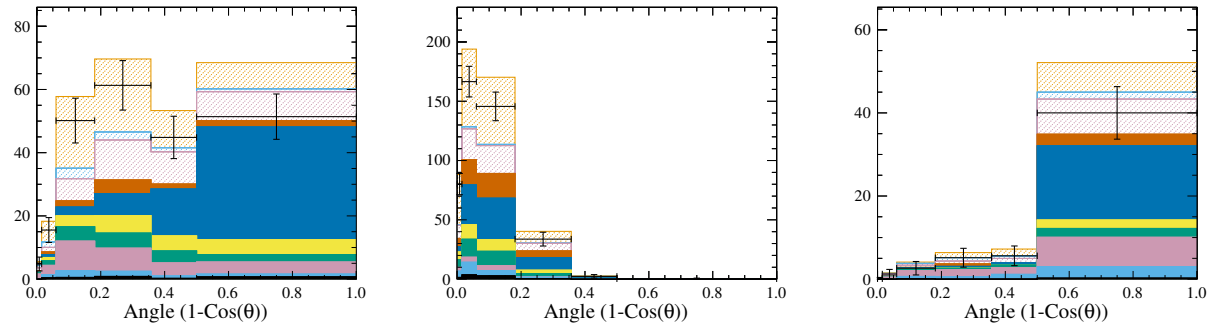

(d) Near Sideband Kalman Contained **(e)** Near Sideband Kalman Exiting **(f)** Near Sideband Cluster

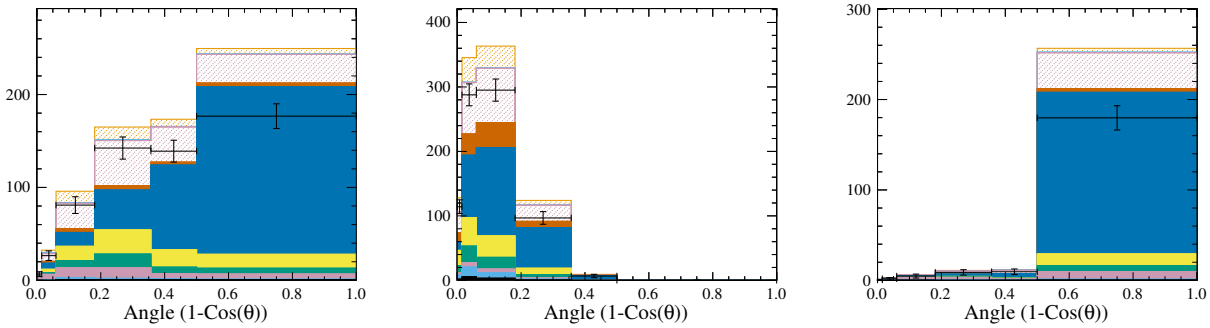

(g) Far Sideband Kalman Contained **(h)** Far Sideband Kalman Exiting **(i)** Far Sideband Cluster

Figure B.44: -1σ Background Cross Section Parameters - Mock Data with Pre-Fit NEUT Templates - Angle Projection

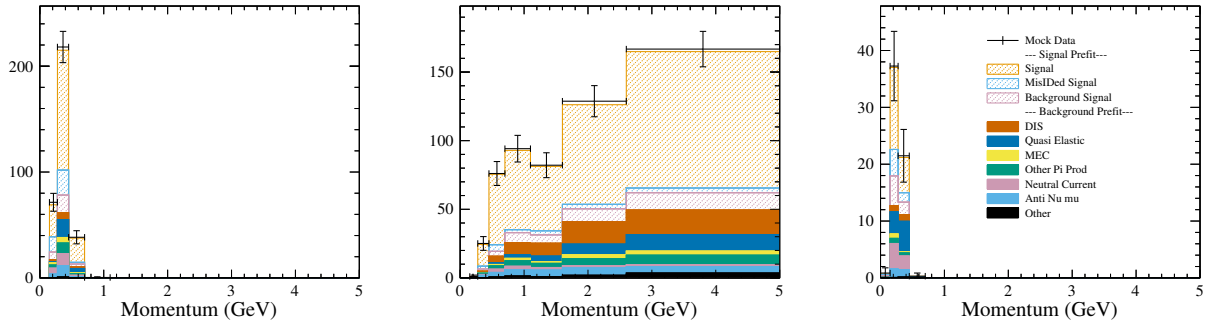

(a) Selected Kalman Contained **(b)** Selected Kalman Exiting **(c)** Selected Cluster

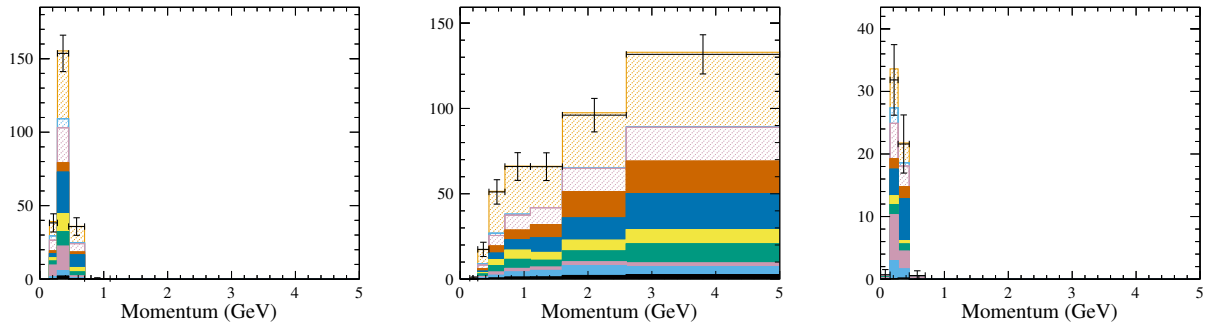

(d) Near Sideband Kalman Contained **(e)** Near Sideband Kalman Exiting **(f)** Near Sideband Cluster

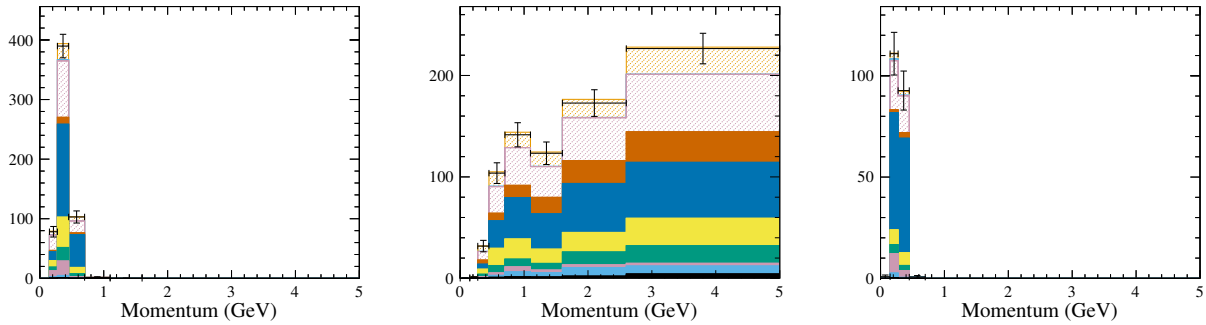

(g) Far Sideband Kalman Contained **(h)** Far Sideband Kalman Exiting **(i)** Far Sideband Cluster

Figure B.45: -1σ Background Cross Section Parameters - Mock Data with Post-Fit NEUT Templates - Momentum Projection

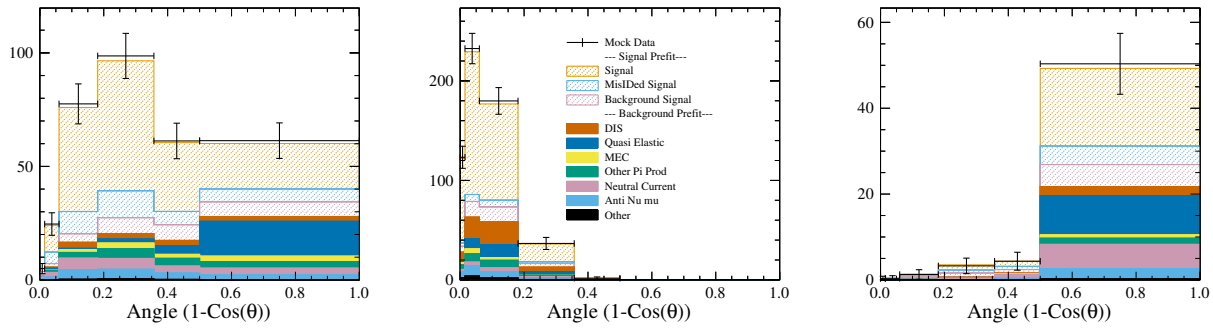

(a) Selected Kalman Contained **(b)** Selected Kalman Exiting **(c)** Selected Cluster

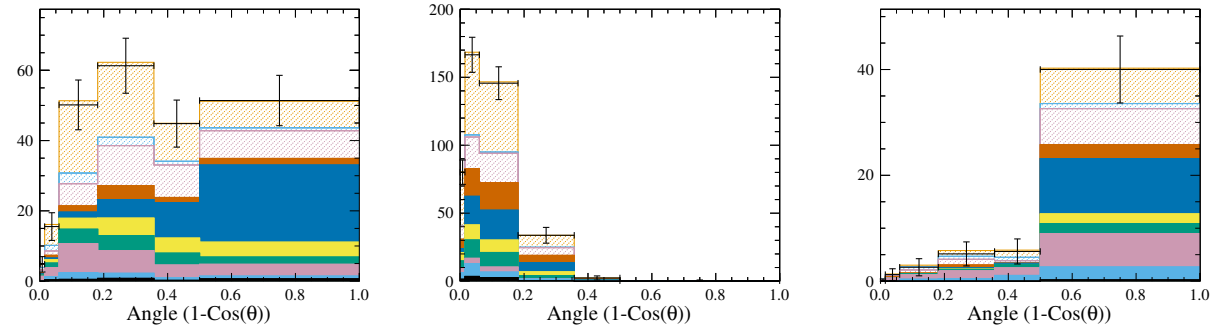

(d) Near Sideband Kalman Contained **(e)** Near Sideband Kalman Exiting **(f)** Near Sideband Cluster

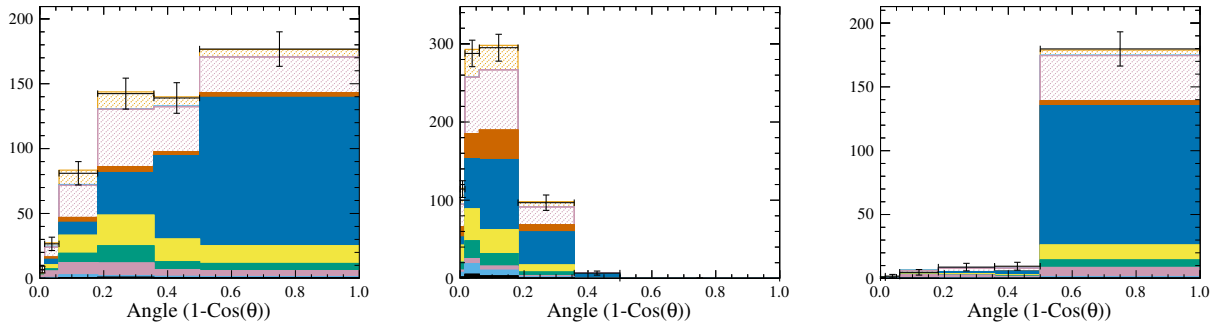

(g) Far Sideband Kalman Contained **(h)** Far Sideband Kalman Exiting **(i)** Far Sideband Cluster

Figure B.46: -1σ Background Cross Section Parameters - Mock Data with Post-Fit NEUT Templates - Angle Projection

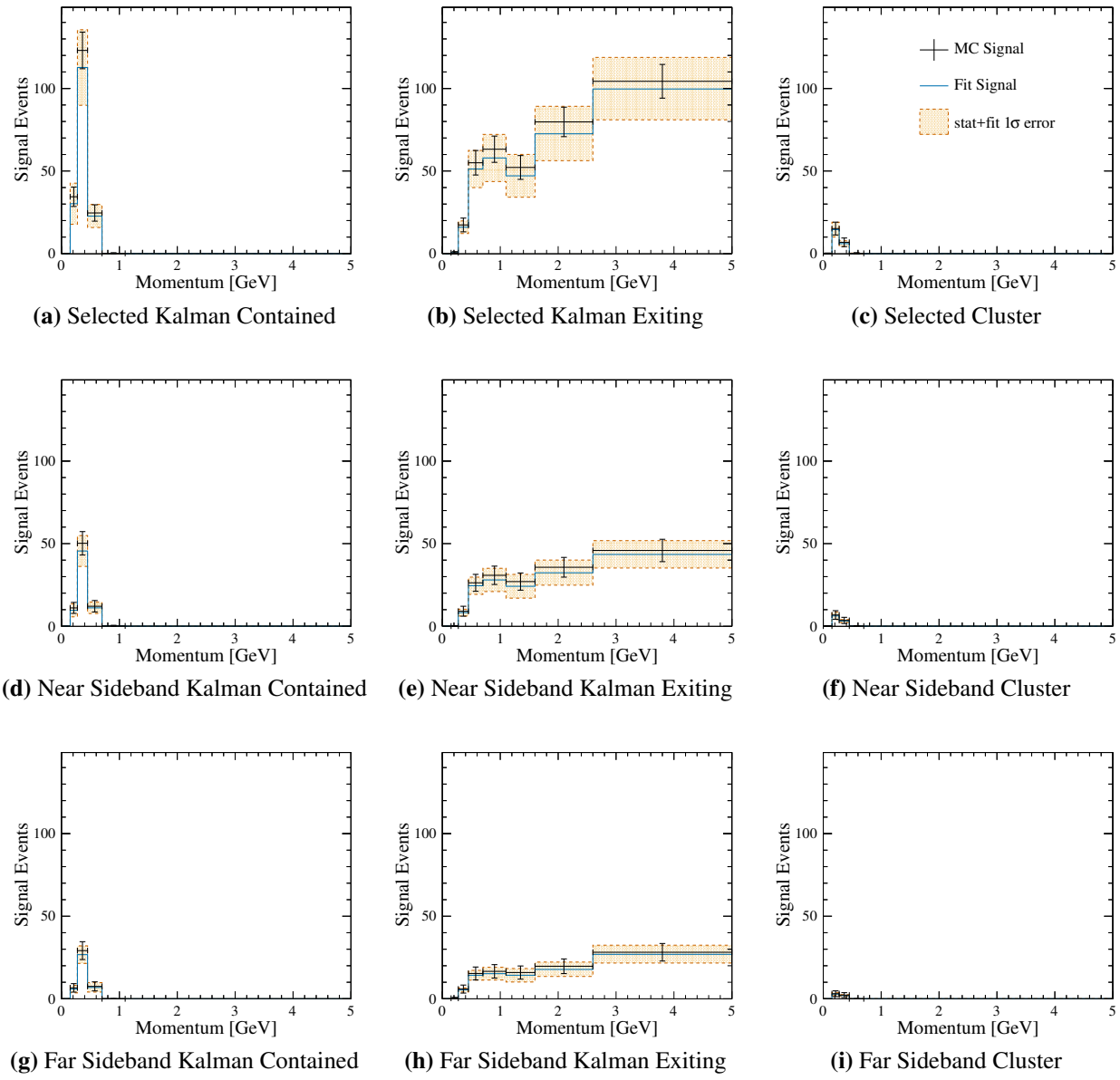

(a) Selected Kalman Contained **(b)** Selected Kalman Exiting **(c)** Selected Cluster

(d) Near Sideband Kalman Contained **(e)** Near Sideband Kalman Exiting **(f)** Near Sideband Cluster

(g) Far Sideband Kalman Contained **(h)** Far Sideband Kalman Exiting **(i)** Far Sideband Cluster

Figure B.47: -1σ Background Cross Section Parameters Study - Signal fit in the muon momentum projection. Black crosses represent the mock data with statistical error bars. The solid blue line is the best fit and the orange region is the error from the fit. - Momentum projection

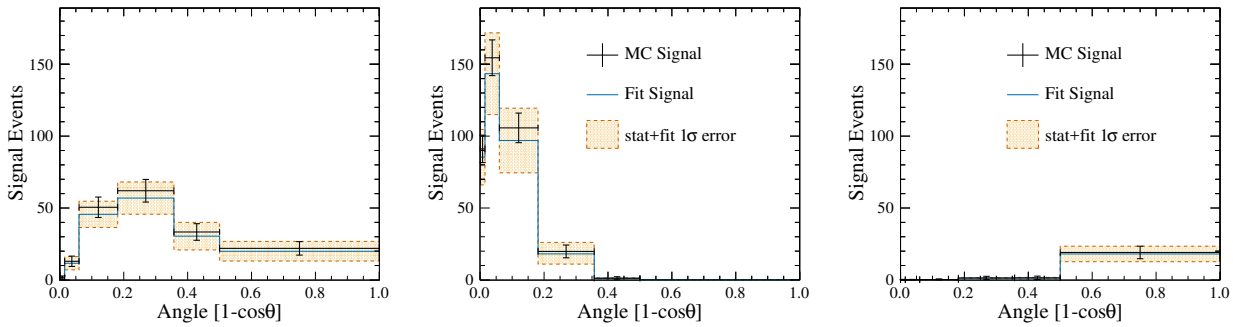

(a) Selected Kalman Contained **(b)** Selected Kalman Exiting **(c)** Selected Cluster

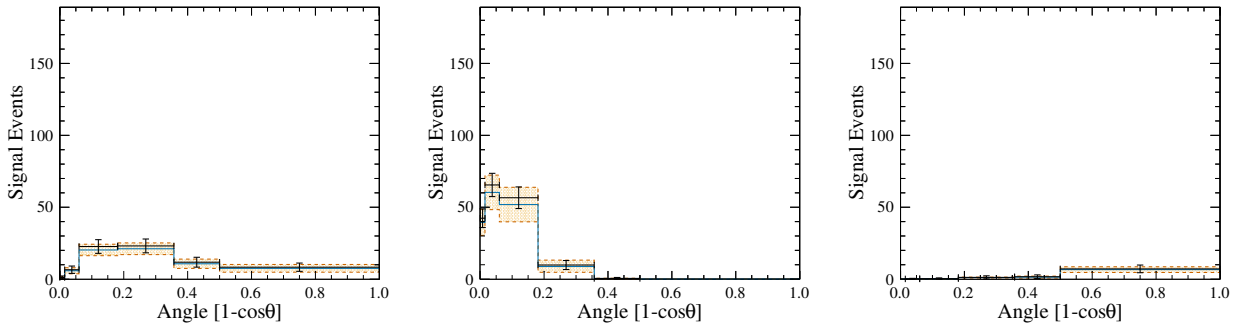

(d) Near Sideband Kalman Contained **(e)** Near Sideband Kalman Exiting **(f)** Near Sideband Cluster

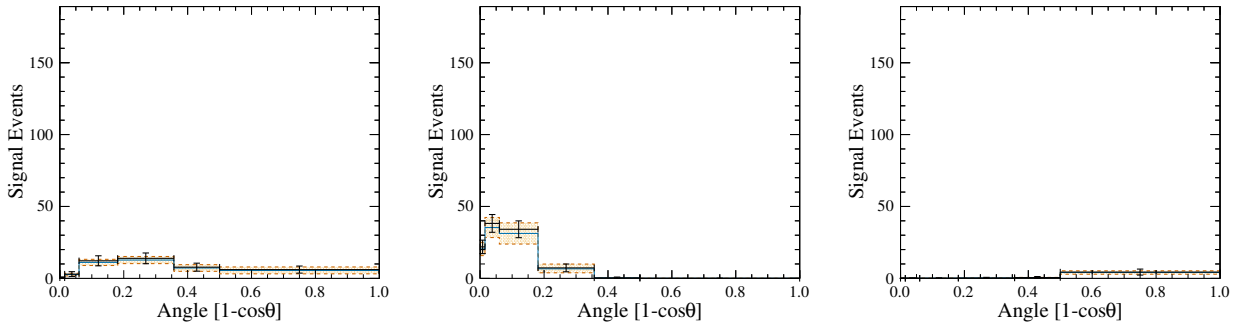

(g) Far Sideband Kalman Contained **(h)** Far Sideband Kalman Exiting **(i)** Far Sideband Cluster

Figure B.48: -1σ Background Cross Section Parameters Study - Signal fit in the muon angle projection. Black crosses represent the mock data with statistical error bars. The solid blue line is the best fit and the orange region is the error from the fit. - Angle projection

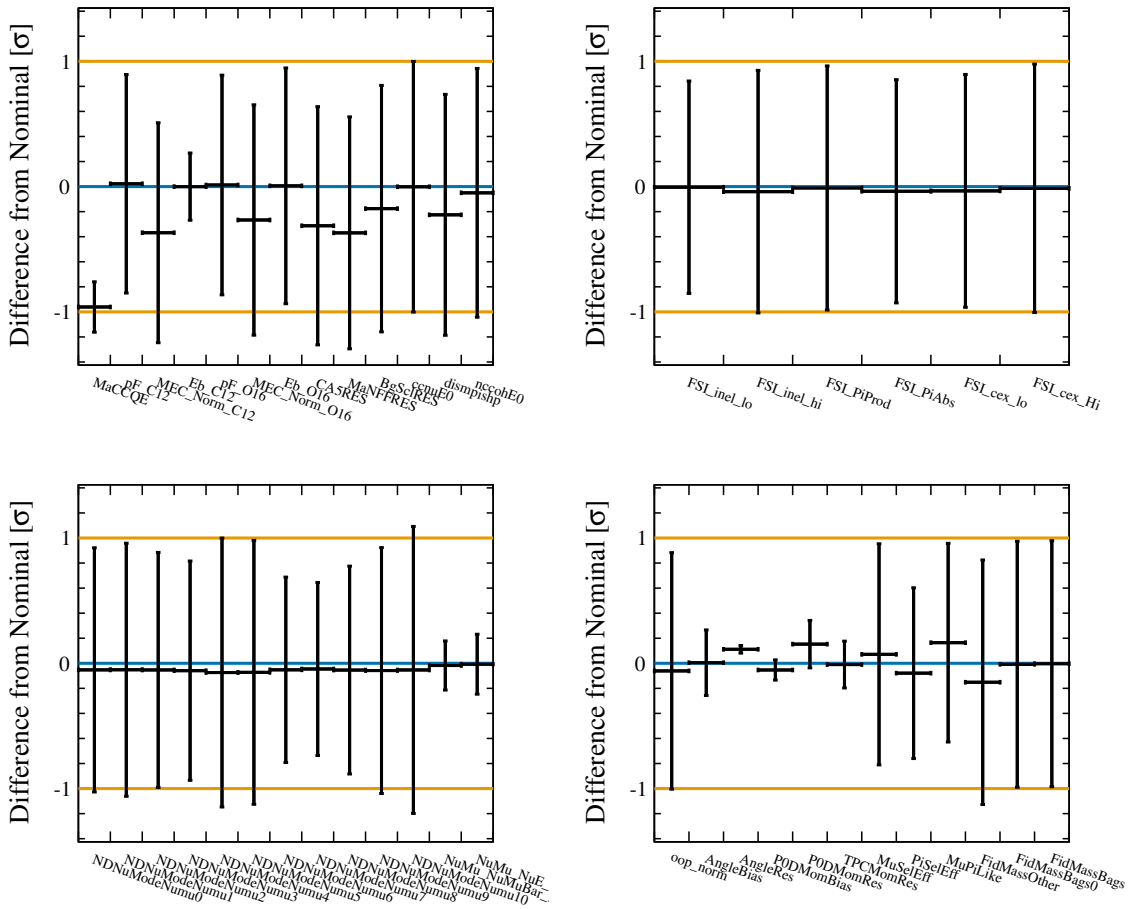

Figure B.49: -1σ Background Cross Section Parameters Study - Fit parameter deviation from nominal. The points in this plot are the best fit parameter value in units of sigma for each dial. The error bars on the points are the error on that parameter from the fit, while the orange lines at +1 and -1 represent the default one sigma error placed on the variable.

the fitter with a changed signal model, exactly what we are looking for. Future tests are adjusting some of the background models underneath this adjustment, to test the robustness of this fit.

Plotted in Figures B.50 and B.51 are the mock data over the pre-fit NEUT templates, while Figures B.52 and B.53 are the mock data over the post-fit NEUT templates. The extracted signal is plotted in figures B.54 and B.55. The fit parameter deviations from nominal and error are plotted in figure B.56.

B.4.2 Minoo's CC Resonant Model

This version of the Minoo resonance model is implemented with the number of resonant events equal between Minoo's and the base NEUT Model. The main effect the Minoo model has on events included in this analysis is shifting the momentum of the pion below the reconstruction threshold of the PØD. Because of this, the main effect of implementing this model is not a shape change in the muon kinematics, but a general decreases in the number of events.

Plotted in Figures B.57 and B.58 are the mock data over the pre-fit NEUT templates, while Figures B.59 and B.60 are the mock data over the post-fit NEUT templates. The extracted signal is plotted in figures B.61 and B.62. The fit parameter deviations from nominal and error are plotted in figure B.63.

B.4.3 GENIE Signal

This study uses the GENIE prediction for the signal channels as mock data in place of the NEUT default prediction.

For GENIE mock data, the analysis was done on GENIE MC files for Run4 Water, and a new set of templates were made. Splines were then created that can make mock data by converting the NEUT templates into GENIE templates. This is not a perfect test, as any kinematic bins for which NEUT has no events, there can be no GENIE events. A study was done to identify if this was a significant problem, and it was found that the only time GENIE had events in a bin that NEUT did not, there were very few events. As the goal of this study is to evaluate the performance of our

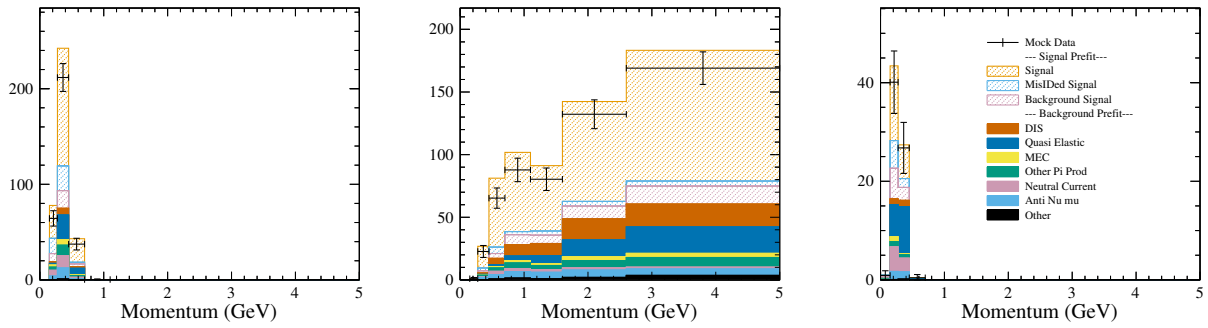

(a) Selected Kalman Contained **(b)** Selected Kalman Exiting **(c)** Selected Cluster

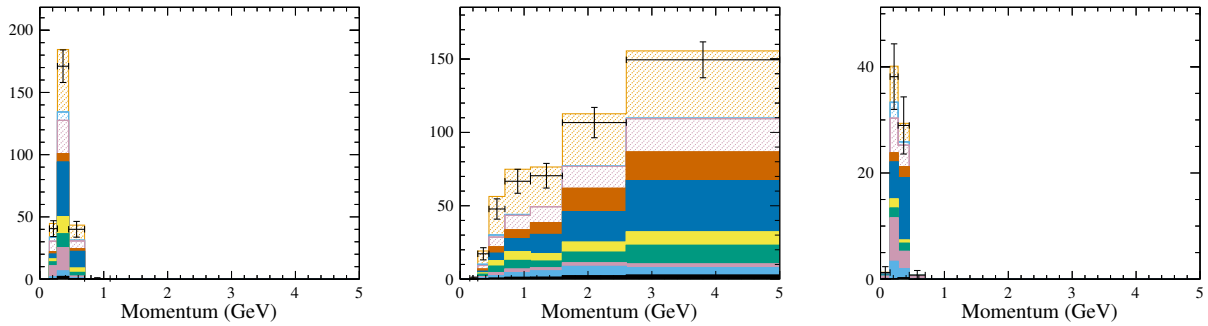

(d) Near Sideband Kalman Contained **(e)** Near Sideband Kalman Exiting **(f)** Near Sideband Cluster

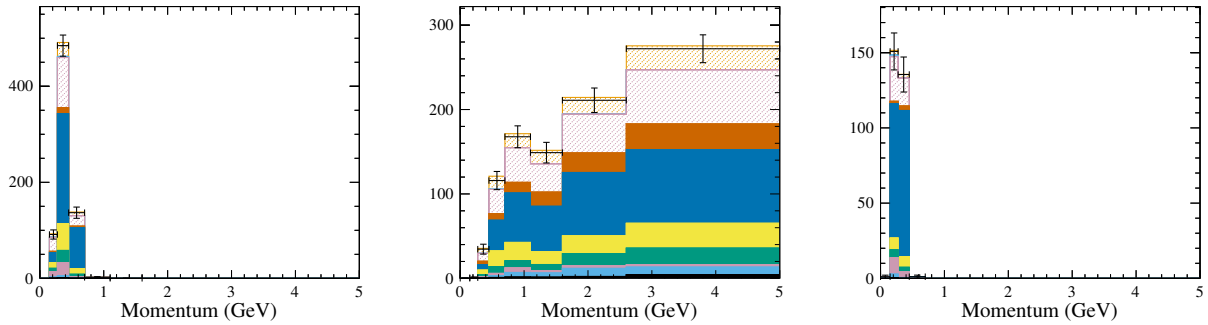

(g) Far Sideband Kalman Contained **(h)** Far Sideband Kalman Exiting **(i)** Far Sideband Cluster

Figure B.50: CC Coherent Model Study - Mock Data with Pre-Fit NEUT Templates - Momentum Projection

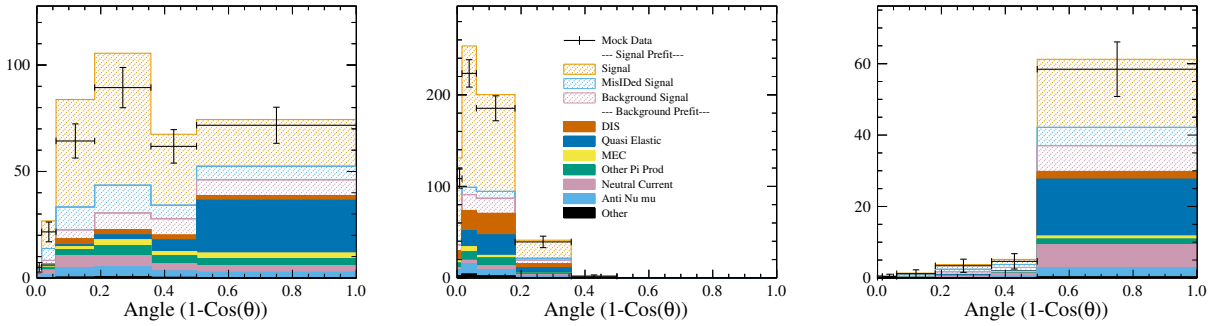

(a) Selected Kalman Contained **(b)** Selected Kalman Exiting **(c)** Selected Cluster

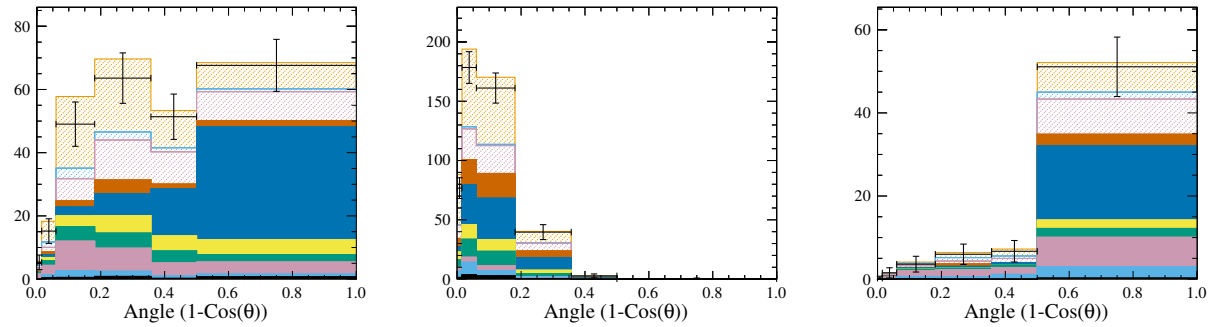

(d) Near Sideband Kalman Contained **(e)** Near Sideband Kalman Exiting **(f)** Near Sideband Cluster

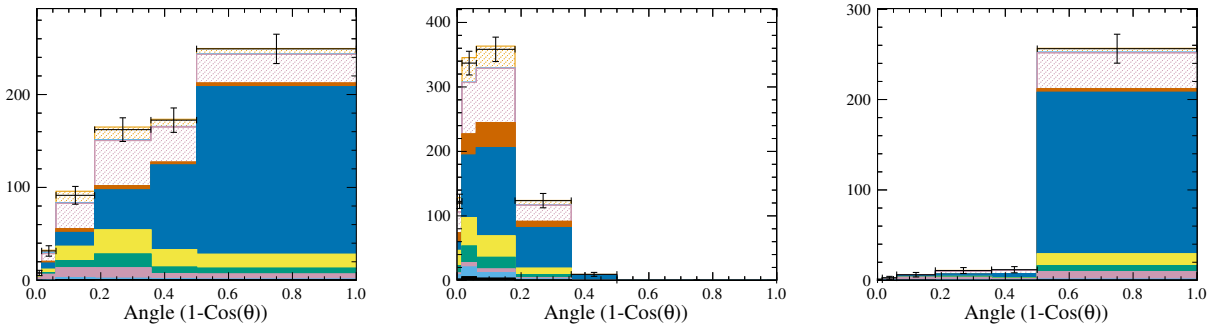

(g) Far Sideband Kalman Contained **(h)** Far Sideband Kalman Exiting **(i)** Far Sideband Cluster

Figure B.51: CC Coherent Model Study - Mock Data with Pre-Fit NEUT Templates - Angle Projection

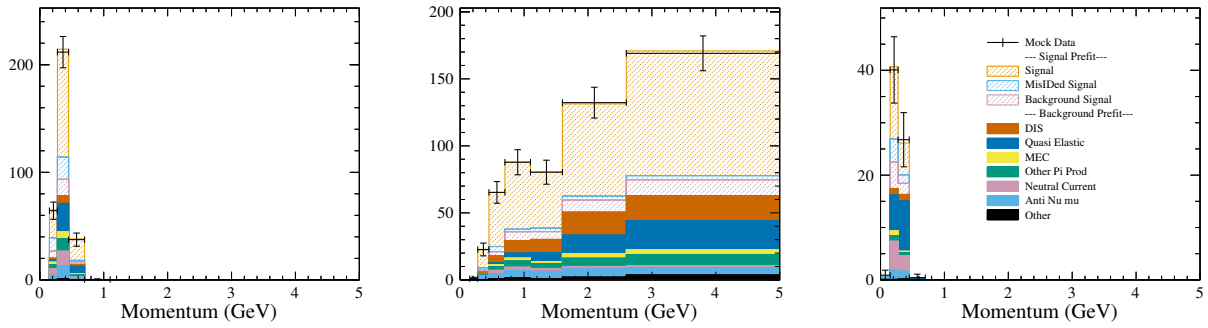

(a) Selected Kalman Contained **(b)** Selected Kalman Exiting **(c)** Selected Cluster

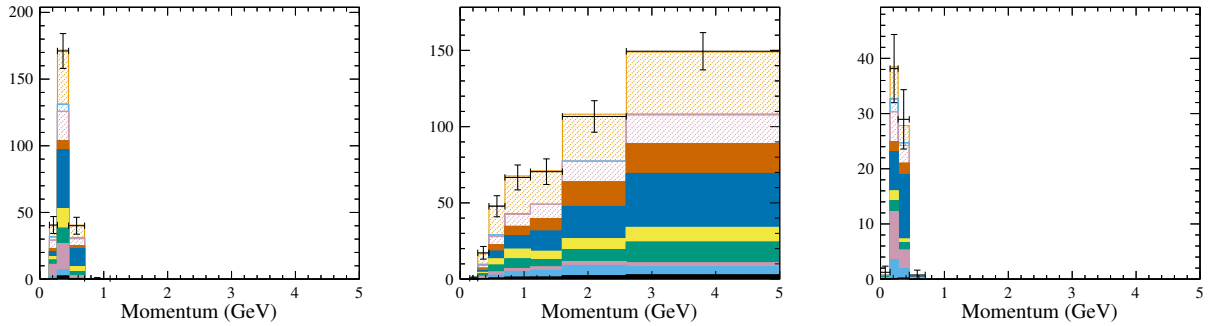

(d) Near Sideband Kalman Contained **(e)** Near Sideband Kalman Exiting **(f)** Near Sideband Cluster

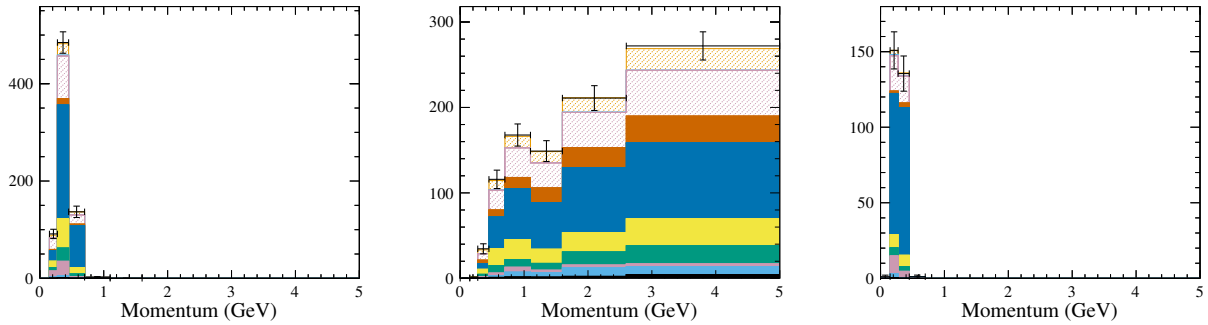

(g) Far Sideband Kalman Contained **(h)** Far Sideband Kalman Exiting **(i)** Far Sideband Cluster

Figure B.52: CC Coherent Model Study - Mock Data with Post-Fit NEUT Templates - Momentum Projection

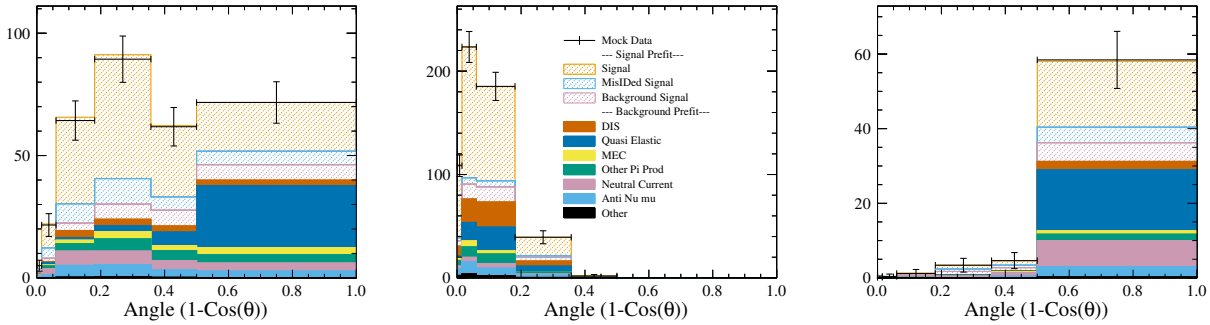

(a) Selected Kalman Contained **(b)** Selected Kalman Exiting **(c)** Selected Cluster

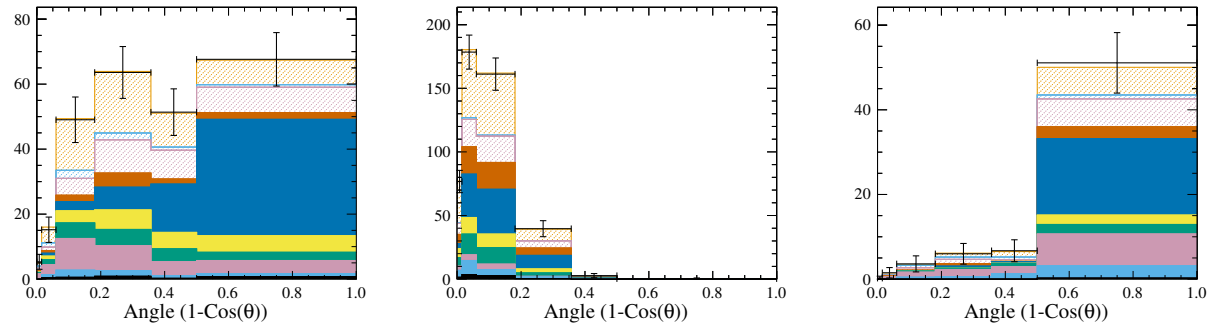

(d) Near Sideband Kalman Contained **(e)** Near Sideband Kalman Exiting **(f)** Near Sideband Cluster

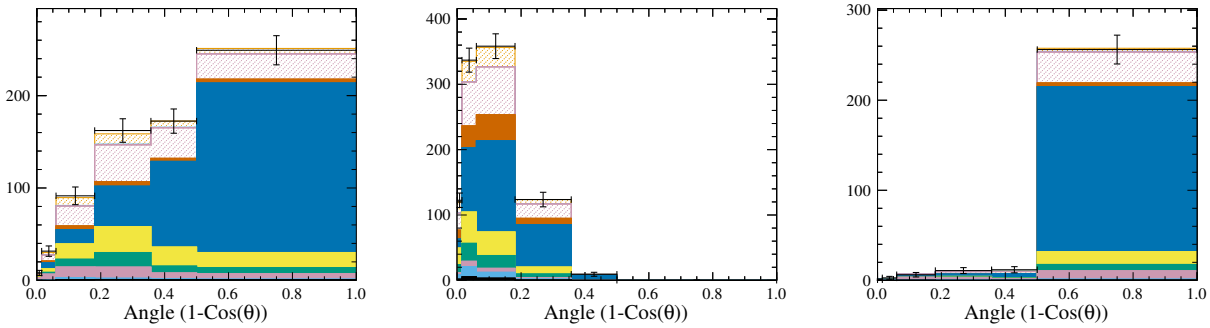

(g) Far Sideband Kalman Contained **(h)** Far Sideband Kalman Exiting **(i)** Far Sideband Cluster

Figure B.53: CC Coherent Model Study - Mock Data with Post-Fit NEUT Templates - Angle Projection

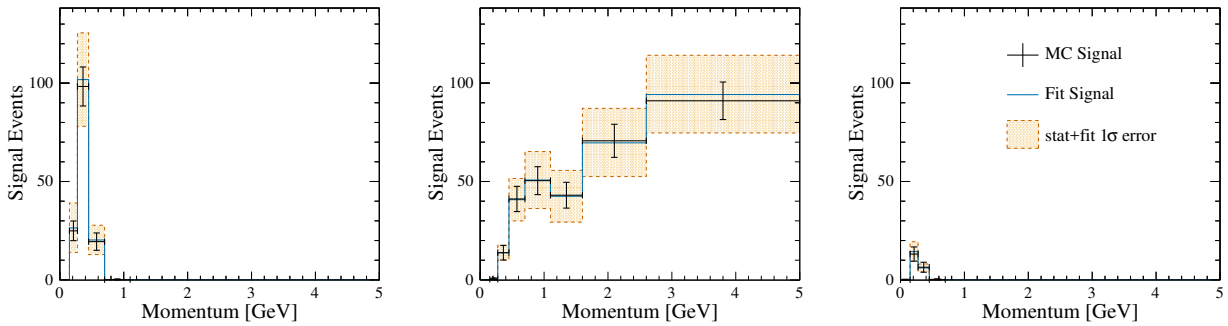

(a) Selected Kalman Contained **(b)** Selected Kalman Exiting **(c)** Selected Cluster

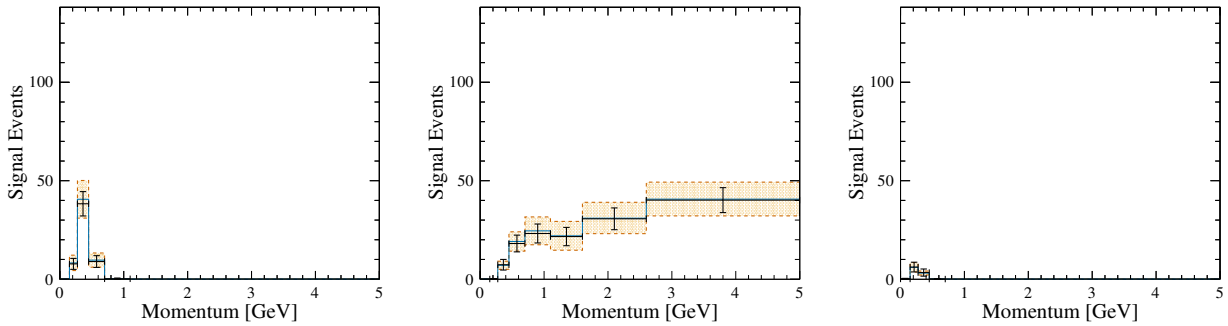

(d) Near Sideband Kalman Contained **(e)** Near Sideband Kalman Exiting **(f)** Near Sideband Cluster

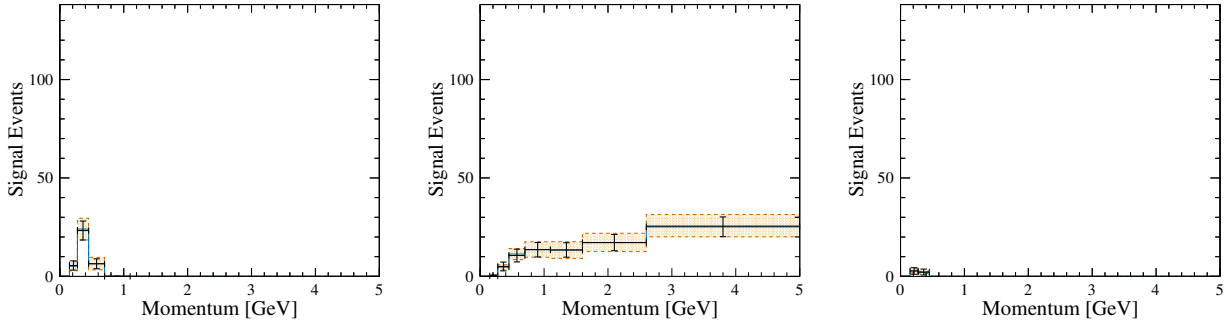

(g) Far Sideband Kalman Contained **(h)** Far Sideband Kalman Exiting **(i)** Far Sideband Cluster

Figure B.54: CC Coherent Model Study - Signal fit in the muon momentum projection. Black crosses represent the mock data with statistical error bars. The solid blue line is the best fit and the orange region is the error from the fit. - Momentum projection

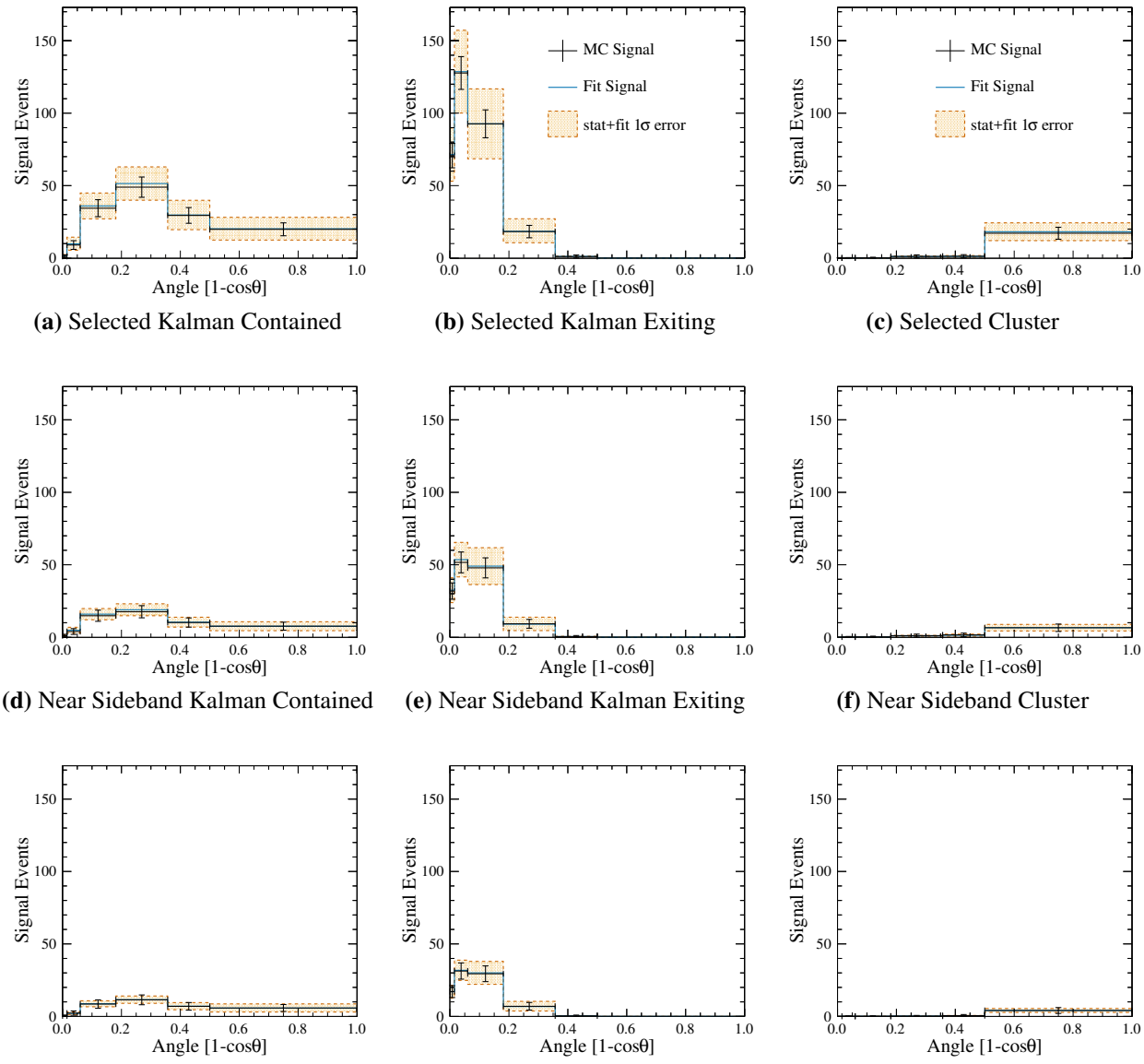

(a) Selected Kalman Contained **(b)** Selected Kalman Exiting **(c)** Selected Cluster

(d) Near Sideband Kalman Contained **(e)** Near Sideband Kalman Exiting **(f)** Near Sideband Cluster

(g) Far Sideband Kalman Contained **(h)** Far Sideband Kalman Exiting **(i)** Far Sideband Cluster

Figure B.55: CC Coherent Model Study - Signal fit in the muon angle projection. Black crosses represent the mock data with statistical error bars. The solid blue line is the best fit and the orange region is the error from the fit. - Angle projection

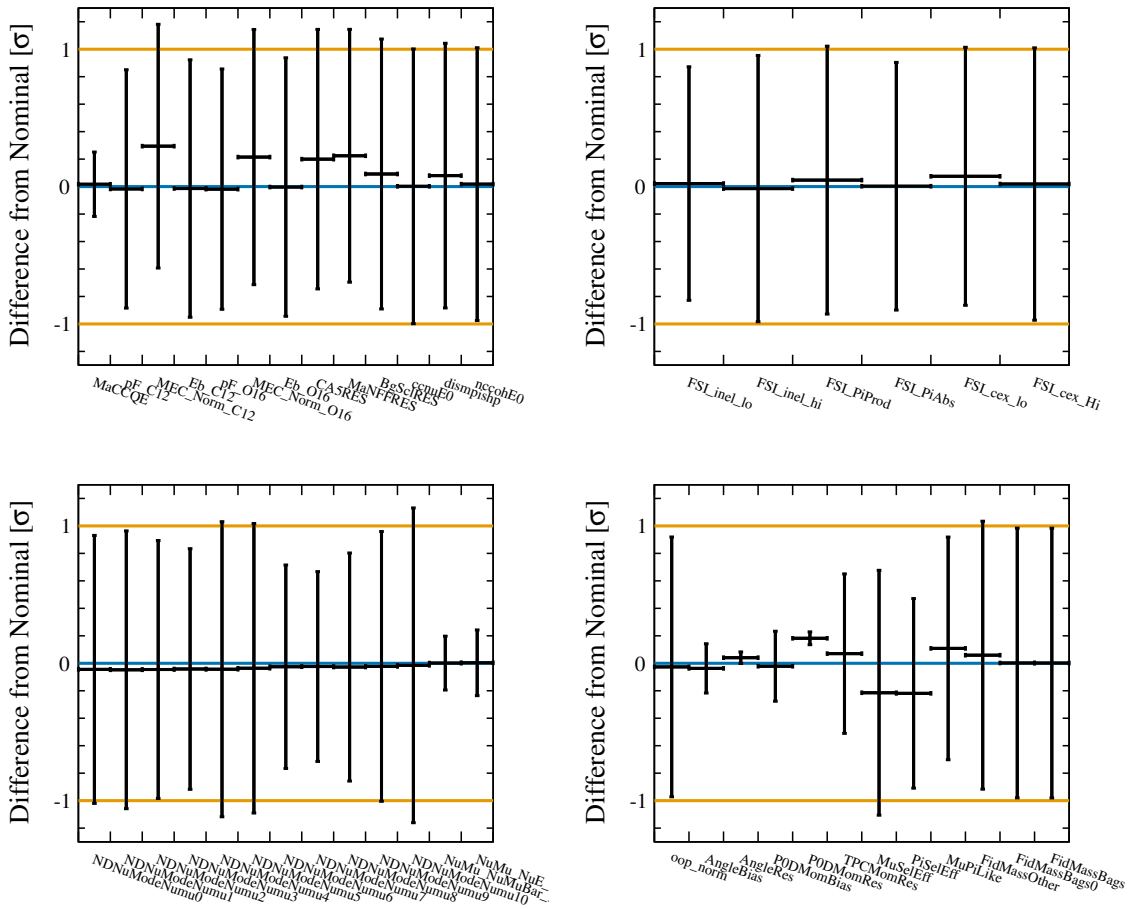

Figure B.56: CC Coherent Model Study - Fit parameter deviation from nominal. The points in this plot are the best fit parameter value in units of sigma for each dial. The error bars on the points are the error on that parameter from the fit, while the orange lines at +1 and -1 represent the default one sigma error placed on the variable.

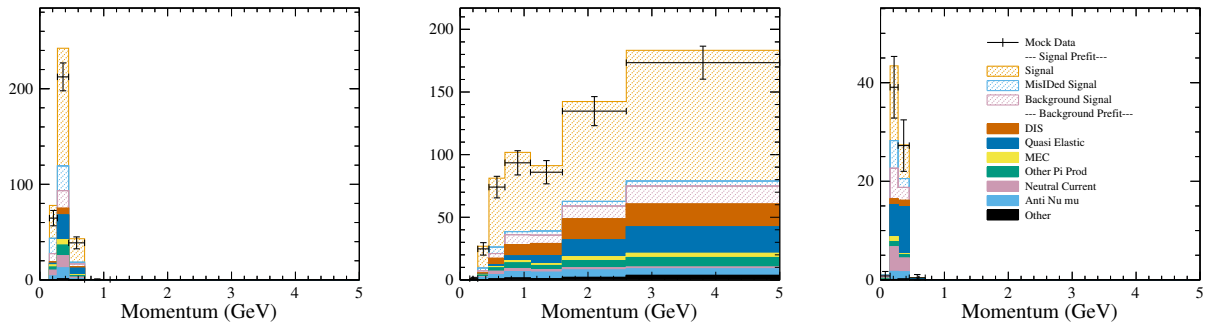

(a) Selected Kalman Contained **(b)** Selected Kalman Exiting **(c)** Selected Cluster

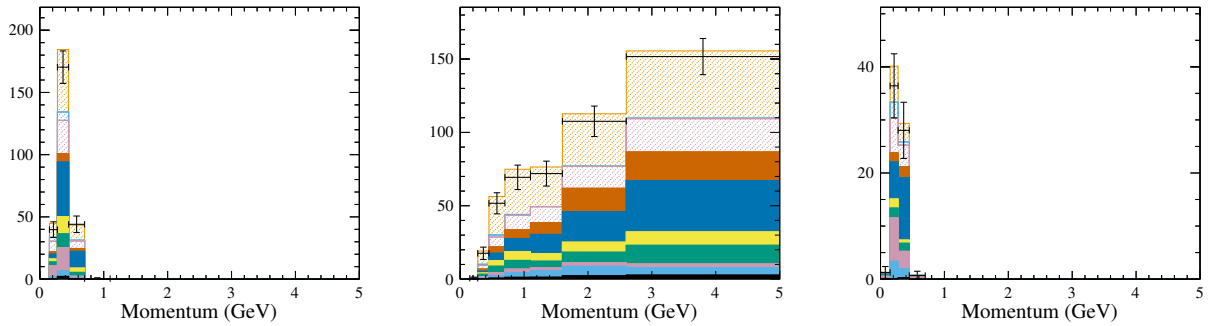

(d) Near Sideband Kalman Contained **(e)** Near Sideband Kalman Exiting **(f)** Near Sideband Cluster

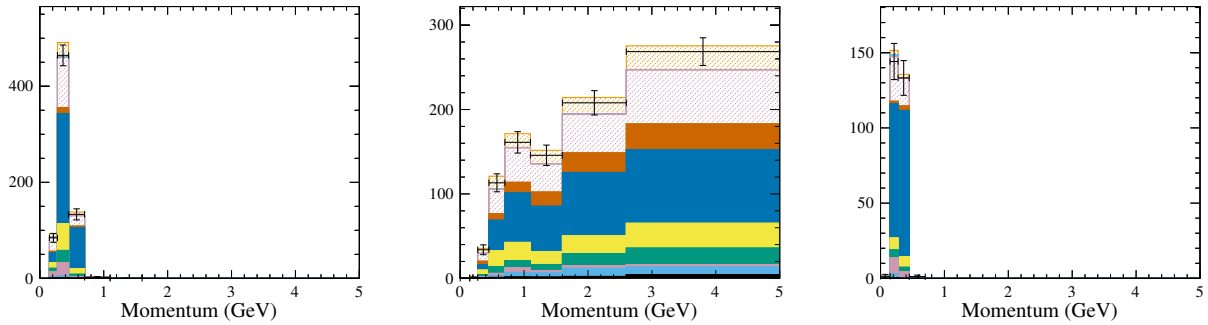

(g) Far Sideband Kalman Contained **(h)** Far Sideband Kalman Exiting **(i)** Far Sideband Cluster

Figure B.57: CC Resonant Model Study - Mock Data with Pre-Fit NEUT Templates - Momentum Projection

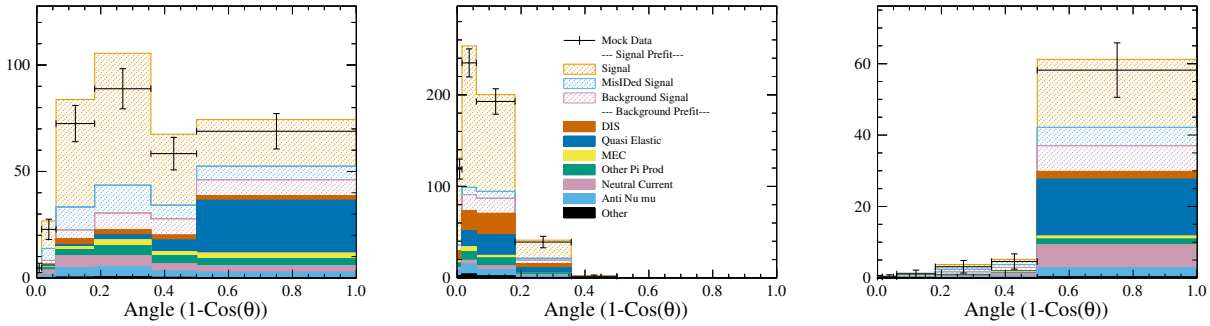

(a) Selected Kalman Contained **(b)** Selected Kalman Exiting **(c)** Selected Cluster

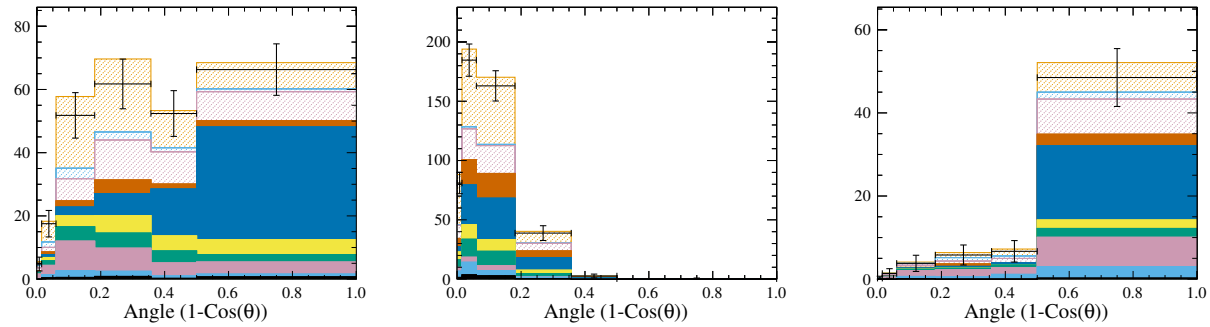

(d) Near Sideband Kalman Contained **(e)** Near Sideband Kalman Exiting **(f)** Near Sideband Cluster

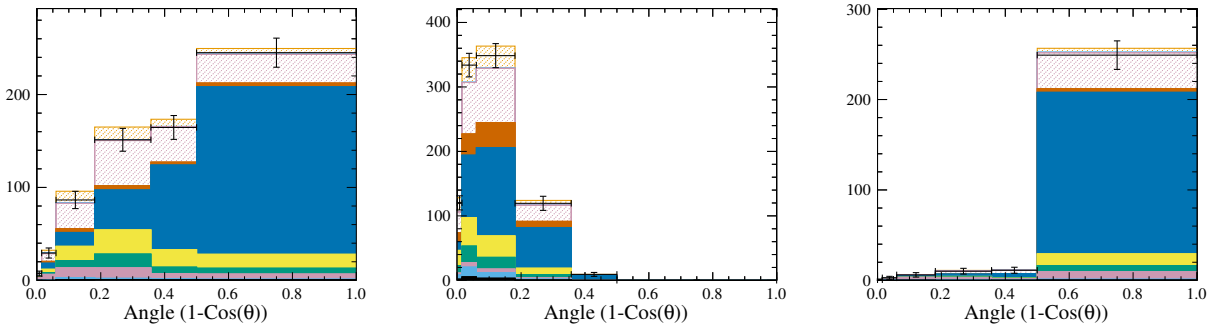

(g) Far Sideband Kalman Contained **(h)** Far Sideband Kalman Exiting **(i)** Far Sideband Cluster

Figure B.58: CC Resonant Model Study - Mock Data with Pre-Fit NEUT Templates - Angle Projection

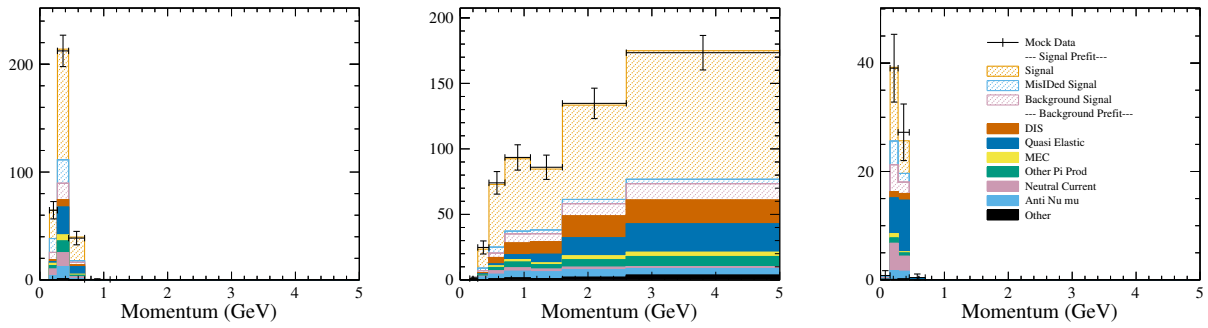

(a) Selected Kalman Contained **(b)** Selected Kalman Exiting **(c)** Selected Cluster

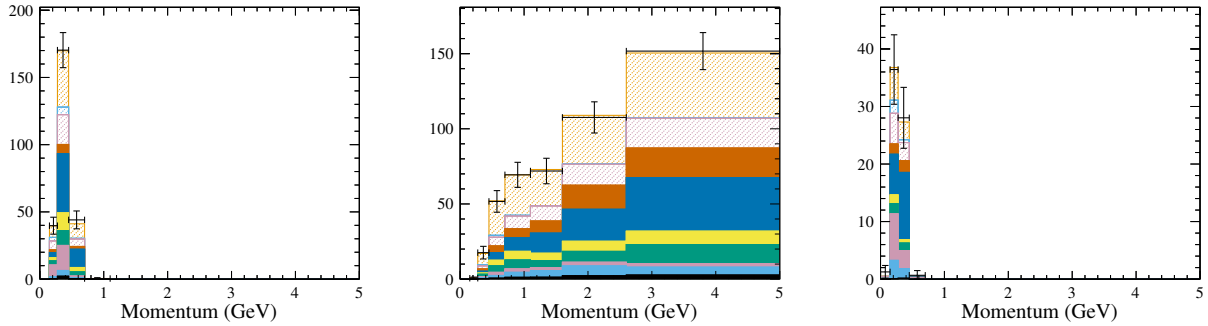

(d) Near Sideband Kalman Contained **(e)** Near Sideband Kalman Exiting **(f)** Near Sideband Cluster

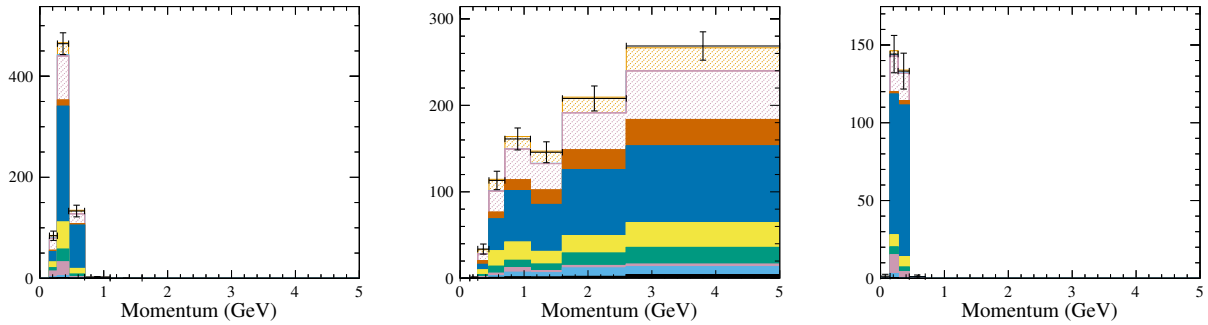

(g) Far Sideband Kalman Contained **(h)** Far Sideband Kalman Exiting **(i)** Far Sideband Cluster

Figure B.59: CC Resonant Model Study - Mock Data with Post-Fit NEUT Templates - Momentum Projection

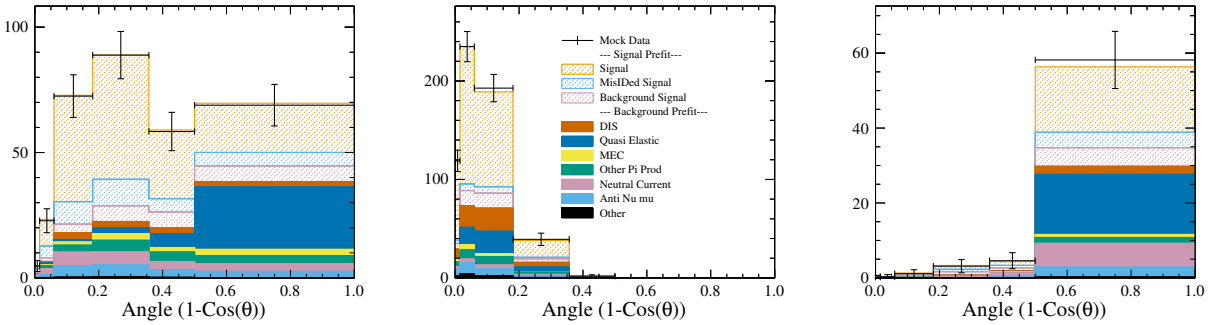

(a) Selected Kalman Contained **(b)** Selected Kalman Exiting **(c)** Selected Cluster

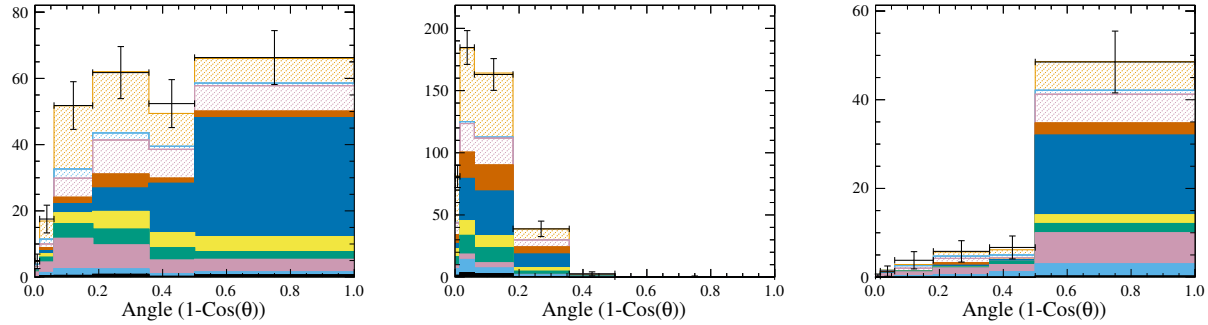

(d) Near Sideband Kalman Contained **(e)** Near Sideband Kalman Exiting **(f)** Near Sideband Cluster

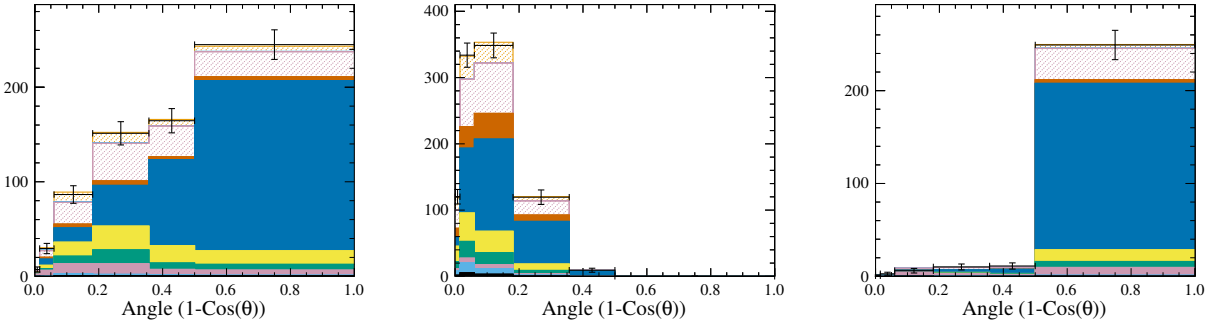

(g) Far Sideband Kalman Contained **(h)** Far Sideband Kalman Exiting **(i)** Far Sideband Cluster

Figure B.60: CC Resonant Model Study - Mock Data with Post-Fit NEUT Templates - Angle Projection

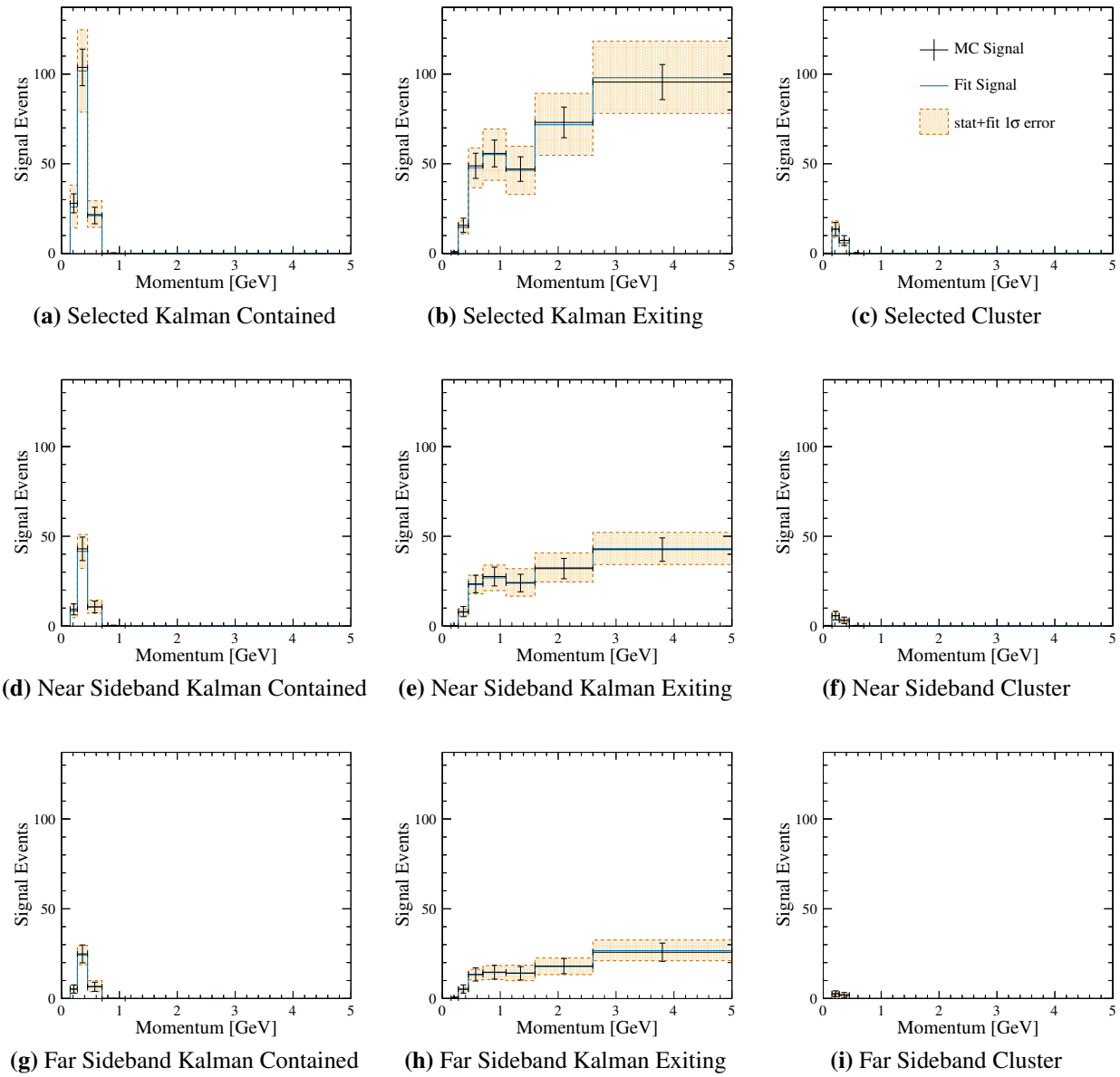

(a) Selected Kalman Contained **(b)** Selected Kalman Exiting **(c)** Selected Cluster

(d) Near Sideband Kalman Contained **(e)** Near Sideband Kalman Exiting **(f)** Near Sideband Cluster

(g) Far Sideband Kalman Contained **(h)** Far Sideband Kalman Exiting **(i)** Far Sideband Cluster

Figure B.61: CC Resonant Model Study - Signal fit in the muon momentum projection. Black crosses represent the mock data with statistical error bars. The solid blue line is the best fit and the orange region is the error from the fit. - Momentum projection

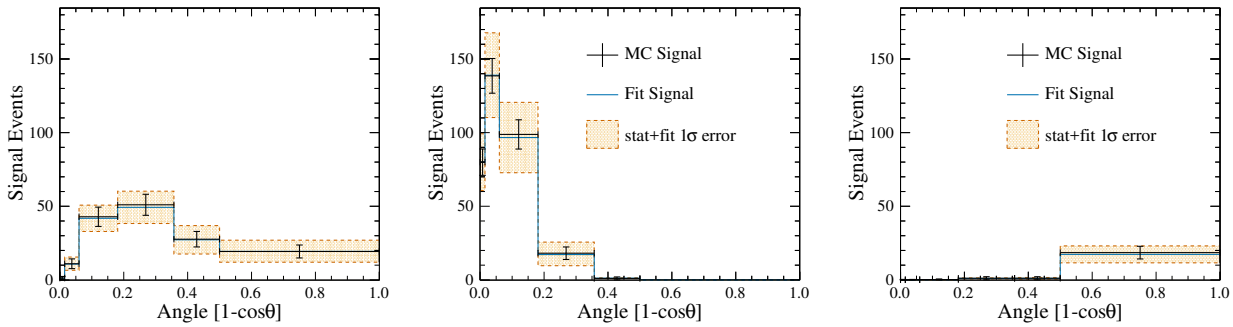

(a) Selected Kalman Contained **(b)** Selected Kalman Exiting **(c)** Selected Cluster

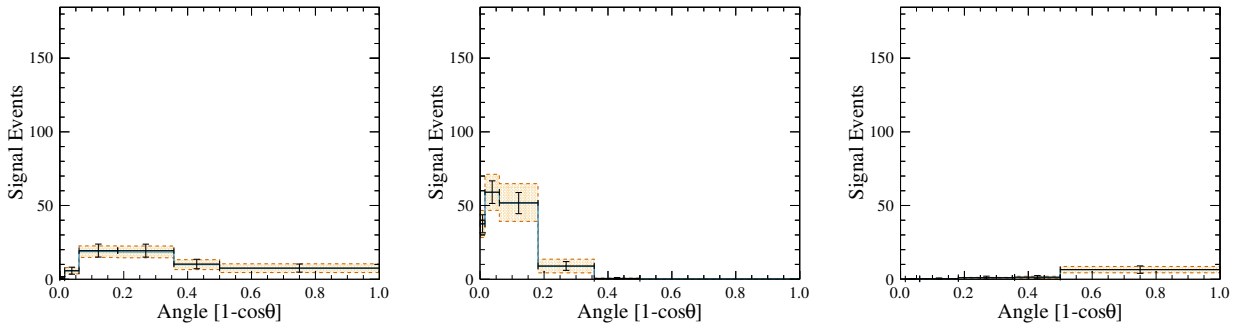

(d) Near Sideband Kalman Contained **(e)** Near Sideband Kalman Exiting **(f)** Near Sideband Cluster

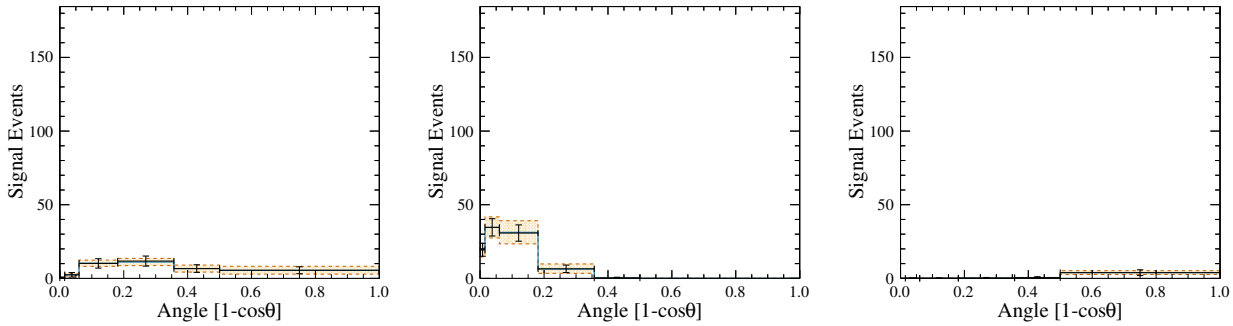

(g) Far Sideband Kalman Contained **(h)** Far Sideband Kalman Exiting **(i)** Far Sideband Cluster

Figure B.62: CC Resonant Model Study - Signal fit in the muon angle projection. Black crosses represent the mock data with statistical error bars. The solid blue line is the best fit and the orange region is the error from the fit. - Angle projection

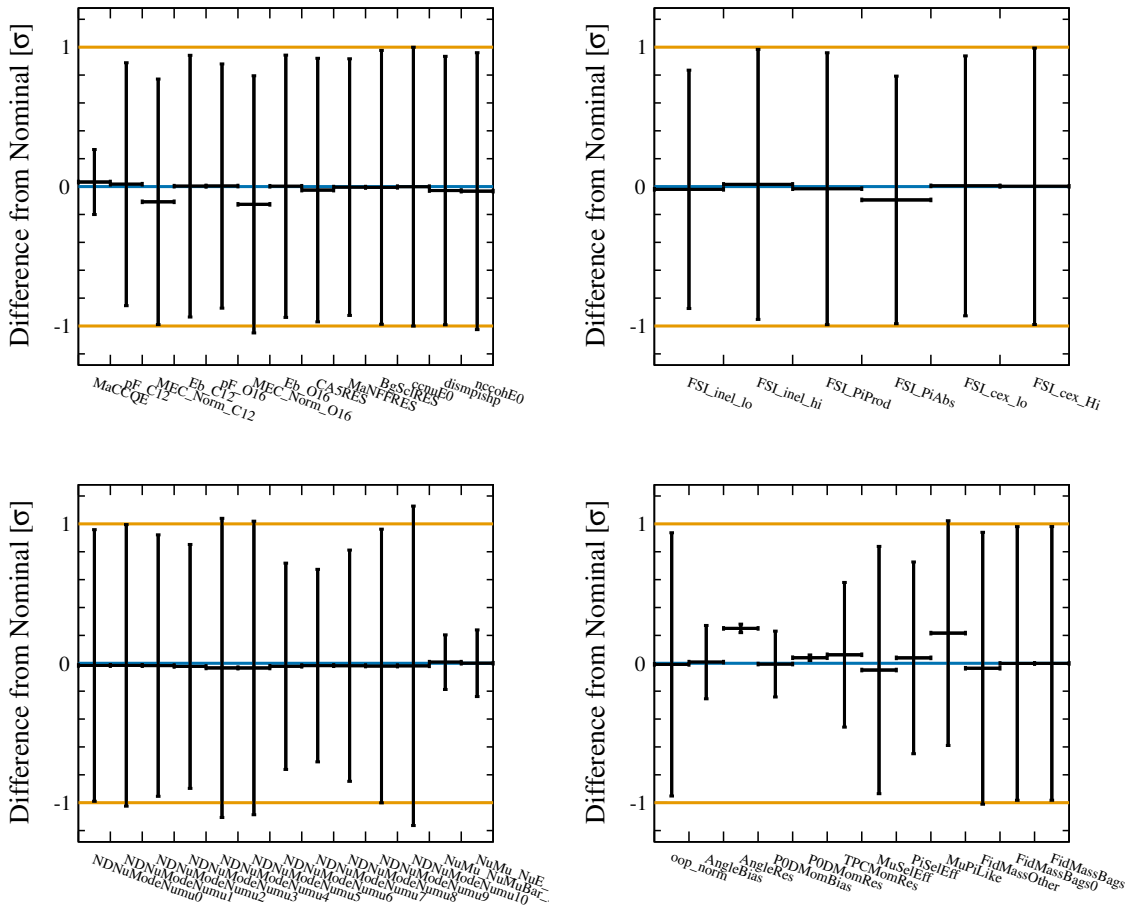

Figure B.63: CC Resonant Model Study - Fit parameter deviation from nominal. The points in this plot are the best fit parameter value in units of sigma for each dial. The error bars on the points are the error on that parameter from the fit, while the orange lines at +1 and -1 represent the default one sigma error placed on the variable.

fitter with different shapes for the different templates, it was determined that this was not enough of a problem to invalidate the study.

Plotted in Figures B.64 and B.65 are the mock data over the pre-fit NEUT templates, while Figures B.66 and B.67 are the mock data over the post-fit NEUT templates. The extracted signal is plotted in figures B.68 and B.69. The fit parameter deviations from nominal and error are plotted in figure B.70.

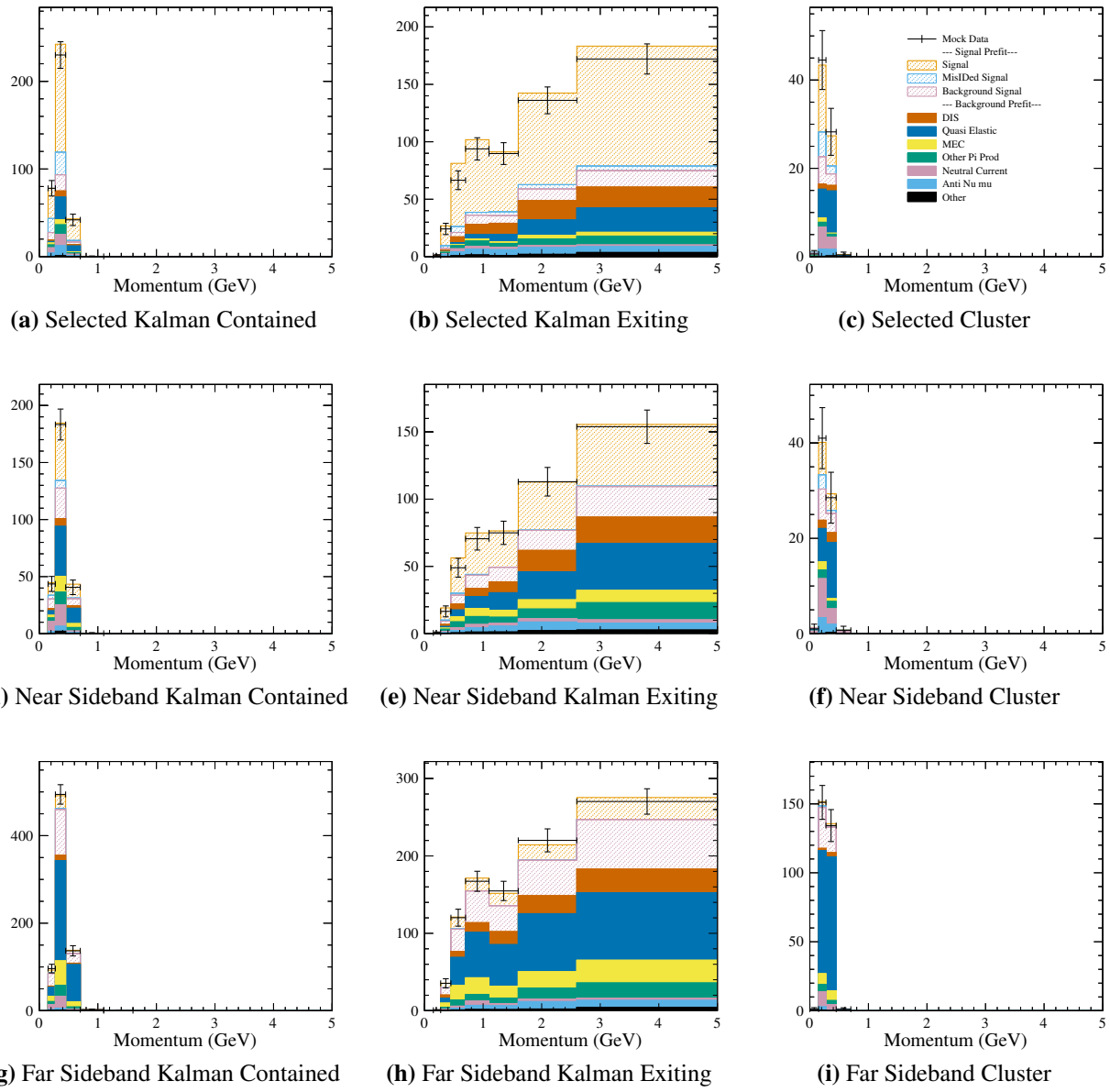

(a) Selected Kalman Contained **(b)** Selected Kalman Exiting **(c)** Selected Cluster

(d) Near Sideband Kalman Contained **(e)** Near Sideband Kalman Exiting **(f)** Near Sideband Cluster

(g) Far Sideband Kalman Contained **(h)** Far Sideband Kalman Exiting **(i)** Far Sideband Cluster

Figure B.64: GENIE Signal - Mock Data with Pre-Fit NEUT Templates - Momentum Projection

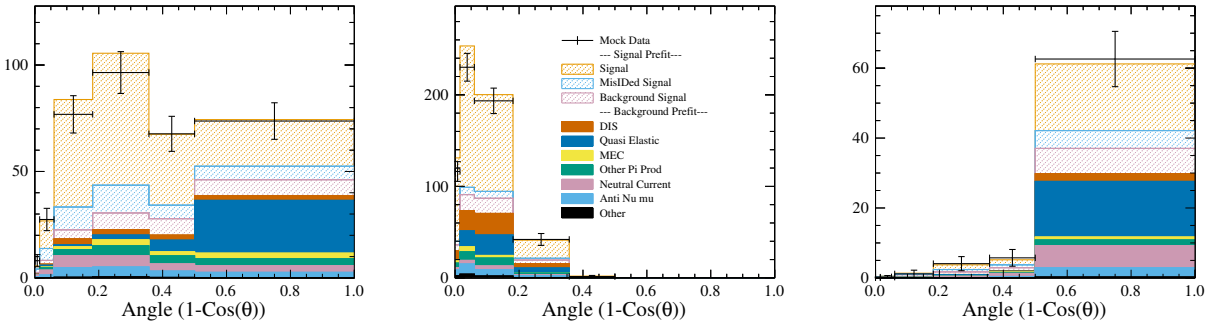

(a) Selected Kalman Contained **(b)** Selected Kalman Exiting **(c)** Selected Cluster

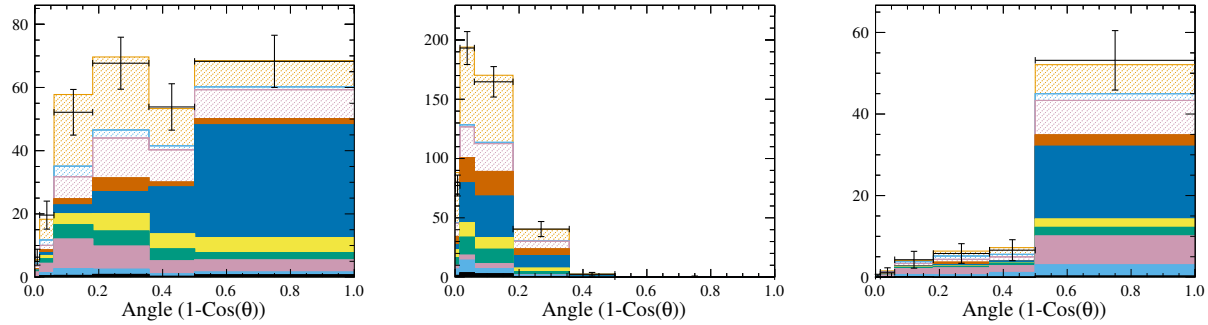

(d) Near Sideband Kalman Contained **(e)** Near Sideband Kalman Exiting **(f)** Near Sideband Cluster

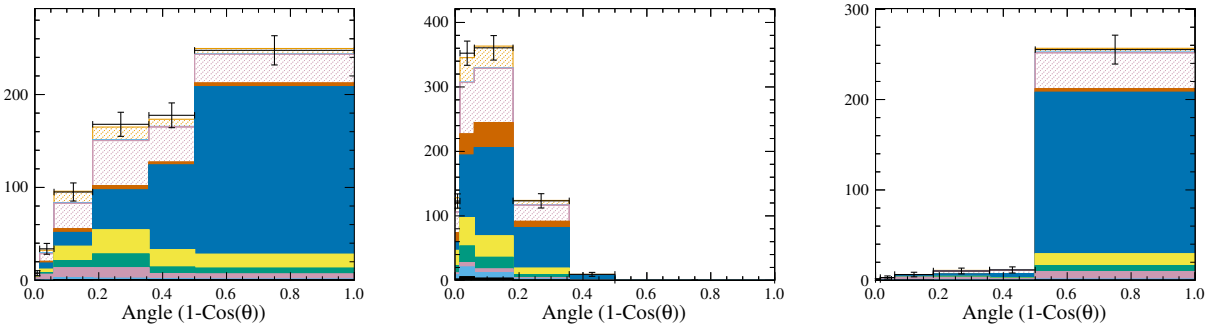

(g) Far Sideband Kalman Contained **(h)** Far Sideband Kalman Exiting **(i)** Far Sideband Cluster

Figure B.65: GENIE Signal - Mock Data with Pre-Fit NEUT Templates - Angle Projection

B.4.4 Res Q^2 signal distortion

As suggested, a test was done applying a Q^2 distortion to the resonant channel to approximate the RPA effect currently modeled for CCQE. This distortion was done using the CCQE RPA model, applied to the resonance events, adjusting the weight of each resonant event as a function of that event's Q^2.

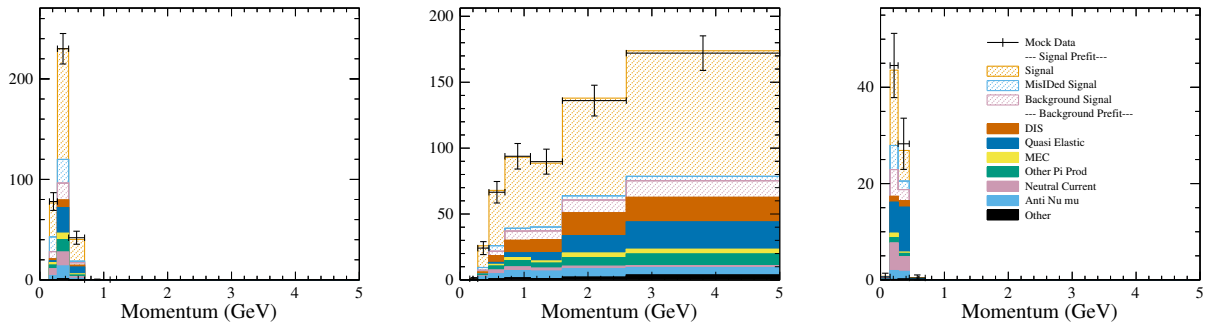

(a) Selected Kalman Contained **(b)** Selected Kalman Exiting **(c)** Selected Cluster

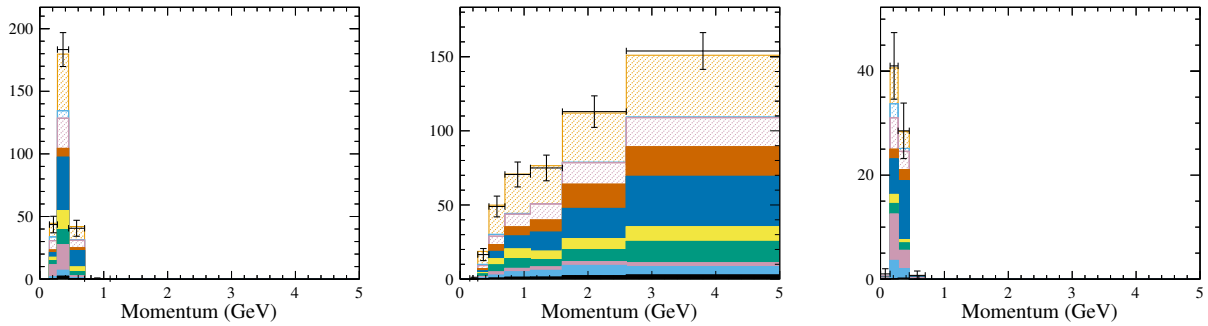

(d) Near Sideband Kalman Contained **(e)** Near Sideband Kalman Exiting **(f)** Near Sideband Cluster

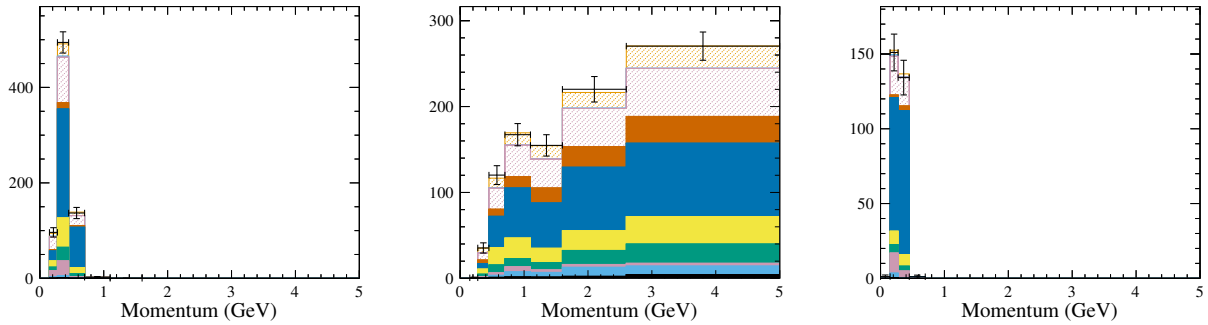

(g) Far Sideband Kalman Contained **(h)** Far Sideband Kalman Exiting **(i)** Far Sideband Cluster

Figure B.66: GENIE Signal - Mock Data with Post-Fit NEUT Templates - Momentum Projection

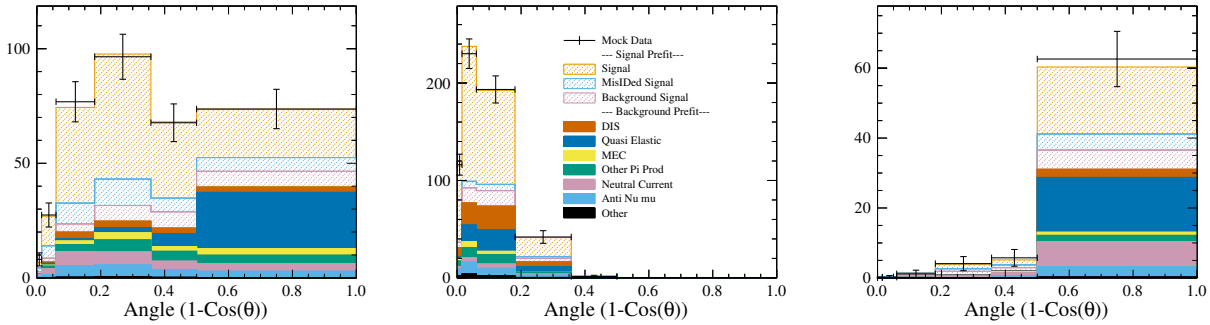

(a) Selected Kalman Contained **(b)** Selected Kalman Exiting **(c)** Selected Cluster

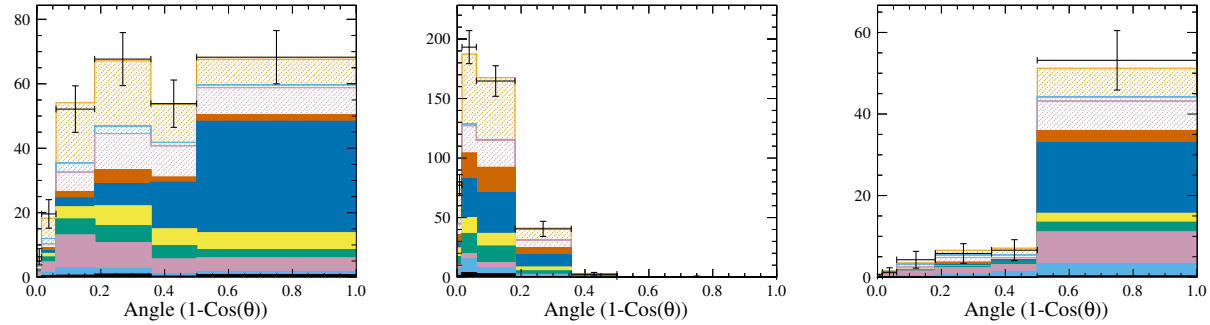

(d) Near Sideband Kalman Contained **(e)** Near Sideband Kalman Exiting **(f)** Near Sideband Cluster

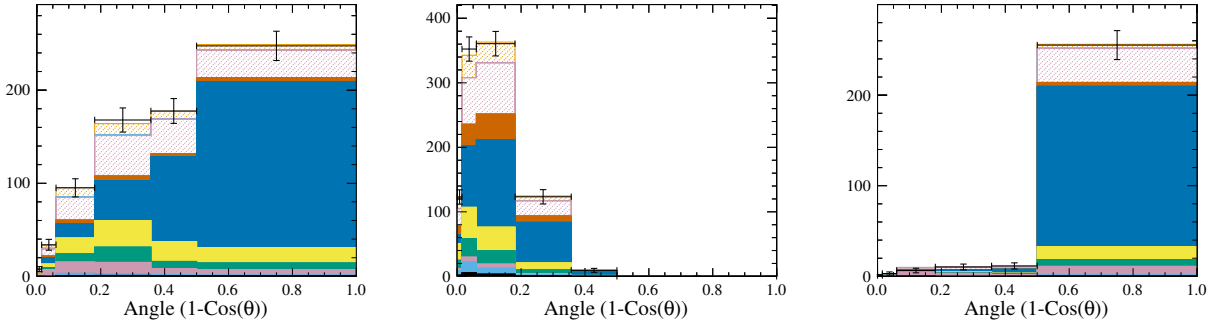

(g) Far Sideband Kalman Contained **(h)** Far Sideband Kalman Exiting **(i)** Far Sideband Cluster

Figure B.67: GENIE Signal - Mock Data with Post-Fit NEUT Templates - Angle Projection

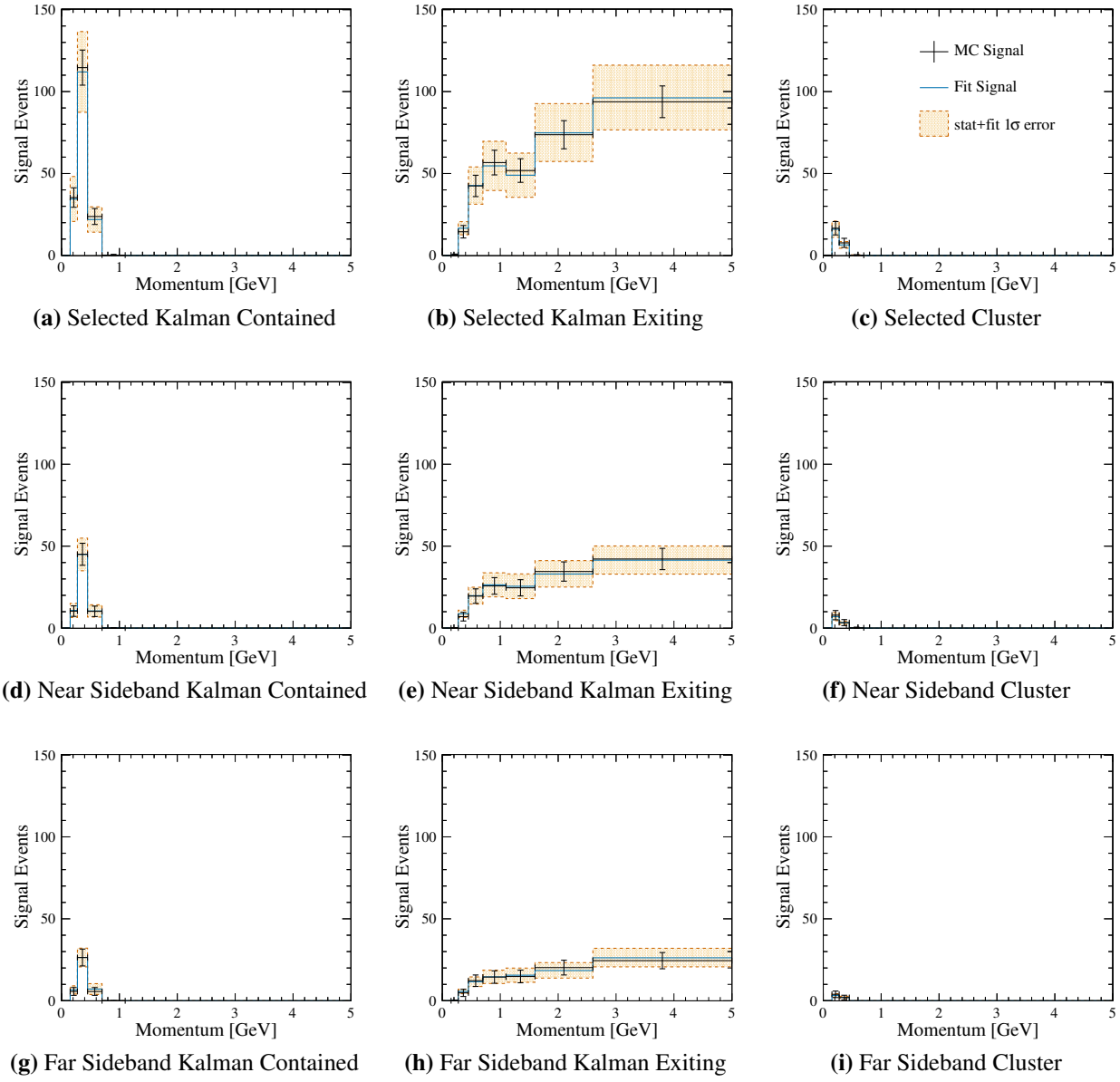

(a) Selected Kalman Contained **(b)** Selected Kalman Exiting **(c)** Selected Cluster

(d) Near Sideband Kalman Contained **(e)** Near Sideband Kalman Exiting **(f)** Near Sideband Cluster

(g) Far Sideband Kalman Contained **(h)** Far Sideband Kalman Exiting **(i)** Far Sideband Cluster

Figure B.68: GENIE Signal Study - Signal fit in the muon momentum projection. Black crosses represent the mock data with statistical error bars. The solid blue line is the best fit and the orange region is the error from the fit. - Momentum projection

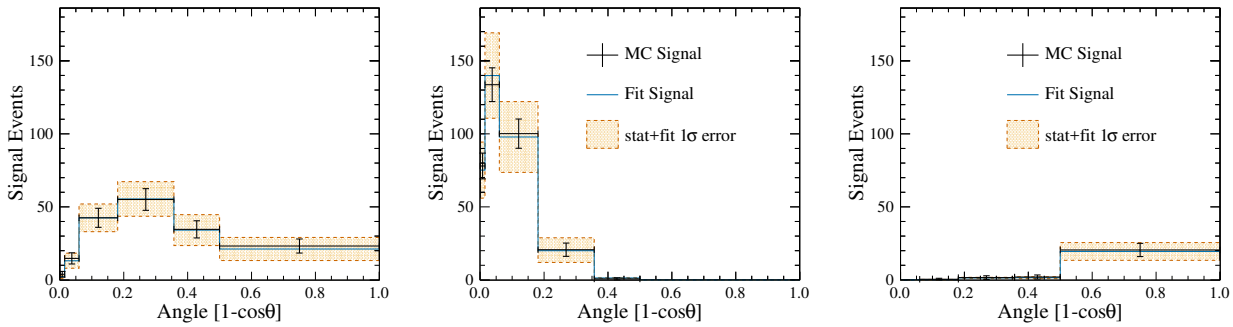

(a) Selected Kalman Contained **(b)** Selected Kalman Exiting **(c)** Selected Cluster

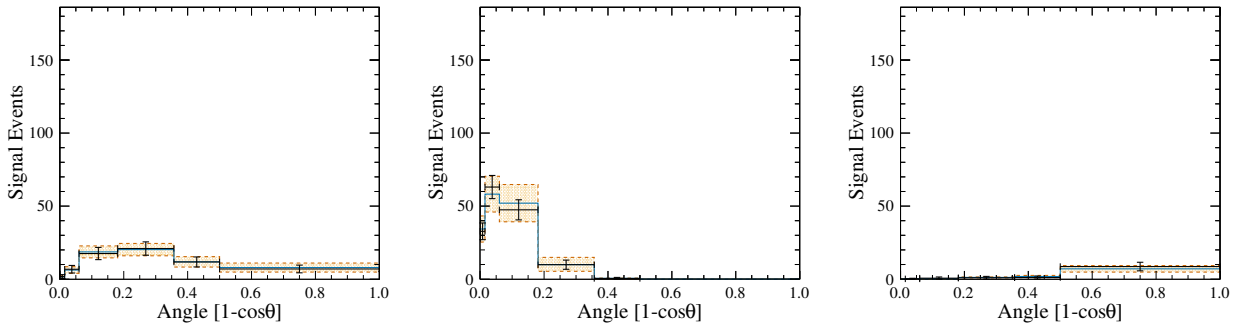

(d) Near Sideband Kalman Contained **(e)** Near Sideband Kalman Exiting **(f)** Near Sideband Cluster

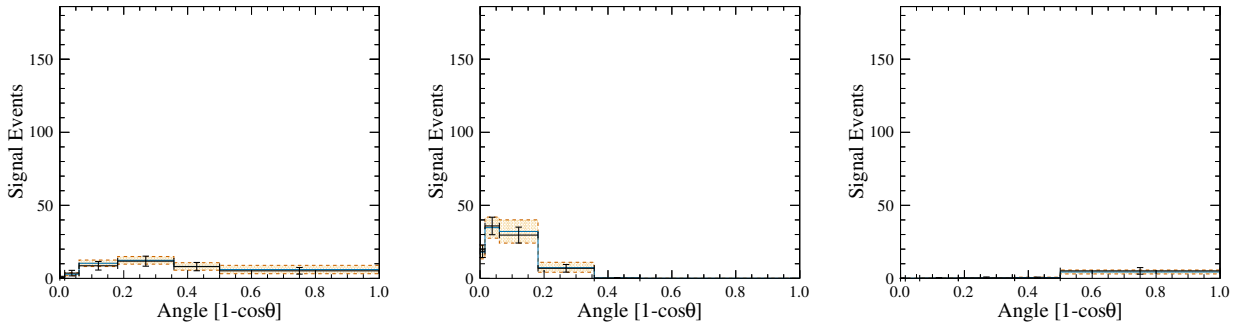

(g) Far Sideband Kalman Contained **(h)** Far Sideband Kalman Exiting **(i)** Far Sideband Cluster

Figure B.69: GENIE Signal Study - Signal fit in the muon angle projection. Black crosses represent the mock data with statistical error bars. The solid blue line is the best fit and the orange region is the error from the fit. - Angle projection

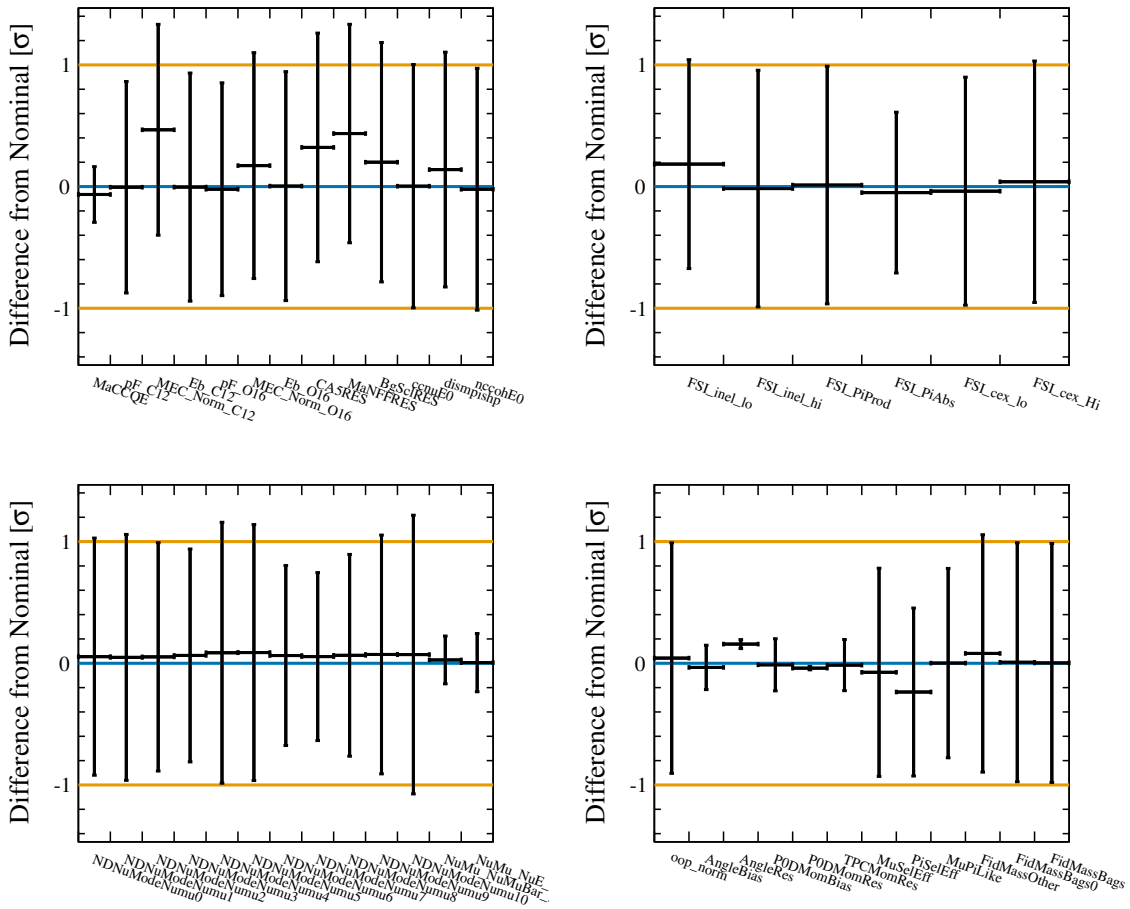

Figure B.70: GENIE Signal Study - Fit parameter deviation from nominal. The points in this plot are the best fit parameter value in units of sigma for each dial. The error bars on the points are the error on that parameter from the fit, while the orange lines at +1 and -1 represent the default one sigma error placed on the variable.

Plotted in Figures B.71 and B.72 are the mock data over the pre-fit NEUT templates, while Figures B.73 and B.74 are the mock data over the post-fit NEUT templates. The extracted signal is plotted in figures B.75 and B.76. The fit parameter deviations from nominal and error are plotted in figure B.77.

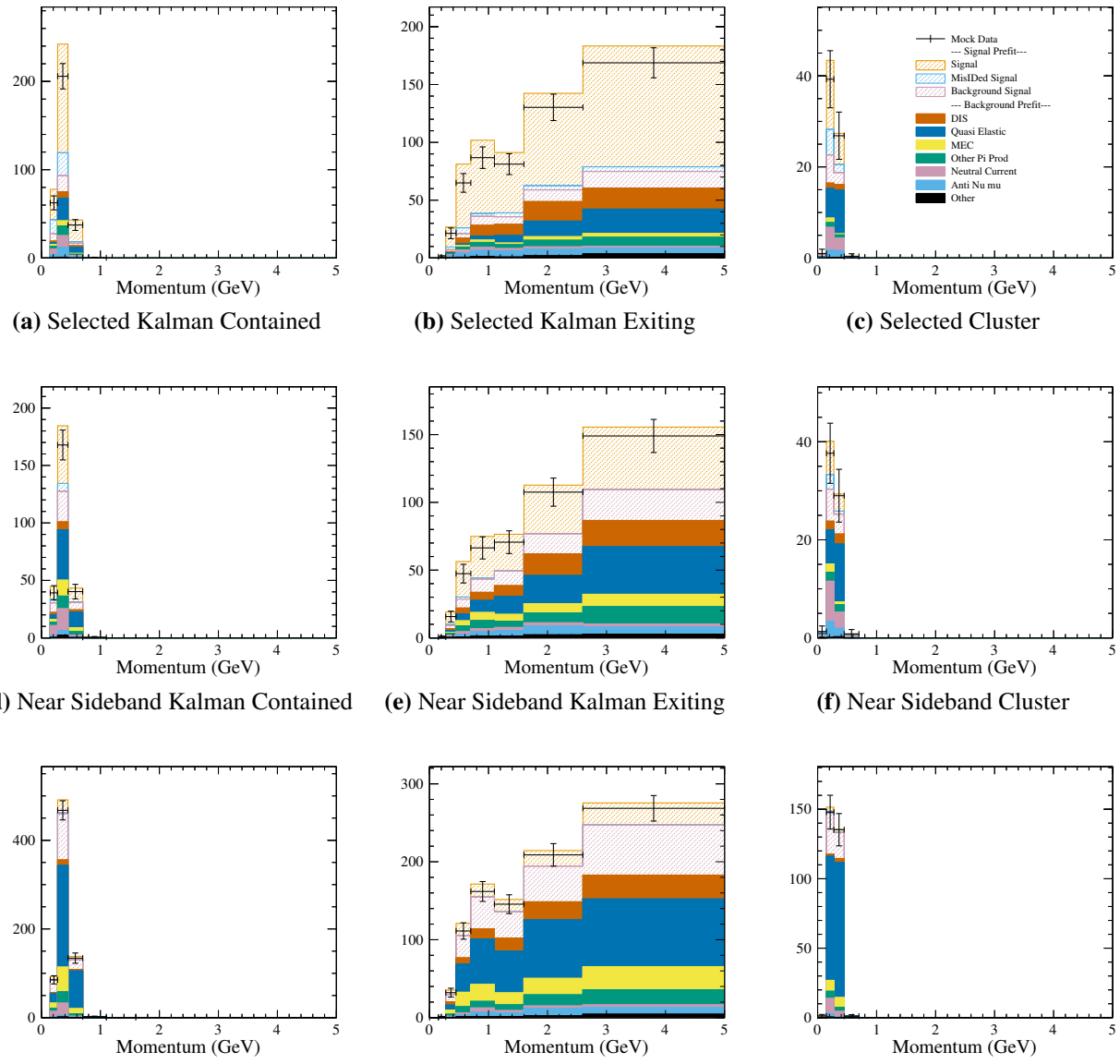

(a) Selected Kalman Contained **(b)** Selected Kalman Exiting **(c)** Selected Cluster

(d) Near Sideband Kalman Contained **(e)** Near Sideband Kalman Exiting **(f)** Near Sideband Cluster

(g) Far Sideband Kalman Contained **(h)** Far Sideband Kalman Exiting **(i)** Far Sideband Cluster

Figure B.71: Resonant Q^2 Distortion - Mock Data with Pre-Fit NEUT Templates - Momentum Projection

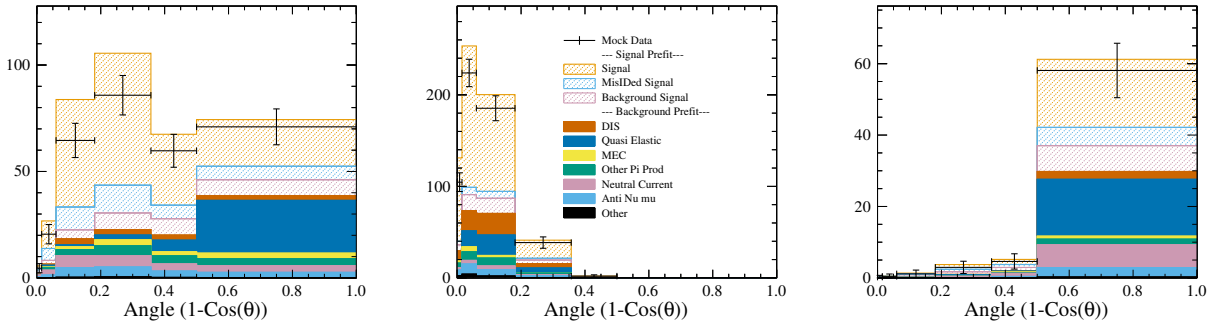

(a) Selected Kalman Contained **(b)** Selected Kalman Exiting **(c)** Selected Cluster

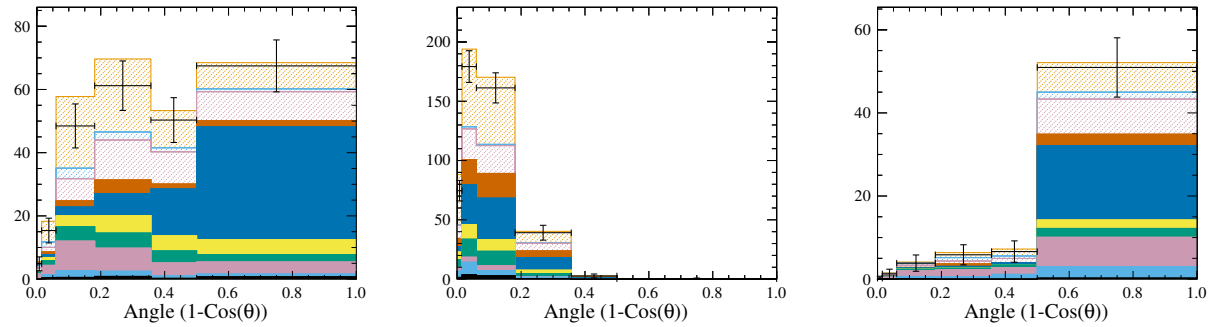

(d) Near Sideband Kalman Contained **(e)** Near Sideband Kalman Exiting **(f)** Near Sideband Cluster

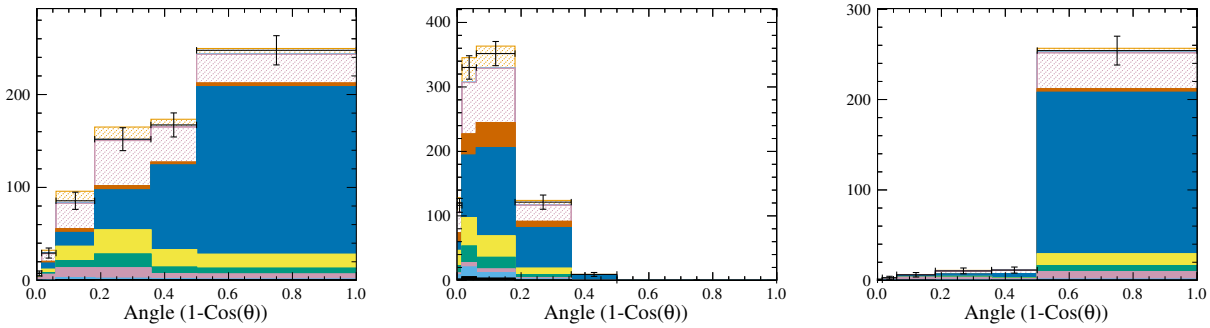

(g) Far Sideband Kalman Contained **(h)** Far Sideband Kalman Exiting **(i)** Far Sideband Cluster

Figure B.72: Resonant Q^2 Distortion - Mock Data with Pre-Fit NEUT Templates - Angle Projection

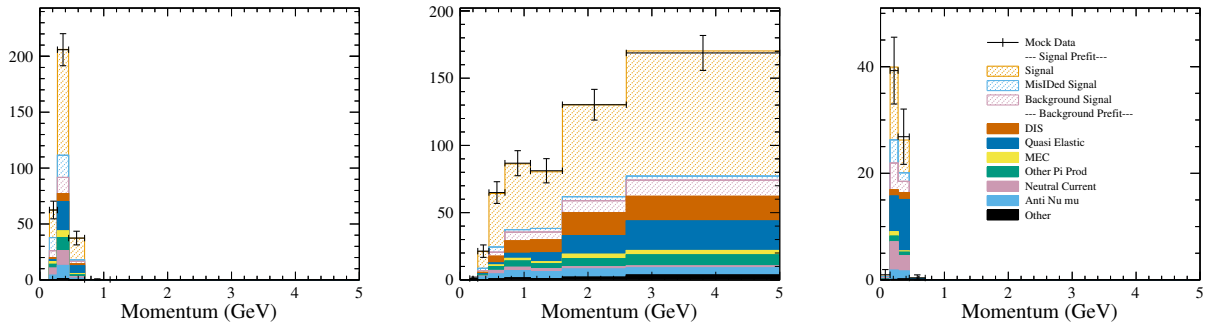

(a) Selected Kalman Contained **(b)** Selected Kalman Exiting **(c)** Selected Cluster

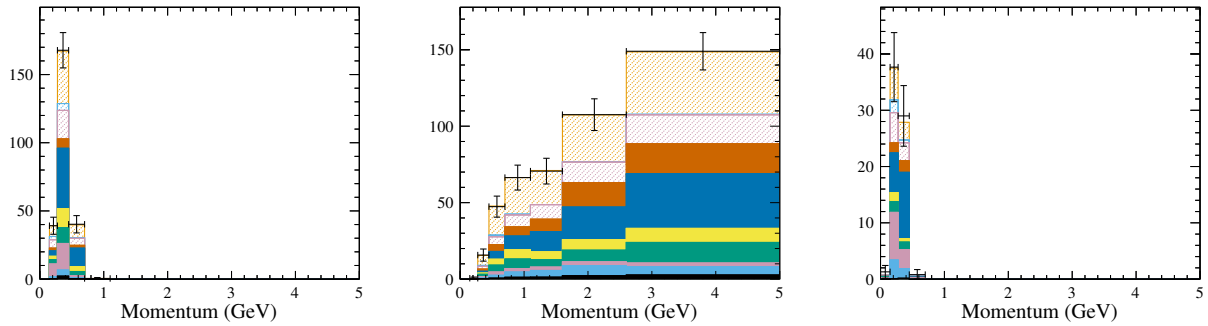

(d) Near Sideband Kalman Contained **(e)** Near Sideband Kalman Exiting **(f)** Near Sideband Cluster

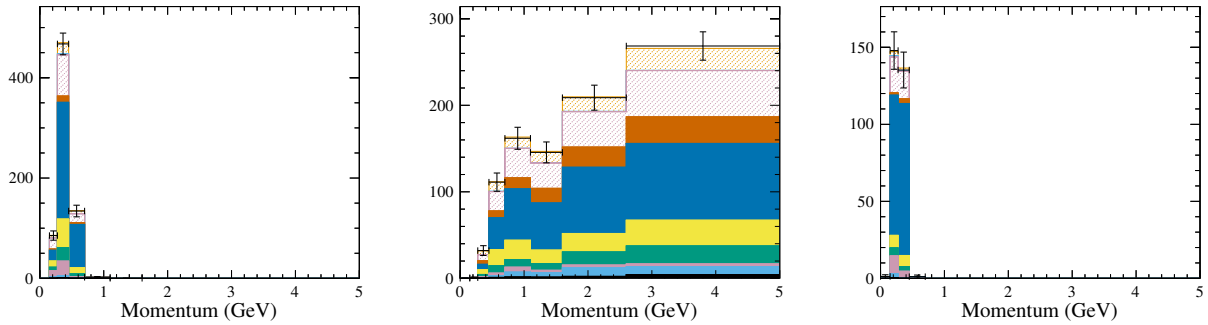

(g) Far Sideband Kalman Contained **(h)** Far Sideband Kalman Exiting **(i)** Far Sideband Cluster

Figure B.73: Resonant Q^2 Distortion - Mock Data with Post-Fit NEUT Templates - Momentum Projection

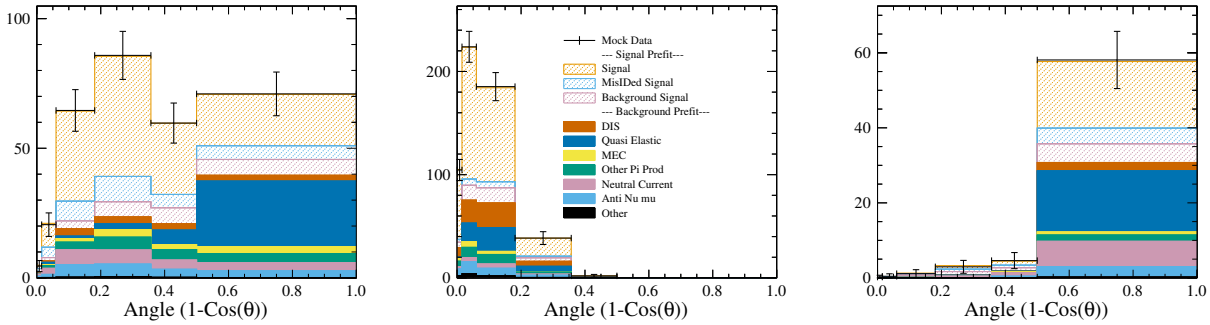

(a) Selected Kalman Contained **(b)** Selected Kalman Exiting **(c)** Selected Cluster

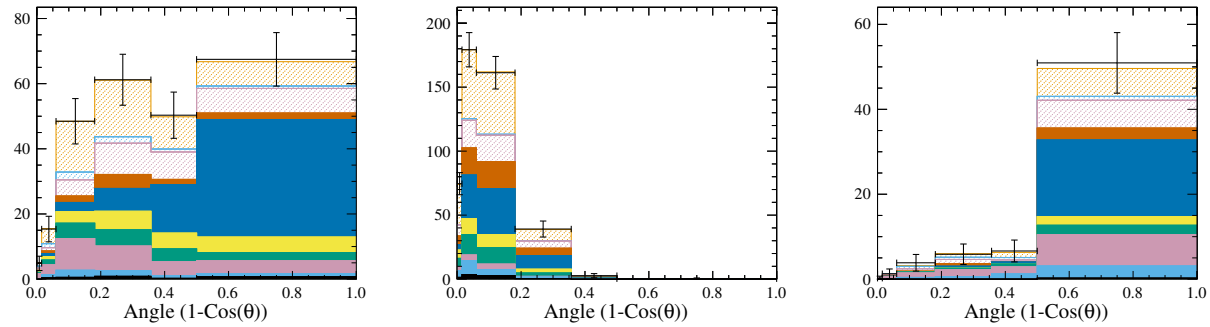

(d) Near Sideband Kalman Contained **(e)** Near Sideband Kalman Exiting **(f)** Near Sideband Cluster

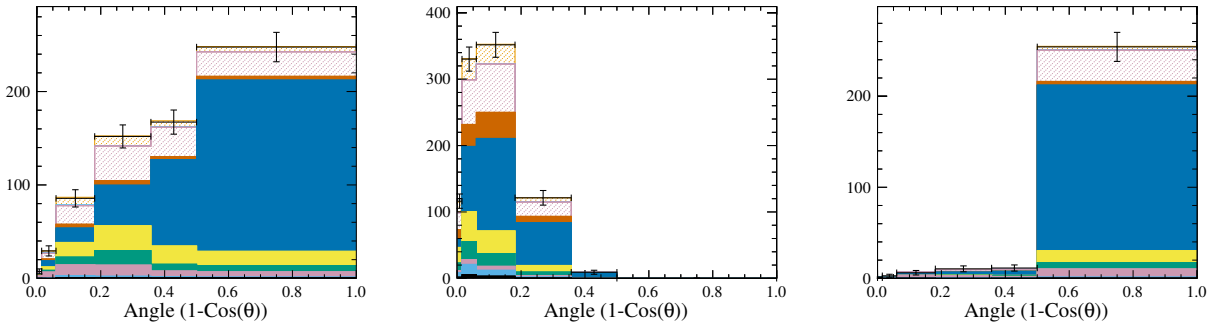

(g) Far Sideband Kalman Contained **(h)** Far Sideband Kalman Exiting **(i)** Far Sideband Cluster

Figure B.74: Resonant Q^2 Distortion - Mock Data with Post-Fit NEUT Templates - Angle Projection

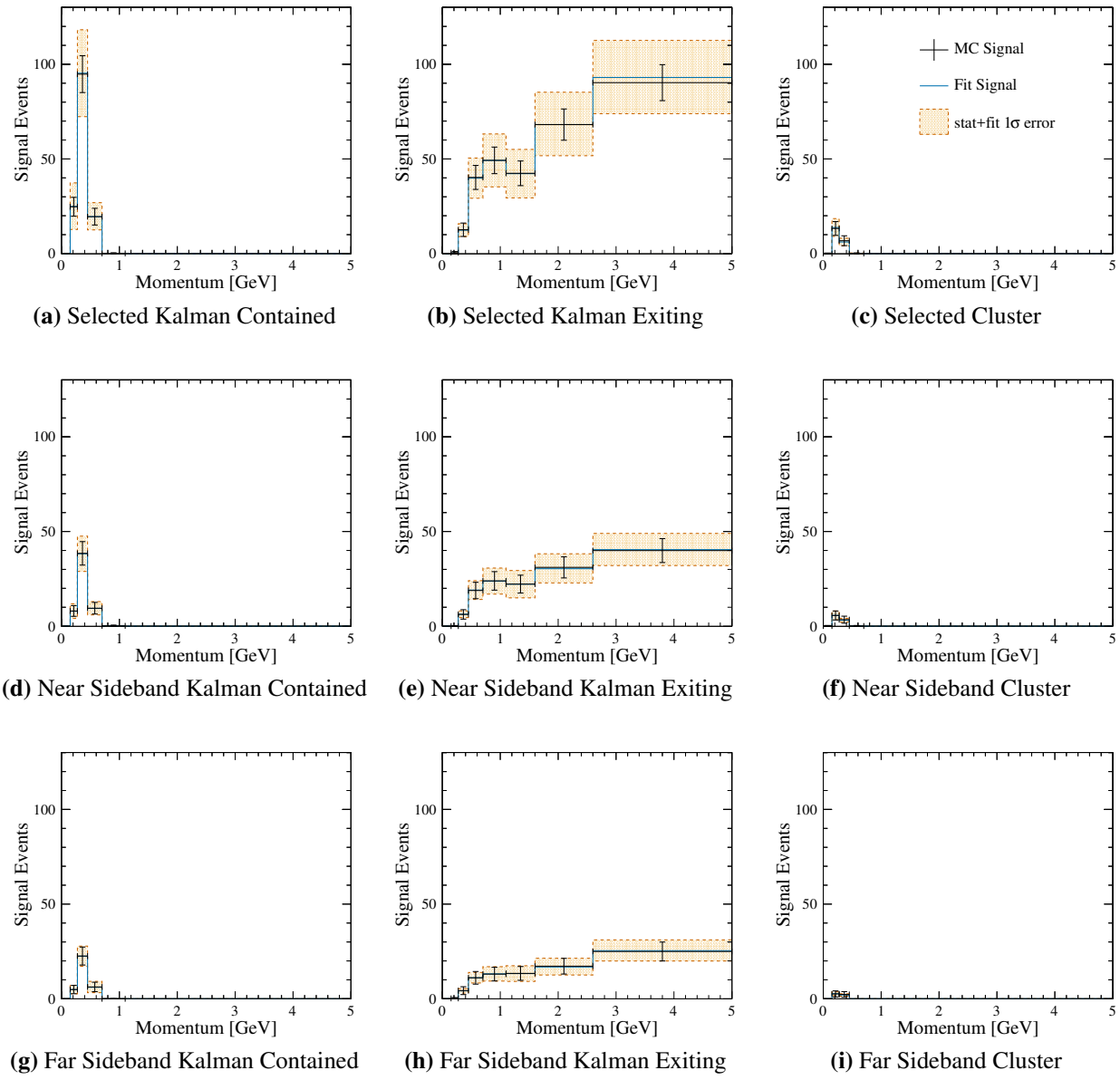

(a) Selected Kalman Contained **(b)** Selected Kalman Exiting **(c)** Selected Cluster

(d) Near Sideband Kalman Contained **(e)** Near Sideband Kalman Exiting **(f)** Near Sideband Cluster

(g) Far Sideband Kalman Contained **(h)** Far Sideband Kalman Exiting **(i)** Far Sideband Cluster

Figure B.75: Resonant Q^2 Distortion Study - Background fit in the muon momentum projection. Black crosses represent the mock data with statistical error bars. The solid blue line is the best fit and the orange region is the error from the fit. - Momentum projection

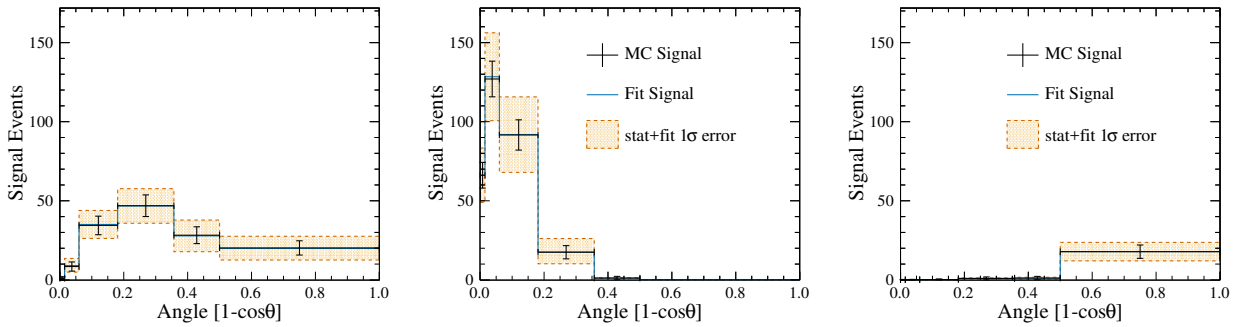

(a) Selected Kalman Contained **(b)** Selected Kalman Exiting **(c)** Selected Cluster

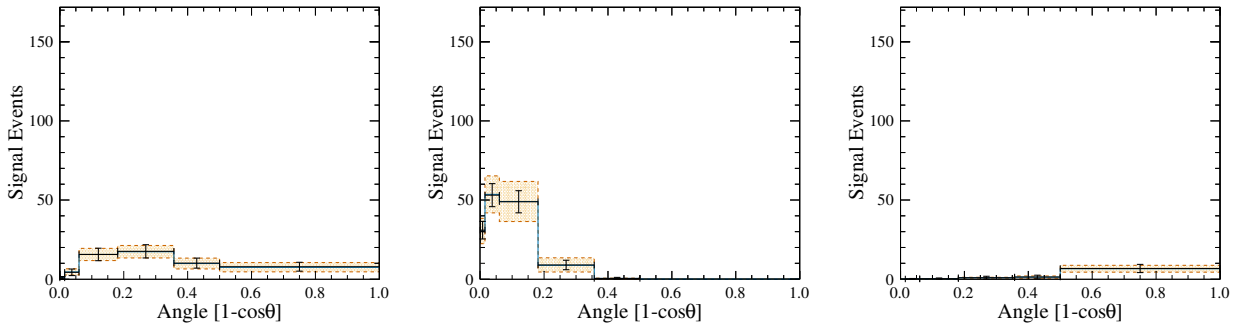

(d) Near Sideband Kalman Contained **(e)** Near Sideband Kalman Exiting **(f)** Near Sideband Cluster

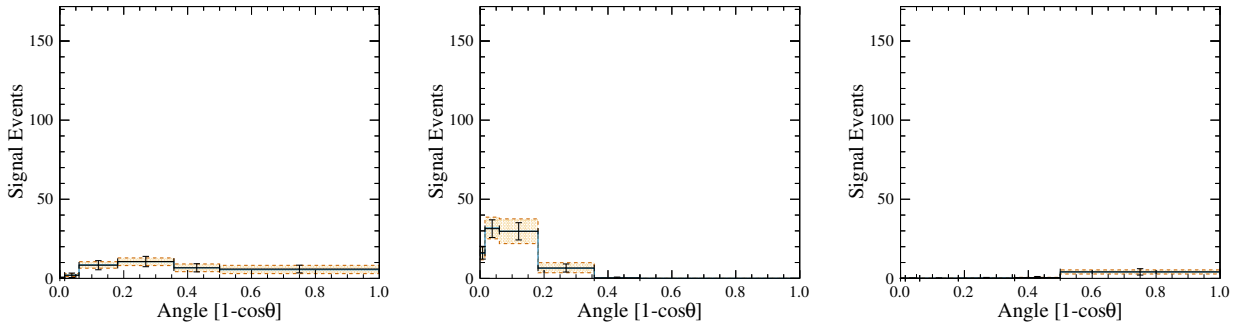

(g) Far Sideband Kalman Contained **(h)** Far Sideband Kalman Exiting **(i)** Far Sideband Cluster

Figure B.76: Resonant Q^2 Distortion Study - Background fit in the muon angle projection. Black crosses represent the mock data with statistical error bars. The solid blue line is the best fit and the orange region is the error from the fit. - Angle projection

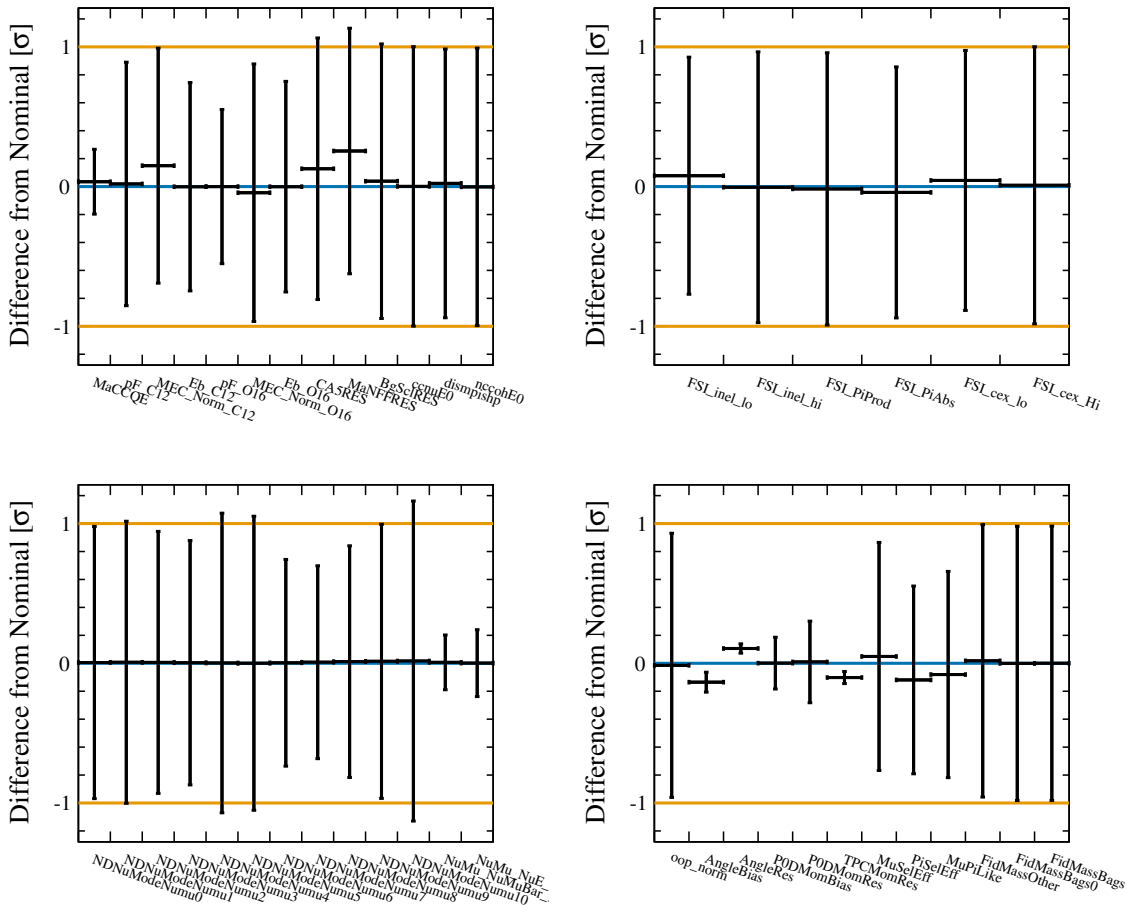

Figure B.77: Resonant Q^2 Distortion Study - Fit parameter deviation from nominal. The points in this plot are the best fit parameter value in units of sigma for each dial. The error bars on the points are the error on that parameter from the fit, while the orange lines at +1 and -1 represent the default one sigma error placed on the variable.

B.5 Mock Data Tests With New Background Physics Models

Adjusting the background models provides a test for the fitter for modes in which varying the fit parameters can not exactly equate the mock data. These fits are important to show the ability of the fitter to fit backgrounds that are different from the default templates and ensure there is enough freedom in the fits.

B.5.1 Spectral Function to RFG with RPA

Two dials are used in conjunction for this test: the Spectral Function to RPA dial as well as the RPA dial. This is one example of a shift in the background by a dial that is not also a fit parameter, and the performance shows the fitter's ability to adapt to data that is different from the NEUT templates and fit parameters.

Plotted in Figures B.78 and B.79 are the mock data over the pre-fit NEUT templates, while Figures B.80 and B.81 are the mock data over the post-fit NEUT templates. The extracted signal is plotted in figures B.82 and B.83. The fit parameter deviations from nominal and error are plotted in figure B.84.

B.5.2 GENIE Background

For this study the Mock Data is made using the GENIE templates for the backgrounds instead of the default NEUT. The same method for generating GENIE signal was used to generate templates for GENIE background.

Plotted in Figures B.85 and B.86 are the mock data over the pre-fit NEUT templates, while Figures B.87 and B.88 are the mock data over the post-fit NEUT templates. The extracted signal is plotted in figures B.89 and B.90. The fit parameter deviations from nominal and error are plotted in figure B.91.

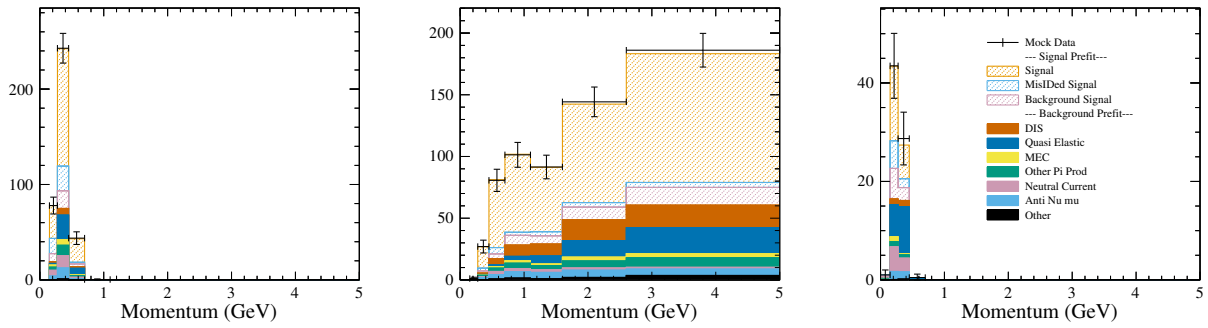

(a) Selected Kalman Contained **(b)** Selected Kalman Exiting **(c)** Selected Cluster

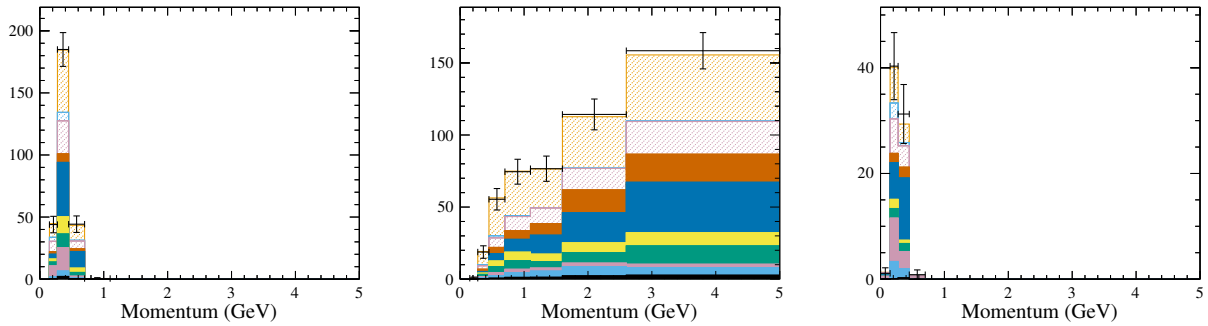

(d) Near Sideband Kalman Contained **(e)** Near Sideband Kalman Exiting **(f)** Near Sideband Cluster

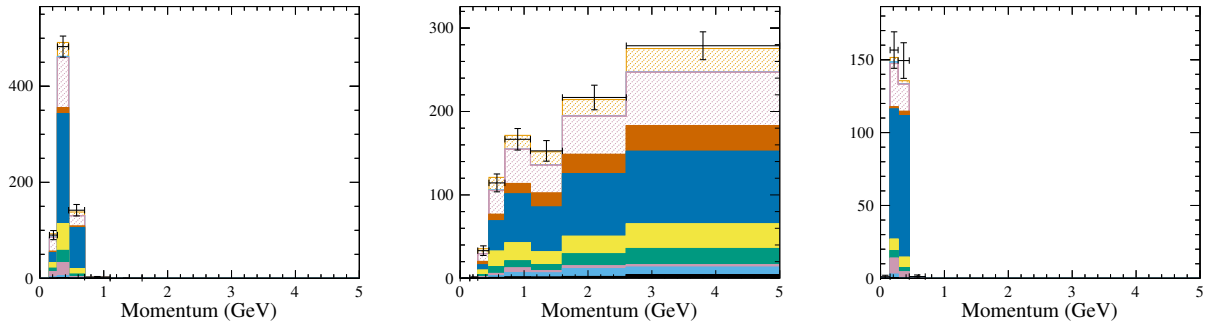

(g) Far Sideband Kalman Contained **(h)** Far Sideband Kalman Exiting **(i)** Far Sideband Cluster

Figure B.78: CCQE Model - Mock Data with Pre-Fit NEUT Templates - Momentum Projection

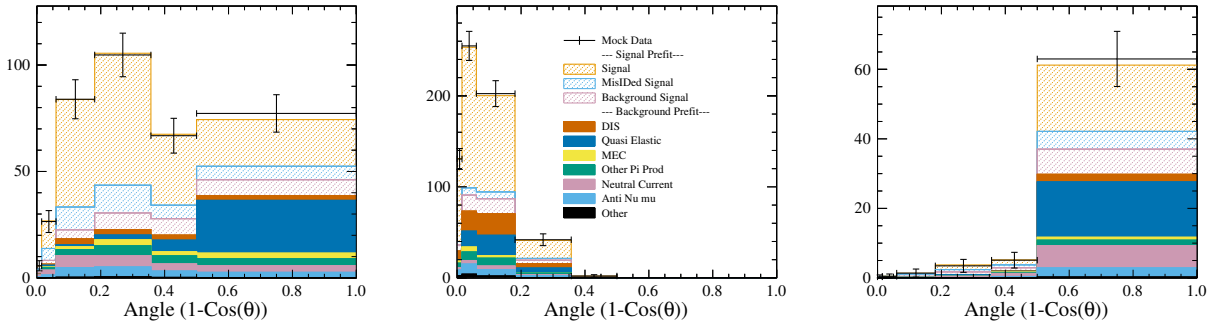

(a) Selected Kalman Contained **(b)** Selected Kalman Exiting **(c)** Selected Cluster

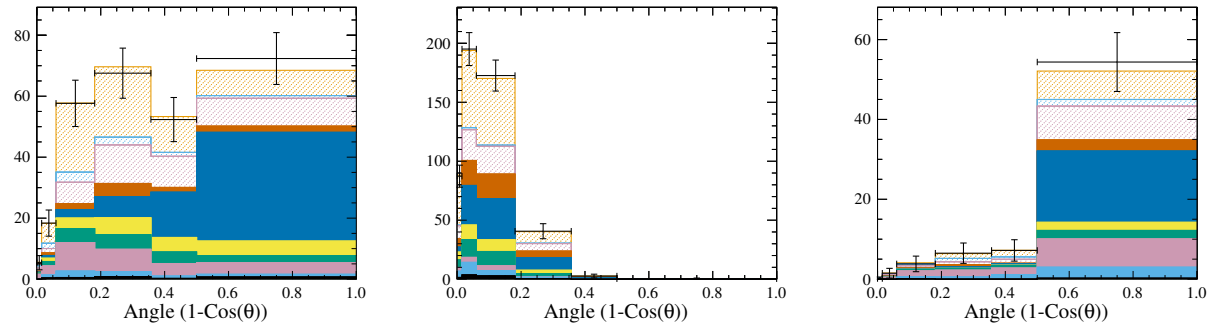

(d) Near Sideband Kalman Contained **(e)** Near Sideband Kalman Exiting **(f)** Near Sideband Cluster

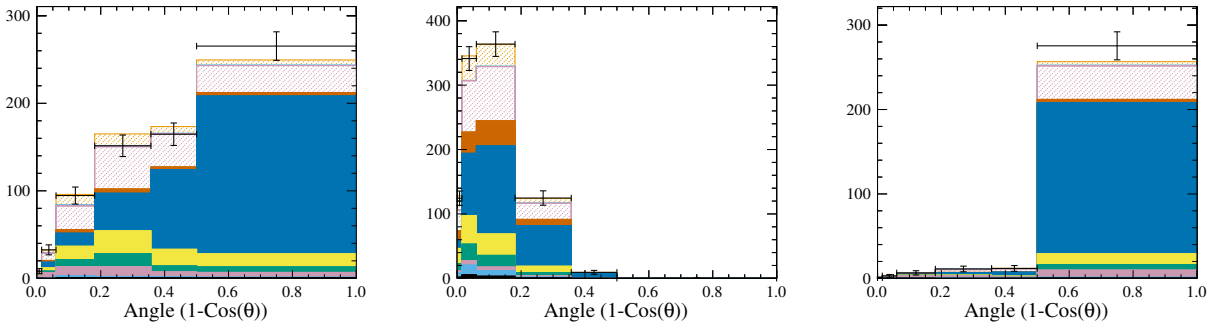

(g) Far Sideband Kalman Contained **(h)** Far Sideband Kalman Exiting **(i)** Far Sideband Cluster

Figure B.79: CCQE Model - Mock Data with Pre-Fit NEUT Templates - Angle Projection

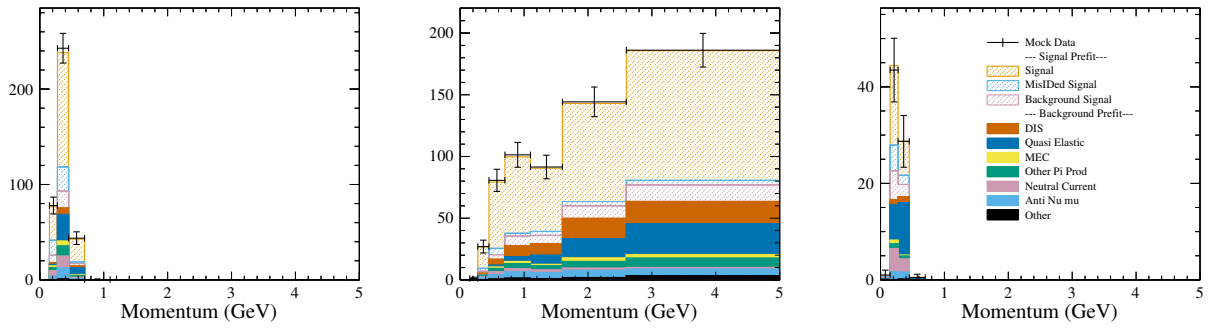

(a) Selected Kalman Contained **(b)** Selected Kalman Exiting **(c)** Selected Cluster

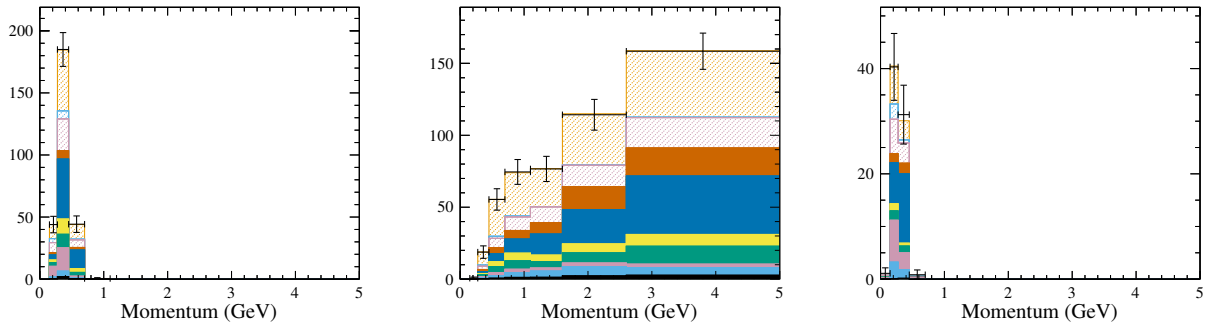

(d) Near Sideband Kalman Contained **(e)** Near Sideband Kalman Exiting **(f)** Near Sideband Cluster

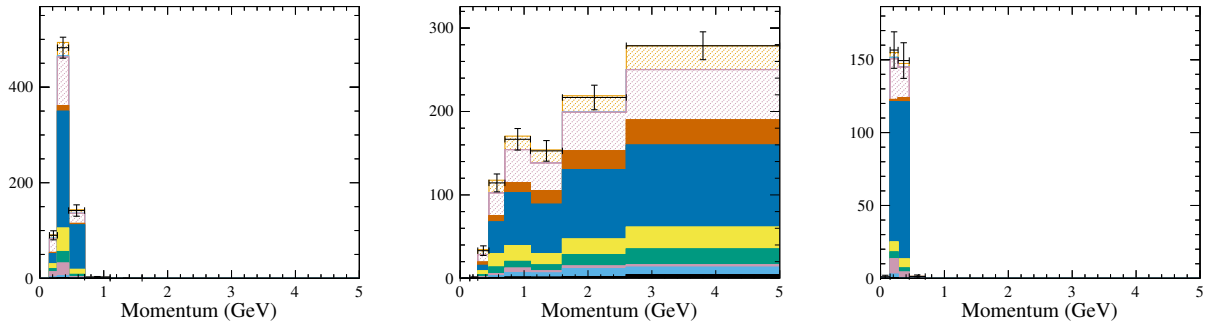

(g) Far Sideband Kalman Contained **(h)** Far Sideband Kalman Exiting **(i)** Far Sideband Cluster

Figure B.80: CCQE Model - Mock Data with Post-Fit NEUT Templates - Momentum Projection

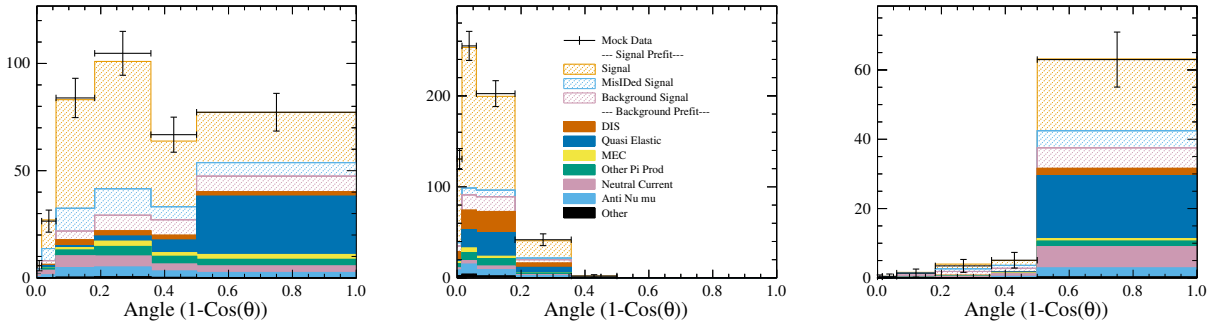

(a) Selected Kalman Contained **(b)** Selected Kalman Exiting **(c)** Selected Cluster

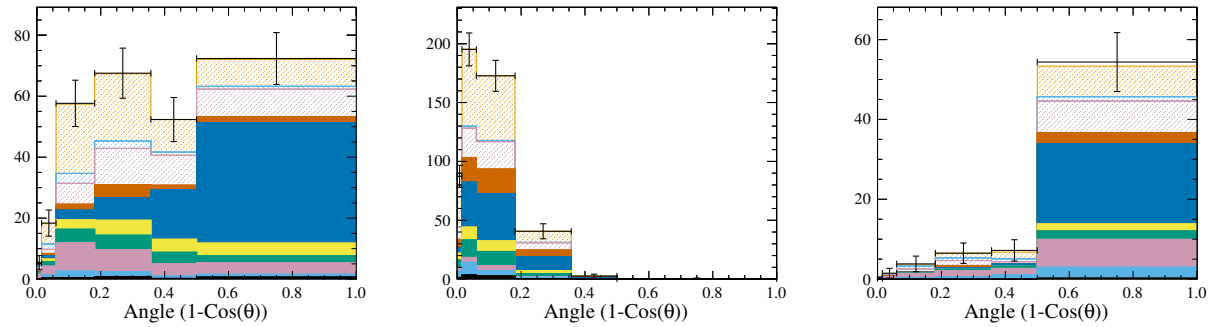

(d) Near Sideband Kalman Contained **(e)** Near Sideband Kalman Exiting **(f)** Near Sideband Cluster

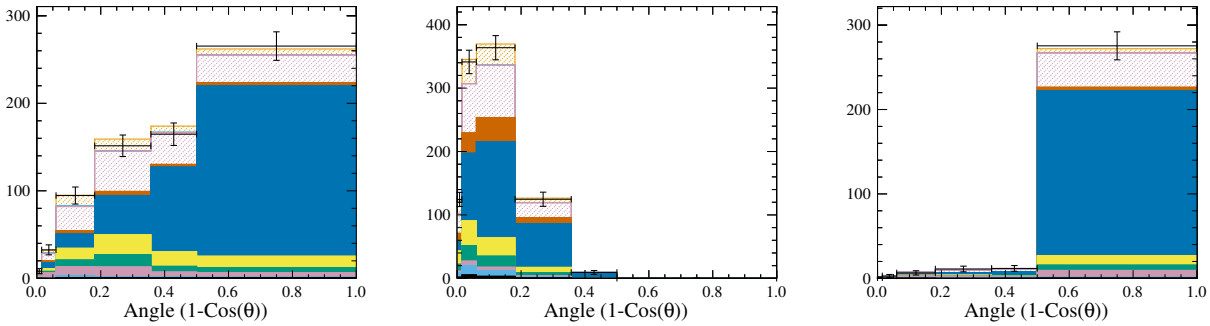

(g) Far Sideband Kalman Contained **(h)** Far Sideband Kalman Exiting **(i)** Far Sideband Cluster

Figure B.81: CCQE Model - Mock Data with Post-Fit NEUT Templates - Angle Projection

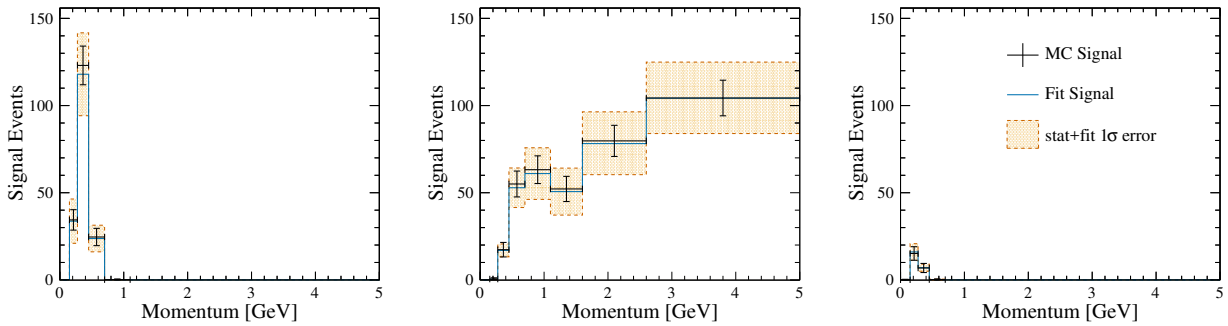

(a) Selected Kalman Contained **(b)** Selected Kalman Exiting **(c)** Selected Cluster

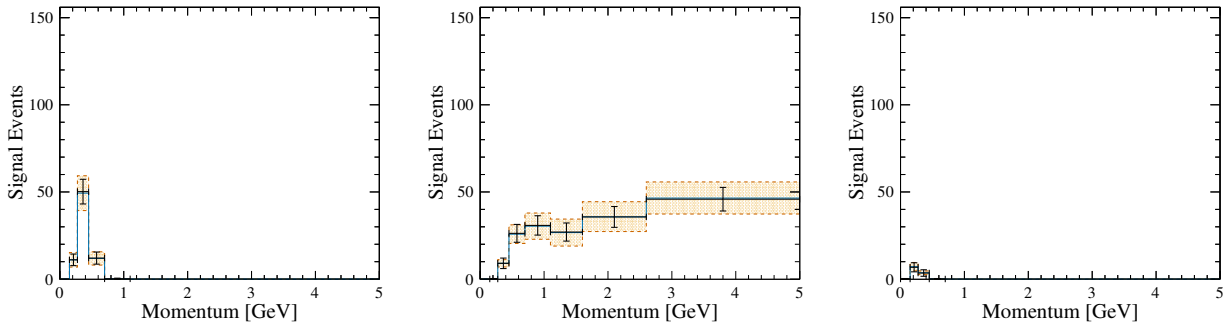

(d) Near Sideband Kalman Contained **(e)** Near Sideband Kalman Exiting **(f)** Near Sideband Cluster

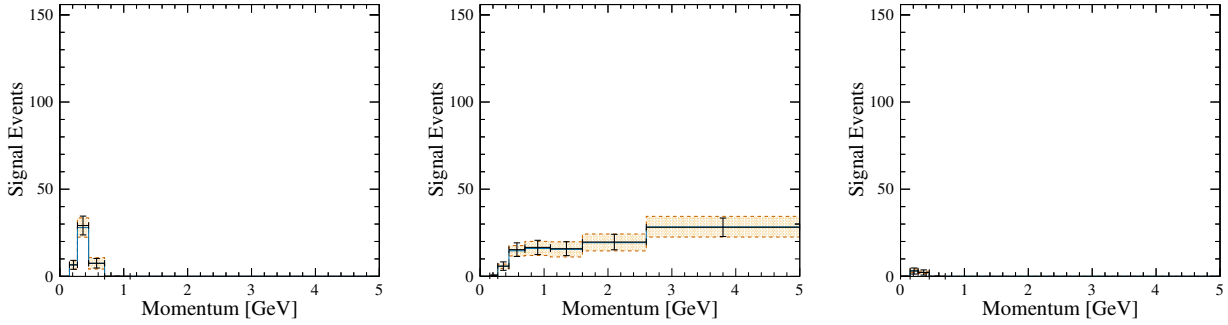

(g) Far Sideband Kalman Contained **(h)** Far Sideband Kalman Exiting **(i)** Far Sideband Cluster

Figure B.82: CCQE Model Study - Signal fit in the muon momentum projection. Black crosses represent the mock data with statistical error bars. The solid blue line is the best fit and the orange region is the error from the fit. - Momentum projection

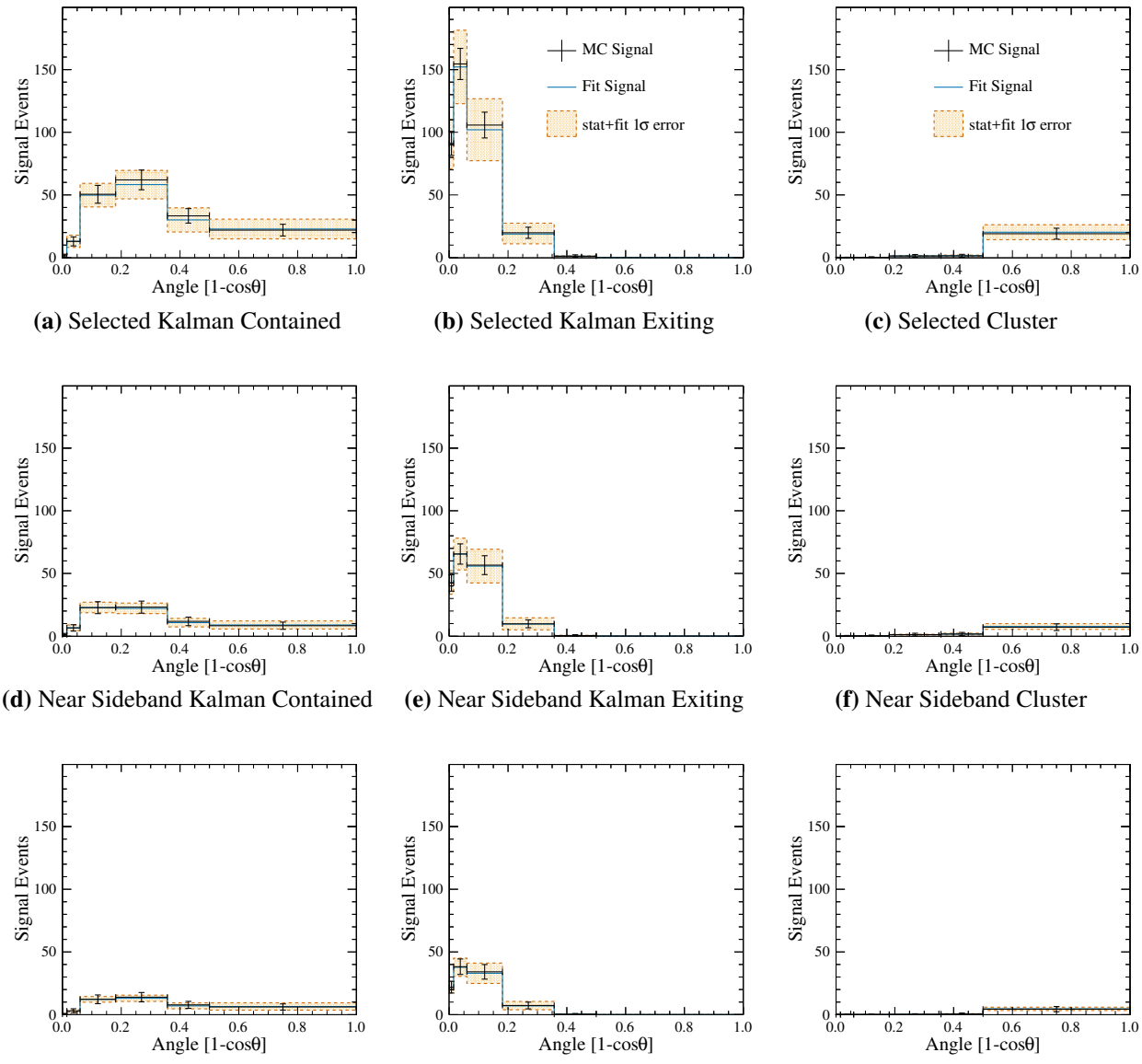

(a) Selected Kalman Contained **(b)** Selected Kalman Exiting **(c)** Selected Cluster

(d) Near Sideband Kalman Contained **(e)** Near Sideband Kalman Exiting **(f)** Near Sideband Cluster

(g) Far Sideband Kalman Contained **(h)** Far Sideband Kalman Exiting **(i)** Far Sideband Cluster

Figure B.83: CCQE Model Study - Signal fit in the muon angle projection. Black crosses represent the mock data with statistical error bars. The solid blue line is the best fit and the orange region is the error from the fit. - Angle projection

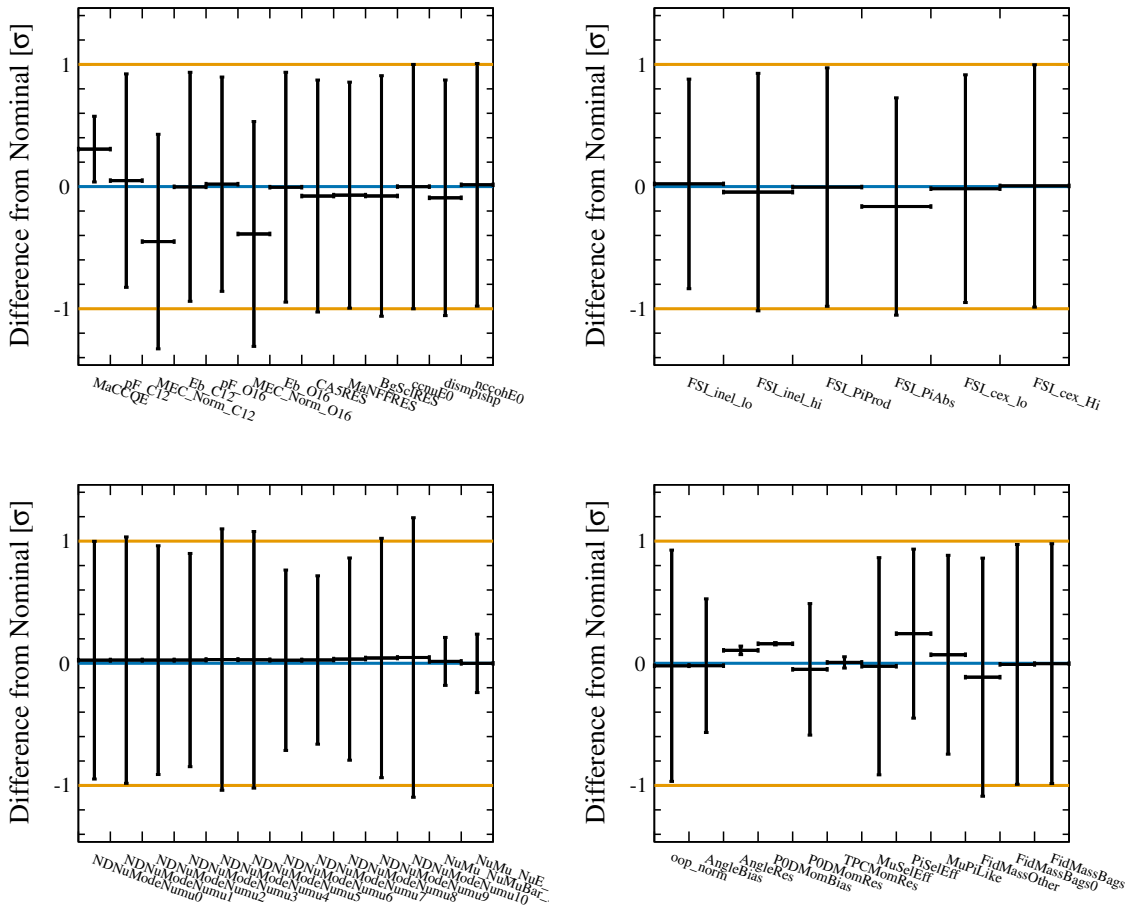

Figure B.84: CCQE Model Study - Fit parameter deviation from nominal. The points in this plot are the best fit parameter value in units of sigma for each dial. The error bars on the points are the error on that parameter from the fit, while the orange lines at +1 and -1 represent the default one sigma error placed on the variable.

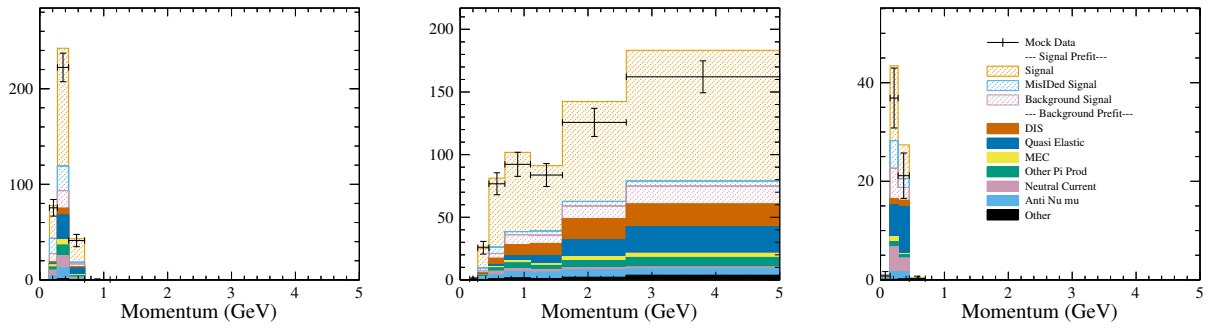

(a) Selected Kalman Contained **(b)** Selected Kalman Exiting **(c)** Selected Cluster

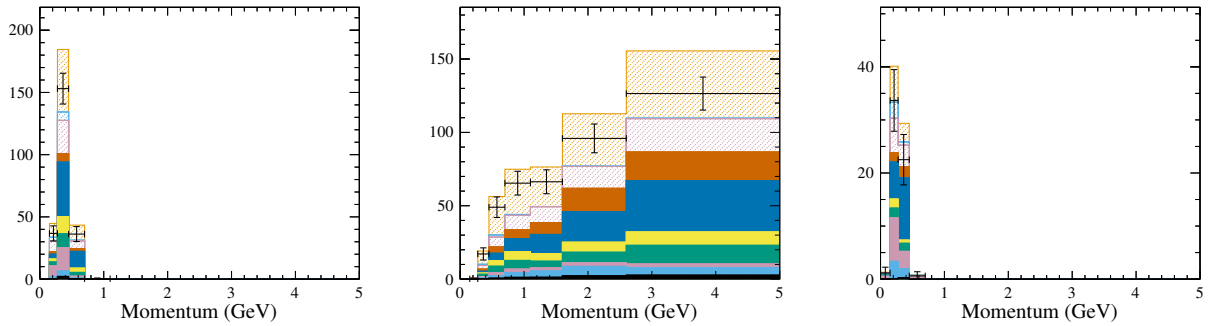

(d) Near Sideband Kalman Contained **(e)** Near Sideband Kalman Exiting **(f)** Near Sideband Cluster

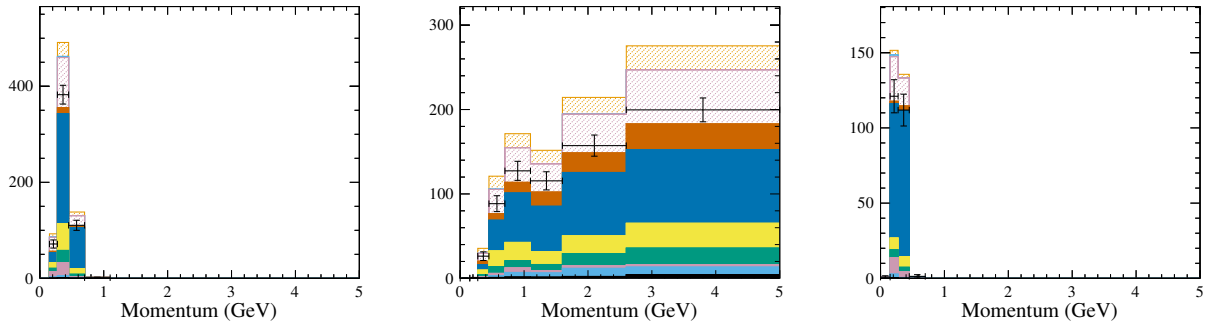

(g) Far Sideband Kalman Contained **(h)** Far Sideband Kalman Exiting **(i)** Far Sideband Cluster

Figure B.85: GENIE Background - Mock Data with Pre-Fit NEUT Templates - Momentum Projection

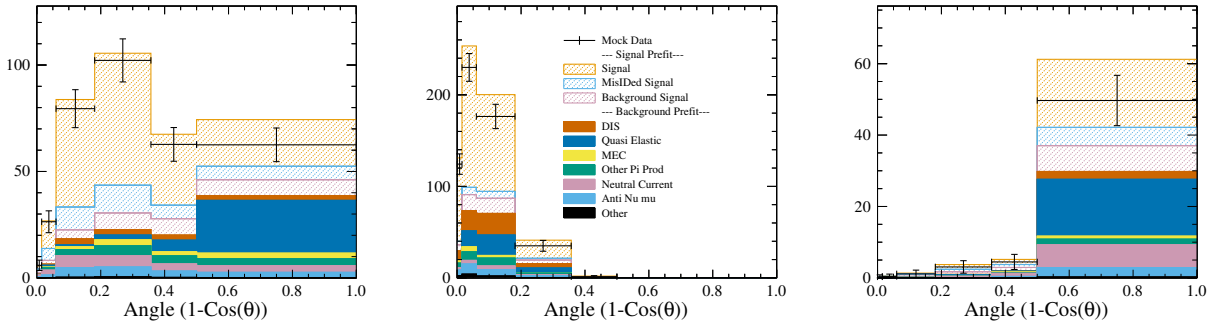

(a) Selected Kalman Contained **(b)** Selected Kalman Exiting **(c)** Selected Cluster

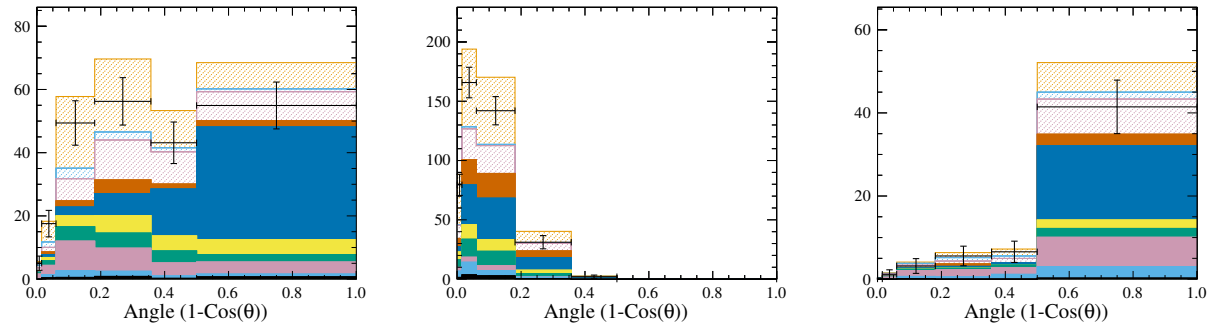

(d) Near Sideband Kalman Contained **(e)** Near Sideband Kalman Exiting **(f)** Near Sideband Cluster

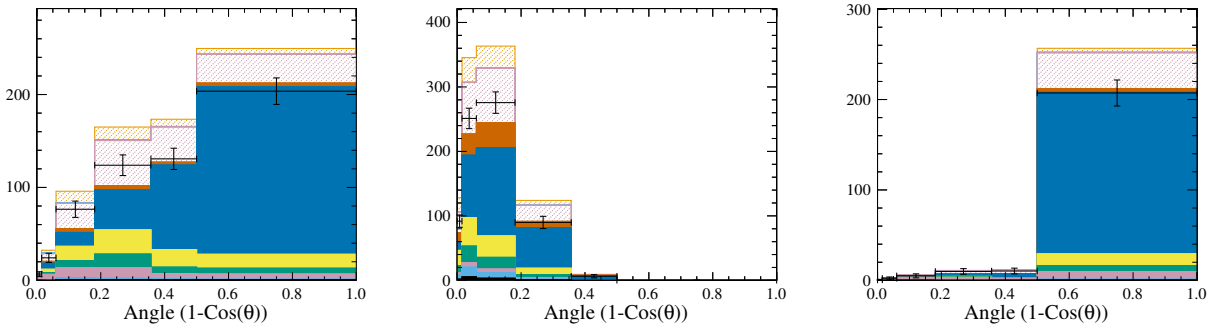

(g) Far Sideband Kalman Contained **(h)** Far Sideband Kalman Exiting **(i)** Far Sideband Cluster

Figure B.86: GENIE Background - Mock Data with Pre-Fit NEUT Templates - Angle Projection

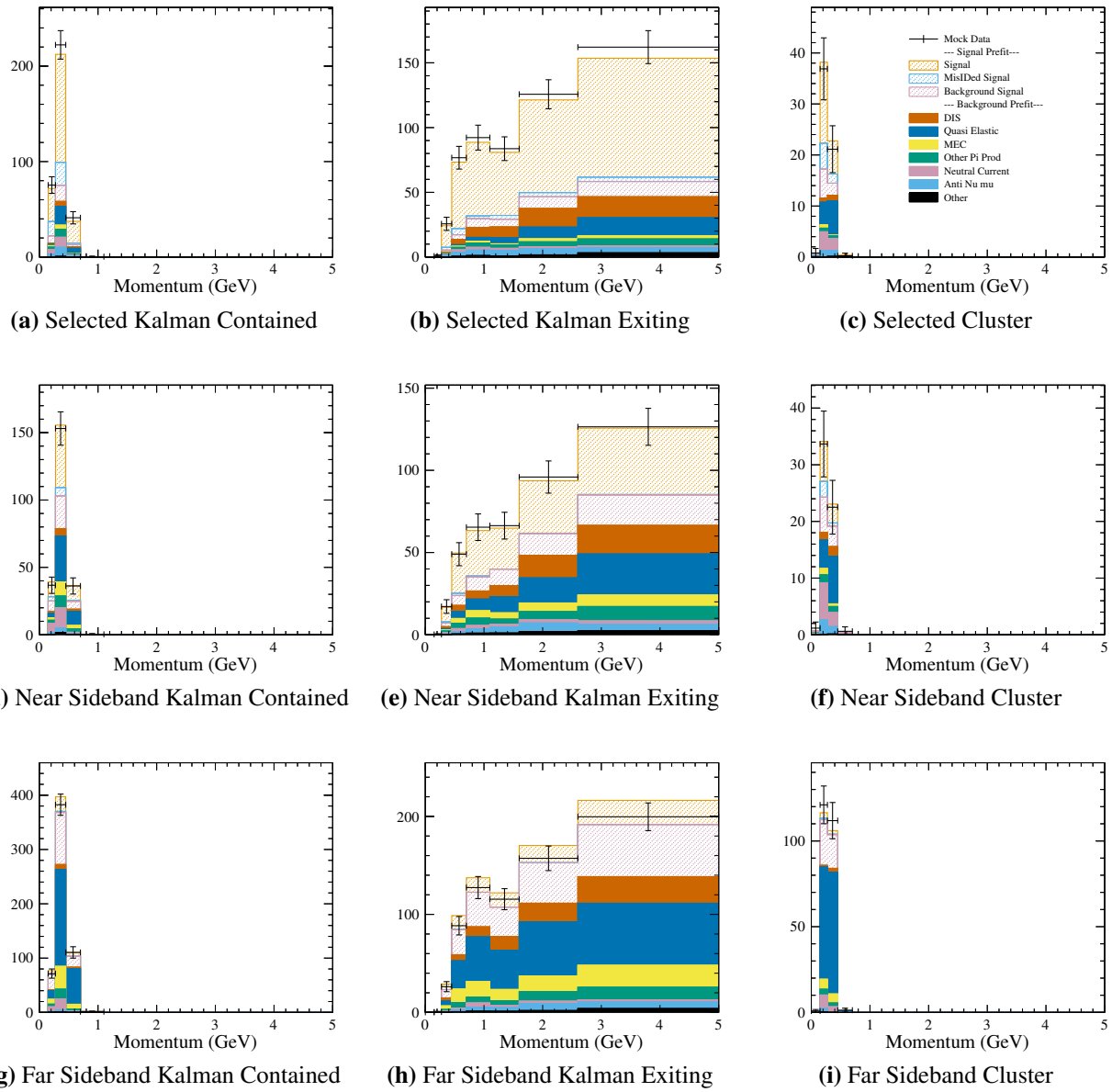

(a) Selected Kalman Contained **(b)** Selected Kalman Exiting **(c)** Selected Cluster

(d) Near Sideband Kalman Contained **(e)** Near Sideband Kalman Exiting **(f)** Near Sideband Cluster

(g) Far Sideband Kalman Contained **(h)** Far Sideband Kalman Exiting **(i)** Far Sideband Cluster

Figure B.87: GENIE Background - Mock Data with Post-Fit NEUT Templates - Momentum Projection

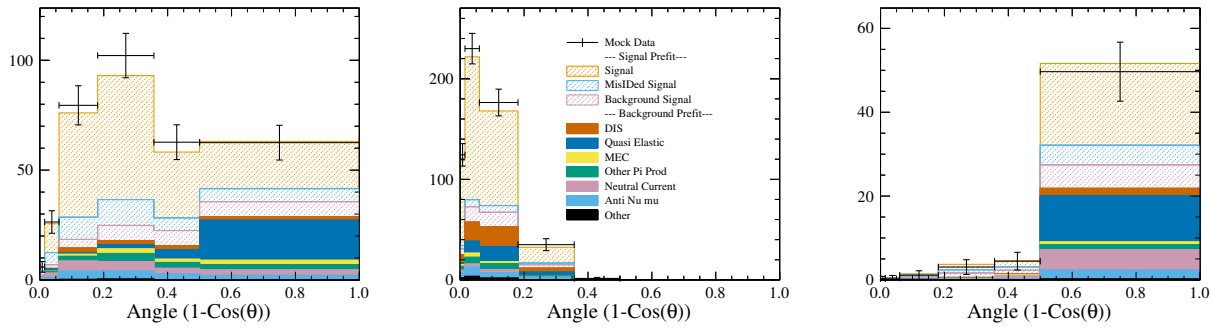

(a) Selected Kalman Contained **(b)** Selected Kalman Exiting **(c)** Selected Cluster

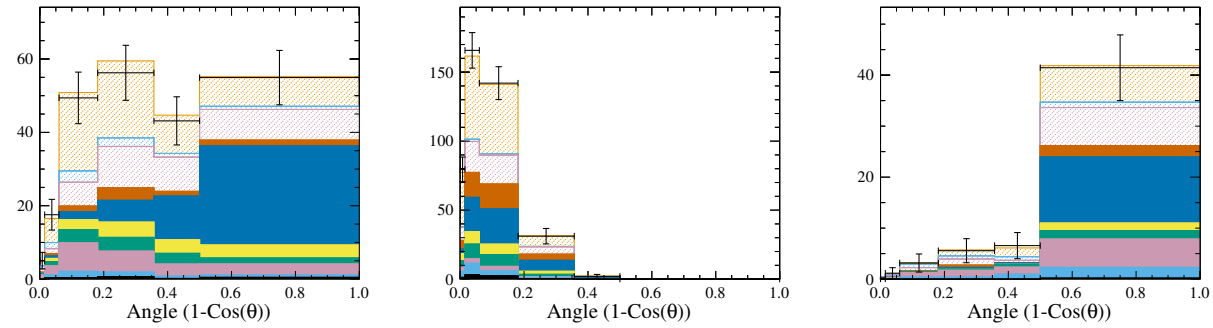

(d) Near Sideband Kalman Contained **(e)** Near Sideband Kalman Exiting **(f)** Near Sideband Cluster

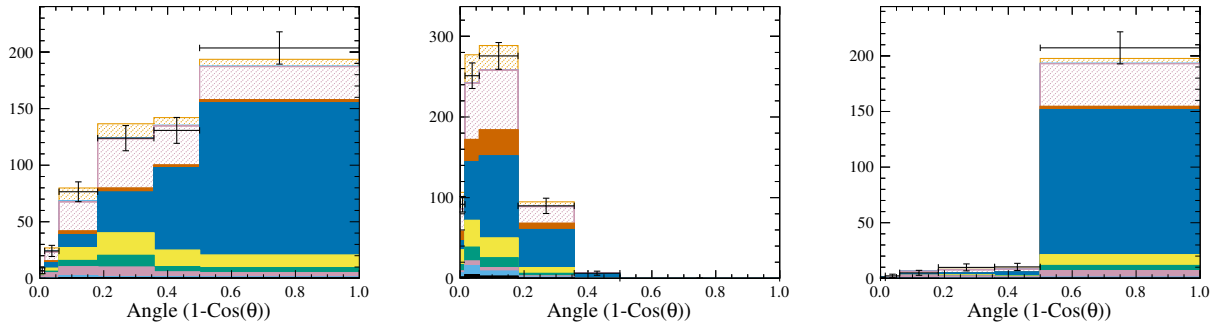

(g) Far Sideband Kalman Contained **(h)** Far Sideband Kalman Exiting **(i)** Far Sideband Cluster

Figure B.88: GENIE Background - Mock Data with Post-Fit NEUT Templates - Angle Projection

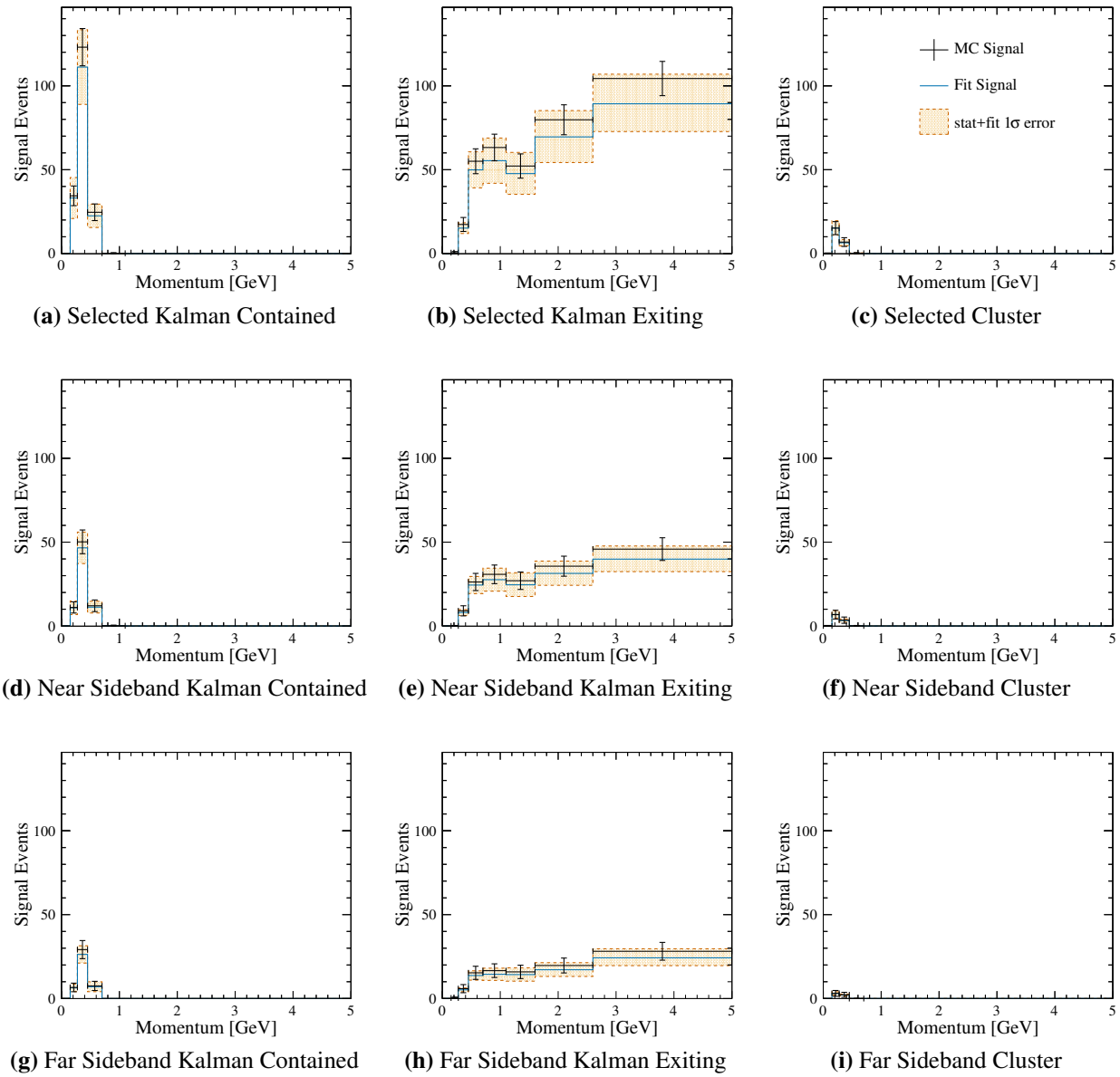

(a) Selected Kalman Contained **(b)** Selected Kalman Exiting **(c)** Selected Cluster

(d) Near Sideband Kalman Contained **(e)** Near Sideband Kalman Exiting **(f)** Near Sideband Cluster

(g) Far Sideband Kalman Contained **(h)** Far Sideband Kalman Exiting **(i)** Far Sideband Cluster

Figure B.89: GENIE Background Study - Background fit in the muon momentum projection. Black crosses represent the mock data with statistical error bars. The solid blue line is the best fit and the orange region is the error from the fit. - Momentum projection

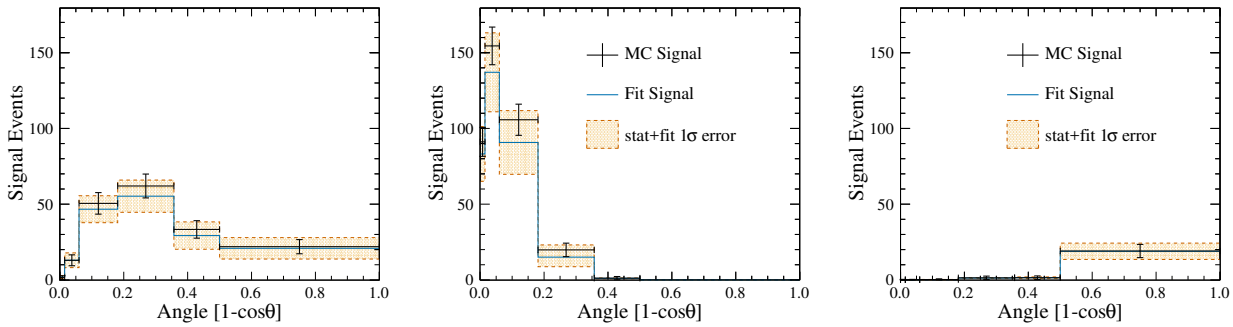

(a) Selected Kalman Contained **(b)** Selected Kalman Exiting **(c)** Selected Cluster

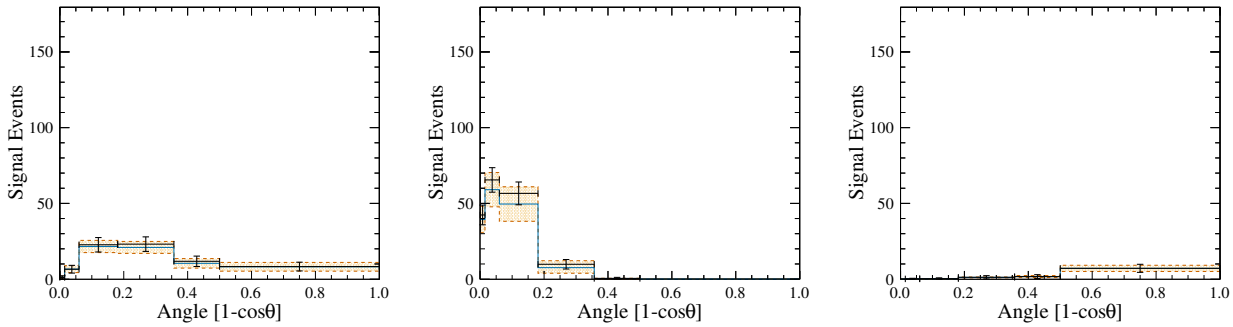

(d) Near Sideband Kalman Contained **(e)** Near Sideband Kalman Exiting **(f)** Near Sideband Cluster

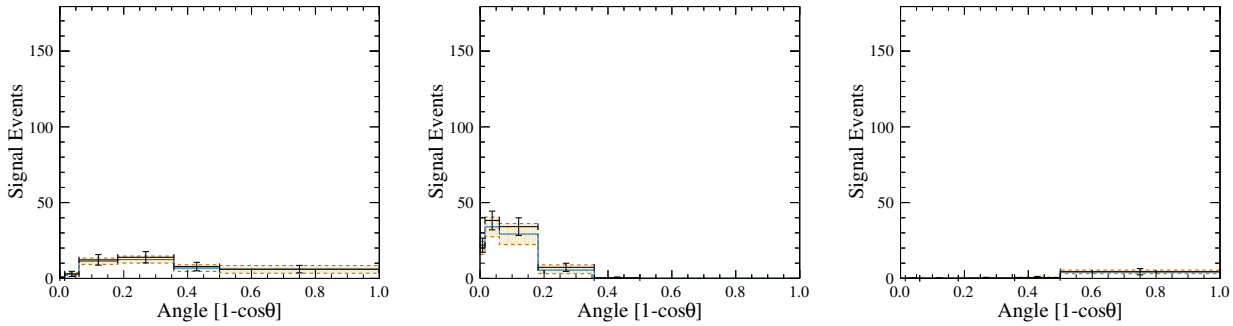

(g) Far Sideband Kalman Contained **(h)** Far Sideband Kalman Exiting **(i)** Far Sideband Cluster

Figure B.90: GENIE Background Study - Background fit in the muon angle projection. Black crosses represent the mock data with statistical error bars. The solid blue line is the best fit and the orange region is the error from the fit. - Angle projection

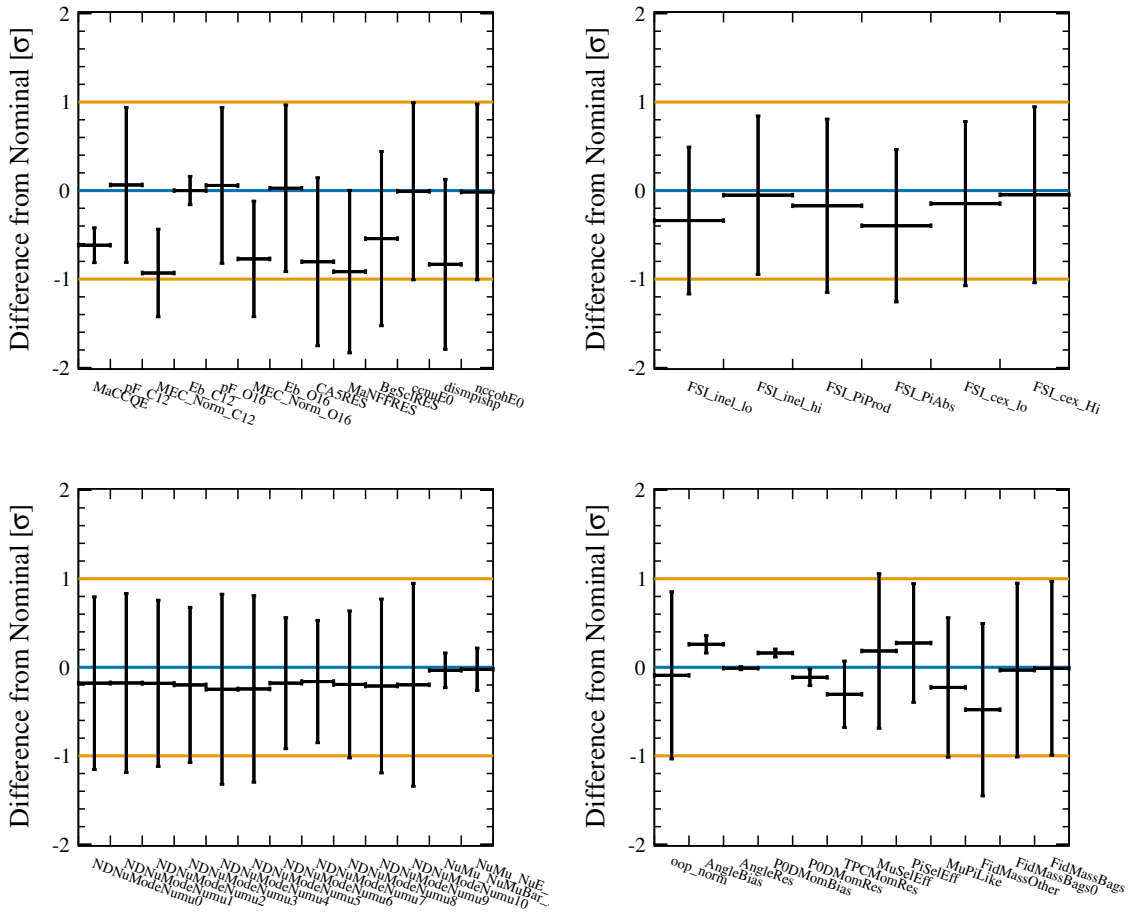

Figure B.91: GENIE Background Study - Fit parameter deviation from nominal. The points in this plot are the best fit parameter value in units of sigma for each dial. The error bars on the points are the error on that parameter from the fit, while the orange lines at +1 and -1 represent the default one sigma error placed on the variable.